CHARACTERISTICS OF MUSCLE ACTIVATION PATTERNS AT THE ANKLE IN STROKE PATIENTS DURING WALKING

By

Thomas Alexander Stone BEng.

A thesis submitted in partial fulfilment of the requirements of
Bournemouth University for the degree of
Doctor of Philosophy

December 2006

Bournemouth University
In collaboration with Salisbury NHS Foundation Trust

I Acknowledgements

I would like to express my sincerest gratitude to Dr Duncan Wood, supervisor during this PhD. The patience and unfailing support shown has been exceptional and is inadequately acknowledged within this passage.

I would also like to extend my appreciation to Prof. Ian Swain for providing me with the opportunity to read for this degree and Prof. Denzel Claremont (School of Design, Computing and Engineering, Bournemouth University) for his supervision and support during this PhD.

I would like to acknowledge the Engineering and Physical Sciences Research Council who funded this work.

Acknowledgments are due to all the clients of the National FES centre, Salisbury District Hospital who participated as volunteers during this project

My Thanks to Dr Steven Crook, Dr Paul Taylor and Mr Rod Lane for technical support and discussion. Also to Geraldine Mann, Catherine Jolly and Ingrid Wilkinson for a clinical perspective. The staff of the Research and Development Support Unit, Salisbury District Hospital for statistical advice and ethical submissions.

Many thanks to Christopher Chamberlin for his friendship, advice and support over the past years. Also to all the staff of the Department of Medical Physics and Biomedical Engineering, Salisbury District Hospital who have helped not only academically but also through their friendship. Additional thanks to Kirstyne, Darren, Salim, Phil and the ELAB, Ingrid and Sam.

I would like to express gratitude to my family who have shown extraordinary tolerance and unerring support over the past years. Indulgently, I must also express my thanks to all those who have helped make, what could have been an invidious affair, a tremendously enjoyable period of my life. Thank you to Chrissie, Bronwen, Wendy, Cat, Emily, Milan and Maj, Mark (for lateral thinking), Lou, Angie, Clare, Nicky, Jo and Vivo.

II Abstract

Stroke causes impairment of the sensory and motor systems; this can lead to difficulties in walking and participation in society. For effective rehabilitation it is important to measure the essential characteristics of impairment and associate these with the nature of disability. Efficient gait requires a complex interplay of muscles. Surface electromyography (sEMG) can be used to measure muscle activity and to observe disruption to this interplay after stroke. Yet, classification of this disruption in stroke patients has not been achieved.

It is hypothesised that features identified from the sEMG signal can be used to classify underlying impairments.

A clinically viable gait analysis system has been developed, integrating an in-house wireless sEMG system synchronised with bilateral video and inertial orientation sensors. Signal processing techniques have been extended and implemented, appropriate for use with sEMG. These techniques have focussed on frequency domain features using wavelet analysis and muscle activation patterns using principal component analysis. The system has been used to measure gait from stroke patients and un-impaired subjects.

Characteristic patterns of activity from the ankle musculature were defined using principal component analysis of the linear envelope. Patients with common patterns of tibialis anterior activity did not necessarily share common patterns of gastrocnemius or soleus activity. Patients with similar linear envelope patterns did not always present with the same kinematic profiles. The relationship between observable impairments, kinematics and sEMG is seen to be complex and there is therefore a need for a multidimensional view of gait data in relation to stroke impairment. The analysis of instantaneous mean frequency and time-frequency has revealed additional periods of activity not obvious in the linear or raw signal representation. Furthermore, characteristic calf activity was identified that may relate to abnormal reflex activity. This has provided additional information with which to group characteristic muscle activity. An evaluation of the co-activation of gastrocnemius and tibialis anterior muscles using a sub-band filtering technique revealed three groups; those with distinct co-activation, those with little co-activation and those with continuous activity in the antagonistic pair across the stride.

Signal features have been identified in sEMG recordings from stroke patients whilst walking extending current signal processing techniques. Common features of the sEMG and movement have been grouped creating a decision matrix. These results have contributed to the field of clinical measurement and diagnosis because interpretation of this decision matrix is related to underlying impairment. This has provided a framework from which subsequent studies can classify characteristic patterns of impairment within the stroke population; and thus assist in the provision of rehabilitative interventions.

III Abbreviations

CVA	Cerebral Vascular Accident
EMG	Electromyography / Electromyogram
FES	Functional Electrical Stimulation
iEMG	integrated Electromyography
LE	Linear Envelope
PCA	Principal Component Analysis
sEMG	surface Electromyography
SENIAM	Surface Electromyography for Non-Invasive Assessment of Muscles
TFR	Time Frequency Representation
ADP	Adenosine Triphosphate
AFO	Ankle Foot Orthoses
ASIS	Anterior Superior Iliac Spine
PCI	Physiological Cost Index
MA	Moving Average
ARV	Average rectified Value
FIR	Finite Impulse Response
MVC	Maximum voluntary Contraction
SD	Standard Deviation
CP	Cerebral Palsy
SCI	Spinal Cord Injury
ECG	Electro-CardioGram
DV	Digital Video
CCD	Charge Coupled Device
RGB	Red, Green, Blue
YUV	Chromatince, Luminance
FPS	Frames Per Second
LAN	Local Area Network
IR	Infra-Red
IC	Integrated Circuit
DAQ	Data Acquisition
PDA	Personal Digital Assistance
WHO	World Health Organisation

IV Publications Arising From This Work

Stone, T. A. and Wood, D. 2006. Surface EMG Analysis of Lower Limb during Un-Impaired and Hemiplegic Walking. In: **Joint ESMAC and GMAS Meeting**, Amsterdam, VU Amsterdam.

Stone, T. A. and Wood, D. E. 2005. Analysing EMG signals from Normal and Hemiplegic walking. In: **The Future of Engineering in Clinical Gait Analysis**, Gordon Museum, Guys Hospital, London, IPEM.

Stone, T. A. and Wood, D. E. 2005. Surface EMG Signals Recorded from the Lower Limb During Un-impaired and Hemiplegic Walking. In: **Biomechanics of the lower limb in health, disease and rehabilitation**, Manchester, Salford. pp 102-103.

Stone, T. A. and Wood, D. E. 2003. Development of a low cost gait analysis system to classify muscle dysfunction in the lower limb after stroke. In: **Biomechanics of the lower limb in health, disease and rehabilitation**, Manchester, Salford. pp 112-113.

V Table of Contents

1 Introduction

Stroke is a debilitating disease that results in patterns of sensory and muscle dysfunction that in turn may cause deficits in motor control. Stroke occurring in one of the hemispheres of the brain will generally result in paresis, partial loss of ability to generate tension in a muscle, effecting the contralateral side of the body, hemiplegia, and produces stereotypical patterns of disability in, for example, walking. Rehabilitation in stroke as defined in Effective Health Care (Effective Health Care bulletins: Stroke rehabilitation 1992) is:

> *"To minimise disability and handicap and to maximise life satisfaction for both patient and carers"*

Rehabilitating those affected by stroke begins at the point of disease onset and can be required for long periods after the initial insult (Outpatient Service Trialist. Therepy-based rehabilitation services for stroke patients at home. 2003; National Clinical Guidlines for Stroke 2ed 2004). However, the effectiveness of rehabilitation modalities is often not assessed, primarily due to their effect not being quantified (Langhorne and Pollock 2002; Toro, Nester et al. 2003). Many attempts have been made to document the pattern of walking or gait in both the non-disabled and disabled communities; these have provided insight into the diverse ways that human locomotion is achieved in normal walking and how the seemingly stereotyped patterns of dysfunction in hemiplegic gait disguise the underlying and individual etiology.

The impairments seen in gait have been measured extensively using both observational (Greenberg, Gronley et al. 1996; Huges and Bell 1994; McNee and Watter 2002; Toro and Farren 2002) and instrumented gait analysis techniques; those systems that use body worn markers, motion sensors and video (Churchill, Halligan et al. 2002; Granat, Maxwell et al. 1995; Perry 1992; Winter, Eng et al. 1995). In addition, electromyography has been integrated with these systems to give insight into the underlying muscle and hence, motor dysfunction that results in gait abnormalities (Nilsson, Federici et al. 1997; Pierrynowski and Galea 2001; Wade, Wood et al. 1987). Traditional observational gait analysis is open to criticism being both subjective and unreliable (Mackey, Lobb et al. 2002); furthermore, comparison between assessments is difficult (Craik and Oatis 1995). Modern gait assessment laboratories can provide extensive and quantitative kinetic, kinematic and muscle activity data. However the use of

these laboratories is often prohibitive due to geography, cost and the required expertise (Toro, Nester et al. 2003). There is a need for a quantitative and well-defined assessment strategy in gait; one that informs the clinician about more functional aspects of gait and that is specific to their questions. Given the research into gait and gait abnormalities, the classification of muscle dysfunction underlying the walking pattern after stroke is still unclear. It is considered important to have a deeper understanding of the characteristics of the different underlying impairments in order that an objective choice of the therapeutic interventions can be made and their impact quantified (Langhorne and Pollock 2002). This project attempts to measure these deficits and characterise gait in pattern groups through sEMG.

Muscle dysfunction during walking was classified by Knuttson et al. (Knutsson 1981). The study employed electromyography (EMG) to capture the activity from multiple leg muscles. The study concluded that impairments fell in to one of three categories:

- Premature activation of the calf muscle (Type I)
- Abolition or marked lowering of electromyographical activity in two or more muscle groups in the paretic limb (Type II)
- Abnormal co activation in several of the limb muscles with no significant decrease in the electromyogram (Type III)

Burridge et al. (Burridge, Wood et al. 2001) tried to quantify the sub-groups observed by Knuttson by comparing the amplitude and timing of impaired and un-impaired surface electromyography signals (sEMG). However, they were not able to measure significant variations in the timing of impaired muscle activity or describe some of the more obvious differences observed between muscle activation patterns. The difficulties of the earlier studies may result from limitations in sEMG processing methodologies and a poverty in the signal features used to identify signal variation. Spectral analysis has provided evidence that the frequency of the sEMG signal can be used to differentiate between impaired and non-impaired subjects (Casale, Buonocore et al. 1994; Wakeling, Pascual et al. 2001). Furthermore, new signal processing techniques for analysing dynamic signals have been shown to be valuable in analysing muscle function during walking (Stefano and Allen 2003; von Tscharner, Goepfert et al. 2003).

The comparison of existing studies is also often confounded by the lack of standardisation of signal acquisition and signal processing methodologies; specifically in methods of amplitude estimation and timing of the sEMG signal. These failings have led to the concerted effort to standardise the area. SENIAM (Surface EMG for Non-Invasive Assessment of Muscles) is a concerted action funded by the EU and the fact that it has

received such funding reflects the maturity and potential benefits of sEMG(Hermens, Freriks et al. 1999). The objectives of the SENIAM project are (1.) To integrate basic and applied research on sEMG at a European level in order to establish European co-operation (2.) To solve key items that prevents a useful exchange of data and [clinical] experience. Thus far the group has developed recommendations on standardisation in three areas: sensors and sensor placement, signal processing and modelling. However, few external studies appear to have embraced the new standards.

The aim of this project was to identify patterns of muscle activity that could be used to characterise walking impairments in stroke patients in order better to understand how these impairments can be mitigated in the future. Although impairments can effect all parts of the lower limb stereotypical impairments can exist at particular joints in particular at the ankle. In this project therefore, focus is given to the ankle. It is believed that surface electromyography can be used to quantify characteristic impairments within the stroke group. Therefore the objectives of this work are:

- To develop gait analysis equipment appropriate for the clinical environment to measure sEMG in relation to walking.
- To identify properties in the sEMG that could be used to characterise gait impairments.
- To identify existing sEMG signal processing techniques that could be useful in analysing impairments.
- To extend these signal processing tools to analyse sEMG with respect to identifying impairment.
- To conduct clinical tests to determine usefulness of sEMG signal processing techniques in hemiplegics patients during walking
- To characterise underlying walking impairments at the ankle in stroke patients.

Chapter 2 begins by outlining the condition of stroke and its impact on the patient and specifically the impact on functional walking. Walking and the mechanisms of the central nervous system that permit un-impaired gait are covered which leads to the specific disruptions of these mechanisms after stroke. Section 2.1.3 then reviews the means by which disturbances to the normal pattern of walking can be assessed and quantified and reflects the wealth and at the same instant the poverty of current methods to quantify the pattern of walking. Section 2.4 reviews the current status of surface electromyography in the clinical field; contemporary methodologies of capturing and processing the sEMG

signal are presented in addition to the restrictions of the techniques. Chapter 3 concludes with a review of the most recent signal processing techniques applied to surface electromyography and identifies techniques that could be particularly useful in analysing gait and impairments after stroke.

In chapter 3 the techniques identified in chapter 2, specifically, principal component analysis and wavelet analysis; are expanded upon. The implementation of each method for this project is described with flow diagrams explaining how each technique relates to one another and thus generate a framework of techniques which are to be applied to the sEMG. In addition, a low cost gait analysis system which addresses some of the issues elucidated in section 3.1 is presented. The specification for each of the systems components is presented and the way in which the specification was achieved. Subsequently, the positive and negative aspects of the system are discussed and reference made to the specific challenges related to the development and future developments of the system.

Data collection for this work was governed by the NHS research ethics which is presented in section 3.4 and presents inclusion and exclusion criteria for the data collection. The assessment protocol including the process for data collection is then given.

The electromyographic and kinematic data collected from stroke patients is reported in chapter 4 sectioln 4.4.4. Firstly, the observational gait analysis results are introduced in graph form. Then, the sEMG data is presented in terms of linear envelope, time-frequency analysis, mean frequency and sub-band filtering. Finally, kinematic data from each limb segment is reported for each subject. A case study is presented for each patient introducing features observed in the sEMG and relating these to kinematic and observational gait analysis results.

The thesis concludes with a discussion of the information gained from the signal processing techniques applied to the sEMG data and a critique of the performance of the gait analysis system. The characteristics of the individual sEMG signals are discussed and a grouping of the patients is proposed through use of the features observed in the sEMG and kinematical data.

2 Literature Review

2.1 Stroke

2.1.1 Prevalence & Incidence

The Office for National Statistics states (5A2 Prevalence of Stroke per 1000 patients, by year: 1994-1998 1998) that for 1994–1998 the number of strokes as a crude rate across all ages in males and females was 2.3 per thousand and 2.2 per thousand respectively (Figure 1).

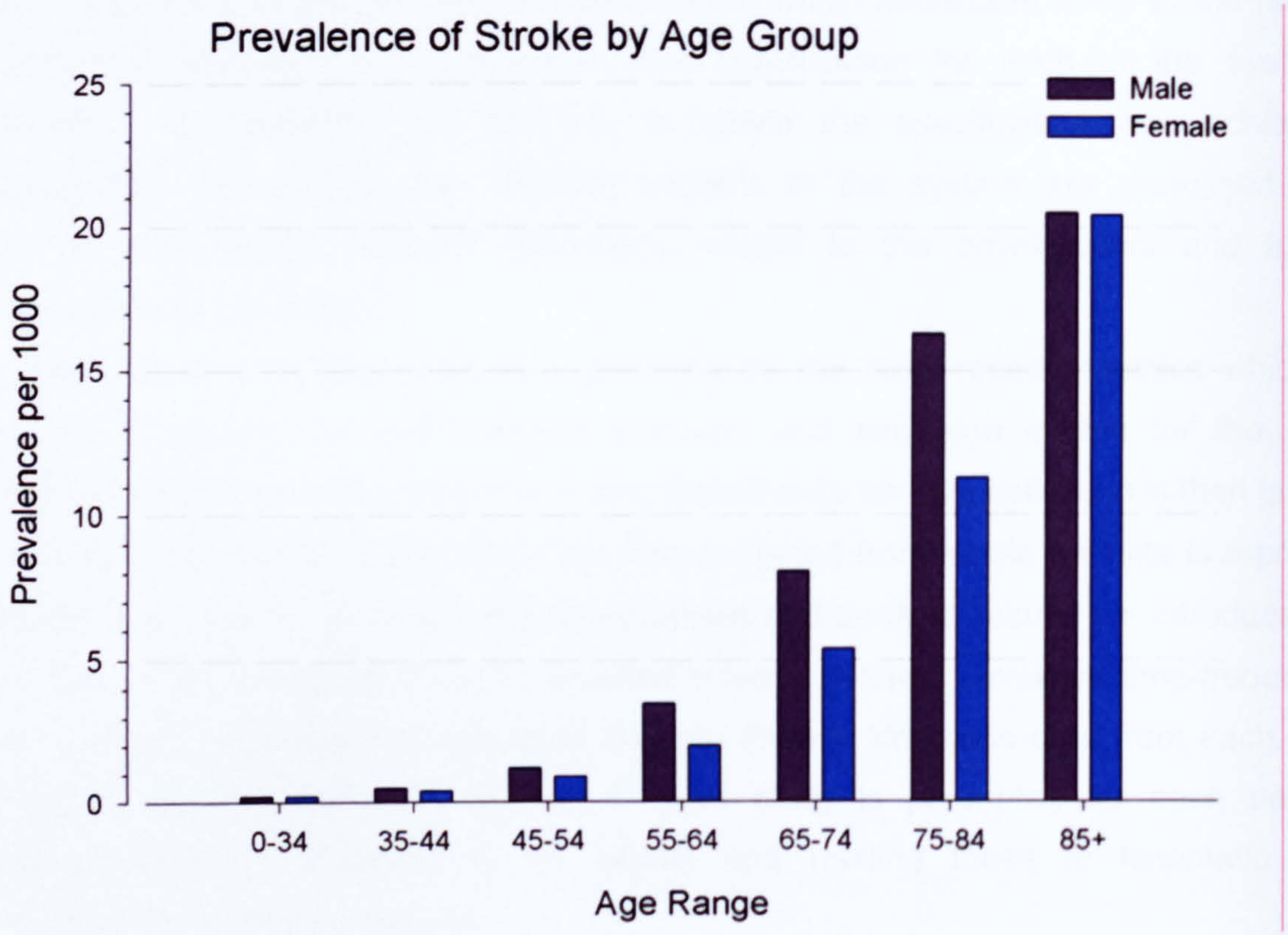

	0-34	35-44	45-54	55-64	65-74	75-84	85+
Male	0.2	0.5	1.2	3.5	8.1	16.3	20.5
Female	0.2	0.4	0.9	2	5.4	11.3	20.4

Figure 1 the prevalence of strokes across ages and gender per 1000

Given an approximate population for the UK of 58 million this translates as a prevalence of approximately 260,000 strokes. The incidence of strokes i.e. the number of new cases is approximately 160,000 in the UK (5A2 Prevalence of Stroke per 1000 patients, by year: 1994-1998 1998), though numbers vary from 258,000 (IS117 Incidence, aetiology and management of stroke 2003) to 125,000 (Mant, McManus et al. 2003). This prevalence and incidence of stroke costs the NHS in the region of 4% (2.3 billion) of its total

expenditure and it is the single biggest cause of disability in the UK and the third highest cause of death (Wade 2000).

Stroke is an all encompassing term for the various forms of cerebral vascular disease which all have in common vascular injury to the brain. The World Health Organisation defines stroke as involving (National Clinical Guidlines for Stroke 2ed 2004):

> *"Rapidly developed clinical signs of focal or global disturbance of cerebral function, lasting more than 24 hours or leading to death, with no apparent cause other than a vascular origin."*

The brain constitutes only 2% of the body's weight yet it requires 20% of the body's oxygen and glucose when the body is at rest (Tortora and Grabowski 2000). Neurons of the brain synthesise adenosine triphosphate (ATP), an important neuro-chemical, almost exclusively from glucose which the brain itself has very little in the way of storage; therefore this large demand must be maintained and any restriction to the flow of blood to the brain can cause permanent damage. The restriction of blood flow to the brain can be caused in a number of ways and in the next section those that come under the umbrella of stroke will be outlined.

2.1.2 Etiology

Stroke consists of divergent subtypes, having in common vascular injury to the brain. Currently cerebral vascular disease is categorised as in Table 1 (International Classification of Disease -10 Chapter IX: Diseases of the Circulatory System 2003):

Group	ICD[1]
Cerebrovascular disease	I60-I69
Subarachnoid haemorrhage	I60
Intracerebral haemorrhage	I61
Other non-traumatic intracranial haemorrhage	I62
Cerebral infarction	I63
Stroke, not specified as haemorrhage or infarction	I64
Occlusion and stenosis of pre-cerebral arteries, not resulting in cerebral infarction	I65
Occlusion and stenosis of cerebral arteries, not resulting in cerebral infarction	I66
Other cerebrovascular disease	I67
Cerebrovascular disorders in disease classified elsewhere	I68
Sequelae of cerebrovascular disease	I69

Table 1 Cerebral Vascular Disease, classification by the World Health Organisation (WHO)

[1] International Classification of Disease (World Health Organisation definition of disease identifier)

Fundamentally stroke can be subdivided into ischaemia and haemorrhage; ischaemia being the deprivation of blood flow to the brain and haemorrhage being bleeding into or around the brain. The mechanism of stroke in addition to the location will define the outcome of the disease with respect to an individual; the location is by far the most important factor. An ischaemic stroke or brain infarct (resulting in permanent injury) may be further subdivided into cerebral thrombosis, cerebral embolism and reduced systemic perfusion. Cerebral infarctions are responsible for 80% of strokes.

An embolism occurs when material from elsewhere in the body occludes a blood flow in a vessel. An embolus tends to arise proximally to the embolism differentiating itself from thrombosis that tends to be a localised process (Harrison and Dyken 1983). Thrombus is the primary source of embolism and primarily from the heart, long vessels, or the venous circulation. Less common are embolisms resulting from tumours or formed from air. The size of the emboli defines to some extent the location of embolism remaining in the extracranial vessels or moving deeper to the intracranial vessels. The other major characteristic of emboli is that they tend to fragment, dislodge and therefore move to distal vessels.

Thrombosis is defined as the condition where the blood changes state from liquid to solid. The important distinction within cerebral thrombosis is that the formation of the thrombus is a localised obstructing process. The lumen of the vessel, hollow centre of the artery or vein through which the blood flows, is narrowed or occluded by the formation of a clot. The Harvard Stroke Registry suggests that 56% of thromboses are caused due to atherosclerosis (Caplan and Stein 1986).

Haemorrhage is divided into subarachnoid and intracerebral haemorrhage. Numbers are slightly less consistent with respect to the incidents of haemorrhage; hospital admissions suggest as many as 20% of strokes can be attributed to haemorrhage, split equally between subarachnoid and intracerebral legions. Other studies would imply fewer numbers for subarachnoid haemorrhage, 5% (Bamford, Sandercock et al. 1990; Ricci, Celani et al. 1991). One thing is certain, the prognosis for haemorrhagic stroke is much worse; subarachnoid haemorrhage as a result of rupture of a sacular aneurysm, the predominate cause of haemorrhage in the subarachnoid space, has a 33% chance of death before the receipt of medical attention. 17 out of 100 will survive, most of whom will suffer from a severe sequela (Caplan and Stein 1986).

A subarachnoid haemorrhage is caused when blood leaks out into the vascular bed on the brain surface and is disseminated via the spinal fluid pathways into spaces around the brain. A ruptured aneurysm will cause rapid bleeding at systemic blood pressure rapidly increasing intracranial pressure. Bleeding directly into the brain is known as

intracerebral haemorrhage, usually caused by increased blood pressure. The haemorrhage, at first soft, dissects along white matter fibre tracks and into the ventricles or to the surface of the brain where it makes contact with cerebrospinal fluid; the blood clots and solidifies causing swelling to adjacent tissue. The blood finally clears, is absorbed and debris cleared leaving a void that may dissect brain pathways. In addition, the very material that protects the brain from the outside world also acts to restrict the swelling of brain tissue and therefore causes hemiation from one compartment of the brain to another (Caplan and Stein 1986; Harrison and Dyken 1983). The damage caused to the brain during haemorrhage can be summarised as the cutting of flow to connecting pathways; localised or generalised pressure injury or the impact of biochemical substances adversely effecting vascular or brain tissue.

Finally, some strokes are the result of a reduced systemic perfusion; this is a generalised lack of flow to the brain often caused by myocardial infarction or arrhythmia. It should be noted that the final three categories of stroke (Table 1) are essentially undefined.

The previous paragraphs have focussed on the physical attack on the brain, the cause and process but not the outcome. As the definition given in section 2.1.1 states, stroke produces a disturbance of cerebral function for more than 24 hours i.e. a lasting disturbance or sequelae; the next section presents the form that this disturbance might take.

2.1.3 Impairment and Disability

Damage to the brain will result in an underlying impairment which in turn will cause disability and finally the probable loss of some social ability, i.e. handicap. As previously mentioned, the location of the brain injury will largely dictate the outcome of the disease as this depends on how the communications within the brain have been damaged. Disabilities from stroke are the result of impairments in various cerebral functions such as cognition, motor and sensory (Caplan and Stein 1986).

The right side of the brain controls the movements of the left side of the body; a stroke in the right side of the brain will therefore cause motor-sensory deficits in the left side of the body including paralysis; left hemiplegia. Right hemisphere stroke will result in impairments in analytical and perceptual tasks such as judging speed, distance, size and position. Furthermore, an impulsive nature can evolve, sufferers becoming assured that they are capable of tasks that they were able to perform before their stroke but are no longer able. Following a right hemisphere stroke a survivor may suffer from left sided neglect where an individual may forget or ignore people and/or objects on their left side;

left sided neglect stems from the impairments of the visual field. Short-term memory problems can also result from a right hemisphere stroke (S-Cook and Woollacott 2001).

Stroke in the left hemisphere of the brain causes motor-sensory deficits in the right side of the body; so called right hemiplegia. In contrast to right-hemisphere stroke, left-hemisphere stroke survivors can develop a cautious behaviour and along with memory problems, making retention of information difficult. These patients generally need frequent instruction and feedback to complete a task. Speech and language problems may occur, known as aphasia, that is generally very specific to the sufferer i.e. they may be able to read and write yet are not capable of forming words, due to paralysis in their speech related muscles, or indeed they may have difficulty using a correct or real word (Caplan and Stein 1986).

Stroke can also occur specifically in the cerebellum or brain stem. The cerebellum's main role is to evaluate the movements initiated by the cerebrum and act as a feedback system to maintain the integrity of the movement and maintain posture and balance smoothing and co-ordinating complex sequences of skeletal muscle contraction; it is phasically active during locomotion. Therefore, stroke in the cerebellum will cause deficiencies in balance, abnormal reflexes and muscle and limb coordination. The brain stem contains nuclei that control subconscious muscular movement including life support functions. It also contains nuclei such as the basal ganglia that help coordinate movement, regulate muscle tone and convey information regarding proprioception and other incoming sensory signals to the rest of the brain. Damage to this part of the brain can be devastating causing bilateral paralysis and impairment of speech, swallowing, eye movement, and impairments in controlling breathing, heart rate and blood pressure (Caplan and Stein 1986).

The inability to walk efficiently is a common disability within the stroke community and has obvious social implications from the purely functional to the aesthetic. In fact, walking is the functional activity that is most valued within the stroke community (Bohannon and Andrews 1995). Mobility after stroke is closely related to the severity of the stroke. The Scandinavian Stroke Scale which has been reported as a good indicator of recovery of and mobility after stroke show those with low scores representing mild motor impairment can often walk without assistance on discharge from hospital, where few with severe motor impairments will recover to walk even with assistance when discharged (Mohapatra and Kelker 2003). A study of 804 stroke patients (Jorgensen, Nakayama et al. 1995) showed that 95% of surviving stroke patients will regain walking function eleven weeks after their stroke. More specifically, the study reported that 50% of patients could walk without assistance after rehabilitation, 11% could walk with assistance and 18% had no

functional gait. Furthermore, the study supported the link between initial mobility scores and outcome. There is certainly variability in the reported outcome after stroke with respect to walking function. For example, a comparative study (Wandel, Jorgensen et al. 2000) reports that only 10% of stroke patients would regain independent walking and in a study focusing on those having minimal rehabilitative intervention, 66% of patients reported that they could walk on discharge (Hale and Eales 1998). Walking without assistance, or the patients testimony to be ability to walk, does not of course specify the quality or the physiological cost of (the effort required by) the patient's gait.

Primary impairments after stroke are usually characterised as diminished muscle strength, an inability to generate voluntary muscle contraction of normal magnitude, and inappropriate timing or grading of a contraction (Olney and Richards 1996). Strength of lower extremity muscles have been correlated with walking performance (Bohannon 1991; Hamrin, Eklund et al. 1982), though it has also been described as a "non-comprehensive determinant of gait performance" when related to other clinical measures such as motor control. Motor control has been strongly associated with walking performance, it is the selective control of proximal lower limb muscles that might be the principal factor in an individual's walking velocity (Bohannon 1987; Chen, Chen et al. 2003). Reduced strength is thought to be attributed to several issues concerning the motor unit; the firing rate of the motor unit may be reduced, there are fewer motor units available to be activated or there is, fundamentally, an inability to excite motor units (Frascarelli, Mastrogregori et al. 1998; Thomas, Butler et al. 2002). An observed decrease in strength can also be associated with competing agonist and antagonist muscles known as co-contraction and is often seen in the ankle of the hemiplegic patient (Olney and Richards 1996). In this case the plantar flexors actively provide a moment of force about the ankle that cannot be overcome by the dorsiflexors or require excessive contribution of the dorsiflexors. Abnormal muscle synergy is one of the hallmarks of hemiplegic walking (Lamontagne, Richards et al. 1998).

Several weeks post stroke, spasticity may become evident in some of the patients muscles. Spasticity is a complex condition that will be addressed in greater depth later in the thesis (see section 2.2.3). However, its effects are, generally speaking, a resistance to lengthening of the muscle and are often referred to in terms of hypertonicity or increased tone. This increased resistance to stretch can be attributed to an abnormal reflex response to a movement, active (positive) influences, or to passive (negative) influences such as a mechanical change within the muscle. Studies report anything from 19% of stroke patients (Sommerfield, Eek et al. 2004) to 38% of stroke patients (Watkins, Leathley et al. 2002) will present with signs of spasticity.

The proportions of those patients who suffer long term walking disability as a result of stroke is evident and supports the case for diagnostic techniques to apply assistive technologies and medical interventions. In order to restore a patient's ability to walk independently, retraining of their gait is often necessary requiring measuring and discriminating deviations in their walking patterns from normal and prescribing the best therapeutic course. It is therefore necessary to understand the characteristics of both normal and pathological gait.

2.2 Walking and Motor Control

Distributed areas of the central and peripheral nervous system interact in complex ways to produce what appears to most as an effortless and everyday activity. Controversy still exists around how the central nervous system integrates afferent information from many centres such as the visual, vestibular and proprioceptive systems. These are believed to modulate some central motor programme to coordinate the timing and degree of activation of muscles required for efficient and goal directed locomotion. Indeed, it has been suggested that there exists more than one central motor programme controlling sub-cortical coordination and reflex modulation mechanisms separately (Duysens and Van de Crommert 1998).

As was mentioned in the previous chapter abnormal walking patterns are often present after stroke; but before one can define what is abnormal it is appropriate to define what is considered normal. This section looks at how the process of walking is described and how gait events are subdivided. The neuro-physiological basis for locomotion is given describing how normal motor control is achieved and how this is disrupted after stroke.

2.2.1 The Gait Cycle

The gait cycle is described by a series of temporal events and is defined between foot strike and foot strike on the same leg. The gait cycle is normalised in time to 100% and subdivided between stance and swing phase, which represent approximately 60 % and 40 % respectively of one stride (see Figure 2 top).

Traditionally sub divisions of the gait cycle represented events related to normal function, this was due to the historical association of clinical gait analysis to the rehabilitation of amputees for which such a description was appropriate. However, this is often not appropriate for deviations due to paresis or paralysis and alternatives were developed predominantly by members of the Rancho Los Amigos Medical Centre (Perry 1989). They describe the two periods of the gait cycle, stance and swing, which are divided into eight functional phases that fulfill the necessary tasks to complete a stride.

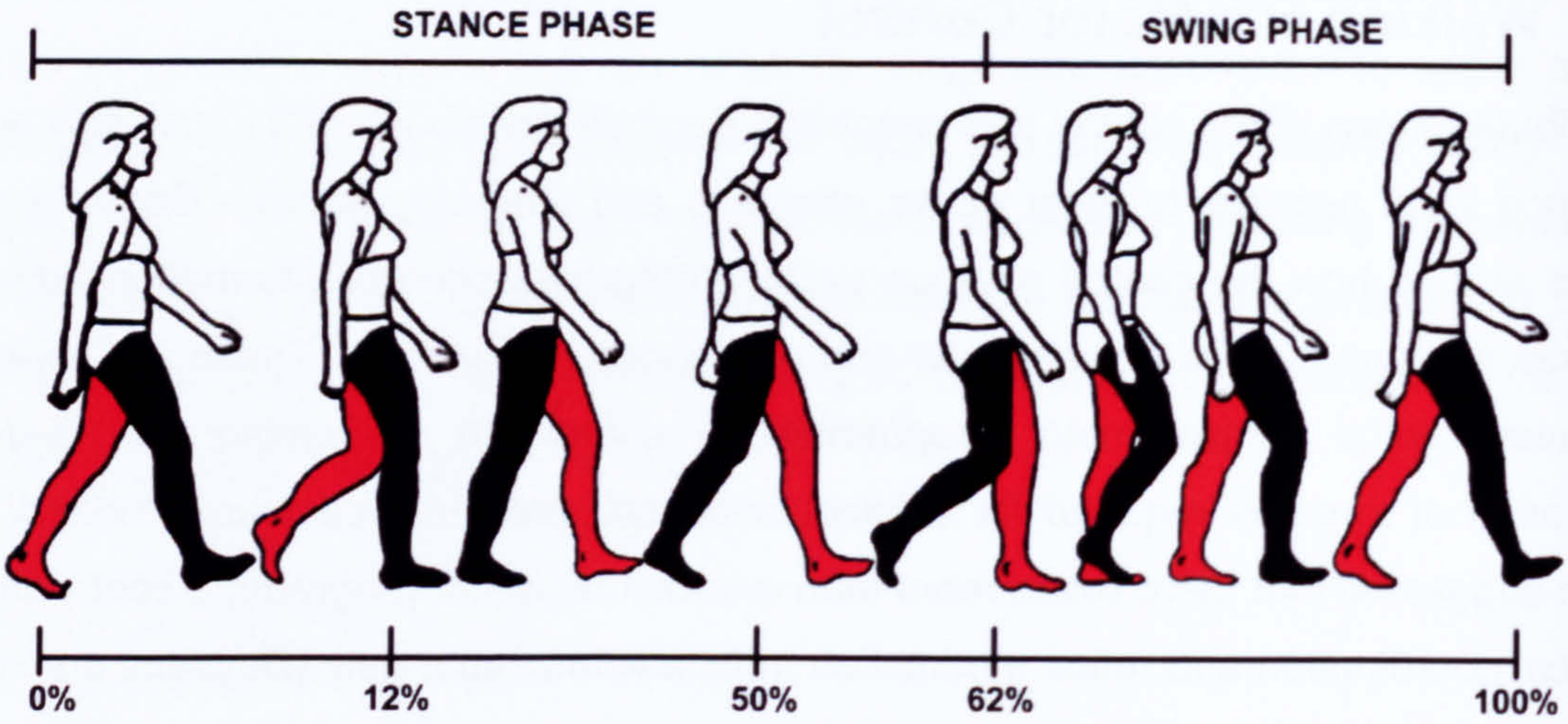

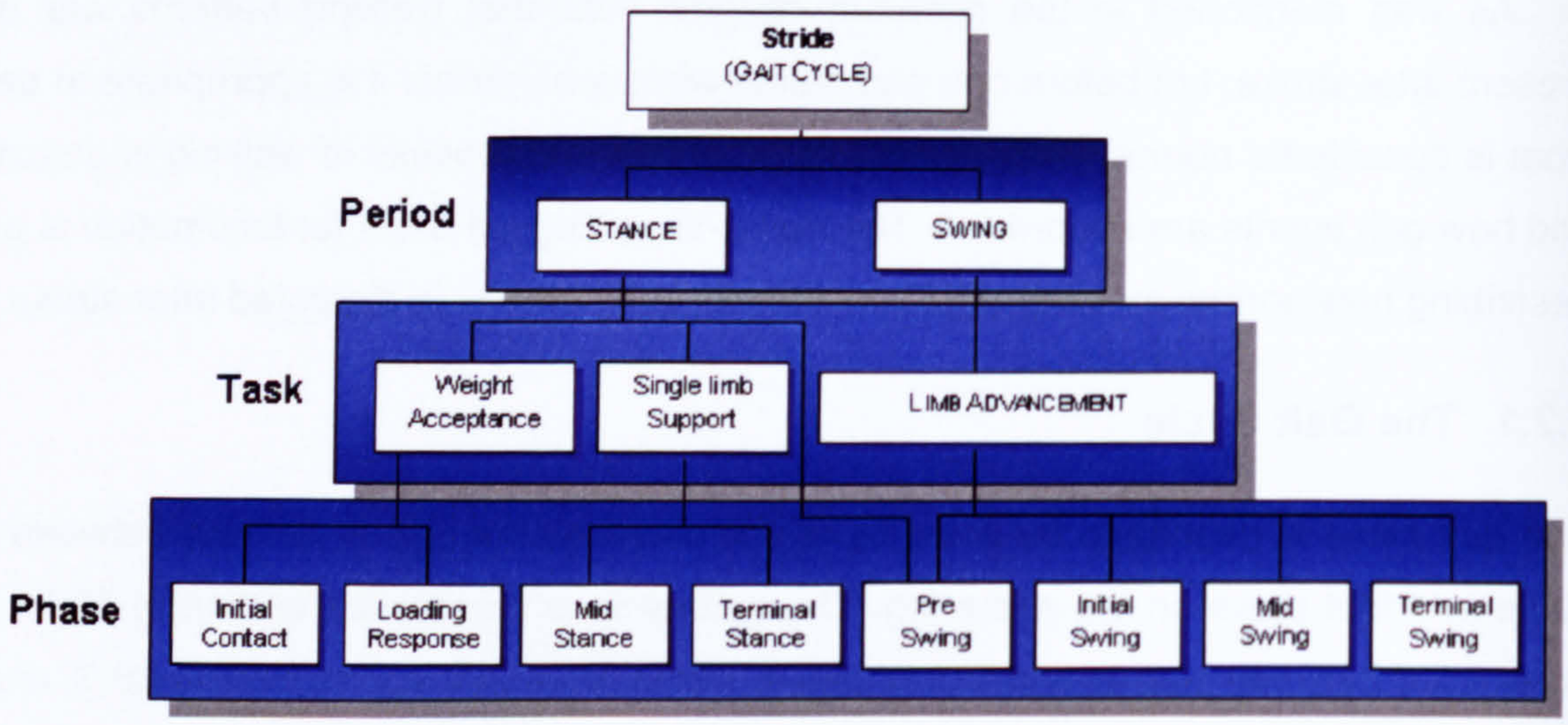

Figure 2 (Top) shows the Gait cycle, expressing several means of describing the aspects of gait. Bottom figure displays the relationship between the terminology. Adapted from the origonal (Rose and Gamble 1994)

The stance phase requires two tasks, weight acceptance and single limb support. Weight acceptance begins with initial contact often defined as foot strike and continues to loading response. Single limb support has three phases: mid stance, terminal stance and pre-swing. The swing phase begins with pre-swing, goes through initial, and mid-swing to terminal swing then ends at initial contact (see Figure 2 bottom).

The descriptions used to differentiate between points in the gait cycle vary. For example, Sutherland et al. (Farmer, Swash et al. 1993) introduced the terminology initial double limb stance, single limb stance and terminal double limb stance. This reflects that there is bilateral foot contact for the first 12% of the gait cycle and for the final 10% of the stance phase (50% – 60% gait cycle). Significantly, during single limb support the body is

supported by only one limb. However, here the description given by Perry (Perry 1992) is used.

The normal gait pattern is consistent and several texts present detailed descriptions of motion, in all anatomical planes (Perry 1992; Winter 1990). Therefore the gait cycle is described with regard to normal walking so far as it introduces the terminology required to analyze pathology in gait and in addition, to reflect the consistency of kinematics and kinetics of non-pathological walking. Descriptions will predominantly focus on sagittal plane motion as this is most prominent.

2.2.1.1 Loading response

The first event in the gait cycle is initial contact, often referred to as heel strike or foot strike. Initial contact is instantaneous and marks the beginning of the loading response phase that is 0 to 10% of the gait cycle, and describes the transference of body weight onto the stance limb. The ankle, which is in a neutral position, is subject to a large plantar flexion moment as the ground reaction force acts posterior to the ankle. If the ankle is observed in the frontal plane and transverse plane, the ankle is seen to rapidly evert and externally rotate during the first 15% of the gait cycle. The passive plantar flexion movement is resisted by the action of the pre-tibial muscles and controls plantar flexion. At initial contact, the knee joint is at full extension. With floor contact, a large extensor moment is created about the knee that is restrained by the knee flexors. This eccentric activity helps prevent the knee hyperextending; this also represents an important power absorption phase for the knee joint. The hip is in flexion and requires the activation of the hip extensors to provide support. The hip must resist a strong abduction and flexion moment as the load is released from the swing limb. The pelvis is supported through the activation of gluteal muscles.

2.2.1.2 Mid Stance

During mid-stance, 10 to 30 % of the gait cycle, plantar flexors eccentrically control the rotation of the ankle preventing the body's centre of mass from dropping, decelerating forward rotation and allowing the knee to selectively and rapidly extend, so-called knee ankle stability linkage. The rotation of the tibia over the tarsus is known as the second or ankle rocker. This permits the limb to advance over the stationary foot. The knee moves from flexion back into extension. This occurs as the vertical component of the ground reaction force moves anterior to the knee and produces passive extension that is controlled by the knee flexors, up to this point quadriceps activity assists extension. The

femur progresses over the tibia that is restrained by the triceps surae muscles. During mid-stance the hip moves into extension as the centre of mass moves forward.

2.2.1.3 Terminal stance

The trunk progresses forward over the stationary foot and the movement of the tibia is restricted and maintains the ankle in approximately 10° of dorsiflexion. This relates to an important phase where mechanical energy is absorbed through the eccentric contraction of the calf muscles. The heel lifts from the ground and the forefoot becomes the fulcrum over which limb pivots, the third or forefoot rocker. At this point the greatest strain is placed on the ankle plantar flexors stabilising the ankle through the phase. The centre of mass is elevated during heel rise permitting the contralateral leg to swing through. The knee having reached its maximum extension during stance begins to move back into flexion; it is at this point that the stance limb must support the pelvis alone and requires the activity of the hip abductors.

2.2.1.4 Pre-swing

The final phase of stance is between 50 and 60 % of the gait cycle; here the weight is transferred to the contralateral limb. The knee moves into flexion, the joint moving to approximately 35° to 40° flexion. This flexion is caused predominantly by action of the hip and ankle rather than active contribution of knee flexors. Knee extension is partly due to a force vector that moves posterior to the knee. The ankle allows the tibia to rotate but the fixed knee naturally makes the fibula rotate forward. Knee flexion is controlled by the activity of the quadriceps principally with a brief contribution of rectus femoris. At this point the ankle reaches 20° to 25° plantar flexion. As weight is transferred, the activity of the plantar flexors reduces as the limb is being unloaded. The hip flexes and moves to neutral. However, in the coronal plane there is a lateral displacement of the pelvis along with the force vector, this generates an adductor torque, towards the midline, and this must be restrained by the stance limb pelvic musculature.

2.2.1.5 Initial swing

The final 40 % of the gait cycle begins as the toe is lifted from the ground and the knee further flexes to the region of 60° through the inertial forces of the limb and activity primarily of bicep femoris. The ankle begins to dorsiflex as the toe leaves the ground. This is the principal power generation phase of the hip as the hip ceases to extend and begins to flex swinging the leg through. The primary function of both knee and ankle is to clear the foot from the floor in order to let the swing limb advance.

2.2.1.6 Mid-swing

During mid-swing, where the tibia becomes vertical, the ankle is dorsiflexed through activity of the tibialis anterior, thus enabling the foot to clear the floor. Floor clearance is achieved through flexion of the hip and ankle as the knee passively begins to extend. Muscle activity at this point is moderate, as much movement is achieved passively. The tibialis anterior is sustaining the movement initiated in initial swing and the hamstrings are beginning the activity in preparation for terminal swing.

2.2.1.7 Terminal Swing

In the final phase of the gait cycle the ankle is held in the neutral position and is maintained in this position in readiness for initial contact. The knee extends further, and rapidly, principally through the action of the vastus muscles. Knee extension advances the tibia in preparation for foot contact. In terminal swing the thigh segment is decelerated by action of the hamstrings and gluteus maximus positioning the limb ready for initial contact. It should be noted that during the swing phase no ground reaction forces act on the limb.

2.2.2 Motor Control

Motor control can be described as the ability to regulate or direct the mechanisms essential to movement. Movement disorders apparent after stroke result from the disruption of normal motor control. However, the understanding of the neural control of locomotion is not definitive.

In the early part of the twentieth century, it was thought that the nervous system facilitated movement by way of reflex chaining i.e. a stimulus would create a response that in turn would create another response; reactions from several parts of the nervous system combining to create action. The theory of reflex action was expanded into a hierarchical model; this top-down structure suggested that higher levels of the system exerted control on those primitive levels below and therefore moved away from the idea that the nervous system is purely reactive. More recently theories regarding the control of mammalian locomotion have established that there exists an innate locomotive pattern that is modulated by sensory feedback and supraspinal centres (Lacquaniti, Grasso et al. 1999; McCrea 2001).

More recently, the term central pattern generator (CPG) describes spinal networks that generate rhythmical movements without the need for control from higher areas of the central nervous system or peripheral feedback. It has been suggested that in mammals each limb is controlled by a separate CPG - that is itself constructed of a unit CPG or burst generator controlling flexors and extensors separately - controlling a set of

synergistic muscles about a joint. This model of control permits the units to activate in and out of phase and equally with variable phasing through reciprocal inhibition and modification of the synaptic strength in the spinal cord (Guadagnoli, Etnyre et al. 2000; Van de Crommert, Mulder et al. 1998; Zajac, Neptune et al. 2003). The exact nature of CPGs is still under debate; but, it would appear that CPGs are populations of neurons that can interrelate in a flexible manner. This relation is not only within but also between the different levels of the central nervous system and can generate global or stereotypical movements. Therefore, though "primitive" rhythmical movements, such as during locomotion, may have their origin within a hard-wired, innate, motor programme the flexibility of the motor system requires the mediation of both supraspinal and peripheral control.

Flexor reflex afferent feedback is known to play a vital role in the control of locomotion; indeed in mammals they play an intrinsic role in the CPG and are a major determinant of its rhythmic nature (McCrea 2001). The action of segmental reflexes in motor control is complex and highly flexible, and with respect to locomotion they cannot be reduced to a generalised action.

Reflex mechanisms are important to allow the system to overcome perturbations in walking and to adapt to variations in the environment; in addition, they support the centrally programmed motor-neuronal drive (Bo Nielsen 2002; Dietz 1997). The influence of monosynaptic reflexes, those that involve one motor neurone and one sensory neurone, can be modulated depending on the sensitivity of muscle spindles and the level of pre-synaptic inhibition in the spinal cord. During normal walking the pattern of contribution of stretch reflexes have been seen to vary depending on muscle group and to be gait phase dependent; acting to both suppress and facilitate activity of a muscle group (Duysens, Trippel et al. 1990). For example, reflex amplitude decreases in the quadriceps during stance and knee flexion for shock absorption (Dietz, Discher et al. 1990; Mrachacz-Kersting, Lavoie et al. 2004). The pattern for calf muscles displays a facilitation of stretch reflex at the end of stance and a suppression of the reflex during swing, respectively to promote activity during push off and reduce it during the dorsiflexion of the ankle in the swing phase (Dietz 1997). However, it is thought that during normal walking monosynaptic inputs to the motor neurones are depressed by pre-synaptic inhibition and thus make a small contribution; it is only when there is a large perturbation in gait that the reflex response is strong enough to overcome the inhibition (Sinkjaer, Andersen et al. 2000). Recently it has been suggested that many of these reflex responses, during perturbations in gait, act as error signals and are mediated by supraspinal centres. Tibialis anterior activity was shown to be affected by long latency reflex activity after rapid plantar flexion

of the ankle during walking (Sinkjaer, Andersen et al. 2000). This allows the central nervous system to apply non-reflex corrections to the motor programme. In addition, many so-called reflexes are in fact anticipated by, and are functionally part of, the motor pattern during walking (Bo Nielsen 2002).

Increasingly the influence of spinal centres to the control of locomotion is becoming clear. Stroke is an insult to the brain and not spinal cord although it cannot be inferred that stroke does not disrupt spinal control directly. Nevertheless, there is evidence for the existence of several locomotor regions within supraspinal centres in humans that are required not only to regulate the rhythm of the locomotor pattern but also to activate it. Therefore consideration must be given to the impact to and between these supraspinal areas after stroke. Within the brainstem there exist four locomotor regions that, when stimulated, generate spontaneous locomotion patterns during animal studies and are believed to exist in humans (McCrea 1996). These locomotor regions are themselves synapsed by many areas of the brain, each with an important role in walking. The mesencephalic locomotor region, for example, integrates signals from the basal ganglia and cortex. The basal ganglia, although still essentially a mystery, is thought to have profound influence on movement. Evidence drawn from impairment associated with diseases of the basal ganglia, for example Parkinson's disease, reflects its important role in gait. The basal ganglia influence movement through the connectivity with the cortex. The cerebral motor cortex, specifically the primary, supplementary and pre-motor cortex, connects with descending motor pathways and synapses with alpha motorneurones and therefore provides a central drive for the activation of muscles. Additionally therefore, the motor cortex is related to generating motor programs, modulating muscle activation and importantly influencing long latency, segmental, reflexes. Both the basal ganglia and motor cortex have neural pathways to and from the cerebellum which, and again mostly through the outcomes of diseases of the cerebellum, is thought to compare descending motor programs with afferent information in order to smooth and coordinate movements.

2.2.3 Disruption of Motor Control after Stroke

Lesions of the upper motor neurone after stroke disrupt the normal mechanisms of motor control due to damage to populations of neurones or the communication between them. Primary motor impairments are those that affect muscle strength, muscle tone, coordination and voluntary muscle activation.

Partial loss of the ability to generate tension in a muscle, referred to as paresis, results from damage to descending motor pathways that prevents normal motor neural drive to the motor units (S-Cook and Woollacott 2001) and thus the precise control of

muscle contractions. The location of a lesion very much dictates the degree of impaired function and the limbs involved. For example, because the origins of the corticospinal tract are distributed in the cortex a lesion is likely to involve impairment of fewer functions. However, if the same lesion were to occur in the subcortical region where the fibres of the corticospinal tract are crowded closer together there would be far greater breadth of impairment. Weakness is the result of inappropriate recruitment of motor units (el-Abd, Ibrahim et al. 1993) or the reduced rate of firing in motor units (Frascarelli, Mastrogregori et al. 1998; Gemperline, Allen et al. 1995) and changes in the mechanical properties of the muscle (Bourbonnais and Vanden Noven 1989). Distal muscle control tends to be affected more profoundly than that of proximal muscles in cerebral lesions due to the reduced ability to modulate motor neurone firing frequencies during small voluntary movements (Frascarelli, Mastrogregori et al. 1998; S-Cook and Woollacott 2001). Its contribution to movement impairments is now being considered increasingly important and within gait more complex (Bourbonnais and Vanden Noven 1989; Lamontagne, Malouin et al. 2001; Nadeau, Gravel et al. 1999; S-Cook and Woollacott 2001). The capacity of a subject to generate tension in a muscle is thought to limit the maximum speed of walking. However, this is not a simple correlation. Weakness in muscles specific to walking certainly inhibits gait speed but only if there is no compensatory strategy to the loss of function due to the weakness (Nadeau, Gravel et al. 1999). The plantar flexors would represent such a muscle group providing significant power during stance to advance the centre of mass (Olney, Griffin et al. 1991). Although plantar flexor weakness has been positively correlated with reduced walking speed, the passive constituent of the muscles also appears to play a significant role in compensating for disrupted motor control (Lamontagne, Malouin et al. 2001).

Pretibial muscle weakness has been put forward as an underlying impairment for excess plantar flexion during swing, and results in an inability to maintain tension against the elastic tension in the calf (Perry 1992). Weakness, or reduced muscle activity in several muscles in the paretic limb also characterises type 2 impairments as described by Knutsson et al. (Knutsson and Richards 1979) – see introduction. However, an inability of the pretibial muscles to generate tension to overcome passive tension in the calf may also reflect positive impairment in the calf (Becher, Harlaar et al. 1998; Burridge, Wood et al. 2001).

Muscle tone ranges from flaccidity, hypotonia, to spasticity and rigidity, abnormal hypertonia. Spasticity can often develop several months after the initial stroke, after 12 months 19% of patients present with spasticity (Watkins, Leathley et al. 2002), though

others report higher numbers. The term spasticity can have a wide clinical perception. However, it is generally defined:

> *"A motor disorder characterised by a velocity dependent increase in tonic stretch reflexes with exaggerated tendon jerks, resulting from hyperexcitability of the stretch reflex, and is one component of the upper motor neuron syndrome" (Lance 1980)*

Though the mechanisms that generate spastic behaviour in muscles are not completely understood, it is widely believed that damage to descending motor systems produce increased excitability of the alpha motor neurone (S-Cook and Woollacott 2001). This was thought to be due to an exaggerated monosynaptic stretch reflex response and poor control of polysynaptic stretch reflex (Farmer, Swash et al. 1993). However, this explanation failed to make clear long and medium latency reflex contribution to spasticity; only recently has it been confirmed that spastic hypotonia depends on the release of group II afferents and results in reduced inhibition of group Ia afferents (Sinkjaer, Andersen et al. 2000). In addition, it excludes findings that show, in some subjects, there is no electrophysiological manifestation in the spastic muscle. The latter suggests that some spastic muscles undergo rheological change generating passive tension (Dietz and Berger 1983). The complexity of clinical manifestations of spasticity has encouraged an alternative definition that emphasises the broader components to spasticity other than just enhanced stretch reflex (Burridge, Wood et al. 2005; Pandyan, Gregoric et al. 2005; Voerman, Gregoric et al. 2005; Wood, Burridge et al. 2005).

> *"Disordered sensori-motor control, resulting from an upper motor neurone lesion, presenting as intermittent or sustained involuntary activation of muscles"(Pandyan, Gregoric et al. 2005; Wood, Burridge et al. 2005)*

The contribution of spasticity to gait performance has often been inferred from static assessments of hypertonicity (Becher, Harlaar et al. 1998; Sinkjaer, Andersen et al. 2000) which in part is supported by the focus of Lance's definition given earlier. Consideration of purely passive contributions to spasticity has been criticised as the presentation of spasticity varies from static to dynamic conditions (Bo Nielsen 2002; Yelnik, Albert et al. 1999). Specifically, Dietz et al. (Dietz 1997) emphasises the weak relationship between physical symptoms observed during clinical examination and altered neural mechanisms underlying impairment in active movements. Electrophysiological methods exist to identify

objectively spasticity during walking (Knutsson and Richards 1979) however, not quantitatively. In this light, a method to quantify spastic contribution during walking was presented by Lamontagne et al. (Lamontagne, Malouin et al. 2001) and demonstrated the locomotion and phase specific nature of spasticity.

Plantar flexor spasticity can be seen in stroke patients and has been reported in several studies (Knutsson and Richards 1979; Olney and Richards 1996). Plantar flexor spasticity is often observed as premature activation of the calf muscles as it is stretched during dorsiflexion. Knuttson et al. (Knutsson and Richards 1979) denoted this as a type 1 activation pattern and observed it in 9 out of 29 patients. These observations were supported by Burridge et al. (Burridge, Wood et al. 2001) who also found low Tibialis anterior activity combined with inappropriate activity of the calf muscle. In an assessment of H-reflex modulation in spastic paretic patients Yang (Yang, Fung et al. 1991) reports that reflex modulation is commonly reduced during stance and the stretch reflex is slightly depressed during swing. This would support the idea that premature calf activity was related to an improperly modulated stretch reflex (Sinkjaer 1997; Yang, Fung et al. 1991). Lamontagne et al. (Lamontagne, Malouin et al. 2001) maintain that the consequence of plantar flexor spasticity is poorly understood as no significant relationship was found between plantar flexor spasticity and moment. Therefore, plantar flexor spasticity is not necessarily a primary contributor to plantar flexor weakness (Lamontagne, Malouin et al. 2001), whereas, passive tension in the plantar flexors do contribute to the plantar flexor moment (Lamontagne, Malouin et al. 2000). The contribution of calf spasticity to the perceived weakness of the tibialis anterior during dorsiflexion has been supported by Knuttson and Burridge however, increased tibialis anterior muscle activity has also been observed with hypertonic calf muscles again reflecting the contribution of excessive plantar flexor stiffness (Lamontagne, Malouin et al. 2001; Nourbahsh and Kukulla 2003).

In all, the literature expresses the complex relationship between spasticity and function. However, most intriguing is the increasing volume of literature that downplays the contribution and prevalence of spasticity, or perceived spasticity, in impairment (Becher, Harlaar et al. 1998; Bohannon and Andrews 1990; O'Dwyer, Ada et al. 1996; Sommerfield, Eek et al. 2004; Watkins, Leathley et al. 2002).

After a stroke, appropriately graded and phased muscle activity is often absent generating stereotypical patterns of movements that cannot be correctly adapted to the environment or specific task. Correct muscle coordination does not reflect on an individual muscle's capacity, but rather how it acts in relation to other muscle groups. However, it cannot be assumed that a muscle can physically permit the activity it is required to. Therefore, influences such as the biomechanical structure of the muscle will affect the

efficacy of the coordinated movement. Abnormal co-activation of several muscles groups was described by Knuttson et al. (Knutsson and Richards 1979) as type 3 impairments. These patterns were only found in 4 of the 29 patients and were combined with normal levels of activity. Indeed it was reported that activity of the muscle might sometimes be increased above that considered normal. In particular, quadriceps, calf and hamstrings became particularly co-activated. Lowered tibialis anterior activity was observed in combination to abnormally phased calf muscles. Abnormal synergies result in characteristic flexor extensor patterns as muscles are simultaneously recruited across multiple joints. Additionally, the phasing of a single muscle may reflect a loss of selective recruitment, for example in the control of plantar flexion at foot strike. Though not quantified, Dimitrijvic et al. (Dimitrijevic, Faganel et al. 1981) also categorises co-activity between the gastrocnemius and tibialis anterior during stance and mid-swing. However this was only present within 3 of the 34 patients within the study. Levels of co-contraction were measured by Lamontagne et al. (Lamontagne, Richards et al. 2000; Lamontagne, Richards et al. 1998) who found that levels of co-activation in the non-paretic limb increases between initial contact and contralateral toe off. This increase in co-activity was linked to decreased levels of postural stability as was the reduction of co-activity on the paretic side. The reduced co-activity was seen in the single limb support phases i.e. swing phase on the contralateral limb. This was not linked with reduced gait speed in the sense that healthy subjects display reduced levels of co-activity when walking slowly (Murray, Mollinger et al. 1984; Yang and WInter 1985). However, levels of co-activity were linked to gait speed in the respect that more severely affected patients, i.e. slower walkers, displayed increased levels of co-activity on the non-paretic side as an adaptive behaviour.

2.2.4 Walking Impairments after Stroke

Disruption to normal motor control generates abnormal patterns of movement either by direct influence or through the adoption of compensatory movements in an attempt to overcome the impairment.

In a review of impairments and possible compensatory strategies Olney et al. (Olney and Richards 1996) lists five kinematic deviations that commonly occur after stroke and reflect early studies by several authors (Knutsson and Richards 1979; Lehmann, Condon et al. 1987). Firstly, limited ankle dorsiflexion at initial contact and during stance could reflect poor control of the triceps surae or an attempt to increase stability at initial contact. Secondly, knee hyperextension in the stance phase could again reflect calf spasticity or abnormal synergy; however, this could also reflect a method of stabilising the knee in response to weakness about the knee and therefore can be used to assist during the

propulsion phase of gait. Mulroy et al. (Mulroy, Gronley et al. 2001) used a statistical method (Cluster Analysis) to assess the primary kinematical contributions to impaired gait and found that those with increased knee extensors to be a prominent group, this was also reflected in work by De Quervain et al. (De Quervain, Simon et al. 1996) who found an equivalent group. Reduced knee flexion in swing might well reflect an inability to activate knee flexors; alternatively, it could be a method of keeping the foot in close proximity to the ground, thus, ready to provide support if necessary. Increased knee flexion during the stance phase is thought to be an impairment of the knee extensors; i.e. an inability to support the knee joint during loading response. Mulroy et al. (Mulroy, Gronley et al. 2001) terms this a buckling knee pattern and again was a prominent sub-group also termed "stiff knee pattern" by De Quervain et al. (De Quervain, Simon et al. 1996). Finally, the common feature of hip hitching and circumduction are compensatory methods of clearing the foot from the ground during the swing phase. This is in response to an inability to dorsiflex the foot or to flex the knee during the swing phase. Inadequate hip flexion will result in difficulty advancing the limb during the swing phase. In order to achieve better limb advancement this can be compensated for by recruiting abdominal muscles; overtly this appears as a lean of the trunk to the posterior. In addition, circumduction, vaulting and contralateral lateral sway may be employed (S-Cook and Woollacott 2001).

Chen et al. (Chen, Patten et al. 2005) recently confirmed many of these findings in a treadmill study at matched speeds with un-impaired subjects. Findings showed that hip joint angles were on average reduced and in addition the variability of the hip angles increased from normal. In the paretic limb the hip was seen to extend less than the non-paretic limb which would impede proper limb advancement. Knee joint angles were characteristically lower at toe-off of the paretic swing limb and suggested poor preparation for the swing phase. Interestingly there was no statistically significant increase in ankle angle on the paretic side during toe-off. This is in contradiction to most clinical observations and earlier kinematic findings. This might relate to the use of a treadmill in the study (Chen, Patten et al. 2005) and the fact that three of the six patients wore an ankle foot orthosis (AFO) during the study. It should be noted that the use of an AFO is very likely to have affected other joint kinematics. Lateral displacement of the paretic limb was significantly increased and suggestive of circumduction in order to clear the swing limb. An increased energy cost was measured in response to hip hitching.

Variations in walking speed affect the pattern of walking and pattern of muscle activation. However, changes in motor control can affect walking speed. Therefore, it is important to distinguish between deviations from a normal gait due to walking speed and

those due to impairment (Andriacchi, Ogle et al. 1977). Walking speed in stroke patients is reported to be lower than in the un-impaired (Chen, Patten et al. 2005; Olney and Richards 1996; vonSchroeder, Coutts et al. 1995) and strongly reflects the level of impairment (Andriacchi, Ogle et al. 1977; Murray, Mollinger et al. 1984; Roth, Merbitz et al. 1997). Cadence and gait symmetry also reflect levels of motor recovery (Brandstater, Bruin et al. 1983). Specifically, cadence is reduced; the period of double support is increased as is the time spent in swing phase on the hemiplegic side (Brandstater, Bruin et al. 1983; Olney and Richards 1996). However, reduced cadence was not reported by Chen et al. (Chen, Patten et al. 2005), indeed, no change was found between un-impaired and stroke patients walking at matched speed. This study was conducted using a treadmill which may explain the apparent contradiction, especially with regard to cadence which has been found to increase significantly between over ground and treadmill walking and stance time which has been found to significantly reduce (Alton, Baldey et al. 1998).

The gait of a stroke patient will vary over time from the initial insult to many months after. The level of impairment varies considerably from patient to patient as does the level of recovery (Wade, Wood et al. 1987). Therefore, one must be careful when generalising about gait; in addition, it demands caution when characterising impairment based on small populations of patients.

2.2.5 Summary

The pattern of walking in un-impaired individuals is very efficient and consistent, yet, the complex manner in which it is thought to be achieved permits an extremely flexible system. This allows an individual to adapt to environmental conditions and to specific tasks. After stroke this adaptability and efficiency is commonly lost, revealing primitive patterns of movement, due to the disruptions of normal motor control systems which make such primitive responses overt. However, their contribution to abnormal walking patterns is itself complex; underlying impairments do not act in isolation and other plastic changes occur resulting in compensatory activity.

The underlying cause of abnormal walking patterns is not always defined by the overt patterns of movement. It is important to quantify these patterns of movement with respect to the pattern of muscle activity in order to understand better the global impairment that culminates in an abnormal walking pattern. Practitioners of clinical gait analysis have utilised various technologies in order to elucidate on the questions referred to earlier, these methods are considered in the following section.

2.3 Gait Analysis

2.3.1 Introduction

It is clear that gait impairments are common after a stroke and, although impairments often present with stereotypical patterns, they can have varying complex underlying causes. Gait analysis attempts to differentiate between those overt impairments that are compensations and those that represent the underlying impairment. Since the early 1930's clinical gait analysis has applied video analysis, force measurements and muscle activity to decompose movement disorders. Gait analysis laboratories today use sophisticated technology to track movements of body segments, energy expenditure through gas analysis, muscle activity and ground reaction forces. Such facilities however, are not widely available and even when they are they are not always ideally suited to a particular patient population (Toro, Nester et al. 2003). As such, attempts have been made to develop alternative methods of gait analysis more suited to the rehabilitation clinical environment and which do not require skilled technical assistance. Gait analysis methods can be technically as simple as measuring walking speed. Walking speed for example has been generally accepted as a valid measure to assess a patient's progress (Andriacchi, Ogle et al. 1977; Roth, Merbitz et al. 1997). However, such methods fail to distinguish between causes and effect, for example, deviations due to walking speed and those due to underlying impairment.

2.3.2 Gait Laboratories

The state-of-the-art for gait analysis is the motion analysis laboratory. The laboratory provides a quantitative description of limb movements and forces in three dimensions. A system for motion analysis consists of a marker tracking system (for example, VICON from VICON Peak, CODA from Charnwood dynamics and Zebris) and one or more force plates (e.g. Bartec, Kistler and AMTI). There are two distinct groups of marker technology, active and passive. Active markers (CODA, Zebris or Polhemus) generate a signal that is captured by sensor array or are themselves the sensor. Active sensors can use a variety of mediums including infrared light, electromagnetic fields and ultrasound. Passive markers (VICON or Qualisys) are used to reflect infrared light generated by specialised infrared cameras.

All motion-tracking systems capture the position of a marker within a calibrated 3D space. Most simply therefore, these system can be used to track the movement of a point on the body within the 3D space. A single marker cannot be used to define the location of

a joint centre and therefore the internal axis of a limb segment, information required for detailed kinematical analysis. Therefore, to measure the kinematics of a limb in three-dimensions a model must be generated that relates the locations of several markers, fixed relative to one another, to anatomical landmarks on a limb segment which themselves define the structure of the limb segment and joint (Wu, Siegler et al. 2002; Wu, van der Helm et al. 2005). There are several commonly used models used in gait analysis. One example uses a cluster of at least three markers, placed on a rigid frame or attached directly to the skin, to define a local coordinate system. Additional markers are used to define the distal and proximal joints of the limb segment and thus the joint coordinate system. The positions of these markers are measured whilst the subject remains static. This defines how the position of the local coordinate system markers must be rotated and translated to define the position of the joint coordinate system markers and therefore defines the orientation of the limb and estimated location of the joint centre with respect to the global coordinate system.

Additional equipment can be employed to 3D motion analysis including oxygen monitoring, electromyography and plantar pressure measurements. The combination of limb kinematics, using the model defining the marker placement on the body, and force plate data permits the calculation of joint moments and forces through the process of inverse dynamics. However, models for marker placement are continuing to evolve and improve, furthermore, additional technology is being integrated into systems, for example, the use of MRI data in line with finite element analysis to model joints (Hemmerich, Merwe et al. 2004). Even though standards and technology are in flux (Robertson and Attfield 2005) motion analysis systems represent the most accurate and complete means of acquiring gait information. If criticisms were to be levelled at movement analysis laboratories then they would be, ironically, at the complexity and breadth of data they provide. In addition, the shear cost of implementing and operating such systems mean they are not widely available (Simon 2004). Finally, the process of a gait analysis assessment using movement analysis systems is very demanding, and therefore not appropriate for all patients and certainly not appropriate for everyday clinical use (Toro, Nester et al. 2003). In addition, there is a debate regarding the efficacy of laboratory based gait analysis for all patients within a group and therefore an argument for more selective use of these facilities (Baker 2005).

In this light, alternative methods of assessing gait and importantly quantifying walking patterns have been presented in literature.

2.3.3 Observational Gait analysis

The visual and quantitative analysis of gait is observational gait analysis. The use of the term quantitative implies only a systematic, formal approach to scoring deviations and not necessarily that the systems employed are strictly objective or repeatable. There is a body of evidence that reveals that some observational gait analysis systems have poor repeatability, lack validity and often correlate poorly with objective quantitative instrumented gait analysis techniques (Craik and Oatis 1994; Huges and Bell 1994; Lord, Halligan et al. 1998; Mackey, Lobb et al. 2002; Pomeroy, Pramanik et al. 2003).

Techniques of observational gait analysis document time and distance parameters and information about walking skills. Furthermore, they often evaluate kinematics. Some observational gait analysis techniques can be described as a method to assess more objectively the ambulatory status of a patient. The systems have tended to be designed for specific patient groups (Carol, Janes et al. 1982; Dimonte and Light 1982; Nelson 1974; Olney, Elkin et al. 1979). These systems are cheap, relatively fast to complete and very simple to implement. Therefore, they have been adopted within many institutions as they provide a more accessible method of gait analysis than instrumented systems.

Though the validity and reliability of these systems have been called into question and few of the systems have undergone validation, ambulation profiles such as that developed by Olney (Olney, Elkin et al. 1979) have been assessed for inter/intra-rater reliability and have proved that ambulation profiles can be reliable and therefore objectively evaluate locomotor skills. Huges and Bell (Huges and Bell 1994) developed a system in response to the need for a sensitive and reliable system on which a plan for treatment of stroke patients could be based. There was a significant agreement between raters for swing phase kinematics but poor agreement for stance phase kinematics and for the general description of the characteristics of gait. This system used video analysis to assess a patients walking and was not compared to "live" assessments of the patient. It has been suggested that agreement between raters can be significant, though variability with respect to raters assessing the patient "live", rather than on video, can be significantly higher (Wiles, Newcombe et al. 2003). Therapists will tend to use a wider range of cues when assessing patients live. Furthermore, only one video camera is often used which can result in error as it only presents a 2-dimensional image. For example, movements in the frontal plane can distort movements in the sagittal plane that would become evident if images of both planes were assessed. Visual analysis of movement via video has been used to assess observational gait analysis (Mackey, Lobb et al. 2002; McNee and Watter 2002; Pomeroy, Pramanik et al. 2003; Wiles, Newcombe et al. 2003) and though there

was consistency within an individual rater, assessment on the quality of movement between raters varied significantly. It was concluded that the reliability was not sufficient for clinical practice.

Lord et. al (Lord, Halligan et al. 1998) have developed a visual gait assessment scale, the Rivermead scale, in answer to the need for an objective assessment of hemiplegic stroke gait that does not rely on broad descriptive terms of quality or purely quantitative analysis. The system has undergone assessments for both validity and reliability; 93.8% of assessments agreed exactly, though collectively 63.2% disagreed by at least 1 point on the scale. The system is based around a four point ordinal scale; it observes trunk and lower limb movements in swing and stance of one side of the body at a time. In addition, walking time, step length and asymmetry are recorded. The Rivermead gait analysis scale purposely does not rely on video analysis, as it is felt that this could be the cause for the moderate reliability of other systems due to the distortions resulting in 2-dimensional video analysis.

There is discussion regarding the scaling methods used to record gait information; ratio scales are considered best for long-term analysis rather than ordinal scales. The aspects of the Barthel index and Fugl-Myer sensory motor tests that represent locomotor function are less sensitive in detecting improvements for performance approaching a maximum value (Craik and Oatis 1995). This is in contrast to a continuous variable such as gait velocity and pulse rate. Furthermore, these may be assessed separately, the variable contributing to improvement singled out, and therefore a determination made of which orthotic or other therapeutic device should be used. Functional scales are however considered useful as screening tools i.e. functional independence performance. The Fugle-Myer is however specifically referenced within the recommendations of the International Classification of Functioning (ICF) (WHO 2003) (Gladstone, Danells et al. 2002).

Yelnik et al (Yelnik, Albert et al. 1999) describe an observational gait analysis guide to assess the role of spasticity in neuropsychological disorders in order that they could select patients before treatment. The system is interesting in that it focuses on the diagnosis of disabling spasticity that is hard to differentiate from other causes of hypertonia such as contracture or changes in the mechanical properties of the muscle.

Perhaps the most refined system for observational gait analysis is that described in the Rancho Los Amigos observational gait analysis handbook (Department 1989). This has been developed over approximately 20 years and has been revised several times. This observational gait analysis technique provides a guide to the importance of each event in the gait cycle with respect to each limb segment including the trunk. The

importance is related to typical gait disorders, for example, knee flexion during mid-swing. The methodology is intended to draw the observer's attention to specific limb segments during particular phases of the gait cycle. However, the technique is not intended to be quantitative but descriptive, therefore providing a consistent framework from which to describe disordered gait. There is no provision to grade the severity of the impairment; it is a binary condition.

The methods of assessing gait analysis systems, for those that have been assessed, have been diverse making it hard to compare results. The comparison between assessments provides perhaps more information regarding their relative strengths than studies that have compared visual gait analysis systems to instrumented systems (Craik and Oatis 1995), which are unarguably more repeatable and accurate.

2.3.4 Energy Cost

An important component of non-pathological walking is efficiency. Motor impairments often result in increased energy expenditure and thus limit function. For example, large excursions of the centre of mass horizontally vertically or transversely are inefficient and therefore require a higher energy cost.

Energy generated by the body can be quantified by two methods; direct and indirect calorimetry. Direct calorimetry is highly accurate though impossible outside specialised laboratories, as it requires a hermetically sealed and insulated chamber allowing the heat generated by the subject during activity to be measured very accurately. Alternatively, indirect calorimetry depends upon the premise that all energy metabolism in the body ultimately depends on the use of oxygen. The difference between oxygen consumption at rest and during steady state activity therefore indirectly estimates energy metabolism. This is true as only a small proportion of energy metabolism results from anaerobic activity under steady state conditions. The accuracy of indirect calorimetry compares well to direct calorimetry (Williams, Katch et al. 1991). Based on the same underlying principle the measurement of heart rate reflects increased metabolic effort (Boyd, Fatone et al. 1999; Nene 1993) and is more commonly used in the clinical environment. Physiological cost index or PCI is a measurement of heart beats per metre (MacGregor 1979).

PCI has been shown to be reliable in un-impaired subjects at sub-maximal levels of exercise in steady and in non-steady state situations (Bailey and Ratcliffe 1995). However, many non-steady state uses of PCI have been criticised and some support the use of the Total Heart Beat Index (Hood, Granat et al. 2002) which divides the total number of heart beats by the total distance travelled. There could still be the criticism that many impaired subjects may not be working sub-maximally and therefore the underlying

principal that they are working aerobically may not be true. Measurements such as PCI are preferred, as they do not require specialised equipment. Additionally, even modern equipment used for indirect calorimetry is cumbersome and may not be appropriate for some patient groups (Hood, Granat et al. 2002).

2.3.5 Motion Sensors

Micro-Electro-Mechanical Systems (MEMS) technology now permits the fabrication of multi-axis accelerometers and gyroscopes at low cost. This in turn makes simple movement sensors a cost effective, though still limited, alternative to traditional kinematic methods. Several studies have used body worn sensors to measure human kinematics and spatio-temporal gait features rather than using marker systems such as described earlier. The work either addresses the need to develop simpler clinical methods to assess gait (Aminian, Najafi et al. 2002; Tong and Granat 1999) or to develop control modalities for orthotic interventions (Ghoussayni, Stevens et al. 2002; Monaghan, Veltink et al. 2004). Tong et al (Tong and Granat 1999) developed a gait analysis device based on two uni-axial gyroscopes, placed on the thigh and the shank, from which they calculated knee angle and segment angular velocities. Furthermore, they concluded that a single gyroscope could be used to calculate cadence and walking speed and presented joint angle data that correlated well with an optical system. Aminian et al (Aminian, Najafi et al. 2002) used wavelet analysis to deconstruct gyroscopic data from the shank in order to pinpoint moments of foot strike and toe off. Stride length, stride time and gait velocity were calculated for un-impaired subjects. By comparing gyroscopic data with an optical Vicon system Mayagoitia et al. (Mayagoitia, Nene et al. 2002) showed the efficacy of using gyroscopes to calculate accurately segment angular velocity and joint angle. Studies thus far have presented little gyroscopic or accelerometer data from pathological gait, these studies do not usually use raw kinematical data but transform it into temporal information of gait. Importantly, literature provides no standardised method of using such movement sensors in the assessment of pathological gait.

Such sensors have the advantage of being relatively easy to fabricate in-house which also means that implementation costs are low. Additionally, MEMS technology accelerometers are capable of withstanding up to 1000g; that is equivalent to being dropped at height onto a hard surface. Housed correctly such devices are robust and harder to damage than technologies such as electrogoniometers. Accelerometers, gyroscopes and magneto-resistive sensors provide a volume of data from which information such as joint angles can be calculated in addition to directly measuring rates of change of rotation and acceleration.

Electrogoniometry can be used to make continuous joint angle measurements. These operate either as potentiometers or strain gauges attached across a joint. They can be uni-axial thus only measuring movement in one plane, or multi-axial. Multi-axial electrogoniometers could potentially measure movements in all planes of movement. Although the use of electrogoniometers is evident in the literature there is little formal evidence of their functionality. The validity of hip kinematics is of particular concern particularly in those with poor hip control (Perry 1992). Additionally, the multiple degrees of freedom of many joints, inaccessibility of some axis of rotation and level of subcutaneous fat all make multi-axis electrogoniometry problematic (Whittle 2002). However, electrogoniometry is still an economic means of measuring planar movements, ranges of movement if not absolute angles, and rates of change of movement. Rose et al (Rose and Gamble 1994). showed the technique to be consistent and provide reliable knee movement data; however, this assessment was only from young healthy subjects, and enforced the requirement for careful and secure placement of the sensors. Electrogoniometry is described in most books on gait analysis but with its description, there is always a caveat to its use.

The durability of electrogoniometers constructed as strain gauges is a concern. They are easily damaged and generally, the environment in which they are used requires durability. Recently it has been suggested that joint segment elevation angles are as important as joint angles. Electrogoniometers would require post-processing to generate this data. Finally, although they are a low-cost alternative, the equipment must still be purchased commercially and, therefore, is still costly.

2.3.6 Low Cost Camera Based Movement Analysis Systems

An area of quite recent development is that of camera systems that either do not require a marker set or require fewer cameras to capture walking kinematics. Work has been done to develop both 2-dimensional and 3-dimensional systems. Industry has contributed to this area by providing increasingly practical object tracking software and real-time video image analysis software. RIVCAM (Churchill, Halligan et al. 2002) is a marker-based system that captures sagittal plane kinematics. Whilst measuring a fixed angle as it moved in front of the camera a standard deviation of less than 1° was achieved. Additionally, errors resulting from the subject moving toward or away from the camera were approximately ±10°. Therefore within ±8cm away from the calibrated line the errors were comparable to that of a commercial optical system. Recently, a method of calculating 3-dimentional movement from video captured from a single camera was presented by Yang (Yang and Yuan 2005). However, this method involved a complex reconstruction process translating

2-dimensional points into 3-dimensional space in conjunction with human biomechanical models. Single camera systems using artificial neural networks to compare human movements with template data have been developed by Hicks et al (Hicks 2005) and multi-camera systems to estimate body poses from a template set was recently implemented by Kersting et al. (Kersting 2005). There is a large volume of literature related to the automated marker-less tracking of human motion and it is at present an area of vigorous research. There are currently no commercial systems available to measure 3D articulated human motion from raw marker-less image data (Hicks 2005).

2.3.7 Plantar Pressure

Devices for measuring plantar pressure have two, not necessarily parallel, roles; firstly, to quantify the distribution of body weight across the plantar aspect of the foot, secondly, to identify certain gait events including foot strike and toe off. The simplest implementations of such devices are pressure sensors placed under the heel and toe. Additional sensors may be placed under the first and fifth metatarsal heads. More complex commercial implementations use large arrays of pressure sensors which give a complete image of the pressure distribution at higher resolution. Such commercial systems include Pedar and FSA. By their very nature the systems are often intrusive and costly to integrate into a broader system.

Footswitches are used to capture phase transitions during gait and therefore allow conclusions to be drawn regarding associated measures such as EMG. Different methods of gait cycle selection from manual to fully automated have been applied in the literature. In un-impaired subjects the method of gait cycle selection does not appear to influence the outcome of associated gait analysis measures. However, the method of gait cycle selection can alter considerably the analysis of pathological gait (De Stefano, Burridge et al. 2004), this related predominately to the reliability of the footswitch signal. Additionally, variations in sensor placement and deviations from the normal foot fall pattern can introduce error into the gait phase measurement especially when smaller footswitches are used.

As was mentioned earlier, gait laboratories use force plates to define gait phases. Although this is not plantar pressure, they represent extremely accurate methods of capturing gait events. However, because of their limited size they can only capture one or two steps and require the subject to be specific about their foot placement. The latter can introduce perturbations within the gait cycle as the subject aims for the force plate.

2.3.8 Electromyography

Electromyography (EMG) is the measurement of bio-potentials resulting from the contraction of skeletal muscles. Electromyography was first used in relation to gait analysis during the 1930's when indwelling or needle electrodes were employed. To date, and with the introduction of non-invasive surface EMG (sEMG), there is very little in the way of standardisation within the field. The strong requests from practitioners (Kleissen, Litjens et al. 1997) for standard databases of EMG patterns and methodologies have yet to be fulfilled. Needle electrodes can be inserted directly into a muscle and provide a high specificity and capability to measure activity from deep musculature. However, the specificity reflects only a very small number of motor units and thus can fail to present the activity of the muscle as a whole. As needle electrodes can isolate a small number of motor units, and therefore individual motor unit action potential trains, they are often used in the assessment of neurological conditions, for example nerve conduction velocities. Surface EMG provides a non-invasive method of measuring activity from superficial muscles and better represents the global activity of a particular muscle, as it is a representation of the superposition of multiple active motor units. Although more modern processing methodologies can allow sEMG signals to be decomposed into individual motor unit action potential trains the common use is to assess muscle fatigue and muscle coordination. Collectively the techniques of EMG are clinically useful in defining motor impairment. Surface EMG is a method reported to be used within many gait laboratories (Freriks, Kleissen et al. 1999). However, diagnostically the technique suffers from a lack of standardised processing methods and the inherent variability between patients due to pathology and anatomical factors. With specific reference to stroke patients there is limited literature relating the use of sEMG to gait analysis. Yet what literature does exist, confirms sEMG as a method for identifying characteristics of muscle activation patterns in hemiplegic gait after stroke (Burridge, Wood et al. 2001; Knutsson and Richards 1979) Equipment for electromyography is in general high cost and requires careful application in order to generate usable results. Nevertheless, it is the only practical method of assessing muscle activity during walking. Electromyography is presented as a very useful tool in assessing underlying motor disorders and the only practical method of assessing muscle activity during walking; however, the methodologies for assessing sEMG have not been standardised. In addition, techniques for quantifying deviations using sEMG do not satisfactorily exist for assessing gait after stroke; in which case, there is a need to review the available methods of acquiring and processing EMG for disrupted gait and specifically that after stroke.

2.4 EMG Assessment in Gait Analysis

2.4.1 Introduction

Electromyography (EMG) is the measurement of the electrical activity generated by a contracting muscle. Therefore, it is the analysis of muscle activity and, by implication, also of muscle function. Basmajian and De Luca define electromyography as:

> *"Electromyography is the study of muscle function through the inquiry of the electrical signal the muscles emanate." (Basmajian 1979)*

Consequently, it provides useful information regarding muscle activity and therefore function. The way in which muscle function is inferred from the electromyogram, that which might be described as information extraction, is very often by visual assessment of the signal. The observational methodology relies on a subjective judgement of parameters such as signal amplitude and phasing (Knutsson and Richards 1979). The aim however is ideally to quantify the signal in some way. The development of mathematical methods and models, in addition to the ever advancing power of computing, has led to many novel methods of processing the signal. The earliest techniques related the firing of motor units to the number of zero crossings or turns in the signal within an epoch. These are simple time series methods that relate to the signal's frequency content. These methods are still used today in the areas of neurophysiology to assess motor unit conduction velocities (Lange, Van Weerden et al. 2002) and fatigue analysis (Umezu, Kawazu et al. 1998) during isometric muscle contraction; in addition to the control of prosthetics (Boostani and Moradi 2003). Similarly the methods of peak counting provide information with regard to frequency content. On-off activity of the sEMG has been related to functional activity such as walking, therefore, relating phases of movement to phases of muscle activity. There is an association of sEMG amplitude to muscle force which has led to the popularity of smoothed or filtered sEMG. The relation of sEMG amplitude to muscle strength (Hermens, Freriks et al. 1999; Knutsson and Richards 1979) relates variation in sEMG amplitude to that of impairments in motor control or physiological change in muscle (Farina and Merletti 2000).

Although there is a long history in the application of sEMG, debate still exists regarding the comparison of two or more sets of sEMG data. Thus normalisation methods whether in time or the frequency domain provoke important questions. The issue of standardisation in the analysis and capture of sEMG is long standing (Kleissen, Litjens et al. 1997). In an attempt to resolve this issue a European funded Concerted Action

SENIAM (part of the BIOMED 2 programme (CORDIS 2001)) worked to provide guidelines on the acquisition and processing of sEMG. These recommendations were published in 1999 and to date they represent the most concise guidelines on sEMG methodology covering a broad range of applications (Hermens, Freriks et al. 1999). As quoted within the SENIAM recommendations the very fact that such a project was funded reflects the maturity and relevance of sEMG today. However, a search of UK National electronic Library for Health (NeLH) (Health 2006) [using the search phrase sEMG or EMG or Surface Electromyography] revealed only three references to evidence involving sEMG and one reference, none related to gait analysis. In the US a guideline released in 2001 [www.guideline.gov] concluded that:

> *"...Surface Electromyography is considered an acceptable tool for kineasiologic analysis of movement disorders ...; for evaluating gait and posture disturbances..."*

This recommendation was based on a strong consensus of evidence from expert opinion, case studies and nonrandomised controls. It would therefore appear that based on the current body of clinical guidelines and review-based evidence, sEMG has not been adopted into the clinical environment. It may perhaps be reasoned that the paucity of such literature intimates that sEMG has not been properly evaluated on clinical grounds. This is therefore a seemingly contradictory position for sEMG. One in which it is widely applied within gait analysis laboratories, in addition to being a long standing research tool, the other where it is ill-defined as a clinically relevant, diagnostic tool for movement disorders.

This section reviews the current literature with respect to sEMG signal processing methods in gait analysis and specifically in the assessment of gait after stroke. These processing techniques rely very much on traditional methods, and for this reason, the scope of the review is broadened to include methodologies from parallel fields. As yet, these techniques have failed to be adopted into clinical gait analysis; although they introduced novel techniques that have not been developed into a wider context.

2.4.2 Basic sEMG Signal Processing Techniques

Perhaps the first example of sEMG study of stroke patients was that of Hirshberg (Hirschberg and Nathanson 1952). Raw patterns of sEMG were captured on an 8-channel ink oscillograph and divided into gait phases by hand, based on foot switch data. No additional processing was reported and periods of on-set and cessation were judged by eye. Though the sEMG data was not quantified, the conclusions drawn in this early paper, with respect to hemiplegic gait, have been supported in subsequent studies. Hirschberg's

study reveals, among other things, that a significant amount of information is contained within the raw sEMG signal. Subsequent processing of the signal however, in addition to being an aid to its visual interpretation, facilitates a basic quantitative analysis of the sEMG signal. These methods are common place in sEMG analysis and can be found referenced in most texts on the subject; see: (Hermens, Freriks et al. 1999; Marris, Lamb et al. 1992; Perry 1992)

2.4.3 sEMG signal Acquisition

Traditionally the Surface EMG signal is acquired using bipolar surface electrodes in a differential configuration; such an electrode attenuates noise present at both terminals of the sensor. The inter-electrode distance additionally acts as a high-pass filter to the acquired signal and will affect the frequency distribution in the signals spectrum (Mayagoitia, Nene et al. 2002). The SENIAM guidelines have acted to try and standardise the sensor construction parameters. The bandwidth of the biological signal is very wide, however, it is generally accepted that sampling between 1kHz and 2kHz subsequent to an anti-aliasing filter, to remove the influence of high frequency harmonics, with a high cut-off frequency of 500 to 1kHz is acceptable (Basmajian 1979; Hermens, Freriks et al. 1999; Mayagoitia, Nene et al. 2002). Subsequent filtering often removes low frequency signals below 10Hz as these are considered to be predominantly movement artefact if present (Rechtien, Gelblum et al. 1996).

2.4.3.1 Full wave Rectification

Full-wave rectification is a process whereby the signal is forced to contain samples with the same polarity (see Figure 3). This ensures that a bipolar signal becomes constructed entirely of data samples with zero or positive magnitude and therefore has a non-negative mean. The raw rectified signal is more visually appealing than the original bipolar signal as it permits an intuitive visual assessment of the signal onset and amplitude. Additionally it allows for additional signal processing stages to be applied to the signal, for example smoothing or filtering, in order to generate a linear envelope, the so-called sample-rectify-smooth process (Clancy 1999).

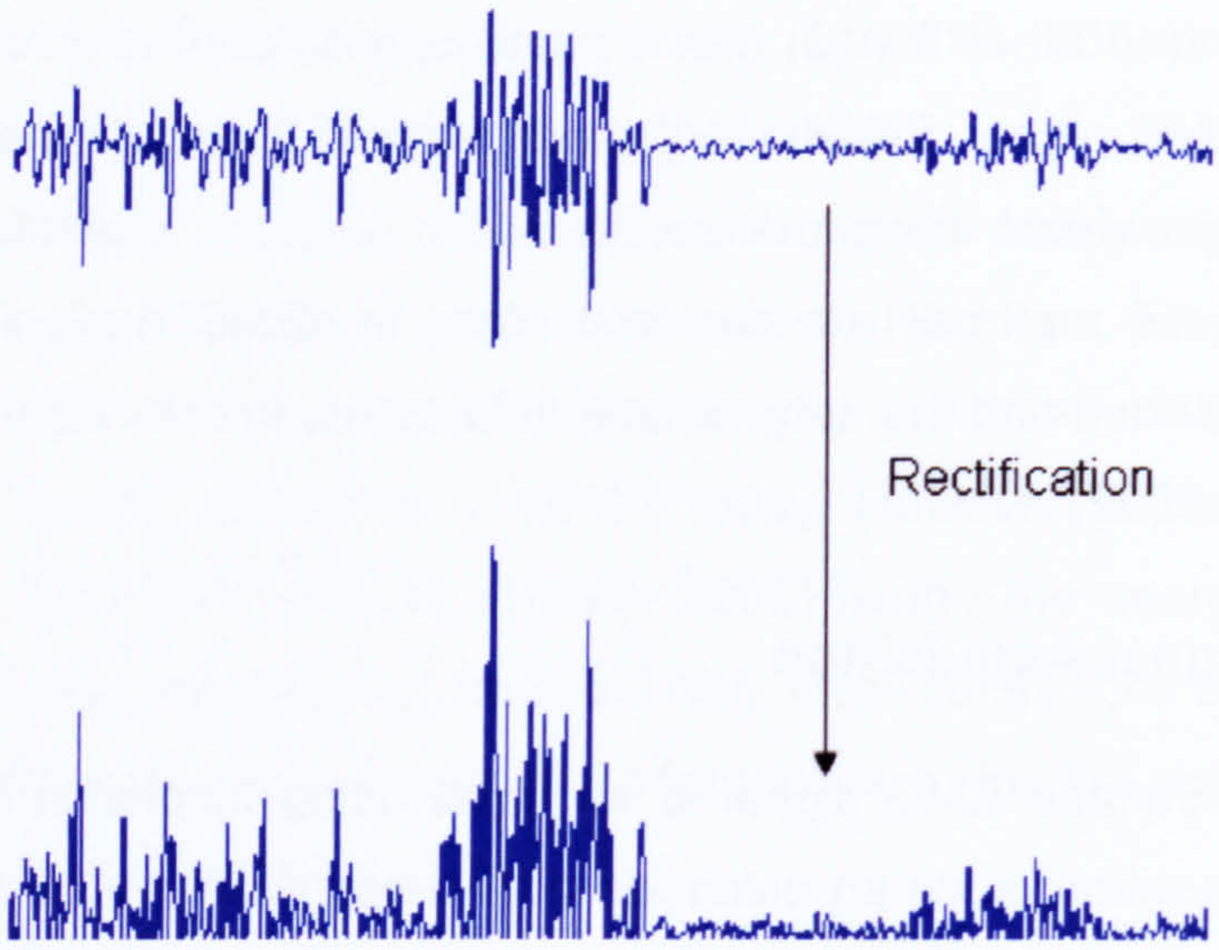

Figure 3 example of a raw sEMG signal (Top) and the same signal after full-wave rectification (Bottom).

2.4.3.2 Linear Envelope Detection

In order to facilitate the estimation of the raw sEMG signal characteristics the high frequency component is often removed leaving the demodulated or linear envelope representation. The Root Mean Square (RMS) representation (Equation 1) reflects the average sEMG signal power. The level of smoothing is defined by the number, N, of samples, x_i, over which the signal is then averaged.

$$RMS = \sqrt{\frac{1}{N}\sum_{i=1}^{N} x_i^2}$$

Equation 1 Root Mean Square

Alternatively the average rectified value (ARV) representation (Equation 2) reflects the average signal amplitude over the averaged samples, where x_i is the sample and N is the averaging number. Unlike the RMS value the ARV does not have a direct physiological linkage (Mayagoitia, Nene et al. 2002). The ARV is equivalent to a moving average (MA) or specific case of a finite impulse response (FIR) digital filter (Mathworks 2006) (see Figure 4). The characteristic of the filter used to smooth the raw rectified sEMG signal largely influences the characteristics of the resulting linear envelope and is generally chosen subjectively (D'Alessio and Conforto 2001).

$$ARV = \frac{1}{N}\sum_{i=1}^{N} |x_i|$$

Equation 2 Average Rectified Value

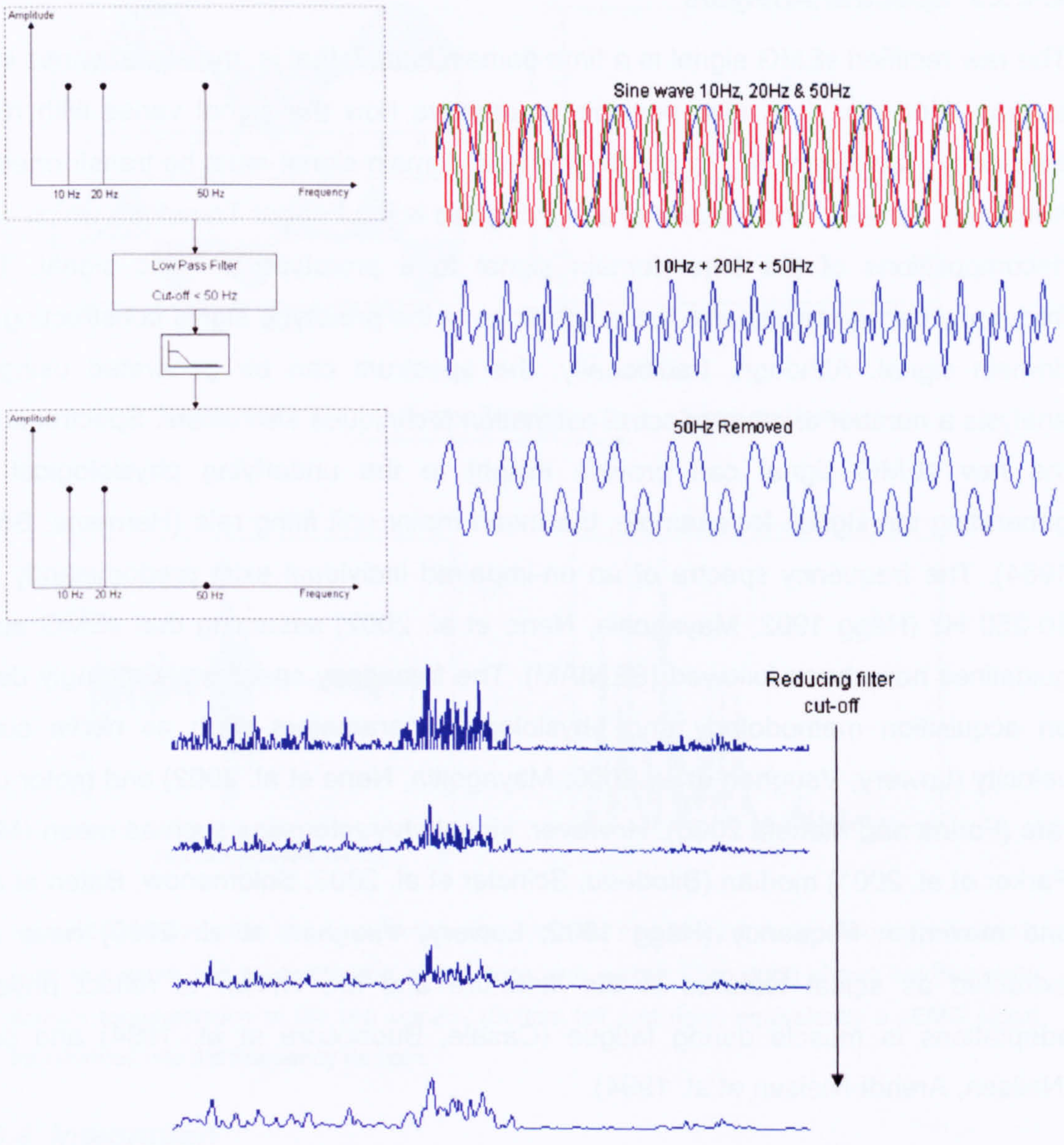

Figure 4 removing frequency components: Low Pass Filtering. (top left) Frequency components shown in the signals (top right) passing through a low pass filter removes the 50Hz component. The resulting signal is shown in the last plot of the top left figure. (Bottom middle) an example of a raw sEMG signal (top) passing through 30Hz, 20Hz and 3Hz low pass filter.

Pathology is known to be generally reflected in the variation of sEMG amplitude from that collected from un-impaired subjects (Knutsson 1981). Although it can therefore be considered as an important characteristic of the sEMG signal, there is continued debate with respect to its precise association with physiological factors (Farina, Merletti et al. 2004) and the validity of conclusions drawn from comparing amplitude estimations between subjects (Kleine, Stegeman et al. 2001).

2.4.3.3 Spectral Analysis

The raw rectified sEMG signal is a time domain signal, that is, the signal varies in relation to time. However, it is also possible to observe how the signal varies with respect to frequency (see Figure 5). To do this the time domain signal must be transformed into the frequency domain. One method of achieving this is the Fourier Transform which correlates decompositions of the time domain signal to a prototype periodic signal. Thus the frequency domain represents the proportions of the prototype signal constructing the time domain signal. Although, traditionally, the spectrum can be generated using Fourier analysis a number of other spectral estimation techniques also exists. Spectral analysis of the raw sEMG signal can provide insight to the underlying physiological process generating the signal, for example, the mean motor unit firing rate (Hermens, Boon et al. 1984). The frequency spectra of an un-impaired individual exist predominantly between 10-250 Hz (Hägg 1992; Mayagoitia, Nene et al. 2002) assuming that sEMG acquisition guidelines have been followed (SENIAM). The frequency spectrum is strongly dependent on acquisition methodology and physiological parameters such as nerve conduction velocity (Lowery, Vaughan et al. 2000; Mayagoitia, Nene et al. 2002) and motor unit firing rate (Farina and Merletti 2000). However, signal characteristics such as mean (MacIssac, Parker et al. 2001) median (Bilodeau, Scindler et al. 2003; Solomonow, Baten et al. 1990) and maximum frequency (Hägg 1992; Lowery, Vaughan et al. 2000) have all been extracted as signal features in the literature and are known to reflect physiological adaptations in muscle during fatigue (Casale, Buonocore et al. 1994) and pathology (Neilsen, Arendt-Nielsen et al. 1994).

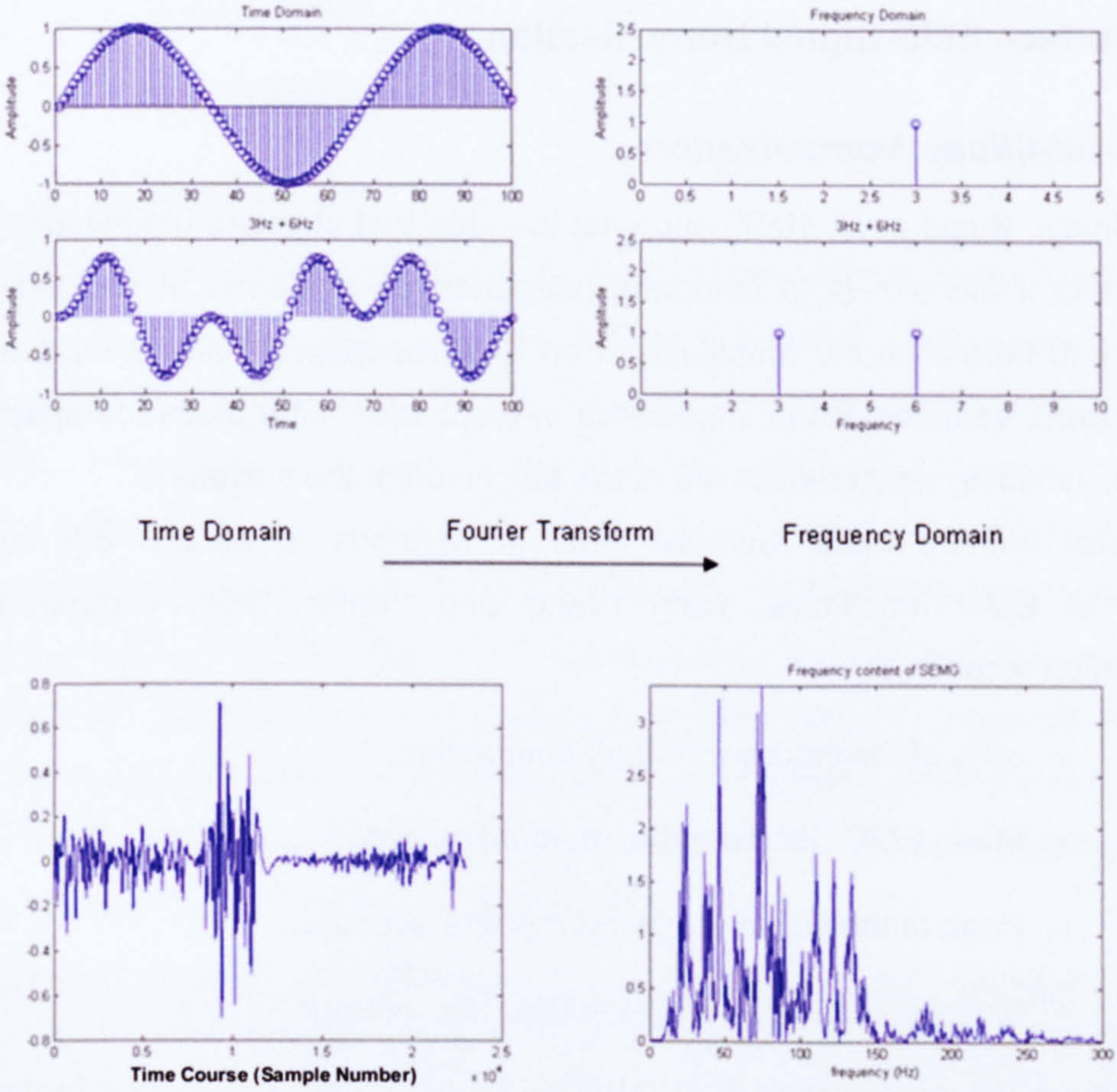

Figure 5 Transformation of a time domain signal into the frequency domain. (Top left) displays a pure sine wave and a combination of two pure sine waves. (Top right) shows the frequency domain representation of the two signals. (Bottom left and right) equivalently a sEMG signal transformed into the frequency domain.

2.4.3.4 Integration

Integration is another technique often referenced in EMG texts (Marris, Lamb et al. 1992) The integrated EMG (iEMG) represents the area under the EMG signal graph and is thought to represent the number of active motor units (Marris, Lamb et al. 1992) However, the link between sEMG amplitude and the number of active motor units is not a simple linear relationship and thus this methodology is open to criticism (Farina, Cescon et al. 2002; Farina, Merletti et al. 2004). The application of iEMG is generally applied to isometric or isokinetic movements.

2.4.4 Surface EMG Signal Normalisation

2.4.4.1 Amplitude Normalisation

Shiavi (Shiavi, Bugle et al. 1987) supports the idea that absolute magnitudes of EMG are meaningless if the aim is to compare independent waveforms across individuals; it is necessary to normalise the amplitude of an EMG waveform. Factors such as superficial fat and tissue, variance in the impedance of electrodes, inter-electrode spacing and skin condition, including temperature, affect the amplitude of the waveform.

Several authors have reported different methods to reduce the inter-individual variation in EMG amplitude. Yang (Yang and Winter 1984) compared four such normalisation techniques:

- 50% of maximum voluntary contraction,
- Mean EMG per isometric moment of force,
- Peak of the within-subject ensemble average,
- Mean of the within-subject ensemble average.

Maximum voluntary contraction (MVC) was calculated using a calibration chair that could measure the maximum moment of force generated over three consecutive maximum contractions of a muscle. A previous study had already provided the rationale for choosing 50% of MVC rather than 100%, see Table 2 (Yang and Winter 1883). A maximum voluntary contraction is hard to maintain without fatigue, furthermore Dubo (Dubo, Peat et al. 1976) showed it not to reduce inter-individual variability. The sub-maximal contraction was maintained for three seconds and repeated three times for each muscle of interest. Choosing a component of EMG where the force was steady for each of the three isometric trials, and averaging them, defined the normalising factor for each muscle. It was shown that values for the 50% MVC method were variable and this resulted in increased variation in EMG patterns where normalising methods calculated based on 50% isometric contractions were involved. This included the second method assessed, mean EMG per isometric moment of force, where the average moment of force was divided by the average EMG value over the three isometric contractions. Coefficient of variation, calculated for each muscle, showed a dramatic increase in variation in all but the vastus lateralis muscle with 50% MVC and in all muscles:

- Rectus femoris,
- Vastus Lateralis,

- Biceps Femoris,
- Tibialis Anterior,
- Soleus;

When the mean EMG per isometric moment of force normalisation was utilised Yang made an interesting distinction between two joint muscles and single joint muscles, suggesting that this may be a source of variation in the measurement of isometric contractions. Furthermore, it was noted that it is difficult to produce a maximum contraction from strong muscles such as the soleus muscle. Therefore, an inability to stabilise two joint muscles combined with an inability to elicit maximum contraction from some muscles combined to produce a large variability in both techniques involving the measurement of 50% maximum contraction. Peak within-subject ensemble averages and mean within-subject ensemble averages, also assessed by Shiavi (Shiavi, Bugle et al. 1987) and Kadaba (Kadaba, Ramakrishnan et al. 1989), proved to be superior at reducing variability in all muscles as represented in Table 3.

Muscle	Un-normalised	Normalised to 50% MVC	Normalised to μV/Nm	Normalised to peak ensemble average	Normalised to mean ensemble average
Rectus Femoris	81	119	167	54	56
Vastus Lateralis	91	79	111	41	40
Biceps Femoris	128	197	148	56	56
Tibialis anterior	49	52	51	37	32
Soleus	52	82	61	35	34

Table 2 Coefficient of variation (as percentage) of four normalisation techniques (Yang and Winter 1984)

Muscle	Normalised to average (Mean) ensemble average	Normalised to maximum (Peak) ensemble average
Tibialis anterior	.50	.55
Gastrocnemius	.64	.72
Soleus	.56	.58
Rectus Femoris	.66	.64
Medial Hamstring	.78	.75
Vastus Lateralis	.88	.79
Gluteus Medius	.58	.58

Table 3 Coefficient of variation (as decimal) of mean and peak ensemble average method of normalisation (Shiavi, Bugle et al. 1987)

It is interesting that Yang draws a distinction between Knutsson's terminology of "average peak amplitude of integrated EMG" and "normalisation to peak ensemble";

justifiably, considering that ensemble averaging would reduce such random features that are perhaps unlikely to occur with temporal consistency. Furthermore, Yang states that normalisation to the peak value over several strides might introduce variability, observing that this might include values resulting from an atypical step. Yang notes a disadvantage in using EMG values normalised to peak or mean values of ensemble averages EMG; these values do not reflect the maximum capacity of the subject to develop tension or a moment of force. Yang further maintains that this information is important in certain situations and suggests that muscle strength tests would be useful in such situations.

Shiavi (Shiavi, Bugle et al. 1987) compared the average value of within-subject ensemble average EMG to the peak within-subject ensemble average EMG. These two techniques were referred to as *pattern average* and *pattern peak* respectively. Though providing similar shaped waveforms they generated different standard deviations, the pattern average method having a smaller standard deviation during quiescent periods and therefore "emphasising periods of activity". Furthermore, Shiavi states that correlation of the fluctuations of the standard deviation with amplitude of the pattern average method is true for all muscles. Therefore, pattern average was used as the normalising parameter during that study. As seen in Table 3 the variability produced by the pattern average, mean ensemble average, is lower in the muscles of the shank than those of the thigh and vice versa for the variability of the pattern maximum, peak ensemble average. Kadaba (Kadaba, Ramakrishnan et al. 1989) assessed between and within day reliability of kinematic and EMG data and normalised the sEMG signal to the peak within each stride. This might be criticised given the preceding discussion. If the stride is atypical then the peak value could be atypical and therefore normalising to that value will distort the pattern. Burden (Burden, Trew et al. 2003) reviewed the use of main normalisation methods during a gait analysis trial. The findings were again similar to those referenced earlier. In particular that the mean dynamic sEMG generated the most non-variable result; in addition, normalisation based on isokinetic and isometric maximum voluntary contraction increased intra-individual variation. Again, it was emphasised that normalisation to percentage MVC provided a measurement of capacity obscured by other normalisation techniques.

2.4.5 Features of the Surface EMG

2.4.5.1 Linear Envelope & Amplitude Estimation

There is a complex interplay of factors that are known to determine the amplitude of the measured sEMG signal (Kleine, Stegeman et al. 2001). De Luca categorises these factors

into causative, intermediate and deterministic groups (DeLuca 1997) (see Figure 6). Causative factors represent the influence of electrode position and orientation in relation to the muscle; motor unit innervation zones and tendon, in addition to the electrode structure itself. The latter De Luca describes as extrinsic factors. The intrinsic factors are physiological; and include the number of active motor units, fibre type, blood flow, motor unit firing rate and their interactions. Intermediate factors are described by De Luca as "physical and physiological phenomena that are influenced by one or more of the causative factors and in turn influence the deterministic factors". Finally, deterministic factors directly influence the measured sEMG interference pattern such as number of measured motor units and motor unit action potential amplitude and shape.

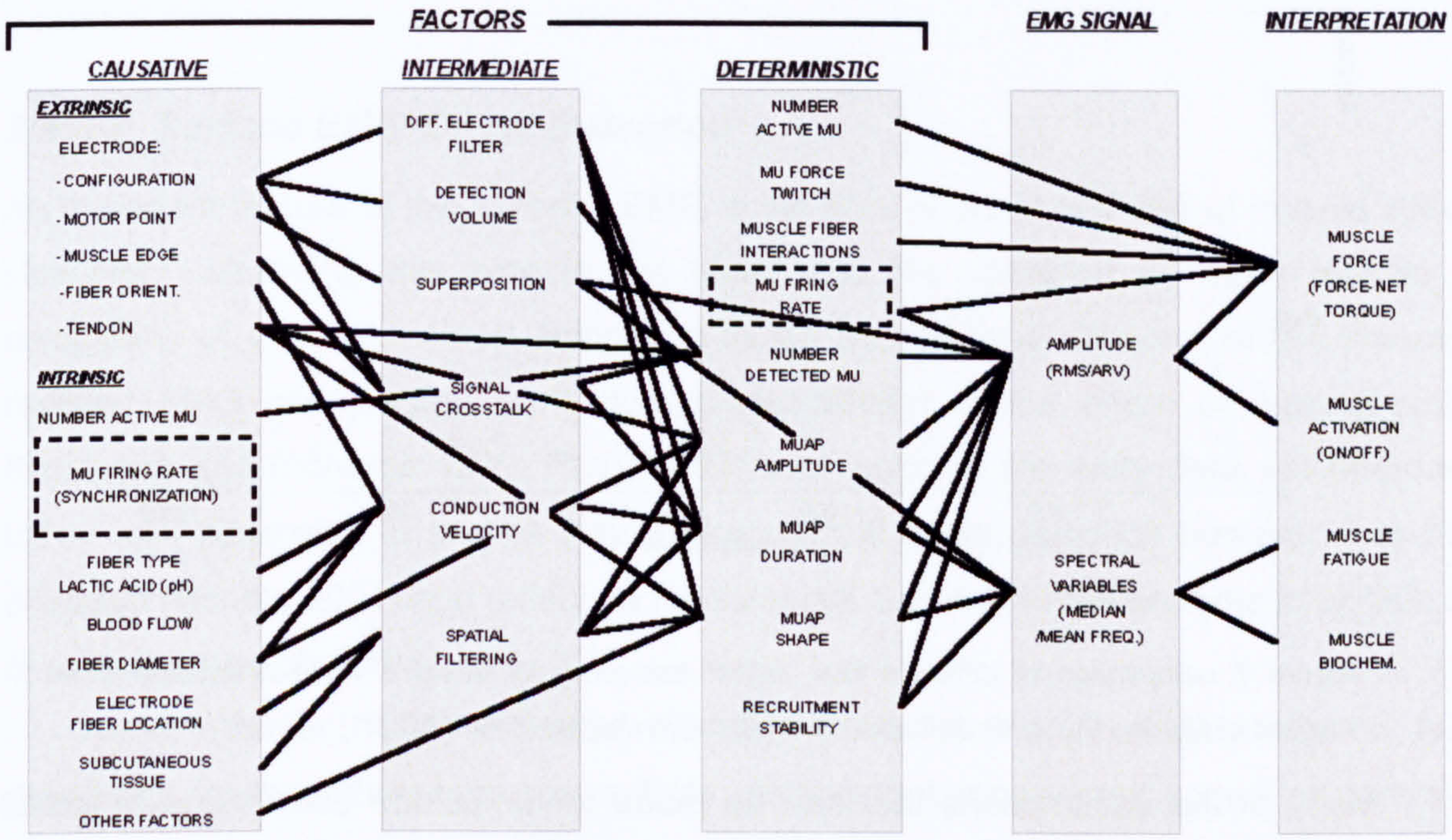

Figure 6 Factors affecting the sEMG signal from De Luca (DeLuca 1997)

The linear envelope is widely used because it is associated with the mechanical force generated by the muscle (Hermens, Freriks et al. 1999). Though caution must be used with such an association, as Figure 6 demonstrates, under certain conditions it is a useful estimate, or in its crudest use, an indication of muscle force generation. This association has also guided the progress of signal processing methodology. From studies of isometric contractions, filter cut-off frequencies of 2Hz have been proposed (Winter 1984). This level of filtering generates a delay of approximately 80ms which relates to the period between the sEMG signal manifestation and the onset of mechanical force. In combination, however, lower cut-off frequencies produce signals with higher signal-to-noise ratios (Hermens, Freriks et al. 1999) with the trade-off that fast movements or rapidly changing bursts of muscle activity can be hidden. In reality, filter characteristics to generate the linear envelope vary in the literature (Clancy 1999; DeLuca 1997; Fullmer,

Meek et al. 1984; Hermens, Freriks et al. 1999; Hershler and Milner 1978; Parker, Stuller et al. 1977), variation in filter characteristics generate variations in the linear envelope representation as can been seen in Figure 7.

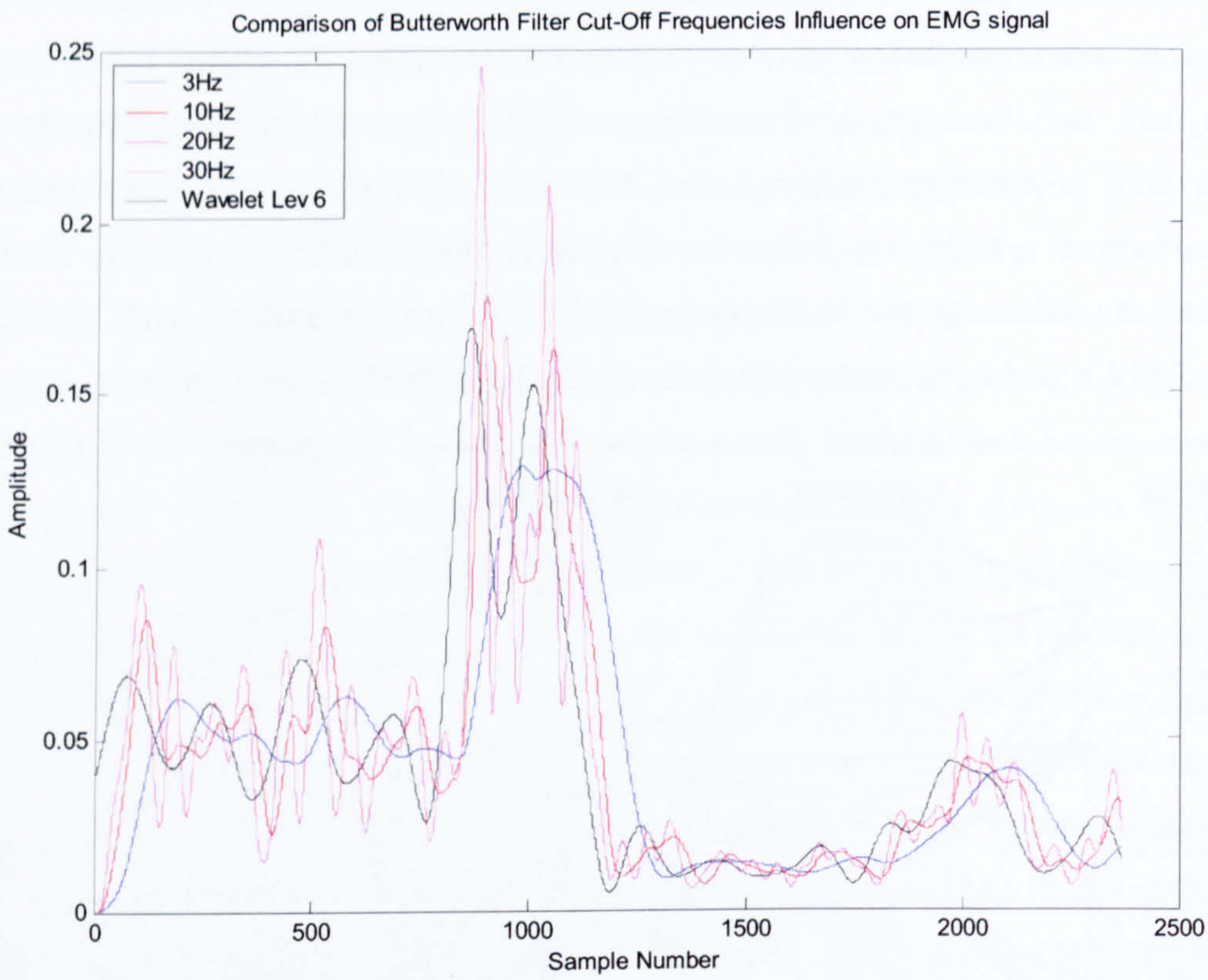

Figure 7 comparison of different filter cut-off frequency including a wavelet decomposition method of filtering that is described in more detail in chapter 2.4.6.1 (p. 61)

Many of the assumptions that can be made for amplitude estimations of isometric contractions cannot be made during the analysis of dynamic contractions (Farina and Merletti 2000; Hermens, Freriks et al. 1999; Ripoli, Belardinelli et al. 1999). The raw rectified sEMG signal is described as a non-stationary stochastic signal (Clancy 1999) when considering long time epochs of dynamic contractions (Hermens, Freriks et al. 1999). The linear envelope representation is also used in an attempt to resolve the problem of estimating the amplitude of such a signal (St-Amant, Rancourt et al. 1998) which has, in turn, led to the development of more advanced sEMG smoothing methods. The non-stationary characteristic of the signal has led some authors to vary adaptively the number of samples over which to average, dependent on some other signal variable. Dependent variables such as sample amplitude and the first derivative of a signal epoch (Clancy 1999; Fullmer, Meek et al. 1984) or signal variance (Parker, Stuller et al. 1977; St-Amant, Rancourt et al. 1998) have been used to vary adaptively the averaging window length. One example is that of Herscler and Milner (Clancy 1999; Hershler and Milner

1978) who developed an algorithm to calculate an optimal window length for varying walking speed. Importantly this work also reflects the subtlety of the signal amplitude to environmental factors. Many of these methods are confounded by the findings of Clancy (Clancy 1999) who concluded that the best fixed length windowing methodology worked as well as the best adaptive length windowing technique. However, this finding was also situation dependent (Hershler and Milner 1978). The most recent amplitude estimation technique was presented by Ricamato et al. (Ricamato and Hidler 2005). This technique used a "metric" to define amplitude, timing and phase properties of sEMG during treadmill re-retraining of gait after stroke and spinal cord injury. The metric compares sEMG activity by calculating the magnitude component that is defined as the similarity in amplitude with a normal data set.

2.4.5.2 Surface EMG Onset Detection

An important feature of the dynamic EMG is the time of onset and end of muscle activity. However, calculating this time is not trivial and the range of literature reflects the complexity of the task. Visual inspection by an experienced observer of the smoothed rectified EMG can provide an accurate assessment of the onset of muscle activity (Knutsson and Richards 1979; Perry 1993) and much of the early data still referenced today was generated in such a way. Observational onset detection however, has been criticised (Bonato 2001) and reflects a fundamental question in the analysis of sEMG; that of reliability and objectivity.

Winter (Winter 1984) criticises the early uses of threshold detection on linear envelopes to characterise muscle activity, stating that many were based on "arbitrary" threshold values. Furthermore, Winter states that as amplitude information is inherently removed in the simple application of threshold detection; both false positive and negative results can be generated. Early studies did not analyse "on and off" patterns in relation to the linear envelopes that generated them (Bekey, Chang et al. 1977; Chong, Vojnic et al. 1978; Close and Todd 1959). Work developing methods to extract onset features from EMG has been motivated by the field of postural control and literature is directed at a variety of tasks including walking but also during elicited and isometric muscle contractions. However, many of these have been assimilated into techniques specifically to characterise patterns of muscle activation during locomotion. Until recently the criticism of onset detection techniques revolved around non-standardised heuristic criteria and the lack of studies confirming their reliability (Staude and Wolf 1999).

Hodges (Hodges and Bui 1996) assessed a combination of parameters applied to an onset detection method. Broadly the methods processed the EMG by low pass filtering the

raw signal, then set a threshold value based on the standard deviation (SD) of the smoothed signal. Finally a period of time was set which the threshold must have exceeded. The degree of smoothing was shown to be critical in the detection accuracy of the technique. Overly smoothed data was seen to vary significantly from the visually assessed onset times. Equivalently, delayed detection occurs when filtering is not sufficient as the more rapid changes in amplitude reduce the mean; inaccuracies in detection were in the same order as over-smoothing. The threshold level described in terms of SD was not found to affect significantly the onset detection in relation to changes in other parameters. However, it is clear that false negative results occurred more frequently with greater threshold levels. Intuitively, the time for which a threshold must be exceeded increased premature detection when short, and delayed detection if longer when compared to visually identified onset times. A 25ms period closely approximated visually assessed signals. In comparison, an earlier study (Bogey, Barnes et al. 1992) applied a 50 point moving average to smooth the raw data and then used a value of 2 SD's of the smoothed signal as a threshold level. Interestingly, the ensemble averaged EMG amplitude was maintained after processing in support of the criticisms of Winter. Bogey (Bogey, Barnes et al. 1992) promotes an EMG representation based on onset and cessation times combined with an intensity representation generated by removing low relative intensities of short duration from the ensemble averaged profile.

Recently, more advanced statistical methods have been applied to the problem of defining EMG onset times. In particular a double threshold detector based on the statistical parameters of raw EMG was developed by Bonato (Bonato 1998). Arguing that conventional onset detection based on the threshold of a linear envelope was counter to standardisation, and generally not satisfactory, the technique introduces a second threshold criterion. The second threshold criterion allows the user to reduce the probability of false positive readings due to low signal-to-noise ratio and maximise the probability of correct onset detection. Most recently the use of statistical onset detection has progressed to combine the greater physiological understanding of sEMG and analysis of stochastic processes. A prominent study by Staude (Staude and Wolf 1999) introduced the approximated generalised likelihood ratio which was adopted in the study of variable gait in cerebral palsy and stroke (Roetenberg, Buurke et al. 2003).

2.4.5.3 Spectral Estimation

The features of the frequency spectrum have been associated with underlying physiological processes. As was mentioned earlier, the main features drawn from the frequency spectrum are the mean, median and maximum frequencies, specifically a shift

of these parameters to lower frequencies during fatigue (Beck, Housh et al. 2005; Bilodeau, Scindler et al. 2003; Hermens, Boon et al. 1984). Time series parameters such as signal zero crossing and signal peaks can be also calculated indirectly from the spectrum (Hermens, Freriks et al. 1999). Hermens (Hermens, Boon et al. 1984) relates the bandwidth between 10-25Hz to the mean firing frequency of the active motor units. Though extending the bandwidth to 40Hz the findings of Hermens (Hermens, Boon et al. 1984) were supported by Hagg (Hägg 1992), though this study clarified that changes in motor unit firing rates only cause significant shifts in the frequency spectrum at low contraction intensities. That is when the probability of contiguous motor unit action potentials (MUAP) overlapping is less likely. Again, the schematic representation of the interplay between many factors in the physiological system presented by De Luca reveals the complexity of the system that generates the frequency spectrum (DeLuca 1997). The intrinsic causative effect on the sEMG spectrum of motor unit firing rate can be small (Hägg 1992). However, this assertion relies on only a small contribution of motor unit synchronisation. This effect has been suggested to decrease the mean frequency of the sEMG spectrum in both model and human trials (Kilner, Baker et al. 2002; Kleine, Stegeman et al. 2001; Marsden, Farmer et al. 1999). Levels of motor unit synchronisation have been observed to vary in patients and be directly associated with functional performance, specifically, a slowing of performance with the loss of synchronisation (Farmer, Swash et al. 1993). However, increased periods of MUAP in stroke patients have also been observed (Datta, Farmer et al. 1991). Yet, the influence on synchronisation is strongly criticised by De Luca, specifically, during spectral compression in fatigue studies (DeLuca 1997) (De Luca, Roy et al. 1993). This was on the grounds that the shift in mean frequency during fatigue is the result of adaptation to the shape of the motor unit action potential, it itself is physiologically linked to conduction velocity (Lowery, Vaughan et al. 2000) due to biochemical changes in the system (Dimitrova and Dimitrov 2003). Though motor unit discharge synchronisation has been shown and alterations to pre-synaptic motor-neurone inputs are evident as a result of diseases of the nervous system, (Farmer, Halliday et al. 1997) De Luca regards such changes as incapable of adapting the sEMG spectrum outside the MUAP firing rate frequency range. The conclusions of Kliene (Kleine, Stegeman et al. 2001) however, would suggest otherwise when considered in relation to the evidence of alteration to the normal firing pattern of the motor neurone in stroke patients (Farina, Cescon et al. 2002). Spectral modification may not be explained by MUAP shape and conduction velocity alone.

The mean and median frequency have been used in the assessment of motor unit recruitment during contraction of increasing intensity and fatigue onset (Gerdle,

Henriksson-Larsen et al. 1991) (Hägg 1992; MacIssac, Parker et al. 2001; Solomonow, Baten et al. 1990) However, caution is needed in drawing a simple relationship between these physiological parameters and the spectral characteristic. Although a linear relationship has been measured between mean or median frequency (Hägg 1992; Hermens, Freriks et al. 1999), the translation of these characteristics to recruitment strategies and is complicated because the measurement of conduction velocities is influenced by motor unit discharge rate and muscle length (Enoka and Fuglevand 2001; Farina, Cescon et al. 2002; Schulte, Dimitrova et al. 2005; Schulte, Farina et al. 2004). Furthermore, it is argued that muscle fibre types are not related to distinct conduction velocity (Enoka and Fuglevand 2001; Jakobsson, Edstrom et al. 1991).

The coefficients of the spectral techniques themselves have been used to characterise movements and to identify pathology. In particular the autoregressive (AR) model (Farina and Merletti 2000; Farmer, Halliday et al. 1997; Hu and Nenov 2004; Pattichis and Elia 1999) and Fourier transform (Beck, Housh et al. 2005; Hostens, Seghers et al. 2003; Zhang, Shiavi et al. 1991) have been applied to both static and dynamic sEMG classification.

Coefficients of the discrete Fourier transform were shown to be able to characterise a linear envelope. However, interestingly the phase spectra was shown to play a far more significant role in defining the shape of the linear envelope (Zhang, Shiavi et al. 1991). In this study AR coefficients were excluded due to poor performance. However, other studies have found coefficients from the AR model to be effective at differentiating signals (Christodoulou and Pattichis 1999; Farina and Merletti 2000; Park and Lee 1998; Pattichis and Elia 1999). The AR model is a parametric model and defined:

$$x(n) = -\sum_{k=1}^{p} a(k)x(n-k) + w(n)$$ Equation 3 Auto Regressive Function

The model bases the value of a signal, $x(n)$, at time t as the linear combination of previous values of the signal, $a(k)x(n-k)$, plus some level of noise $w(n)$. Spectral components can be calculated using the AR model. One assumes that the signal under observation is the result of a linear system driven by white noise. Spectral components can be calculated by finding the coefficients (parameters) of the system that hypothetically generates the signal. In a study assessing motor unit firing rates in the upper limb (un-impaired, Parkinson's disease and stroke), Kang et al. (Kang, Cheng et al. 1996; Kang, Shiu et al. 1995) utilised parametric modelling to estimate the dominant MU firing frequency and to characterise abnormalities during isometric contractions. They used short time epochs of sEMG and therefore the assumptions regarding linearity and

stationarity remained justified. Autoregressive coefficients were also extracted as features in an upper limb study of spinal injured patients and un-impaired subjects (Chen, Sun et al. 1997). The study compared the AR coefficients to linear predictive coefficients derived cepstral coefficients. Cepstral coefficients are features generated from the inverse log of the Fourier power spectrum but can be calculated directly from the autoregressive model (Pattichis and Elia 1999). Again this study represents a use of parametric modelling, although here to discriminate between upper limb movements by generating features for pattern classification. This study did not represent the same restrictions in terms of requiring isometric contractions and generated features that related to the synergy between two muscles. The cepstral coefficients were shown to be superior at discriminating between movements. Cepstral coefficients were also investigated by Boostani (Boostani and Moradi 2003) as a feature for prosthetic control which also identifies them as a time varying features. Most recently the coefficients from the AR model have been integrated into a classification methodology by Itiki (Itiki 2005) which succeeded in achieving a 96% discrimination rate between pathological and non-pathological needle EMG signals.

The coefficients of the spectral estimation techniques can provide time varying parameters for dynamic contractions; directly however, they are not known to represent underlying physiological processes. Time-frequency techniques can provide instantaneous values of frequency parameters (Englehart, Hudgins et al. 1999; MacIssac, Parker et al. 2001). The Gabor or Short-Time Fourier Transform (STFT) essentially applies the traditional Fourier transform to small epochs of the signal thus maintaining the stationarity requirement. Unfortunately the STFT suffers because a trade-off has to be made, which is governed by the Heisenberg uncertainty principle, between resolving features in the time domain and frequency domain (Mallat 1989; Merletti 1999). More advanced techniques such as wavelet analysis however have overcome this requirement (Englehart, Hudgins et al. 1999).

2.4.6 Advances in sEMG Signal Processing

2.4.6.1 Wavelet Analysis

In recent years wavelet analysis has seen a rise in popularity within biomedical engineering. With respect to gait analysis and sEMG, the application of this signal processing method has been limited. This is in light of useful findings when applied to sEMG acquired from isometric contractions. Wavelet analysis has shown clear advantages over traditional time-frequency analysis at resolving both frequency and time

domain properties. This could be particularly useful for analysing dynamic contractions, such as those acquired during walking, where the non-stationary nature of sEMG makes traditional frequency domain analysis inappropriate. Furthermore, the manner in which the frequency of the sEMG signal varies over the time of a stride could yield useful characteristic differences between those with a walking impairment. First the background of the technique is examined.

2.4.6.1.1 Background

The continuous wavelet transform of a function f at scale s and translation u is given by (Mallat 1999):

$$Wf(u,s) = \int_{-\infty}^{+\infty} f(t)\psi^*(t)dt = \langle f, \psi_{u,s} \rangle .$$

Equation 4Continuous Wavelet Transform

This means the function f is correlated with the dilated and translated wavelet:

$$\psi_{u,s}(t) = \frac{1}{\sqrt{s}}\psi\left(\frac{t-u}{s}\right).$$

Equation 5 Wavelet Definition

The wavelet is a special function ψ which conforms to particular rules such as it has a zero average and finite energy, the prototype of which is called the mother wavelet (Mallat 1999). In other words the wavelet transform decomposes a signal over a dilated and translated function, the mother wavelet. Figure 8 shows some examples of wavelet families, the Daubechies and Complex Gaussian wavelets are shown with different orders which results in increasing the number of oscillations in the signal. The term $\frac{1}{\sqrt{s}}$ is used to normalise the power of the wavelet. The features of the different wavelets make them suitable for different signal processing purposes. The dilated and translated wavelets are well localised in both time and frequency. Therefore, transient signal components can be observed (Mallat 1999). By comparing the local time and frequency supports for the traditional Fourier and Short Time Fourier transforms with the discrete wavelet transform the advantage becomes clear. Figure 9 shows that the discrete wavelet transform allows a higher temporal resolution, short epoch wavelets, at high frequencies and higher frequency resolutions at low frequencies, long epoch wavelets; i.e. longer periods of oscillation equate to lower frequencies. The output of the wavelet transform over a varying frequency and amplitude signal is shown in Figure 10. Therefore, the energy of a signal

can be well specified over the whole time-frequency plane. An extension to the wavelet transform, the wavelet packet transform, permits an even more specific time-frequency plane, tailored to the signal being analysed (Englehart, Hudgins et al. 1999).

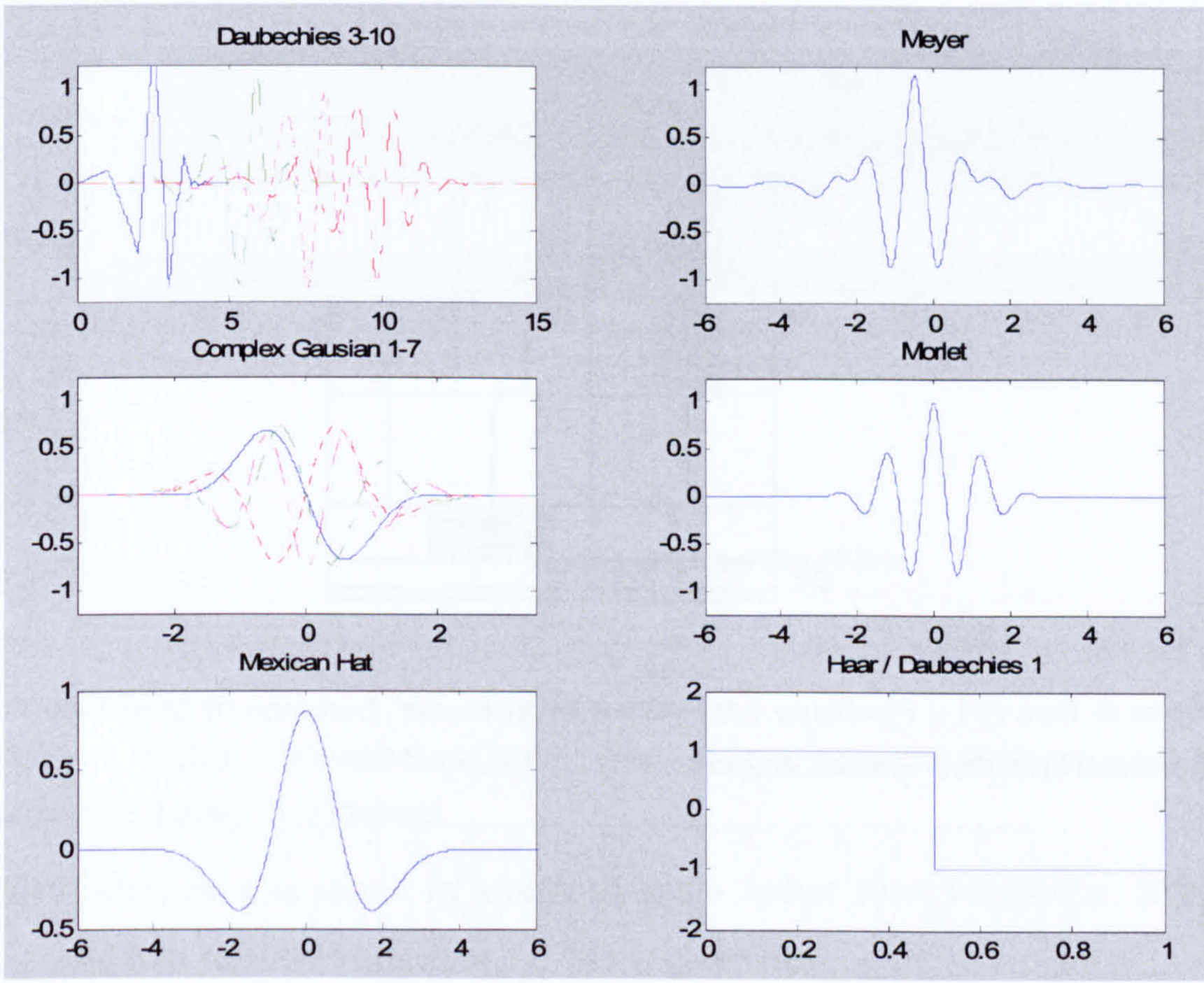

Figure 8 Families of wavelets (Generated during this study using the MATLAB Wavelet Toolbox)

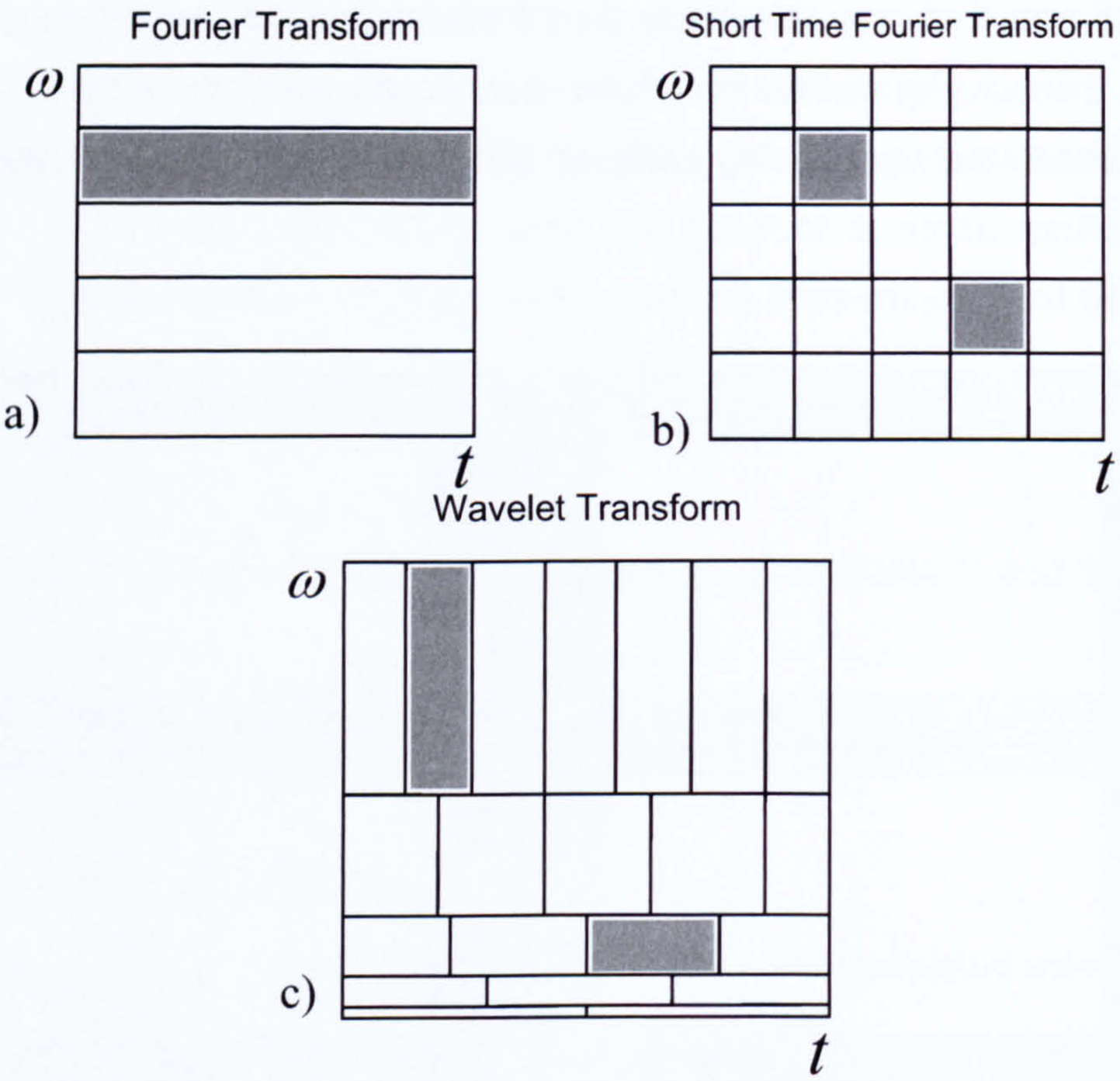

Figure 9 Time (t) – Frequency (ω) planes for a) Fourier Transform b) Short-Time Fourier Transform c) Discrete Wavelet Transform

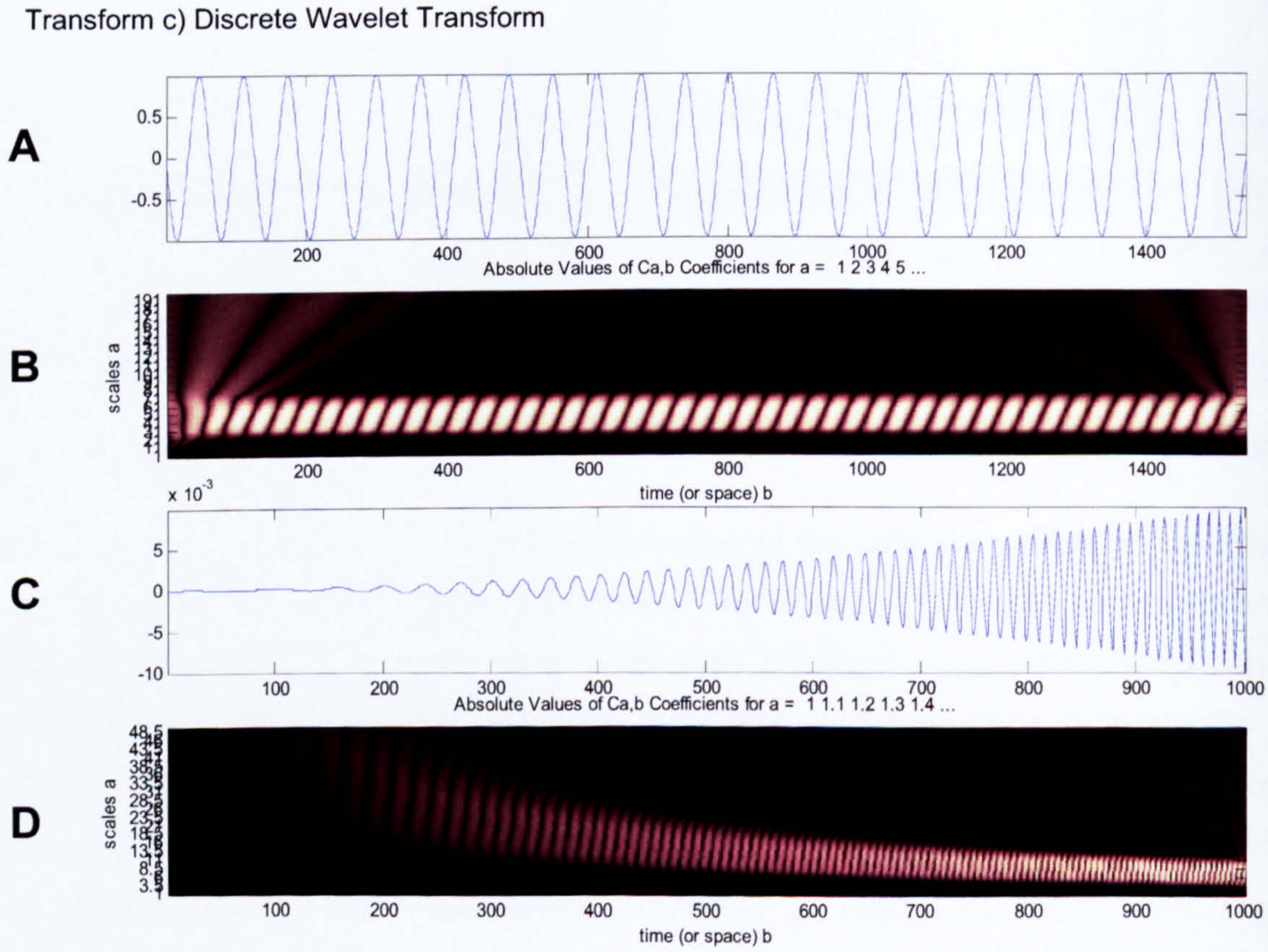

Figure 10 Sine wave **A** & continuous wavelet transform **B**, Chirp wave **C** & continuous wavelet transform **D**

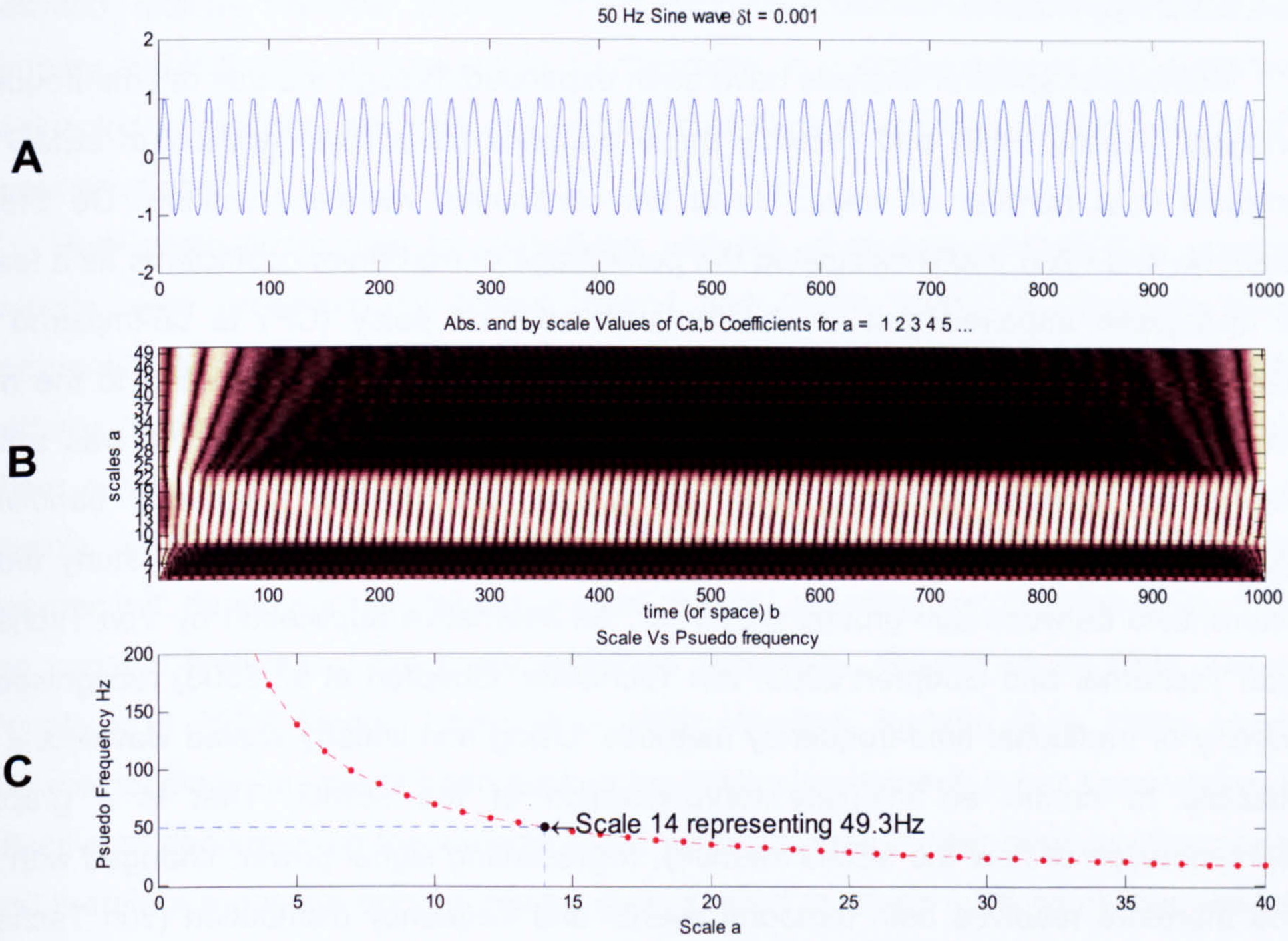

Figure 11 Relation of Wavelet Scale to Frequency. **A)** 50Hz sine wave. **B)** Continuous wavelet transform. **C)** Scale vs. frequency.

In wavelet analysis it is usual to speak of scale rather than frequency. Scale can be directly linked to a pseudo frequency f_a, this is given by:

$$f_a = \frac{f_c}{a\Delta t}$$

Equation 6 Wavelet Scale to Frequency Conversion

Where, f_c is the centre frequency of the wavelet, a is the scale (2^a is displayed on the y axis of Figure 11 **C**) and Δt is the signal sampling period (Mathworks 2006).

The choice of wavelet to use when analysing sEMG is not consistent in the literature, De Stefano et al. (Stefano and Allen 2003) uses a complex Gaussian of order 3 whereas Von Tsharner (von Tscharner 2000; von Tscharner 2002; von Tscharner and Goepfert 2003) uses a Phil or Meyer wavelet. Karlsson et al. (Karlsson, Gerdle et al. 1998) uses a Morlet or modulated Gaussian wavelet. These choices are not well defined and there are many commonly used wavelets to choose from. The advice for choosing an appropriate wavelet for an analysis points towards choosing a wavelet shape that represents the prototype of the signal being analysed (Torrence and Compo 1998).

2.4.6.1.2 Application

Methods of spectral analysis have been expanded through the use of time-frequency analysis (Mallat 1989) and recently these methods have been applied to sEMG gait analysis in a number of ways. Using the continuous wavelet transform De Stefano (Stefano and Allen 2003) calculated the percentage of maximum coefficients as a feature to distinguish impaired gait of children with cerebral palsy (CP) to un-impaired age matched children. Additionally, an instantaneous frequency corresponding to the mean coefficient at a particular time epoch was extracted as a feature. This was able to distinguish between impaired and un-impaired over limited frequency bandwidths (gastrocnemius 70 – 100 Hz tibialis anterior 70 – 90 Hz). However, the study did not differentiate between sub-groups within CP. An alternative application by Von Tscharner (von Tscharner and Goepfert 2003; von Tscharner, Goepfert et al. 2003) recognised the poverty of traditional time-frequency methods. Using non-linearly scaled wavelets it was possible to create an intensity representation of the sEMG. That is a graphical representation of how the sEMG intensity, representing signal power, changed with time and therefore resolves both temporal events and frequency distribution (von Tscharner 2000). In addition, the intensity representation generated a pattern space from which principal patterns can be identified using principal component analysis (von Tscharner and Goepfert 2003) therefore providing a method to classify muscle activation patterns. This method has not yet been extended to pathological walking. It has the advantage that the raw sEMG signal is processed and therefore information is not removed through the filtering process. This method is mathematically complex; the output, though appealing, specifically that it represents an sEMG signal in time, amplitude and frequency, requires the understanding of frequency decomposition and is abstracted from the original sEMG signal. It does therefore, not allow for simple communication of results to therapists. This problem is amplified if using the raw wavelet decomposition spectrum which visually does not relate directly to the sEMG linear envelope.

2.4.6.2 Multivariate Statistical Methods

Jansen et al. (Jansen, Miller et al. 2003) developed a novel analysis method to assess muscle synergy patterns during walking, extending this to the analysis of trajectories, when the linear envelope of one muscle is plotted against another. The trajectories can be clustered into templates (representative muscle synergy patterns), the frequency at which these templates appear during a series of strides provides insight into the structure of the muscle activity. Although this technique has not been applied to pathological gait it addresses an important component in pathological gait, similarly to co-

activation indices. However, it does so by quantifying similarities in the way muscles act in synergy and is therefore more subtle. Furthermore, in a similar manner to the application of principal component analysis, the method quantifies structural similarities to the sEMG linear envelope.

Multivariate techniques for classifying patterns of muscle activation in unimpaired walkers were presented by Shiavi (Shiavi and Griffin 1981). By applying principal component analysis (Karhunen-Loeve expansion, see next page) to linear envelope patterns these were reduced to a few patterns representing the variance across all the linear envelopes. Cluster analysis was then applied to the reduced data set for each muscle. Similar application of principal component analysis has been used in order to determine if, during normal walking, a small number of underlying patterns existed amidst the variable features of the linear envelope (Ivanenko, Grasso et al. 2003; Ivanenko, Popple et al. 2004; Merkle, Layne et al. 1998; Wootten, Kadaba et al. 1990). However, this methodology has never been applied to walking impairment. It has been shown to be effective at decomposing the variable linear envelope to a smaller number of components and therefore a dataset appropriate for classification methods such as cluster analysis. It also has the advantage of being associated to the control aspect of gait, specifically the principle of dynamic systems analysis approach (Craik and Oatis 1995; Full and Koditschek 1999; Webber and Zbilut 1994; Zajac, Neptune et al. 2003). This principle reduces the degrees of freedom of the anatomical and physiological system that generates movement. For example, the complexity of controlling inter-segmental joint angles, ankle, knee and hip, might be viewed as a series of individual segment elevations such as the foot or thigh or global kinematical goals (Ivanenko, Grasso et al. 2003; Olney, Elkin et al. 1979).

It is known that un-impaired walking can be described by relatively few patterns of muscle activity representing the varied sEMG linear envelopes captured from multiple muscle groups (Ivanenko, Popple et al. 2004). The premise with regard to un-impaired walking is that multiple muscle groups could be controlled by a few underlying activity generators (Ivanenko, Popple et al. 2004). However, it should also be possible to characterise impaired activity in a similar way. It may be possible to describe deviations in the sEMG linear envelope by a small number of patterns. Alternatively, deviations from the factors representing un-impaired activity could be used to characterise poor or inappropriate muscle activity.

2.4.6.2.1 Principal Component Analysis

Principal Component Analysis is a method by which a set of variables is reduced to a new parsimonious set of variables based on a linear combination of the original data. The new variables are the principal components of the original set of variables. The first principal component is the linear combination of the original data that reflects the maximum variance out of all the possible linear combinations. The second, third, and fourth principal component are then defined as the subsequent combinations that reflect the maximum variance in addition to being uncorrelated with the previous components. The p principal components, $y_1, y_2, \cdots, y_p$, are (Jolliffe c1986):

$$\begin{aligned} y_1 &= a_{11}x_1 + a_{12}x_2 + \ldots + a_{1p}x_p \\ y_2 &= a_{21}x_1 + a_{22}x_2 + \ldots + a_{2p}x_p \\ &\vdots \\ y_p &= a_{p1}x_1 + a_{p2}x_2 + \ldots + a_{pp}x_p \end{aligned}.$$

Equation 7 Principal component Analysis

Where a is defined such that: $\sum_{j=1}^{p} a_{ij}^2 = 1$ for all $i = 1, \cdots, p$ $j = 1, \cdots, p$ and ensures the requirement for maximum variance and each principal component being un-correlated. The coefficients are calculated by finding the eigenvalues and eigenvectors of the co-variance, or correlation, matrix of the original data set $\mathbf{X}$. The correlation matrix $\mathbf{R}$ is calculated:

$$\mathbf{R} = (1/p)\mathbf{X}\mathbf{X}^{\mathsf{T}}.$$

Equation 8 Correlation Matrix

The eigenvectors of $\mathbf{R}$ represent the coefficients $a_1, a_2, \cdots, a_p$ of Equation 7 and the eigenvalues represent the relative power of its corresponding eigenvector. Alternatively, the process can be described by calculating a set of weighting values $\mathbf{W}$ for the basis vectors (eigenvectors) $\boldsymbol{\lambda}$ to construct the original data set $\mathbf{X}$ (Wootten, Kadaba et al. 1990)

$$\mathbf{X} = \boldsymbol{\lambda}\mathbf{W}. \qquad \text{Equation 9}$$

Therefore,

$$\mathbf{W} = \boldsymbol{\lambda}^{\mathsf{T}}\mathbf{X}. \qquad \text{Equation 10 PCA Weighting Factors}$$

The principal component methodology requires the sEMG to be represented as a linear envelope. In this way the dimensionality of the data is reduced from the outset,

though the method would not perform well using raw high-dimensional data. However, little justification is given for the values chosen in literature. Wootten et al. (Wootten, Kadaba et al. 1990) created a data vector based on the linear envelope by integrating the signal to create a 32-point data vector. Ivanenko et al. (Ivanenko, Popple et al. 2004) also generated a linear envelope but defined it using 200 data points. In order to generate a data set with the smallest dimensionality it is reasonable to reduce the number of data points representing the linear envelope. For example, a linear envelope generated using a 15Hz cut-off frequency need only be represented by greater than 30 samples for a 1 second period, in order to confidently reconstruct the pattern of the signal. Thus the implementation of Wootten et al. (Wootten, Kadaba et al. 1990) is justifiable. However, the implementation by Ivanenko et al. (Ivanenko, Popple et al. 2004) creates a high redundancy in the linear envelope and therefore over specifies the signal.

The specification of a normalisation technique is important as implicitly it dictates the resulting principal components. Wootten et al. (Wootten, Kadaba et al. 1990) normalised the linear envelope to the maximum within each signal. Therefore the assumption is that the relative amplitude should not reflect in the resulting principal components. For the un-impaired this is not an unreasonable assumption, and is possibly desirable as it reduces variability (Hermens, Freriks et al. 1999). However, to make the same assumption within the impaired group, where the relative amplitude could be a feature of pathology, is not reasonable. Therefore application of this methodology to an impaired group requires a consideration of these normalisation techniques.

2.4.6.3 Non-Linear Methods

Processing methodologies in areas other than gait analysis have probably seen the most development over the past 20 years, and they probably reflect the most advanced signal processing methods in the use of sEMG. Although direct transfer of techniques to clinical gait analysis is generally not possible, the principal aims of sEMG classification related to movement could motivate applications within gait analysis. Several good reviews reflect most of the development (Bonato 2001; Conte and Merletti 1995; Langhorne and Pollock 2002; Merletti and Conte 1995).

Non-linear time series analysis has been a relatively recent tool in the analysis of biological systems. Although terms related to non-linear time series analysis, such as fractals, chaos and strange attractors, were known to the fields of theoretical mathematics and physics and in the field of biological systems analysis, it is only recently that it has been adopted in the analysis of physiological systems. The ability of a dynamic assessment to help disentangle the complex structure of many biomedical signals and

systems has shown it to be a valuable analysis technique. The technique has found application in monitoring foetal ECG, human breath rate, autonomic control of heart rate and sEMG. Though primarily applied to understanding the underlying physiological system - that is one likely to be constructed of multiple subsystems interacting and producing structurally complex systems of control (Allen 1999) and thus presenting the possibility of deconstructing the control mechanisms in gait - the technique is equally applicable for quantifying underlying changes in signals of dynamical systems. Non-linear time series analysis tools have been applied to isometric sEMG patterns in the assessment of fatigue (Mewett, Reynolds et al. 2001; Nieminen and Takala 1996) but as yet there is no evidence in the literature of this technique being applied to dynamic EMG, surface or otherwise, during locomotion.

Fractal analysis has been applied to movement analysis (Ripoli, Belardinelli et al. 1999). The technique attempts to classify signals based on some underlying parameter that should reflect the dynamics of the phenomenon. It therefore does not rely on the comparison of "specific pattern features" such as spectral or amplitude features which is advantageous when the exact physical model for the processes is unknown. Computationally such methods can be very efficient and as mentioned before do not require the transformation of the original signal. Ripoli et al. (Ripoli, Belardinelli et al. 1999) suggests good results in characterising particular movements, however it is not clear the extent to which this classification can relate to pathology.

Recurrence plots are a non-linear technique that have been applied to sEMG measured from isometric contractions (Webber, Schmidt et al. 1995). Recurrence plot analysis does not make any constraints on the data set being analysed in terms of statistical distribution, stationarity or data set size (Filligoi and Felici 1999). Thus, it was suggested that they would be suitable for physiological data. During heavy loading, in isometric contractions, non-linear variables indicated the onset of fatigue faster than traditional linear techniques (Webber, Schmidt et al. 1995). However, it should also be noted that when lower forces were applied to a limb both linear and non-linear techniques gave quasi steady states over time.

Neural networks and fuzzy techniques have been applied to sEMG in the assessment (Su and Wu 2000) of gait, and the control of orthoses (Micera, Sabatini et al. 1999), also specifically during gait (Lauer, Smith et al. 2005). All have reported good results in classifying either gait events or impaired from un-impaired walkers and upper limb movements. However, they do not comment on the physiological deficits that cause the particular movements.

2.4.7 Surface EMG in the assessment of Hemiplegic Gait

Herschler (Hirschberg and Nathanson 1952) was said to have been the first to have applied sEMG to the analysis of hemiplegic gait. It was noted that latterly other authors had confirmed many of Hershlers observations but in addition, tried to quantify the outcomes by using onset-offset detection (Dimitrijevic, Faganel et al. 1981; Perry, Waters et al. 1978), though this also excluded amplitude information. Knutsson (Knutsson and Richards 1979) applied linear envelope detection and therefore retained amplitude information, in order to characterise particular patterns of impaired activation. The linear envelope was created by calculating the average rectified value using an averaging period of 0.2 seconds. This time was justified using the relationship between the delay introduced to the signal and the onset of mechanical force.

Knutsson reports that different groups presented with fundamentally different patterns of disturbed muscle activation. In particular four groups were defined, each characterised by common features. Type 1 were characterised by premature activation of the calf muscle. Type 2 included those who appear to have abolished or marked lowering of the sEMG activity in two or more muscle groups in the paretic limb. Type 3 characteristics were abnormal co-activation of several of the limb muscles but with no significant decrease in the amplitude of muscle activity. Premature muscle activation of the ankle appeared in the period of dorsiflexion i.e. when the muscle was lengthening and it was suggested that premature activation was due to hyperactive stretch reflex. Some subjects in this group presented with clonus, represented by a 5Hz oscillation in the EMG. Eight of the patients presenting with this form of dysfunction suffered from hemiparesis because of stroke. It is felt that the discontinuity between the numbers of stroke patients (23) to MS and cerebral tumours (3) suggests that little can be drawn from the numbers; less to state that dysfunction as a result of stroke was seen across all groups. Co-activation was only found in four hemiparetic patients all having suffered a stroke. Reciprocal activation was disrupted which manifested as a disorganisation of the normal sequential shifts of activity in different muscles. The final group, type 4, included those with no clear affinity to the other three groups. Although Knutsson's study represents the first to subdivide impairments in stroke patients using sEMG, it was not possible to quantify these sub-grouping.

Extending this work Burridge et al. (Burridge, Wood et al. 2001) worked to develop indices that described abnormalities in muscle activation causing drop foot. Similar to Knuttson, Burridge et al. focused on three areas of impairment; activity in tibialis anterior during the swing phase, premature calf activity in early stance phase and calf activity

during push off. The indices were defined from visual inspection of sEMG and foot switch data. The linear envelope was defined by calculating the ARV, however the time constant recorded in their paper was 13.8 seconds which is equivalent to several gait cycles and unlikely to have been used to generate the supporting linear envelopes. Noting that the tibialis anterior had two bursts of activity between toe off and toe strike the tibialis anterior index was defined as:

$$\frac{\sum_{toestrike}^{toeoff} TAactivity}{\sum_{100\%GC}^{0\%GC} TAactivity}$$

Where GC = gait cycle. The premature calf activity index assumed, based on visual inspection, no calf activity in the first 20% of the gait cycle. Premature calf activity due to passive stretch during early stance would produce activity early in the stance phase; the index was therefore defined as:

$$\frac{\sum_{0\%GC} NormCalfActivity + 20\%GaitCycle}{\sum_{100\%GC} CalfActivity}$$

The push off index relied on observations that the average period of calf activity was 11% of the gait cycle before heel rise to 9% of the gait cycle after heel rise. The push off index was defined:

$$\frac{\sum_{9\%AfterHeelRise}^{11\%BeforeHeelRise} ClafActivity}{\sum_{100\%GC}^{0\%GC} CalfActivity}$$

It was reported that although the indices alone did not appear to fully describe impaired muscle activation, they did identify differences between hemiplegic and normal calf muscle activation; specifically whether the dysfunction was due to inappropriate activity early in the stance phase or reduced sEMG at push off. Importantly it was reported that the hemiplegic muscle pattern of the tibialis anterior during swing phase was not dissimilar to that of the un-impaired subject. Furthermore it was noted that drop foot might be the result of increased calf activity as much as it is the result of weakness of the tibialis anterior muscle. Some of the subjects could not be classified in terms of Knuttson's sub-groupings, although the subjects that did fall into one of the groups did not change from

one group to another; this suggests validity in this classification over the course of the study.

Conclusions with respect to co-contraction are somewhat in contradiction to Lamontagne (Lamontagne, Malouin et al. 2001; Lamontagne, Richards et al. 2000; Lamontagne, Richards et al. 1998) who specifically studied co-activation in hemiplegic stroke patients. Lamontangne observed that co-activation was increased in non-disabled subjects in comparison to stroke patients. The co-activation index introduced in Lamontangne's study was developed from a study of cerebral palsy children (Crenna 1998). This method used a threshold of 20μV to define a significant activity of the linear envelope above noise. The index was generated by dividing the average period of co-activity with the period of the gait phase. Significantly no normalisation technique was used; however, the generation of the linear envelope was also not fully defined.

Additional contributions have been made by Chen (Chen, Huseh et al. 1994) and Ricamato et al. (Ricamato and Hidler 2005). However, these studies have not focused on the interpretation of sEMG within a stroke group but rather in developing means to describe the differences between stroke and un-impaired walking. The conclusions of Chen (Chen, Huseh et al. 1994) reflect the temporal differences in muscle activation elucidated by early studies (National Clinical Guidlines for Stroke 2ed 2004; Nelson 1974) but failed to generate further diagnostic information. Again the linear envelope, generated using a 15Hz moving average filter, was used to observe the coordination of muscle activity. Ricamato et al. (Ricamato and Hidler 2005) applied a novel amplitude estimation technique (see 2.4.5.1 Linear Envelope & Amplitude Estimation) with MVC and peak ensemble normalised linear envelopes. However, this methodology was used with treadmill walking and has not been applied to sEMG from patients walking freely. Furthermore it did not propose to differentiate different impairments.

2.4.8 Conclusions

Technological advances in the past sixty years since sEMG was first used have not produced equivalent advances in the analysis of sEMG with respect to hemiplegic gait after stroke. Although filtering methods have advanced permitting the use of digital filters in addition to complex amplitude and spectral estimation techniques, quantification of the linear envelope or raw sEMG has not been effectively addressed. As was mentioned earlier, little additional information has been obtained with respect to impaired muscle timing since the earliest studies. Methods to quantify deviations in sEMG relating to motor impairment after stroke do not appear to be adequately addressed in the literature.

Work on sEMG signal analysis appears to have been approached from many directions by researchers from a variety of backgrounds. This has produced many novel methods for signal analysis; however, there is less in the way of a logical progression of methodologies. Although it is clear that creative methods have been published in the literature, in some cases specifically directed at gait analysis, the literature involved with the classification of gait deficits, specifically after stroke, does not reflect these developments. There appears little consistency between methods of generating linear envelopes in even quite recent studies and little justification for the varied implementations; this should be considered in relation to the recent publication of the SENIAM guidelines.

Of particular interest to this thesis are multivariate statistical approaches that have been shown to be effective at differentiating patterns of muscle activation, but have not been extended to be used in the analysis of pathological gait. Cluster, factor and principal component analyses are comparatively simple mathematical techniques which make them advantageous. In particular, principal component analysis also relates to neurological control of multiple muscle groups and therefore may also be able to contribute to the understanding of disrupted control and muscle synergy.

Spectral components in the sEMG during walking has received limited investigation particularly so for stroke patients. Many traditional spectral analysis techniques have not been suitable for the analysis of the non-stationary dynamic sEMG; however, recent advances in time-frequency analysis have presented exciting possibilities in observing the instantaneous changes in both the time and frequency domain. Such analysis has not been completed for stroke patients and may help relate spectral changes in the sEMG during walking to impairment.

3 Methodology

3.1 Equipment

3.1.1 Introduction

Traditional gait analysis laboratories are not always appropriate for clinical assessment of gait (see section 2.3). For this project, alternative equipment was sourced and developed, providing appropriate and clinically relevant measurements, yet low cost. The system combines sEMG, movement and video analysis and provides a modular framework for the development of a clinically viable gait assessment system. As each component was designed to work independently, there were two specifications; a broad requirement that additional modules could integrate synchronously with one another and the specific requirements of the particular module. This chapter sets out the specification for each module and implementation. In addition, as this part of the project intends to provide a framework for future development, criticisms of the current implementation and suggestions for development are given.

The system combines three components. The video component provides the facility to analyse a subject's walking pattern using observational gait analysis techniques. A video record of a subject walking can be very useful in understanding movement data from other sensors. For example, if the subject were to stumble or stop walking for any reason, these may not be immediately evident in raw sensor data. Therefore, the video information can augment and elucidate other sensor data. The sEMG component records simultaneous electro-potentials from multiple lower limb muscles and, within the scope of this study, is used to answer key questions on the phasing and characteristics of lower limb muscle activity. The third component utilises orientation sensors to measure 3D kinematics of the lower limb that can be associated with video, observational techniques and sEMG data to compare different movement strategies with the underlying pattern of muscle activity. Body worn sensors such as these are potentially a low-cost means of acquiring lower limb kinematics and therefore an alternative to using marker-based systems.

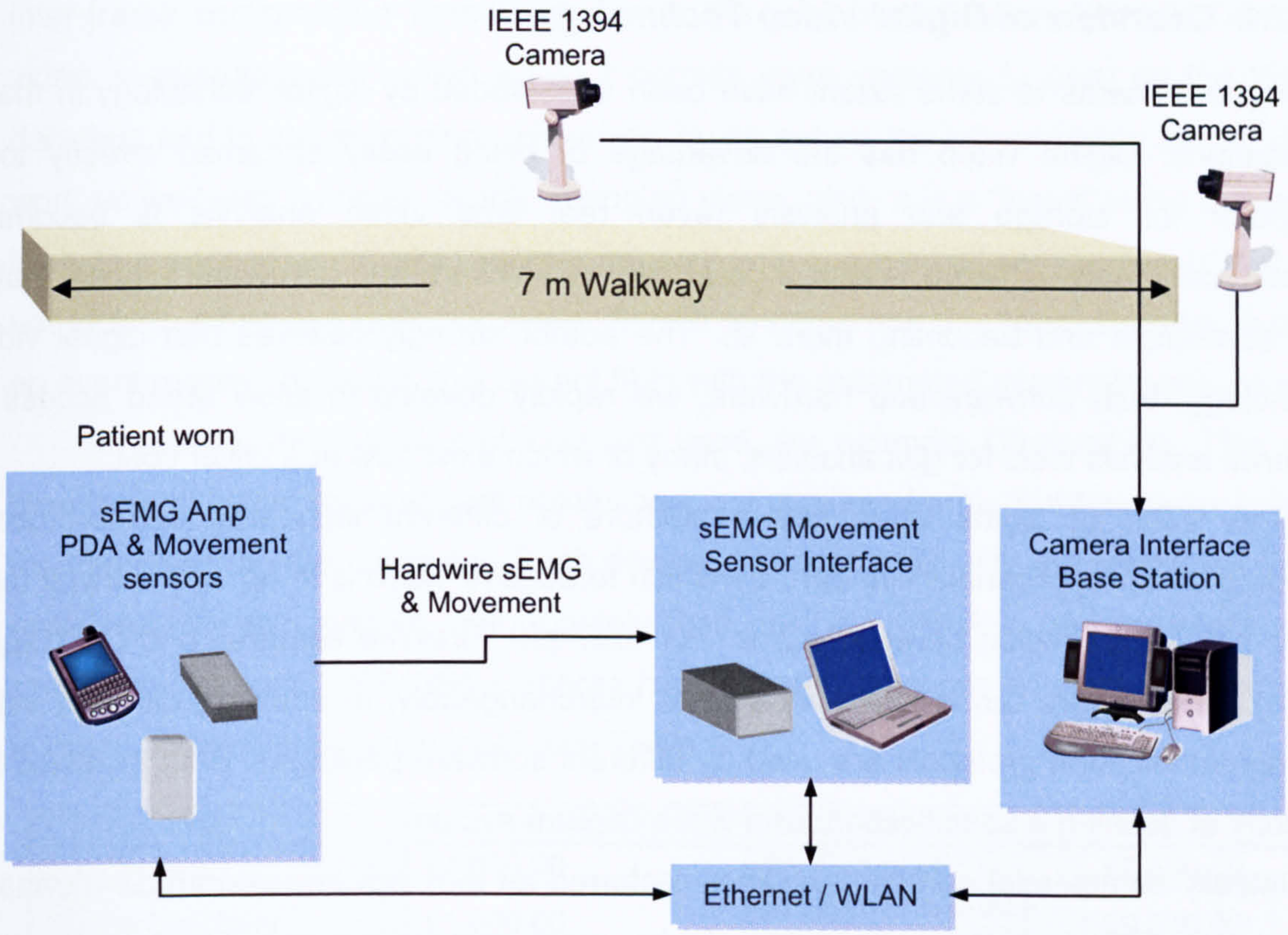

Figure 12 the gait analysis system developed during this project. The system contains bi-lateral video, wired or wireless sEMG sensors using a PDA device and movement measurements using body worn orientation sensors. The sEMG and motion sensors are interfaced via a LAN to a laptop and both laptop and cameras are controlled by a base station unit.

3.1.2 Video system

3.1.2.1 Specification

The camera system was to have two cameras capturing simultaneous video for the coronal and sagittal views of a subject walking that could be analysed. The video data needed to be synchronised with the motion and EMG measurements and support the modular framework consistent with the specification of the elements within the wider system. The video format was required to be portable such that video could be transferred and easily analysed on other computers. The system had to be implemented economically, that is, such camera systems already exist although their cost is generally prohibitive. Motion analysis systems found in gait laboratories require high frame rates (1000 frames per second and greater) and high resolutions (typically above 1024 x 768) to ensure that marker positions can be well defined. However, such high specifications are not required for visual gait analysis, the frame rate will only be required to be between 25 and 30 FPS consistent with those systems reported in literature (Kirtley 2005). A schematic of the system developed is shown in Figure 12 above.

3.1.2.2 Overview of Digital Video Technology

Analogue cameras to some extent have been superseded by digital technology in many applications. Digital video has the advantage of being easily streamed directly to a computer for storage and analysis (even real time video analysis is becoming economically viable). There is also a great deal of software and hardware support that is now accessible and becoming more so. The author strongly believes that digital video technology, both software and hardware, will rapidly develop to allow broad access to powerful analysis tools for gait analysis, many of which exist now at a lower cost.

The world of digital video has a plethora of different standards and protocols. Deciding on an appropriate standard by which to acquire video is in no way a trivial task. There can be confusion between terms. For example, FireWire cameras and DV (Digital Video) cameras are terms sometimes used interchangeably; in addition, different video and communication protocols are used by different software packages. Both increase the difficulty of defining a specification for a video capture system.

Initially commercial camcorders were preferred as they are an economical means of producing relatively high quality video. Today most camcorders can stream video to a computer via a FireWire (Apple) or i.Link (Sony) card using the DV protocol. IEEE 1394 is a communications protocol designed for high-speed communications (developed by Apple in the 1980's) over short distances. The standard provides a communication mode with a fixed bandwidth channel for the transmission of live video. In the UK, the DV standard is DV-PAL, a standard that captures 25 frames per second with a resolution of 768×576 and 4:2:0 YUV (see description below) encoding. The method of image encoding impacts on the technology used to retrieve ultimately the image. There are two types of output from a digital camera, compressed and uncompressed. Uncompressed video comes in four forms; raw, RGB, YUV and monochrome, terms described below. A raw camera output is purely the output from the CCD (Charge Coupled Device) in the camera; it would appear as a meaningless image unless further processed and converted to another format. RGB represents an image by encoding each pixel by a combination of Red Green and Blue; this is a 32-bit image, 8-bits encoding each of the colours and the final 8-bits that are not always implemented. RGB is undesirable because of the size of the image file; YUV can achieve equivalent quality but more economically. YUV results from the human eye being more sensitive to variations in luma or brightness (Y) and chroma or differences in colour (U & V). Thus, an image is encoded to represent it in these terms. The luma of the image corresponds exactly to the monochrome image whereas the chroma represents the colour information. There are several types of YUV, each characterised by how many bits are used to encode Y, U and V; these vary in quality from 4:4:4 to 4:2:0. Importantly, DV is an

inter-frame compression format (similar to the jpeg compression format). Compressed video is advantageous in two ways; it permits more cameras to exist on the IEEE1394 data bus and is easier to store. However, by its nature the compression format does not work as well with complex rapidly changing video, also, it is a "lossy" video format that is likely to reduce video quality. Another concern with commercial camcorders is that they do not include external trigger hardware. Similar systems use the audio channel to generate an event marker; however, this did not fit in with the automated system for this project.

In industry, alternative protocols are used, for example CameraLink. This protocol permits high frame rates at high resolutions, but requires frame grabber cards to interface the cameras with the computer. Such devices fit in very well with the control methodology envisioned for this system, unfortunately their cost is prohibitive and therefore were not considered further. IEEE1394 cameras have recently become an economical alternative to many conventional vision tools (see Table 4.)

Camera Link		IEEE 1394	
2 x Cameras	£4,000.00	2 x Cameras	£2,500.00
Frame Grabbers	£1,600.00	IEEE1394 interface card	£0,030.00
Cabling	£0,200.00	Cables	£0,090.00
Software	£2,000.00	Software	£2,600.00
Power supply	£0,160.00	Repeaters	£0,100.00
Total	£7,960.00	Total	£5,290.00

Table 4 the cost comparison of a Camera Link camera system to D-Cam camera system

The frame rates of IEEE1394 cameras are usually slower camera link cameras and the cost of implementation is much lower. IEEE1394 cameras differ from DV camcorders because their outputs are not compressed (D-Cam specification, which interfaces different cameras to the DV standard) and use either raw or YUV video formats. Although the frame rates of IEEE1394 are faster than DV cameras, they are also more expensive and tend not to have lenses attached due to the breadth of applications to which they might be applied. Because they are intended for industrial use, they usually have external trigger capabilities.

3.1.2.3 Hardware Implementation

Two IEEE1394 cameras (Sony DFW-VL500) were used to implement the system. The DFW-V500 is capable of acquiring 30 fps at VGA resolution (640 x 480). A higher resolution would always be desirable – the higher the resolution the easier it is to identify anatomical detail- but VGA resolution is the same the DV-PAL standard and therefore the same as most low cost cameras commonly used for visual gait analysis (Kirtley 2005). Although colour images can be acquired at up to 4:4:4 YUV, monochrome images were

used to achieve the best resolution. The camera benefited from an integral 12X zoom lens similar to that found in camcorders and appropriate for field of view in this application.

Figure 13 the Sony DFW-VL500 camera

Two PCI FireWire cards connected the two cameras to the base station computer. The software written to control video capture and commercial software was able to measure the time for the acquisition of each frame of video. From this it was possible evaluate the frame rate of the system. This information indicated that frames were being "dropped" – if a new frame is requested before the first has been processed from the video buffer this frame of video is lost. In addition, comparing coronal and sagittal frames indicated the cameras were unsynchronised by at least one frame. It was recognised that one reason for this was that a single FireWire bus was used to transmit data from both cameras. With a single data bus, its bandwidth must be split between the data stream from both cameras. The video format used was uncompressed video and required the largest possible bandwidth of IEEE1394 protocol. To help resolve this problem a second FireWire bus was added.

Because of the distributed nature of this application, long data cables were required. Although FireWire should not operate effectively over cable lengths more than four metres, it was found that two six-metre cables connected by a 9 volt UniBrain FireWire line driver effectively transmitted the camera data.

The base station computer consisted of a 2.6GHz Pentium processor with 2GB of SDRAM and a 180GB internal serial ATI hard disk with a 120GB parallel ATI removable hard disk. Video data was recorded to the internal hard disk but then transferred to the removable hard disk. This could be stored in a secure location for data protection purposes.

An additional multifunction National Instruments (NI) 6024E data acquisition PCI card was also fitted to the base station in order to use the external trigger capabilities of the cameras and to provide a synchronisation and control architecture for future applications.

3.1.2.4 Software Implementation

LabVIEW was used as the environment to implement the control and user interface for the whole system. This development software was used because it provided a rapid prototyping and implementation environment. The software could have been implemented in a lower level language such as C++; LabVIEW has a C++ core, however, using a lower level language would have required a longer period for prototyping and implementation. In addition, there was a more transparent integration between user interface, signal processing and data acquisition with a high-level language. The structure of LabVIEW is implicitly hierarchical which therefore supported the modular design outlined in the introduction to this chapter. In addition to the LabVIEW full development software, the NI IMAQ IEEE1394 camera driver was required to connect the windows kernel to the LabVIEW architecture. The LabVIEW driver provides additional virtual instruments with which to control the IEEE1394 cameras. One of the benefits of the IEEE1394 standard is the control it provides over the cameras. In order to generate usable video, parameters such as iris aperture, gain and brightness must be configured correctly. In variable light conditions, a flexible means of controlling these parameters is advantageous. Such light conditions were present in the clinic space available during this project. In general, very few institutions are likely to have rooms that are, or could be, specifically designed to provide consistently appropriate lighting for professional quality video. For this project, blue curtains were used to insulate part of the room from external light sources, unfortunately additional external sources from doors and side rooms could not be controlled. In addition, by reducing the external light sources the overhead lighting then became insufficient and required higher gain values for the digital video. One final lighting problem was the frequency of the overhead fluorescent lights. It was necessary to set the shutter of the camera speed to 10ms to compromise on removing the strobe effect from the overhead lights and retain shutter speed that did not produce blurring of the video image during the fastest movements. The drawback to a faster shutter speed is that a greater light intensity is required to generate the same quality of video image as for a slower shutter speed; therefore, this exacerbated the lighting problem previously mentioned.

There was no provision included within LabVIEW or the NI IMAQ IEEE1394 driver to generate a video container and save video. Three methods have been implemented to

overcome this, block diagrams and front panel illustrations can be found in Appendix C.I. One option was to use an alternative software environment to capture AVI video; however, this is not desirable as it failed to integrate the video system completely with the other system modules. Alternatively, third party demonstration code was implemented to generate AVI video. However, the first approach was to snap individual images from the IEEE1394 bus and convert each acquired frame to a jpeg or bitmap image. Video could be played back by iterating through these images, much like a flick book. This approach generated smooth pseudo video at an average 23 FPS, which can be converted to AVI video through third party software. The frame rate was calculated by timing one iteration of the while-loop that acquires an image; a special version of the acquisition software was created specifically to measure the frame rate. Although this frame rate is above the requirements for perceptively smooth video, and is therefore acceptable, it is below the specification for the system and the capabilities of the cameras.

An alternative software package and software driver, Fire-i, was used to capture multiple AVI's at the full frame rate of the cameras. At that time, it was the only commercially available software discovered that could record from multiple Firewire cameras simultaneously. A user guide developed by the author for the use of this system by clinicians is included in the appendix. This is commercial software from UniBrain and although generated the best results was not controlled by the LabVIEW system implementation and thus was not fully integrated into the wider system. Therefore video capture was not truly synchronised, specifically, the video was only synchronised with respect to time. This in itself was not a criticism as the video could still be synchronised with the wider system to within one frame acquisition time (1/30 of a second). However, the desired system would not require such manual synchronisation.

The third method used demonstration virtual instruments (IVision7.2) that create AVI from a stream of images. These virtual instruments do not require the IEEE1394 IMAQ driver and they instead use Microsoft DirectShow that interfaces equipment that conforms to the Windows Driver Model. This would include compressed video formats from DV camcorders. The collection of virtual instruments also included basic image analysis and object tracking. Although this implementation was not used because its robustness could not be demonstrated, however it demonstrated a flexible method of acquiring video in addition to a method of implementing basic image analysis for calculating kinematics.

Both the first and second method were used in this project to collect data form patients, However, the final video used for visual gait analysis was captured using method two, the fire-i software.

The camera software was the hub of the wider system; data acquisition from all modules was initiated through the communication of the base station to the other components. Data acquisition was initiated by pressing the record button and ended by pressing the stop button. The user had to update the session identifier before continuing. The progress of the acquisition was displayed to the user through LED's on the front panel.

3.1.2.5 Criticisms & Future Development

There is a significant amount of development possible within the camera system, and several routes that could be taken. The current implementation fails to fulfil the maximum capabilities of the cameras. It is entirely possible to achieve the specification for the system through additional software modules of which there are several commercially available. These additional modules however only implement generically functions that are available through Microsoft DirectShow and so specific solutions could be developed for this system.

Video synchronisation through the LAN is acceptable; however, it would be preferable to trigger the camera acquisition to ensure that both cameras do expose an image simultaneously. Triggering can easily be achieved using the trigger input of the DFW-VL500 and the output lines of the multifunction DAQ installed in the base station.

The base station itself could be upgraded to improve the robustness of the system. At present only short periods of video can be captured at any one time. Although this is acceptable within the procedure for data acquisition in this project, the system is susceptible if video longer than approximately 30-40 seconds is acquired. This vulnerability currently makes the system difficult to use for clinicians. By increasing the level of SDRAM (4GB is suggested) and using two internal hard disks in a RAID configuration this problem could be significantly reduced.

The Firewire standard is currently changing to a faster bandwidth (800 Mbs^{-1} from $400Mbs^{-1}$), although this would require an upgrade in the cameras, it would open the possibility of utilising higher resolution video or adding more cameras. This suggestion relates to the users requirements.

3.1.3 Motion Sensors

3.1.3.1 Specification & Justification

The system requirement is to capture kinematic information regarding the lower limb using body worn sensors. Although there are a variety of sensors that are able to measure components of motion such as acceleration and rate of change of rotation, literature does not support a standardised means of generating kinematic data during pathological walking. Therefore, it was more appropriate to use a device that was able to integrate the movement components in order to measure absolute limb segment angles. Such a device exists in the form of the Xsens MT9 orientation sensor. Limb segment angles have been used as an alternative to joint angle measurements and related to human gait control in some literature (Ivanenko, Grasso et al. 2003). For this reason, and to simplify the implementation of the system, limb segment elevation angles have been adopted in this project. Orientation sensors are able to provide pitch data of the limb segment. The use of limb segment elevation angles does not preclude the calculation of joint angles.

3.1.3.2 Introduction to the Xsens MT9 and XBus Master

The MT9 is a 3-dimentional orientation sensor that consists of accelerometer, gyroscope and magneto-resistive sensors; the information from which is combined to generate orientation information in three dimensions. Additionally each of the three raw kinematic variables can be accessed individually.

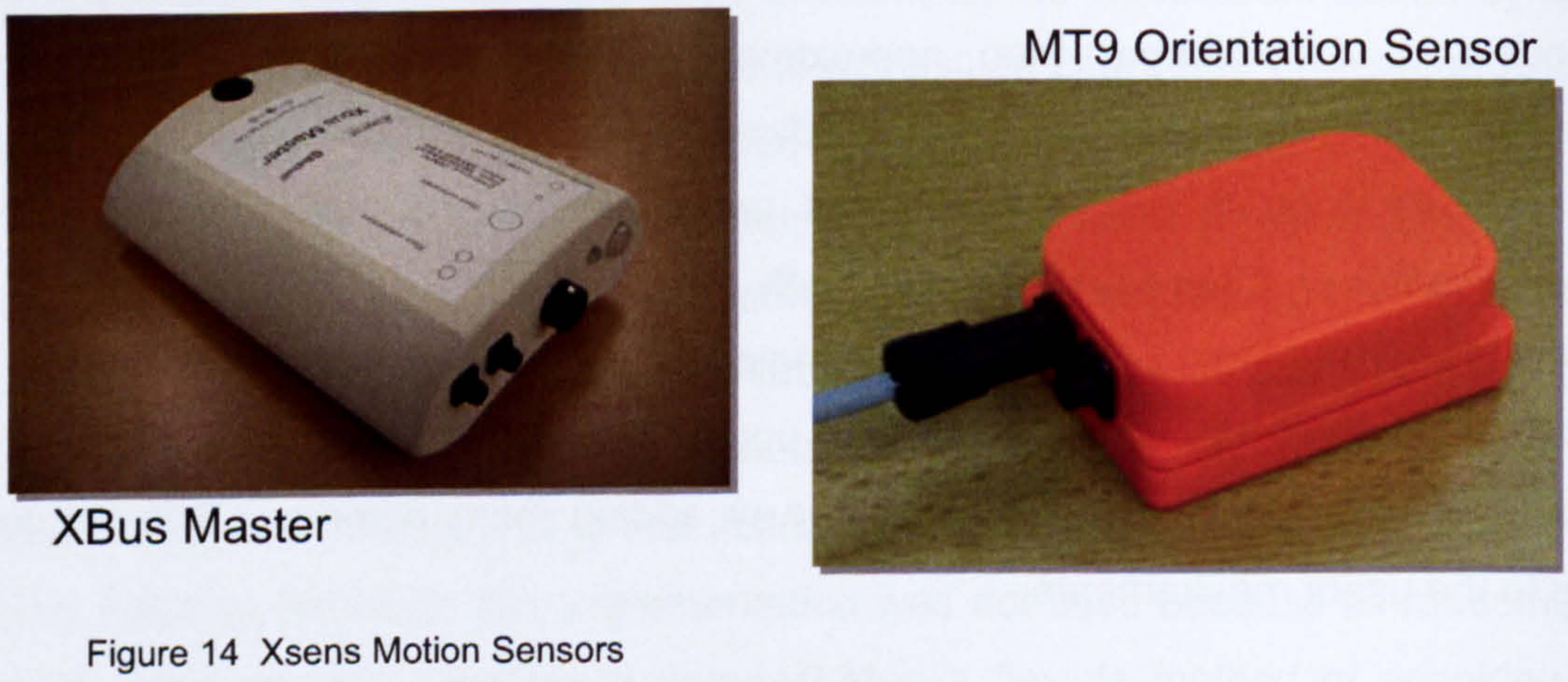

Figure 14 Xsens Motion Sensors

The MT9 sensor interfaces with a belt worn unit that integrates the information from each of the three orientation sensors and interfaces the controlling computer through a serial cable or through a Bluetooth connection. The orientation of the sensor is calculated by the difference of the sensor coordinates to a global coordinate system.

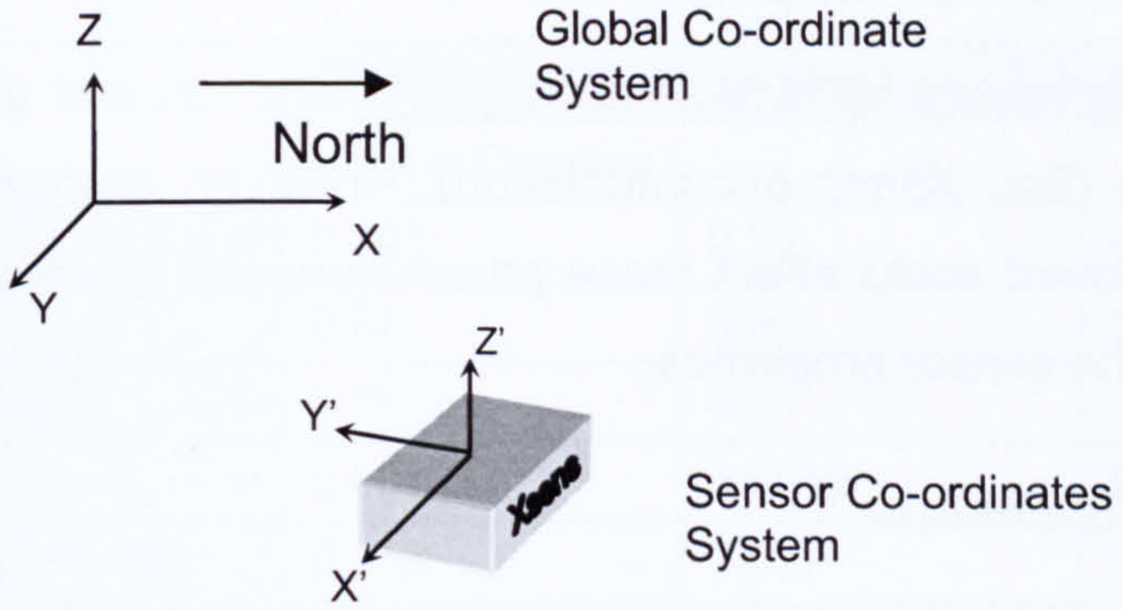

Figure 15 Global and sensor reference system

It is possible to re-define the orientation of the global coordinate system by orienting the sensors to the new coordinate system and performing a "reset", a function provided in the software accompanying the sensors. For example, the sensor can be reset to reflect the surface on which it is placed. This aligns the sensor co-ordinate system with the surface. No reset was used during walking tests, except for global reset for calibration, as it would assume a common starting angle, for those with pathologies this would not be a reasonable assumption. Therefore, all measurements were made in relation to the global coordinate system to the sensor axis. The sensor axis is not aligned with the surface.

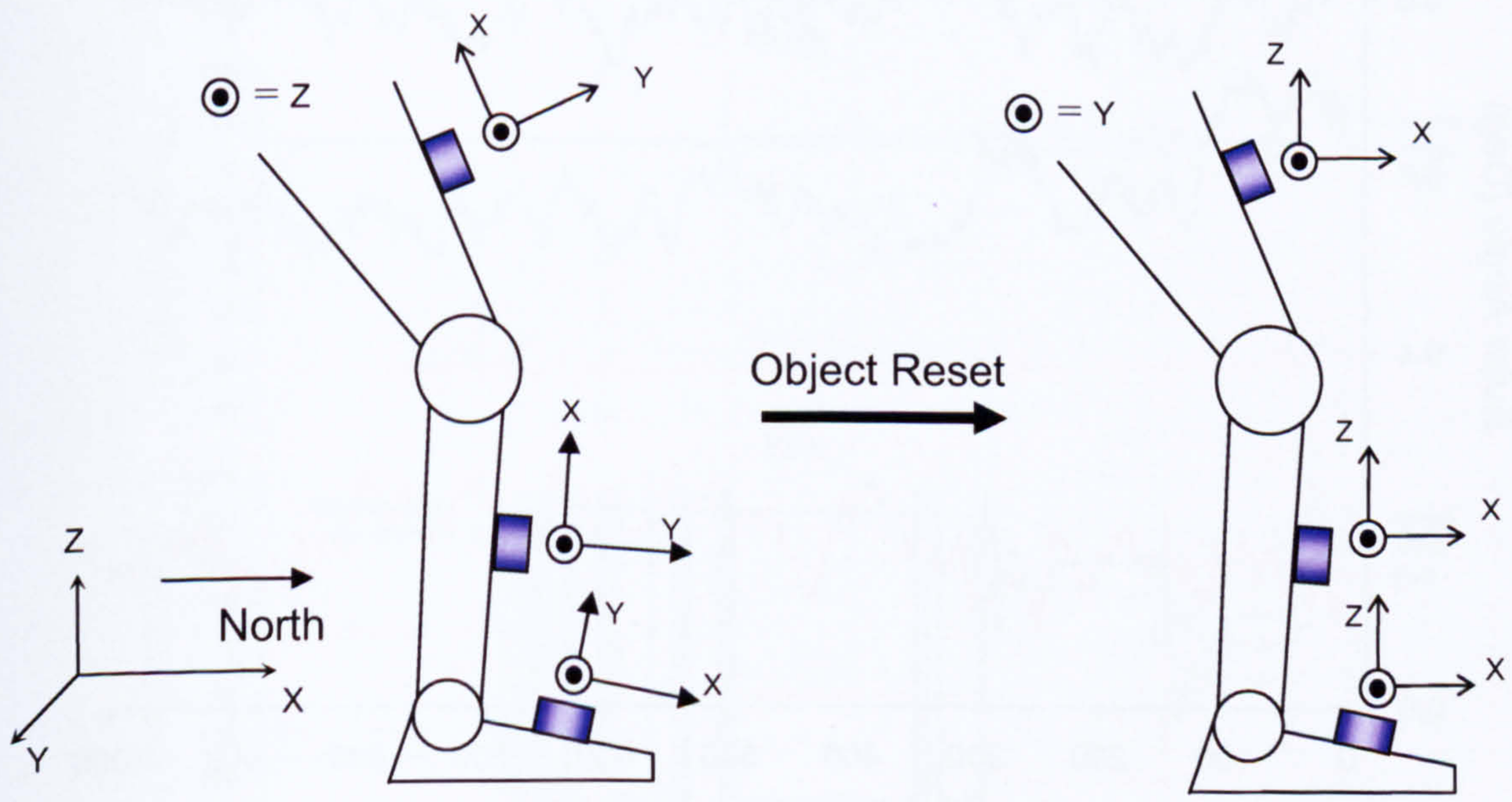

Figure 16 Example of object reset

3.1.3.3 Confirmation of sensor properties

The MT9 is reported to have a dynamic accuracy of 3 degrees and a static accuracy of less than one degree (See Xsens documentation). However, environmental conditions and the type of movement could affect these parameters and therefore an assessment was made to confirm the sensor properties.

3.1.3.4 Static Measurements

Sensor agreement for static measurements was assessed by attaching the sensors to a horizontally and vertically aligned surface. Finally, directional influences on joint angle calculations were measured. Horizontal and vertical measurements were taken from the sensor over a 40-second period that permitted an assessment of stability of the sensor over the estimated period of a single walk within a walking assessment these results are shown in Figure 17 and Table 5. Cumulative results over 10 static tests are shown in Table 6 - Table 9.

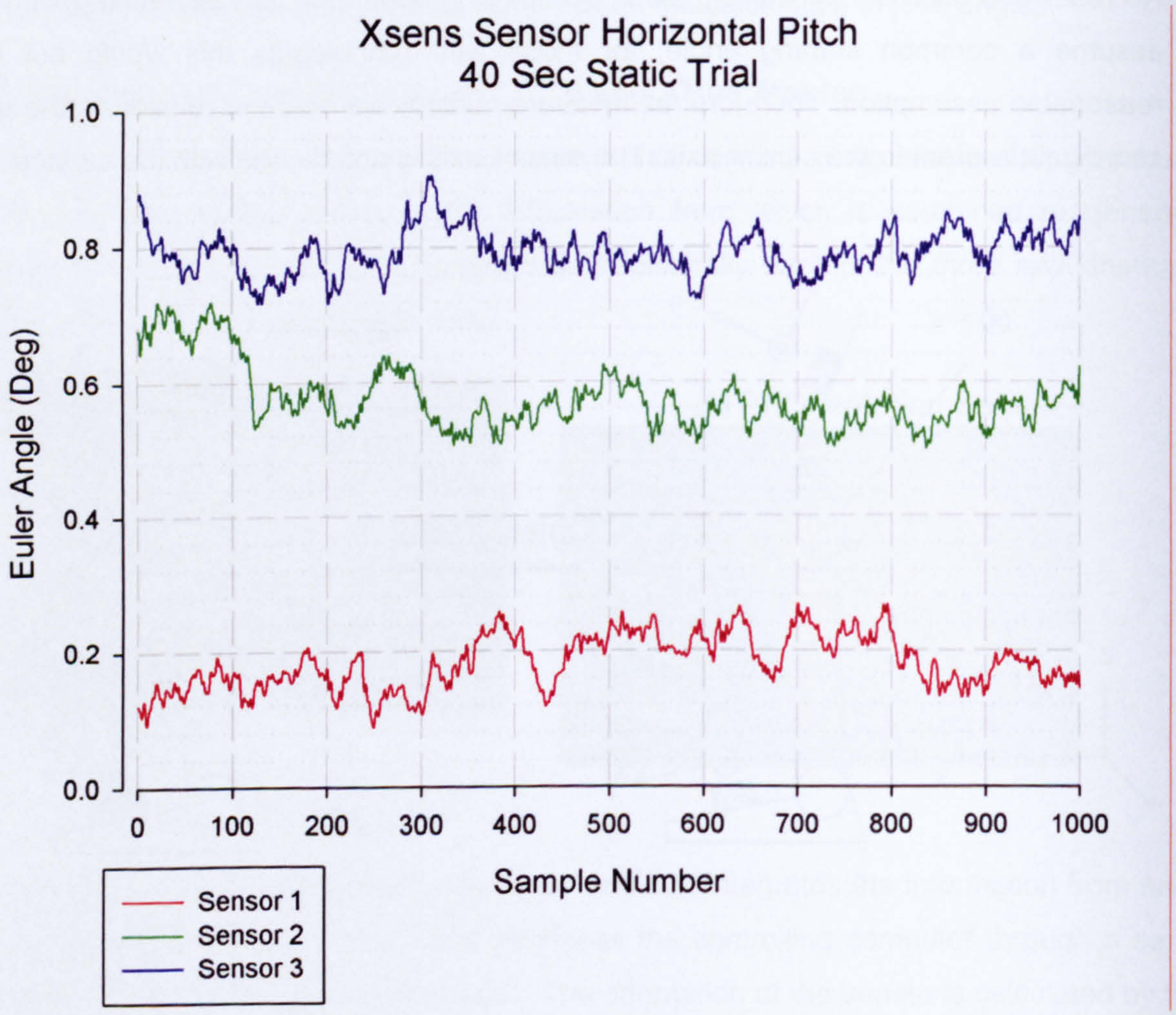

Figure 17 Sensor stability, 40 second segment (Pitch)

	Sensor 1	Sensor 2	Sensor 3
	Units in Degrees		
Min:	0.091	0.72	0.5
Max:	0.27	0.90	0.72
Mean:	0.18	0.79	0.57
Variance	0.0015	0.0010	0.0024
Standard Dev	0.038	0.032	0.049

Table 5 results from static horizontal long-term stability sensor tests

Static measurements were also made whilst the sensors were attached to the thigh, shank and foot. The effect of direction to the orientation measurements was assessed by having the subject turn to face four directions. The sensor readings are shown in Figure 12 and Figure 19.

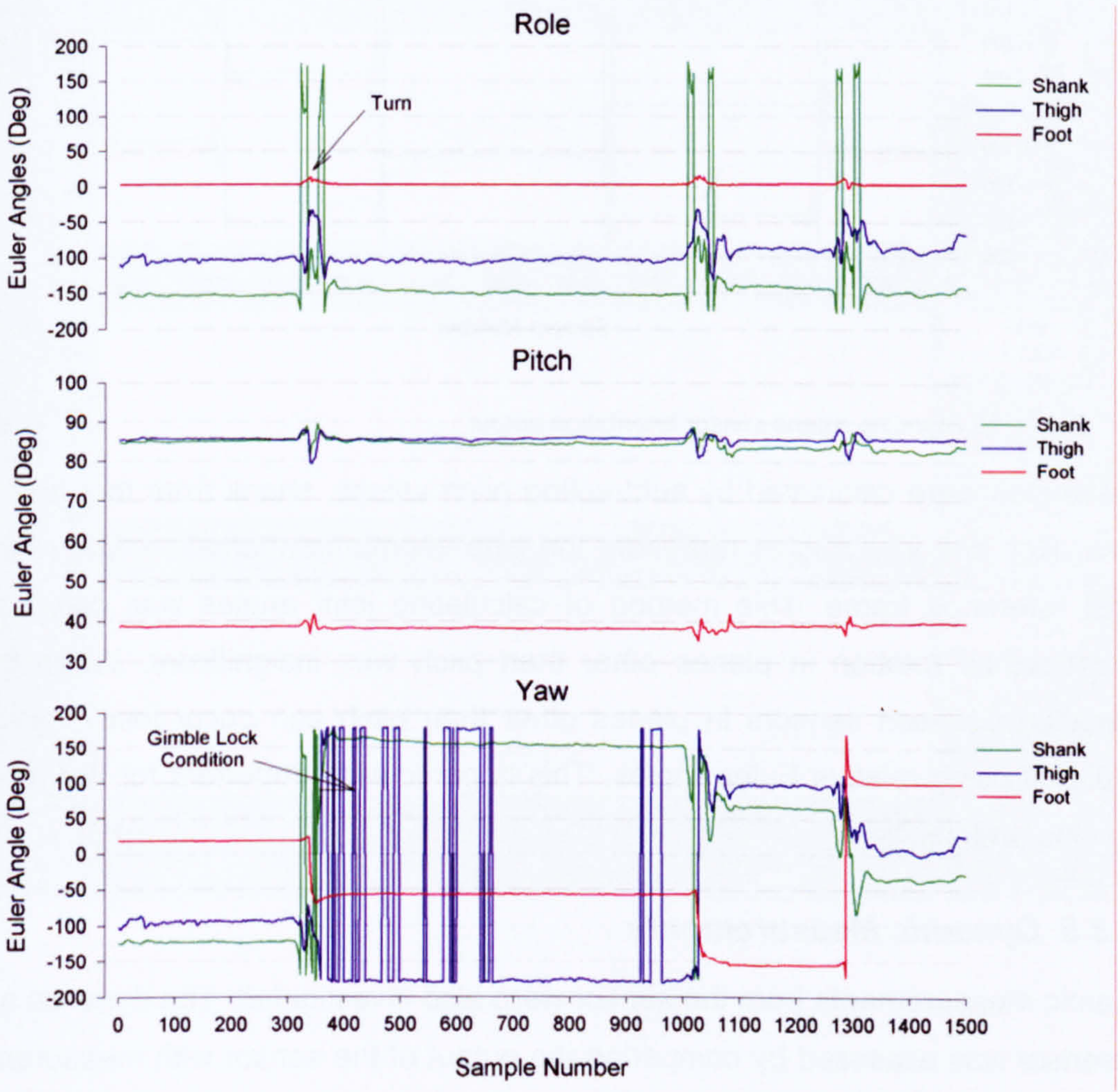

Figure 18 Standing joint angle Xsens sensor output.

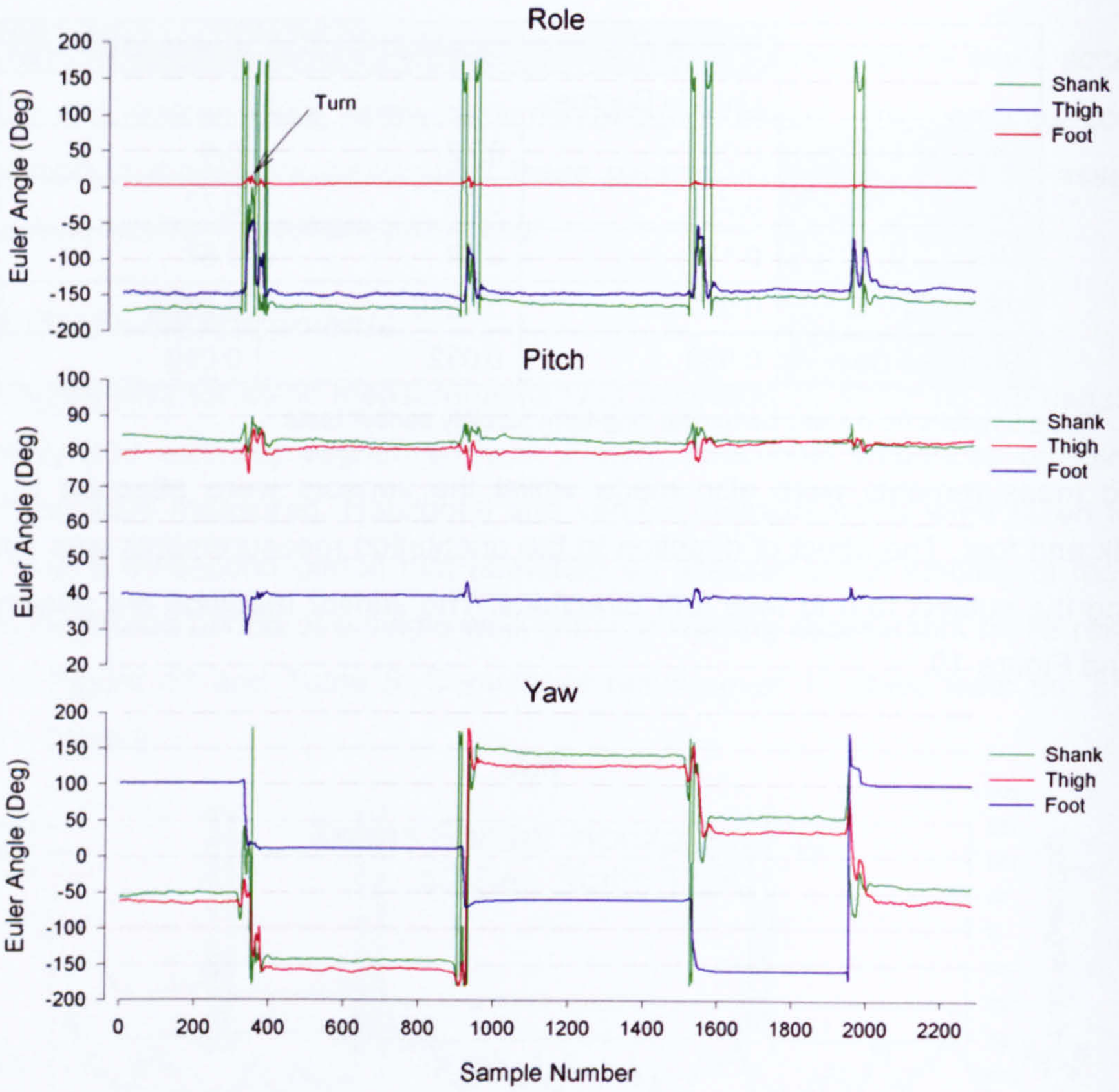

Figure 19 Standing Xsens sensor orientation output

Joint angles were calculated by subtracting pitch values, shank from foot and thigh from shank. Roll and yaw angles represent the limb segments orientation with respect to the global reference frame. This method of calculating joint angles was only used in this evaluation, as rotation in planes other than pitch was insignificant. When the relative orientation between sensors in planes other than pitch can occur joint angles must be calculated using relative Euler angles. This is particularly important for the articulation of the ankle and pelvis.

3.1.3.5 Dynamic Measurements

Dynamic measurements from the sensor were also investigated. The dynamic accuracy of the sensor was assessed by comparing the output of the sensor with measurements from an optical movement analysis system (CODA motion system, Charnwood dynamics) during postural movements. To understand the sensor output with respect to walking, pilot assessments were made in combination with footswitch data to associate kinematical data

from the MT9 sensors to gait events. As with the static assessment, the sensors were aligned using a global reset provided in the Xsens software package.

The MT9 sensors were compared to the CODA motion system by attaching three IR LED markers to the corners of the MT9 sensor. These three markers defined two vectors of the orientation sensor; by performing a cross product between these vectors, the third vector can be calculated. Therefore, the three markers generated a rigid body simulating the orientation sensor and from which Euler angles could be calculated. The results from postural movements display significant variability in Euler angles representing the yaw of the sensor although this may be due in part to optical marker occlusion. However, variation of this nature can be seen in the Euler angles roll and pitch which do not suffer the apparent offset seen with yaw in Figure 20. The agreement between the two systems are shown in Table 10.

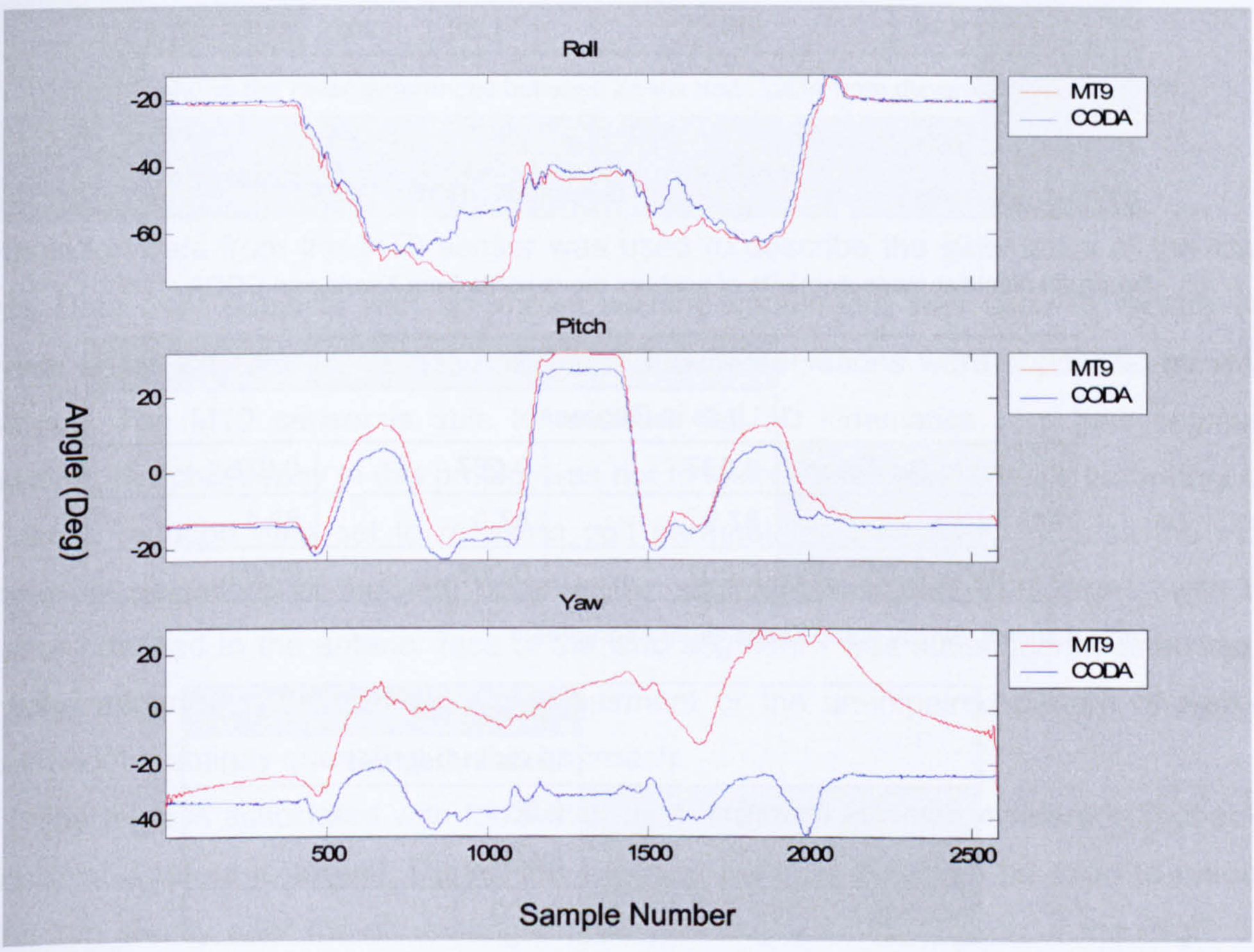

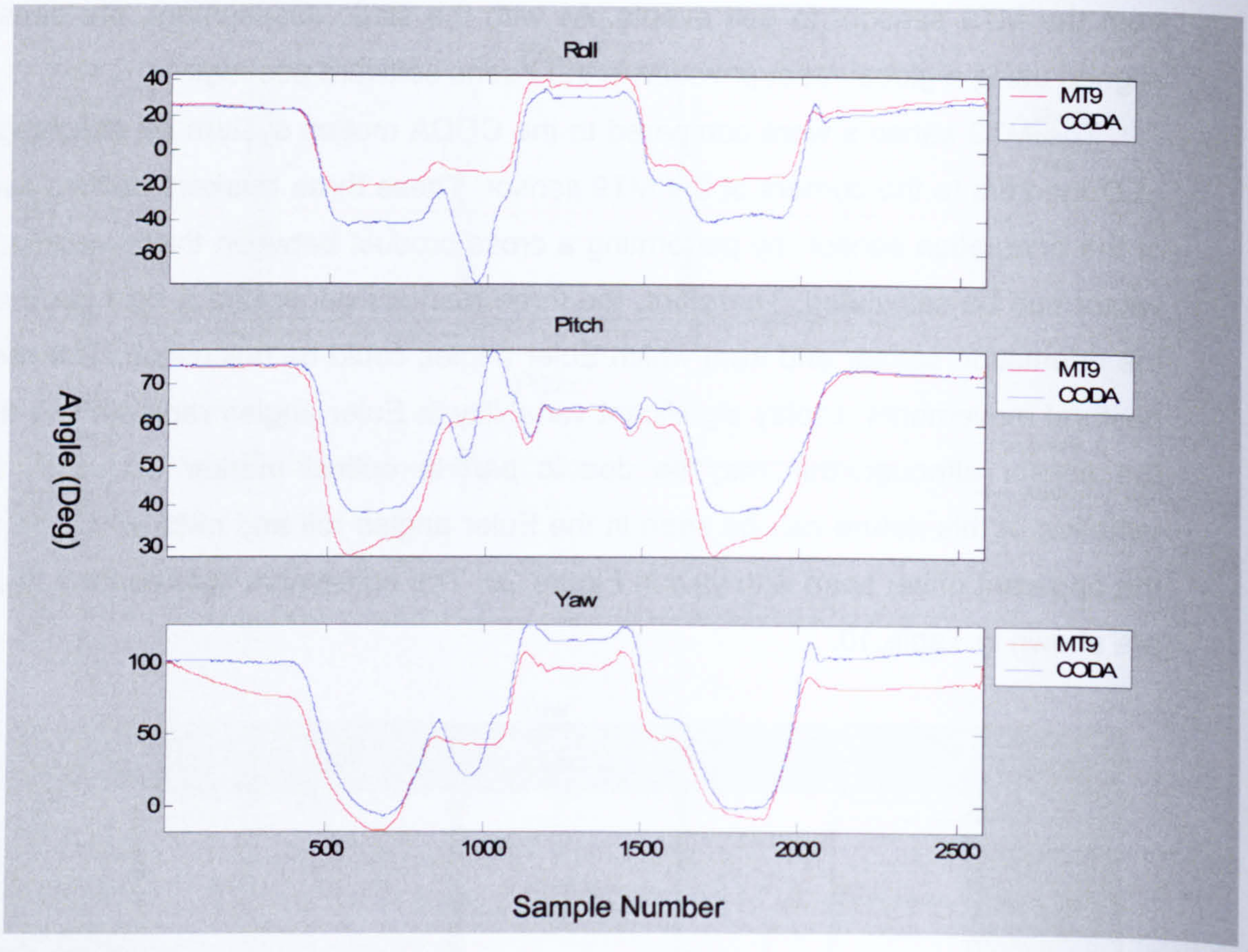

Figure 20 displays measurements of postural movements from Xsens and CODA.

	Sensor 1	Sensor 2	Sensor 3
	Units in Degrees		
Standard Deviation	0.037	0.087	0.038
Mean	87.9	87.9	88.1
Variance	0.001	0.008	0.001

Table 6 shows vertical static Xsens sensor agreement

	All Sensors
	Units in Degrees
Standard Deviation	0.09
Mean	88.0
Variance	0.009

Table 7 displays vertical static Xsens sensor agreement results for all sensors

	Sensor 1	Sensor 2	Sensor 3
	Units in Degrees		
Standard Deviation	0.04	0.03	0.05
Mean	0.18	0.8	0.57
Variance	0.001	0.001	0.002

Table 8 shows horizontal static Xsens sensor agreement

	All Sensors
	Units in Degrees
Standard Deviation	0.26
Mean	0.52
Variance	0.066

Table 9 displays horizontal static Xsens sensor agreement results for all sensors

		MT9 Mean	CODA Mean	Diff
		Units in Degrees		
Sensor 1	Roll	42.26	38.81	3.45
	Pitch	3.27	6.58	3.31
	Yaw	1.14	31.18	30.04
Sensor 2	Roll	9.96	1.82	8.14
	Pitch	57.91	61.45	3.54
	Yaw	58.17	72.99	14.8

Table 10shows the mean differences between Xsens and CODA from dynamic movement trial

3.1.3.5.1 Description of orientation data from walking

Orientation data from the MT9 sensor was used to describe the kinematics of the lower limb. Data from subjects with no known walking impairment was used to identify key events in the unimpaired walking patterns. These observations were supported by video analysis. The MT9 sensor is able to measure full 3D kinematics of a limb segment, however, the philosophy in this project was not to imitate a full gait analysis laboratory but to use a reduced data set to measure gait parameters. Therefore, because the most prominent deviations of the limb occur in the sagittal plane only, limb pitch – with the sensor attached to the anterior face of the limb segment - was subsequently analysed. It is fully recognised that subtleties of impairment or the un-impaired pattern of walking would not be entirely quantified by this approach.

The thigh is associated with footswitch data in Figure 21 Point 4 refers to foot-strike and point 3 refers to toe-off. During the swing phase, the thigh can be seen to reach a minimum shortly after toe-off relating to the maximum anterior rotation of the thigh. The thigh then rapidly flexes passing the midline at the maximum value of elevation angle. Prior to foot-strike the segmental angle reduces relating to forward flexion reaching a minimum at foot-strike. The thigh returns to vertical during stance and gradually reduces in elevation angles as it rotates posteriorly.

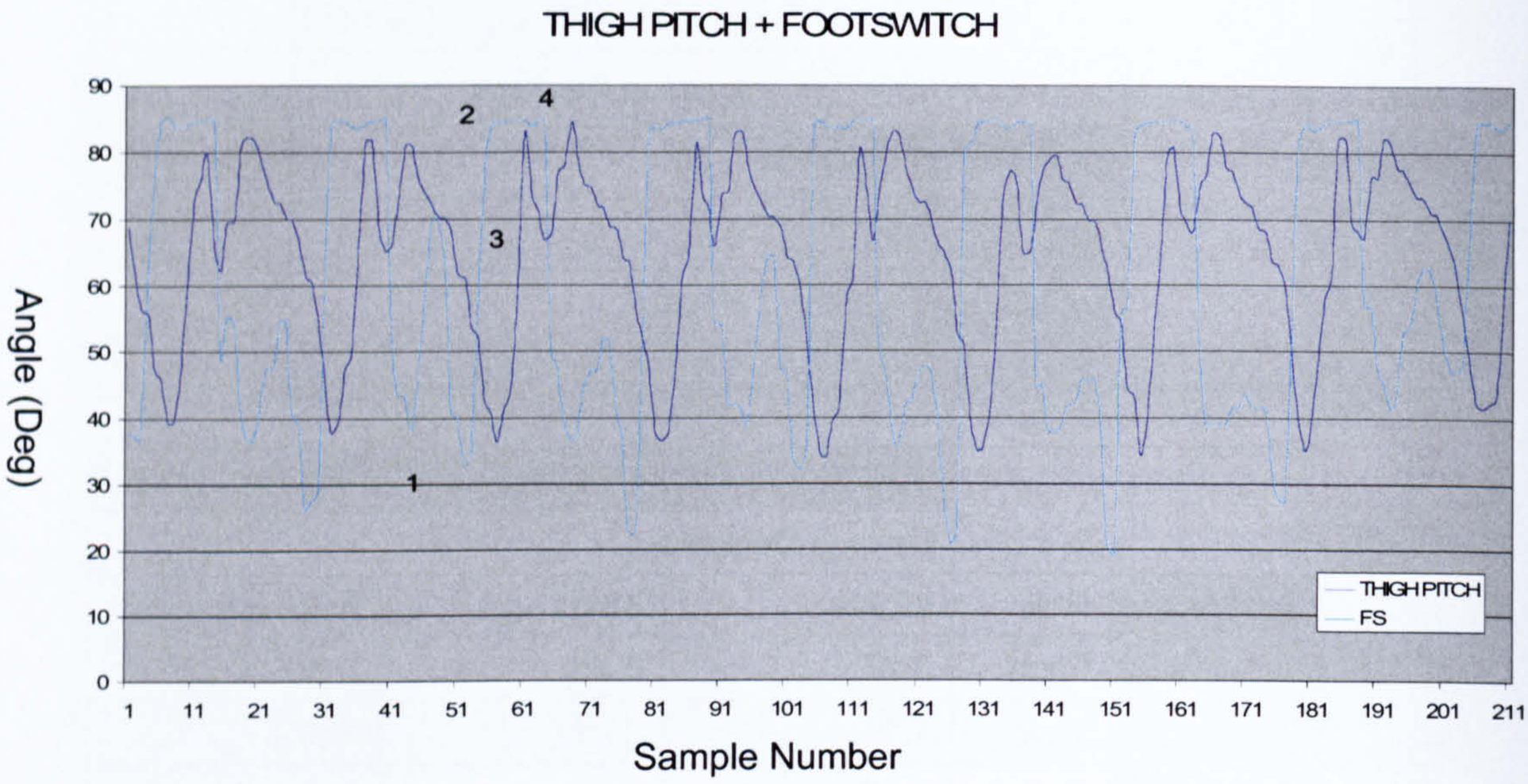

Figure 21 Thigh sensor pitch angle compared to footswitch signal. Un-impaired subject

The foot is related to the thigh segmental angle in Figure 22. It should be remembered that the foot sensor is not attached horizontally on the foot; therefore, the sensor naturally sits at an angle. During the stance phase, the foot rapidly plantar flexes to foot flat where the segmental angle remains constant for a short while. Prior to toe-off the foot plantar flexes rapidly to a maximum value of segmental angle relating to the sensor becoming more vertical. A mixture of dorsiflexion and forward rotation of the tibia create a net reduction in elevation angle prior to a significant reduction as the foot swings through during the swing phase, at foot strike the sensor is almost horizontal.

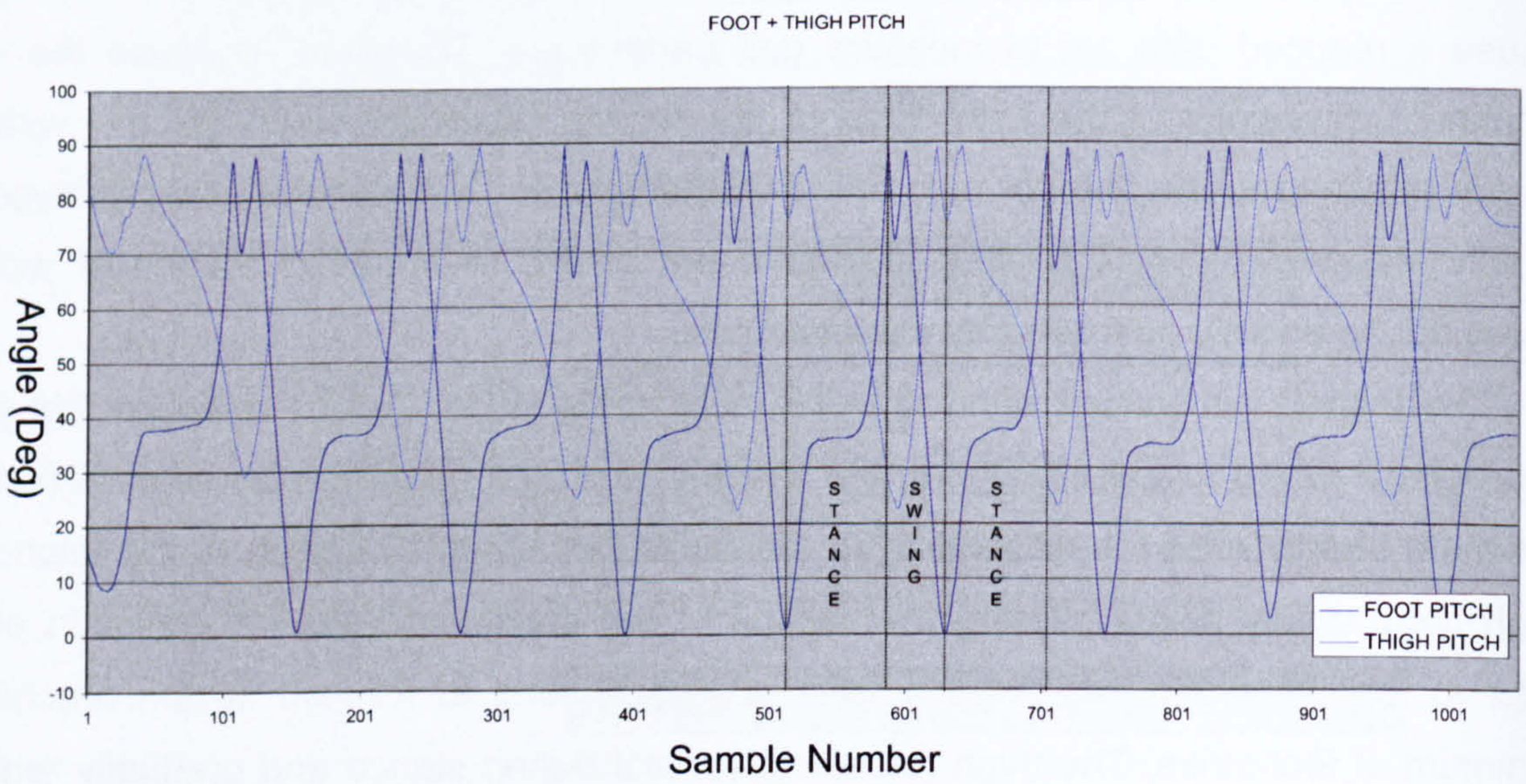

Figure 22 shows the foot sensor pitch angle in comparison to the thigh sensor pitch angle. The data is from an un-impaired subject.

Figure 23 displays the pattern of shank elevation angle related to the thigh sensor data. Due to the articulation of the shank, the pattern of elevation angle is the most complex. At foot-strike, loading response causes a small perturbation in the shank pattern. Subsequently the shank rotates backwards and the sensor becomes increasingly vertical passing through mid-stance. Past mid-stance, the shank continues posteriorly reaching a minimum just prior to toe-off. The shank does not reach a minimum elevation angle at toe-off due to the roller action at the foot that begins the anterior rotation of the shank before toe-off. After the toe-off, the forward rotation of the thigh rapidly increases the elevation angle, as the sensor becomes increasingly vertical, passing the midline and subsequently reducing. Just prior to foot-strike, a small increase in elevation angle relates to preparation for initial contact and posterior rotation of the thigh.

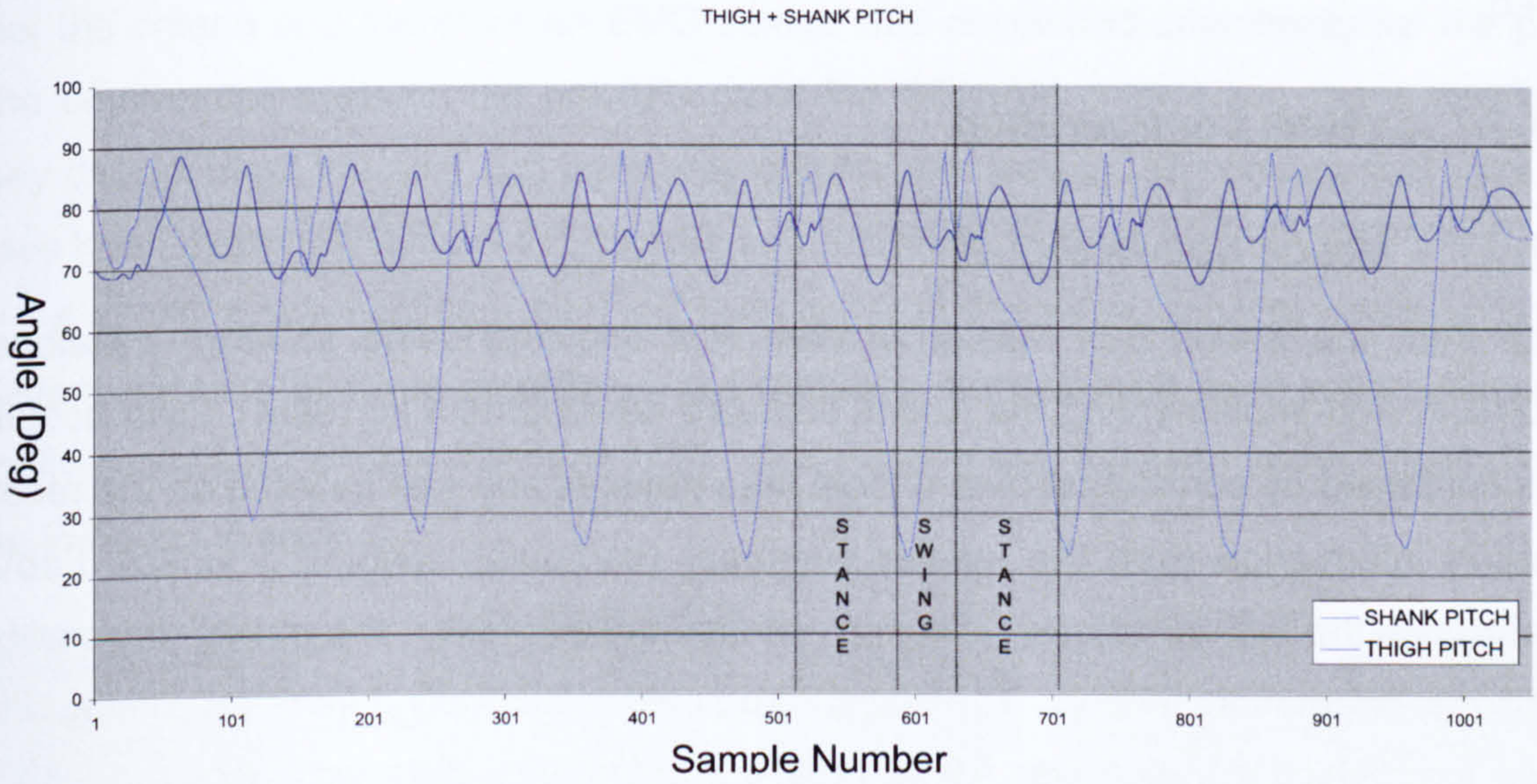

Figure 23 Shank sensor pitch angle compared to thigh sensor pitch angle. Un-impaired subject

3.1.3.6 Conclusions from Confirmation of sensor properties

Static assessments made on the vertical and horizontal surfaces demonstrated that the sensors were consistent and accurate. There was some drift in the values; however, this was less 0.01 degrees over 30 seconds for all three sensors. The inter-sensor variance for the orientation values was less than 0.01 degrees suggesting a consistent measurement can be made between sensors as long as they are calibrated together. Static accuracy was within 2 degrees of the vertical and within less than one degree of the horizontal.

The assessment of effect of direction on the output of the orientation sensors demonstrated that joint angle calculations estimated the true angle of each joint consistent

with a standing posture. Furthermore, there was no directional influence on the pitch and yaw values. The roll values naturally changed with direction and did so logically in steps of 90 degrees in conjunction with a turn.

Dynamic assessments showed the dynamic accuracy to be less than that stated in the Xsens system literature. However, some measurement error was introduced due to occlusion of the optical sensors during the assessment. Marker occlusion error could not explain significant drift seen in some orientation values; however, these were restricted to yaw. However, it is proposed only to use pitch values to calculate joint segmental elevations and joint angles as was justified earlier.

Walking assessments on non-pathological subjects demonstrated the consistency of the segment elevation angles (see Appendix B.VII). Furthermore, for each limb segment gait events could be identified and were consistent with the observed walking pattern from video.

3.1.3.7 System configuration

3.1.3.7.1 Motion Software

Data from the Xsens Bus Master System was acquired using software developed in LabVIEW and implementing the Xsens software development kit (SDK). Data acquisition was controlled by connection over a local area network and was initiated on the receipt of session information from the master computer (computer controlling video). LabVIEW configured the XBus master initiating communication over the serial port with the individual orientation sensors. The software defined the sampling frequency using a timed while loop which duration was 10ms (100Hz). Orientation data was acquired with each iteration of the while loop as a two-dimensional array corresponding to each axis of each sensor and saved to a text file. Calibrated data was not acquired during the clinical walking assessments. The LabVIEW block diagram can be found in Appendix D.II.

3.1.3.7.2 Hardware configuration

The thigh sensor was placed at the midline between the anterior superior iliac spine (ASIS) and superior part of the patella. The shank sensor was placed on the midline along the anterior aspect of the tibia. The foot sensor was placed on the dorsal aspect of the foot in line with the shank sensor whilst standing.

3.1.4 sEMG sensor

3.1.4.1 Specification and Justification

The sEMG device had to conform to the recommendations given by the SENIAM project. It was necessary that the device could be integrated into a broader system, that is, the sEMG data should be synchronously acquired with motion and video data. The cost of the device had not to be prohibitive. As the device was to be used in a clinical environment, safety was a strong concern. Wireless communications between the patient bourn device and the acquisition equipment was preferred in order to remove trailing wires that may impede the progress of the subject. Measurements were to be taken from eight muscles; therefore, the device had to have at least eight channels.

A review of current commercial solutions was first made; however, no system fully met the criteria and therefore an EMG device was developed specifically for the project. The commercial systems did not fully meet the SENIAM criteria but, most significantly, they did not meet the cost and portability criteria; this lead to the concern that they would have been extremely difficult to integrate into a broader system.

A sEMG system configuration is shown below in Figure 24. Broadly speaking a sEMG system consists of a pre-amplifier, main amplifier, transmission over some channel and finally some form of user interface. This configuration was followed in the development of the in-house system.

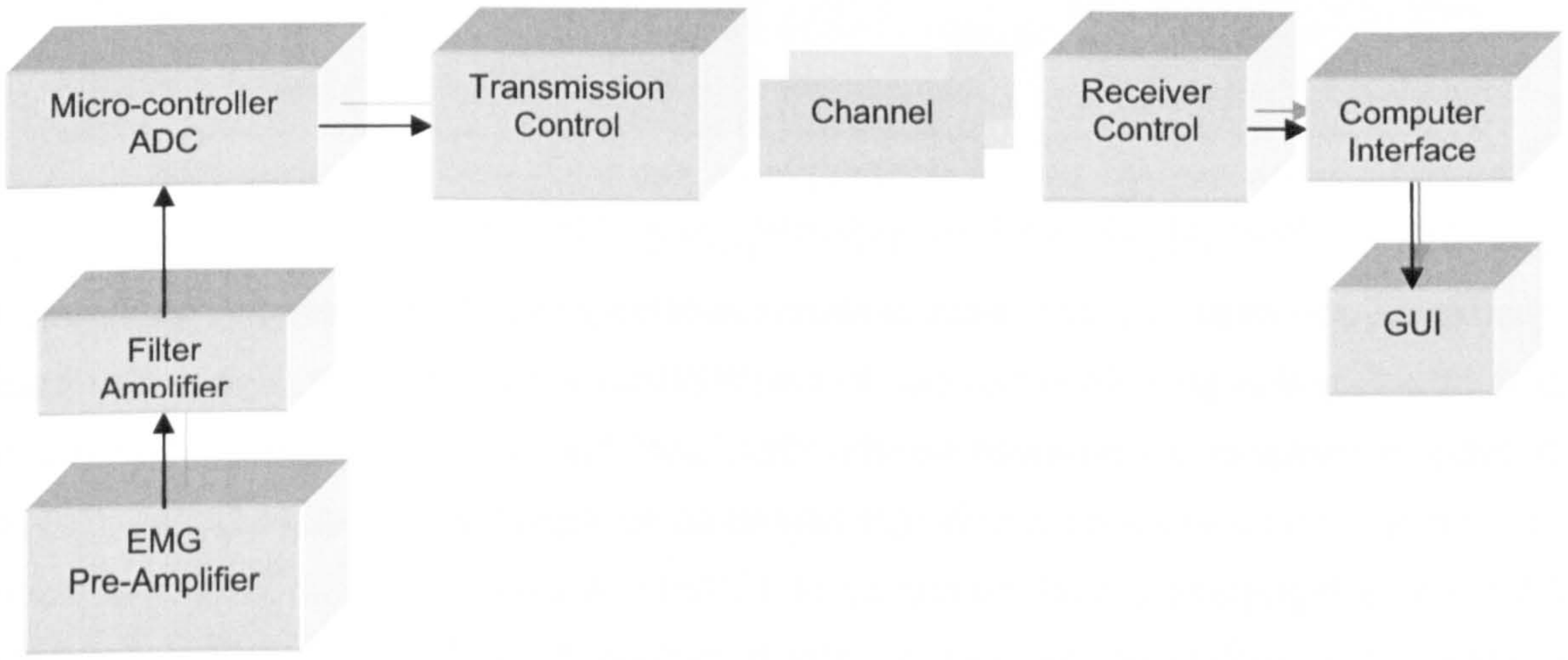

Figure 24 standard sEMG system configuration

3.1.4.2 Pre-Amplifier Design

Movement artefacts can be introduced into an EMG signal due to the inertial effects of the pre-amplifier and therefore a low profile sensor was developed. The minimum length and width of the sensor is defined by the inter-electrode distance that the SENIAM guidelines

suggest to be 20mm. A design using a fixed inter-electrode distance was also proposed by SENIAM and was implemented in this project.

Pre-amplification was achieved using an Analog Devices differential ADM620 instrumentation amplifier (gain 10). The SMT footprint was small and therefore took up very little in space on the PCB. The pre-amplifier was interfaced using SMT mini B USB connectors. This permitted pre-fabricated USB cables to be used between the pre-amplifier and the patient module. Electrodes were interfaced using snap connectors that allowed that most commercially available ECG electrodes could be used with the sensor. Finally, the entire sensor was encased in low heat melt glue.

3.1.4.3 Patient Module Design

The patient module is the most complicated component of the EMG system (image shown in Figure 12). Its role is two-fold; first to transmit EMG information to the base station and secondly to condition the EMG signal from the pre-amplifier in order that it may be sampled and transmitted.

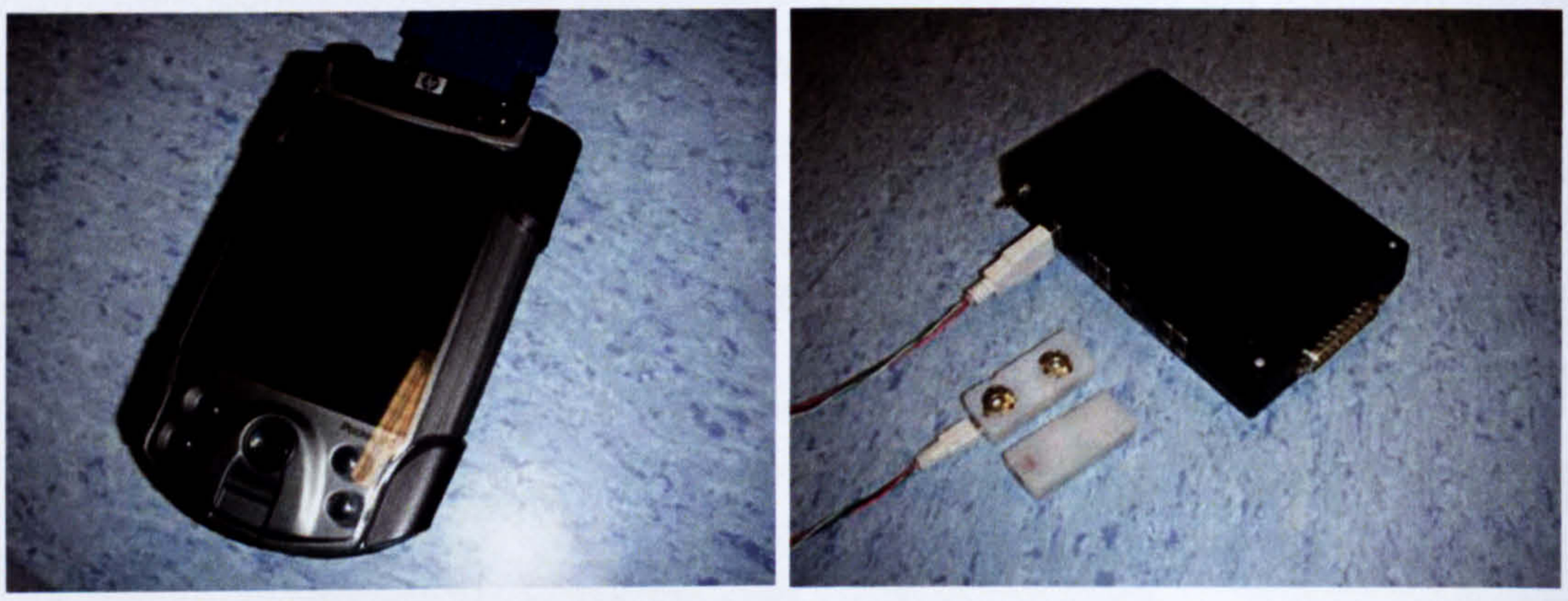

Figure 25 Patient Module (left) PDA (right) sEMG pre-amplifier and low pass filter

The signal conditioning component design is relatively straightforward; its parameters are prescribed by the guidelines set out in the SENIAM standards. The signal conditioning circuitry consists of a non-inverting amplifier (gain 100) and a low pass filter. A Linear Technology filter integrated circuit (IC) was used to implement a 4-pole Bessel low-pass filter with a high-pass cut-off frequency of 1000Hz. A filter IC was chosen over discrete component to implement the filter in order to reduce the space required for each of the circuit components, eight such filters needed to be implemented. The IC filter was also likely to have properties that were more consistent than a discrete implementation.

LabVIEW was chosen as the environment in which to implement the user interface and signal analysis components of the system. This environment was chosen as it could easily implement a friendly user interface for the system but most importantly, it supported

the modular nature of the design; in addition, it is relatively simple to interface data acquisition equipment with the computer and software. The data acquisition (DAQCard 6024E National Instruments, Figure 26) equipment was chosen to digitise the sEMG signal from the patient module.

Figure 26 National Instruments DAQCard - 6024E Multifunction PCMCIA data acquisition card

Although the DAQCard simplified the data acquisition stage of the system, it generated a problem with respect to signal communication. Specifically the latter configuration requires that the data acquisition equipment would need to be carried by the subject. This problem was overcome by using a wireless LAN enabled PDA running a reduced version of LabVIEW (LabVIEW PDA module). The data acquisition card is a buffered 16-channel PCMCIA analogue acquisition system that samples at 12.5KS/s per channel with a 16-bit resolution. Samples are read from a circular buffer on to the PCMCIA bus and streamed to solid-state memory on the PDA.

An alternative, and less desirable, configuration for the system was implemented by using the controlling computer (battery powered) to interface the data acquisition equipment instead of the PDA. A shielded cable connected the patient module to the data acquisition equipment through a connector block at the computer and via a 32-pin D-type connector at the patient module. This configuration required an adapted version of the acquisition software that was run on the controlling computer.

3.1.4.4 EMG Software

The EMG software is composed of two parts; first, the PDA module software is responsible for acquiring data from the DAQCard and maintaining communications with the base station. The second is a component of the base station that initiates data acquisition and then receives data from the PDA when the acquisition has finished (LabVIEW block diagram appendix D.III).

When the record button was pressed on the base station a "start" signal, consisting of the session identifier that is the bases for the data log file name, is transmitted to the PDA. Data acquisition begins after the next five second multiple has passed, which was implemented to ensure synchronisation with the other measurement devices. The PDA continues to log data until the TCP/IP connection is closed by the base station. At this point, the TCP/IP connection is re-established; the logged sEMG data is converted to a text stream and transmitted to the base station over the wireless network were the sEMG is then displayed to the user. Real time sEMG acquisition and display was not implemented in the system see Appendix D.II and D.III.

The first implementation of the acquisition software did not achieve the correct sampling frequency. The error in sampling frequency occurred for two reasons; firstly, the original driver for the DAQCard installed on the PDA was equivalent to the traditional data acquisition driver used in full version of LabVIEW and was not optimised for the PDA. This problem was resolved by installing a new version of the driver, DAQmx Base. This driver is specifically for use in windows CE and Pocket PC applications. The second problem was that the data acquisition virtual instruments were highly inefficient. This was for two reasons; a highly redundant implementation which was resolved through reorganisation of the virtual instruments and the use of 32-bit data value representation. The PCMCIA data bus is 16-bits wide; therefore, data representation was changed to a 16-bit unsigned character.

The adapted software for the alternative implementation of the system did not need to implement network communications but used the same data acquisition configuration as the PDA software although this was achieved with virtual instruments appropriate for the LabVIEW full development system rather than for the Windows CE platform.

3.1.4.5 Criticisms & Suggestions for Development

The real time representation of the sEMG is not essential; however, it does make it easier to identify poor quality signals quickly and therefore it should be implemented in this system. The original software configuration used TCP/IP in an attempt to achieve real-time sEMG display. It is felt that a user-defined protocol (UDP) would introduce fewer network overheads and therefore could be efficient enough for a real-time implementation.

The method of triggering the system, although effective, should be adapted to use a trigger input of the data acquisition equipment. Ideally, this would be generated by another multifunction data acquisition card available in the base station. The affect would be twofold; data acquisition would be synchronised with respect to the acquisition equipment onboard clock rather than the respective system clocks. Secondly the PDA software

would not have the overhead introduced by using the network for triggering the acquisition and could therefore be used to implement alternative control functions.

The role of the pre-amplifier and the signal conditioning aspect of the patient module should be combined. The size and imposition of the patient module is excessive especially in terms of its signal-routing components; these could be fitted around the PDA to produce a more compact design.

3.2 Surface EMG Analysis

3.2.1 Introduction

Section 2.4 presented a variety of signal processing methods that have been applied to the study of sEMG and they reflect many years application of sEMG analysis. Currently these methodologies have not been able to provide answers to clinically relevant questions i.e. to guide therapeutic interventions. However, some of the methods reflect possibly useful outcome measures. In this section those methods identified in section 2.4, specifically, principal component analysis and wavelet analysis will be developed into methods to describe better sEMG for classification of walking impairment after stroke. Little information exists on the frequency content of SMEG in the hemiplegic patient, therefore, to support the use of more advanced techniques, basic frequency analysis was applied. In addition, some traditional methods are re-applied. Linear envelope detection is commonly referenced in the literature to define periods of muscle activity that can then be used in a qualitative manner to define the sEMG signal. Firstly therefore, the characteristics and implementation of the linear envelope detector are given.

The sEMG acquisition equipment provides a band-limited version of the raw sEMG, as shown in Figure 27; this provides the basis from which all other signal processing techniques are applied. Subsequently each methodology is described including a flow diagram providing the input requirement of the process and the output signal. Together, these link to provide a structure of the analytic techniques.

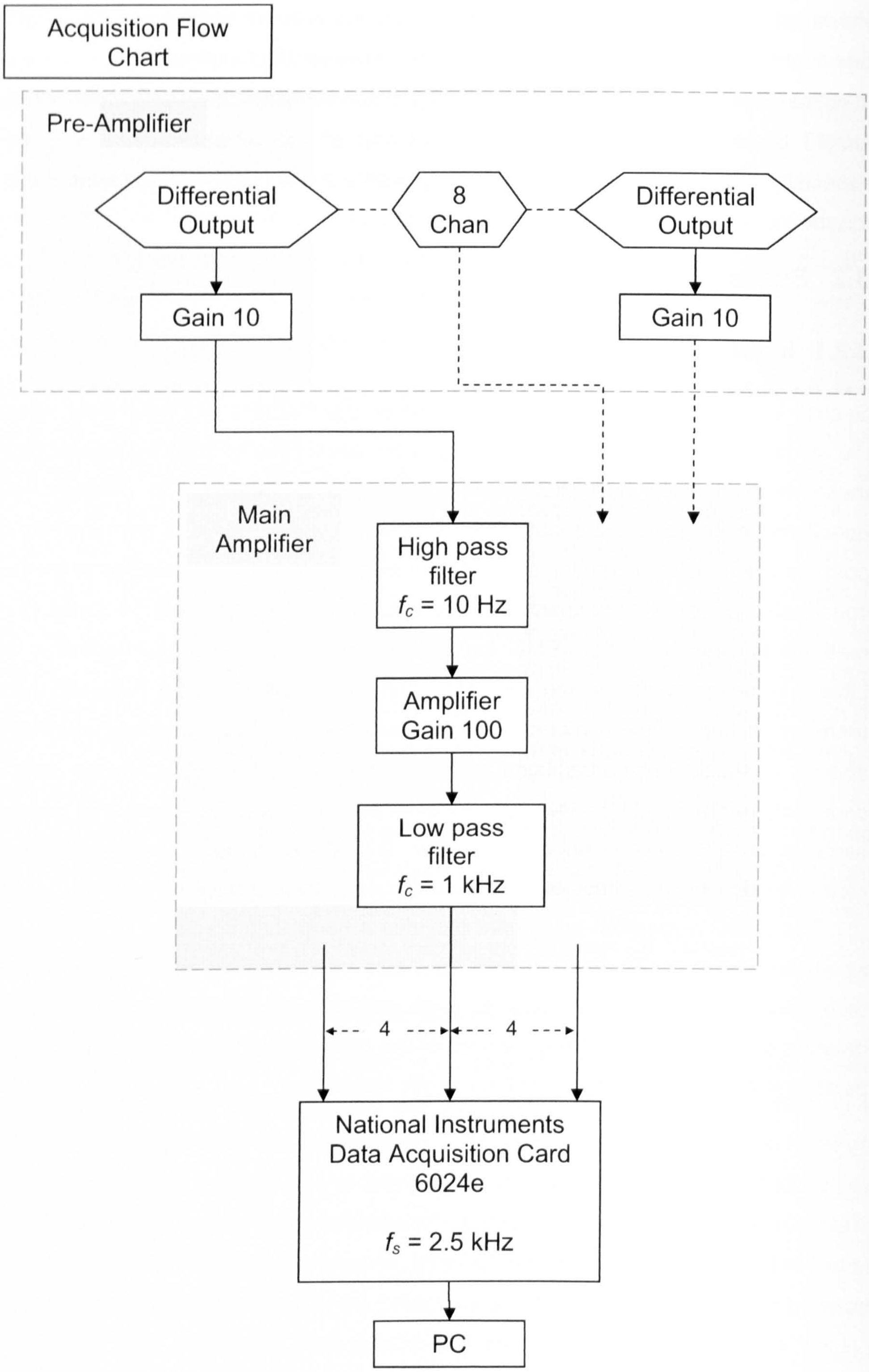

Figure 27 sEMG Acquisition Flow Diagram

3.2.2 Linear Envelope Detection

The linear envelope is a smoothed representation of the raw interference pattern. The characteristics of the signal are defined by the method of smoothing applied. Traditionally the linear envelope is generated by applying a low-pass filter or smoothing function. In the existing literature, the motivation for choosing the filter cut-off frequency at 2Hz was to reduce variability in the signal but also the linkage between sEMG and onset of muscle force. However, and almost by definition, such a low cut-off frequency will remove subtle changes in the linear envelope, that is, the higher frequency components.

The rational for the 2Hz cut-off frequency, as mentioned above, is only appealing if the removal of signal variability is desirable and the representative delay is relevant to the study design. It cannot be assumed that the variability in the linear envelope using higher cut-off frequencies is not representative of different impairment. There appears to be no rationale other than the reduction of signal variability. This is only reasonable in un-impaired groups where the underlying muscle activity might be assumed to be quite consistent. It is difficult to define criteria against which a decision could be made for linear envelope detection specifically related to analysis of impaired subjects. This is amplified when the understanding of the high frequency and signal variability is limited with respect to its relation to pathology. Surface EMG from un-impaired walkers was used to develop the implementations of the selected methods. Even with subjects from a relatively narrow age range and physical abilities, that is they had no known pathology, the frequency spectrum of the sEMG varied and furthermore the spectrum varied from muscle to muscle. Muscle to muscle variations are not surprising given that different requirements of the muscle would lead to different structures of muscle fibres and types. Furthermore, there is evidence to show that these can vary even in time according to the nerve innervating them. Therefore, it is reasonable to suggest variations between people whose lifestyles vary, the sedentary compared to the athlete for example.

One criterion against which to make a rational decision about filter characteristics is the use of the linear envelope. For example principal component analysis would operate poorly if a signal was used that was highly changeable, that is having high dimensionality. Yet a method of ratios and indices would, perhaps, show greater subtlety and discrimination when a greater number of frequency components were present. Where a method relies on a statistical technique the dimensionality of the signal dramatically affects the capacity of the method to generate meaningful results. Similarly, where two or more muscle activity patterns are to be compared, the stochastic nature of the raw sEMG signal requires an estimate of the signal to be generated. In the two extremes, too little

smoothing fails to remove the random element and too much removes information. From initial results of un-impaired sEMG, it can be seen that variations of the filter characteristics produce significant deviations in the timing of the muscle activity (see Figure 28) and reflects results presented in the SENIAM guidelines (Hermens, Freriks et al. 1999).

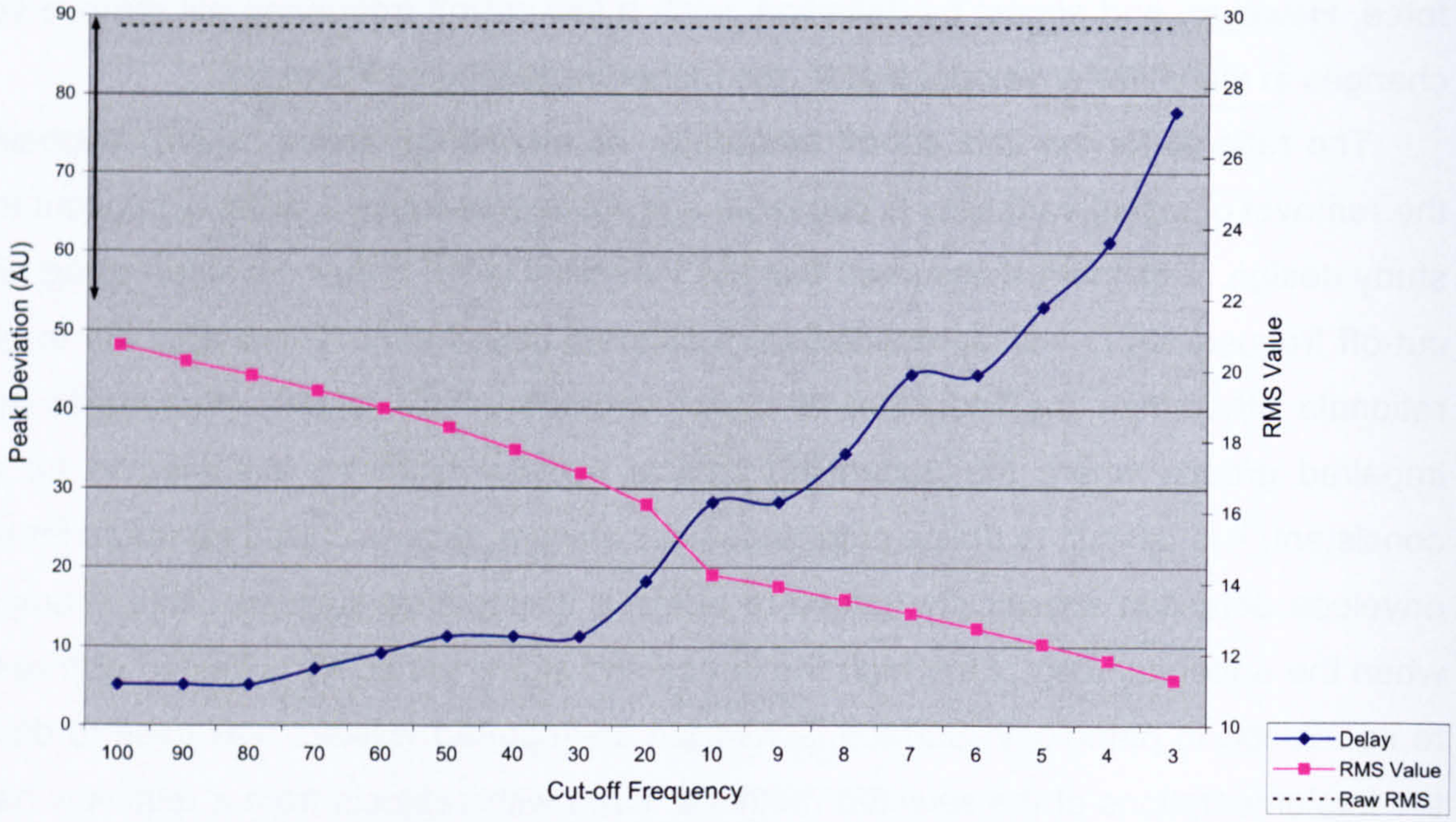

Figure 28 filter cut-off frequency Vs RMS value and peak delay

In this project, the linear envelope representation was to be used with the principal component analysis technique and to generate a simplified visual representation of the raw sEMG signal. Therefore, the primary criterion for linear envelope generation was to reduce the dimensionality of the signal. As a product of applying wavelet analysis (see section 3.2.6) a method of linear envelope generation, that reduced delay and amplitude attenuation (see Figure 7), was introduced. Wavelet decomposition uses a filter called a quadrature mirror filter (see section 3.2.5 and Figure 37). The filter generates approximations that are the low frequency components and details that are the high frequency components. Therefore, the wavelet transform itself can be used as a linear envelope detector. The frequency content of the linear envelope is defined by the level to which the signal is deconstructed. Furthermore, redundant information within the signal is removed as part of the filtering process (see section 3.2.4 Principal Component Analysis), yet at any level the signal can be reconstructed to restore temporal information. This is shown in Figure 29 where the raw sEMG signal is decomposed and subsequently reconstructed. The linear envelope in this project was constructed in this way (see Figure

30) an alternative using a Bessel filter and ARV sEMG was also implemented but altimately not used to analyse subject data as a result of the data shown in Figure 28, the Bessel filter implementation flow diagram is shown in Figure 31).

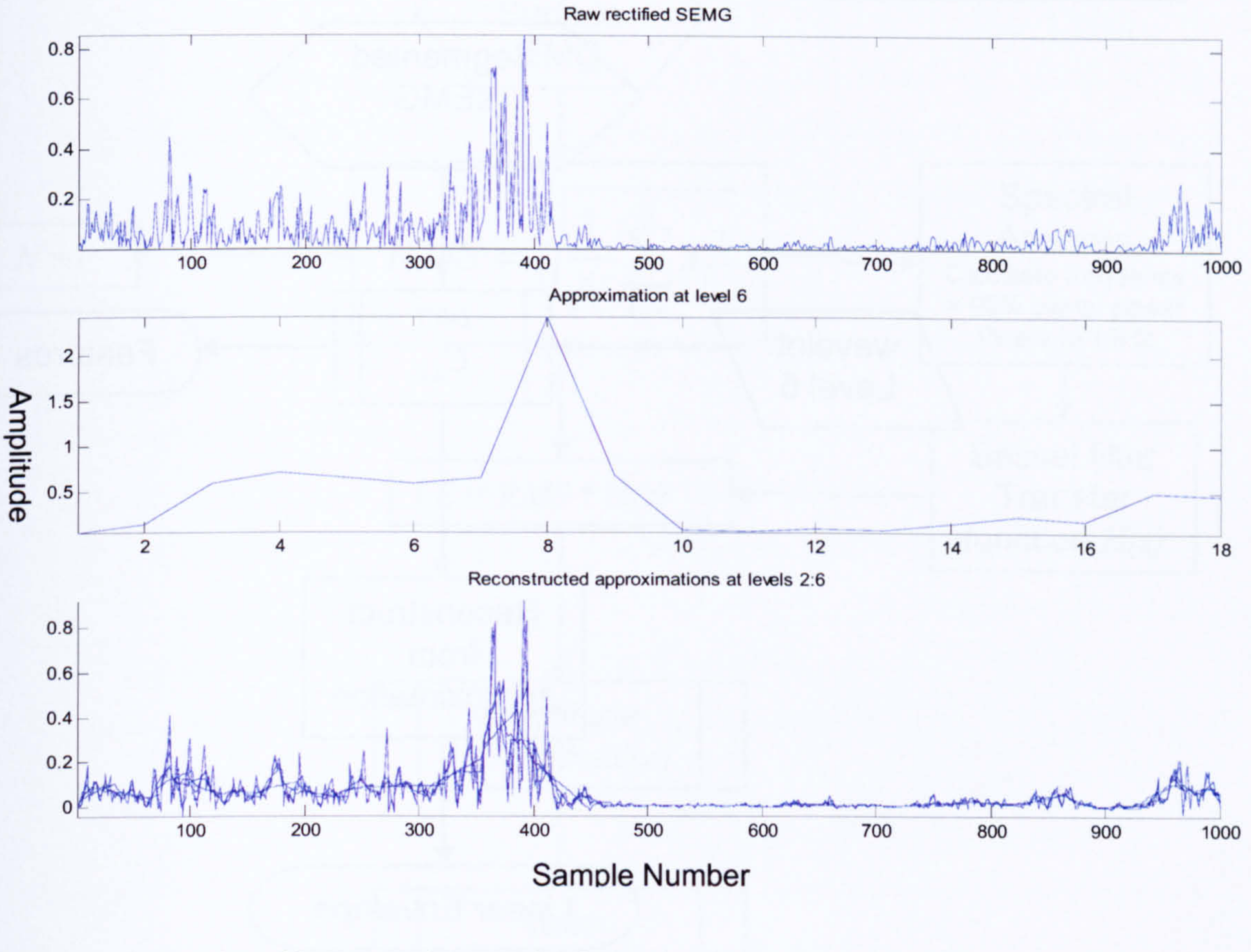

Figure 29 Generation of features using wavelet deconstruction

The linear envelope was normalised to within subject peak amplitude. This is contrary to the literature presented in section 2.4.4; however, the goals of these studies are different to those in this project. Here, the linear envelope is not used to compare the relative amplitude between subjects but to generate a characteristic pattern of the subject's sEMG. Normalising to the peak within subject amplitude merely simplifies the visual interpretation of the sEMG pattern in terms of within subject variability and footswitch data but is not a requirement. The principal component analysis technique implemented in this project does not require amplitude normalised sEMG (See section 3.2.4).

The linear envelope representation was also normalised in time by a FFT method of interpolation (see MATLAB user manual and Appendix B for MATLAB implementation) to represent 0 - 100% gait cycle. The traditional representation of the gait cycle, as presented in section 2.2.1, relates 0% gait cycle to foot strike. Unfortunately, because of the automated subdivision of the gait cycle in this thesis 0% gait cycle relates to toe-off.

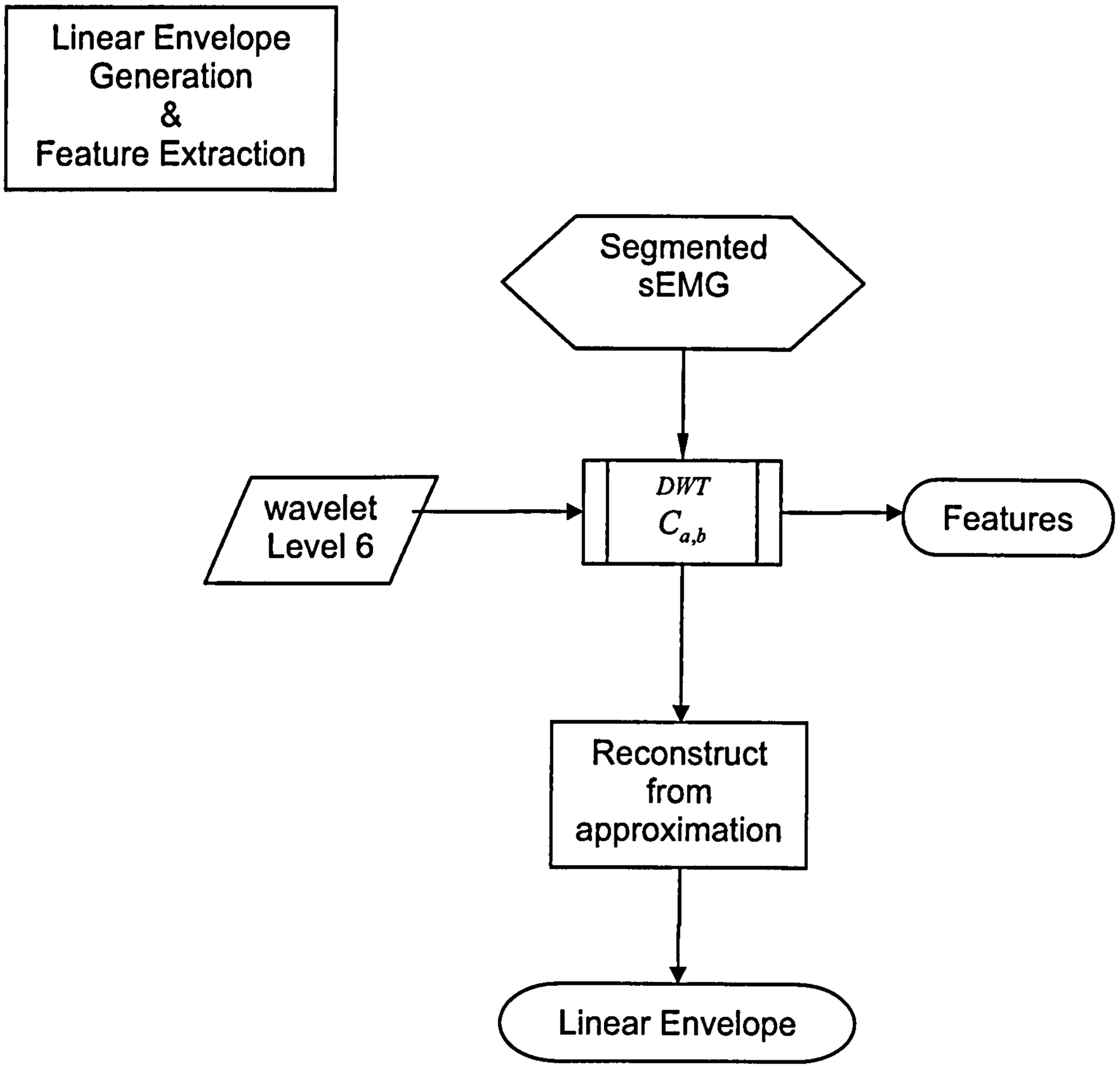

Figure 30 shows the wavelet method of linear envelope generation. The segmented raw sEMG signal is transformed by a discrete wavelet transform of wavelet level 6, this signal is then reconstructed to restore the temporal information.

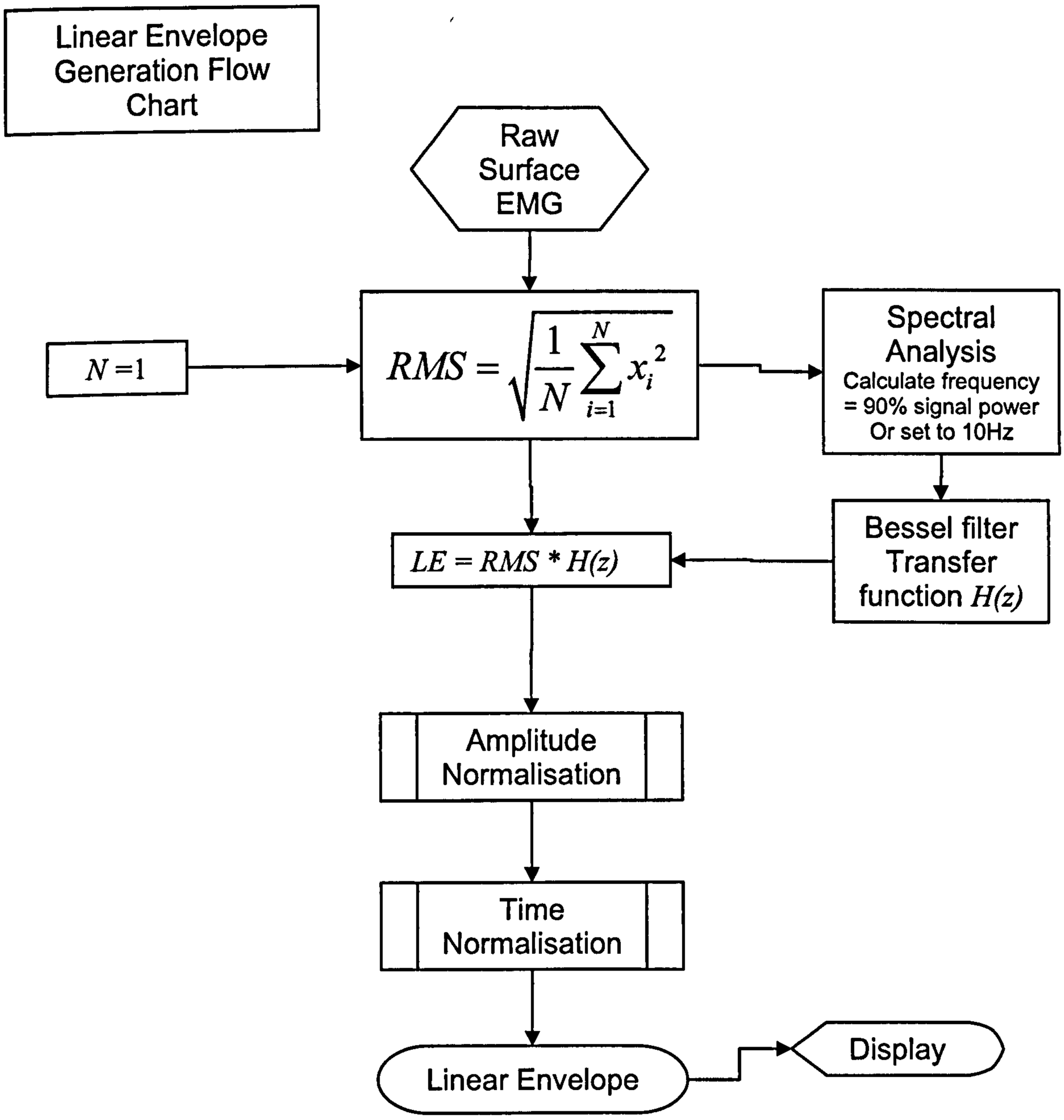

Figure 31 Generation of Linear Envelope (Bessel filter method)

3.2.3 Basic Frequency Analysis

No information could be found during the review of the literature regarding the frequency constituents of sEMG from hemiplegic stroke patients. Therefore, Fourier analysis was applied to the segmented sEMG to inform the necessity of more advanced techniques. Fourier analysis was accomplished in LabVIEW using the power spectrum virtual instrument (for information see LabVIEW documentation (National Instruments 2006)) with rectified raw sEMG. The mean frequency (Equation 11) and the frequency at which the maximum coefficient were calculated:

$$Mean\ Frequency = \frac{1}{f}\sum_{i=1}^{f} f.c_f$$

Equation 11 Fourier analysis, mean frequency calculation

The mean frequency response can be found in Appendix B.II. No statistical significance can be drawn from these results; this is because the number of subjects included does not support this. However, results suggest a lowering of mean frequency in many of the impaired subjects; it also suggests varying mean frequency muscle to muscle. Therefore, further investigation was deemed appropriate.

3.2.4 Principal Component Analysis

Principal Component Analysis (PCA) reduces a set of variables to a new parsimonious set of variables. The mathematical basis of this technique was given in section 2.4.6.2. The generation of the principal components is a relatively simple process, a flow diagram is given below (Figure 33), and the MATLAB script can be found in the appendix (Appendix C). The technique uses the linear envelope representation. Features can be generated from the linear envelope by averaging over the signal. The averaging value is chosen to reduce the number of samples representing the linear envelope to only the number required to retain the maximum frequency content of the linear envelope. A process of integration can be used as shown in the flow diagram in Figure 32. However, features in this porject were generated through wavelet analysis using wavelet deconstruction (see section 3.2.5 & 3.2.2). A correlation matrix of the linear envelope features is then generated using Equation 8. Eigenvectors of the correlation matrix are retrieved then, following the work of Wootten et al. (Wootten, Kadaba et al. 1990), weighting coefficients are created (see Equation 9) which can then be used to reconstruct the signal with a reduced number of basis vectors (eigenvectors). The closeness of the reconstructed signal to the original can be assessed by calculating the mean square error (Wootten, Kadaba et al. 1990) or coefficient of variance (Winter and Yack 1987). The quality of the reconstruction is shown in Appendix B.VI& Appendix Figure 103. The number of eigenvectors used to reconstruct the signal was chosen based on the amount of variance they described. Enough eigenvectors are included to describe 90% of the variance within the feature matrix (Wootten, Kadaba et al. 1990). In chapter 2 (section 2.4.4) it was noted that the normalisation technique used to form the linear envelopes that make up the correlation matrix was important to the conclusions to be drawn from the technique. It was decided not introduce linear envelope amplitude as a possible variable. As different amplitudes existed between the sEMG signals this would reduce the significance of some

activation patterns and thus its presence might not be appreciated. Furthermore, the relative amplitudes of the sEMG signal can be evaluated separately and novel methods, superior to linear envelope representation, exist (Ricamato and Hidler 2005). Therefore, the results of this technique represent the patterns of activation with no regard to the respective amplitudes of the signal.

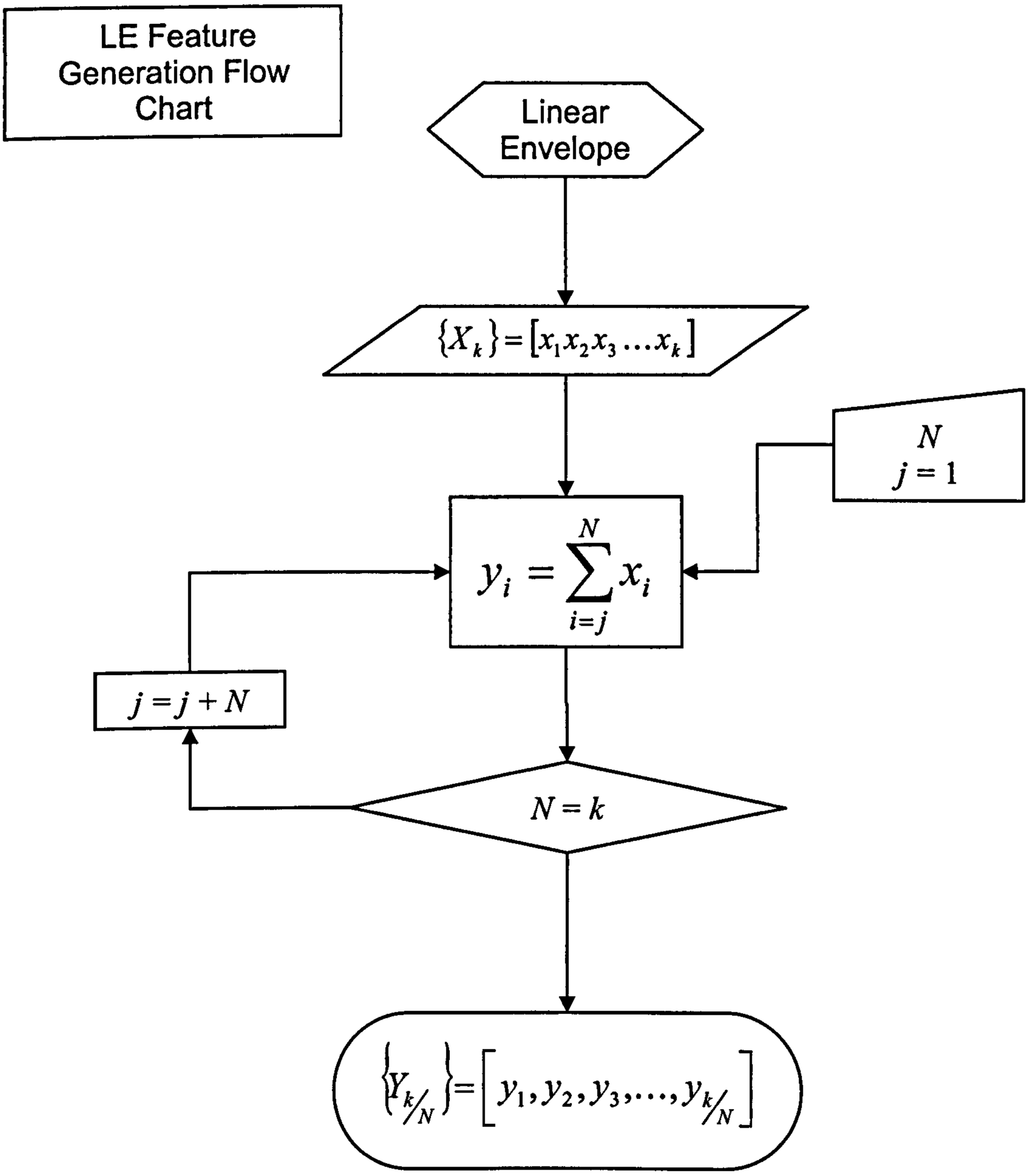

Figure 32 Feature Extraction Flow Diagram (Averaging Method)

Principal Component Analysis Flow Chart

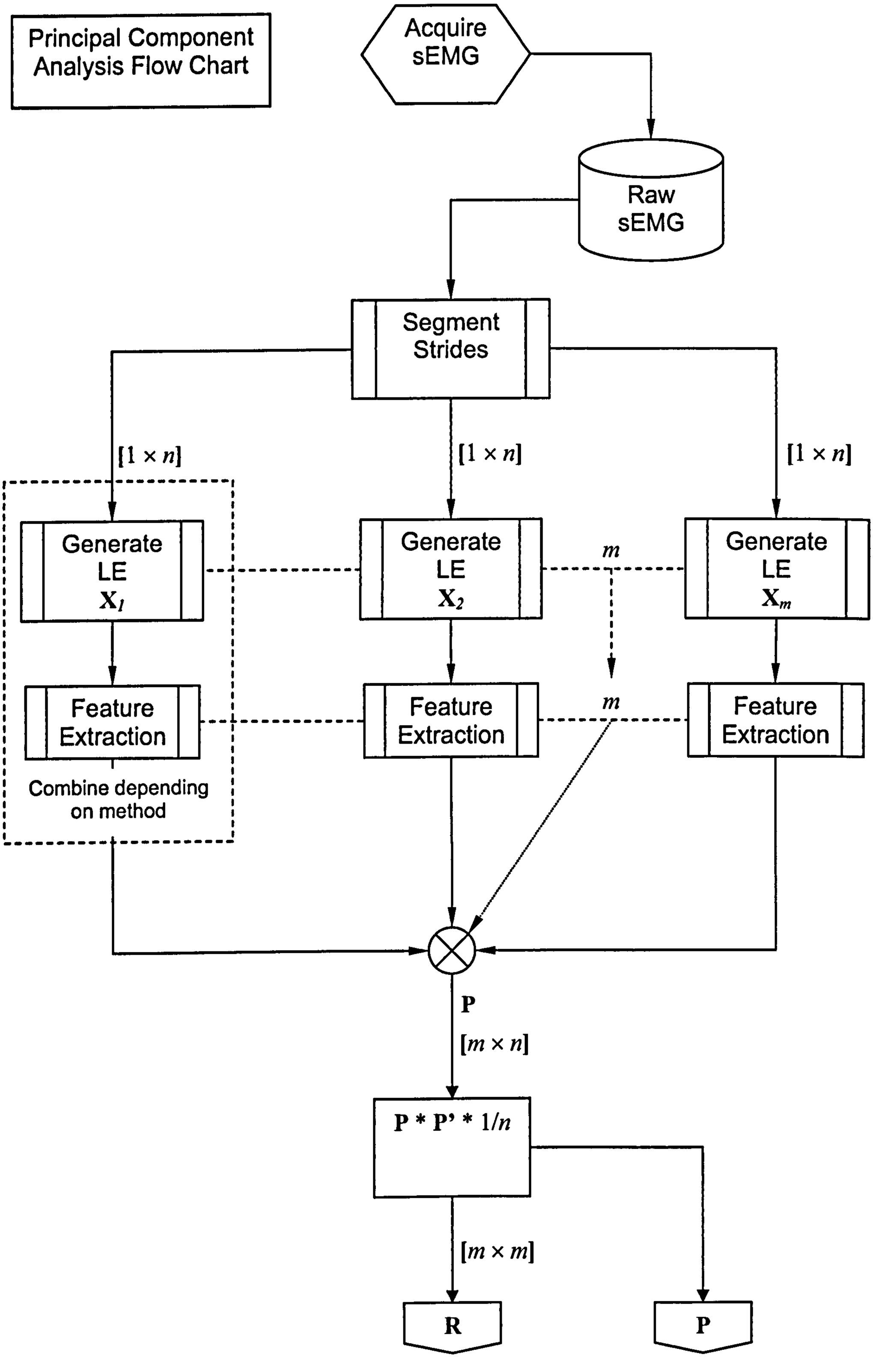

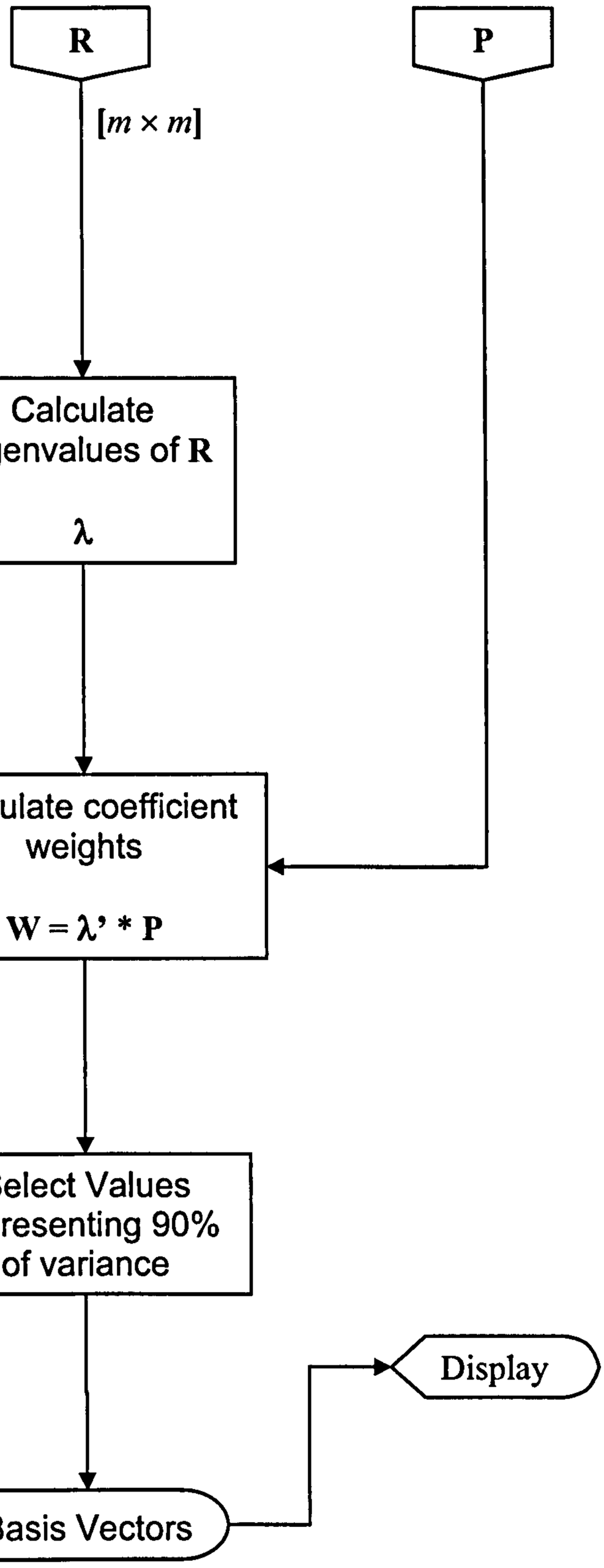

Figure 33 Principal Component Analysis Flow Diagram

3.2.5 Wavelet Analysis

Based on the analysis of the Fourier frequency spectrum, variations in the sEMG frequency analysis were further analysed using 2D time frequency analysis. Surface EMG signal processing techniques using Wavelets were implemented using the MATLAB wavelet toolbox 2.2. A block diagram of the methodology is shown in Figure 34. The continuous wavelet transform (CWT) was used to analyse the rectified sEMG at different frequency resolutions. Following the work of De Stephano (Stefano and Allen 2003) the Gaussian wavelet of order 3 was used. The scale level to which the signal was decomposed was set to be equivalent to the bandwidth of the filtered sEMG. The decomposition permits the calculation of the instantaneous mean frequency and maximum frequency coefficient over a period of activity as shown in Figure 34. The wavelet coefficients were calculated using the continuous wavelet transform command.

```
COEFS = cwt(s, scales, 'wname', PLOTMODE);
```

where '`s`' is the signal under analysis, '`scales`' defines the starting level, interval and end level, for example, 1:5:256 starts at level 1 and increments the level by 5 up to the level 256. The argument '`wname`' refers to the wavelet type and '`PLOTMODE`' defines the display output. '`COEFS`' is a 2D array of coefficients from the wavelet transform calculated from applying Equation 4. The coefficients can be displayed in one of four ways depending on the '`PLOTMODE`' argument. The colouration can be given as intra-scale magnitudes, or as a relative inter-scale magnitude. Alternatively, the absolute magnitudes can be represented graphically; again, represented as intra or inter-scale colouration. These different representations can be used to focus on the significance either of a frequency bin or of a time epoch with respect to frequency.

3.2.6 Wavelet filtering & Burst Detection

The inadequacies of traditional smoothing when applied to impaired sEMG were resolved by using characteristics of the wavelet transform that allow selective filtering of a signal. By applying techniques described by Conforto (Conforto, D'Alessio et al. 1999) artefacts within the sEMG could be removed in addition to identifying periods of muscle activity. The Flow diagram for this process is given in Figure 36.

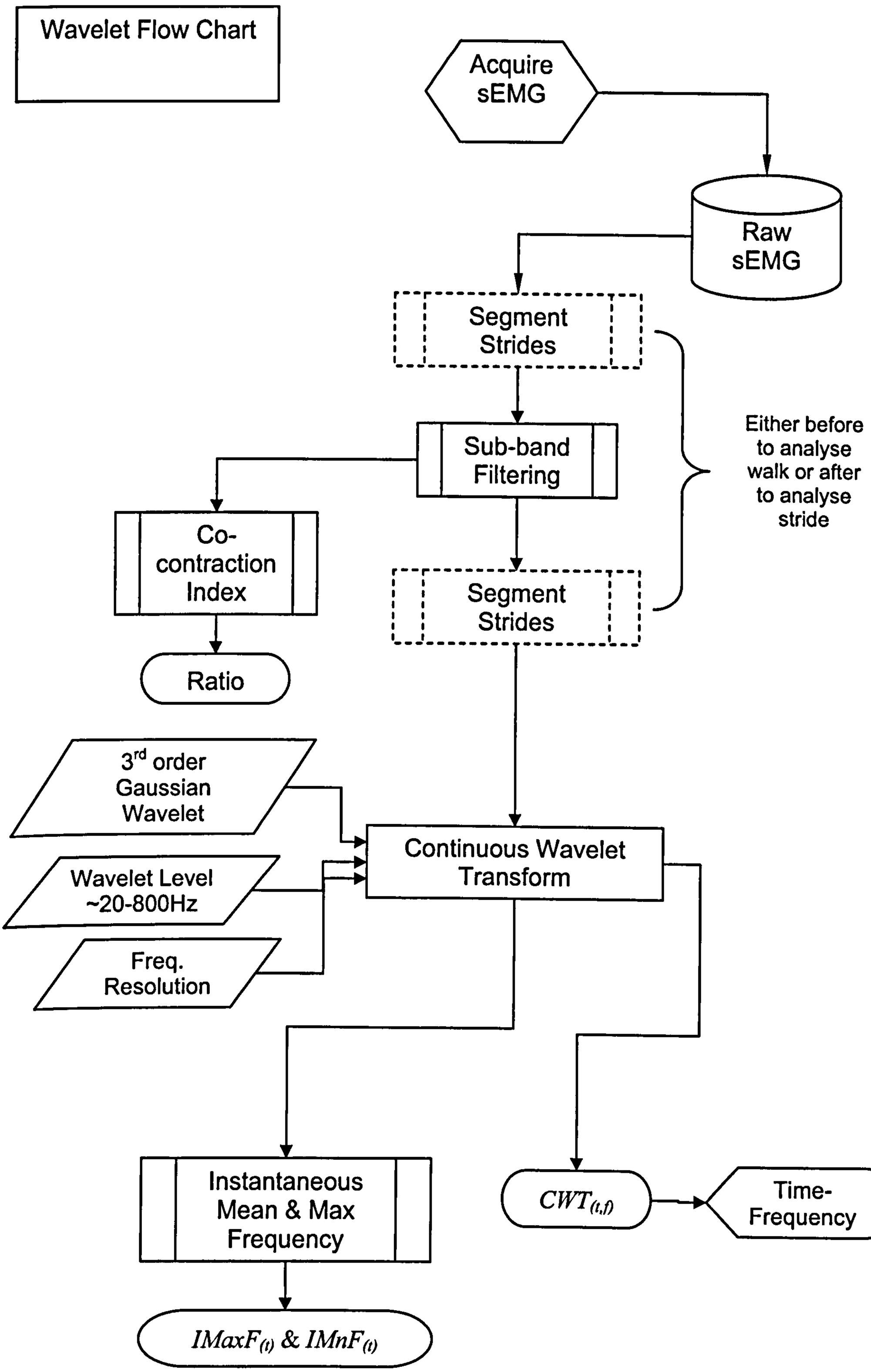

Figure 34 Continuous Wavelet Transform Flow Diagram

Because the wavelet transform decomposes the signal into different frequency bands, it is possible to filter the signal at each of the separate sub-bands. If the coefficients relating to noise artefacts are identified, they can be set to zero and the signal reconstructed from the processed coefficients will be the original signal minus the noise artefacts. Additionally, the sub-band that is assumed to characterise sEMG activity most strongly can be used to identify periods of activity without the contribution of artefact. This method uses the discrete wavelet transform and a special wavelet, the digital Mayer wavelet.

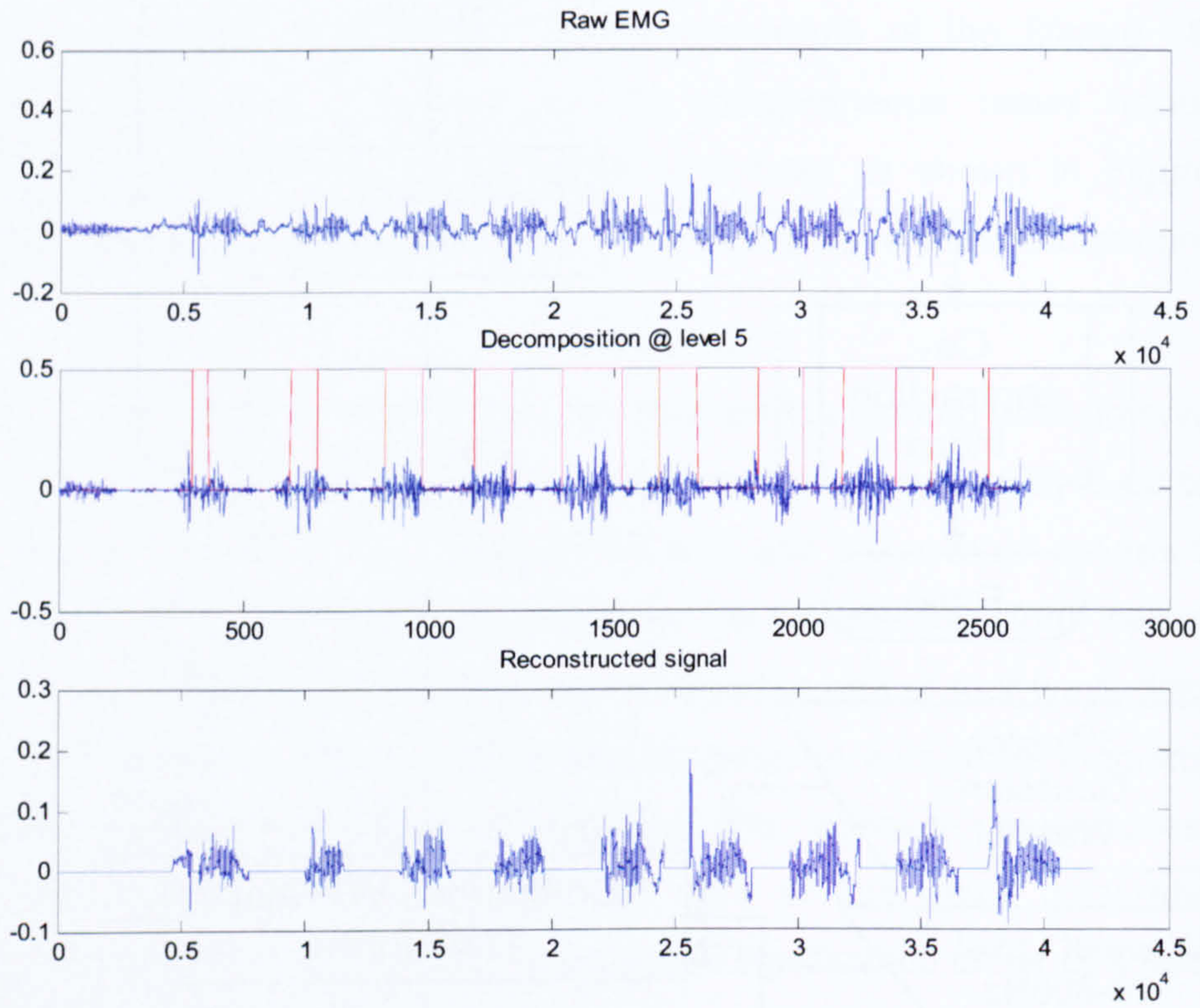

Figure 35 Raw sEMG signal decomposed and divided crudely into burst and inter-burst periods. Inter-burst periods set to zero

This has properties necessary for discrete signal processing and follows the methodology presented by Conforto (Conforto, D'Alessio et al. 1999). The signal is decomposed over 8 levels using the MATLAB wavelet toolbox. Each level, or scale, represents a particular frequency bandwidth as described earlier. The wavelet coefficients are calculated using the discrete wavelet function:

```
[Ca, Cd] = dwt (X,'dmey','mode');
```

The output from the 'dwt' function is two 1D arrays, '`Ca`' represents the approximation coefficients or the low frequency components, '`Cd`' represents the detail coefficients of the high frequency components. The signal for deconstruction is given by '`X`', at the first

deconstruction x is the original signal, for each subsequent level of deconstruction x is given by the previous variable cd. The decomposition scale is therefore given by the number of iterations of this process. The argument 'mode' is important in this implementation as it defines the method of handling border distortion due to convolution on finite length signals [see MATLAB wavelet toolbox (Mathworks 2006)]. Furthermore, 'mode' defines how to deal with signals that are not dyadic i.e. with a length 2^n, n = 1, 2.... Here periodic-padding is used to simplify the interpolation of burst and inter-burst periods between decomposition levels; i.e. to use the indices of the array describing the burst period in one level to describe the burst period in a lower decomposition level, the array must be made smaller whilst retaining the temporal relationship between the two. This is complicated if a non-dyadic relationship exists between decomposition levels. Using the scale representing the higher frequencies (smaller scales) it can be assumed that there is only a very small contribution of low frequency artefact. Therefore, all the coefficients relate to only sEMG activity. A crude determination of burst and inter-burst periods is made by applying a threshold to the signal coefficients at this lower scale. The threshold value is determined by the standard deviation of the rectified signal. If the coefficients within a window translated along the signal are below half the standard deviation of the rectified signal, the coefficient representing the centre of the window is defined as in an inter-burst period. Based on this crude assignment the power of the signal within burst and inter-burst periods is calculated. The power is then used to generate a threshold adapted to the particular sub-band. The newly optimised threshold is then applied to the signal to identify a better estimate of burst and inter-burst periods. The coefficients that characterise noise, as identified by the power of the coefficients within the inter-burst periods, can be set to zero. Having identified the periods of activity lower frequency bands can be filtered by following the same process of calculating the power of burst and inter-burst periods and therefore generating an optimised threshold for each wavelet scale. The signal can be reconstructed by applying the inverse discrete wavelet transform using the new set of coefficients, and finally samples within the inter-burst periods are set to zero. In an addition to the methodology presented by Conforto (Conforto, D'Alessio et al. 1999) filtering of high frequency artefacts was also implemented by setting to zero coefficients greater than twice the average power within a burst period. Again, this threshold is adapted for each frequency band or wavelet scale.

It is possible to create a function whose translations and dilations produce a wavelet orthogonal basis over which a signal can be decomposed. These dilations carry variations in the signal at different resolutions, thus the transform creates multi-resolution approximations of the signal. The signal can be reconstructed by adding the signal

approximation to the detail variation between each approximation level. Interestingly a wavelet function that generates an orthonormal basis can be completely characterised by a particular type of filter called a quadrature mirror filter. This class of filter is used to implement fast wavelet algorithms. The process of burst detection is described diagrammatically in Figure 36. The decomposition process using quadrature mirror filters is shown diagrammatically in Figure 37.

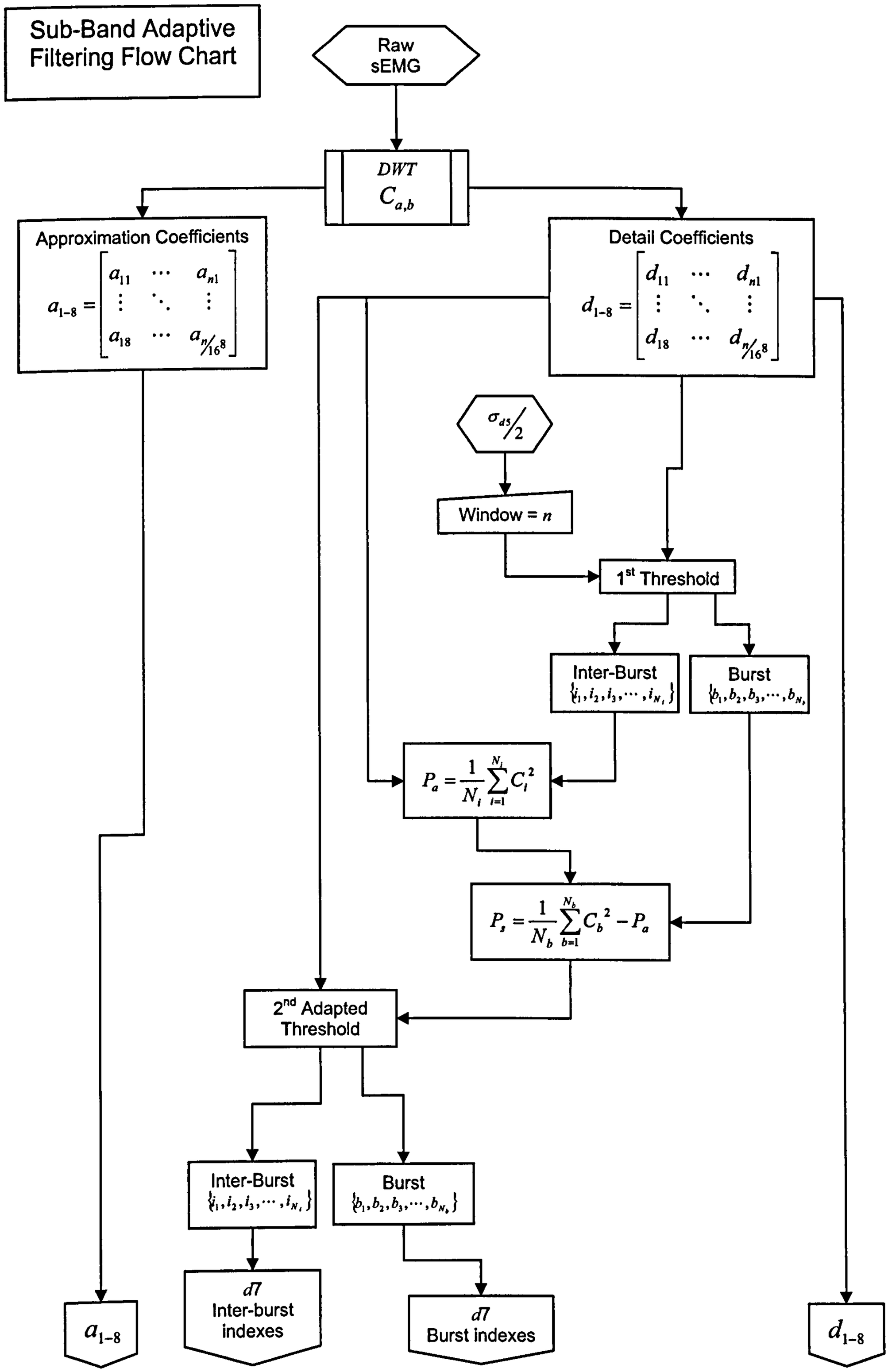
Sub-Band Adaptive Filtering Flow Chart
Raw sEMG
DWT
$C_{a,b}$
Approximation Coefficients
$a_{1-8} = \begin{bmatrix} a_{11} & \cdots & a_{n1} \\ \vdots & \ddots & \vdots \\ a_{18} & \cdots & a_{n/16^8} \end{bmatrix}$
Detail Coefficients
$d_{1-8} = \begin{bmatrix} d_{11} & \cdots & d_{n1} \\ \vdots & \ddots & \vdots \\ d_{18} & \cdots & d_{n/16^8} \end{bmatrix}$
$\sigma_{ds}/2$
Window = n
1st Threshold
Inter-Burst $\{i_1, i_2, i_3, \cdots, i_{N_i}\}$
Burst $\{b_1, b_2, b_3, \cdots, b_{N_b}\}$
$P_a = \frac{1}{N_i}\sum_{i=1}^{N_i} C_i^2$
$P_s = \frac{1}{N_b}\sum_{b=1}^{N_b} C_b^2 - P_a$
2nd Adapted Threshold
Inter-Burst $\{i_1, i_2, i_3, \cdots, i_{N_i}\}$
Burst $\{b_1, b_2, b_3, \cdots, b_{N_b}\}$
$d7$ Inter-burst indexes
$d7$ Burst indexes
a_{1-8}
d_{1-8}

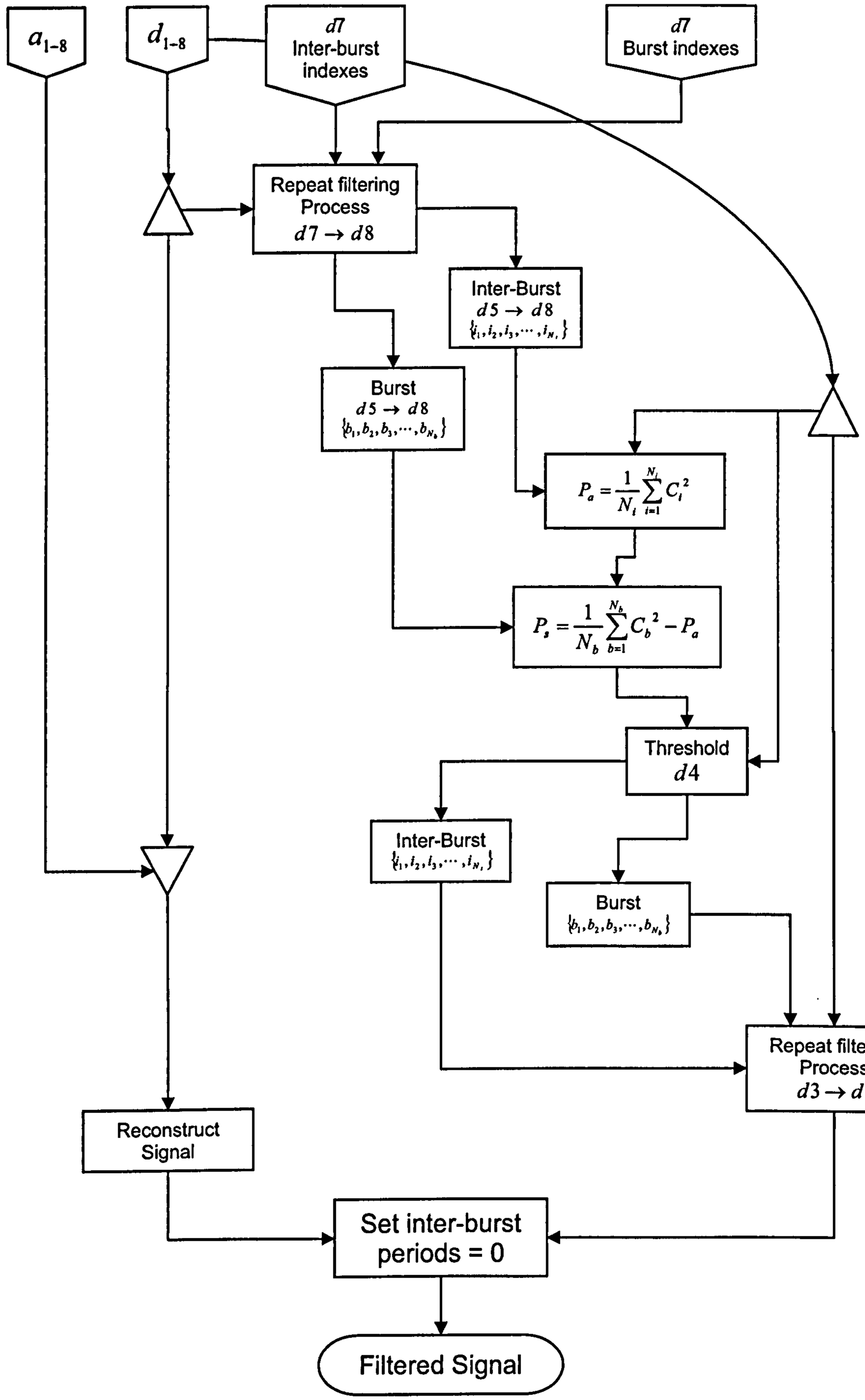

Figure 36 Wavelet Burst Detection Flow Diagram

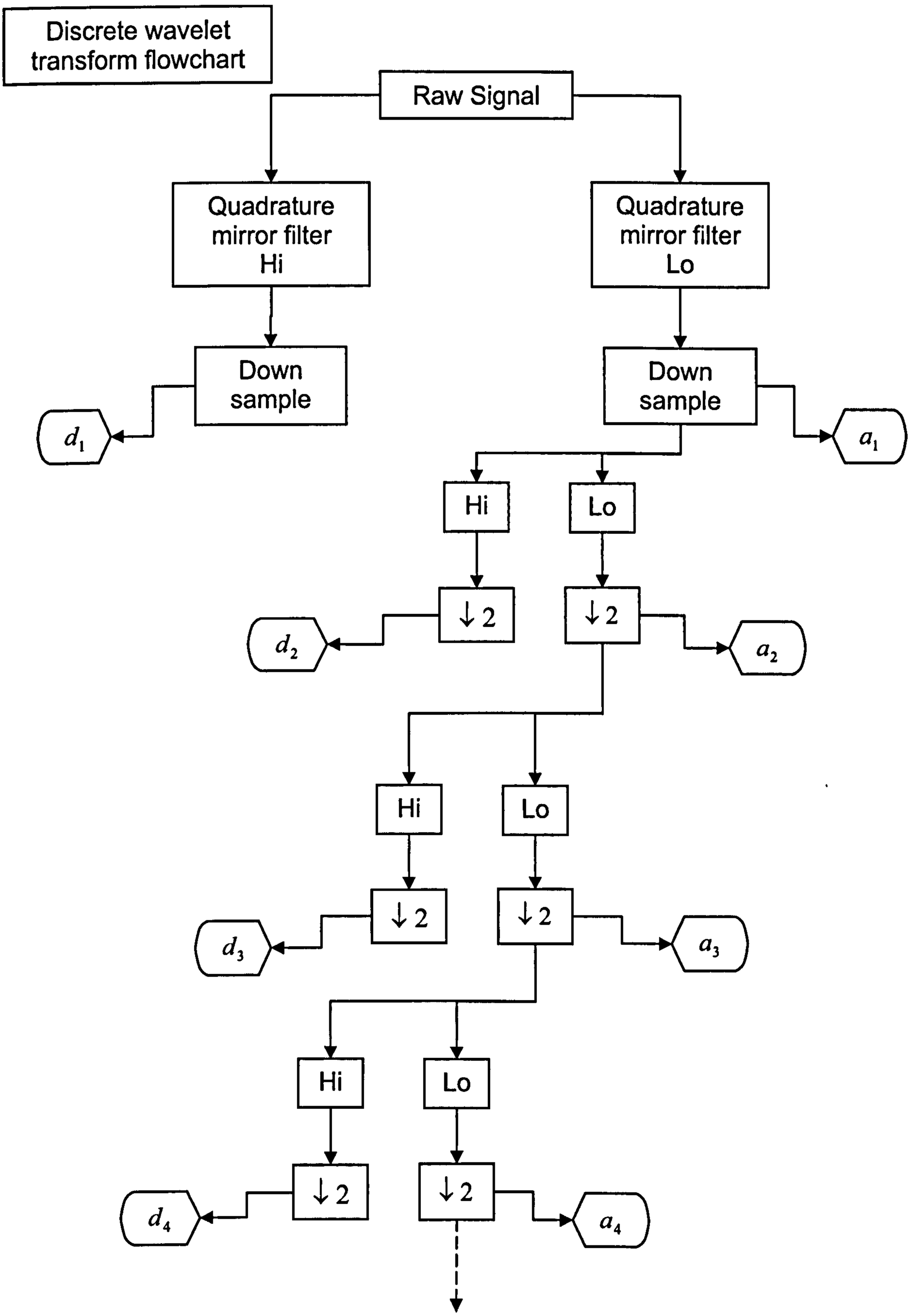

Figure 37 Discrete Wavelet Decomposition using Quadrature Mirror Filter

3.3 Video Analysis

3.3.1 Introduction

Three methods of analysing walking were subsequently applied to the video captured during each assessment. Two observational gait analysis techniques and one commercial video processing technique were used in order to support or deny the kinematic data collected from the instrumented system. The observational techniques are those found in current clinical practice and therefore could provide information equivalent to that most commonly acquired during clinical assessments. This was intended to characterise particular pathological gait using a contemporary scale. The two observational techniques used were the Rivermead gait scale and the Los Amigos gait analysis scale.

3.3.2 Rivermead Gait Analysis Scale

The Rivermead gait scale identifies common impairments in hemiplegic gait and ascribes a score depending on the severity. The scale is divided according to the gait cycle, separating the stance and swing phases. Each side of the patient's body is observed and measured using a separate form, thus, each lower limb is assessed for impairment. A copy of the gait scale can be found in Appendix F.II.

3.3.3 Los Amigos Gait Analysis Scale

The Los Amigos gait scale does not ascribe a level of severity to a gait deviation but simply identifies its existence. Again, the scale is divided into phases of the gait cycle from left to right. Deviations from the gait cycle are listed vertically and a grey scale is used to describe the significance of the deviation to a particular period of the gait cycle. The gait scale can be found in Appendix F.I. As with the Rivermead scale, the analysis is conducted on the left and right leg separately.

3.4 Clinical Protocol

The study was required to undergo an ethical review by the local research ethics committee in line with the research governance framework for health and social care. A research protocol and supporting material was submitted to the Salisbury and South Wiltshire research ethics committee who gave a favourable opinion.

3.4.1 Inclusion criteria

To be included in the study patients had to have suffered a cerebral vascular accident (CVA) as defined by the world health organisation, without reference to etiology, and are at least 6 months post CVA. Furthermore, the patient must have been using the Odstock Drop Foot Stimulator for at least six months. Participants were required to live within 25 miles of Salisbury District Hospital in order that travelling to the research site was not prohibitive. The participants had to be able to ambulate safely over the 7m course and be able to understand and follow verbal and or written instructions.

3.4.2 Exclusion criteria

Due to the limited number of subjects in this study those with pathology in addition to CVA that might contribute to a disrupted pattern of gait, for example hip / knee replacement or osteoarthritis were excluded. In addition, those who rely on a walking aid for safe ambulation were also excluded. It would be reasonable to conceive these subjects as a further subdivision of the groups being studied. Those already taking part in a research project were not approached.

3.4.3 Recruitment

Patients were recruited from the patient database of the functional electrical stimulation clinic in the Department of Medical Physics and Biomedical Engineering Salisbury District Hospital. A lead clinician selected prospective participants based on the inclusion and exclusion criteria after having reviewed their patient notes. The department Caldicott guardian asked permission of the prospective participant to be approached by the investigators. On receipt of permission from the prospective participant, an invitation letter was sent to them. The first appointment was made after any queries had been addressed. In total 28 patients were suitable for the study of which 15 agreed to be approached.

3.4.4 Consent

In line with the ethical requirements of the study, informed consent was obtained from each participant at the time of the first appointment. Two consent forms were required, one specifically to gain permission to video the participant during the assessment and the other to gain consent to make and retain measurements for the assessment. An information sheet was included with the invitation letter; this detailed everything that was to happen to the participant during the study. Specific consent was gained to inform the participants GP or consultant that they were taking part in the study. The participant, and carer/friend if present, was introduced to all the equipment to be used in the study and the process of the assessment, and finally the consent form was read through with them. After all the participant's questions had been answered, the consent form was signed and copied; the original form was retained by the researcher, one copy was kept by the participant and one was kept in the patient's medical notes.

3.4.5 Assessment

All the data for each participant was collected during a gait analysis session lasting approximately 2 hours, a flow diagram for the assessment process can be found in Appendix D. A significant proportion of the session was spent placing the sEMG sensors. Each sensor was placed according to the measurement between two anatomical landmarks. These positions are those defined in the SENIAM guidelines for sensor placement and can be found in appendix I. Sensors were placed:

1) Tibialis Anterior
2) Soleus
3) Gastrocnemius
4) Vastus lateralis
5) Rectus Femoris
6) Biceps Femoris

- The skin area was cleaned and slightly abraded using an isopropanol swab. 3M blue spot paediatric ECG electrodes were attached to the preamplifiers and then attached to the skin using the adhesive surface of the electrode.
- The preamplifiers were secured using Micropore surgical tape. Movement of the sensor with respect to leg was minimised. Sensor cables were taped to the participant's leg to avoid movement artefact due to tension in the cables.
- Force sensitive resistors were placed in the participants shoe

- MT9 orientation sensors were placed on the leg. The orientation sensors were attached using Velcro straps. The foot sensor was placed around the base of the shoe of the participant. Both the shank and thigh attachments were made around the leg. The position of the sensor was defined by the measurement between anatomical landmarks but such that they would not interfere with the sEMG sensors during movement (see section 3.1.3).
- It was ensured that the participant's leg movement was not restricted by the attachment of the cables, this was a safety consideration as much as a data quality issue and therefore time was spent repositioning the cables until the participant was comfortable
- The interface equipment, XBus master, footswitch driver and sEMG interface were held in a bag worn around the patients waist. Sensor cables were attached and the sensor, sensor placement and corresponding sensor channel was recorded.
- An assessment was made of the integrity of the data channels and of the operation of the system. Any sEMG sensors exhibiting poor skin attachment or cable attachment were adjusted and the assessment repeated. Whilst standing, a static measurement of the orientation sensors made.
- The participant was asked to walk, at a self-selected speed, a seven metre straight and level course. Patients were again reminded of the trailing instrument wires. If the patient required a walking stick for safe ambulation, they were encouraged to use it.
- One seven-metre course constituted one walk. The first walk was used to assess the quality of the acquired data. Any sensors exhibiting movement artefact were checked and repositioned. The patient was given the opportunity to rest.
- The patient was asked to make four walks, after each walk the sEMG data was checked for any excessive movement artefact and sensors attachments improved if required. The patient was able to rest at these points.
- The system was reset and the patient prepared for the next walk.
- The assessment was stopped after a maximum of six walks or at any point if the participant requested.
- At the end of the assessment, the sensors were removed in the reverse of the way they were attached.

4 Results

4.1 Introduction

This chapter presents the groupings found from the results of the walking assessments. The chapter begins by introducing the graphs that will be used for the presentation of the results. An overview of the results from un-impaired subjects is given in section 4.3. In section 4.4.2 groupings of subjects according to observational gait analysis are shown and section 4.4.3 gives the groupings from the segmental elevation angles. Section 4.4.4 then presents the results of the sEMG analysis of impaired subjects. In sections 4.4.4.1 to 4.4.4.5, patterns of muscle activity in three ankle muscles during a stride are presented in terms of time-domain, frequency domain, characteristics of muscle phasing and agonist antagonist co-activity. Due to the small number of subjects and the combination of both the common features and individual characteristics of each subject, section 4.6 presents a case study presentation of each impaired subject.

The results shown in this chapter for impaired subjects reveal the characteristics that can be used to group subjects according to underlying impairment. The characteristics are used in section 4.5 to produce a prototype decision matrix that gives a structure to define underlying impairment. The graphs in this chapter therefore are used to represent the groupings that were found and are not the results in entirety. The results for each subject are presented in full within the Appendix (see Appendix A). All the kinematic and sEMG data are shown in the appendix in terms of four graphs;

- firstly the linear envelope representation of sEMG for each muscle,
- secondly, the time frequency representation of sEMG for each muscle,
- thirdly, the instantaneous mean frequency response from each muscle,
- and finally, the graph of co-activation between tibialis anterior and gastrocnemius.

The next four subsections describe how these graphs are presented and are shown in Figure 38, Figure 39, Figure 40 and Figure 41.

4.2 Presentations of Graphs

4.2.1 Linear Envelope Representation

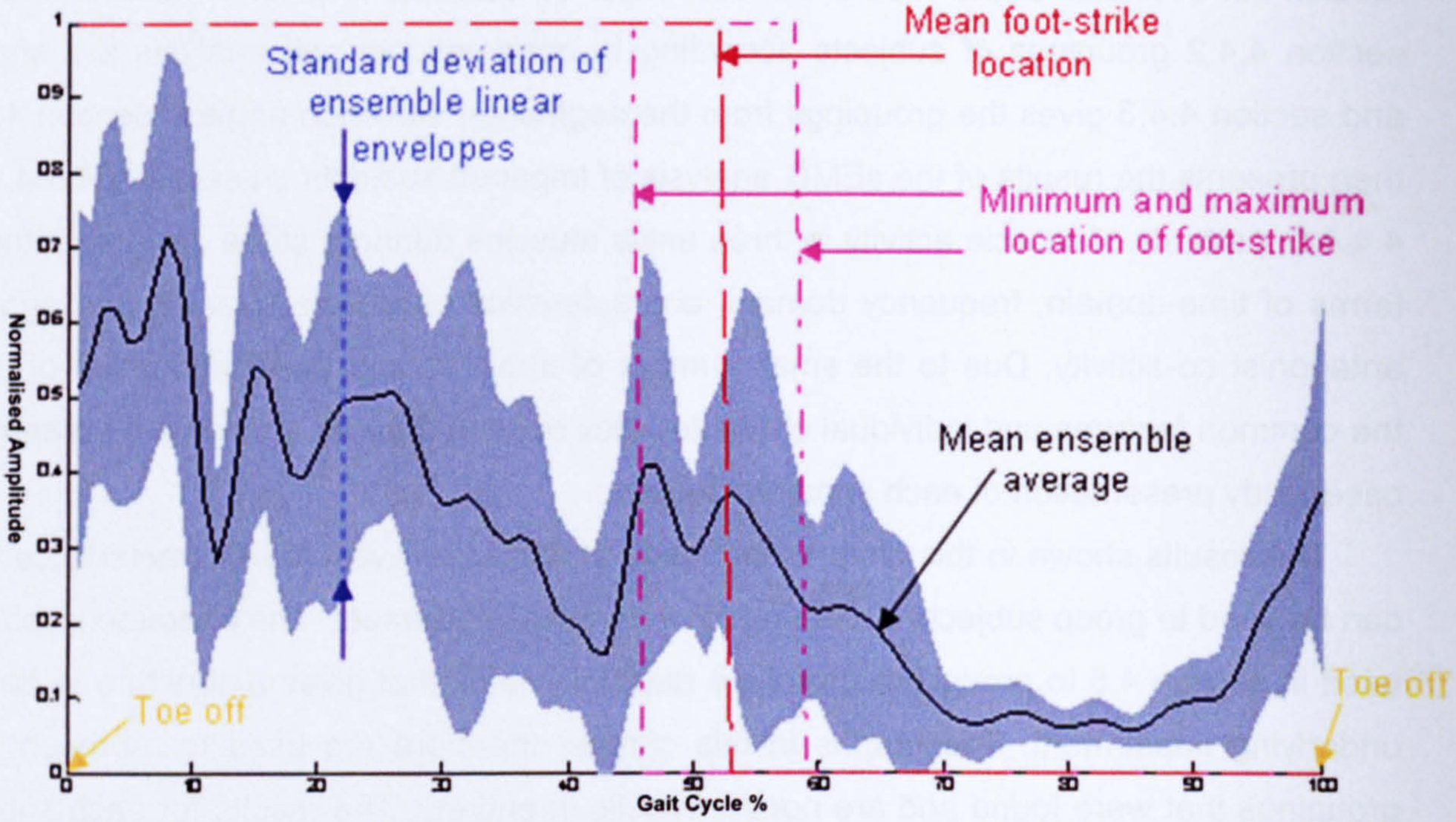

Figure 38 Explanation of the linear envelope representation used within the results chapter of this thesis

Figure 38 shows how the linear envelope is represented. The linear envelope is represented as the mean ensemble average of the normalised linear envelope (normalised to maximum of within ensemble). The gait cycle is represented from toe-off to toe-off (0-100%). Foot-strike is given by the mean foot-strike (red line) and the maximum and minimum foot-strike (mauve line).

4.2.2 Time-frequency Representation

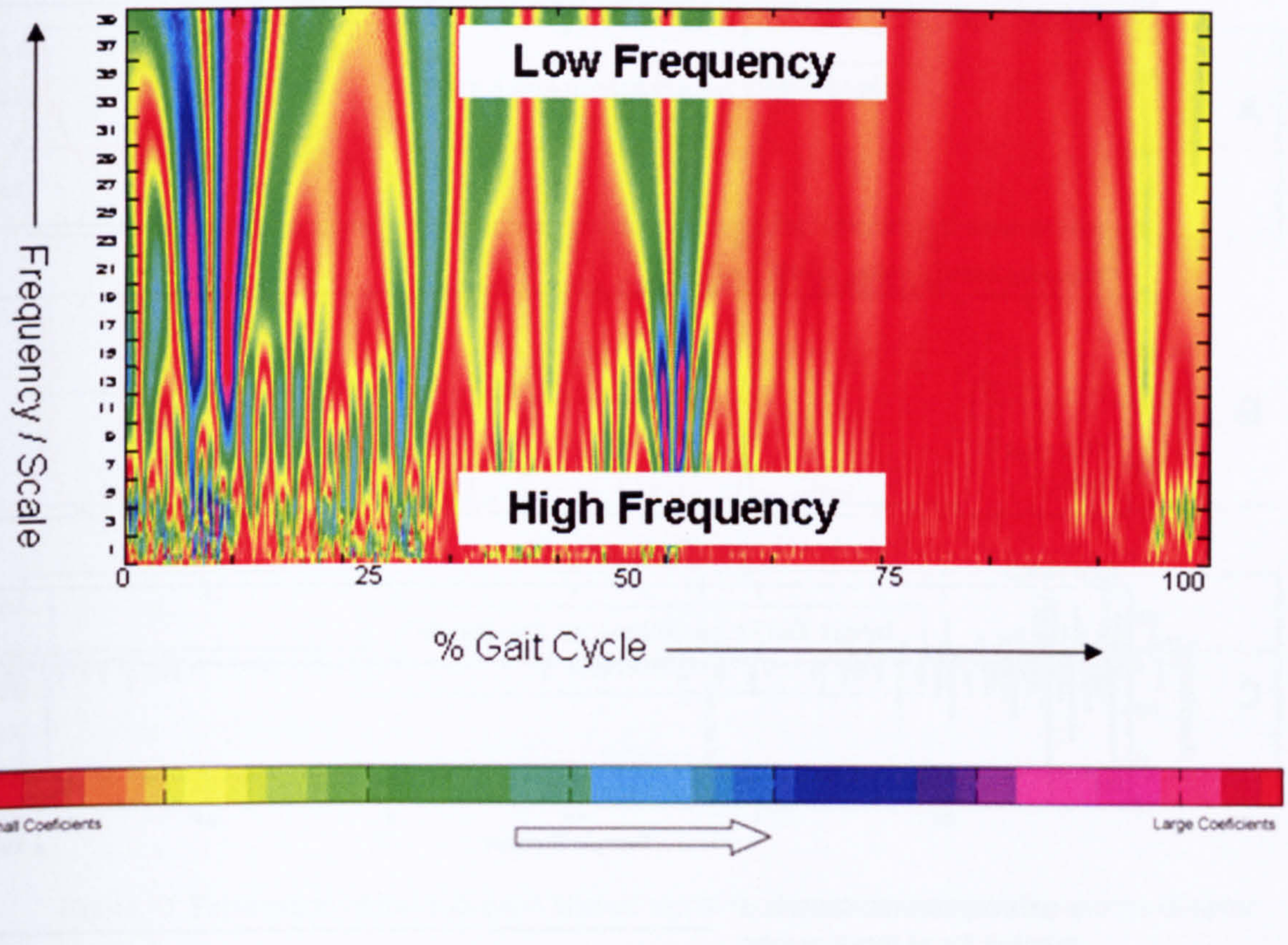

Figure 39 Explanation of the time-frequency representation used in the results chapter of this thesis

Figure 39 shows how the time-frequency representation is presented in the thesis. From left to right represents a single stride divided into 0-100%. The y-axis displays the wavelet scale applied this relates to frequency high scale values represent low frequencies and vice versa. The amplitude of the wavelet coefficient are represented by the colour and shown in the colour map above.

4.2.3 Instantaneous Mean Frequency

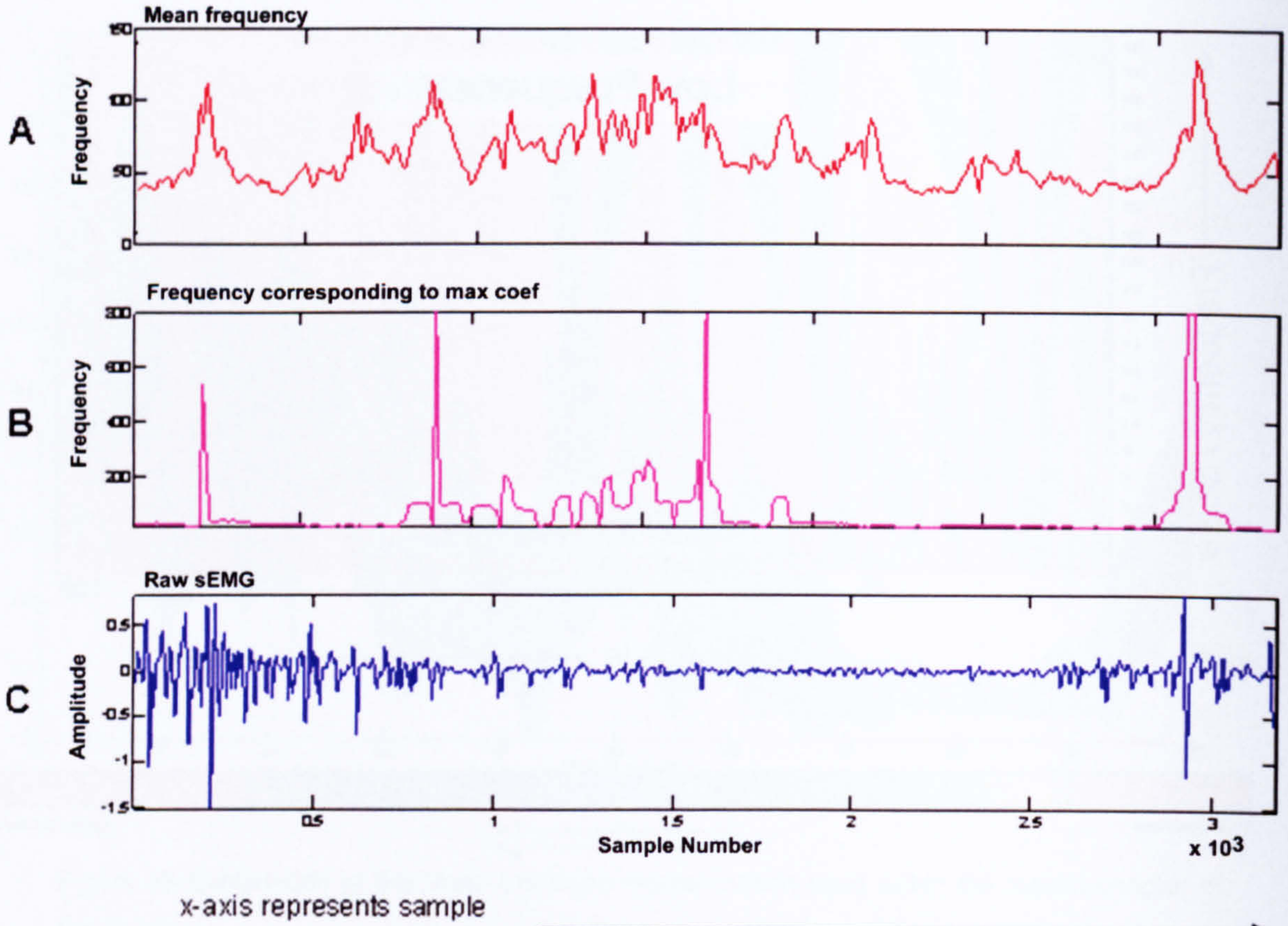

Figure 40 Explanation of the instantaneous mean frequency representation used in the results chapter of this thesis

Figure 40 describes the three graphs which are used to evaluate the change in frequency across a single stride and represented by the mean value. Figure 40 **A** shows the mean frequency for every time epoch of the time frequency diagram. Figure 40 **B** shows the frequency corresponding to the maximum coefficient in the time-frequency diagram. Figure 40 **C** shows the raw sEMG signal representing a single stride.

4.2.4 Co-activation

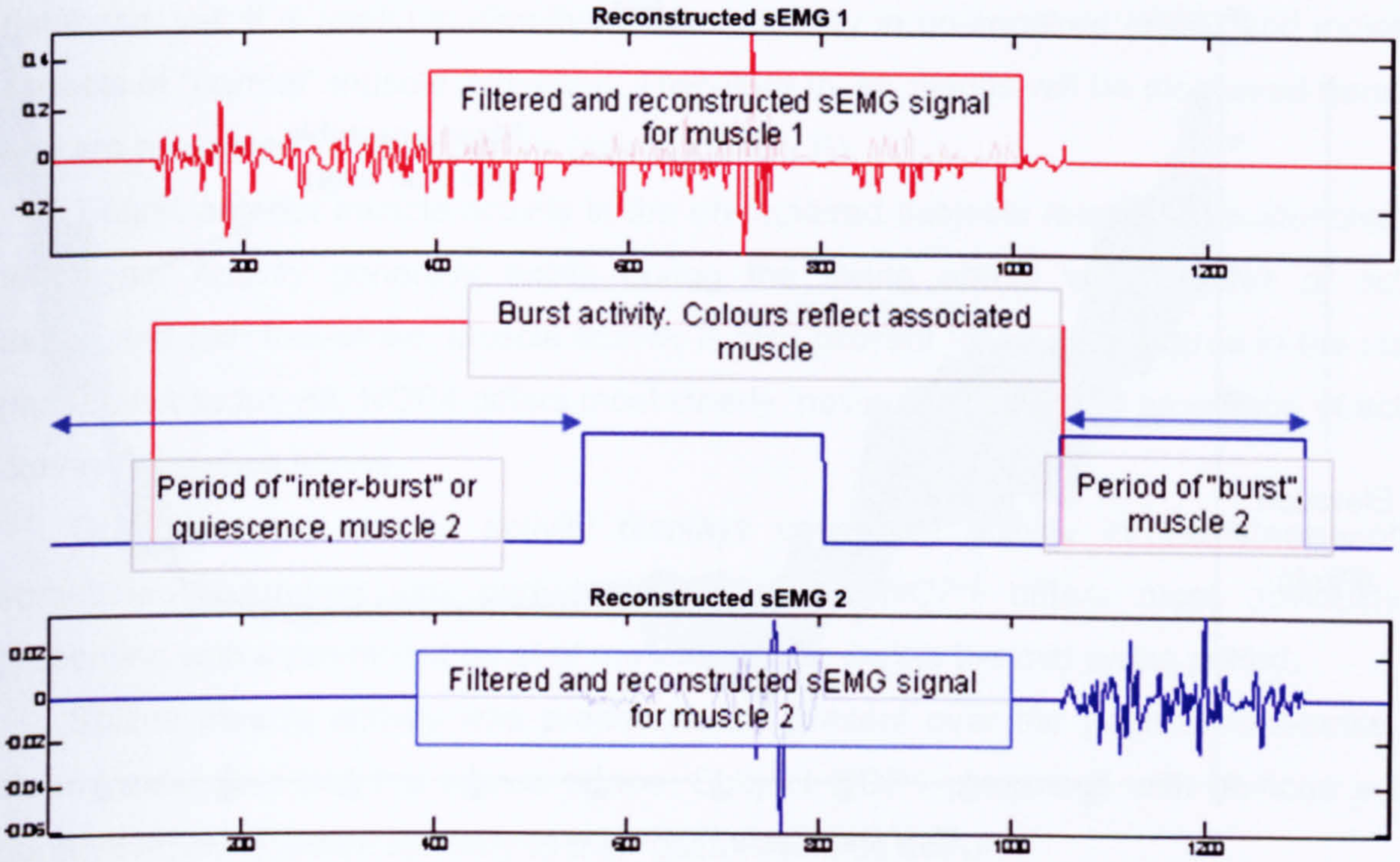

Figure 41 Explanation of the sub-band filtered signal representation used in the results chapter of this thesis.

In Figure 41 two muscles are depicted and shown as their filtered (after n level wavelet decomposition) and reconstructed signal. The centre plot shows the burst activity calculated from the technique, the colours show to which muscle the activity relates. The x axis defines the sample number. The Y axis for all but the centre graph shows amplitude of the raw sEMG.

4.2.5 Segment Elevation Angles

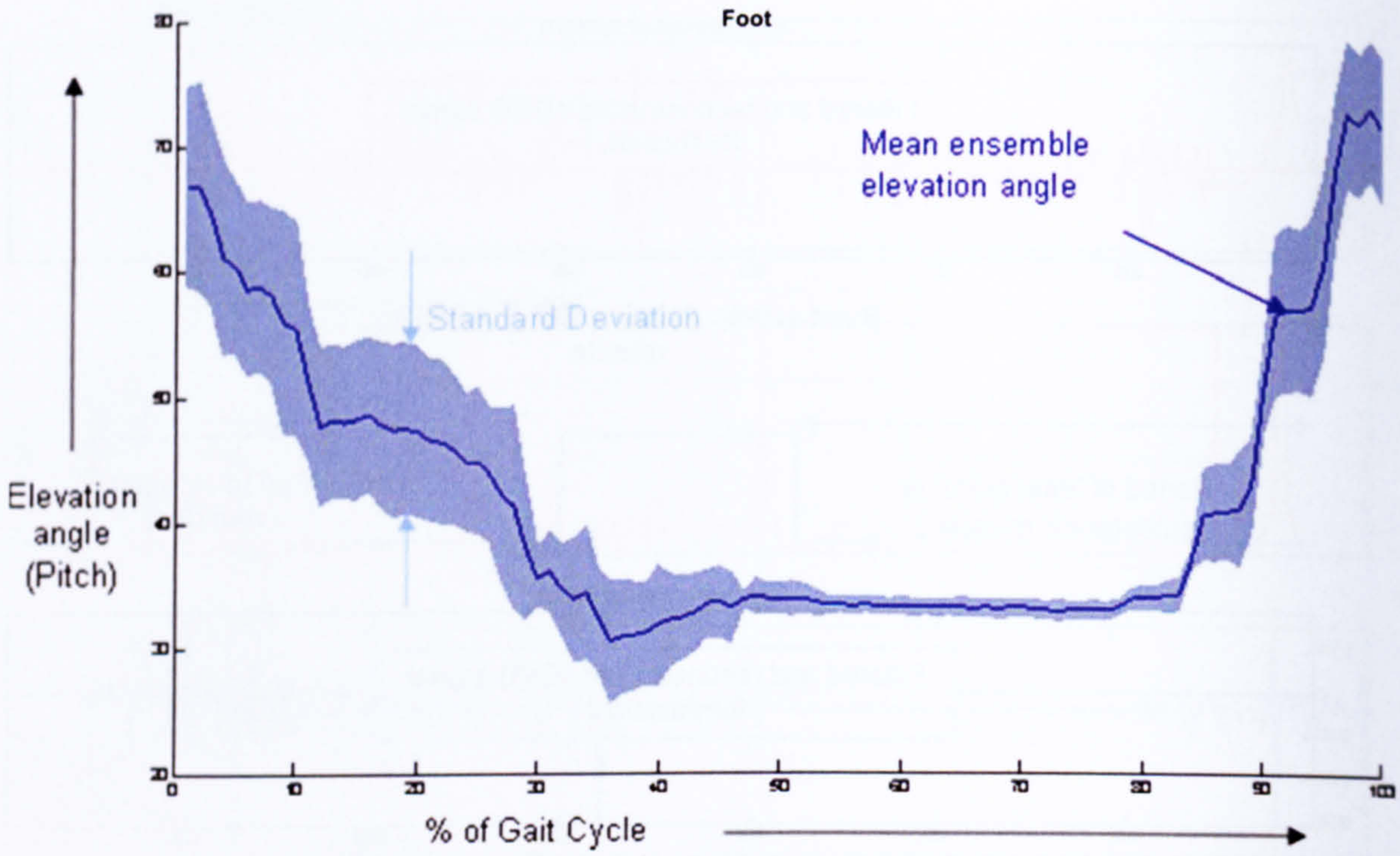

Figure 42 Explanation of the limb segment elevation angles used in the results chapter of this thesis.

In Figure 42 the x-axis is presented as one gait cycle (0 – 100% toe-off to toe-off). The data is presented as the mean ensemble average of n strides with the standard deviation of the data. The pitch of the motion sensor described in Euler angles is given on the y-axis. The graph describes the pitch of a limb segment during a stride. Because the shank articulates about the knee and ankle posterior rotation about the knee will appear the same as anterior rotation about the ankle. As such the direction of rotation is given relative to one of the joints in the text. Note should be taken of the phase in which the activity exits; during the stance phase rotation will about the ankle and thus anterior.

4.3 Un-Impaired Subjects Results

Un-impaired data was collected from four male subjects (average age 30) as part of the gait analysis equipment development. It is not intended to represent a normative database; yet, it is useful in identifying the variability in un-impaired sEMG and indicating aspects of "normal" muscle activation. Therefore these results will be discussed generally and are presented in the appendix (see Appendix B).

Tibialis anterior muscle activity in the un-impaired subjects reveals consistencies and variations. Activity generally exists during the swing phase with a peak of activity associated with foot-strike. Muscle activity is also present to a lesser degree in the stance phase prior to toe-off. NOP4 differs most clearly, having an increased proportion of activity during the stance phase.

Gastrocnemius muscle activity displays consistent activity in the stance phase sometimes extending into early stance. Subject NOP1 differs most obviously by presenting with a prominent burst of muscle activity during the mid swing period.

Soleus muscle activity was predominantly present over the point of foot-strike and clearly extending into the stance phase. Subject NOP1 presented with obvious activity during the swing phase similarly to their gastrocnemius activity.

Similarly to the linear envelope representation the time-frequency representation displays similarities in phasing of muscle activity for the respective muscles. Where prominent bursts of activity are present it generally extends across frequency bins and is distinct from periods of sEMG quiescence. However, the time-frequency representation displays variations in the structure of the muscle activity not communicated by the linear envelope representation specifically that phases of activity are not homogenous in nature. The patterns of onset and off-set of activity varies in subjects.

Patterns of mean frequency activity relate to the periods of raw sEMG activity. Some subjects displayed additional increases in instantaneous mean frequency during periods of quiescence with respect to the linear envelope.

4.4 Impaired Subjects Results

4.4.1 Participant Information

The following details each of the subjects making up the impaired group;

- CVA03 is a 62 year old male suffered a right side cerebral vascular accident (CVA – embolic) in 2000 resulting in left side hemiplegia. He does not use a stick and can walk approximately 100 metres un-aided.
- CVA06 is a 67 year old male suffered a right side CVA, subarachnoid haemorrhage, in 1996 and has been left with severe hemiparesis on the left side. Uses a stick and can walk approximately 500 meters.
- CVA07 is a 48 year old male patient suffered a right sided CVA (embolic) which occurred in 2000 and suffers left hemiplegia. The patient can walk ¾ of a mile unaided.
- CVA10 is a 65 year old male patient who suffered a left side CVA (embolic) resulting in right side hemiplegia. The patient can walk only a short distance, 100 metres, un-aided.
- CVA11 is a 51 year old female who suffered a right side CVA, inter-cerebral haemorrhage, in 1993 and suffers with left hemiplegia. The patient can walk short distances un-aided.
- CVA14 is a 68 year old male who suffered a left side CVA (embolic) in 1999 and suffers right side hemiplegia. The patient sometimes requires a walking stick and can walk approximately ½ a mile unaided.
- CVA15 is a 75 year old male who suffered a left side CVA (embolic) in 1999 and suffers from a right side hemiplegia. The patient can walk ¼ to ½ a mile unaided.
- CVA05 – The data from this subject was unusable due to technical failure.
- CVA02 – The subject withdrew from the study as they felt they could not complete the minimum number of walks safely.
- CVA00 – The subject withdrew from the study due to illness.

4.4.2 Observational Gait Analysis

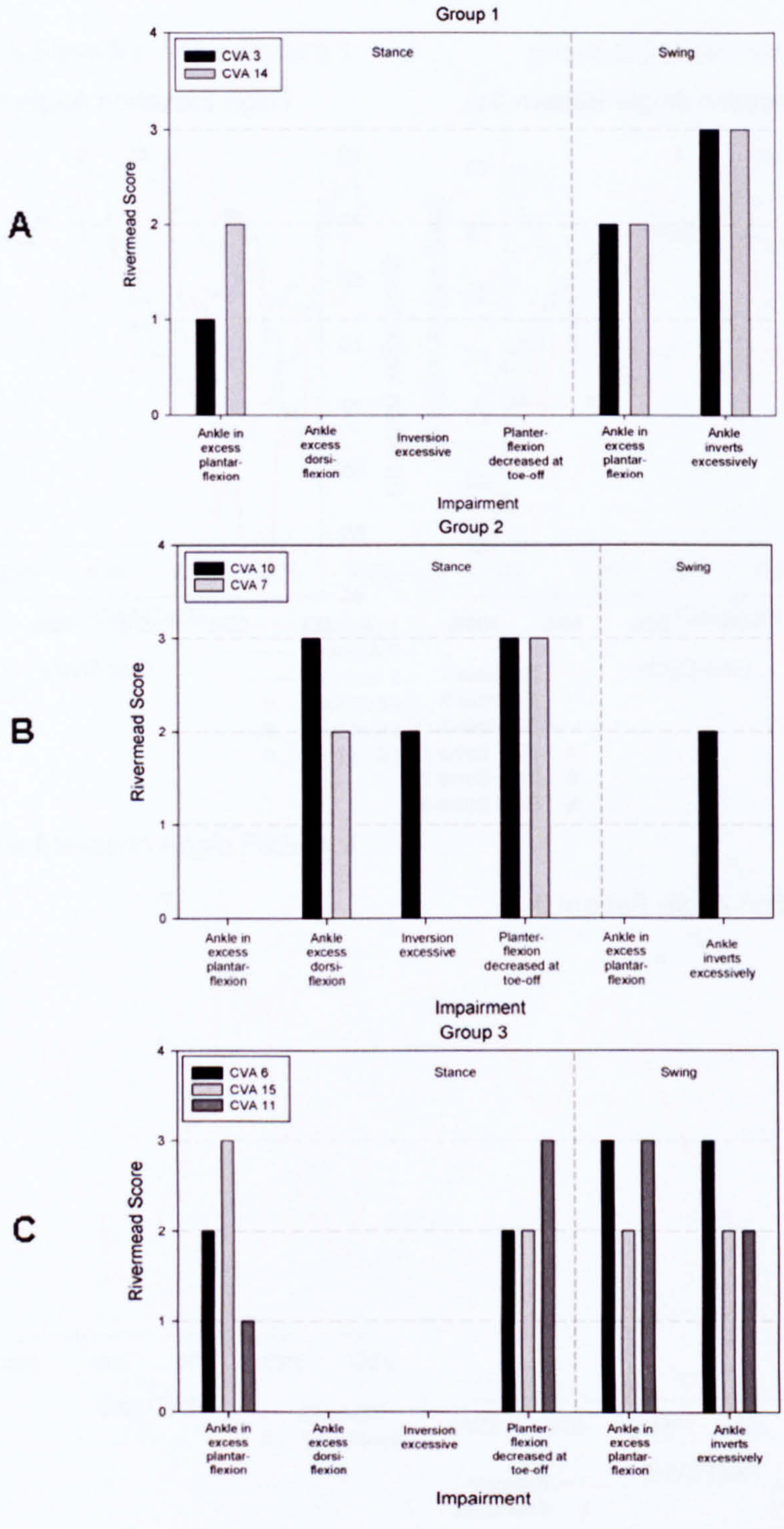

Figure 43 Observational Gait analysis Patterns and Groups

Three groups are presented from the observational gait analysis. The ankle impairments distinguish most from patients and are shown in Figure 43. Group 1 shows plantar flexion in stance but no decreased plantar flexion at toe off (**A**). Group 2 shows excess dorsiflexion in stance but with no excess planter flexion during the stance or swing phase but with decreased plantar flexion at toe off (**B**). Group 3 shows excess plantar during stance but with decreased plantar flexion at toe off (**C**).

4.4.3 Limb Segmental Elevation Angles

4.4.3.1 Thigh

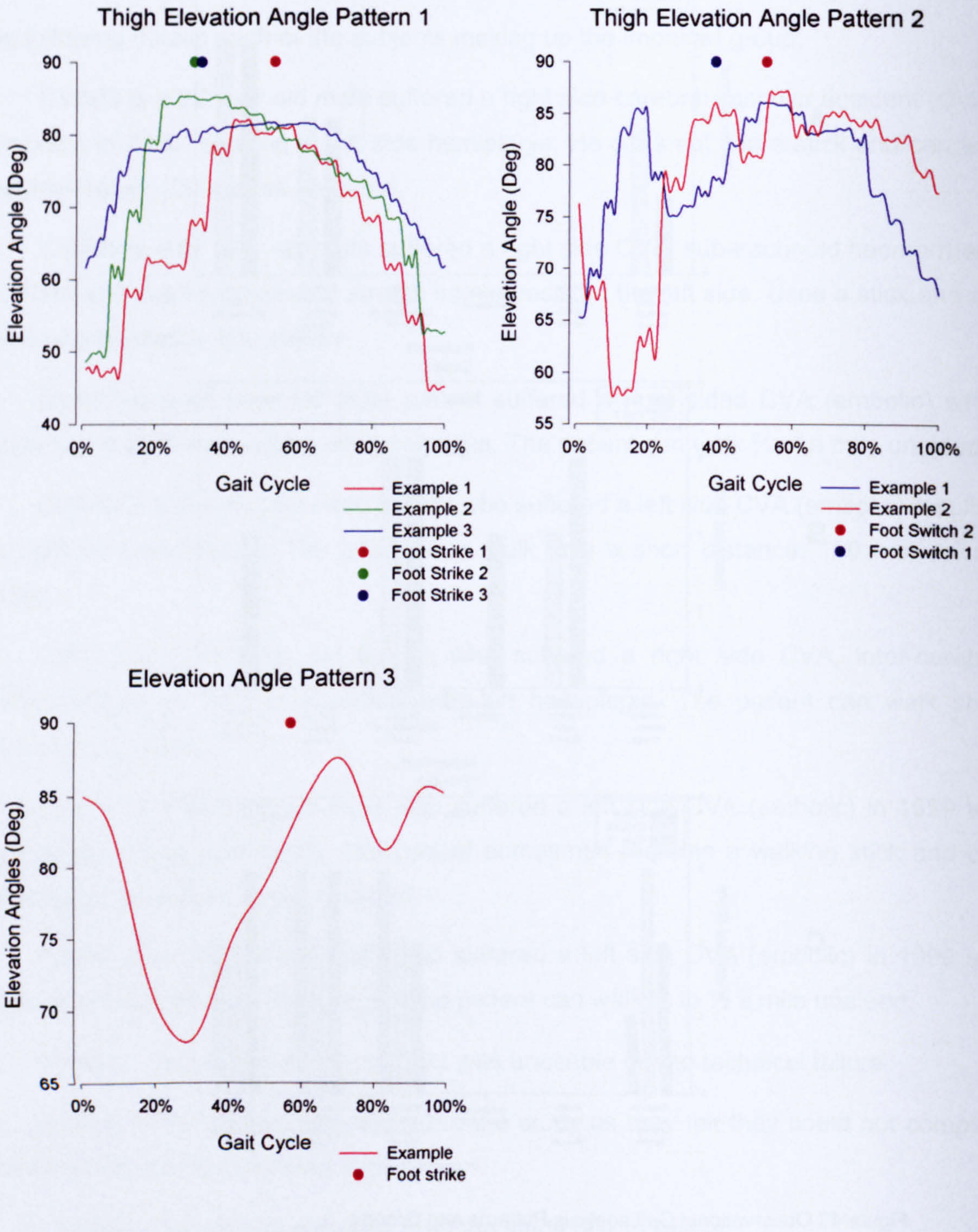

Figure 44 Thigh elevation patterns and groups

Three patterns of thigh elevation angle are shown in Figure 44. The patterns can be summarised as a rapid increase in angle followed by a gradual decline. The second pattern shows a similar pattern as to one but with a short period of decreased angle during the swing phase. Pattern 3 shows a gradual increase in angle throughout swing with a perturbation during late stance.

4.4.3.2 Shank

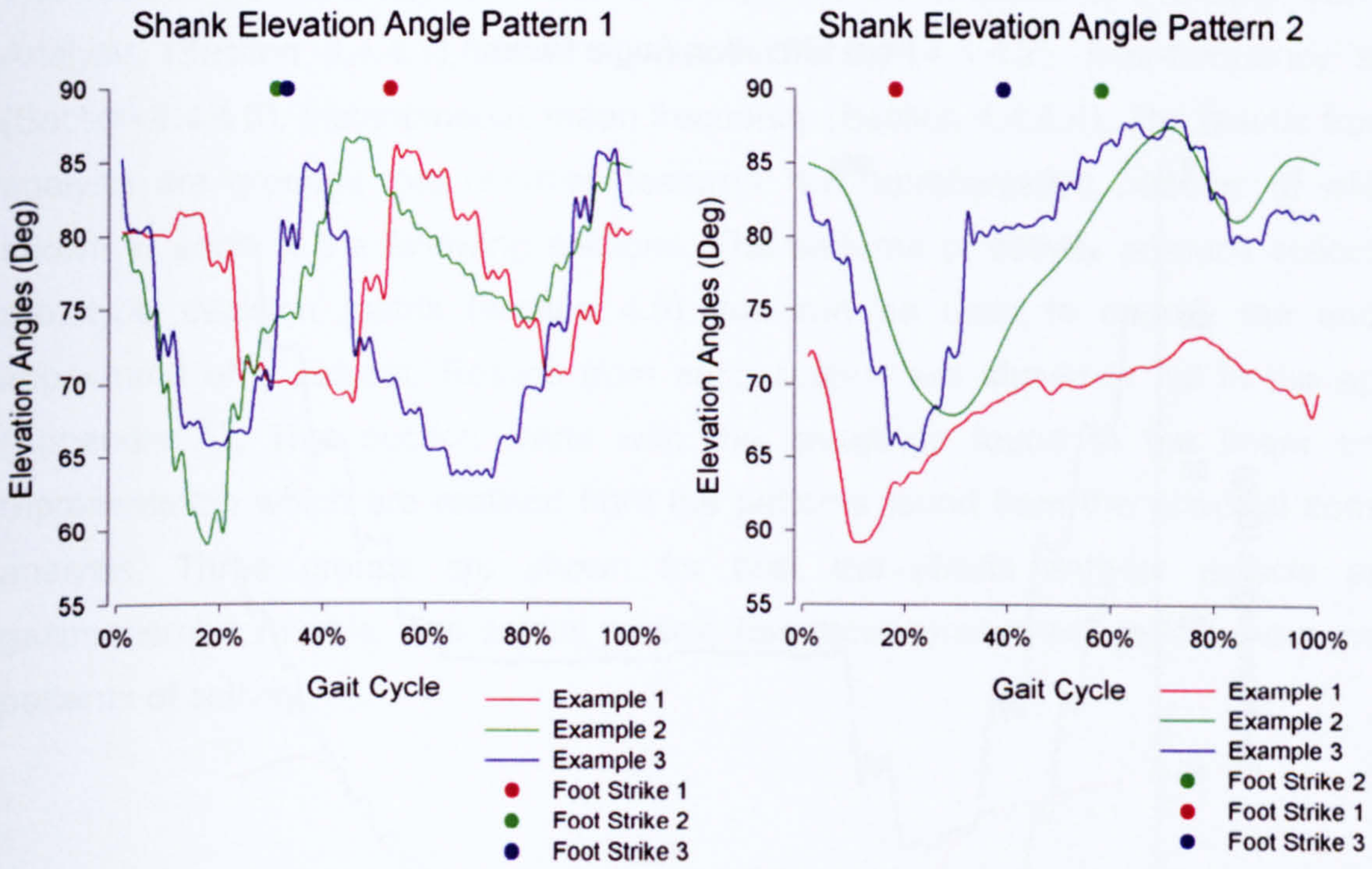

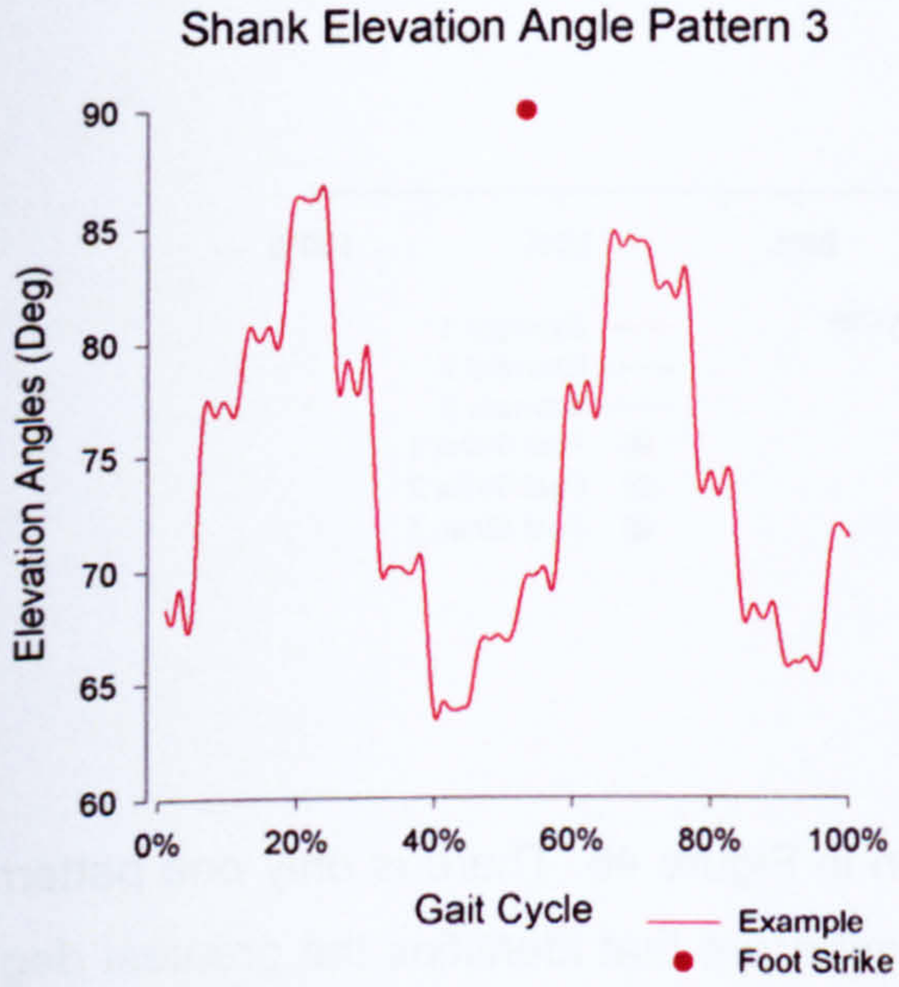

Figure 45 Shank elevation angle patterns

The patterns observed from the shank elevation angles are shown in Figure 45. Pattern 1 shows a decrease in elevation angle during the swing phase and a second reduction in angle during the stance phase. Pattern 2 is similar to pattern 1 except that the reduction in elevation angle during the stance phase is much smaller. Pattern 3 is the inverse of pattern 1 with two increases in elevation angle during stance phase and swing phase respectively.

4.4.3.3 Foot

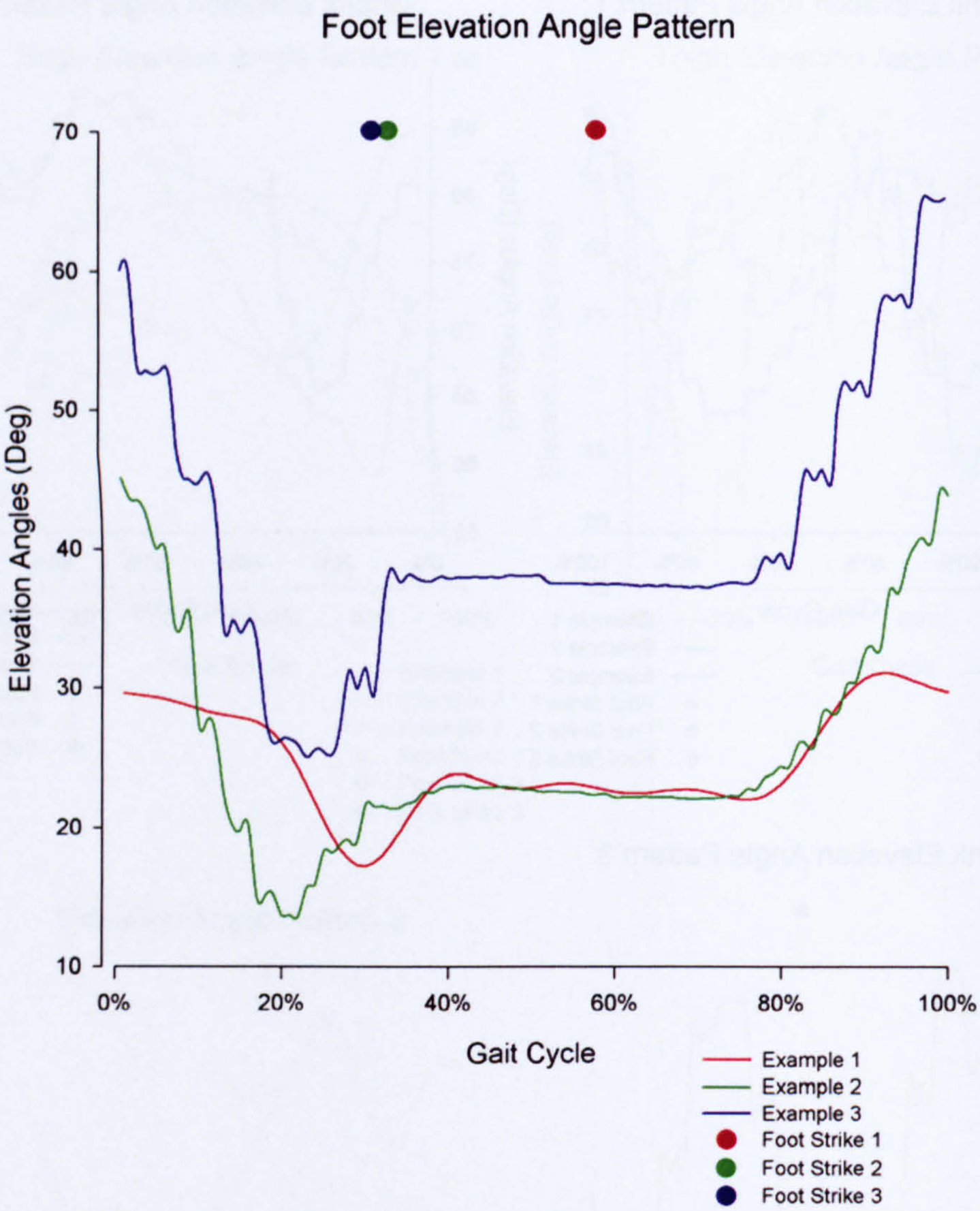

Figure 46 Foot elevation angle pattern

The patterns of foot elevation angle are shown in Figure 46. There is only one pattern of foot elevation angle identified that includes a minimum that identifies the greatest degree of plantar flexion. The rapid increase in elevation angle during swing phase, however, does always relate to foot strike and passive plantar flexion.

4.4.4 Surface Electromyography

The results for the analysis of sEMG are presented in terms of Principal Component Analysis (Section 4.4.4.1), linear envelope (Section 4.4.4.2), time-frequency analysis (Section 4.4.4.3), Instantaneous mean frequency (Section 4.4.4.4). The results from each analysis are grouped into common features, the representative patterns of which are shown in each of the following sections. The patterns of activity produce collectively a prototype decision matrix (section 4.5) that can be used to specify the underlying impairment of a subject. Results from each subject are shown in full in the appendix (Appendix A). This section starts with the groupings found in the linear envelope representation which are realised from the patterns found from the principal component analysis. Three groups are shown for both the tibialis anterior muscle and the gastrocnemius muscle. The soleus muscle has more groups that reveal more individual patterns of activity.

4.4.4.1 Principal Component analysis

4.4.4.1.1 Tibialis Anterior

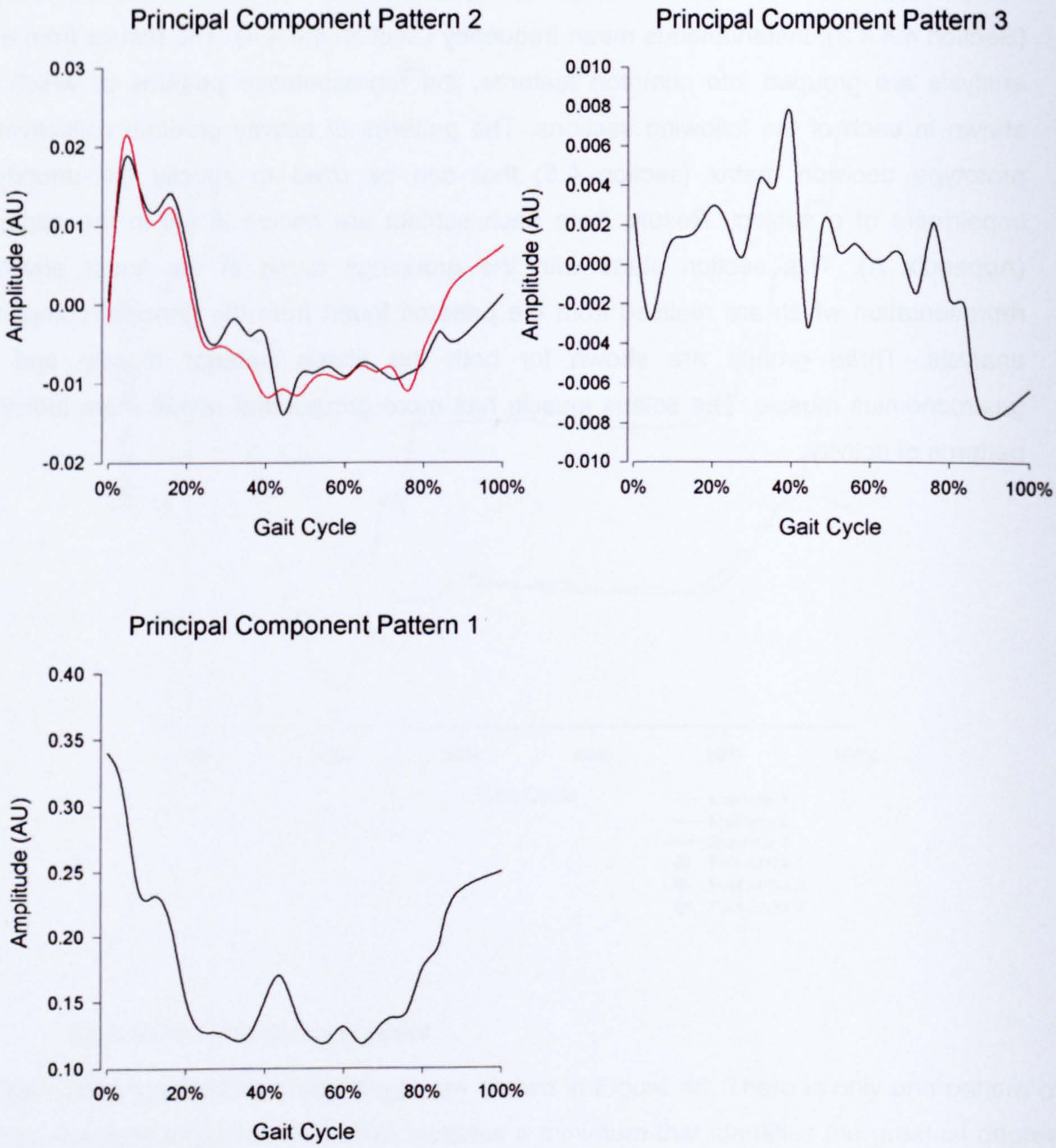

Figure 47 Principal component analysis patterns of Tibialis Anterior muscle

Figure 47 reveals the patterns of tibialis anterior muscle activity in term of the linear envelope representation generated from principal component analysis. Pattern 1 shows activity in the swing phase and during terminal stance, there is an additional burst of activity foot strike. Pattern 2 shows a large peak of activity in early stance that gradually reduces over the gait cycle and increases subtly during terminal stance. Pattern 3 shows minimal activity in stance and swing but with a large increase in activity at foot strike.

4.4.4.1.2 Gastrocnemius

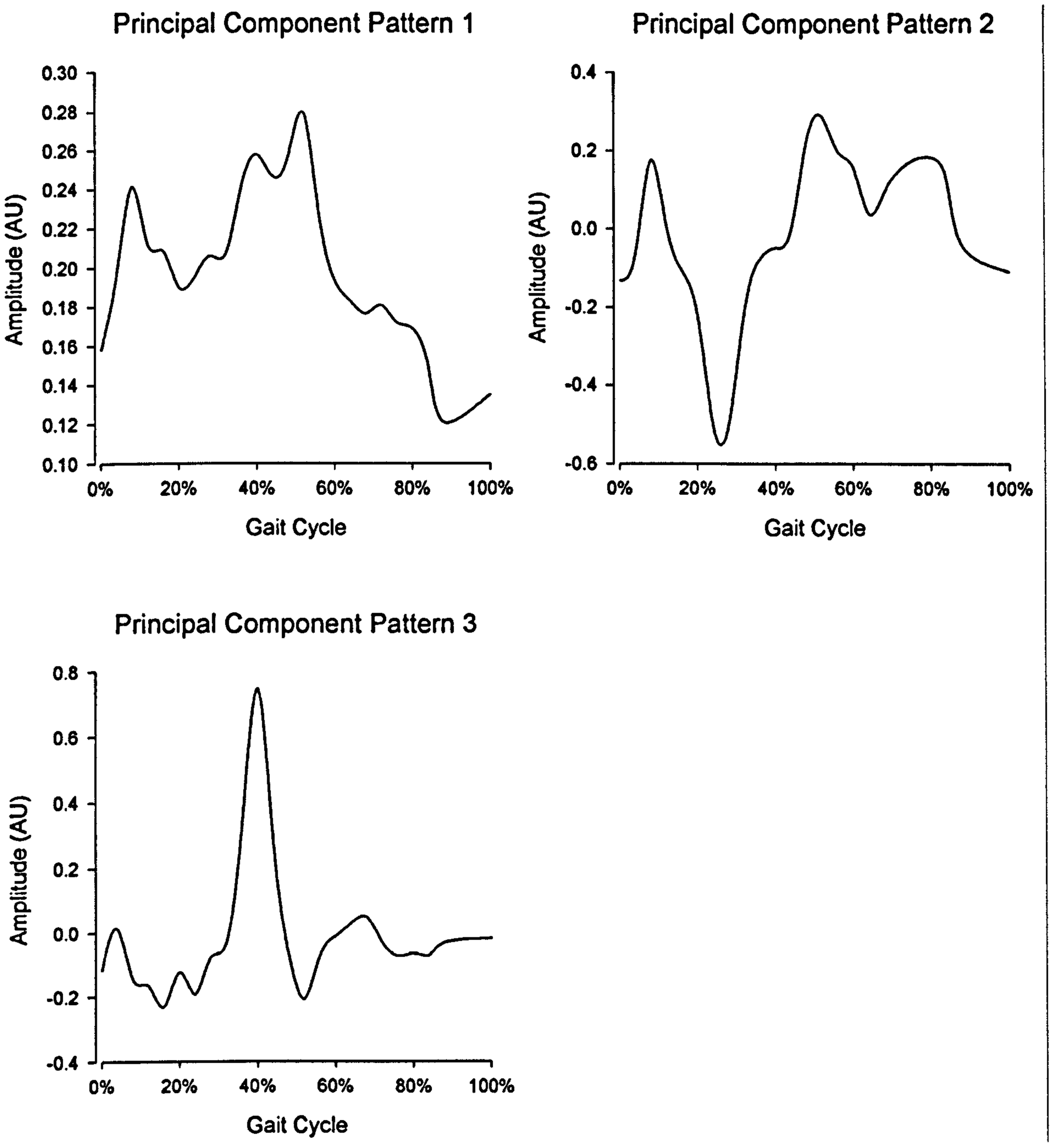

Figure 48 Principal component patterns for Gastrocnemius muscle

Figure 48 show the patterns of gastrocnemius muscle activity in terms of the linear envelope representation generated form principal component analysis. Pattern 1 shows continuous activity throughout the stride predominating in the swing phase and mid stance. Pattern 2 shows a pattern of activity in swing phase and another burst of activity in the stance phase. Pattern 3 shows a significant burst at or around the point of foot strike. This pattern also shows a small amount of activity during the stance phase.

4.4.4.1.3 Soleus

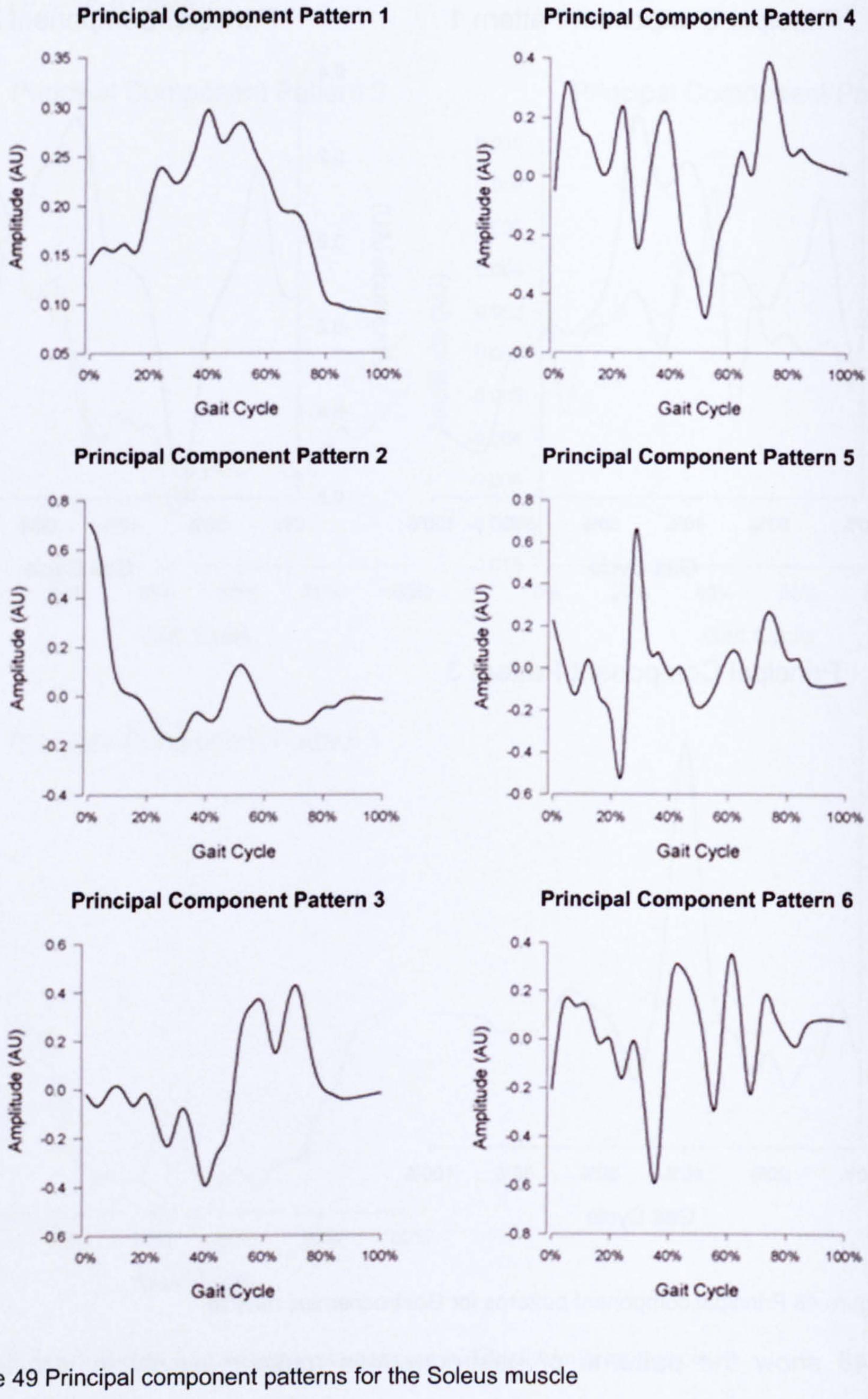

Figure 49 Principal component patterns for the Soleus muscle

Figure 49 shows the patterns of activity in terms of linear envelope of the soleus muscle generated form the principal component analysis. There are far more patterns of activity for the soleus muscle showing more independent characteristics. However, the three primary patterns are; continuous activity that peaks at foot strike. Pattern 2 shows activity in early swing phase and a second peak mid way through the gait cycle. Pattern 3 shows activity extending from foot strike.

4.4.4.2 Linear Envelope

4.4.4.2.1 Tibialis Anterior

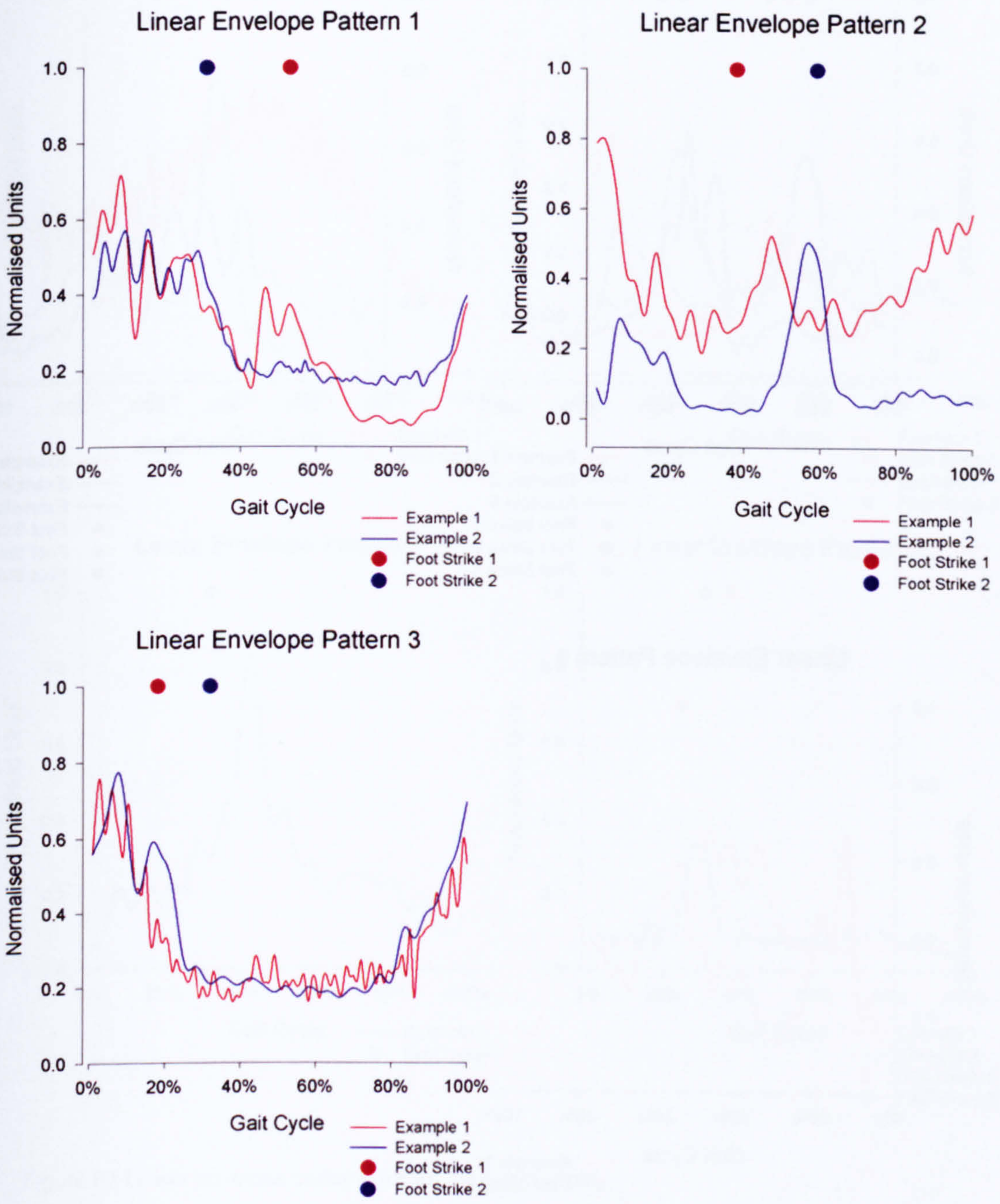

Figure 50 Linear envelope patterns for the Tibialis Anterior muscle

Figure 50 shows examples of the linear envelope patterns found for the tibialis anterior muscle and mirrored by the patterns shown from the principal component analysis (see Figure 47). Pattern 1 shows a rapid onset over the stance – swing phase transition followed by a gradual reduction in activity over the swing phase. Pattern 2 shows activity in early swing phase with a burst of activity at foot strike and some activity during the stance phase. Pattern three shows activity across the stance – swing phase transition extending into the swing phase.

4.4.4.2.2 Gastrocnemius

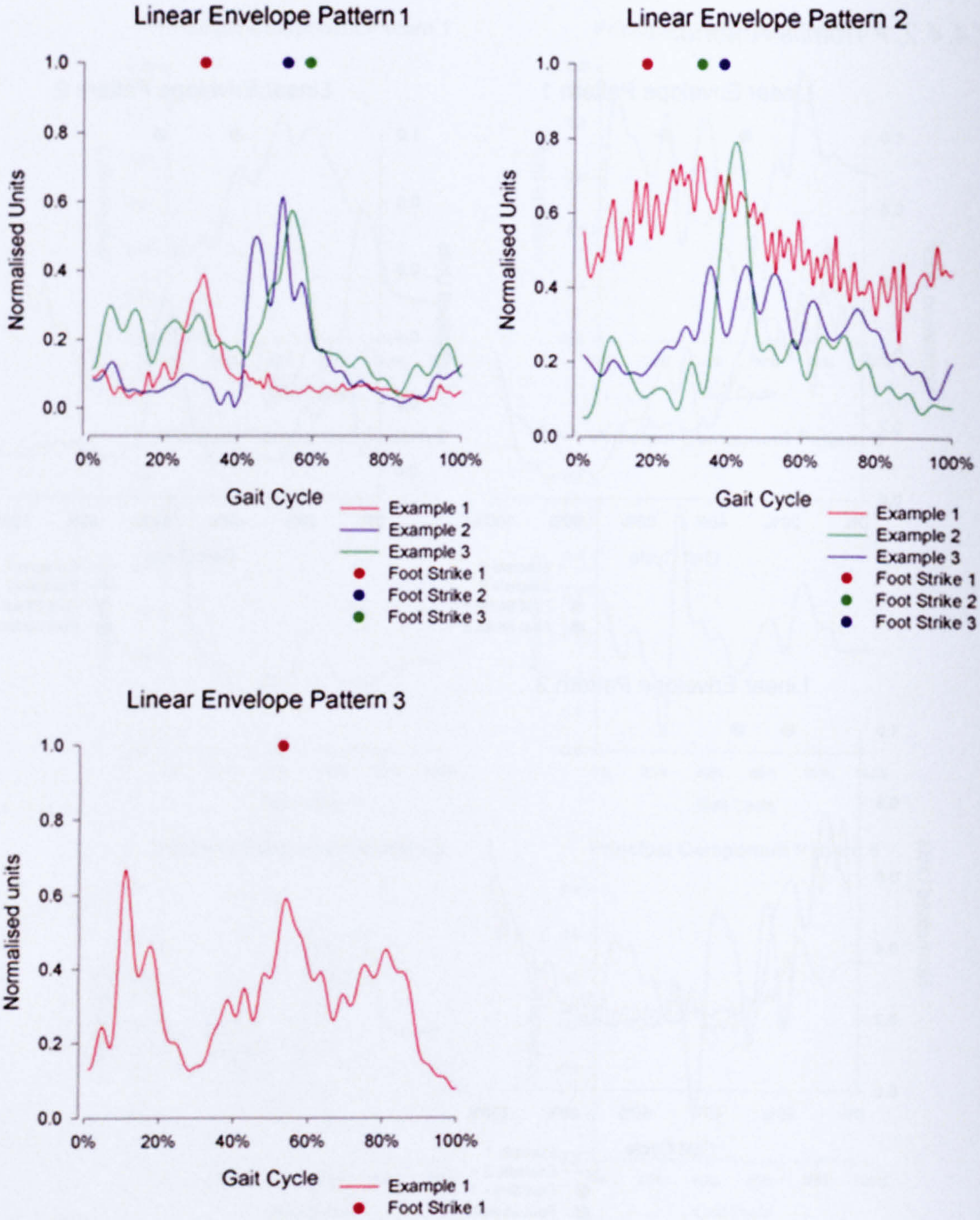

Figure 51 Linear envelope patterns for the Gastrocnemius muscle

Figure 51 shows examples of linear envelope patterns found from the gastrocnemius muscle. These patterns are also shown in Figure 48 from the principal component analysis. Pattern 1 shows a prominent burst of activity at foot strike with a small proportion of activity sometimes visible in the swing phase. Pattern 2 shows activity across the gait cycle possibly with an increased burst of activity at foot strike. Pattern 3 shows two bursts of activity, first in the swing phase the second continuous in the stance phase.

4.4.4.2.3 Soleus

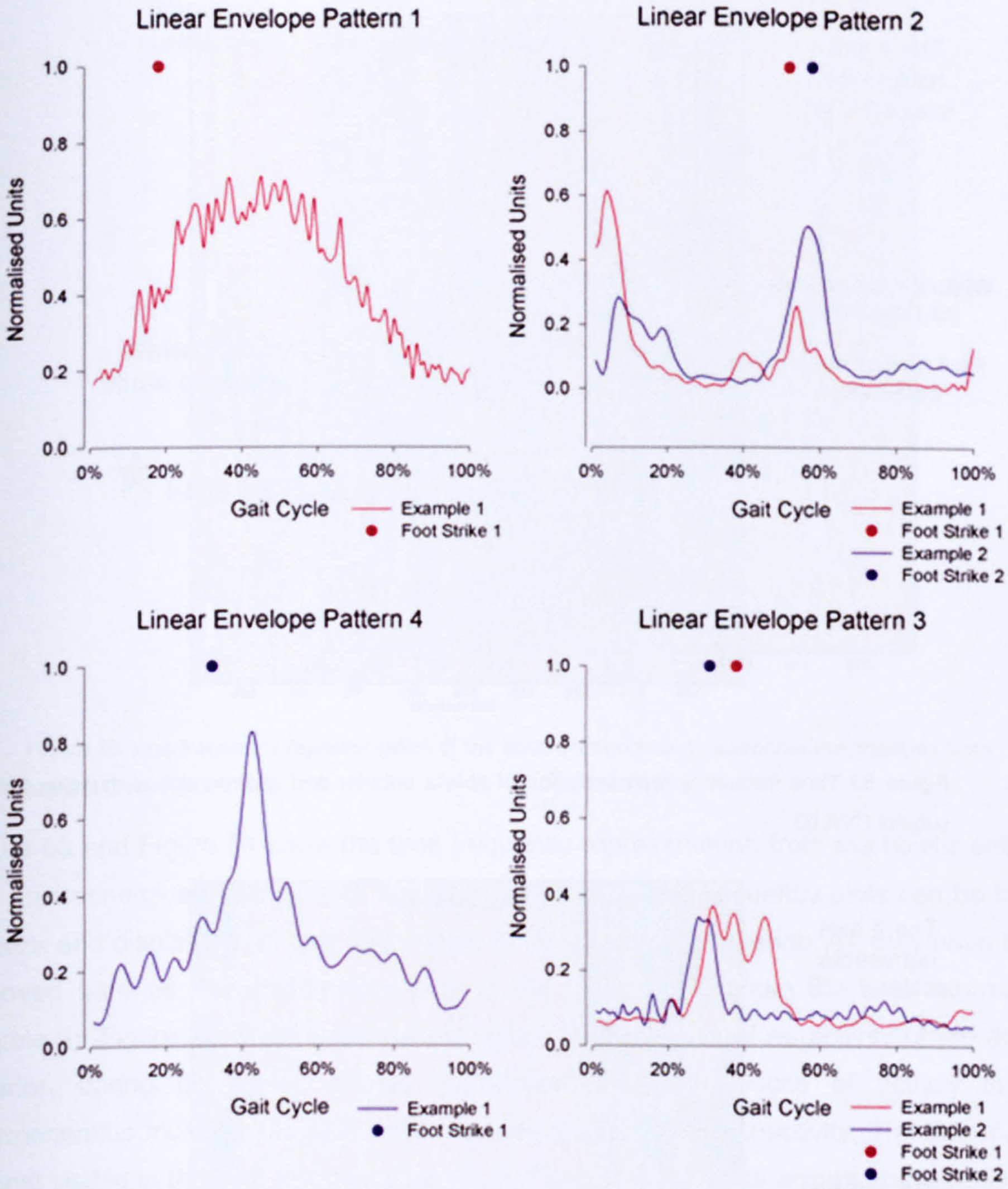

Figure 52 Linear envelope patterns for the Soleus muscle

Figure 52 shows example patterns of soleus muscle activity that reflect the patterns seen from the principal component analysis (see Figure 49). Pattern 1 shows activity that peaks at foot strike that reduces subsequently. Pattern 2 shows a short period of activity in the swing phase and a second period of activity at foot strike but little or no activity in the stance phase. Pattern 4 shows activity in the swing phase and the stance phase but also with a prominent burst of activity at foot strike. Pattern 3 displays a single prominent burst of activity at foot strike that extends slightly into the stance phase. The rest of the stance phase often shows a very small level of activity.

4.4.4.3 Time-Frequency Analysis

The Y axis represents scales 1 - 39

White arrows reveal no coactivity

Blue arrows show co-activity

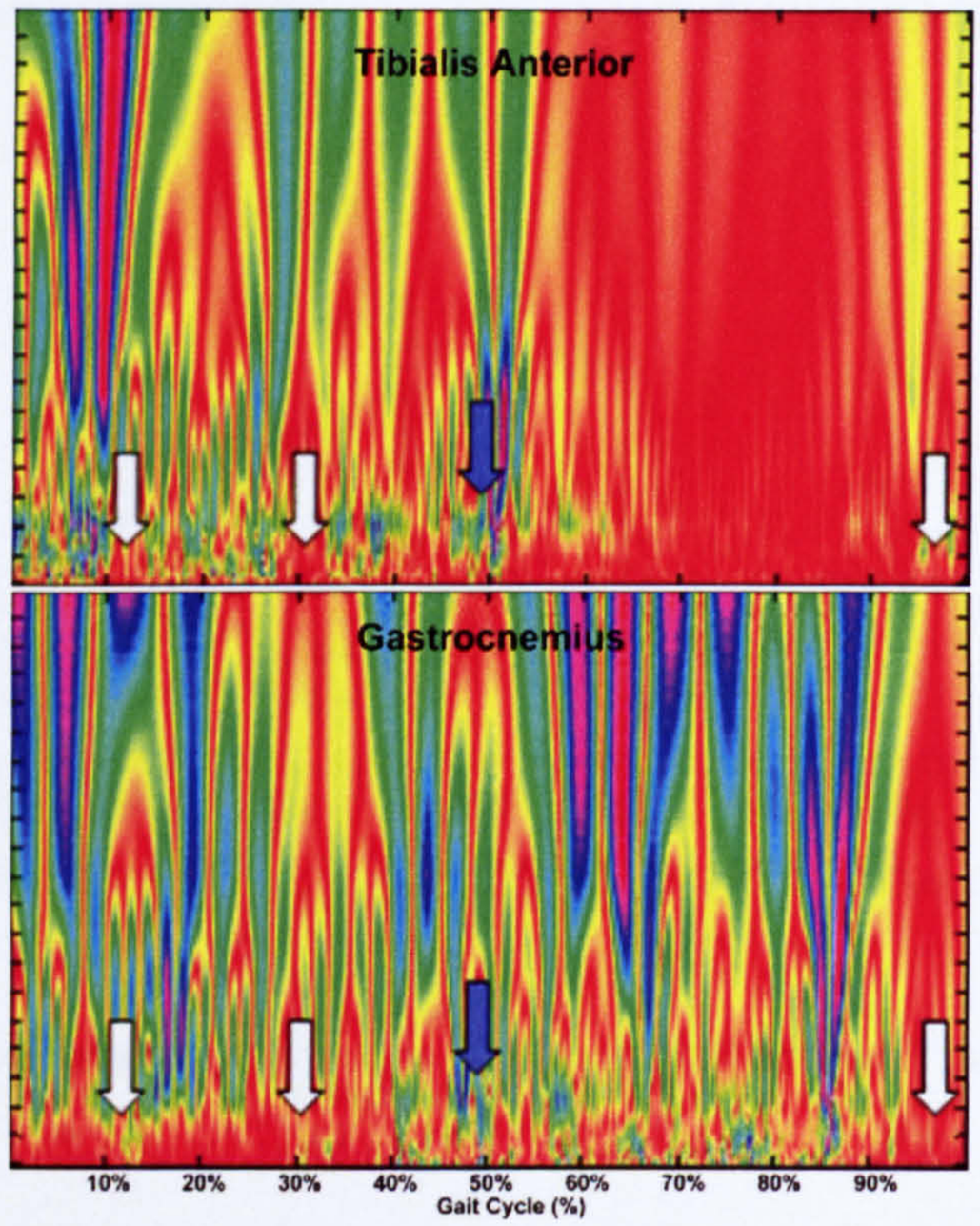

Figure 53 Time frequency representation of tibialis anterior and gastrocnemius muscles from subject CVA 03

The Y axis represents scales 1 - 39

Blue arrows show co-activity

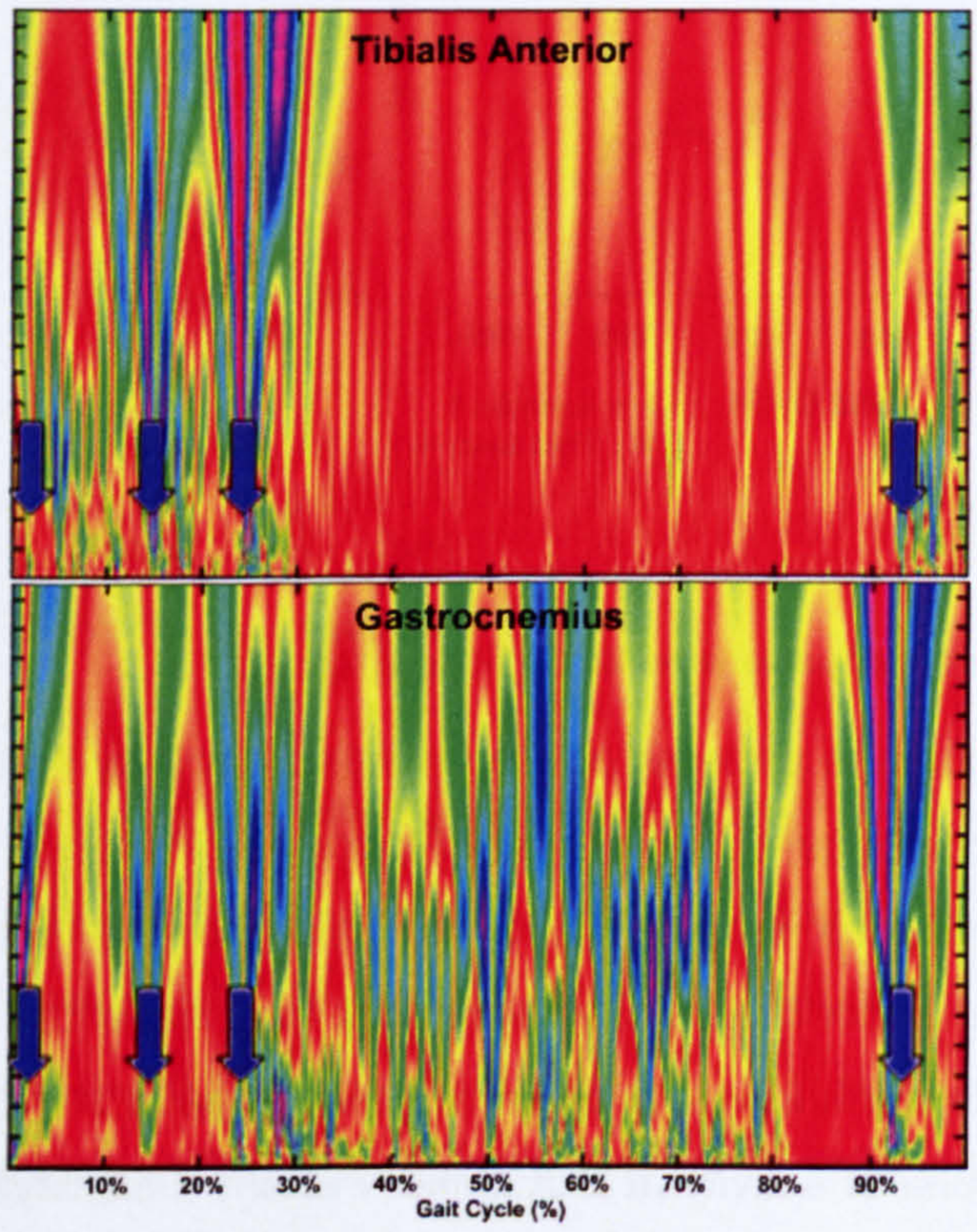

Figure 54 Time frequency representation of the tibialis anterior muscle and gastrocnemius muscle from subject CVA 06

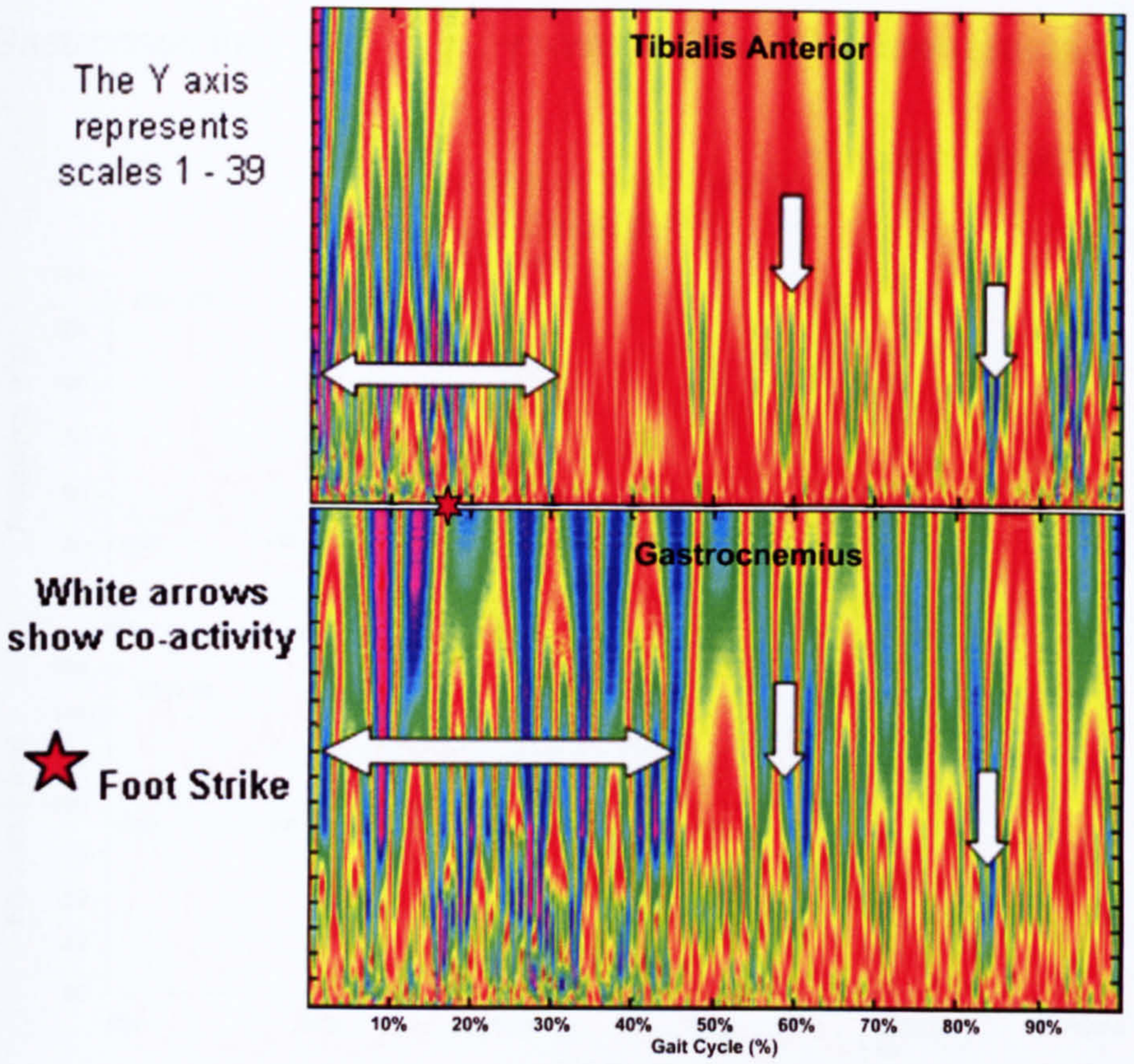

Figure 55 time-frequency representation of the tibialis anterior and gastrocnemius muscles from subject CVA 10

Figure 53 and Figure 54 show the time frequency representation from the tibialis anterior and gastrocnemius muscles from two subjects. These time frequency plots can be found full size and displaying full axis information in the appendix (Appendix A), they have been removed here as the presentation size of the plots would make the axis information illegible. In Figure 53 white arrows show where short periods of no activity of the tibialis anterior, during the swing phase, correspond to short epochs of activity in the gastrocnemius muscle. The blue arrow reveals where there is coactivity. The information is most visible in the high frequency bands. In Figure 54 the white arrows show periods of co-activity in the gastrocnemius muscle during the swing phase and late stance phase. Figure 55 displays a third example of time frequency representation. The pattern reveals increased and sustained, not short epochs, activity across the frequency bands during the swing phase in the gastrocnemius muscle that overlaps periods of activity in the tibialis anterior. In addition epochs of co-activation can be seen over the remainder of the stance phase.

4.4.4.4 Instantaneous Mean Frequency

4.4.4.4.1 Tibialis Anterior

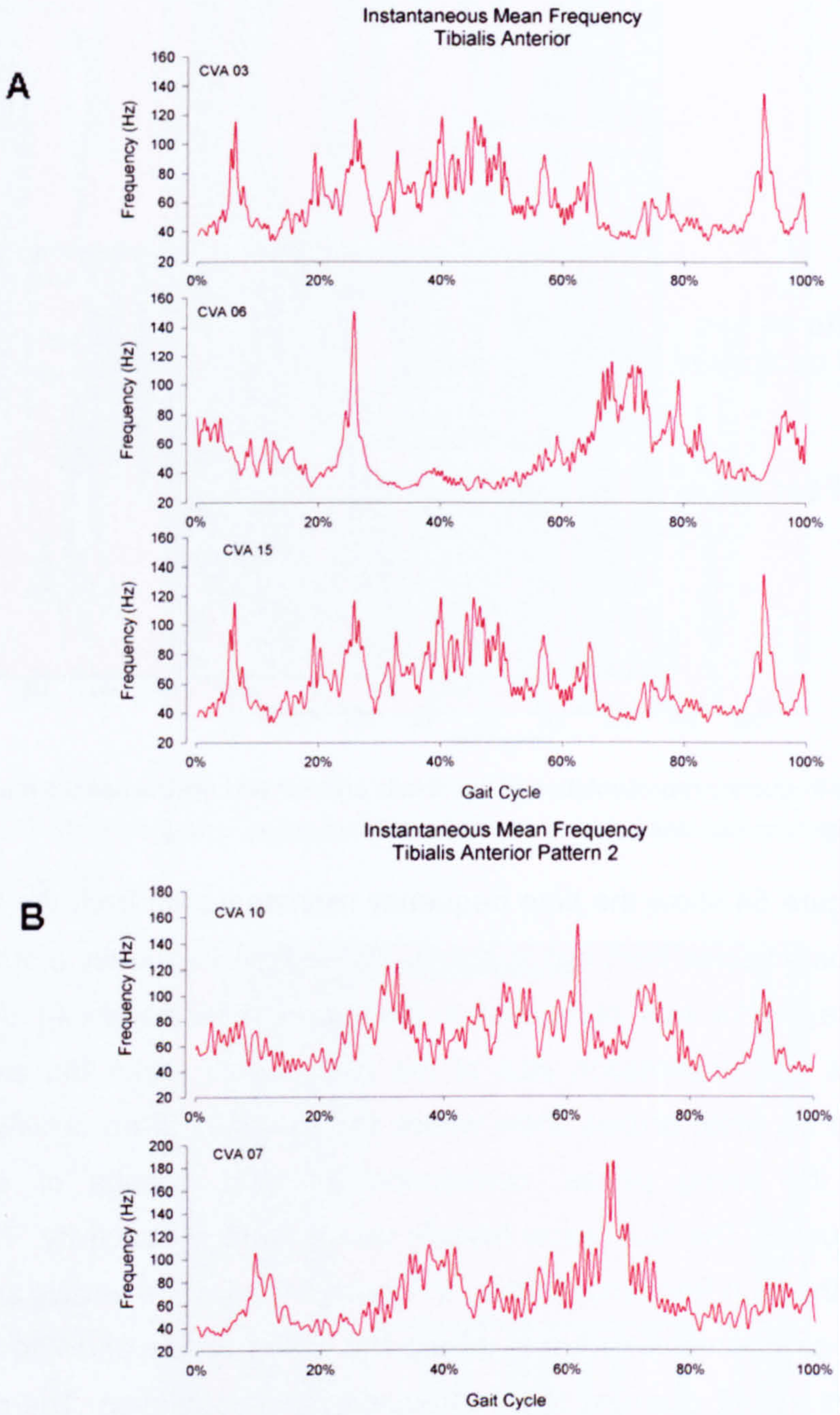

Figure 56 Patterns of instantaneous mean frequency of the tibialis anterior muscle. **A** shows pattern 1. **B** shows pattern 2.

Figure 56 shows examples of the patterns of activity in terms of instantaneous mean frequency for the tibialis anterior muscle. Pattern 1 should be considered in terms of raw sEMG activity. These patterns relate to increases in mean frequency, either in stance phase swing phase or both, but without concomitant increase in raw sEMG activity. Pattern 2 shows a continuous mean frequency activity and with no increase at the key gait events.

4.4.4.4.2 Gastrocnemius

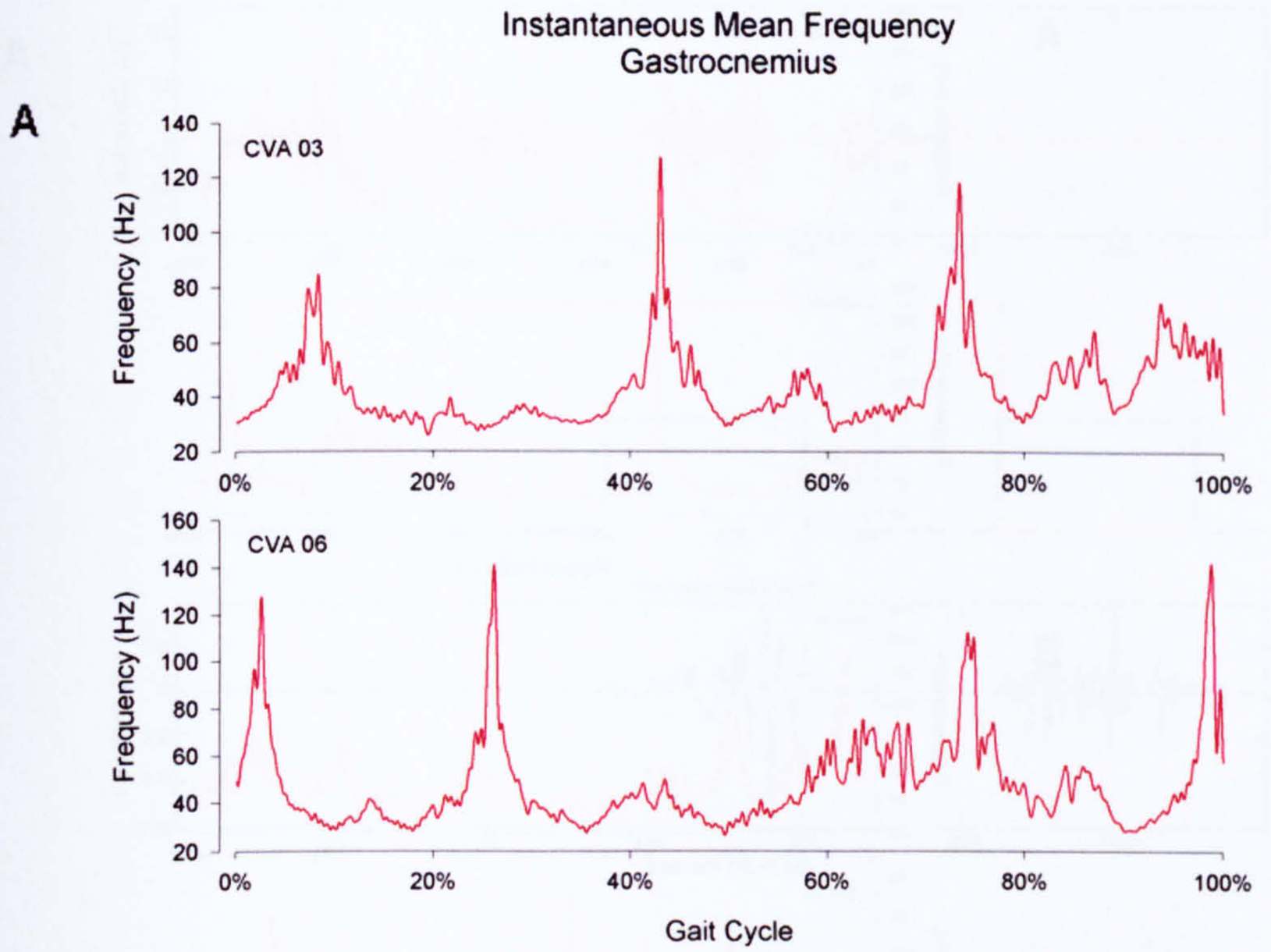

Figure 57 displays instantaneous mean frequency patterns of the gastrocnemius muscle. **A** shows pattern 1. **B** shows pattern 2.

Figure 57 shows the patterns of activity in terms of instantaneous mean frequency from the gastrocnemius muscle. Pattern 1 (**A**) relates to increases in instantaneous mean frequency at key gait events and points at which raw sEMG activity is seen to cease. Pattern 2 (**B**) shows activity that appears continuous but has a pulsatile nature across the stride.

4.4.4.4.3 Soleus

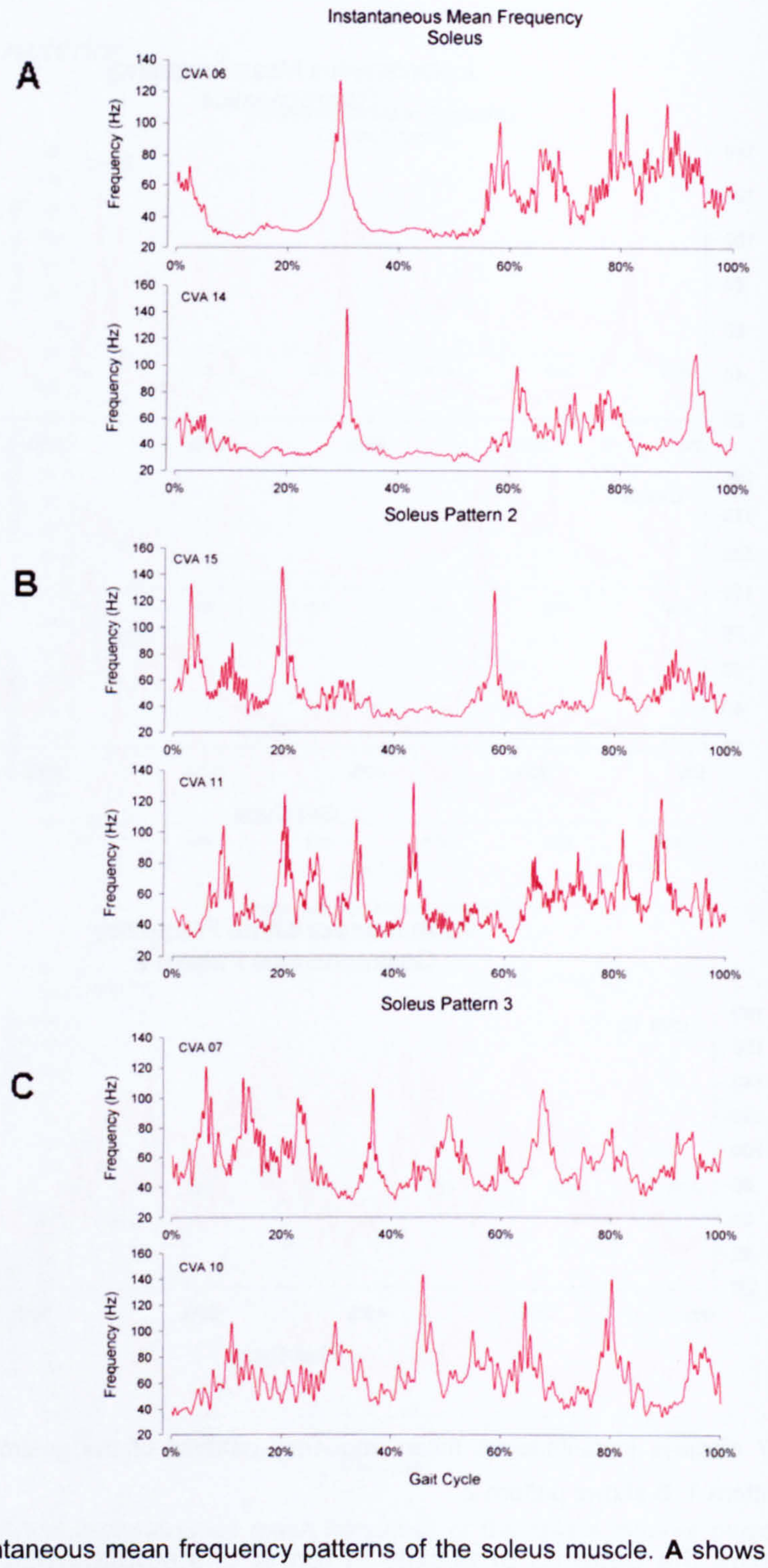

Figure 58 Instantaneous mean frequency patterns of the soleus muscle. **A** shows pattern 1. **B** pattern 2. **C** shows pattern 3.

Figure 58 shows the pattern of activity in terms of instantaneous mean frequency of the soleus muscle. Pattern 1 (**A**) reveals continuous activity in late stance usually accompanied with a prominent burst of activity at foot strike. Pattern 2 (**B**) reveals a pulsatile activity in the swing phase followed by a period of quiescence then some activity, often reduced, in the stance phase. Pattern 3 (**C**) shows a continuous pulsatile activity across the stride.

4.4.4.5 Co-activation Analysis

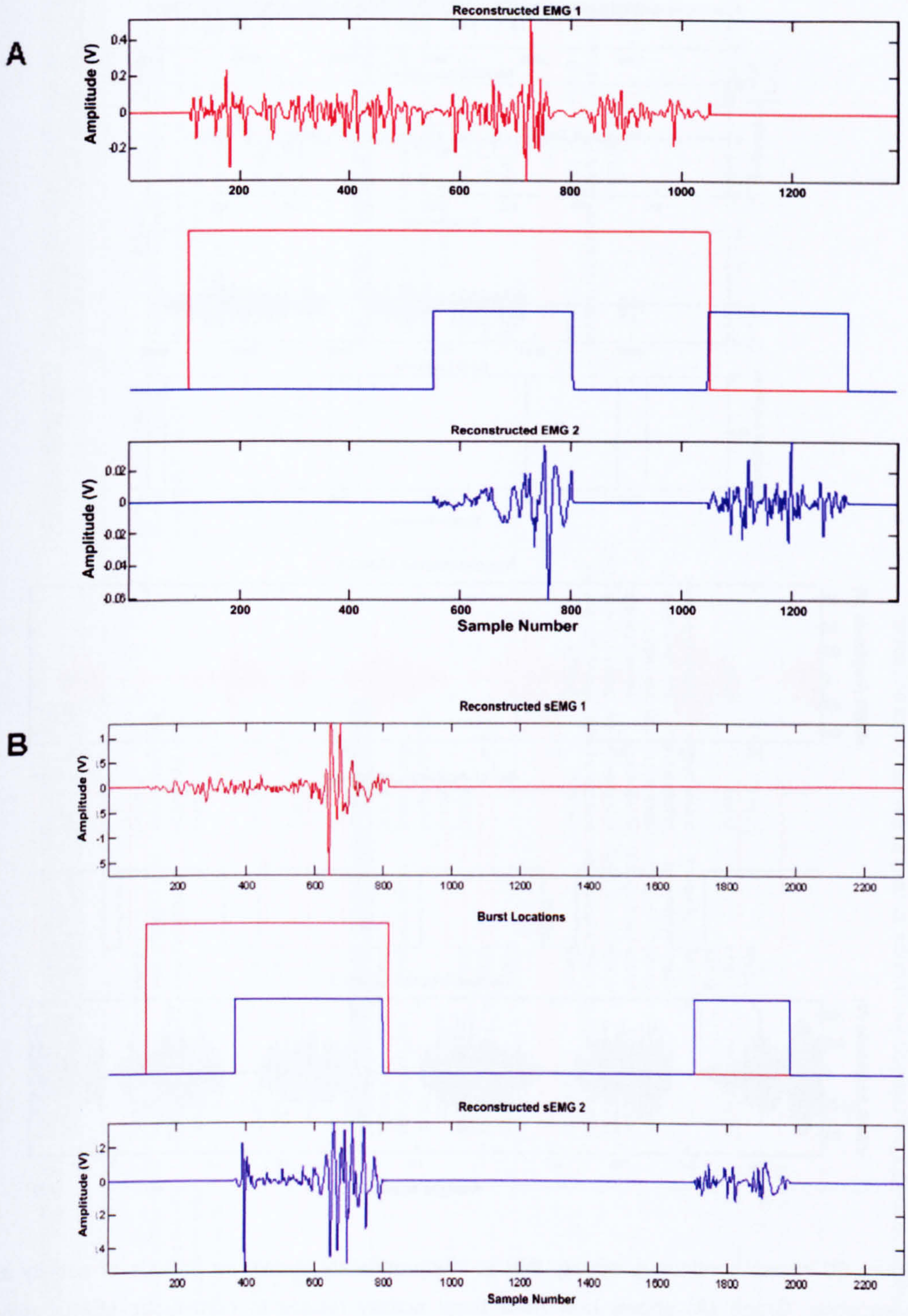

Figure 59 shows patterns of co-activity revealing premature calf activity. Graph (A) shows burst activity from CVA11. Graph (B) shows burst activity from CVA14.

Figure 59 displays an example of co-activation of the gastrocnemius with the tibialis anterior during the swing phase with a subsequent period of gastrocnemius activity during the stance phase. Comparative phasing to unimpaired subjects can be found in Appendix B.IV.

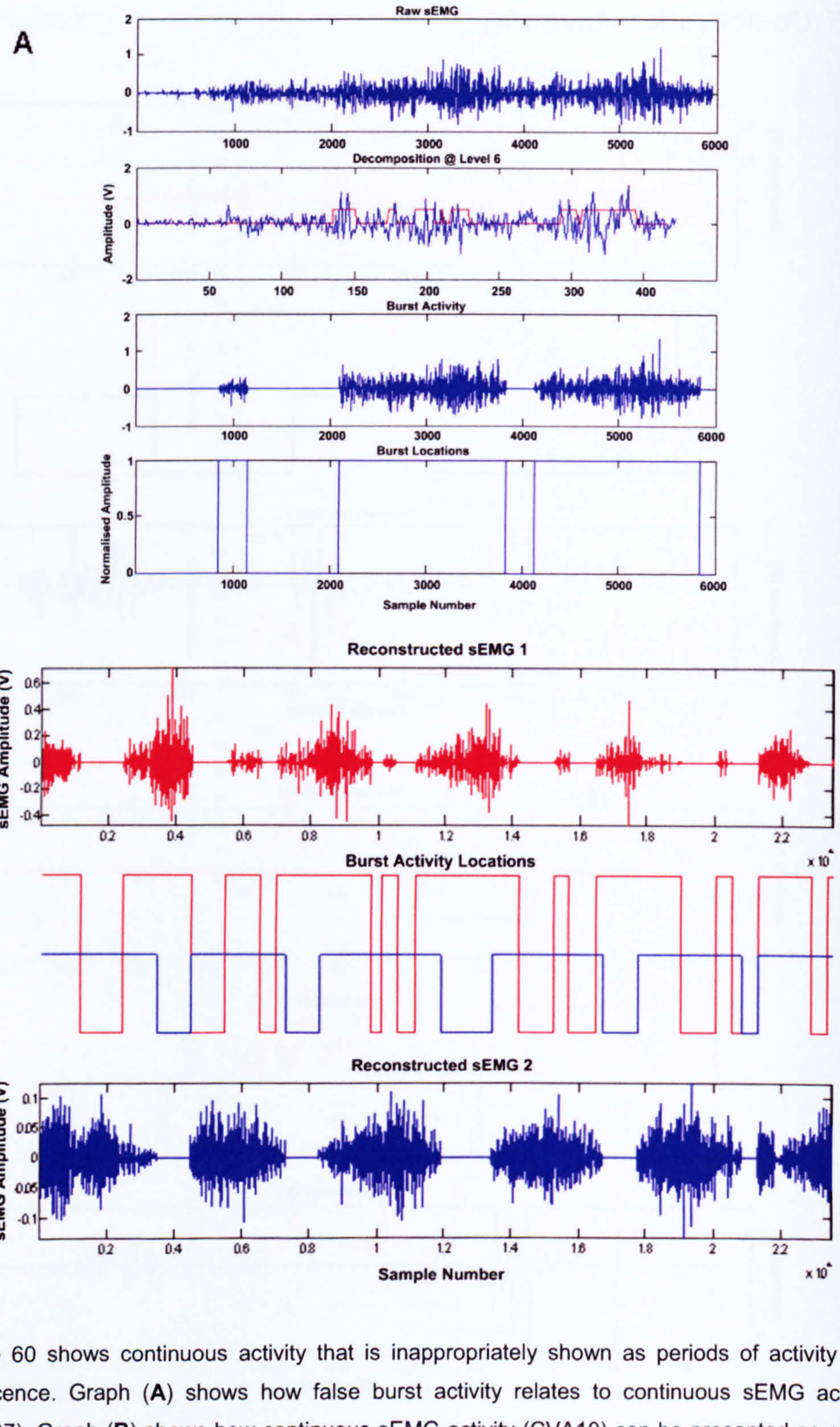

Figure 60 shows continuous activity that is inappropriately shown as periods of activity and quiescence. Graph (**A**) shows how false burst activity relates to continuous sEMG activity (CVA07). Graph (**B**) shows how continuous sEMG activity (CVA10) can be presented as on-off periods of activity.

Figure 60 displays examples of inappropriately divided burst activity. Although periods of burst activity are identified by the technique, Figure 60 **A**, shows how the periods of "inter-burst" do not, in this case, relate to periods of raw sEMG quiescence. Figure 60 **B** is the result from subject CVA10 whose linear envelope and time-frequency response reveals continuous activity.

4.5 Prototype Decision Matrix

Observational Gait Analysis			Linear Envelope			Amplitude		Instataneous Mean Frequency		
			Tibialis Anterior					Tibialis Anterior		
			Group 1	Group 2	Group 3	Group 1	Group 2	Group 1		Group 2
plantar flexion in stance but no decreased plantar flexion at toe off	Excess dorsiflexion in stance but with no excess plantar flexion in the in swing and reduced plantar flexion at toe off	Excess plantar flexion in stance but with decreasedplantar flexion at toe off	Activity in swing phase with gradual decrease after rapid initial onset	With additional burst near foot strike	Activity during late stance and early swing	Similar amplitude TA to GA	Greater TA to GA	increase in the mean frequency during late swing, late stance, or both, without corresponding increases in sEMG amplitude		continuous increase in mean frequency across the stride and did not show relative increases at the key gait events
CVA03	CVA10	CVA06	CVA03	CVA11	CVA07	CVA03	CVA10	CVA06	CVA15	CVA10
CVA14	CVA07	CVA15	CVA06	CVA14	CVA10	CVA06	CVA11	CVA03	CVA11	CVA07
		CVA11			CVA15	CVA07	CVA15		CVA14	
						CVA14				
			Gastrocnemius					Gastrocnemius		
			Group 1	Group 2	Group 3			Group 1		Group 2
			Burst prior to foot strike	Continuous activity	Burst in swing continuous activity in stance			Three peaks of activity relating to toe-off, foot-strike and cessation of sEMG activity		Pulsatile response, continuous
			CVA06	CVA10	CVA03			CVA06	CVA14	CVA10
			CVA11	CVA15				CVA03	CVA11	
			CVA07	CVA14				CVA15	CVA07	
			Soleus					Soleus		
			Group 1	Group 2	Group 3	Group 4		Group 1	Group 2	Group 3
			activity that peaks at foot strike that reduces subsequently	shows a short period of activity in the swing phase and a second period of activity at foot strike but little or no activity in the stance phase	displays a single prominent burst of activity at foot strike that extends slightly into the stance phase	shows activity in the swing phase and the stance phase but also with a prominent burst of activity at foot strik		Activity in late stance	Activity in swing phase	Continous activity
			CVA10	CVA14	CVA07	CVA11		CVA14	CVA11	CVA07
				CVA06	CVA15			CVA06	CVA15	CVA10
										CVA15

Figure 61 shows a prototype decision matrix expressing the groups shown in the previous sections.

4.6 Participant Overview

4.6.1.1 CVA03

Observational gait analysis reveals that the subject excessively plantar flexes their ankle during the stance phase (Appendix Figure 1). Excess plantar flexion is also seen in the swing phase in addition to increased inversion. There is a small "undershoot" visible in the ankle kinematics which means very little or no active dorsiflexion was achieved (active dorsiflexion is dorsiflexion as a result of muscle activity), additionally, the kinematics reveal how fast the foot plantar flexes during terminal stance implying poor ankle control during this phase of gait (Appendix Figure 8). During the swing phase the tibialis anterior activity diminishes after toe-off but increases a small amount prior to foot strike. The activity before foot strike is preparatory in order to try and lift the foot for correct placement at initial contact. Tibialis anterior activity (Appendix Figure 29) increases again during terminal stance; once more, this activity is preparatory to control the ankle prior to toe off. This amplitude is not sustained over the swing phase. Furthermore, the preparatory activity prior to foot strike is low in amplitude when compared to the peak amplitude of the linear envelope. The muscle is therefore capable of generating activity equivalent in amplitude to, for example, that seen in un-impaired subjects but is unable to sustain this level of activity (for example see Appendix A).

Observational gait analysis shows that knee extension is excessive throughout the stance phase and knee flexion is reduced throughout swing. This is also seen in the difference between shank and hip kinematics. Furthermore, the pattern of the shank's motion shows that it is almost vertical at foot strike, which supports the observation of reduced hip flexion during the swing phase and that initial contact is made with the foot flat. The severity of "decreased knee flexion through range" is low as there is an increase in knee flexion seen in Appendix Figure 9 (period A) and Appendix Figure 10. This corresponds to a period where the rate of hip flexion reduces and the rate of shank posterior rotation increases. It is also related to a period of increased gastrocnemius activity (Appendix Figure 30) which may therefore explain the increased knee flexion during this period. The subject hitches the hip during the swing phase and this is represented by the reduced rate of change of hip elevation (Appendix Figure 10 period A) i.e. the hip does not flex and translation of the swing leg is achieved through the rocker action of the contralateral ankle.

Another characteristic of this subjects gait is the extended period of the swing phase. The swing phase is extended and video analysis reveals the increased period of swing phase

corresponds to an increased period of double support, yet the subject's stride time is 1.3 seconds.

The time frequency plot of the tibialis anterior muscle shows how its activity extends into the stance phase. A small level of activity is in fact present throughout the stride. The activity can also be seen to decrease in amplitude and increase in frequency (see Appendix Figure 32). Other characteristics of the tibialis anterior activity are the phasic high frequency bursts of activity that become more obvious as the stride progresses. The preparatory activity just prior to foot strike is clear in the time frequency graph; it is interesting to note how the time frequency pattern differs from the early swing phase activity. The change in the frequency distribution across the stride is also clear in the instantaneous mean frequency (Appendix Figure 35) and supports the earlier observation that the frequency of the muscle activity increases over the stride. The triceps surie activity reveals several interesting points; firstly the frequency content of the gastrocnemius muscle in early stance does not contain the highest frequency components seen during the stance phase (Appendix Figure 33 Appendix Figure 34). This may suggest a different mode of muscle activity for example, the recruitment of slower fatigue resistant muscle fibres. Secondly, the two bursts of activity seen in the raw sEMG appear lower frequency and similar in nature. Because of their proximity to foot-strike and toe-off they might relate to movement artefact. However, the time-frequency plot reveals high frequency components within both bursts suggesting muscle activity. Furthermore, because this activity corresponds closely with the time of toe-off and foot-strike they could reveal a response to these two ankle stabilising phases. The instantaneous mean frequency further supports that these points are related to inappropriate muscle activity. The increase in mean frequency during the swing phase (Appendix Figure 36 and Appendix Figure 37) corresponds to the period of increased knee flexion described earlier, furthermore the second increase seen prior to foot strike corresponds to the decreased level of ankle dorsiflexion. There is appropriate activity of the gastrocnemius visible in the stance phase. The terminal period of calf activity suggested by the increased linear envelop amplitude is also the period of increased mean frequency. During terminal stance, the sEMG amplitude reduces yet the mean frequency increases. Again this may suggest a change in the muscle activation characteristic.

A large degree of co-contraction is suggested by the sub-band filtering technique (Appendix Figure 38). It is also able to identify subtler peaks of activity throughout the stride of both muscles that are also identifiable in the time frequency and mean frequency representations, but which are not obvious in the linear envelope.

4.6.1.2 CVA06

The subject CVA06 had extensive impairments with respect to observational gait analysis (Appendix Figure 2). At the ankle the subject excessively plantar flexes but more severely than the previous two subjects. This is particularly true for the swing phase. The foot elevation angles do reveal a reduced range of movement compared to CVA03 but simultaneously an increased level of absolute dorsiflexion (CVA06 = 8°, CVA03 = 4°). A significant difference is the time spent in swing phase, which reduces when compared to the standard gait cycle. The tibialis anterior is active throughout the swing phase, but the characteristic increase in amplitude seen in the previous two subjects is absent or less visible. However, in an inversion of the time-frequency activity seen in CVA03 the amplitude of the lower frequency coefficients increase over the period of activity (Appendix Figure 42 - Appendix Figure 44). Although the amplitude does not substantially increase prior to foot strike, as reflected in the linear envelope, the frequency activity across all frequency bins is seen to. This is supported by the mean frequency plot that shows an increase in mean frequency prior to foot strike, whereas the mean frequency activity of CVA03 gradually increased from toe-off, subject CVA06 displays a gradual reduction in mean frequency followed by a dominant peak of activity prior to foot-strike. A reduced range of shank elevation angle can be seen compared to CVA03 but greater than CVA11. Again CVA06 is reported to have reduced hip extension during stance and decreased hip flexion during swing, both of these are combined with excessive trunk and pelvic deviation (Appendix Figure 9 and Appendix Figure 10). The shank kinematics (Appendix Figure 11) reveal a reduced range of movement specifically during the stance phase, a pattern similar to CVA11 that implied reduced rotation of the shank over the foot. In contrast to CVA11 however, the gastrocnemius activity revealed in the linear envelope is reduced during the stance phase but similarly displays one prominent burst that occurs at foot strike. Yet, the time-frequency representation (Appendix Figure 44) does reveal the existence of stance phase activity. This activity exists more prominently in the higher frequency bands then seen in other patients. The instantaneous mean frequency (Appendix Figure 46) also shows a gradual increase in amplitude during terminal stance. The relatively large amplitude burst of activity seen in the linear envelope at foot-strike diminishes the significance of the subsequent activity during the stance phase which is approximately half the amplitude of that seen in the tibialis anterior. Yet, much of this activity is appropriately phased. Additionally, an increase in mean frequency can be seen mid to terminal stance in the tibialis anterior muscle (Appendix Figure 39) that corresponds to the increase in mean frequency in both the gastrocnemius and soleus muscles (Appendix Figure 46 and Appendix Figure 47). Therefore, although the linear envelope indicates little co-activation during stance phase, the time-frequency and mean

frequency representation implies that low amplitude co-activation does exist. This is in addition to the substantially increased amplitude response from the triceps surie at foot strike and a period of gastrocnemius activity that begins at the end of period C in Appendix Figure 43. The period coincides with the beginning of anterior rotation of the shank and plantar flexion of the foot. At this point the activity of the gastrocnemius ceases and soleus activity diminishes and only the tibialis anterior displays low amplitude activity. At 90% gait cycle, however, time-frequency analysis reveals that all three ankle muscles become active simultaneously. This pattern is also reflected in the mean frequency graphs (Appendix Figure 45 - Appendix Figure 47).

A pattern of sEMG activity, of short epoch high frequency activity, is again seen simultaneously in the tibialis anterior and gastrocnemius muscles (Appendix Figure 42 and Appendix Figure 43, see points *e* and *f*). This activity occurs at the point where the shank rotation changes direction and begins to rotate forward during the swing phase and occurs between the start and end of hip hitching. Hip hitching was identified during observational gait analysis but hip kinematics also reveals the characteristic pattern related to hip hitching seen in CVA03 (comparing Appendix Figure 10 and Appendix Figure 13).

Sub-band filtering successfully identifies the extended period of tibialis anterior activity and the low amplitude gastrocnemius activity during the stance phase (Appendix Figure 48). Furthermore, sub-band filtering identifies the coactivity prior to toe-off. The co-activation ratio of 0.66 is substantially higher than the 0.26 maximum ratio observed in the un-impaired subjects and all other impaired subjects (see Appendix A.III).

4.6.1.3 CVA07

Subject CVA07 displays lower levels of impairment than the other subjects with respect to observational gait analysis (Appendix Figure 3). The most significant impairment occurred in the ankle during the stance phase and in the knee during the swing phase. Increased ankle dorsiflexion was seen throughout the stance phase leading to decreased plantar flexion at toe-off. Increased knee extension was present, but was less obvious than, for example, CVA06; also present is a moderate level of decreased hip extension. In the swing phase the prominent impairment was severely reduced knee flexion. Of all the participants CVA07 only achieved obvious heel strike at initial contact. This is also evident in the foot kinematics, where there is a small level of plantar flexion related partially to the posterior rotation of the shank (Appendix Figure 15). At foot strike there is a rapid plantar flexion movement of amplitude greater than seen in any other subject. The rapidity of this plantar flexion reflects an inability to restrain the foot against the plantar flexion moment created at initial contact.

The activity of the tibialis anterior is similar to that seen in CVA10, where activity reduces from toe-off to mid-swing and increases again during the stance phase until the termination of the gait cycle. There is a small increase just prior to foot strike also present in CVA10 however; in this subject the swing phase is extended and thus this activity coincides with preparation for foot-strike (Appendix Figure 49). The linear envelope of the gastrocnemius shows a sudden increase in amplitude prior to foot-strike. This activity is clearly premature and corresponds to the end of the period of ankle dorsiflexion and maximum shank anterior rotation (with respect to the knee) which combine to stretch of the triceps surie (Appendix Figure 50). Less obvious in the linear envelope, but present in the time-frequency graph, is a similar increase in activity during early swing. This corresponds to activity in the tibialis anterior, a perturbation to the anterior rotation of the shank and the progression of the foot into dorsiflexion. Again, similarly to CVA10 the time-frequency activity of the tibialis anterior reveals sustained activity throughout the stride (Appendix Figure 52). Furthermore, there are increases in moderate to low frequency activity that is concomitant with similar activity in the triceps surie and correspond to periods of stretch in the calf muscles (kinematics shown in Appendix Figure 14 and Appendix Figure 15, muscle activity shown in Appendix Figure 53 and Appendix Figure 54). This activity is visible in the mean frequency (Appendix Figure 56) where the gastrocnemius displays three prominent increases in amplitude. The soleus mean frequency however, displays greater periodic activity in the swing phase although increased amplitude mean frequency occurs during the stance phase and relates to increased tibialis anterior activity (Appendix Figure 57). Importantly, comparing the amplitude of both muscles the peak amplitude of the tibialis anterior is equivalent to the peak amplitude of the gastrocnemius muscle suggesting that the muscles have more or less equal capacity.

Sub-band filtering was not appropriate for this subject because of the continuous activity of the tibialis anterior muscle (Appendix Figure 58 and Appendix Figure 59); this is discussed in section 5.2.

4.6.1.4 CVA10

Observational gait analysis revealed that the subject had extensive swing phase impairments in the hip, knee and high levels of trunk deviation (Appendix Figure 4). In the stance phase there was increased lateral and posterior/anterior trunk displacement in addition to moderate pelvic deviations specifically lateral displacement and contralateral drop. The subject also presented with severe excessive knee flexion. At the ankle the subject showed excessive ankle dorsiflexion and inversion, one of two subjects (CVA10 and CVA07) to display this impairment. Tibialis anterior activity was continuous throughout

the swing phase and extended into the stance phase - the stance phase was contracted. The tibialis anterior activity then returns during terminal stance. The onset and cessation of tibialis anterior activity is very gradual and reflects the reduced cadence of this subject. The subject had great difficulty lifting his foot from the ground, to the extent that swing phase could not always be clearly distinguished. The ankle kinematics show a reduced range of movement similar to CVA11 and CVA06. However, the distinctive "undershoot", in foot kinematics, has a shallower gradient revealing a gradual movement of the ankle into plantar flexion (see period **B** of Appendix Figure 17). Much of this movement relates to the invertion of the foot during weight bearing. The shank kinematics show a slow and limited shank rotation over the tarsus during stance phase after rapid forward rotation during the swing phase (see period **B** to point *c* in Appendix Figure 18).

The gastrocnemius can be seen to become active early during the swing phase as does the soleus muscle (see Appendix Figure 61 and Appendix Figure 62 period **A**). This is related to the limited additional dorsiflexion of the foot during the swing phase and suggests the activity exists to maintain the ankle angle. The linear envelope of the ankle muscles suggests a reduction in triceps surie activity during mid to terminal stance phase. The time-frequency analysis and median frequency graphs (see Appendix Figure 64 - Appendix Figure 65 and Appendix Figure 67 - Appendix Figure 68) support the increased activity represented by the linear envelope but also imply continuous, though reduced, activity of the triceps surie throughout the remainder of the stance phase. However, the ankle kinematics shows that the foot plantar flexes during terminal stance in the presence of increasing tibialis anterior activity and limited triceps surie activity. This implies little active push-off and activity predominately to stabilise the ankle. At toe off and during swing the foot is kept close to the floor, a response that either relates to incapacity or a readiness to provide support, i.e. cautiousness (De Quervain, Simon et al. 1996). The ankle plantar flexion occurs passively, restrained by tibialis anterior activity, reflected by the thigh rotating forward and the shank displaying little posterior rotation (see Appendix Figure 18, between foot strike and point *b*, see also Appendix Figure 19, between period **B** and point *c*). The mean frequency activity of the tibialis anterior (see Appendix Figure 66 period **C**) reveals a period in which the subject actively tries to lift the foot from the floor. Ankle and shank kinematics also display ankle plantar flexion and subtle changes in shank rotation that relate to attempted foot lift (see Appendix Figure 17 and Appendix Figure 18 period **C**). The mean frequency of the calf muscles activity also increases at this time.

Sub-band filtering subdivided the activity of the tibialis anterior and gastrocnemius and reported a co-activation ratio of 0.38. However, the raw sEMG, mean frequency and time-frequency analysis suggests almost continuous activity in both muscles. Sub-band

filtering did identify the increase in tibialis anterior activity (see Appendix Figure 69 periods **A** and **B** see also Appendix Figure 63 point *f*).

4.6.1.5 CVA11

Subject CVA11 reveals a similar pattern of ankle impairment to CVA03 with respect to observational gait analysis but with an increased level of ankle plantar flexion during the swing phase (see Appendix Figure 5). The ankle kinematics also reveals a similar pattern of movement. The degree of dorsiflexion prior to foot-strike is approximately the same, yet, the range of motion across the stride is, in comparison, reduced. In addition, there is the same rapid plantar flexion during terminal stance (comparing Appendix Figure 8 and Appendix Figure 20).

The activity of the tibialis anterior increases during terminal stance and continues during the swing phase. The activity increases in amplitude prior to foot-strike (Appendix Figure 70, period **B**). Similarly to CVA10 this activity may correspond to periods where the ankle needs to be stabilised either to prevent the foot from excessively plantar flexing or to provide dorsiflexion for foot clearance during the swing phase. The activity is sustained through the swing phase however, unlike CVA03 (see Appendix Figure 29 for comparison), the amplitude of the tibialis anterior activity at foot-strike is greater than that during the rest of the swing phase.

Knee flexion is reported to be increased throughout the stance phase (see Appendix Figure 5); however, the limited range of movement revealed by the kinematics of both hip and shank would suggest there was also inappropriate knee extension (see Appendix Figure 21 and Appendix Figure 22, stance phase). The stance phase range of the shank is reduced in comparison to that seen with CVA03 (see Appendix Figure 21 and Appendix Figure 9 for comparison), this implies that the second rocker action of the ankle is greatly reduced, and the shank does not rotate appropriately over the foot. The activity of the gastrocnemius increases at foot-strike and both sub-band filtering and mean frequency support this observation. Interestingly though, the mean frequency representation also shows related peaks of activity in both the tibialis anterior and the gastrocnemius (see Appendix Figure 76, periods **B**, **C** and **D** and Appendix Figure 77, periods **B** and **C**). There is also an increase of mean frequency in the gastrocnemius during early swing which is related to both the increase in linear envelope activity and mean frequency of the tibialis anterior. The mean frequency and linear envelope activity at initial contact and toe-off is also mirrored by the soleus mean frequency activity (see Appendix Figure 78 period **C**). There are strong indications of a stretch reflex or clonic response where the stretch of the triceps surie stimulates activity that is restrained by the activity of the tibialis anterior. The time frequency graphs suggest a sustained activity from all the ankle muscles and multiple

small epoch bursts that can relate to similar bursts in the antagonist muscle. The overall characteristic of the activity is one of being disorganised, the clear phasing seen in the un-impaired time frequency graphs (see B.III) is absent and that there is a systemic disruption to normal muscle activation.

4.6.1.6 CVA14

The activity of the tibialis anterior muscle is similar to that seen in subjects CVA07, CVA10 and CVA15 (see Appendix Figure 80 and Appendix Figure 49, Appendix Figure 60 Appendix Figure 90 for comparison). Activity increases in swing phase with a small increase just prior to foot-strike which relates to an attempt to dorsiflex the foot ready for foot strike, yet, the kinematics imply little active dorsiflection at foot strike (comparing Appendix Figure 23 and Appendix Figure 24 period **B**). This is supported by the observational gait analysis that reports initial contact with foot flat and excess plantar flexion during the swing and stance phase. Tibialis anterior muscle activity returns early in stance phase, this is also evident from the instantaneous mean frequency representation, however, the time-frequency representation reveals only a small amount of activity during stance (see Appendix Figure 83). This implies that the amplitude may often be very small which can be seen in the example of raw sEMG in Appendix Figure 86. There is activity present during mid-stance which continues to toe-off. Because of the presence of increased plantar flexion during stance phase, identified by the observational gait analysis (see Appendix Figure 6), the tibialis anterior activity may well be acting to help stabilise the ankle throughout the stance phase against gastrocnemius muscle activity. The gastrocnemius muscle is active throughout the stride (see Appendix Figure 81). The limited forward rotation during the stance phase revealed in the shank kinematics (see Appendix Figure 24) suggests that the calf muscles are unable to permit this; furthermore, this may explain the increased plantar flexion during the stance phase and swing phase (see Appendix Figure 6). Tibialis anterior time-frequency analysis reveals high amplitude and high frequency activity to be present just prior to and during foot strike that diminishes subtly during the stance phase and returns just prior to toe off (see Appendix Figure 83). The activity in the latter part of the stance phase corresponds to bursts of increased mean frequency in the calf and continuous increase in mean frequency in the tibialis anterior. This may imply a conflict between the two muscles during stance. The soleus muscle shows an increase in instantaneous mean frequency at a similar time (see Appendix Figure 88) and like the tibialis anterior shows a continuous higher frequency activity during mid to terminal stance in the time-frequency representation that introduces lower frequency bands (see Appendix Figure 85, period **E**). The linear envelope does not reveal

this activity. Both calf muscles display a high amplitude response during foot strike (see Appendix Figure 84, period **B** & **D**, and Appendix Figure 85, period **B**, **C** & **D**), again, implying both muscles have some response to stretch.

The amplitude of tibialis anterior muscle raw sEMG is reduced; however, the tibialis anterior activity response at foot-strike is, in fact, greater in amplitude to the unimpaired subjects. The gastrocnemius peak activity is again equivalent to un-impaired responses (see Appendix A.V). However; during the stance phase - appropriate phasing - the amplitude of the gastrocnemius muscle is lower than the activity in the tibialis anterior muscle of this subject. Therefore the tibialis anterior appears to present with reduced capacity but also acts to resist inappropriately phased triceps surie activity.

Observational gait analysis (see Appendix Figure 6) reveals that the pelvis is abnormally raised during the swing phase this contributes of the period shown in the hip kinematics (see Appendix Figure 25, period **B**). To allow the swing leg to clear the floor the thigh is externally rotated and adducted this causes an apparent increase in hip flexion. A similar response can be observed in subject CVA07 and to a lesser extent CVA06 (see Appendix Figure 13 and Appendix Figure 16 for comparison).

The burst locations from the sub-band filtering show co-contraction of the tibialis anterior and gastrocnemius during the swing phase. Some activity of the gastrocnemius is identified during the stance phase though much of the activity identifiable visually is not recognised as an inter-burst period. The co-activation ratio of 0.43 is the second largest value of all the subjects (see Appendix Figure 89).

4.6.1.7 CVA15

The most prominent impairment revealed by observational gait analysis is excess ankle plantar flexion during the stance and swing phase and poor knee control (see Appendix Figure 7). The foot is noted to make initial contact with the forefoot; this is also revealed by the foot kinematics where after maximum dorsiflexion the foot again plantar flexes. At this point initial contact occurs and the following dorsiflexion appears to be a resultant and passive movement. The level of dorsiflexion denoted by the "undershoot" seen in Appendix Figure 26 and is equivalent to CVA11 (see Appendix Figure 20, period *a* to *b*) and greatly reduced compared to CVA07 (see Appendix Figure 14, period denoted by *undershoot*). This suggests that the active range of the ankle is impaired. Although the overall range of the mean elevation angle for the ankle is 45° this is predominately achieved through the rotation of the shank (see Appendix Figure 27, period **A**). Foot strike occurs further into the gait cycle and extends the period of weight bearing similar to that seen in CVA06 and CVA10 (see Appendix Figure 39 and Appendix Figure 60 for foot-strike locations). The linear envelope activity of the tibialis anterior is similar to that seen in

CVA10 where there is an increase in amplitude during the swing phase and during mid to terminal stance (see Appendix Figure 90, periods **A** & **B** respectively). The amplitude of the tibialis anterior muscle activity is greater than that seen in the gastrocnemius and soleus muscles. The peak amplitude is equivalent to that seen in un-impaired subjects (see Appendix A.V). The gastrocnemius muscle activity occurs early during the swing phase, where there is an abnormally high amplitude burst of activity – abnormally high when compared to normally phased activity of the subject's gastrocnemius muscle. An additional burst of gastrocnemius muscle activity is seen during the stance phase that diminishes before toe-off. This pattern of muscle activity during terminal stance is similar in the soleus muscle which suggests therefore little active push-off (see Appendix Figure 91 and Appendix Figure 92).

Time-frequency analysis and the instantaneous mean frequency representation of the tibialis anterior muscle reveal that activity is extended into and through the stance phase (see Appendix Figure 93, period **C,** and Appendix Figure 96,periods **B** & **C**). This activity is greater than is suggested by the linear envelope representation of the tibialis anterior (see Figure 38). There is a prominent burst of activity during terminal stance that is related to toe-off. Observational gait analysis and kinematics both show this was unsuccessful (see Appendix Figure 7 and Appendix Figure 26 - Appendix Figure 27, period **B**).

Instantaneous mean frequency activity during terminal stance of the gastrocnemius and soleus muscles may suggest why apparently normal amplitude tibialis anterior muscle activity was not affective at lifting the foot. Instantaneous mean frequency activity of the tibialis anterior - Appendix Figure 96, period **B** - relates to the increased plantar flexion prior to foot-strike. This activity corresponds to that present in the instantaneous mean frequency of the soleus but not the gastrocnemius (see Appendix Figure 97 and Appendix Figure 98, period **A**). There is a prominent burst of gastrocnemius and soleus activity (denoted by Appendix Figure 97, period **B**). This activity relates to the stretch of the triceps surie as the foot passively dorsiflexes and the shank rotates forward. An increase in mean frequency can be seen in all three muscles and therefore implies that the tibialis anterior muscle is acting to stabilise the ankle in the stance phase (see Appendix Figure 96 - Appendix Figure 98). Similarly, when the shank is at its maximum forward rotation during the stance phase there is activity in the triceps surie and tibialis anterior muscle again suggesting the sensitivity of the calf to stretch.

Sub-band filtering supports the existence of co-contraction between the gastrocnemius muscle and tibialis anterior muscle (see Appendix Figure 99) that was not revealed by observation of the tibialis anterior and gastrocnemius muscle linear envelope.

5 Discussion

In this project three analytic techniques have been applied to surface electromyography data (sEMG) and related to kinematic variables of walking in stroke patients. These techniques and observations from the kinematic data have led to the development of a framework for analysing sEMG. From each technique the patients have been grouped and by identifying the group in which they have been placed, it is proposed that a decision matrix could be constructed to help identify underlying impairment (see Figure 61). The prototype decision matrix constitutes the significant contribution of this thesis as it provides a structure to fully address the final objective in this project, specifically, to characterise the underlying walking impairments at the ankle in stroke patients. Implicitly this strategy would also contribute to the holistic aspects of gait impairments after stroke. Because of the small number of subjects in the study it is important to note that this project may not reflect results that might be found in a more representative stroke population. However, as stated earlier it does provide the groundwork from which representative groupings can be generated. In this chapter, firstly the patient groupings for each analysis method identified in Chapter XX Section 2.4.6 are presented; the components of the gait analysis system are then discussed. Subsequently the performance of the analytical techniques is discussed. Finally the project method is discussed with reference to the strengths and problems encountered in the protocol.

5.1 Characterisation of Impairment

Patients were grouped by observing similar patterns in each sEMG analysis method and kinematic measurements. Results from each analysis method and measurement will be discussed individually, and ultimately, an example is given of the way these elements, in relation to the prototype decision matrix shown in section 4.5, can be combined to characterise impairments seen in an individual subject.

5.1.1 Limb Segment Elevation Angles

The limb segment elevation angles displayed clear differences from those seen in un-impaired subjects and between those seen from impaired subjects (see Appendix B.VII). Using limb segment angles rather than presenting joint angles followed an example in recent literature (Ivanenko, Popple et al. 2004) in which limb segmental angles are described as being more closely related to the control mechanisms of locomotion. Overall the phasing of the pattern was temporally shifted, for example, peak absolute plantar flexion at the ankle occurred longer into the swing phase for un-impaired subjects, this relates to the impaired subjects trailing foot not being lifted after toe-off but being moved forward immediately after toe-off. Subtle movement patterns observed in un-impaired

subjects were also absent in impaired motion patterns. For example, the small dip (marked as "undershoot" in Appendix Figure 1) reveals active dorsiflexion after toe-off which is again absent from the impaired subjects motion pattern. Kinematic data supports and quantifies the observational gait analysis with respect to range of movement.

Subjects who displayed similar impairments in terms of observational gait analysis did not necessarily display similar patterns of segmental elevation angles. Therefore the common observable impairment is generated through different interactions of limb segment elevation angles.

At the thigh, three patterns can be observed; most commonly, CVA03, CVA06, CVA15 and CVA10 display a single curve increasing from the start of swing peaking around foot-strike and then reducing again towards toe-off. This shows the rapid flexion of the hip during swing and the gradual extension of the hip during stance. Subjects CVA07 and CVA14 are similar to the previous group but display an additional hip extension period just prior to foot-strike. Finally, subject CVA11 displays a small range of hip movement during the swing phase and then an interesting flexion extension pattern during stance.

- The first pattern describes a "step-to" movement with the thigh never crossing the midline of the body, the leg either moves from the posterior to the mid-line or from the midline anteriorly.
- Pattern 2 describes some level of increased hip extension though this could include knee-hyperextension and must be compared to the location of foot-strike to assess whether the extended hip is weight bearing, if not it may be suggestive of circumduction.
- Pattern 3 describes a situation where the hip is not flexed during swing and therefore implies pelvic elevation though swing (hip hitching). The small shallowing of the gradient seen in both CVA06 and CVA03 thigh elevation angle during mid-swing also implies increased hip elevation.

Shank movements also displayed three groups of activity. Subjects CVA03, CVA06, CVA15 displayed a pattern with two "troughs", the first occurring just prior to foot-strike the second occurring at approximately heel-rise. Subjects CVA11, CVA10 and CVA14 displayed a similar pattern to the latter but with the second trough minimised or completely absent. Finally, CVA07 represents pattern 3, an inversion of the first shank pattern and reflects a less impaired movement, the shank posterior rotation being at almost maximum at toe off, reaching the mid point at mid swing and then maximum anterior rotation at approximately foot-strike. This pattern has a striking similarity to the un-impaired results.

- The shank pattern 1 shows that instead of the shank passing the body's midline (at its most vertical) at mid swing or stance it is at its most horizontal. In addition, the shank is near vertical at foot-strike and approaching vertical at toe-off.
- The second shank pattern modifies the latter by reducing the degree of shank rotation over the tarsus during the stance phase.

All subjects displayed very similar ankle movement patterns with no clear discriminating characteristic other than by their ranges of movement; however, CVA07 displays a more appropriate pattern at foot-strike with an increased level of dorsiflexion. In addition, toe-off occurs in a similar fashion to that seen in un-impaired subjects implying the subject was able to extend the knee and support the trailing leg more than other subjects.

5.1.2 Linear Envelope characterisation

Principal component analysis was used to find representative patterns of activation using the linear envelope from each of the ankle muscles, extending the technique described by Wootten et al. (Wootten, Kadaba et al. 1990) to stroke patients and also to the identification of characteristic impairment. Subjects were then grouped by relating their muscle activation pattern to the most significant of those from the PCA. There is a large degree of interpretation involved with analysing the principal component results; in addition, the small number of subjects within this study clearly precludes extension of these results to the wider community. However, within this group of subjects, subdivisions of muscle activation patterns were found; the quality of these underlying groups is shown by the ability of the technique to reconstruct a linear envelope using the fundamental activity patterns (see Appendix A.IV, Section A.IV.d Reconstruction). This suggests they are indeed representative of the key characteristics of all the muscle activation patterns combined within the patient group. With a greater number of subjects it is proposed this technique would be more effective at describing the characteristics of a wider group.

The activity of the tibialis anterior muscle displayed three patterns into which subjects could be grouped together. Subjects CVA03 and CVA06 showed activity in the swing phase only with a gradual decrease in amplitude from the initial rapid onset. Subjects CVA11 and CVA14 displayed a similar pattern to the latter but was characterised by a second prominent burst just prior to and during foot-strike. Finally CVA07, CVA10 and CVA15 showed two phases of activity; one during the swing phase decreasing in amplitude from the initial onset and the second beginning during late to terminal stance that increased in amplitude to toe-off.

Three groups existed with respect to activity of the gastrocnemius muscle, those with a prominent burst just prior to or during foot-strike, those with continuous activity throughout the stride and those with burst around foot strike and continuous activity in the stance phase. Subjects; CVA06, CVA07 and CVA11 showed an additional burst of activity during early swing phase, in addition to some activity in the stance phase. However, the stance phase activity decreased during mid-stance and increased at terminal stance and toe-off. The second group CVA10, CVA15 and CVA14 showed continuous activity throughout the stride. The third group, CVA03, displayed both continuous muscle activity in the stance phase and a prominent burst of activity during the swing phase.

Soleus linear envelope activity was more complex to classify, each subject displaying more individual patterns of activity than is seen with the other muscles. Subjects CVA10 and CVA03 displayed patterns of activity consistent with principal components 1 & 2 respectively (see Figure 131 section 4.10.3). Subject CVA11 individually displayed a pattern consistent with principal component 3, gradually increasing activity from foot strike. Subjects CVA14 and CVA06 displayed a single burst of activity at foot strike that was consistent with principal component 5. Subjects CVA07 and CVA15 did not display an activation pattern consistent with any one principal component but shared characteristics with principal component 1 modified with principal components 4 & 5. This pattern has increasing activity during the swing phase peaking just prior to foot-strike or during the early stance phase. The peak is much sharper than that seen with subject CVA10 and therefore the additional components are required.

An example of how these observations might be combined to describe impairment is given in section 5.1.5 of this chapter. We might relate these groups to Knuttson's grouping; for example CVA03 is placed in group 1 of tibialis anterior activity but in group 3 of the gastrocnemius activity. Both muscles appear to show some correct phasing except the gastrocnemius displays additional activity in swing and the tibialis anterior activity reduces inappropriately. Without reference to the relative amplitude of the two muscles it could be argued that this pattern relates to Knuttsons group 3, abnormal co-activation with no significant decrease in electromyogram. Subject CVA06 also has a group 1 tibialis anterior pattern but has a group 1 gastrocnemius pattern as well which relates to a single prominent burst of activity at foot strike and little activity during stance. This might be related to premature activity of the calf muscle (Knutsson type 1) but could also relate to marked lowering of activity in the muscle group (Knutsson type 2) but with additional activity not previously noted. This interpretation is assisted by relating the pattern to the relative amplitude of the agonist and antagonist muscles. Comparing the mean amplitude of the sEMG, inferred in this thesis from the raw sEMG (see instantaneous mean

frequency figures), CVA06 can be seen to have similar amplitude in both tibialis anterior and gastrocnemius muscles. Subjects CVA10, CVA11 and CVA15 however, displays a marked decrease in the sEMG amplitude of the gastrocnemius muscle activity with respect to the tibialis anterior muscle.

Patients do not fall into groups consistently, that is, CVA06 is grouped with CVA03 for tibialis anterior muscles and with CVA07 and CVA11 for gastrocnemius activity. This is not unreasonable and with such a small subject size it may be that groups have not been identified. It is the combination of activity patterns that may inform the underlying impairment that exists in the subject and it is not necessary for two subjects to present with the same impairment in the same way. This can be reflected in the manner un-impaired subjects present with different patterns of activity yet achieve a gait pattern consistent with "normality" (Arsenault, WInter et al. 1986; Ivanenko, Popple et al. 2004) (see also Appendix A.I).

Although patterns of muscle activity can be related to those observed by Knuttson (Knutsson and Richards 1979), and therefore Burridge et al (Burridge, Wood et al. 2001). Conceptually the use of PCA differs. With this method characteristic patterns of muscle activation are inherently extracted, the relation of these to those previously reported in literature acts to support and objectify the validity of those existing patterns. Importantly, these muscle activation prototypes may have strong relation to motor control strategies (Jansen, Miller et al. 2003) although this may only be revealed through the investigation of a large stroke population and, as in this project, the parallel evaluation of kinematics.

5.1.3 Time-Frequency Analysis

Wavelet analysis was used to decompose the sEMG signal representing different frequency constituent. This allowed that a sEMG signal could be viewed in terms of a time-varying mean frequency, instantaneous mean frequency. Instantaneous mean frequency of impaired muscles revealed unexpected results. In several subjects the mean frequency of the tibialis anterior increased across the stride at times where there was not an equivalent increase in sEMG amplitude. In many of the subjects (CVA06, CVA03, CVA15, CVA11 and CVA14) there was increase in the mean frequency during late swing, late stance, or both, without corresponding increases in sEMG amplitude. These points in the gait cycle relate to points where the ankle is in or preparing for foot-strike or toe-off events. Therefore this activity may represent a strategy for supporting the ankle during these gait events. Clearly the activity needs to be placed in a wider context i.e. kinematics and synergistic muscle activity. Subjects CVA10 and CVA07 shared a similar pattern of mean frequency activity. Both displayed continuous increase in mean frequency across

the stride and did not show relative increases at the key gait events previously mentioned. The maximum frequency displayed in these subjects was sometimes greater than those seen in un-impaired subjects. This is contrary to what might be expected through impaired recruitment due to upper motor neurone disorders (el-Abd, Ibrahim et al. 1993; Rothwell 1996) and changes in modulation of motor neurone firing frequencies (S-Cook and Woollacott 2001). Subject CVA11 showed a unique pattern of activity during the stance phase, displaying larger amplitude bursts of activity; these corresponded to similar bursts of activity in the soleus and gastrocnemius muscles.

The analysis of instantaneous mean frequency has identified common patterns of activity in the gastrocnemius muscle. The most common was that which included three prominent peaks. The first just after toe-off, the second in the proximity of foot-strike and the third corresponding to the cessation of the sEMG activity. The timing of these bursts is therefore similar to that described for tibialis anterior. All but CVA10 displayed this pattern of activity. The instantaneous mean frequency response from subject CVA10 was of a pulsatile nature and of an amplitude consistent with that seen in un-impaired subjects. The activity was sustained throughout a large proportion of the gait cycle. It is interesting to note that subject CVA07 does not share this same pattern, although the mean frequency response for the tibialis anterior was similar in both subjects. Although the peak frequency of the gastrocnemius was equivalent to that seen in the un-impaired subjects between bursts, the amplitude of the mean frequency was substantially lower even during periods of clear activity in the sEMG signal.

The instantaneous mean frequency of soleus muscle provided additional insight into the underlying activity. Subjects CVA14 and CVA06 both revealed prominent periods of activity in late stance that was not clear from the sEMG signal alone; this was also true for CVA11 and CVA15. These subjects also displayed periods of inappropriately phased activity during the swing phase. Subjects CVA07, CVA10 and CVA03 all displayed continuous activity with respect to mean frequency across the stride with a pulsatile pattern of mean frequency.

The implication of changes in instantaneous mean frequency is still not clear (see section 2.4.5.3) however, it is reasonable to assert that an increase in instantaneous mean frequency relates to an increase in “muscle activity”. Yet it is not possible, in this case, to assert the functional implication of the increase or decrease. One might expect a decrease in the mean frequency of a stroke patient, in line with results suggesting motor unit synchronisation (Farmer, Halliday et al. 1997; Farmer, Swash et al. 1993) or disrupted recruitment patterns (el-Abd, Ibrahim et al. 1993). It has also been shown that for stroke patients the disuse of high threshold motor units cause a transform from type 1 to type 2A

and type 2B fibres (Jakobsson, Edstrom et al. 1991). All subjects are long term users of functional electrical stimulation (FES) to correct drop foot through stimulation of the common peroneal nerve to activate the tibialis anterior muscle. Functional ES has been shown to increase the proportion of type 2A fibres, yet, with long term FES use the proportion of type 1 fibres increase (Kwende, Jarvis et al. 1995; Sutherland, Salmons et al. 2006). Therefore, a short term FES usage and stroke may reasonably result in a shift to higher frequency components in the sEMG frequency spectrum. Yet long term FES usage may counteract this change and subsequently produce a shift to lower frequency components. Therefore, there is possibly a contradictory process occurring with stroke patients. In view of the fact that literature previously referenced relates to isometric activity it may be that functional activities such as walking reveal more task oriented responses related also to the subject's impairment and compensatory strategy. Thus time-frequency analysis may reveal frequency shifts related to specific gait events which are more individual. In addition, it may be expected that different responses should be found with muscles involved with FES, i.e. the tibialis anterior, and those not directly stimulated; though there appears to be no evidence about the effect of antagonist muscles to stimulation of the agonist.

What has not been evaluated fully in this project is the way in which the mean frequency changes over specific phases of the stride and thus focussing more specifically on control. Frascarelli et al. (Frascarelli, Mastrogregori et al. 1998) report a difficulty of stroke patients to modulate the firing of motor units during minimal effort voluntary movements; in this project increases in mean frequency have been observed out of the normal phase for the muscle and sometimes with frequencies greater than that seen in un-impaired subjects.

Decreased values of mean frequencies during appropriate muscle activity have also been seen. Although irregular patterns of mean frequency have been identified, further work is required to correlate subtler variations in mean frequency to impairment.

5.1.4 Co-activation Ratio

Sub-band filtering was implemented in order to better differentiate between periods of muscle activity and muscle latency and therefore be used to quantify the level of coactivity between the tibialis anterior and the gastrocnemius. The results from un-impaired subjects displayed the capacity of this technique to differentiate between burst and inter-burst periods. When applied to sEMG from impaired subjects there were mixed results and called into question one of the underlying premises of the signal processing method. The technique performs well with impaired sEMG activity which has clearly divisible periods of

burst activity for example this can be seen with subject CVA03. The technique makes the assumption that there are periods of activity and periods of latency. As can be seen with subjects CVA10 and CVA07 this assumption is not always supportable with respect to impaired sEMG signals. Therefore, this technique should be used selectively i.e. where it is known that the sEMG signal is constructed of "on – off" burst activity. Results do suggest though that in appropriate situations sEMG signals, even with reduced amplitude and signal to noise ratio, can be separated into periods of burst and inter-burst and therefore permit a quantitative evaluation of co-contraction. Subjects CVA10 and CVA07 all display inappropriate activity for this technique, as activity in one of the muscles never ceases and requires artificially creating periods of zero activity. However, the technique overcomes a clear difficulty with existing co-activation indices based on linear envelopes (Burridge, Wood et al. 2001). Linear envelopes can change with respect to their phasing and/or amplitude, therefore a ratio of activity for two high amplitude signals largely out phase could be equivalent to two low amplitude signals largely in phase. This could be the case with subjects who presented with normal amplitude tibialis anterior activity and reduced amplitude gastrocnemius sEMG.

5.1.5 Characteristics of Impairment

Although it is not possible to give a definitive decision matrix it is possible to provide an example of how the measurements made during this project could used to characterise an underlying impairment and link to existing groups suggested by earlier investigators.

Subjects that shared similar motion patterns for example CVA06 and CVA15 can be seen to have substantially different muscle activation patterns. For example; these subjects displayed different patterns of tibialis anterior activation; CVA06 showed activity predominately in the swing phase whereas CVA15 had activity during early swing and terminal stance. The mean frequency responses showed increased activity in late stance for CVA06 and increased activity in swing for CVA15. Gastrocnemius muscle activity was similar in terms of linear envelope pattern; however, the mean frequency response of CVA06 was more gradual than the lower amplitude short epoch bursts of activity seen with CVA15. The relative amplitude of gastrocnemius to tibialis anterior was reduced in CVA15 but similar with regard to CVA06. Soleus activity was inappropriately phased with respect to mean frequency in CVA06 but CVA15 displayed increased activity in the late stance phase. Finally, the levels of co-activation ratio were double for CVA06 than for CVA15.

Therefore CVA15 presents with marked lowering of the sEMG amplitude and mean frequency in combination with ostensibly appropriate phasing in all muscles. Subject

CVA06 displays inappropriate phasing and no significant lowering of amplitude or mean frequency in tibialis anterior or the triceps surae. Returning to Knuttson's classification (Knutsson and Richards 1979), by comparing the principal component grouping with the time-frequency and specifically mean frequency responses and furthermore by evaluating the relative amplitude between antagonistic muscles it is possible to make an assignment to one of Knuttson's four groups. The patterns of activity described for subject CVA15 relate to Knuttson's group 2 and the patterns of activity described for subject CVA06 relate to Knuttson's group 3.

5.2 Gait Analysis System

A system for gait analysis was developed for this project and was presented in chapter 3 section 3.1. The system was to be appropriate for a clinical environment and provide measurements relevant to this project. The system combined video analysis, kinematic and sEMG data. In addition, the system provided a variety of signal processing tools for sEMG which were subsequently used to analyse sEMG from stroke patients.

Principally the system was successful in integrating off-the-shelf technology to provide synchronised measurements from several different systems, both commercial and in-house. The system was successful in using a generic wireless local area network (wLAN) to synchronise different pieces of motion analysis equipment. The LabVIEW language provided a transparent environment to control the wLAN and thus a relatively simple architecture was developed.

The system integrated a low cost wireless sEMG system. The high cost of commercial wireless sEMG was prohibitive and a review of commercial sEMG equipment did not reveal equipment that fully met SENIAM recommendations and suitability for clinic use. Finally, integrating commercial systems into the wider gait analysis system was complicated by software and triggering (synchronisation) requirements. Therefore an in-house system was developed; this too was principally developed from off-the-shelf components. The system was successful in utilising new commercially available data acquisition hardware with a commonplace personal data assistant (PDA). Additional signal conditioning hardware was required but yet again it was possible to implement this with specialised integrated circuit components, specifically, analogue filters and instrumentation amplifiers. The total material cost of the in-house wireless sEMG system was less than £1500 (Commercial systems range from £15000 - £35000). Although the system removed the need for wires trailing from the patient, wires connecting the preamplifiers to the patient worn acquisition system were still present. These wires proved to be cumbersome especially with the number of sEMG sensors attached to the patient.

They significantly increased the time required to attach the sensors and, without care, affected the positioning and adherence of the sEMG preamplifiers and thus the subsequent data. Because of this problem (which is commonly recognised when using sEMG even with commercial systems) the absence of real time sEMG data was amplified; specifically, that the process of checking good sensor positioning and signal quality was made more difficult and time consuming. In this sense the system requires development to make it acceptable for clinical use. It is important to recognise that the system is currently at a prototype stage and therefore, although the size of the signal conditioning stage may be excessive, this could be reduced in subsequent design iterations. The feasibility of such a system can be seen in recent commercial developments by BTS (Bioengineering 2006) who have implemented a wireless sEMG system based around a PDA, wLAN and wireless pre-amplifiers.

Video analysis was achieved using two machine vision Sony DCAM firewire cameras. These were controlled by a purpose designed desktop computer that acts as a digital video processing hub. Bilateral video is a very useful tool in gait analysis and usually achieved through multiplexing analogue cameras. Digital video offers greater flexibility in analysis however, it is a non-trivial task to synchronise several cameras. Common video protocols are not usually used in this way and there was only one piece of commercial software that facilitated multi-camera systems using Firewire. The system was successful at recording bilateral video in formats such as mpeg and AVI; alternatively, the system captured stationary images that were synchronised with other measurement devices. Some issues remain with respect to the video system. Specifically, certain user requirements such as portable video were not fully implemented in the initial system; this is predominately due to the breadth of video formats available and the lack of a local standard. Furthermore, traditional use of video by some analysts tends towards long recording periods; this was not envisaged in the initial specification primarily because it is not encouraged (Kirtley 2005). These are effectively issues of flexibility and as such can be addressed in future design iterations but require user involvement to specify the most appropriate functions and to define good practice. Though simple in concept, the development of a bilateral synchronised camera system is a useful contribution and provides a simple method of recording walking in a clinical environment and can be expanded to utilise image processing tools and can be replicated with ease.

The system employed commercially available inertial orientation sensors to measure the movement of the lower limb. Very often electrogoniometers would be employed to measure joint angles when optical motion analysis systems were not available, however, MT9 inertial sensors introduce the possibility of measuring segmental movements of the

limb and as such could be used to construct a crude segmental model. In this project only sagittal plane kinematics were evaluated as these are the most prominent movements during the walking pattern. However, it became clear that utilising a small proportion of the possible data provided useful information for discriminating between patients. The evaluation of the sensors showed that the accuracy during dynamic movements was lower than that suggested in the commercial literature (a dynamic accuracy of 10° was measured – see chapter 3 Section 3.1.3.5), though, it was accepted that the level of accuracy would not match that of an optical movement analysis system. In addition, the measurements from optical motion analysis systems have a variable accuracy due to marker placement and marker movement errors which can be as high as 10° (Baker 2006). The sensors were simple to attach to the patient, however, the sensor's size proved to be intrusive to the patient. The additional wires from the sensor to the control box were also a problem especially when combined with the wires of the sEMG preamplifiers. Trailing wires from the control box to the base station was restrictive and there is a clear advantage to implementing the wireless connection now possible with the Xsens system.

The equipment exists as a prototype system designed for this purpose; however, it is clear that from a usability point of view development is required. Although the graphical user interface was designed to be as simple to use as possible, the subsequent analysis functions still require a great deal of expertise to use. Designing the system to fit within the confines of normal clinical practice will require further work to crystallise macro-ergonomic issues. The software usability and means of reporting results of the analysis were not considered strongly during the development of the system but are vital for the future usability of the system.

5.3 Analytic Techniques

The linear envelope representation of sEMG was the basis of the principal component analysis (PCA) analysis method and was useful in providing a simple representation of the sEMG to observe amplitude and phasing. In this project discrete wavelet filtering was used to provide a representation with reduced lag and amplitude attenuation than was achievable using Bessel filters developed in the MATLAB signal processing toolbox (see Figure 7; chapter 2, section 2.4.5.1). This is a relatively novel approach to the generation of a linear envelope and became useful when calculating parameters for the PCA due to the natural decomposition of the signal that occurs. An algorithm for automatically sub-dividing the strides of a walk and subsequently calculating basic statistics, such as mean pattern and standard deviation, was implemented as part of the gait analysis system. This

automation provided a simple means of constructing the sEMG linear envelope for analysis.

Time-frequency analysis was achieved using the MATLAB wavelet toolbox and existing wavelet families. There exists a specific wavelet for use in the analysis of sEMG however, its use is restricted. Although it would have been possible to develop a wavelet family specific to the sEMG signal it was decided to use existing wavelet families, a decision supported by their use in other studies (Conforto, D'Alessio et al. 1999; Stefano and Allen 2003). Differences between impaired and un-impaired subjects did not reveal such obvious differences as was expected. For example, there was no obvious shift to lower frequencies which may be expected from, for example, disordered recruitment strategies (el-Abd, Ibrahim et al. 1993; Hermens, Boon et al. 1984). The results from time-frequency analysis with respect to each patient are discussed in section 5.1.3. The use of time-frequency analysis was useful in identifying the phasing of activity and anecdotally describing frequency constituents however, a clear means of quantifying these differences was not developed. The work of Von Tscharner (von Tscharner 2000; von Tscharner 2002) has provided some framework to do this using patterns of sEMG intensity calculated from wavelet coefficients. However, this has not been developed to provide information on pathological sEMG where it could provide significant insight into different patterns of impaired muscle activity and the underlying impairment.

PCA used the linear envelope representation in order to identify key patterns of muscle phasing within each muscle. The technique was dependent on the method by which the linear envelopes were constructed. Specifically, the linear envelope was normalised in such a way that relative differences in amplitude between patients was removed. This enforces the point that PCA, in this project, determines groups based on phasing of the activity and not relative amplitude. This means that discrimination based on amplitude must be achieved by alternative means. It is important also to note that this technique cannot be used in isolation. However, isolating particular aspects of the sEMG signal then evaluating them collectively could provide a more appropriate means of classification. Grouping of subjects using PCA was achieved through observation. Ideally this would be automated using a classification technique such as cluster analysis (Jansen, Miller et al. 2003; Shiavi and Griffin 1981).

Sub-band filtering enabled a selective removal of sEMG at different frequency bands and proved to be efficient at differentiating burst and inter-burst periods of un-impaired muscle activity. However it was only selectively appropriate for use with stroke patients; this is discussed more fully in section 5.1.4.

5.4 Assessment

Subjects only attended a single gait analysis session, therefore day to day variations could not be evaluated. In addition, some patients presented with severe walking impairments that prevented them from completing more than two "walks" and increased the time required for them to ambulate the course. In one respect this affected the operation of the system requiring long measurement times that were clear in retrospect but not envisaged originally. In respect of day to day variations, literature supports using a single analysis session to acquire representative walking patterns (Winter and Yack 1987). In addition, Burridge et al reported that subjects did not tend to migrate from one group of sEMG characteristics to another (Burridge, Wood et al. 2001) between assessments suggesting that sEMG during walking are relatively consistent between assessments.

It could be a criticism that although for visual gait analysis a validated system was implemented, a second rater (observer) was not also used. However, observational gait analysis was used to support other analysis techniques and principally to structure the observations from the video. The analysis of the video was also supported by discussion with physiotherapists in the author's department.

The gait analysis system was used to analyse the walking pattern of stroke patients in order to investigate possible features that could be used to characterise gait deficits. Using the system to measure the walking patterns of stroke patients raised issues that were not identified when used with unimpaired subjects. The application of the sEMG sensors was often complicated by the lack of a prominent muscle belly. Although placement was guided by measurement this was not always sufficient properly to place the pre-amplifier. It was sometimes difficult to locate anatomical landmarks by palpation. Due to skeletal malformation measurement between anatomical landmarks was inaccurate. Therefore some estimation and trial and error was required in the placement of sEMG sensors beyond being guided purely by measurement as defined by recent standards (Hermens, Freriks et al. 1999). It was important to realise that the standards for positioning require some user discretion.

6 Conclusion

In this project a cost-effective gait analysis system was used to capture the kinematics and surface electromyographic (sEMG) data from the lower limb of stroke patients whilst walking. A framework of signal processing software and analysis techniques was implemented and applied to the sEMG signals and kinematics data. This data was assimilated to provide a broad description of each of the subjects gait impairment. Furthermore, the data was used to group the subjects according to their predominant underlying impairment.

Commercially available, and relatively low cost 3D orientation sensors, were used to capture the kinematics of the lower limb. Utilising a small proportion of the possible data from such devices yielded significant insight into the subject's pattern of walking when combined with simple video gait analysis techniques.

Linear envelope analysis of impaired sEMG was extended through the application of principal component analysis (Ivanenko, Popple et al. 2004; Shiavi and Griffin 1981; Wootten, Kadaba et al. 1990). Although the numbers in the study were small, principal component analysis objectively identified the characteristic patterns of muscle activation in the subject group. The characteristic patterns of muscle activation were used to group subjects by comparing their linear envelope activity with those of the principal components. The use of this technique to a wider stroke population, supported with the application of signal classification techniques, was promoted.

In an attempt to retain the subtleties of the raw sEMG signal time-frequency analysis was applied to the sEMG data. Fourier analysis suggested a reduction in the mean frequency of the raw sEMG. However, instantaneous mean frequency was not obviously reduced in many subjects and in some cases peaks of mean frequency actually exceeded those seen in un-impaired subjects. The most interesting outcome was the increase in instantaneous mean frequency related to small increases in the amplitude of the raw sEMG. Equally so was the relationship of increased instantaneous mean frequency to the termination of bursts of sEMG. Therefore, time-frequency analysis was able to identify periods of increased sEMG activity not clearly identifiable from either the raw representation of sEMG or more importantly from either the linear envelope representation.

In an extension of time-frequency analysis and the work of Conforto et al. (Conforto, D'Alessio et al. 1999) a method of sub-band filtering was applied to the raw sEMG signal from the tibialis anterior and gastrocnemius. This technique was able to, in the presence of low amplitude and inappropriately phased activity, distinguish burst and inter-burst activity. This was in turn used to calculate a co-activation ratio between the two muscles. The application of this method unexpectedly identified the inappropriateness of assuming distinct patterns of burst activity in all subjects.

It is asserted that each of the techniques discussed can be developed into a framework to describe the impairment of the subject in terms of motion and electrophysiology. The earliest work to identify patterns in electromyographic signals in stroke patients has offered broad descriptions of impaired muscle activation patterns. Here the activation patterns of three ankle muscles have been evaluated in terms of phasing, amplitude, synergy and instantaneous frequency. Computational methods have been implemented to quantify some of these aspects and thus have provided a framework, particularly in terms of a prototype decision matrix, for the development of a quantitative evaluation technique.

With respect to the original objectives;

- Gait analysis equipment was developed and has been used in a clinical context within and beyond this project.
- Patterns of activity, phasing, co-activation and instantaneous frequency were identified as useful properties in characterising impairments.
- From existing literature principal component analysis and wavelet analysis were identified as already useful sEMG analysis techniques that could be developed for analysis of impairment.
- The analysis techniques were developed and implemented for use within this project.
- Clinical tests were conducted with a small number of patients and the results analysed with relation to underlying motor impairment.
- Groupings were made of the subjects and presented in terms of a decision matrix and, although the robustness of these could not be demonstrated due to the small number of participants, the groups were related to characteristic impairments previously reported in the literature.

This work has shown that existing signal processing techniques, extended for use within this project, can be used to identify characteristics of impairments in stroke patients and that these techniques are now presently available in the context of an in-house gait analysis system.

The project has provided a framework, from which the signal processing techniques and gait analysis equipment can be used within a larger patient group and classify characteristic patterns of impairment within the stroke population, information which will be useful better to direct therapy and promote recovery after stroke.

7 Recommendations for Further Work

The gait analysis system, although efficacious for this project, could be developed to simplify the data acquisition process and thus facilitate further the acquisition of gait data to progress this work.

- Currently the in-house sEMG system does not provide a real-time presentation of the signal. This would be very useful to evaluate the signal quality from each sensor.
- The Xsens system could be developed in two ways; (1) by developing the lower limb model to produce full three-dimensional kinematics. (2) The wireless capabilities of the latest version of the Xsens system to facilitate a fully wireless gait analysis system.
- Usability of the system to further enable data collection should be improved; this should be done in relation to clinical pressures and an understanding of the macro ergonomics of the scenarios in which a system might be used.

Signal processing routines presented in this project can be developed to extend this work.

- The generation of a database of sEMG from stroke patients would provide greater scope to develop outcome measures from wavelet analysis, particularly in relation to key phases in the gait cycle.
- Extension of technique, specifically with regard to work of De Stefano (Stefano and Allen 2003) and Von Tscharner (von Tscharner 2002). Generation of outcome measures from these techniques which are ecologically valid in the rehabilitation field.
- A broader patient group is required to produce characteristic patterns to provide utility of the PCA analysis and subsequently address the environmental validity of this technique. This therefore also requires the generation of a representative database of sEMG from stroke patients.
- Extension of techniques to additional lower limb muscle groups. Elevation angles were measured from three lower limb segments, as was sEMG, yet focus was given to the ankle. A rigorous understanding of lower limb impairments will require relating impaired muscle activation patterns from many muscle groups to kinematic data.

To facilitate the above, clinical trials involving a broader group of stroke patients should be undertaken; this will also provide the representative data to facilitate the classification of impairment in relation to underlying motor impairment during walking

- Collection of data from a broad demographic of stroke patients.
- Evaluation of day to day variation and effect on processing methods.
- Evaluation of environmental influences on data, for example, footwear.

8 References

Office of National Statistics, 1998, 5A2 Prevalence of Stroke per 1000 patients, by year: 1994-1998,

Allen, R. 1999. Editorial. Medical Engineering & Physics, 21(6-7), pp 377.

Alton, F., Baldey, L., Caplan, S. and Morrissey, M. C. 1998. A kinematic comparison of overground and treadmill walking. Clin Biomech (Bristol, Avon), 13(6), pp 434-440.

Aminian, K., Najafi, B., Bula, C., Lyvraz, P.-F. and Robert, P. 2002. Spatio-temporal parameters of gait measuredby an ambulatory system using miniture gyroscopes. J Biomechanics, 35, pp 689-699.

Andriacchi, T. P., Ogle, J. A. and Galante, J. O. 1977. Walking speed as a basis for normal and abnormal gait measurements. J Biomechanics, 10, pp 261-268.

Arsenault, B. A., Winter, D. A. and Marteniuk, R. G. 1986. Is there a "normal" profile of EMG activity in gait? Medical and Biological Engineering and computing, 24, pp 337-343.

Bailey, M. J. and Ratcliffe, C. M. 1995. Reliability of Physiological Cost Index Measurements in Walking Normal SUbjects Using Steady-state, Non-steady-state and Post-exercise Heart Rate Recording. Physiotherapy, 81(10), pp 618-623.

Baker, R. 2005. The search for patients with abnormalities bigger thanour measurement errors. In: Biomechanics of the lower limb in Health, Disease and Rehabilitation,5-7th September, Salford, UK, University of Salford. pp 2-5.

Baker, R. 2006. Baumann Lecture: Measurement Error in Clinical Gait Analysis:

A Thing of the Past? In: Joint ESMAC & GCMAS Meeting,25-30th September 2006, Amsterdam, VU University. pp 48-49.

Bamford, J., Sandercock, P., Dennis, M., Burn, J. and Warlow, C. 1990. A prospective study of acute cerebrovascular disease in the community stroke project -1981-86. 2. Incidence, case fatality rates and overall outcomes at one year of cerebral infarction, primary intracerebral, primary intracerebral and subarachnoid haemorrhage. Journal of Neurology Neurosurgery Psychiatry, 53, pp 16-22.

Basmajian, J. V., 1979. Muscles Alive - Their function revealed by electromyography, 4th ed, Williams and Wilkins.

Becher, J. G., Harlaar, J., Lankhorst, G. J. and Vogelaar, T. W. 1998. Measurement of impared muscle function of the gastrocnemius, soleus and tibialis anterior muscles in spastic hemiplegia: a preliminary study. Journal of Rehabilitation Research and Development, 35(3), pp 314-326.

Beck, T. W., Housh, T. J., Johnson, G. O., Weir, J. P., Cramer, J. T., Coburn, J. W. and Malek, M. H. 2005. Comparison of Fourier and wavelet transform procedures for examining the mechanomyographic and electromyographic frequency domain responses during fatiguing isokinetic muscle actions of the biceps brachii. Journal of Electromyography and Kinesiology, 15(2), pp 190-9.

Bekey, G., Chang, C., Perry, J. and Hoffer, M. 1977. Pattern recognition of multiple EMG signals applied to the description of human gait. Proceedings of the IEEE, 65(5), pp 674-681.

Bilodeau, M., Scindler, S. I., Williams, D. M., Chadran, R. and Sharma, S. S. 2003. EMG frequency content changes with increasing forceand during fatigue in the quadraceps femoris muscle of men and women. Journal of Electromyography and Kinesiology, 13(1), pp 83-92.

BTS PocketEMG. http://www.bts.it/eng/proser/pocemg.htm. 29/11/06

Bo Nielsen, J. 2002. Motoneuronal drive during human walking. Brain Res Brain Res Rev, 40(1-3), pp 192-201.

Bogey, R. A., Barnes, L. A. and Perry, J. 1992. Computer algorithms to characterize individual subject EMG profiles during gait. Archive of Physical and Medical Rehabilitation, 73(September), pp 835-831.

Bohannon, R. W. 1991. Strength deficits also predict gait performance in patients with stroke. Percept Mot Skills, 73(1), pp 146.

Bohannon, R. W. and Andrews, A. W. 1990. Correlation of knee extensor muscle torque and spasticity with gait speed in patients with stroke. Arch Phys Med Rehabil, 71(5), pp 330-3.

Bohannon, R. W. and Andrews, A. W. 1995. Relationship between impairments and gait performance after stroke: a summary of relevant research. Gait & Posture, 3, pp 236-240.

Bohannon, W. R. 1987. Gait performance of hemiparetic stroke patients: selected variables. Arch Phys Med Rehabil, 68(November), pp 777-781.

Bonato, P. 1998. A Statistical method for the measurement of muscle activation intervals from surface myoelectric signal during gait. IEEE Transactions on Biomedical Engineering, 45(3), pp 287-299.

Bonato, P. 2001. Recent advancements in the analysis of dynamic EMG data. IEEE Eng Med Biol Mag, 20(6), pp 29, 32.

Boostani, R. and Moradi, M. H. 2003. Evaluation of the forearm EMG signal features for the control of a prosthetic hand. Physiological Measurement, 24(2), pp 309-19.

Bourbonnais, D. and Vanden Noven, S. 1989. Weakness in patients with hemiparesis. Am J Occup Ther, 43(5), pp 313-9.

Boyd, R., Fatone, S., Rodda, J. and Olesch, C. 1999. High- or low-technology measurements of energy expenditure in clinical gait analysis? Developmental Medicine & Child Neurology, 41, pp 676-682.

Brandstater, M. E., Bruin, H. d., Gowland, C. and Clark, M. B. 1983. Hemiplegic gait analysis of temporal variables. Archive of Physical and Medical Rehabilitation, 64, pp 583-587.

Burden, A. M., Trew, M. and Baltzopoulos, V. 2003. Normalisation of gait EMGs: a re-examination. Journal of Electromyography and Kinesiology, 13(6), pp 519-532.

Burridge, J. H., Wood, D. E., Hermens, H. J., Voerman, G. E., Johnson, G. R., van Wijck, F., Platz, T., Gregoric, M., Hitchcock, R. and Pandyan, A. D. 2005. Theoretical and methodological considerations in the measurement of spasticity. Disabil Rehabil, 27(1-2), pp 69-80.

Burridge, J. H., Wood, D. E., Taylor, P. N. and McLellan, D. L. 2001. Indices to describe different muscle activation patterns, identified during treadmill walking, in people with spastic drop-foot. Medical Engineering and Physics, 23, pp 427 - 434.

Caplan, L. R. and Stein, R. W., 1986. Stroke a clinical approach. Stoneham, Butterworths.

Carol, N. C., Janes, D. and Maschuich, W. 1982. Evaluation pertinant to the gait of children myelomerningocele. Prosthet Orthot Int, 6, pp 27-34.

Casale, R., Buonocore, M., Massa, A. D. and Setacci, C. 1994. Electromyographic Signal Frequency Analysis in Evaluating Muscle Fatigue of Patients with Peripheral Arterial Disease. Archive of Physical and Medical Rehabilitation, 75(October), pp 1118-1121.

Chen, C. L., Chen, H. C., Tang, S. F., Wu, C. Y., Cheng, P. T. and Hong, W. H. 2003. Gait performance with compensatory adaptations in stroke patients with different degrees of motor recovery. Am J Phys Med Rehabil, 82(12), pp 925-35.

Chen, G., Patten, C., Kothari, D. H. and Zajac, F. E. 2005. Gait differences between individuals with post-stroke hemiparesis and non-disabled controls at matched speeds. Gait & Posture, 22(1), pp 51-56.

Chen, J. J., Sun, T. Y., Lin, T. H. and Lin, T. S. 1997. Spatio-temporal representation of multichannel EMG firing patterns and its clinical applications. Medical Engineering and Physics, 19(5), pp 420-430.

Chen, J.-J. J., Huseh, T.-C., Liou, J.-J., Hwang, I.-S. and Lin, S.-I. 1994. Assessment of Asymetric gait in Hemiplegia using electromyographic phasic activity. Biomedical Engineering Application, Basis & Communications, 6(2), pp 211-217.

Chong, K. C., Vojnic, C. D., Quanbury, A. O. and Letts, R. M. 1978. The assessment of the internal rotation gait in cerebral palsy: an electromyographic gait analysis. Clin Orthop Relat Res(132), pp 145-50.

Christodoulou, C. I. and Pattichis, C. S. 1999. Unsupervided pattern recognition for the classification of EMG signals. IEEE Trans Biomed Eng, 46(2), pp 169-78.

Churchill, A. J., Halligan, P. W. and Wade, D. T. 2002. RIVCAM: a simple video-based kinematic analysis for clinical disorders of gait. Comput Methods Programs Biomed, 69(3), pp 197-209.

Clancy, E. A. 1999. Electromyogram amplitude estimation with adaptive smoothing window length. IEEE Trans Biomed Eng, 46(6), pp 717-29.

Close, J. R. and Todd, F. N. 1959. The phasic activity of the muscles of the lower extremity and the effect of tendon transfer. Journal of Bone and Joint Surgery, 41-A(2), pp 189-208.

Conforto, S., D'Alessio, T. and Pignatelli, S. 1999. Optimal rejection of movement artefacts from myoelectric signals by means of a wavelet filtering procedure. Journal of Electromyography and Kinesiology, 9(1), pp 47-57.

Conte, L. R. L. and Merletti, R. 1995. Advances in processing of myoelectric signals part 2. Medical and Biological Engineering and computing, 33, pp 373-384.

Biomedicine and Health (BIOMED 2) 1994-1998. http://cordis.europa.eu/biomed/home.html. 09/06

Craik, R. L. and Oatis, C. A., 1994. Gait Analysis: Theory and Application, Mosby.

Craik, R. L. and Oatis, C. A., 1995. Gait Analysis: Theory and Application, Mosby.

Crenna, P. 1998. Spasticity and 'spastic' gait in children with cerebral palsy. Neurosci Biobehav Rev, 22(4), pp 571-8.

D'Alessio, T. and Conforto, S. 2001. Extraction of the envelope from surface EMG signals. IEEE Eng Med Biol Mag, 20(6), pp 55-61.

Datta, A. K., Farmer, S. F. and Stephens, J. A. 1991. Central nervous pathways underlying synchronization of human motor unit firing studied during voluntary contractions. J Physiol, 432, pp 401-425.

De Luca, C. J., Roy, A. M. and Erim, Z. 1993. Synchronization of motor-unit firings in several human muscles. J Neurophysiol, 70(5), pp 2010-2023.

De Quervain, I. A., Simon, S. R., Leurgans, S., Pease, W. S. and McAllister, D. 1996. Gait pattern in the early recovery period after stroke. J Bone Joint Surg Am, 78(10), pp 1506-14.

De Stefano, A., Burridge, J. H., Yule, V. T. and Allen, R. 2004. Effect of gait cycle selection on EMG analysis during walking in adults and children with gait pathology. Gait Posture, 20(1), pp 92-101.

DeLuca, C. J. 1997. The use of surface electromyography in biomechanics. Journal of Applied Biomechanics, 13(2), pp 135-163.

Pathokinesiology Department Physical Therapy Department, 1989, Observational Gait Analysis Handbook, CA,

Dietz, V. 1997. Neurophysiolgy of gait disorders: preseent and future applications (invited reviews). Electroencephalography & Clinical Neurophysiology, 103, pp 333-355.

Dietz, V. and Berger, W. 1983. Normal impaired muscle stiffness in gait: a new hypothesis. Experimental Neurology, 79, pp 680-687.

Dietz, V., Discher, M., Faist, M. and Trippel, M. 1990. Amplitude modulation of the human quadriceps tendon jerk reflex during gait. Exp Brain Res, 82(1), pp 211-3.

Dimitrijevic, M. R., Faganel, J., Sherwood, A. M. and McKay, W. B. 1981. Activation of paralysed leg flexors and extensors during gait in patients after stroke. Scandinavian Journal of Rehabilitation Medicine, 13, pp 109-115.

Dimitrova, N. A. and Dimitrov, G. V. 2003. Interpretation of EMG changes with fatigue: facts, pitfalls, and fallacies. J Electromyogr Kinesiol, 13(1), pp 13-36.

Dimonte, P. and Light, H. 1982. Pathoechanics, gait deviations and treatment of the rhuematoid foot. Physical Therapy, 62, pp 1148-1156.

Dubo, H. I. C., Peat, M., Winter, D. A., Quanbury, A. O., Hobson, A. D., Steinke, T. and Reimer, G. 1976. Electromyographic temporal analysisof gait: normal human locomotion. Archive of Physical and Medical Rehabilitation, 57, pp 415-420.

Duysens, J., Trippel, M., Horstmann, G. A. and Dietz, V. 1990. Gating and reversal of reflexes in ankle muscles during human walking. Exp Brain Res, 82(2), pp 351-8.

Duysens, J. and Van de Crommert, H. W. 1998. Neural control of locomotion; The central pattern generator from cats to humans. Gait & Posture, 7(2), pp 131-141.

Cetre for Reveiws and Dissemination, 1992, Effective Health Care bulletins: Stroke rehabilitation,

el-Abd, M. A., Ibrahim, I. K. and Dietz, V. 1993. Impaired activation pattern in antagonistic elbow muscles of patients with spastic hemiparesis: contribution to movement disorder. Electromyogr Clin Neurophysiol, 33(4), pp 247-55.

Englehart, K., Hudgins, B., Parker, P. A. and Stevenson, M. 1999. Classification of the myoelectric signal using time-frequency based representations. Medical Engineering & Physics, 21(6-7), pp 431-438.

Enoka, R. M. and Fuglevand, A. J. 2001. Motor unit physiology: some unresolved issues. Muscle Nerve, 24(1), pp 4-17.

Farina, D., Cescon, C. and Merletti, R. 2002. Influence of anatomical, physical, and detection-system parameters on surface EMG. Biological Cybernetics, 86(6), pp 445-456.

Farina, D. and Merletti, R. 2000. Comparison of algorithms for estimation of EMG variables during voluntary isometric contractions. Journal of Electromyography and Kinesiology, 10(5), pp 337-349.

Farina, D., Merletti, R. and Enoka, R. M. 2004. The extraction of neural strategies from the surface EMG. J Appl Physiol, 96(4), pp 1486-1495.

Farmer, S. F., Halliday, D. M., Conway, B. A., Stephens, J. A. and Rosenberg, J. R. 1997. A review of recent applications of cross-correlation methodologies to human motor unit recording. J Neurosci Methods, 74(2), pp 175-87.

Farmer, S. F., Swash, M., Ingram, D. A. and Stephens, J. A. 1993. Changes in motor unit synchronization following central nervous lesions in man. J Physiol, 463, pp 83-105.

Filligoi, G. and Felici, F. 1999. Detection of hidden rhythms in surface EMG signals with a non-linear time-series tool. Medical Engineering and Physics, 21, pp 439-448.

Frascarelli, M., Mastrogregori, L. and Conforti, L. 1998. Initial motor unit recruitment in patients with spastic hemiplegia. Electromyogr Clin Neurophysiol, 38(5), pp 267-71.

Freriks, B., Kleissen, R. and Hemensn, H. 1999. The performance of SEMG equipment used in different European laboratories. In: H. J. Hermens, R. Merletti, H. Rix and B. Freriks (Editors), SENIAM - Deliverable 7- State of the art on signal processing methods for surface electromyography.

Full, R. J. and Koditschek, D. E. 1999. Templates and anchors: neuromechanical hypotheses of legged locomotion on land. J Exp Biol, 202(Pt 23), pp 3325-32.

Fullmer, R. R., Meek, S. G. and Jacobsen, S. C. 1984. Optimization of an adaptive myoelectric filter. In: Annu. Int. Conf. IEEE Eng. in Med.

and Biol. Soc. pp 586–591.

Gemperline, J. J., Allen, S., Walk, D. and Rymer, W. Z. 1995. Characteristics of motor unit discharge in subjects with hemiparesis. Muscle Nerve, 18(10), pp 1101-14.

Gerdle, B., Henriksson-Larsen, K., Lorentzon, R. and Wretling, M. L. 1991. Dependence of the mean power frequency of the electromyogram on muscle force and fibre type. Acta Physiol Scand(142), pp 457–465.

Ghoussayni, S., Stevens, C., Durham, S. and Ewins, D. 2002. Gait Event Detecion: A comparison of force platform, visual inspection, and kinematic algorithm based methods.

Gladstone, D. J., Danells, C. J. and Black, S. E. 2002. The Fugl-Meyer Assessment of Motor Recovery after Stroke: A Critical Review of Its Measurement Properties

10.1177/154596802401105171. Neurorehabil Neural Repair, 16(3), pp 232-240.

Granat, M. H., Maxwell, D. J., Bosch, C. J., Ferguson, A. C. B., Lees, K. R. and Barbenel, J. C. 1995. A body-worn gait analysis system for evaluating hemiplegic gait. Medical Engineering and Physics, 17(5), pp 390-394.

Greenberg, M. B., Gronley, J. A., Perry, J. and Lewthaite, R. 1996. Concurrent validity of observational gait analysis using the vicon motion analysis system. Gait & Posture, 4, pp 167-208.

Guadagnoli, M. A., Etnyre, B. and Rodrigue, M. L. 2000. A test of a dual central pattern generator hypothesis for subcortical control of locomotion. Journal of Electromyography and Kinesiology, 10(4), pp 241-7.

Hägg, G. M. 1992. Interpretation of EMG spectral alterations and alteration indexes at sustained contraction. Journal Applied Physiology, 73, pp 1211-1217.

Hale, L. A. and Eales, C. J. 1998. Recovery of walking function in stroke patients after minimal rehabilitation. Physiother Res Int, 3(3), pp 194-205.

Hamrin, E., Eklund, G., Hillgren, A. K., Borges, O., Hall, J. and Hellstrom, O. 1982. Muscle strength and balance in post-stroke patients. Ups J Med Sci, 87(1), pp 11-26.

Harrison, M. J. G. and Dyken, M. L. 1983. Hypertension in stroke. In: M. J. G. Harrison, M. L. Dyken, A. K. Asburyet al (Editors), Neurology 3: Cerebral Vascular Disease, London, Butterworths. pp 48.

National electronic Library for Health. http://www.nelh.nhs.uk/. 09/02/2006

Hemmerich, A., Merwe, W. v. d. and Vaughan, C. L. 2004. Three-Dimentional in vivo Motion Analysis of Knee Joint Laxity under Torsional Loading. Am. J. Sports Med, 32(2), pp 369-375.

Hermens, H., Freriks, B. and Merletti, R., Eds. (1999). European Recomendations for Surface Electromyography, Biomedical Health Research Program.

Hermens, H. J., Boon, K. L. and Zilvold, G. 1984. The Clinical use of surface EMG. Electromyography & Clinical Neurophysiology, 24, pp 243-265.

Hershler, C. and Milner, M. 1978. An optimality criterion for processing electromyographic (EMG) signals relating to human locomotion. IEEE Trans. Biomed. Eng., BME-25, pp 413–420.

Hicks, Y. 2005. Markerless Motion Capture with a Single Video Camera. In: Biomechanics of the lower limb I Health, Disease and Rehabilitation,5-7th September, Salford, UK, University of Salford. pp 76-77.

Hirschberg, G. and Nathanson, M. 1952. Electromyographic recording of muscular activity in normal and spastic gaits. Archives of Physical Medicine, 33(April), pp 217-225.

Hodges, P. W. and Bui, B. H. 1996. A comparison of computer-based methods for the determination of onset of muscle contraction using electromyography. Electroencephalography and Clinical Neurophysiology/Electromyography and Motor Control, 101(6), pp 511-519.

Hood, V. L., Granat, M. H., Maxwell, D. J. and Hasler, J. P. 2002. A new method of using heart rate to represent energy expenditure: the Total Heart Beat Index. Arch Phys Med Rehabil, 83(9), pp 1266-73.

Hostens, I., Seghers, J., Spaepen, A. and Ramon, H. 2003. Validation of the wavelet spectral estimation tchnique in Biceps Brachii and Brachioradialis fatigue assessment during prolonged low-level static and dynamic contractions. Journal of Electromyography and Kinesiology, UK(UK), pp UK.

Hu, X. and Nenov, V. 2004. Multivariate AR modeling of electromyography for the classification of upper arm movements. Clin Neurophysiol, 115(6), pp 1276-87.

Huges, K. and Bell, F. 1994. Visual Gait assessment of hemiplegic gait following stroke: pilot study. Archive of Physical and Medical Rehabilitation, 75(October), pp 1100-1107.

International Classification of Disease -10 Chapter IX: Diseases of the Circulatory System. www.www3.who.int/icd/vol1htm2003/gi60.htm. Oct

Avon Health Authority, 2003, IS117 Incidence, aetiology and management of stroke, London,

Itiki, C. 2005. Dynamic Programming and Diagnostic Classification. Journal of Optimization Theory and Applications, 127(3), pp 579-586.

Ivanenko, Y. P., Grasso, R., Zago, M., Molinari, M., Scivoletto, G., Castellano, V., Macellari, V. and Lacquaniti, F. 2003. Temporal components of the motor patterns expressed by the human spinal cord reflect foot kinematics. J Neurophysiol, 90(5), pp 3555-65.

Ivanenko, Y. P., Popple, R. E. and Lacquaniti, F. 2004. Five basic muscle activation patterns account for muscle activity during human locomotion. Journal Physiology, 556(1), pp 267-282.

Jakobsson, F., Edstrom, L., Grimby, L. and Thornell, L. E. 1991. Disuse of anterior tibial muscle during locomotion and increased proportion of type II fibres in hemiplegia. Journal of the Neurological Sciences, 105(1), pp 49-56.

Jansen, B. H., Miller, V. H., Mavrofrides, D. C. and Stegink Jansen, C. W. 2003. Multidimensional EMG-based assessment of walking dynamics. IEEE Trans Neural Syst Rehabil Eng, 11(3), pp 294-300.

Jolliffe, I. T., c1986. Principal component analysis. New York, Springer-Verlag.

Jorgensen, H. S., Nakayama, H., Raaschou, H. O. and Olsen, T. S. 1995. Recovery of walking function in stroke patients: the Copenhagen Stroke Study. Arch Phys Med Rehabil, 76(1), pp 27-32.

Kadaba, M., Ramakrishnan, H., Wootten, M., Gainey, J., Gorton, G. and Cochran, G. 1989. Repeatability of kinematic, kinetic, and electromyographic data in normal adult gait. Journal of Orthopaedic Research, 7(6), pp 849-860.

Kang, W. J., Cheng, C. K., Lai, J. S., Shiu, J. R. and Kuo, T. S. 1996. A Comparitive analysis of various EMG pattern recognition methods. Medical Engineering and Physics, 18(5), pp 390-395.

Kang, W. J., Shiu, J. R., Cheng, C. K., Lai, J. S., Tsao, H. W. and Kuo, T. S. 1995. The application of cepstral coefficients and maximum likelihood method in EMG pattern recognition. IEEE Trans Biomed Eng, 42(8), pp 777-85.

Karlsson, S., Gerdle, B. and Akay, M. 1998. Analyzing Surface Myoelectric Signals Recorded During Isokinetic Contractions. IEEE Transactions on Biomedical Engineering, 45(3), pp 97-105.

Kersting, U. G. 2005. Silhouette-Based Human Motion Estimation. In: Biomechanics of the lower limb in Health, Disease and Rehabilitation,5-7th September, Salford, UK, University of Salford. pp 78-79.

Kilner, J. M., Baker, S. N. and Lemon, R. N. 2002. A novel algorithm to remove electrical cross-talk between surface EMG recordings and its application to the measurement of short-term synchronisation in humans 10.1113/jphysiol.2001.012950. J Physiol (Lond), 538(3), pp 919-930.

Kirtley, C., 2005. Clinical Gait Analysis: Theory and Practice, Churchill Livingstone.

Kleine, B. U., Stegeman, D. F., Mund, D. and Anders, C. 2001. Influence of motoneuron firing synchronization on SEMG characteristics in dependence of electrode position. J Appl Physiol, 91(4), pp 1588-1599.

Kleissen, R. F. M., Litjens, M. C. A., Baten, C. T. M., Harlaar, J., Hof, A. L. and Zilvold, G. 1997. Consistency of surface EMG patterns obtained during gait from three laboratories using standerdised measurement tecnique. Gait & Posture, 6, pp 200-209.

Knutsson, E. 1981. Gait control in hemiparesis. Scandinavian Journal of Rehabilitation Medicine, 13, pp 101-108.

Knutsson, E. and Richards, C. 1979. Different types of distributed motor control in gait of hemiperetic patients. Brain, 102, pp 405-430.

Kwende, M. M., Jarvis, J. C. and Salmons, S. 1995. The input-output relations of skeletal muscle. Proceedings Biological Society, 261(1361), pp 193-201.

Lacquaniti, F., Grasso, R. and Zago, M. 1999. Motor Patterns in Walking. News Physiol Sci, 14, pp 168-174.

Lamontagne, A., Malouin, F. and Richards, C. 2001. Locomotor-SpecificMeasure of Spasticity of plantarflexor Muscles After Stroke. Archive of Physical and Medical Rehabilitation, 82(December), pp 1696-1704.

Lamontagne, A., Malouin, F., Richards, C. and F, D. 2001. Mechanisms of disturbed motor control in ankle weakness during gait after stroke. Gait & Posture, 15, pp 244-255.

Lamontagne, A., Malouin, F. and Richards, C. L. 2000. Contribution of passive stiffness to ankle plantarflexor moment during gait after stroke. Archives of Physical Medicine and Rehabilitation, 81(3), pp 351-358.

Lamontagne, A., Richards, C. L. and Malouin, F. 2000. Coactivation during gait as an adaptive behavior after stroke. Journal of Electromyography and Kinesiology, 10, pp 407-415.

Lamontagne, A., Richards, C. L. and Malouine, F. 1998. Coactivation at the ankle during gait on the non-paretic limb of persons with hemiperesis. Can J Rehab, 11, pp 210-211.

Lance, J. W. 1980. Symposium synopsis. In: R. G. Feldman, R. R. Young and W. P. Koella (Editors), Spasticity: disordered motor control, Chicago, Year book medical publishers. pp 485-494.

Lange, F., Van Weerden, T. W. and Van Der Hoeven, J. H. 2002. A new surface electromyography analysis method to determine spread of muscle fiber conduction velocities. J Appl Physiol, 93(2), pp 759-64.

Langhorne, P. and Pollock, A. 2002. What are the components of effective stroke unit care? Age Ageing, 31(5), pp 365-71.

Lauer, R. T., Smith, T. B. and Betz, R. R. 2005. Application of a Neuro-Fuzzy Network for Gait Event Detection Using Electromyography in the Child with Cerebral Palsy. IEEE Transactions on Biomedical Engineering, 52(9), pp 1532-1540.

Lehmann, J. F., Condon, S. M., Price, R. and deLateur, B. J. 1987. Gait abnormalities in hemiplegia: Their correction by ankle-foot orthoses. Archives of Physiotherepy and medical Rehabilitation, 68, pp 763-771.

Lord, S. E., Halligan, P. W. and Wade, D. T. 1998. Visual gait analysis: the development of a clinical assessment and scale. Clinical Rehabilitation, 12, pp 107-119.

Lowery, M. M., Vaughan, C. L., Nolan, P. J. and O'Malley, M. J. 2000. Spectral compression of the electromyographic signal due to decreasing muscle fiber conduction velocity. IEEE Trans Rehabil Eng, 8(3), pp 353-61.

MacGregor, J. 1979. The objective measurement of physical performance with long term ambulatory physiological survallance equipment (LAPSE). In: 3rd International Symposium on Ambulatory Monitoring, London, Academic Press. pp 29-39.

MacIssac, D., Parker, P. A. and Scott, R. N. 2001. The short-time transform and muscle fatigue assessment in dynamic contractions. Journal of Electromyography and Kinesiology, 11, pp 439-449.

Mackey, A., Lobb, G., Walt, S. and Stott, N. S. 2002. The reliability and validity of the observational gait scale in children who have spastic diplegia. Developmental Medicine & Child Neurology: Abstracts 2002, 44(August), pp 13.

Mallat, S., 1999. A Wavelet Tour of Signal Processing, Academic Press.

Mallat, S. G. 1989. A Theory for MultiresolutionSignal Decomposition: The Wavelet Representation. IEEE Transactions on Pattern Analysis and Machine Intellegence, 11(7), pp 674-693.

Mant, J., McManus, R. J., Hare, R. and Mayer, P. 2003. Identification of stroke in the community: a comparison of three methods. Br J Gen Pract, 53(492), pp 520-4.

US Department of Health and Human Services (National Institute for Occupational Safety and Health), 1992, Selected Topics in Surface Electromyography for Use in the Occupational Setting: Expert Perspective,

Marsden, J. F., Farmer, S. F., Halliday, D. M., Rosenberg, J. R. and Brown, P. 1999. The unilateral and bilateral control of motor unit pairs in the first dorsal interosseous and paraspinal muscles in man. J Physiol (Lond), 521(2), pp 553-564.

Mathworks 2006. Signal Processing Toolbox Ver. 6.0. In: MATLAB User Manual.

Mathworks 2006. Wavelet Toolbox Ver. 6.0. In: MATLAB User Manual.

Mayagoitia, R. E., Nene, A. V. and Veltink, P. H. 2002. Accelerometer and rate gyroscope measurement of kinematics: an inexpensive alternative to optical motion analysis system. J Biomechanics, 35, pp 537-542.

McCrea, D. A. 1996. Supraspinal and segmental interactions. Canadian Journal of Physiology andPharmacology, 74, pp 513-517.

McCrea, D. A. 2001. Spinal circuitry of sensorimotor control of locomotion. Journal Physiology, 533(Pt 1), pp 41-50.

McNee, A. E. and Watter, P. 2002. Is the observational gait scale reliable. Developmental Medicine & Child Neurology: Abstracts 2002, 44(October), pp 37.

Merkle, L. A., Layne, C. S., Bloomberg, J. J. and Zhang, J. J. 1998. Using factor analysis to identify neuromuscular synergies during treadmill walking. J Neurosci Methods, 82(2), pp 207-14.

Merletti, R. 1999. The Traditional Fourier Approach to EMG AnalysisDuring Voluntary or Evoked Sustained Contractions. In: H. J. Hermens, R. Merletti, H. Rix and B. Freriks (Editors), SENIAM - Deliverable 7 - State of the art on Signal Processing.

Merletti, R. and Conte, L. R. L. 1995. Advances in processing of myoelectric signals part 1. Medical and Biological Engineering and computing, 33, pp 373-384.

Mewett, D., Reynolds, K. and Nazeran, H. 2001. Embedding Space Normalisation in Recurrence Quantification Analysis of EMG. In: 2nd Conference of the victorian chapter IEEE Engineering in Medicine & Biology Society, Victoria.

Micera, S., Sabatini, A. M., Dario, P. and Rossi, B. 1999. A hybrid approach to EMG pattern analysis for classification of arm movements using statistical and fuzzy techniques. Med Eng Phys, 21(5), pp 303-11.

Mohapatra, S. and Kelker, R. S. 2003. Study on Relationship Between Initial Stroke Severity and Recovery of Mobility Function in Acute Stroke Inpatients. The Indian Journal of Occupaional Therapy, 35(3).

Monaghan, C. C., Veltink, P. H. and Riel, W. J. B. M. V. 2004. Gyroscope Control of Planterflexors for Push-Off of Stroke Subjects. In: 9th IFESS conference,6-9th September 2004, Bournemouth, Salisbury Health Care NHS Trust. pp 280-281.

Mrachacz-Kersting, N., Lavoie, B. A., Andersen, J. B. and Sinkjaer, T. 2004. Characterisation of the quadriceps stretch reflex during the transition from swing to stance phase of human walking. Exp Brain Res, 159(1), pp 108-22.

Mulroy, S., Gronley, J., Wiess, W., Newsam, C. and Perry, J. 2001. Use of cluster analysis for gait pattern classification of patients following stroke. Gait & Posture, 13, pp 309-310.

Murray, M. P., Mollinger, L. A., Gardner, G. M. and Sepic, S. B. 1984. Kinematic and EMG patterns during slow, free, and fast walking. Journal of Orthopaedic Research, 2, pp 272-280.

Nadeau, S., Gravel, D., Arsenault, A. B. and Bourbonnais, D. 1999. Plantarflexor weakness as a limiting factor of gait speed in stroke subjects and the compensating role of hip flexors. Clinical Biomechanics, 14(2), pp 125-135.

Royal Colledge of physicians, 2004, National Clinical Guidlines for Stroke 2ed, London,

National Instruments. www.ni.com. 09/06

Neilsen, J., Arendt-Nielsen, L. and Pedotti, A. 1994. Power Spectrum analysis of the rectified Electromyogram during gait for normals and patients. Electromyography and Kinesiology, 4(June), pp 105-115.

Nelson, A. J. 1974. Functional ambulation profile. Physiotherapy, 54, pp 1059-1065.

Nene, A. V. 1993. Physiological Cost Indexof Walking in Able-Bodied Adolescents and Adults. Clinical Rehabilitation, 7, pp 319-326.

Nieminen, H. and Takala, E. P. 1996. Evidence of deterministic chaos in the myoelectric signal. Electromyogr Clin Neurophysiol, 36(1), pp 49-58.

Nilsson, J., Federici, C. and Panizza, M. 1997. Analysis of electromyographic signals using the "EMGLAB" software. Electroencephalography & Clinical Neurophysiology, 103(1), pp 220.

Nourbahsh, M. R. and Kukulla, C. G. 2003. Relationship between muscle length and moment arm on EMG activity of human triceps surae muscle. Journal of Electromyography and Kinesiology, 14, pp 263-273.

O'Dwyer, N. J., Ada, L. and Neilson, P. D. 1996. Spasticity and muscle contracture following stroke. Brain, 119 (Pt 5), pp 1737-49.

Olney, S. J., Elkin, N. D. and Lowe, P. J. 1979. An ambulation profile for clinical gait evaluation. Physiotherapy Canada, 31, pp 85-90.

Olney, S. J., Griffin, M. P., Monga, T. N. and McBride, I. D. 1991. Work and power in gait of stroke patients. Archive of Physical and Medical Rehabilitation, 72, pp 309-314.

Olney, S. J. and Richards, C. 1996. Hemiparetic gait following stroke. Part 1: Characteristics. Gait & Posture, 4, pp 136-148.

The Cochrane Database of Systematic Reviews, 2003, Outpatient Service Trialist. Therepy-based rehabilitation services for stroke patients at home.,

Pandyan, A. D., Gregoric, M., Barnes, M. P., Wood, D., Van Wijck, F., Burridge, J., Hermens, H. and Johnson, G. R. 2005. Spasticity: clinical perceptions, neurological realities and meaningful measurement. Disabil Rehabil, 27(1-2), pp 2-6.

Park, S. H. and Lee, S. P. 1998. EMG pattern recognition based on artificial intelligence techniques. IEEE Trans Rehabil Eng, 6(4), pp 400-5.

Parker, P. A., Stuller, J. A. and Scott, R. N. 1977. Signal processing for the multistate myoelectric channel. Proc. IEEE, 65, pp 662-674.

Pattichis, C. S. and Elia, A. G. 1999. Autoregressive and cepstral analyses of motor unit action potentials. Medical Engineering & Physics, 21(6-7), pp 405-419.

Perry, J., 1989. Observational Gait Analysis Handbook. CA, Pathokinesiology Department Physical Therapy Department.

Perry, J., 1992. Gait Analysis: Normal and Pathological Function. Thorofare, Slack.

Perry, J. 1993. Determinents of muscle function in spastic lower extremity. Clin Orthop Relat Res, pp 288.

Perry, J., Waters, R. L. and Perrin, T. 1978. Electromyographic analysis of equinovarus following stroke. Clin Orthop Relat Res, 131, pp 47-53.

Pierrynowski, M. R. and Galea, V. 2001. Enhancing the ability of gait analyses to differentiate between groups: Scailing gait data to body size. Gait & Posture, 13, pp 193-201.

Pomeroy, V. M., Pramanik, A., Sykes, L., Richards, J. and Hill, E. 2003. Agreement between physiotherapists on quality of movement rated via videotape. Clinical Rehabilitation, 17, pp 264-272.

Rechtien, J. J., Gelblum, J. B., Haig, A. J. and Gitter, A. J. 1996. Technology assessment: Dynamic electromyography in gait and motion analysis. Muscle & Nerve, 19(3), pp 396-402.

Ricamato, A. L. and Hidler, J. M. 2005. Quantification of the dynamic properties of EMG patterns during gait. Journal of Electromyography and Kinesiology, In Press, Corrected Proof.

Ricci, S., Celani, M. G. and LaRosa, F. 1991. SEPIVAC: a community-based study of stroke incidence in Umbria, Italy. Journal of Neurology Neurosurgery Psychiatry, 54, pp 695-698.

Ripoli, A., Belardinelli, A., Palagi, G., Franchi, D. and Bedini, R. 1999. An effective algorithm for quick fractal analysis of movement biosignals. J Med Eng Technol, 23(6), pp 216-21.

Robertson, Z. C. and Attfield, S. F. 2005. Investigation into the Role of the Bioengineer. In: IPEM Future of Engineering in Gait Analysis, Guys Hospital, London.

Roetenberg, D., Buurke, J. H., Veltink, P. H., Cordero, A. F. and Hermens, H. J. 2003. Surface electromyography analysis for variable gait. Gait & Posture, 18, pp 109-117.

Rose, J. R. and Gamble, J. G., 1994. Human Walking, 2nd ed. Baltimore, Williams & Wilkins.

Rose, J. R. and Gamble, J. G. 1994. Kinematics of normal human walking. In: Human Walking, Baltimore, Williams & Wilkins.

Roth, E. J., Merbitz, C., Mroczek, K., Dungan, S. A. and Suh, W. W. 1997. Hemiplegic gait: relationship between walking speed and other temporal parameters. American Journal of Physical Medicine and Rehabilitation, 76(2), pp 128-137.

Rothwell, J., 1996. Control of Human Volutary Movement, 2nd ed. London, Chapman & Hall.

Schulte, E., Dimitrova, N. A., Dimitrov, G. V., Rau, G. and Disselhorst-Klug, C. 2005. Estimation of the muscle fibre semi-length under varying joint positions on the basis of non-invasively extracted motor unit action potentials. Journal of Electromyography and Kinesiology, 15(3), pp 290-299.

Schulte, E., Farina, D., Merletti, R., Rau, G. and Disselhorst-Klug, C. 2004. Influence of muscle fibre shortening on estimates of conduction velocity and spectral frequencies from surface electromyographic signals. Med Biol Eng Comput, 42(4), pp 477-86.

S-Cook, A. and Woollacott, M. H., 2001. Motor Control Motor Control: Theory and Practical Applications, 2nd ed. London, Lippincott Wiliams & Wilkins.

Shiavi, R., Bugle, H. J. and Limbird, T. 1987. Electromyographic gait assesment, part 1: Adult EMG profiles and walking speed. Journal of Rehabilitation Research and Development, 24(2), pp 13-23.

Shiavi, R. and Griffin, M. P. 1981. Representing and Clustering electromyographic gait patterns with multivariate techniques. Medical and Biological Engineering and computing, 19, pp 605-611.

Simon, S. R. 2004. Quantification of human motion: gait analysis-benefits and limitations to its application to clinical problems. J Biomech, 37(12), pp 1869-80.

Sinkjaer, T. 1997. Muscle, reflex and central components in the control of the ankle joint in healthy and spastic man. Acta Neurol Scand Suppl, 170, pp 1-28.

Sinkjaer, T., Andersen, J. B., Ladouceur, M., Christensen, L. O. and Nielsen, J. B. 2000. Major role for sensory feedback in soleus EMG activity in the stance phase of walking in man. Journal Physiology, 523 Pt 3, pp 817-27.

Solomonow, M., Baten, C., Smit, J., Baratta, R., Hermens, H., D'ambrosia, R. and Shoji, H. 1990. Electromyogram power spectral frequencies associated with motor unit recruitment stratergies. Journal Applied Physiology, 68, pp 1177-1185.

Sommerfield, D. K., Eek, E., Svensson, A.-K., Holmqvist, L. W. and Arbin, M. H. 2004. Spasticity After Stroke: Its Occurences and association with Motor Impairments and Activity Limitations. Stroke, 35, pp 134-140.

St-Amant, Y., Rancourt, D. and Clancy, E. A. 1998. Influence of smoothing window length on electromyogram amplitude estimates. IEEE Trans Biomed Eng, 45(6), pp 795-800.

Staude, G. and Wolf, W. 1999. Objective motor reponse onset detection in surface myoelectric signals. Medical Engineering and Physics, 21, pp 449-467.

Stefano, A. D. and Allen, R. 2003. Application of Complex Wavelets for EMG Analysis During Gait of Asymptomatic and Pathological Subjects. International Journal of Wavelets, Multiresolution and Information Processing, 1(4), pp 425-448.

Su, F. C. and Wu, W. L. 2000. Design and testing of a genetic algorithm neural network in the assessment of gait patterns. Med Eng Phys, 22(1), pp 67-74.

Sutherland, H., Salmons, S., Ramnarine, I. R., Capoccia, M., Walsh, A. A. and Jarvis, J. C. 2006. Adaptive conditioning of skeletal muscle in a large animal model (Sus domesticus). Journal of Anatomy, 209(2), pp 165-77.

Thomas, C. K., Butler, J. E. and Zijdewind, I. 2002. Patterns of pathological firing in human motor units. Adv Exp Med Biol, 508, pp 237-44.

Tong, K. and Granat, M. H. 1999. A Practical Gait Analysis System Using Gyroscopes. Medical Engineering and Physics, 21, pp 87-94.

Toro, B. and Farren, P. 2002. Review of observational gait analysis in clinical pratice. Physiotherapy, 88(11), pp 701.

Toro, B., Nester, C. J. and Farren, P. C. 2003. The status of gait assessment among physiotherapists in the United Kingdom ,. Archives of Physical Medicine and Rehabilitation, 84(12), pp 1878-1884.

Torrence, C. and Compo, G. 1998. A Practical Guide to Wavelet Analysis. Bullitin of the American Meteorological Society, 79(1), pp 60-78.

Tortora, G. J. and Grabowski, S. R., 2000. Principles of Anatomy and Physiology, 9th ed, John Wiley & Son, Inc.

Umezu, Y., Kawazu, T., Tajima, F. and Ogata, H. 1998. Spectral electromyographic fatigue analysis of back muscles in healthy adult women compared with men. Arch Phys Med Rehabil, 79(5), pp 536-8.

Van de Crommert, H. W., Mulder, T. and Duysens, J. 1998. Neural control of locomotion: sensory control of the central pattern generator and its relation to treadmill training. Gait & Posture, 7(3), pp 251-263.

Voerman, G. E., Gregoric, M. and Hermens, H. J. 2005. Neurophysiological methods for the assessment of spasticity: the Hoffmann reflex, the tendon reflex, and the stretch reflex. Disabil Rehabil, 27(1-2), pp 33-68.

von Tscharner, V. 2000. Intensity analtsis in time-frequency space of surface myoelectric signals by wavelet of specified resolution. Journal of Electromyography and Kinesiology, 10, pp 433-445.

von Tscharner, V. 2002. Time-frequency and principal-component methods for the analysis of EMGs recorded during a mildly fatiguing exercise on a cycle ergometer. Journal of Electromyography and Kinesiology, 12(6), pp 479-492.

von Tscharner, V. and Goepfert, B. 2003. Gender dependent EMGs of runners resolved by time/frequency and principal pattern analysis. Journal of Electromyography and Kinesiology, 13(3), pp 253-272.

von Tscharner, V., Goepfert, B. and Nigg, B. M. 2003. Changes in EMG signals for the muscle tibialis anterior while running barefoot or with shoes resolved by non-linearly scaled wavelets. Journal of Biomechanics, 36(8), pp 1169-1176.

vonSchroeder, H., Coutts, R., Lyden, P., Billings, E. and Nickel, V. 1995. Gait Parameters following Stroke: A Practical Assessment. Journal of Rehabilitation Research and Development, 32(1), pp 25-31.

Royal Colledge of physicians, 2000, National Clinical Guidlines for Stroke, London,

Wade, D. T., Wood, V. A., Heller, A., Maggs, J. and Hewer, R. L. 1987. Walking after stroke: Measurement and recovery over the first three months. Scandinavian Journal of Rehabilitation Medicine, 19, pp 25-30.

Wakeling, J., Pascual, S., Nigg, B. and Tscharner, V. 2001. Surface EMG shows distinct populations of muscle activity when measured during sustained sub-maximal exercise. European Journal of Applied Physiology, 86(1), pp 40-47.

Wandel, A., Jorgensen, H. S., Nakayama, H., Raaschou, H. O. and Olsen, T. S. 2000. Prediction of walking function in stroke patients with initial lower extremity paralysis: the Copenhagen Stroke Study. Arch Phys Med Rehabil, 81(6), pp 736-8.

Watkins, C. L., Leathley, M. J., Gregson, J. M., Moore, A. P., Smith, T. L. and Sharma, A. K. 2002. Prevalence of spasticity post stroke. Clinical Rehabilitation, 16(5), pp 515-22.

Webber, C. L., Schmidt, M. A. and Walsh, J. M. 1995. Influence of isometric loading on biceps EMG dynamics as assessed by linear and nonlinear tools. Journal Applied Physiology, 79, pp 814-822.

Webber, C. L. and Zbilut, J. B. 1994. Dynamical assessment of physiological systems and states using recurrence plot stratergies. Journal Applied Physiology, 76(2), pp 965-975.

Whittle, M. W., 2002. Gait Analysis an Introduction, 3rd ed. Oxford, Butterworth-Heinemann.

International Classification of Functioning. http://www3.who.int/icf/icftemplate.cfm. 03/10

Wiles, C. M., Newcombe, R. G., Fuller, K. J. and Price, M. 2003. Use of videotape to assess mobility in a controlled randomized crossover trial of physiotherapy in chronic multiple schlerosis. Clinical Rehabilitation, 17, pp 256-263.

Williams, D. M., Katch, F. I. and Katch, V. L., 1991. Excersise Physiology: Energy, nutrition and Human Performance, 3rd ed. London, Lea & Febiger.

Winter, D. and Yack, H. J. 1987. EMG profiles during normal walking: stride to stride and intersubject variability. Electroencephalography & Clinical Neurophysiology, 67, pp 402-411.

Winter, D. A. 1984. Pathologic Gait Diagnosis with Computer-Averaged Electromyographic Profiles. Archives of Physiotherepy and medical Rehabilitation, 65(July), pp 383-398.

Winter, D. A., 1990. The biomechanics and motor control of human gait, 2nd ed, Wiley-Interscience.

Winter, D. A., Eng, J. J. and G, I. M. 1995. A Review of Kinetic Parameters In Human Walking. In: R. L. Craik and C. A. Oatis (Editors), Gait Analysis: Theory and Application, St Louis, Mosby. pp 252-270.

Wood, D. E., Burridge, J. H., van Wijck, F. M., McFadden, C., Hitchcock, R. A., Pandyan, A. D., Haugh, A., Salazar-Torres, J. J. and Swain, I. D. 2005. Biomechanical approaches applied to the lower and upper limb for the measurement of spasticity: a systematic review of the literature. Disabil Rehabil, 27(1-2), pp 19-32.

Wootten, M. E., Kadaba, M. P. and Cochran, G. V. 1990. Dynamic electromyography. I. Numerical representation using principal component analysis. J Orthop Res, 8(2), pp 247-58.

Wu, G., Siegler, S., Allard, P., Kirtley, C., Leardini, A., Rosenbaum, D., Whittle, M., D'Lima, D. D., Cristofolini, L., Witte, H., Schmid, O. and Stokes, I. 2002. ISB recommendation on definitions of joint coordinate system of various joints for the reporting of human joint motion--part I: ankle, hip, and spine. International Society of Biomechanics. J Biomech, 35(4), pp 543-8.

Wu, G., van der Helm, F. C., Veeger, H. E., Makhsous, M., Van Roy, P., Anglin, C., Nagels, J., Karduna, A. R., McQuade, K., Wang, X., Werner, F. W. and Buchholz, B. 2005. ISB recommendation on definitions of joint coordinate systems of various joints for the reporting of human joint motion--Part II: shoulder, elbow, wrist and hand. J Biomech, 38(5), pp 981-992.

Yang, F. and Yuan, X. 2005. Human movement reconstruction from video shot by a single stationary camera. Ann Biomed Eng, 33(5), pp 674-84.

Yang, J. F., Fung, J., Edamura, M., Blunt, R., Stein, R. B. and Barbeau, H. 1991. H-reflex modulation during walking in spastic paretic subjects. Can J Neurol Sci, 18(4), pp 443-52.

Yang, J. F. and Winter, D. A. 1883. Electromyography reliability in maximal and submaximal isometric contractions. Archive of Physical and Medical Rehabilitation, 64, pp 417-420.

Yang, J. F. and Winter, D. A. 1984. Electromyographic amplitude normalization methods: improving their sensitivity as diagnostic tools in gait analysis. Arch Phys Med Rehabil, 65, pp 517-521.

Yang, J. F. and Winter, D. A. 1985. Surface EMG profiles during different walking cadences in humans. Electroencephalography & Clinical Neurophysiology, 60, pp 485-491.

Yelnik, A., Albert, T., Bonan, I. and Laffont, I. 1999. A clinical guide to asses the role of lower limb extensor overactivity in hemiplegic gait disorders. Stroke, 30, pp 580-585.

Zajac, F. E., Neptune, R. R. and Kautz, S. A. 2003. Biomechanics and muscle coordination of human walking: part II: lessons from dynamical simulations and clinical implications. Gait & Posture, 17(1), pp 1-17.

Zhang, L.-Q., Shiavi, R., Hunt, M. A. and Chen, J.-J. J. 1991. Clustering analysis and pattern discrimination of EMG linear envelopes. IEEE Transactions on Biomedical Engineering, 38(8), pp 777-784.

A Appendix

Impaired Subject Data

A.I Observational Gait analysis results

The following are the results from the Rivermead gait analysis, observational gait analysis, scale. The results form each observational gait analysis form have been plotted on a bar chart to aid interpretation. The bar chart plots the level of severity as defined in the gait analysis scale from 0 – 3, three being the most severe. The chart progresses from left to right, from common stance phase impairments to common swing phase impairments. All the results are for the subject's paretic leg. A description of the impairment being graded forms the x-axis of the chart.

A.I.a CVA03

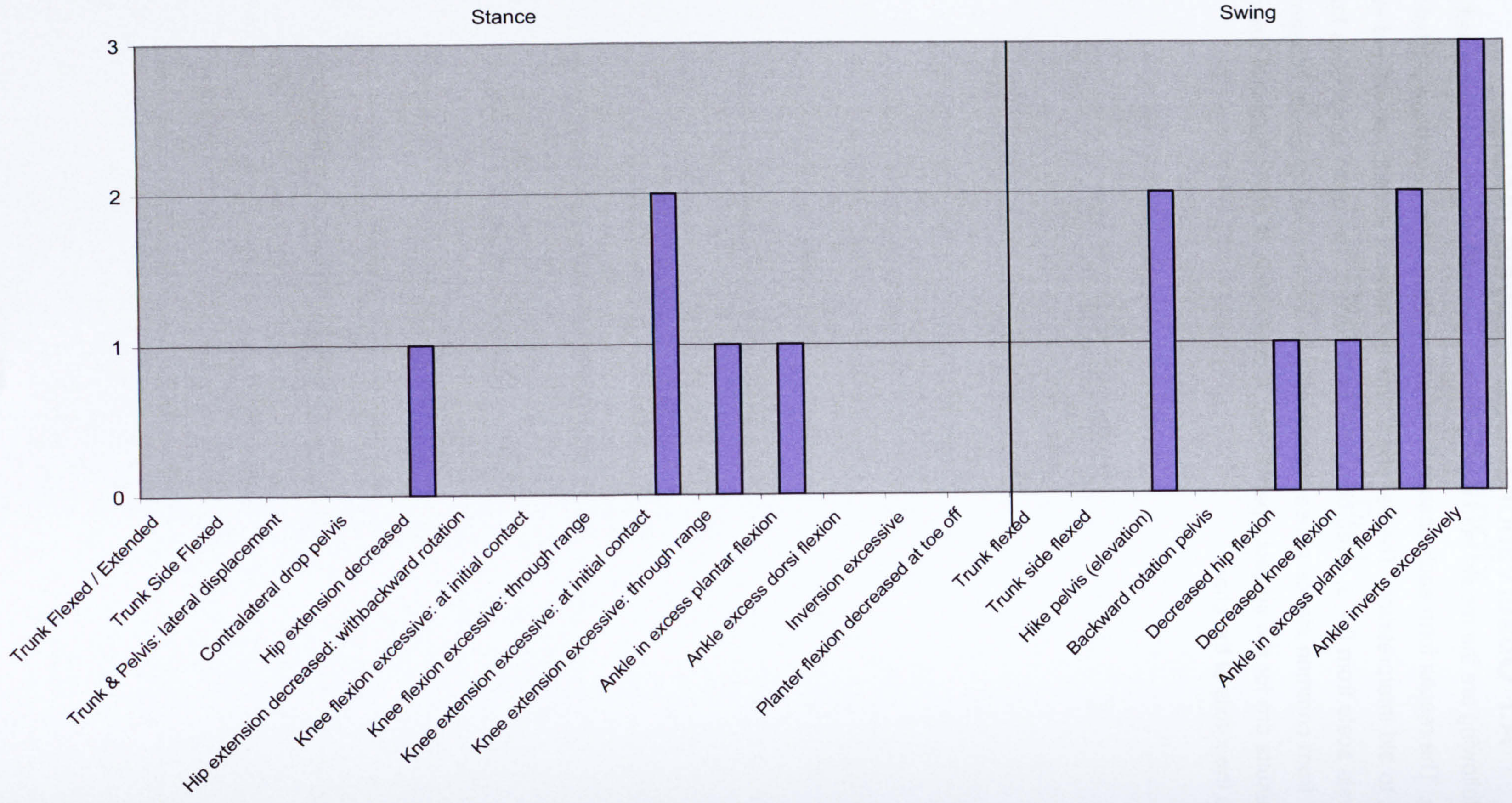

Appendix Figure 1 Rivermead observational gait analysis scale for subject CVA03

A.I.b CVA06

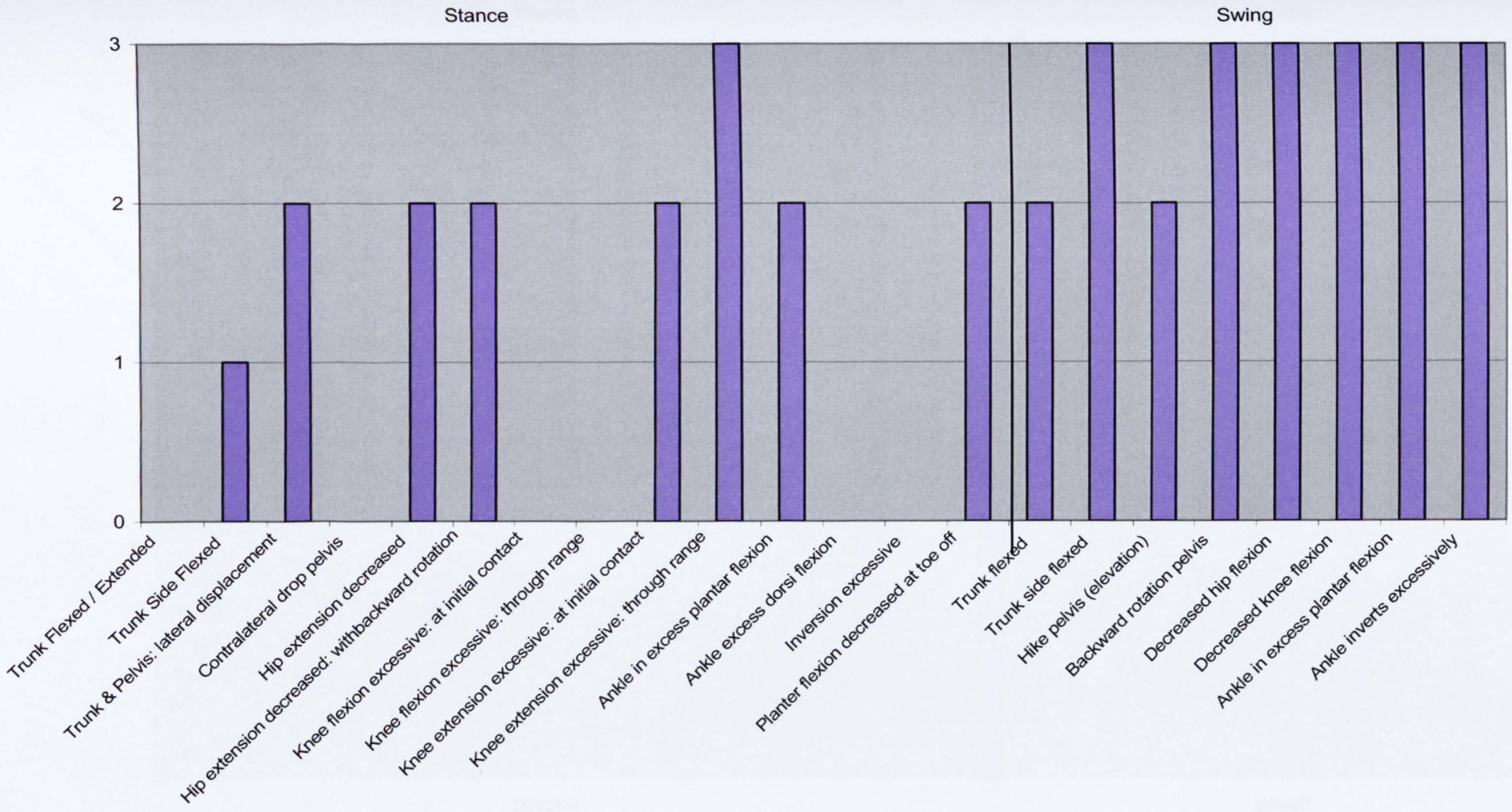

Appendix Figure 2 Rivermead observational gait analysis scale for subject CVA06

A.I.c CVA07

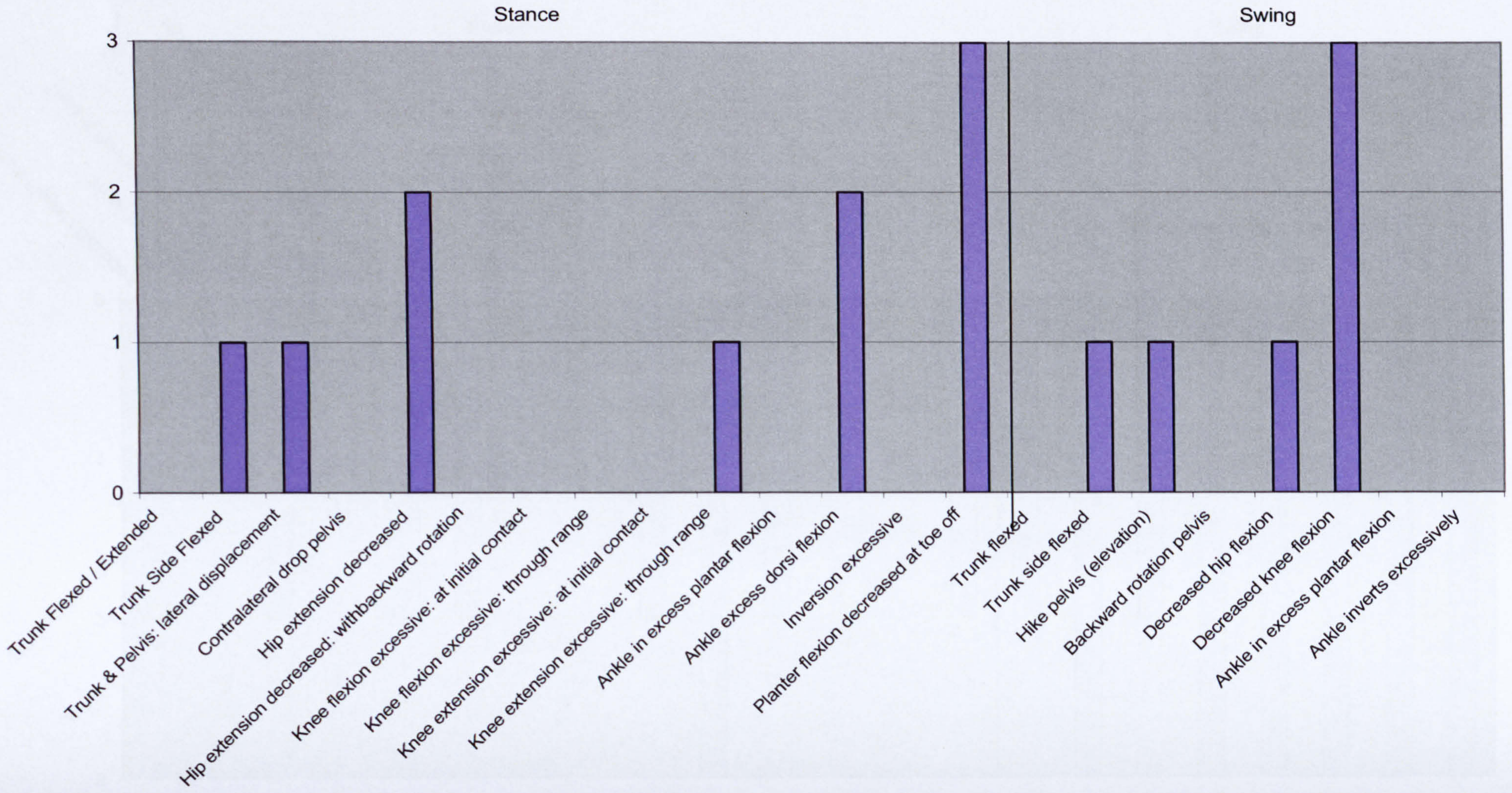

Appendix Figure 3 Observational gait analysis for subject CVA07

A.I.d CVA10

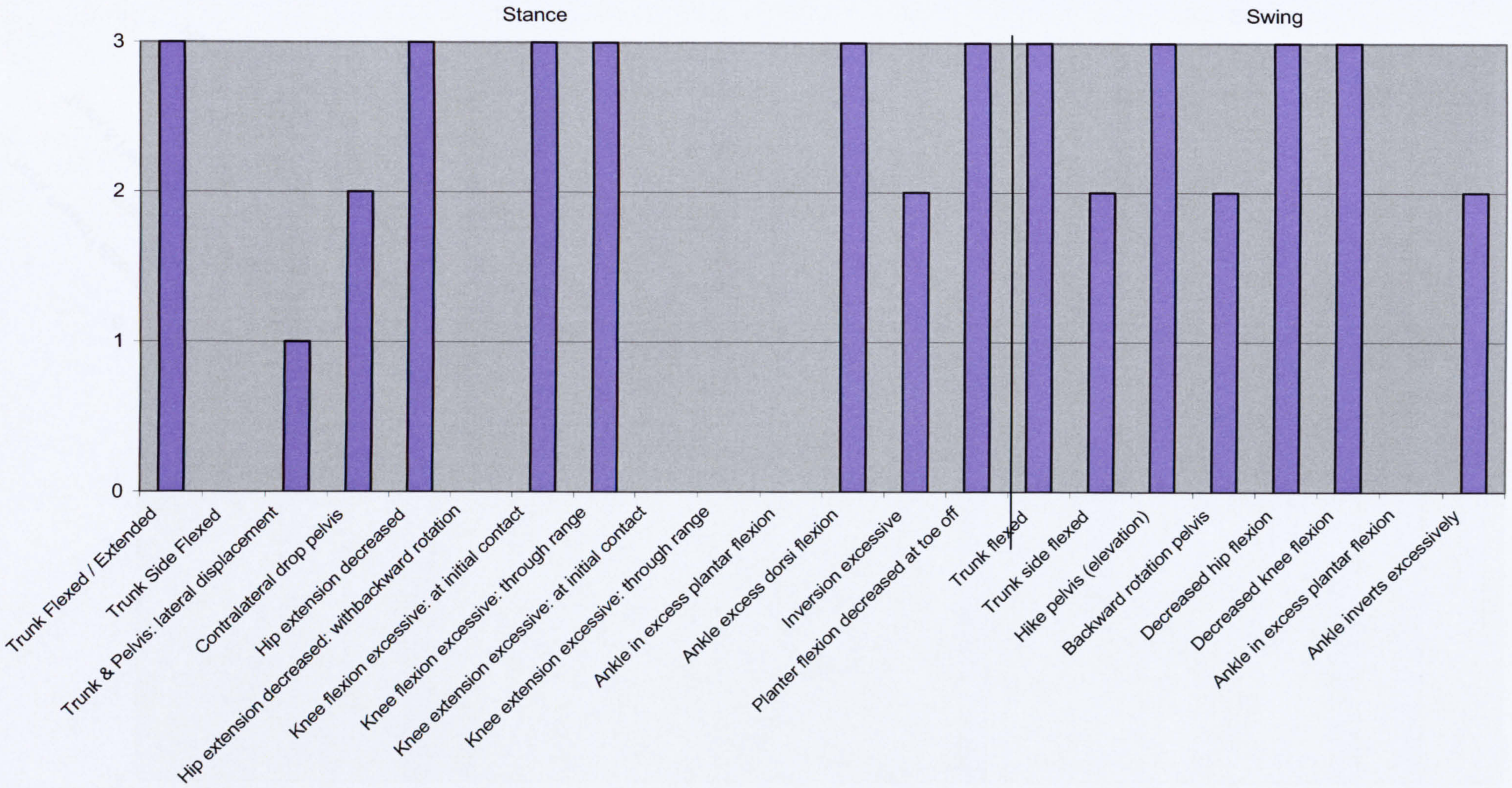

Appendix Figure 4 Observational gait analysis for subject CVA10

A.I.e CVA11

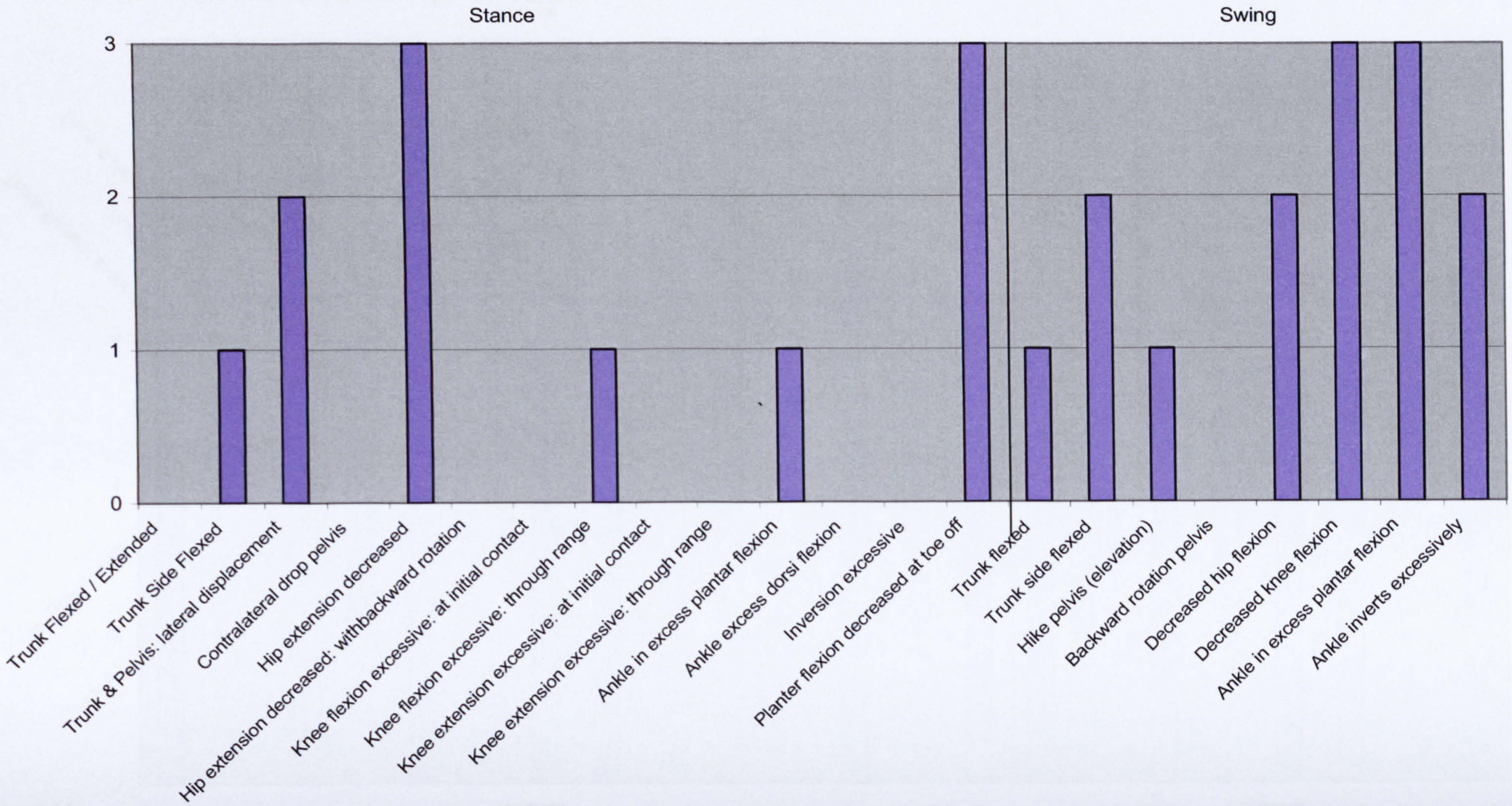

Appendix Figure 5 Rivermead observational gait analysis scale CVA11

A.I.f CVA14

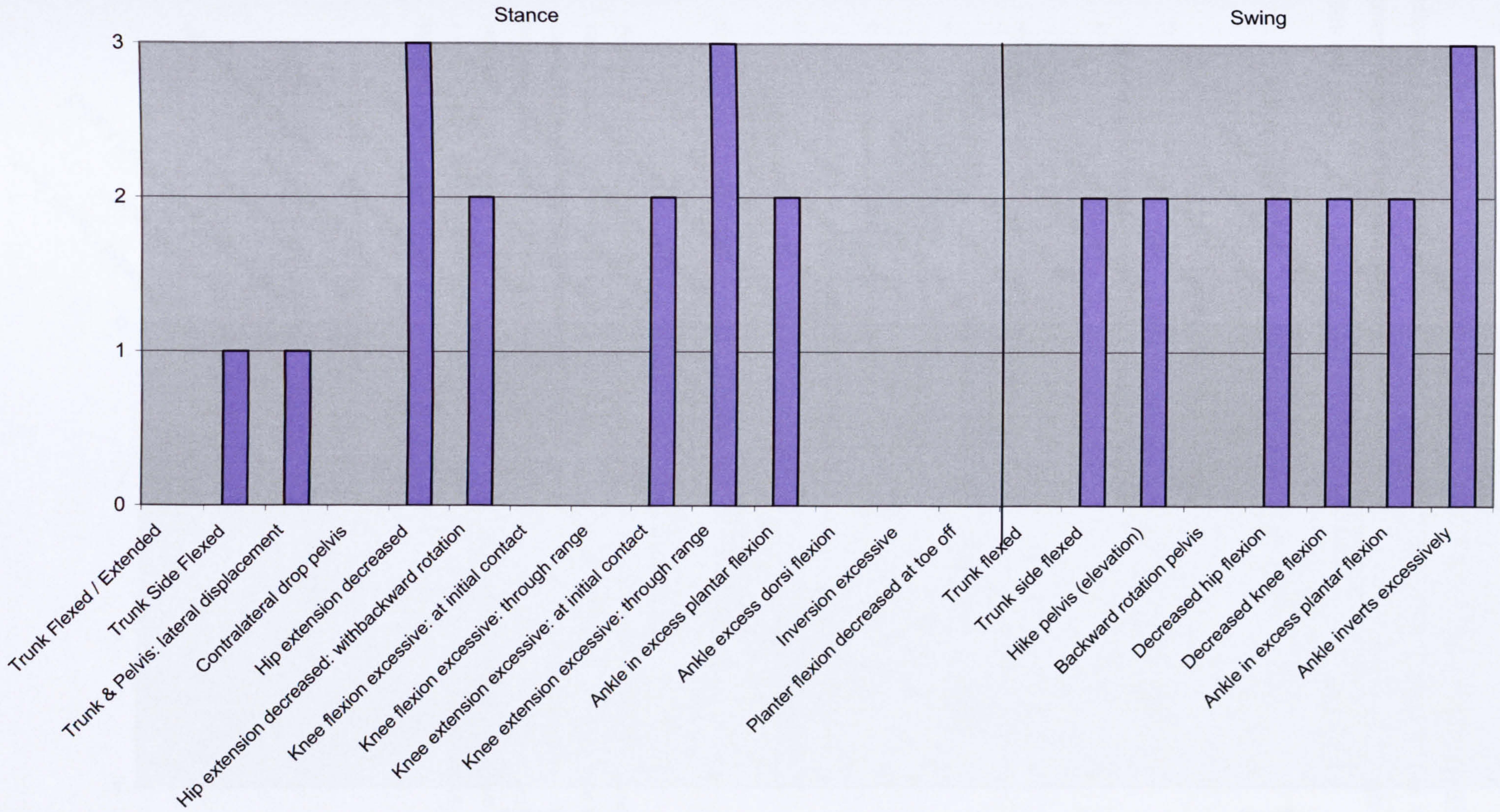

Appendix Figure 6 Observational gait analysis for subject CVA14

A.I.g CVA15

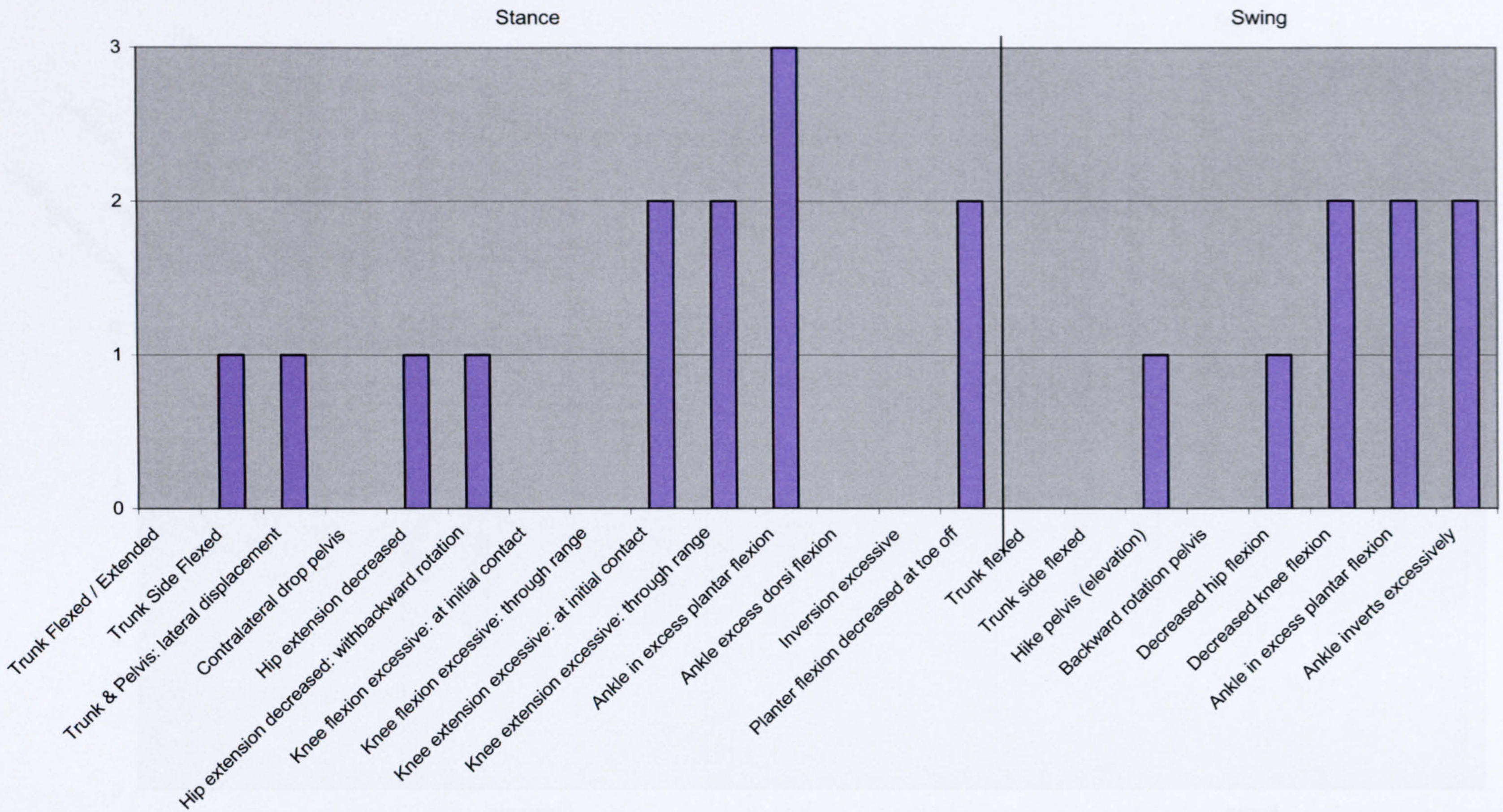

Appendix Figure 7 Observational gait analysis for subject CVA15

A.II Limb Segment Elevation Angles - Kinematics

Section A.II displays results from the Xsens sensors. These results reflect the individual segment angles of the hemiplegic leg. For each subject the foot, shank and thigh segment angles are given.

A.II.a CVA03

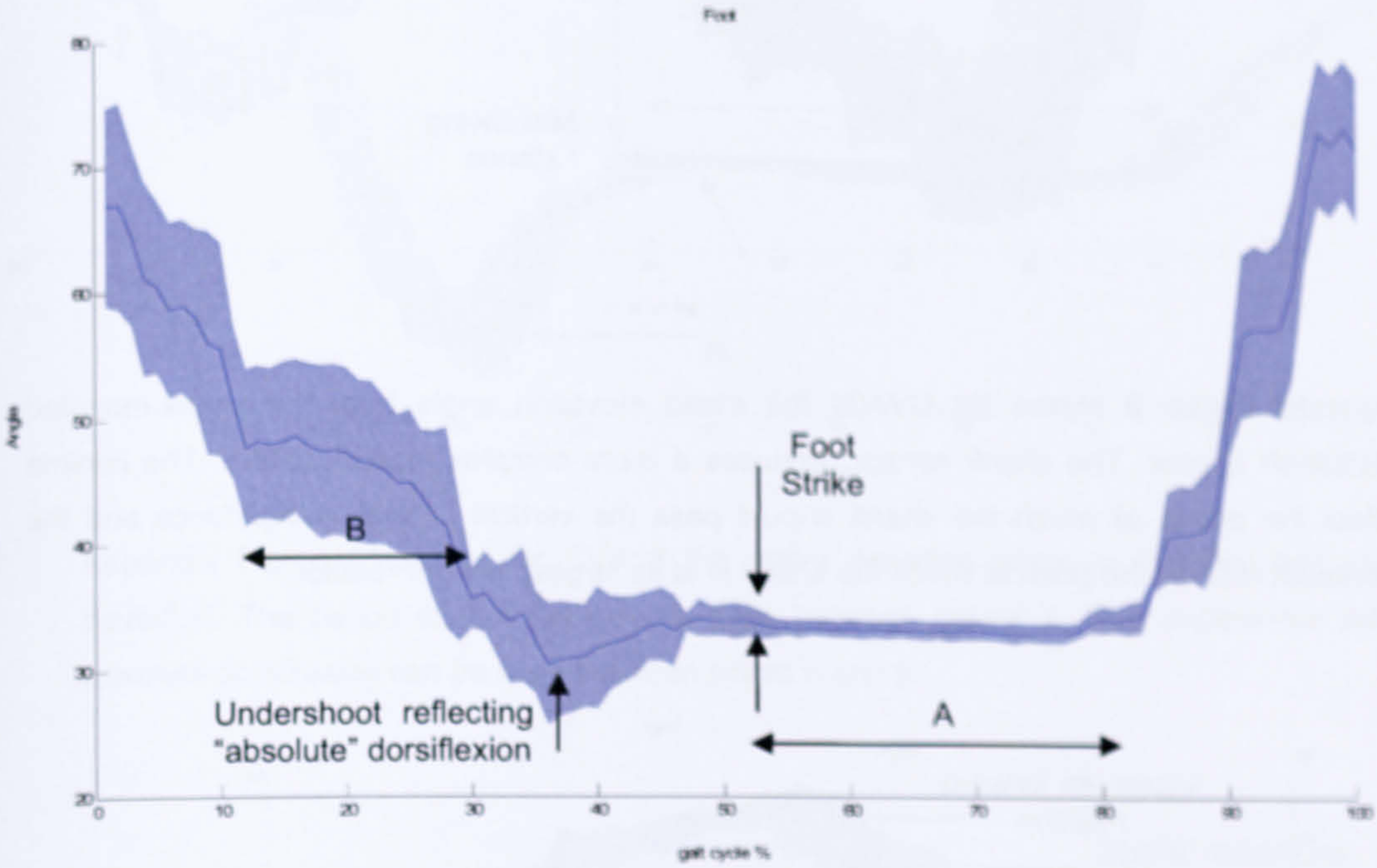

Appendix Figure 8 shows for CVA03 the mean segmental elevation angle of the foot. It should be recognised that because of the angle that the sensor was set, foot flat does not produce a 0° value. Static trial data can be found in the Appendix that display the starting angles each of the sensors. Foot strike is identified. The level of undershoot noted on the Figure reveals the amount of "absolute" dorsiflexion prior to foot strike and is 4°. That is, the angle of the foot not relative to the shank but as absolute elevation angles. Period A shows the period of foot-flat. Period B shows a stunted dorsiflexion during terminal swing through.

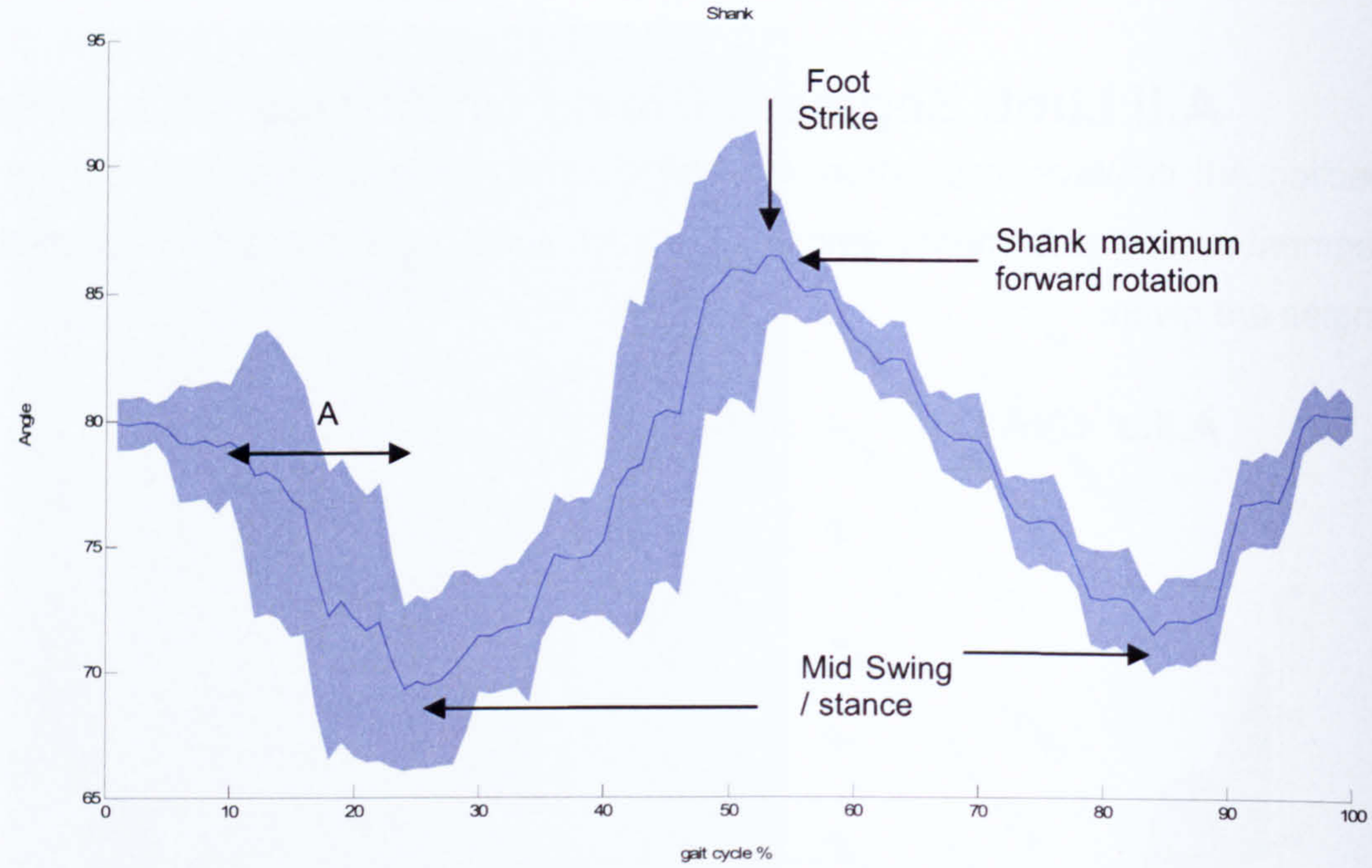

Appendix Figure 9 shows for CVA03 the mean elevation angle from the shank-mounted orientation sensor. The shank sensor produces a more complex motion pattern. The minima reflect the points at which the shank should pass the vertical or mid swing/stance and the maximum reflects the point at which the shank is at its largest forward rotation.

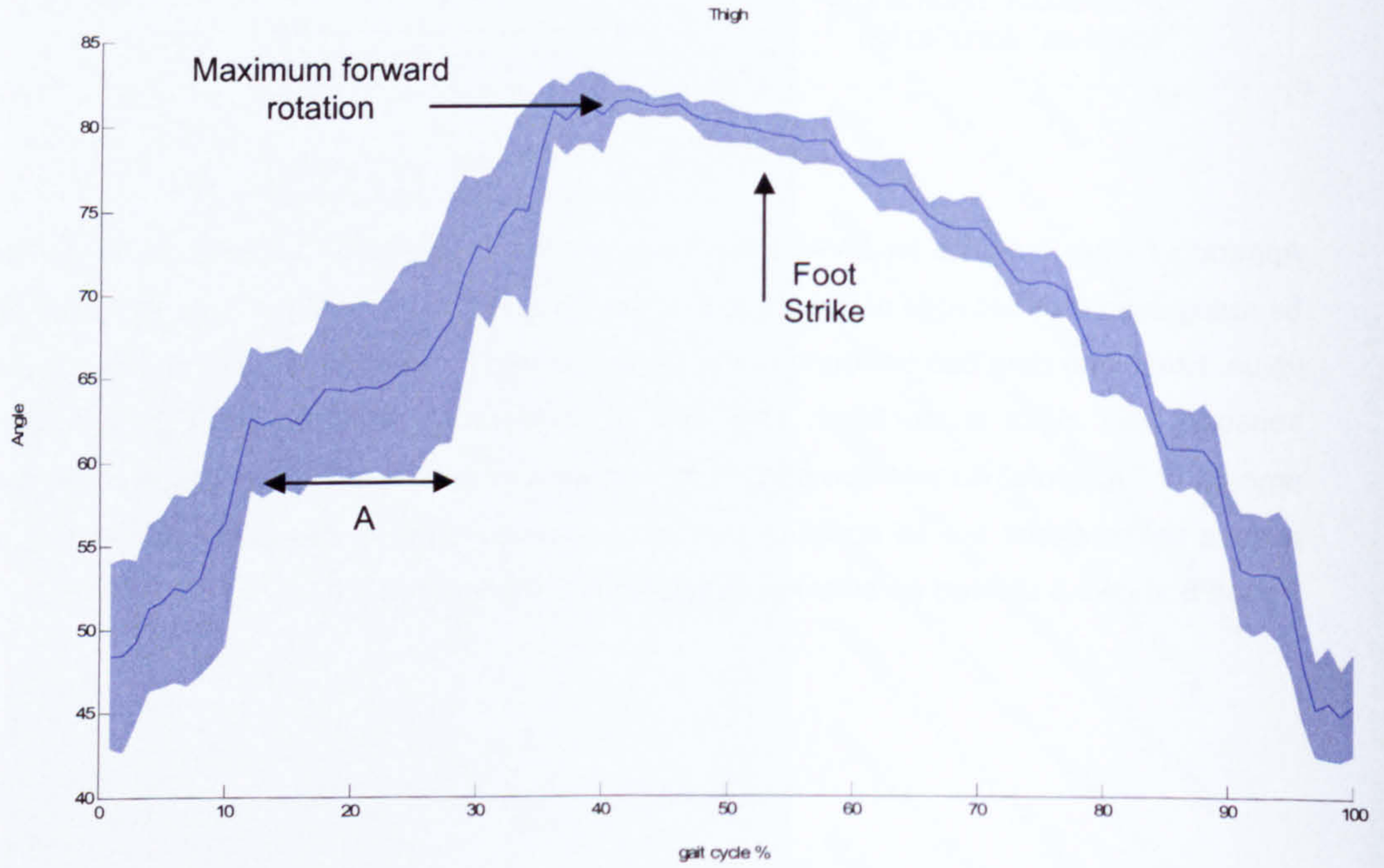

Appendix Figure 10 shows for CVA03 the mean elevation angle from the thigh-mounted orientation sensor. The maximum forward rotation occurring at 43% gait cycle. The gradient of the first 43% of the gait cycle is steeper than the subsequent 57%; between 43 – 60% and 12 – 25% there is a particularly low gradient phase. The first occurs during mid-swing and the second just subsequent to foot strike. The range of mean elevation angle of the thigh is 38°.

A.II.b CVA06

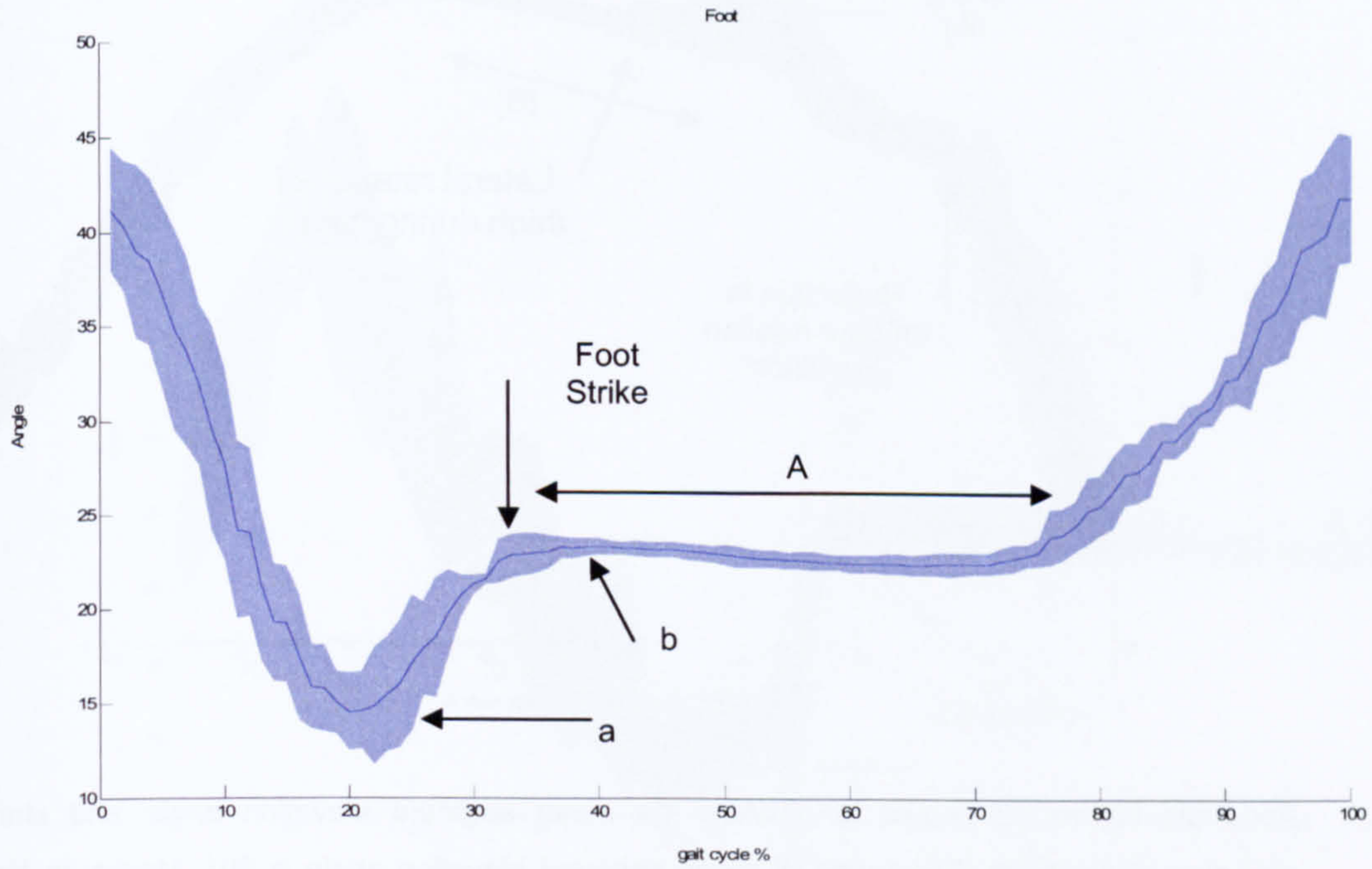

Appendix Figure 11 shows for CVA06 the mean elevation angle of the foot and standard deviation. The period of foot flat can be seen between period A. The undershoot reflecting absolute dorsiflexion can be seen between points a and b.

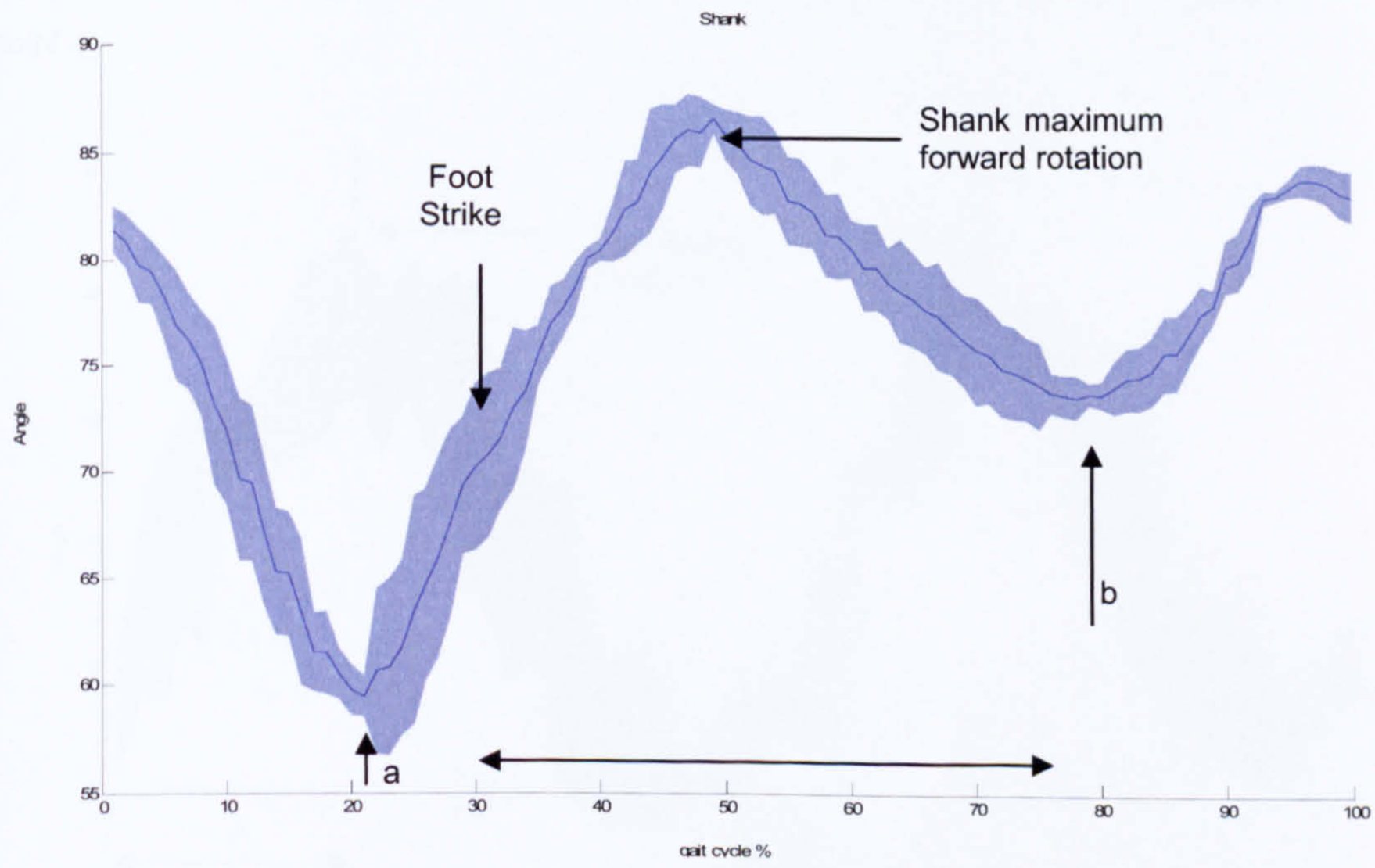

Appendix Figure 12 shows for CVA06 the mean elevation angle and standard deviation of the shank. The range of the mean segment elevation angle is 22°. The elevation angle at mid-swing and mid-stance can be seen between points a and b. Backward rotation can be seen from toe-off to point a changing to anterior rotation up to shank maximum forward rotation. Posterior rotation changes gradually to anterior rotation in the final 50% gait cycle.

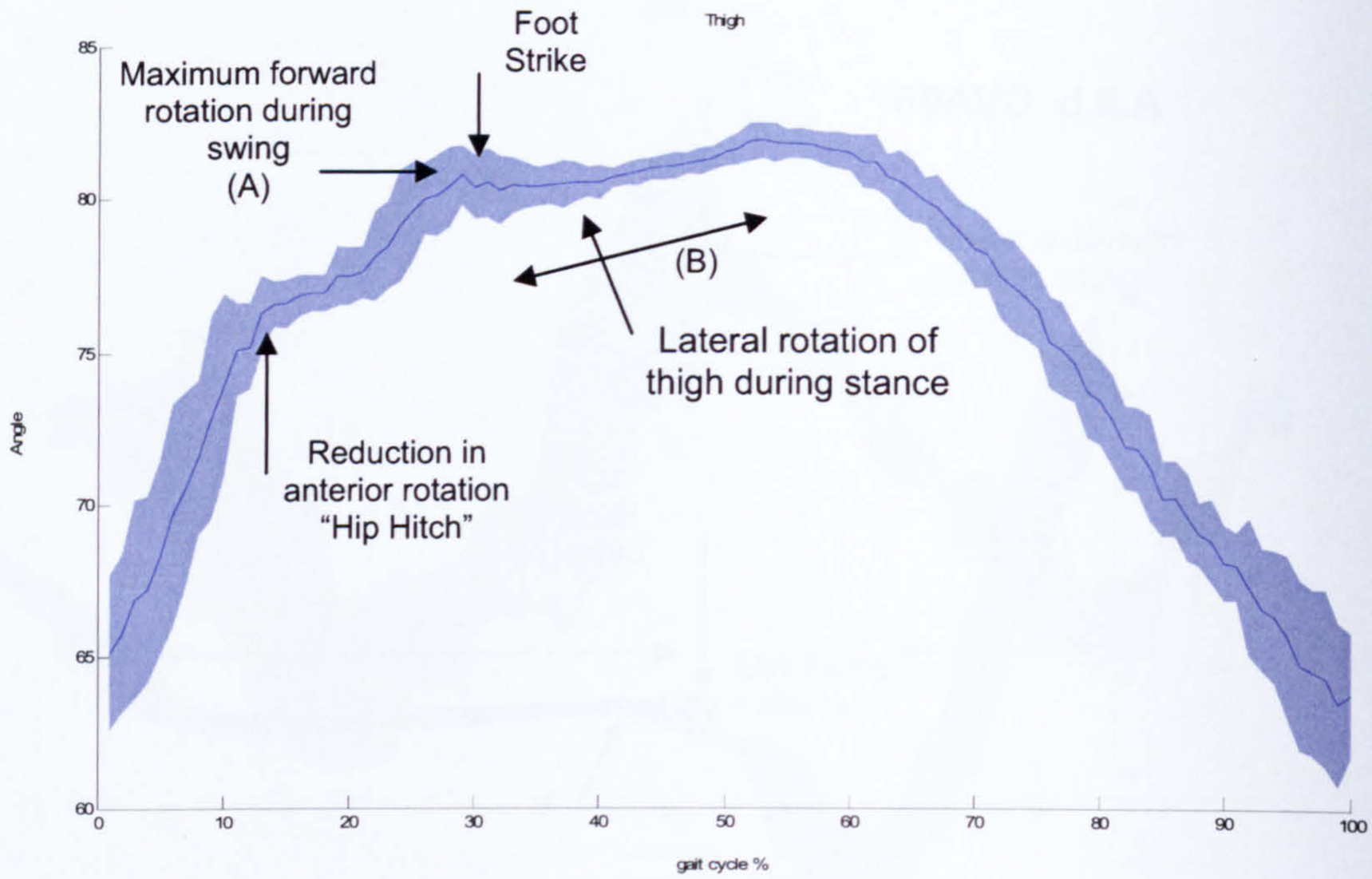

Appendix Figure 13 shows for CVA06 the mean segment elevation angle and standard deviation of the thigh. The range of mean segment elevation angle is 20°. Maximum forward rotation during swing occurs at point A, just prior to this there is a reduction in the gradient of the curve. Between period B forward rotation continues before returning back to a posterior rotation in the later part of the stance phase.

A.II.c CVA07

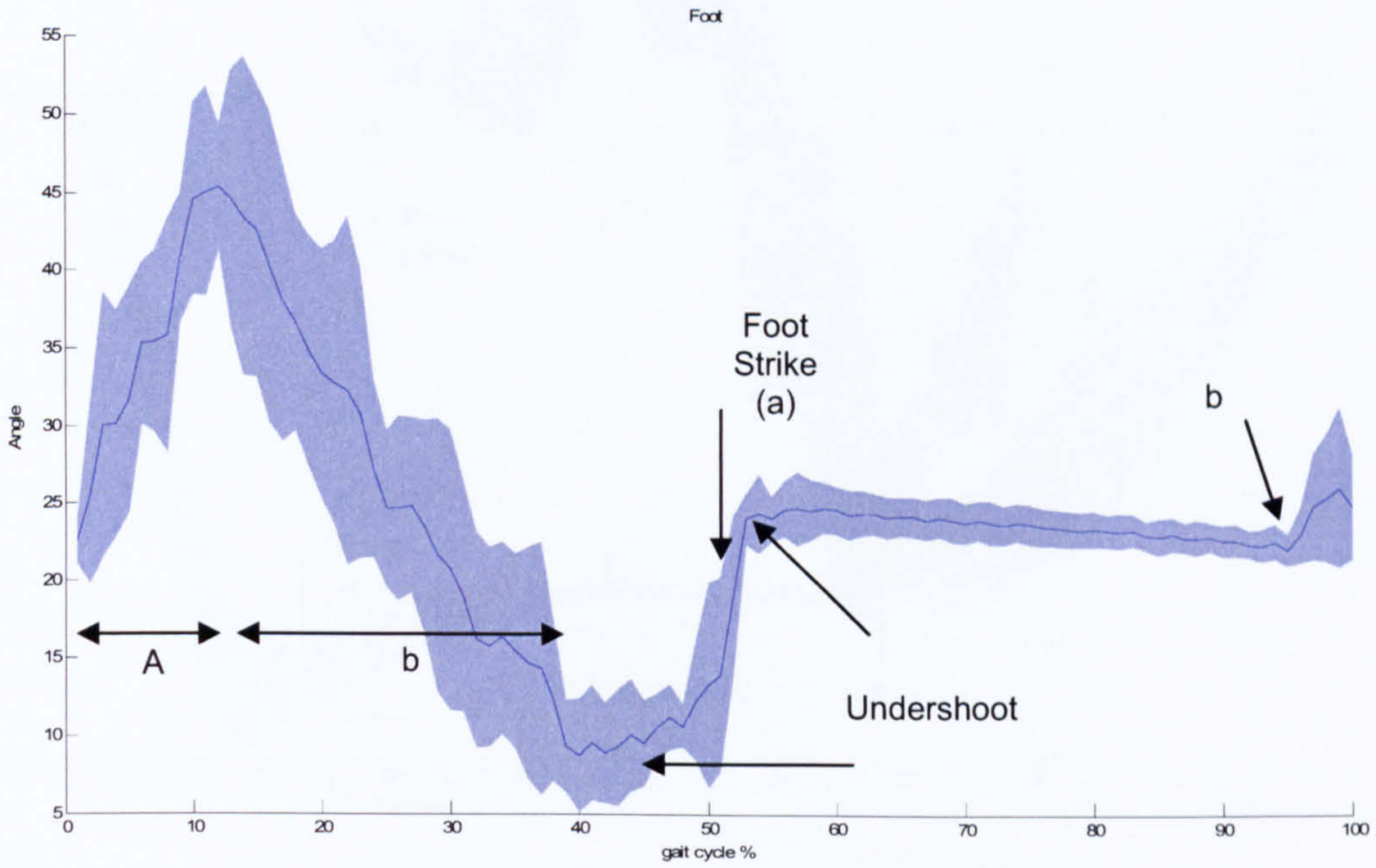

Appendix Figure 14 shows for CVA07 the mean elevation angle and standard deviation of the foot. The range of the mean elevation angle is 35°. Foot strike is shown at point a, foot flat progresses from foot strike to point b. over period A the foot plantar flexes then rapidly dorsiflexes over period B. At point a there is rapid plantar flexion to foot flat which continues until point b.

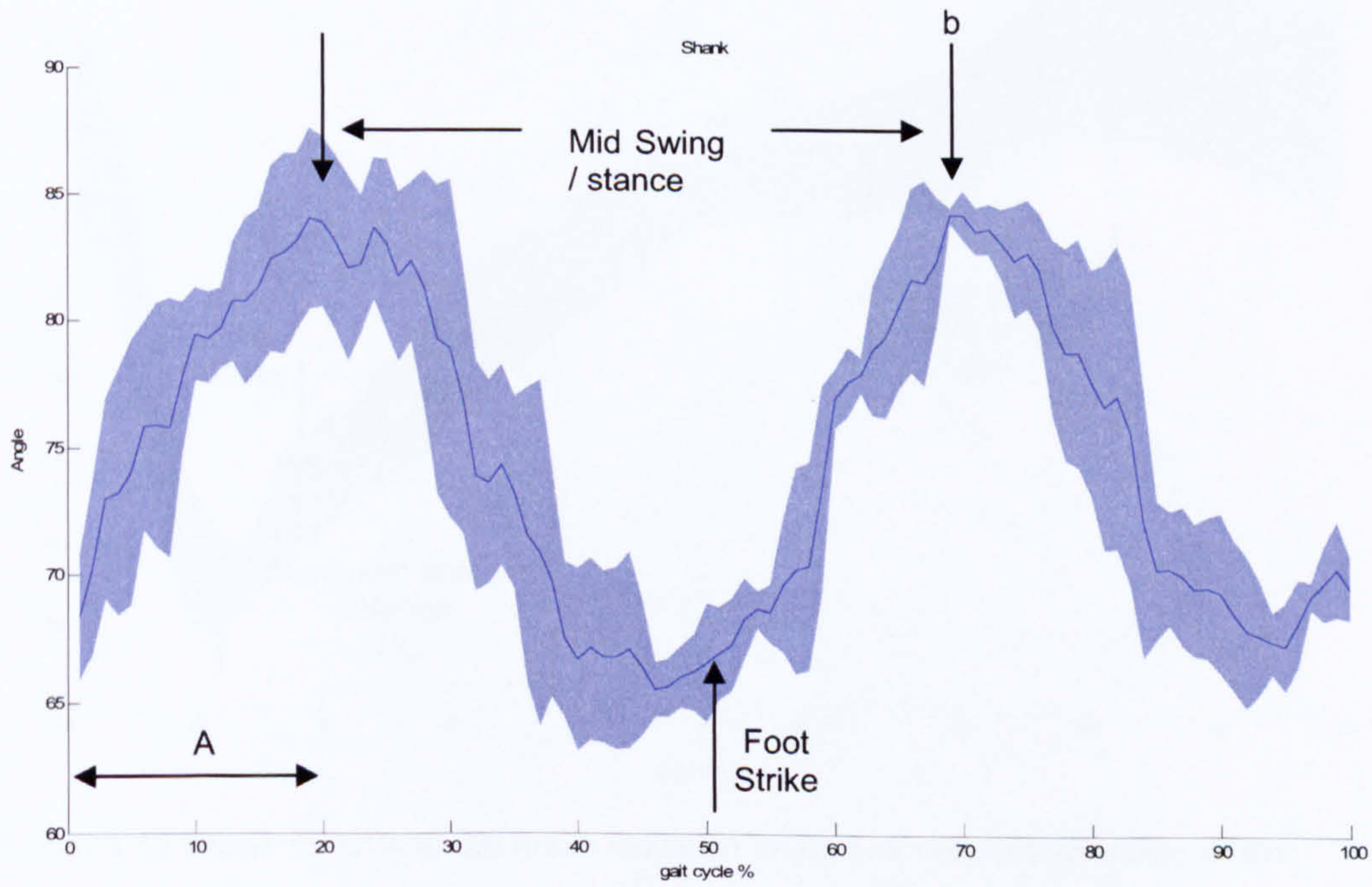

Appendix Figure 15 shows for CVA07 the mean elevation angle and standard deviation of the shank. Over period A the shank rotating to the posterior then rotates anteriorly just prior to foot strike the shank rotates posteriorly again. After foot strike the shank continues to rotate to the posterior until point b where it returns to an anterior rotation. The range of the mean elevation angle is 30°.

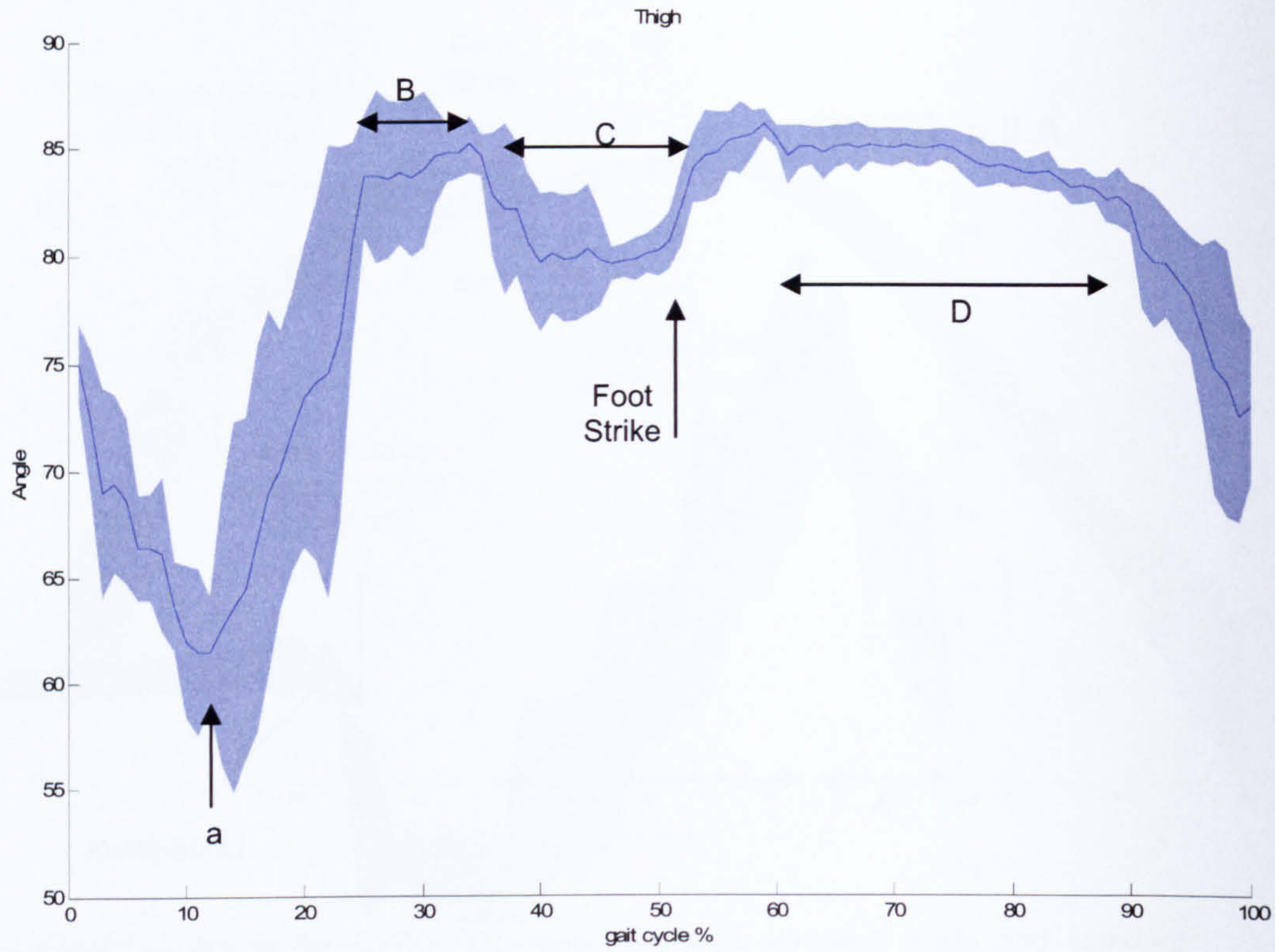

Appendix Figure 16 shows for CVA07 the mean elevation angle and standard deviation of the thigh. The thigh is first seen to rotate anteriorly then at point a begins to rotate forward. Between period B the gradient of this slope decreases, at the end of this period the thigh rotates backwards then forwards, period C. Foot strike occurs in the final third of this epoch. Over period D there is little change in the angle of the thigh that then rapidly rotates forwards. The range of the mean elevation angle is 23°.

A.II.d CVA10

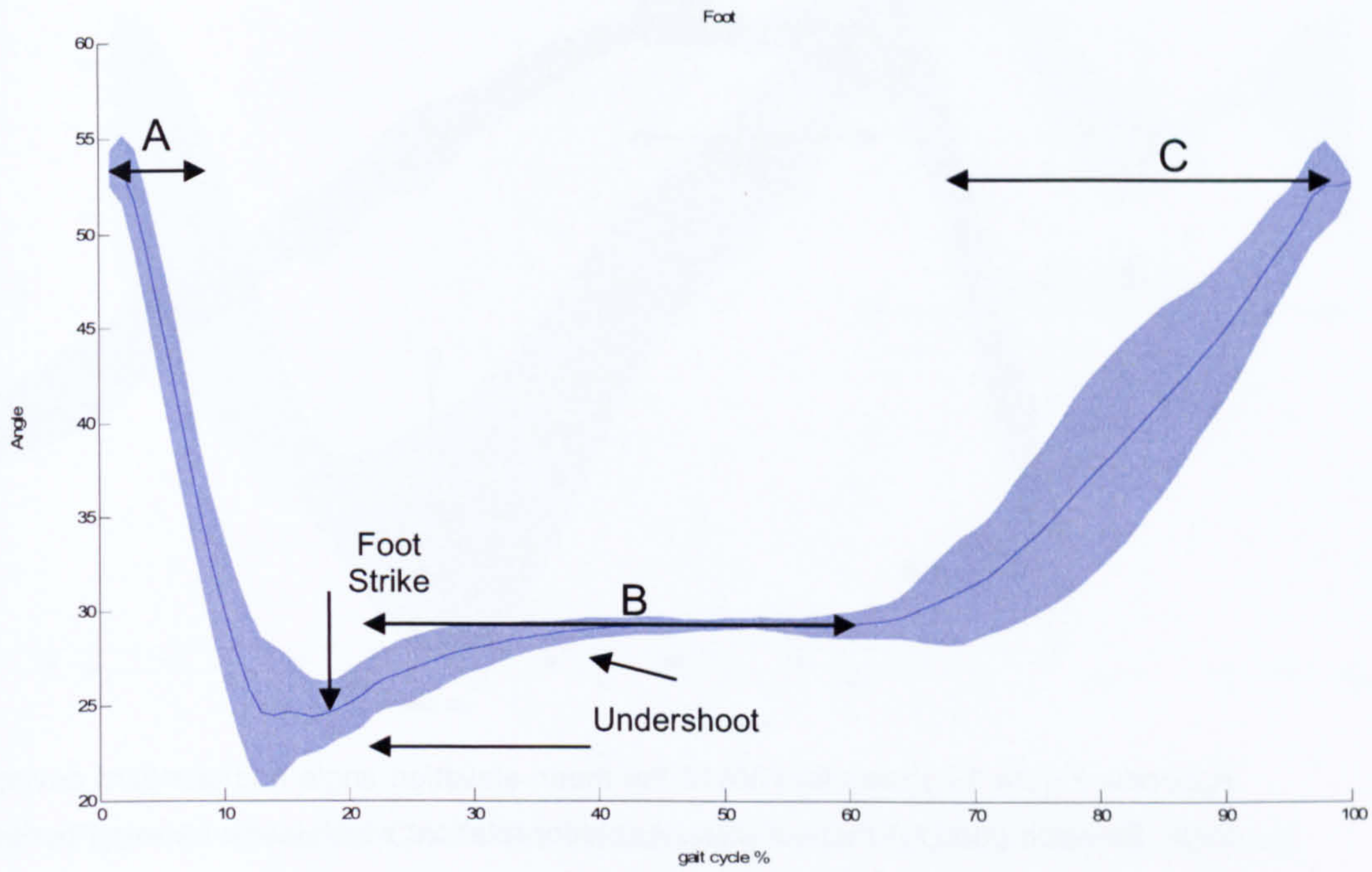

Appendix Figure 17 shows for CVA10 the mean elevation angle and standard deviation of the foot. Over period A the foot dorsiflexes, at foot strike the foot rapidly plantar flexes. A period of foot flat can then be seen shown by B. Over period C the foot plantar flexes. The range of mean elevation angles for the ankle is 29°.

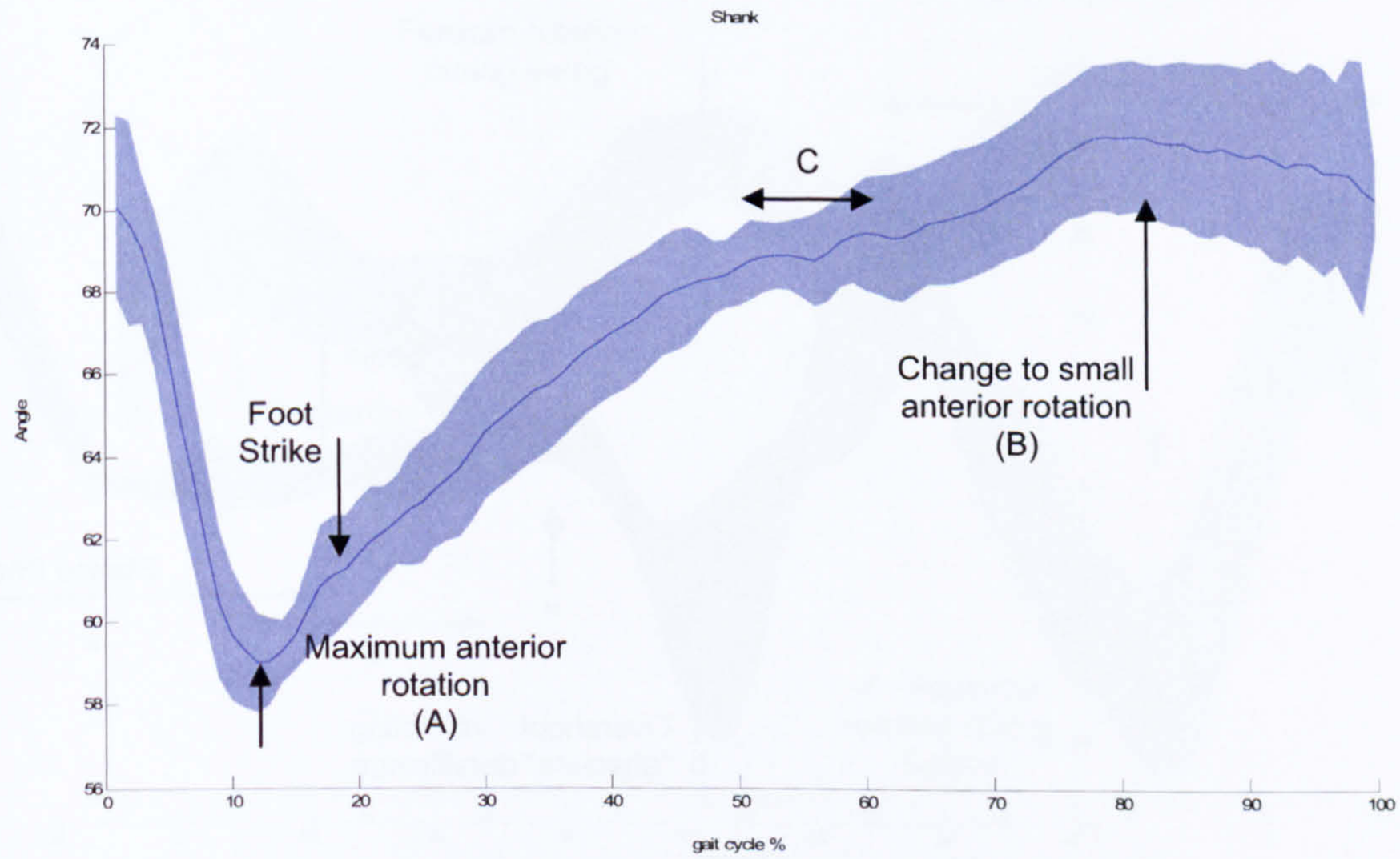

Appendix Figure 18 shows for CVA10 the mean elevation angle and standard deviation of the shank. The maximum anterior rotation is shown at point A. The range of the mean elevation angle is 13°. There is a rapid anterior rotation up to point A and subsequently there is a slow posterior rotation. At point B the slow posterior rotation changes to a small anterior rotation. Period C reveals perturbations related to attempted foot lift.

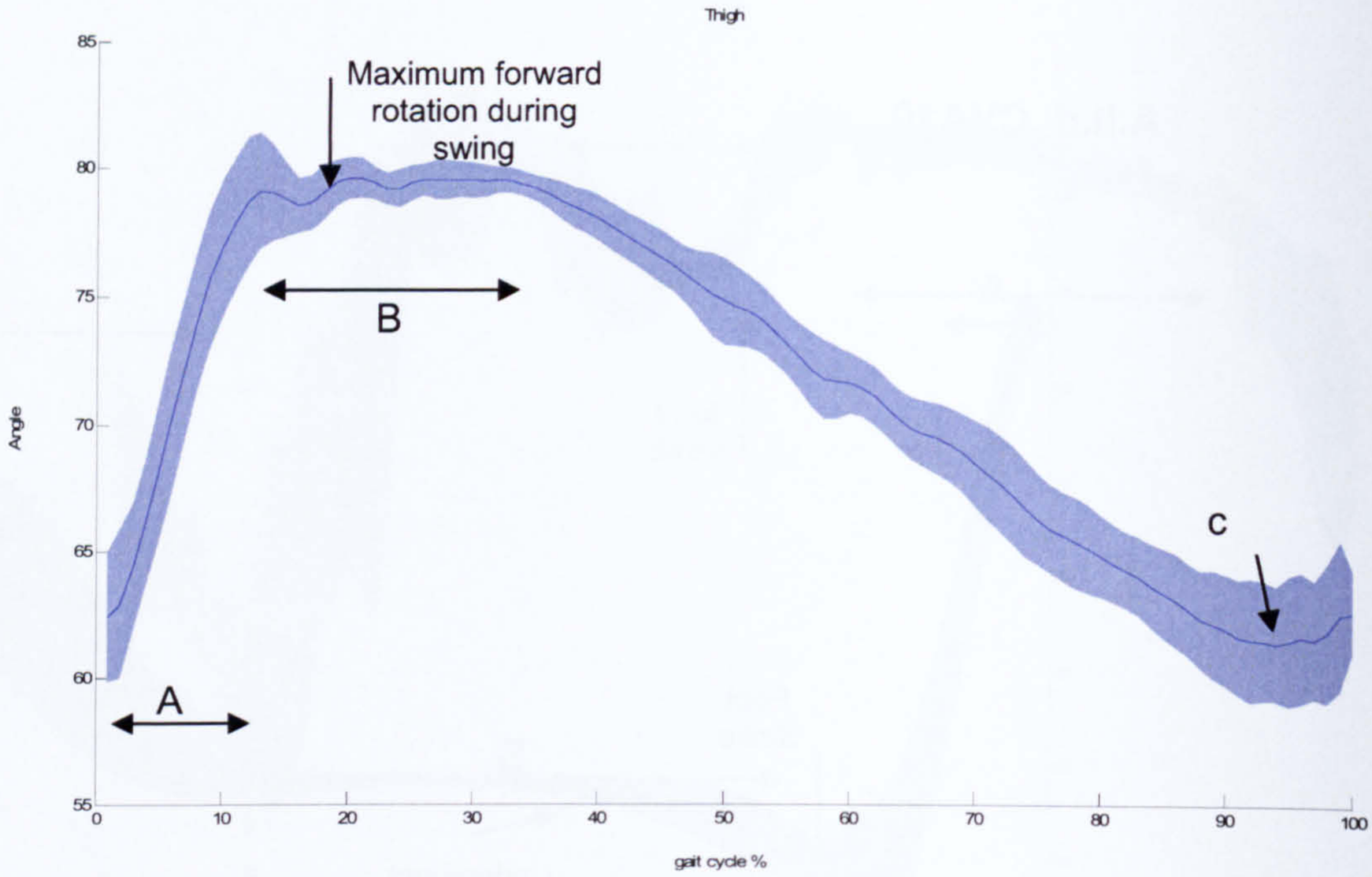

Appendix Figure 19 shows for CVA10 the mean elevation angle and standard deviation of the thigh. Between period A there is a rapid anterior rotation, which levels between period B (there is a small oscillation and which then becomes a gradual posterior rotation. From point c the rotation begins change direction very slightly. The range of mean elevation angle is 18°.

A.II.e CVA11

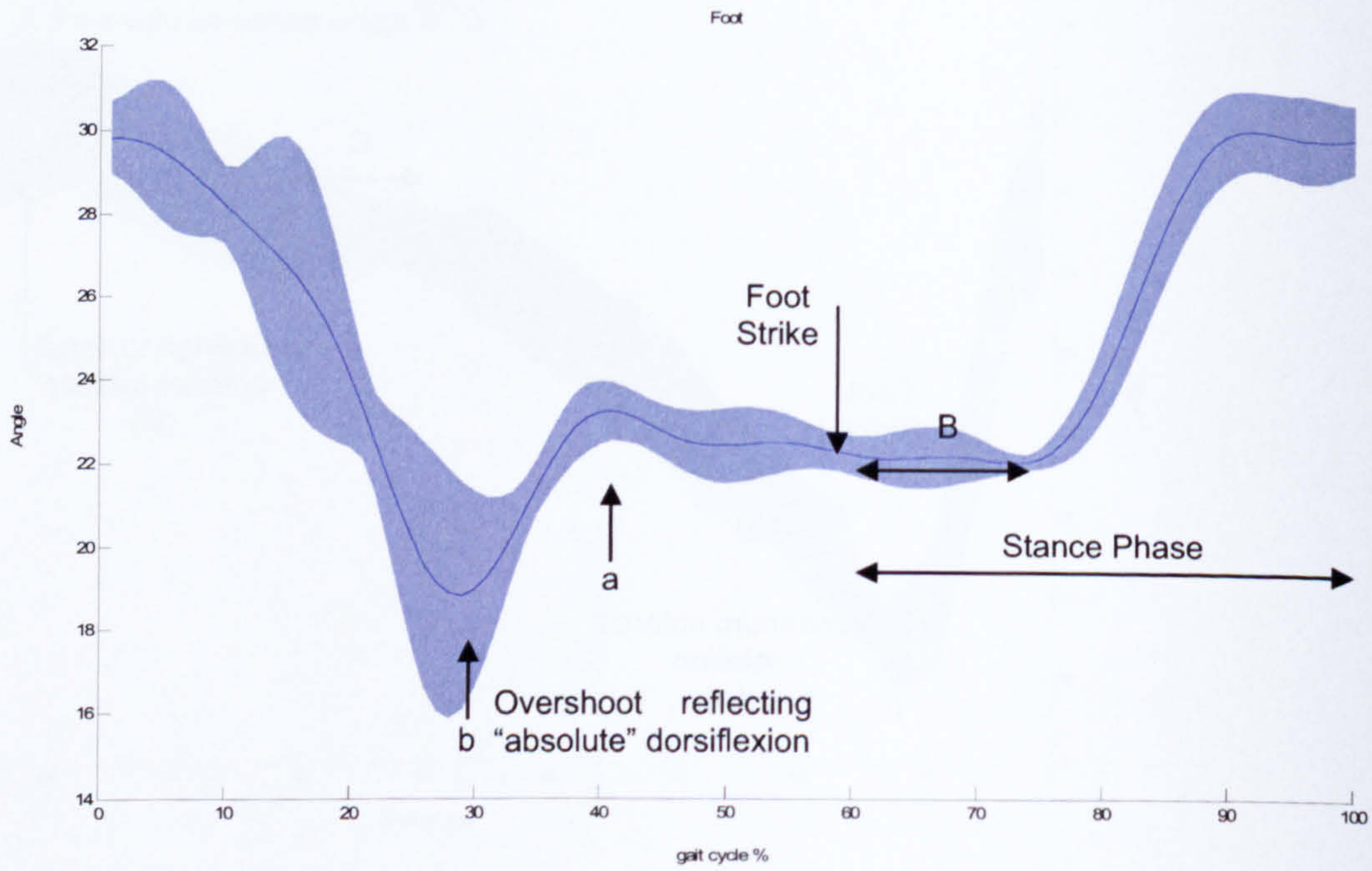

Appendix Figure 20 shows for CVA11 the elevation angles of the foot. At point a the foot is at its maximum forward rotation. The stance phase can be seen as identified, the period of of B shows foot flat. The period between a and b reflects the level of absolute dorsiflxion during swing.

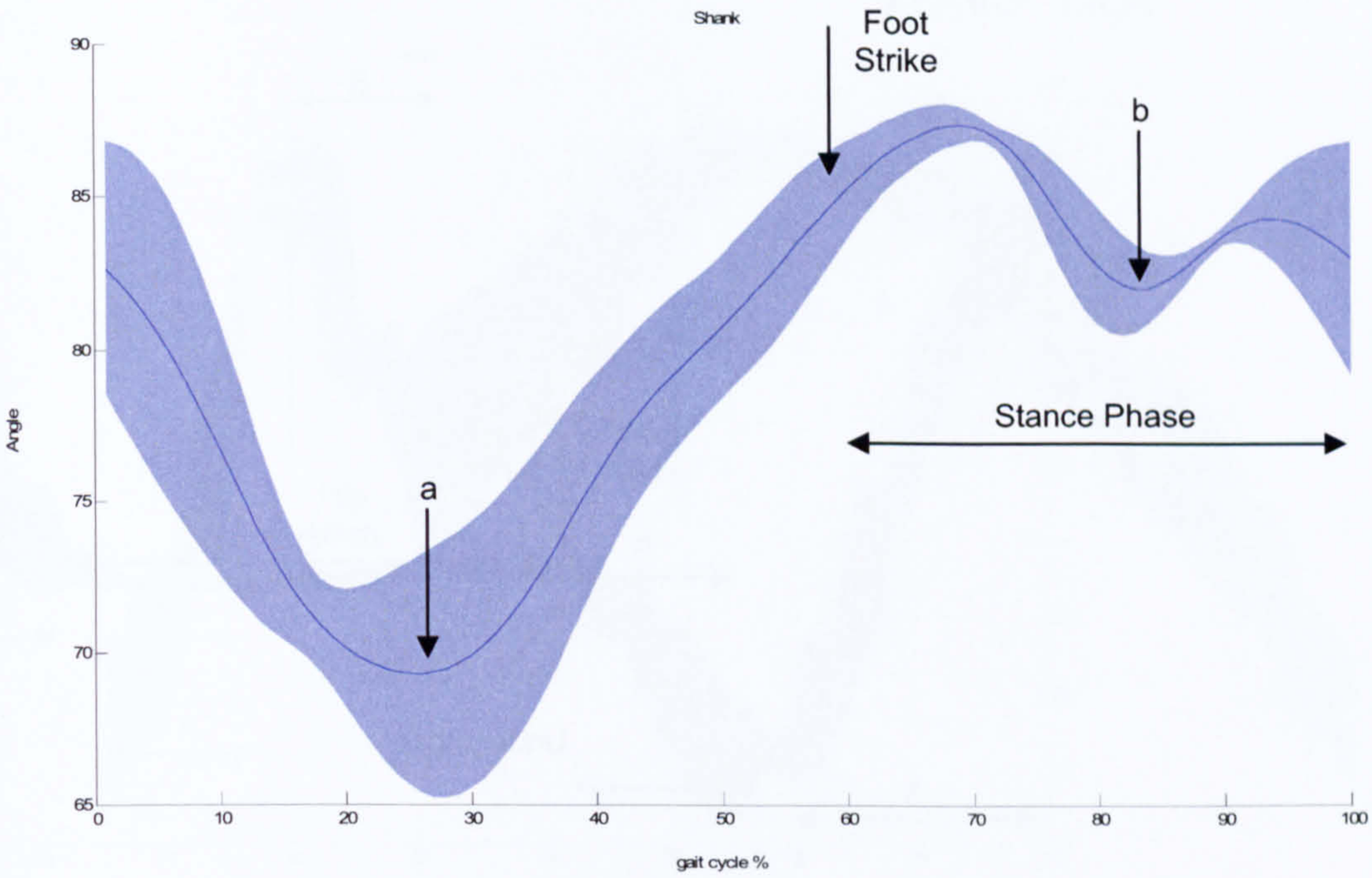

Appendix Figure 21 shows for CVA11 the elevation angles for the shank. During the swing phase the minimum at point a reflects the maximum forward rotation of the shank and occurs at approximately mid swing. Another minimum occurs during mid stance, point b, as the shank moves over the foot.

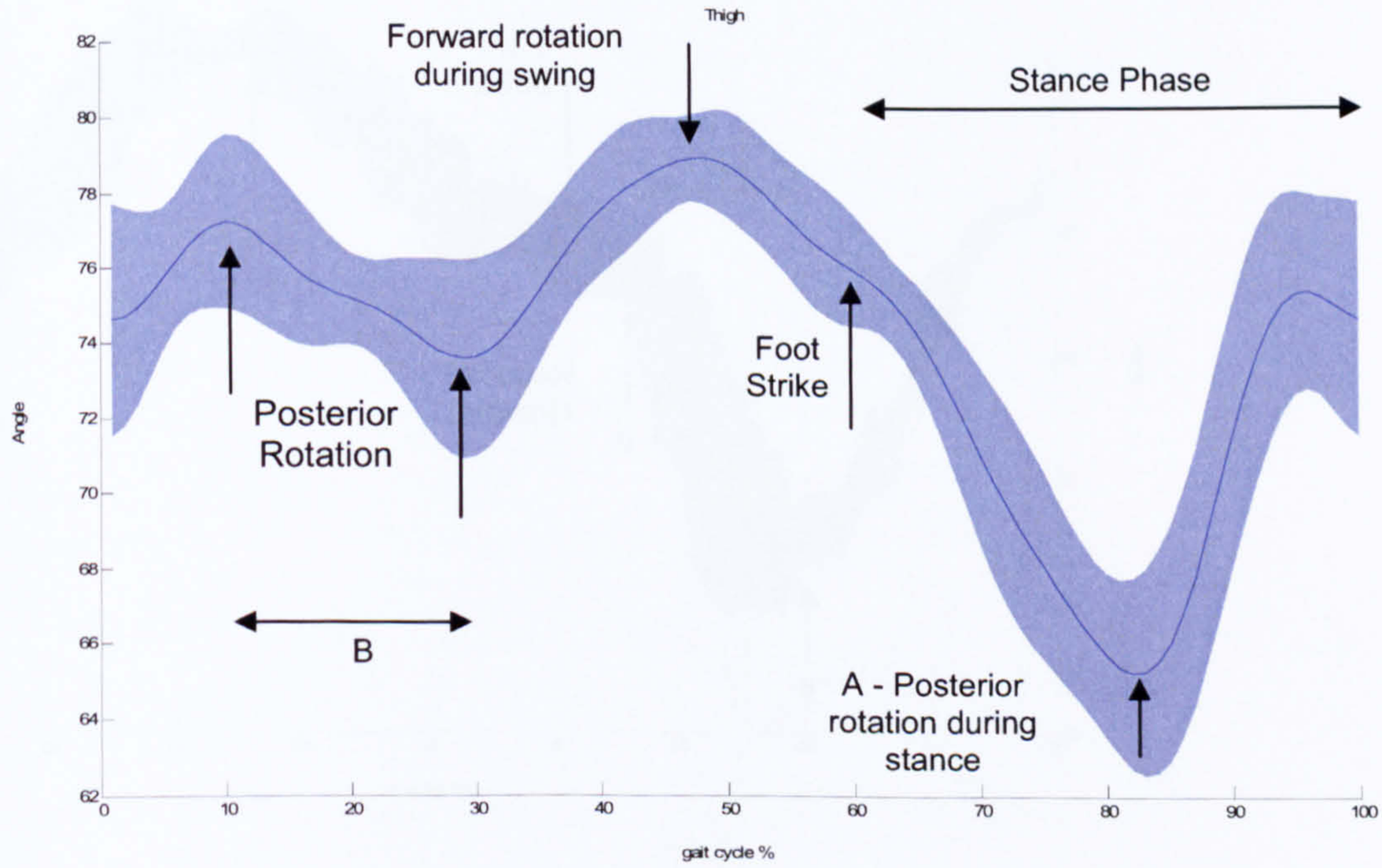

Appendix Figure 22 shows for CVA11 the elevation angles for the thigh. During the stance phase the minimum that occurs at point A reflects the posterior rotation of the thigh during stance. It is interesting to note the posterior rotation between period B in swing phase.

A.II.f CVA14

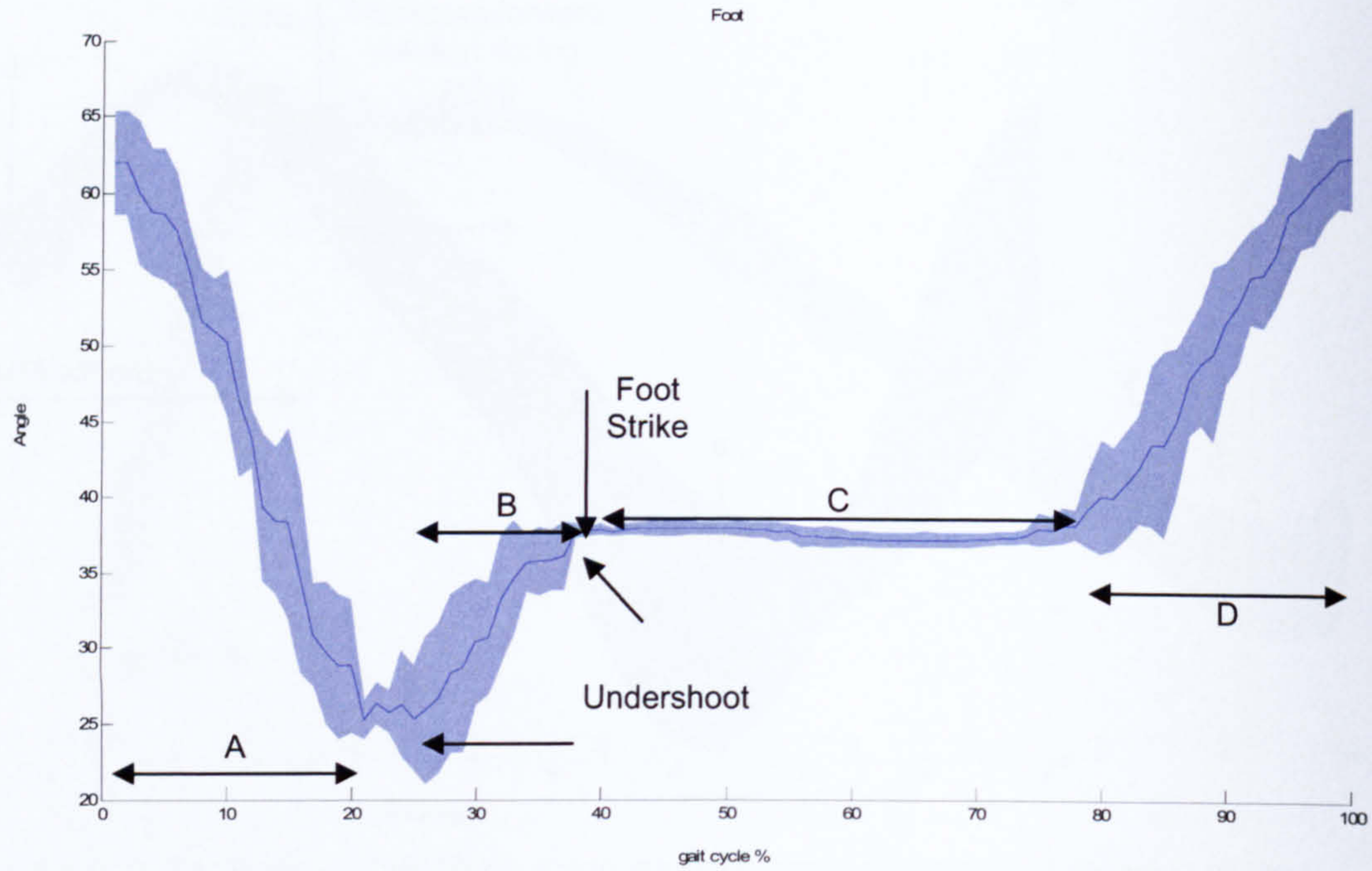

Appendix Figure 23 shows for CVA14 the mean elevation angles and standard deviation of the foot. Over period A the foot dorsiflexes. Subsequently, the foot plantar flexes where for period C the foot is in foot flat phase. over period D the foot plantar flexes until toe-off. The range of mean elevation angle of the foot is 37°.

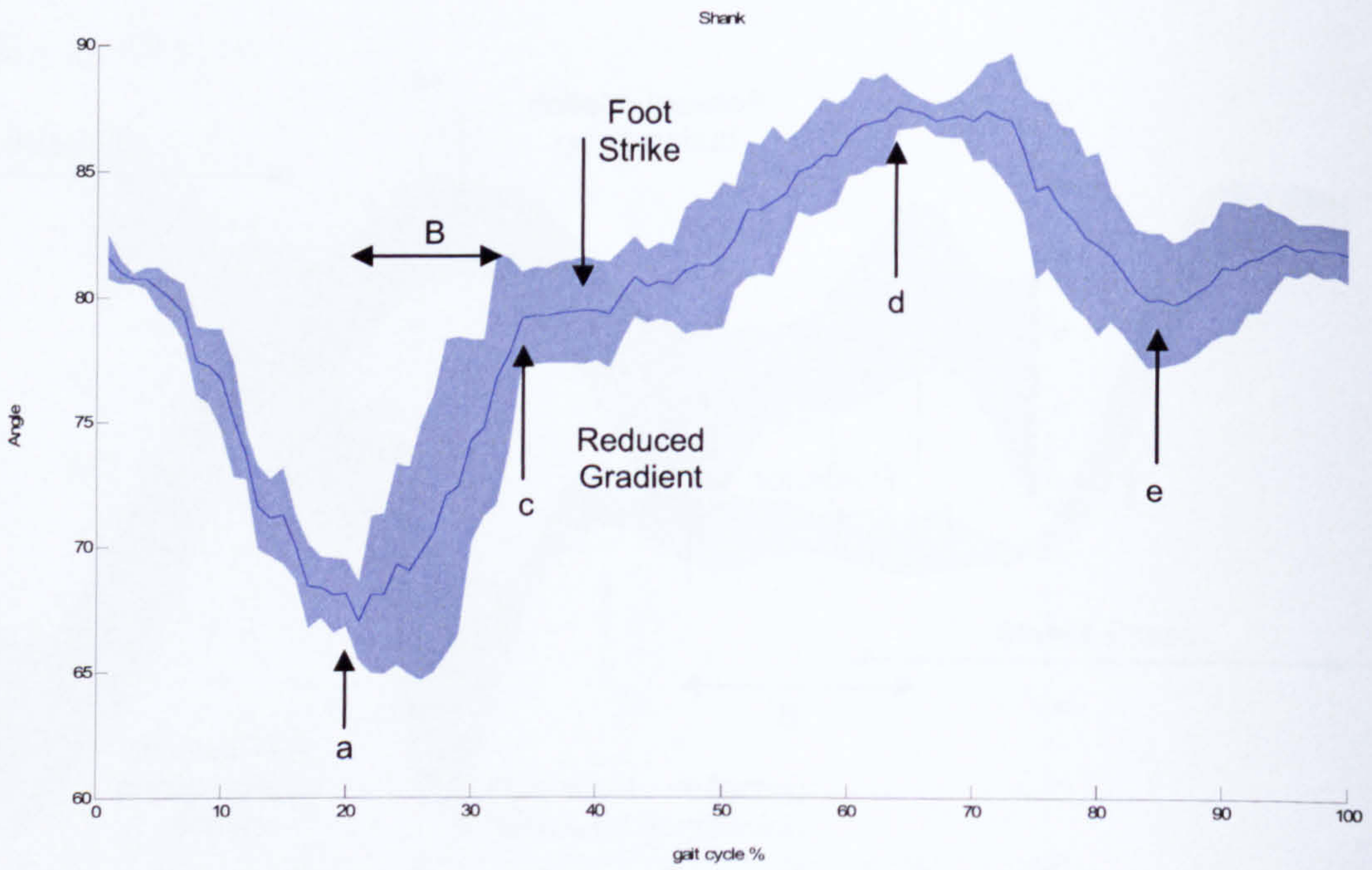

Appendix Figure 24 shows for CVA14 the mean elevation angles and standard deviation of the shank. The shank at first rotates anteriorly up to point a. Over period B the shank rotates posteriorly. At point c the gradient of the change in angle reduces, though continues to rotate to the posterior, until point d. At this point the direction of rotation reverses until point e where it again changes to a posterior rotation. The range of the mean elevation angle of the shank is 19°.

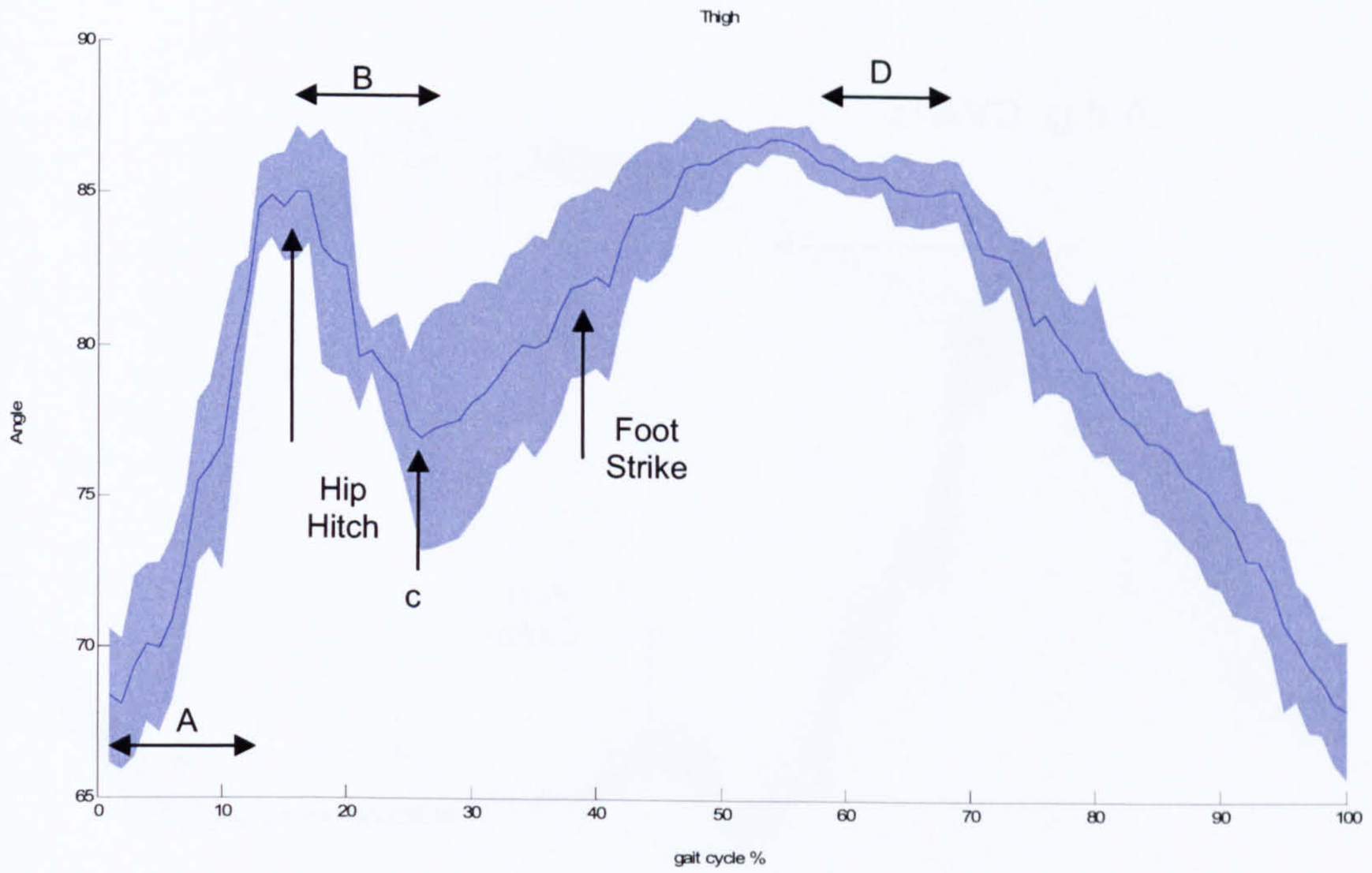

Appendix Figure 25 shows for CVA14 the mean elevation angles and standard deviation of the thigh. Over period A the thigh rotates posteriorly. Over period B the thigh rotates anteriorly before reversing again up to point c. Over period D there is a small rate of change of elevation angle before the anterior rotation gradient increases until toe-off. The range of the mean elevation angle is 18°.

A.ll.g CVA15

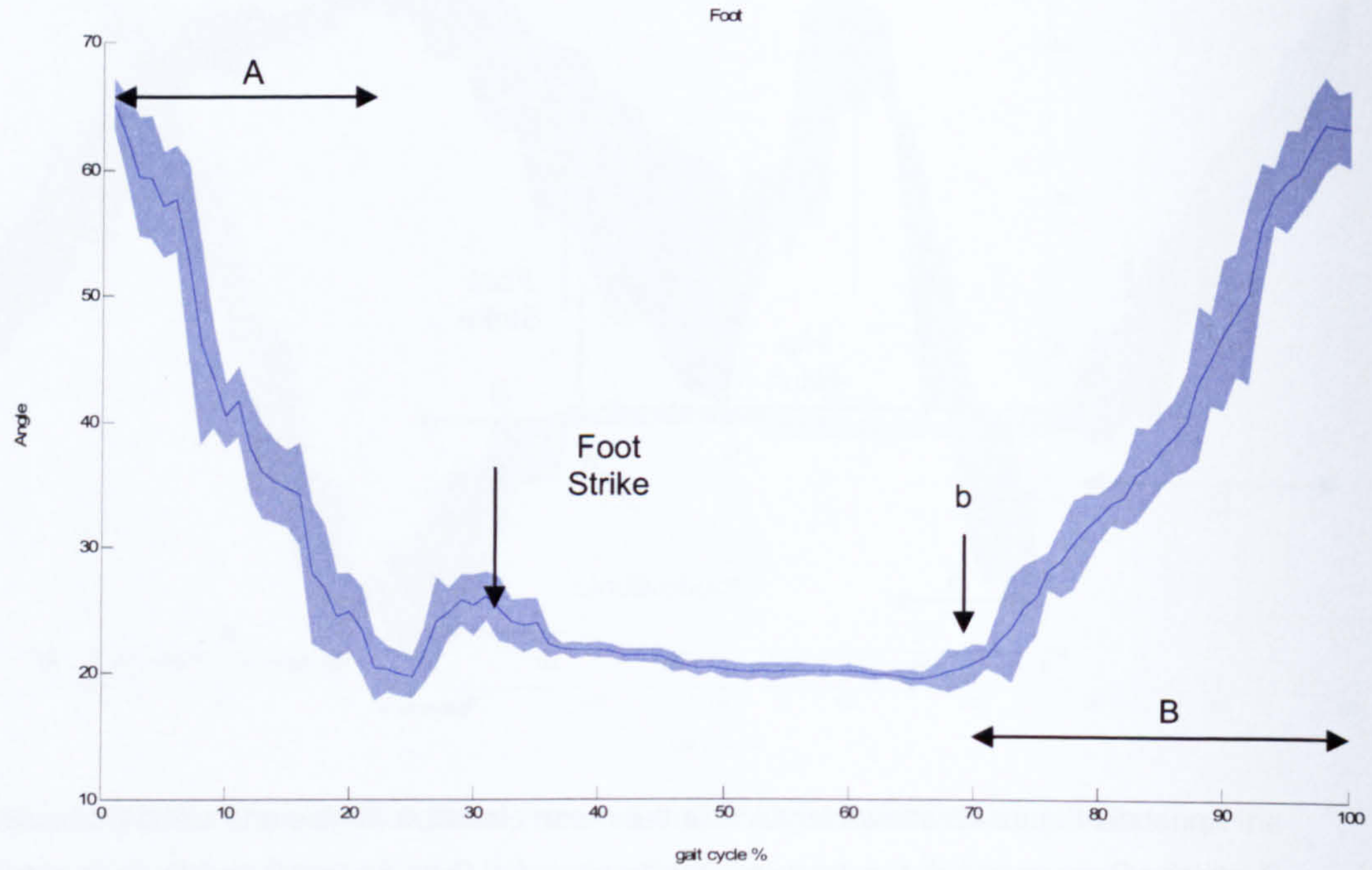

Appendix Figure 26 shows for CVA15 the mean elevation angle and standard deviation of the foot. Period A reveals the foot to dorsiflex, the foot then rapidly plantar flexes and then dorsiflexes again at which point the foot remains in the foot-flat phase until point b. Over point B the foot rapidly plantar flexes. The range of the mean elevation angle is 45°.

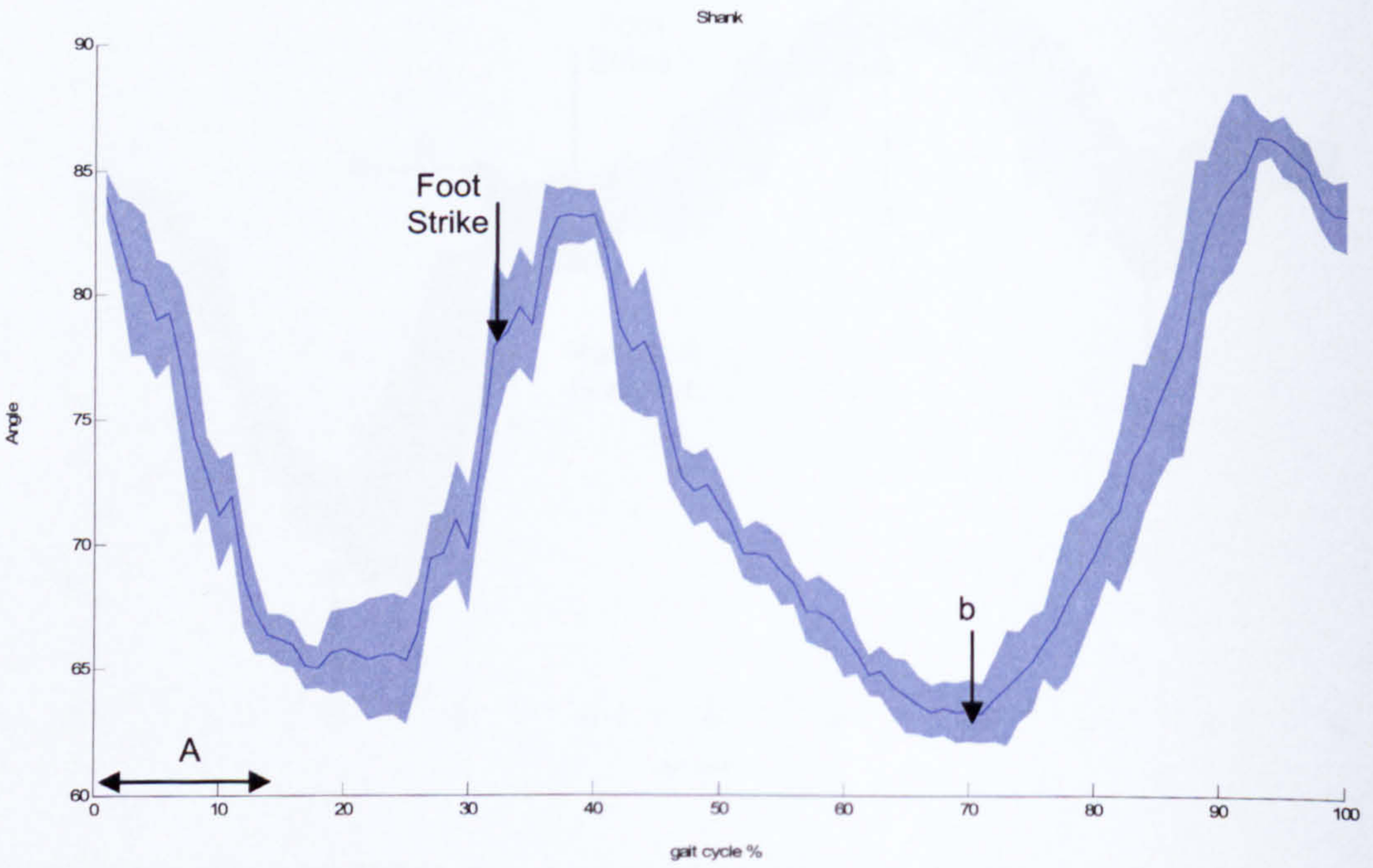

Appendix Figure 27 shows for CVA15 the mean elevation angle and standard deviation of the shank. Over period A the shank rotates anteriorly where the gradient of rotation reduces gradually where the shank begins to rotate posteriorly. Subsequent to foot strike the shank begins to rotate forward until point b where the direction of rotation again reverses. The range of the mean elevation angle is 23°.

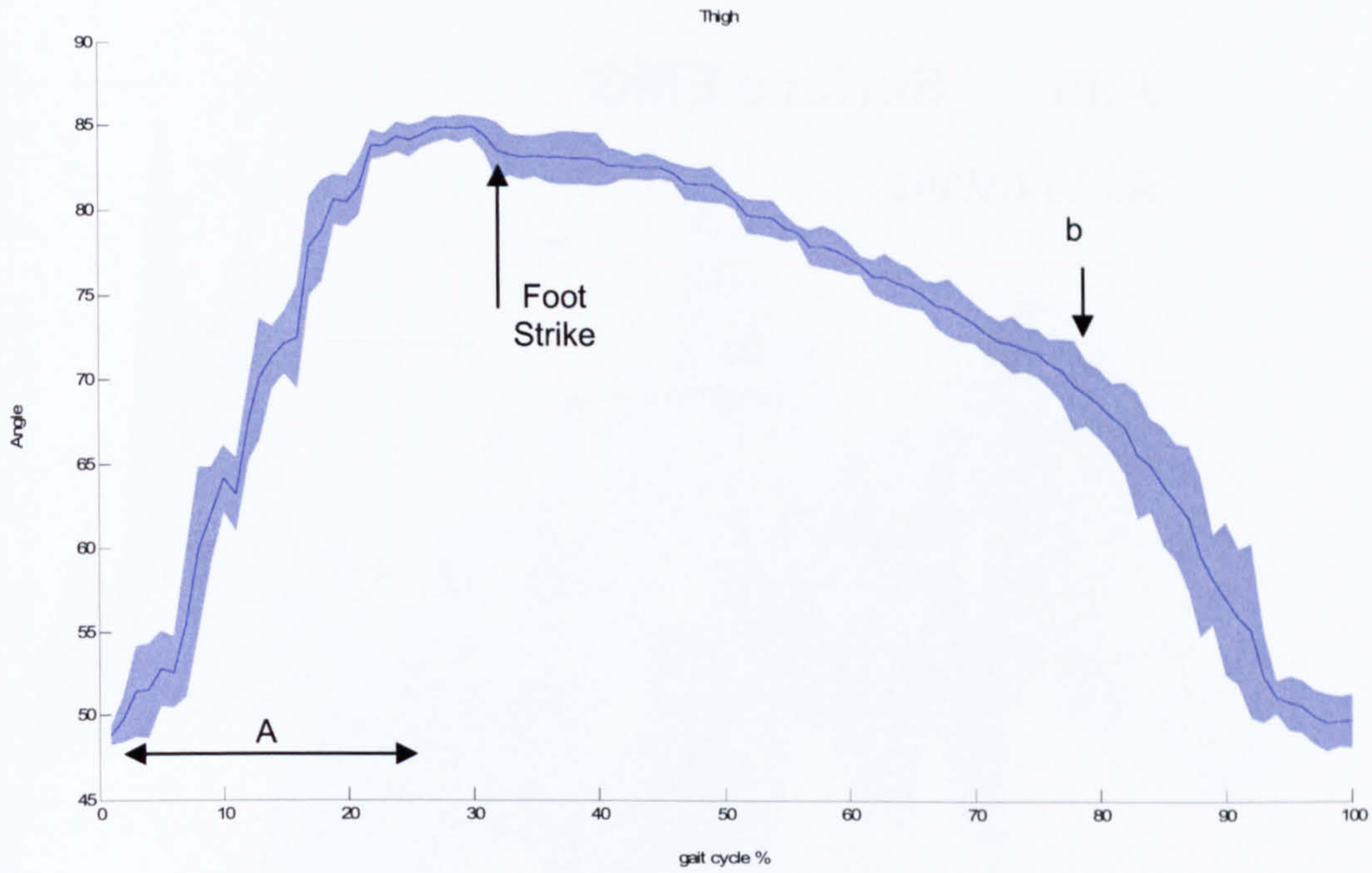

Appendix Figure 28 shows for CVA15 the mean elevation angle and standard deviation of the thigh. Over period A the thigh rotates anteriorly, the gradient of rotation then reduces until foot strike where the direction of rotation reverses. The gradient of rotation remains gradual, shallower than period A, and constant until point b where the rate of change of angle increases. The range of the mean elevation angle for the thigh is 36°.

A.III Surface EMG

A.III.a CVA03

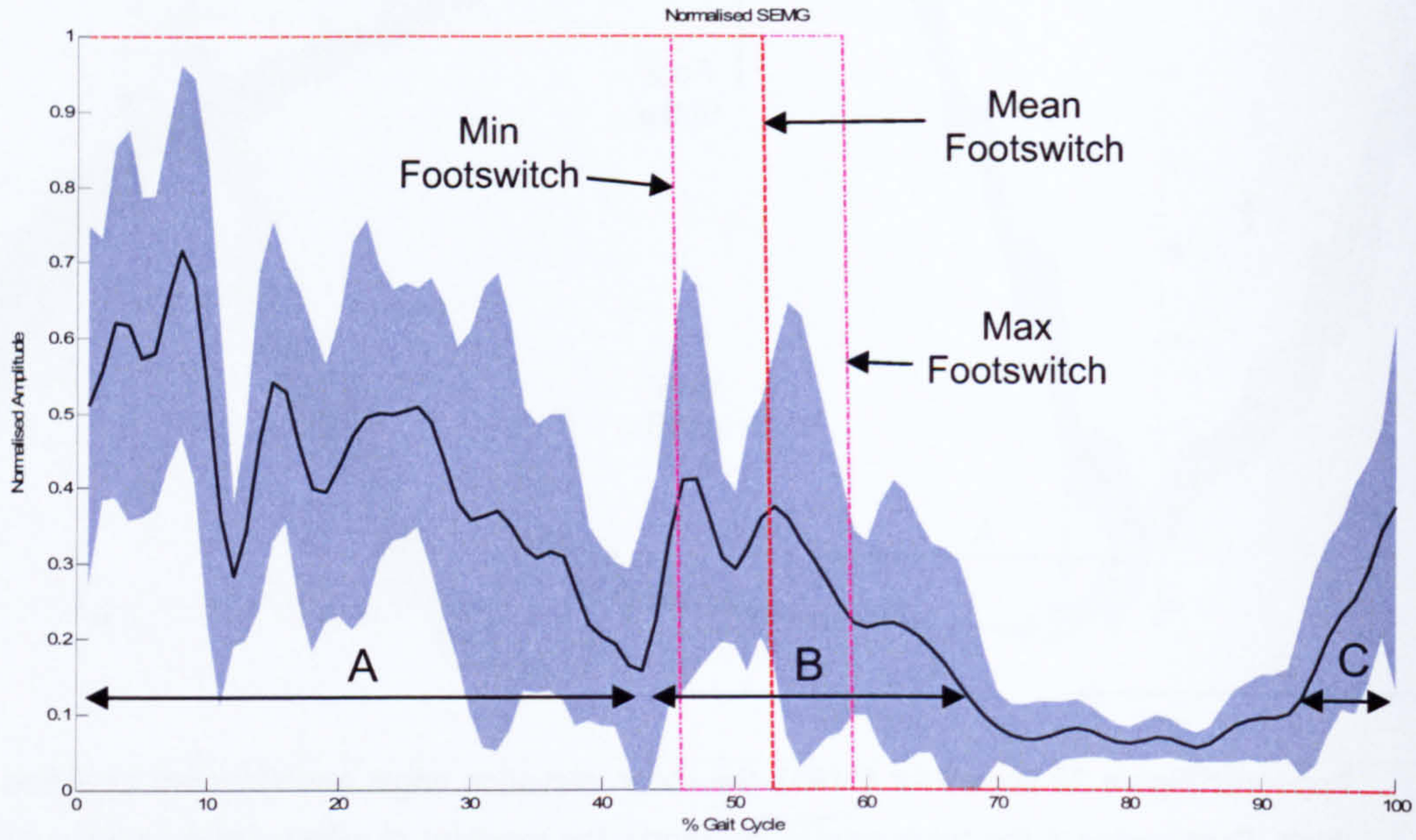

Appendix Figure 29 CVA03 linear envelope representation of the mean tibialis anterior muscle activity and standard deviation. Activity can be seen to decrease from toe off to foot strike, period A. Activity then increases slightly, prior to foot strike, designated by C. Activity can be seen to increase towards terminal stance, C. The broken red line displays the mean location of foot strike the period of the swing phase is shown to be increased.

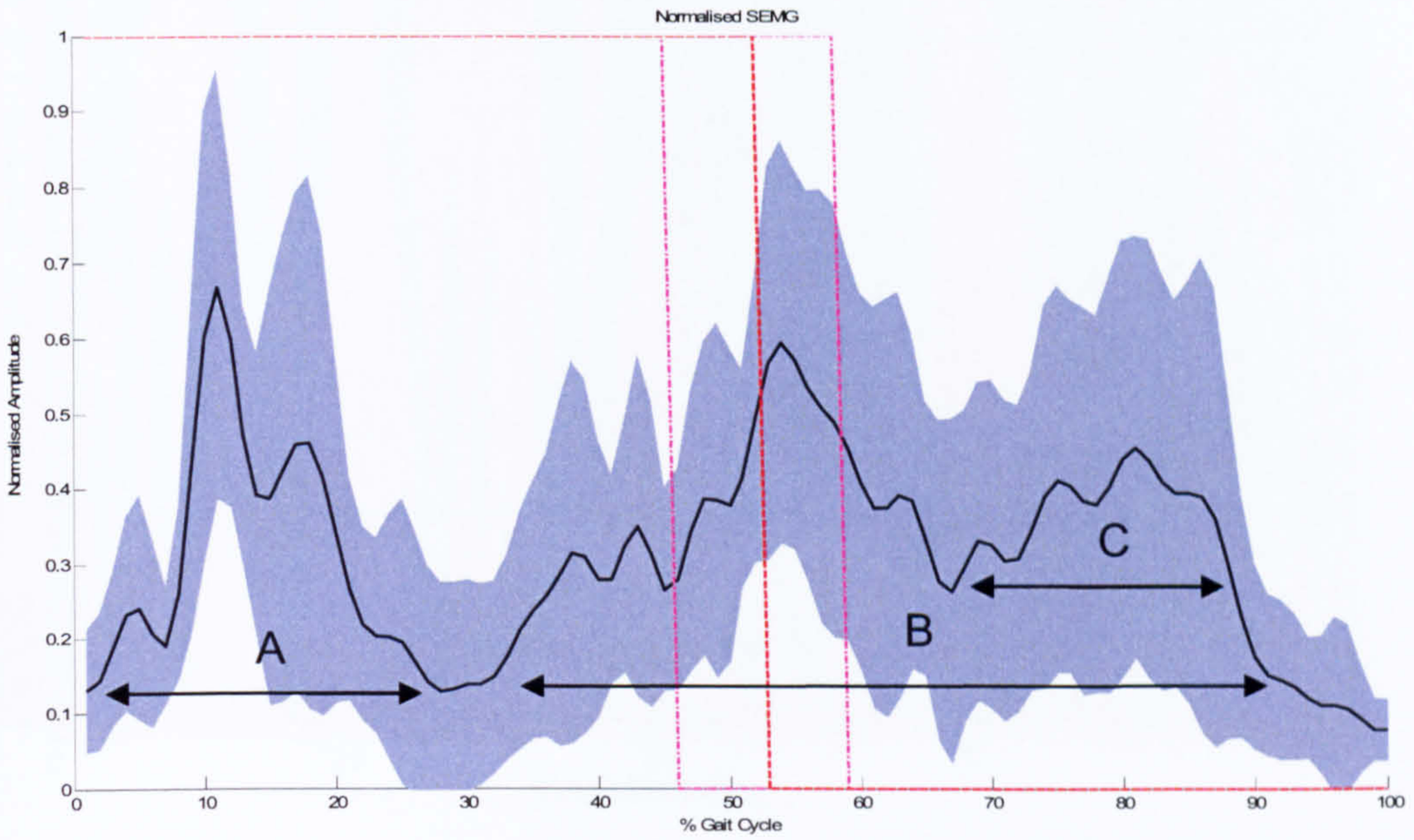

Appendix Figure 30 CVA03 mean linear envelope and standard deviation of the gastrocnemius muscle. The Figure reveals two prominent bursts of gastrocnemius activity. The first burst of activity occurs at initial toe-off and is shown in period A. The second burst begins almost immediately increasing in amplitude to foot-strike then diminishing gradually until toe-off, shown by B. There is a third less prominent burst of activity within the second burst that is designated by C.

Appendix Figure 31 CVA03 mean linear envelope activity and standard deviation of the soleus muscle. The activity consists of two prominent bursts; the first occurs during early swing phase shown by A. The second burst begins during terminal swing phase and continues through early stance phase shown by period B. A brief period of activity can be seen just prior to toe-off, period C.

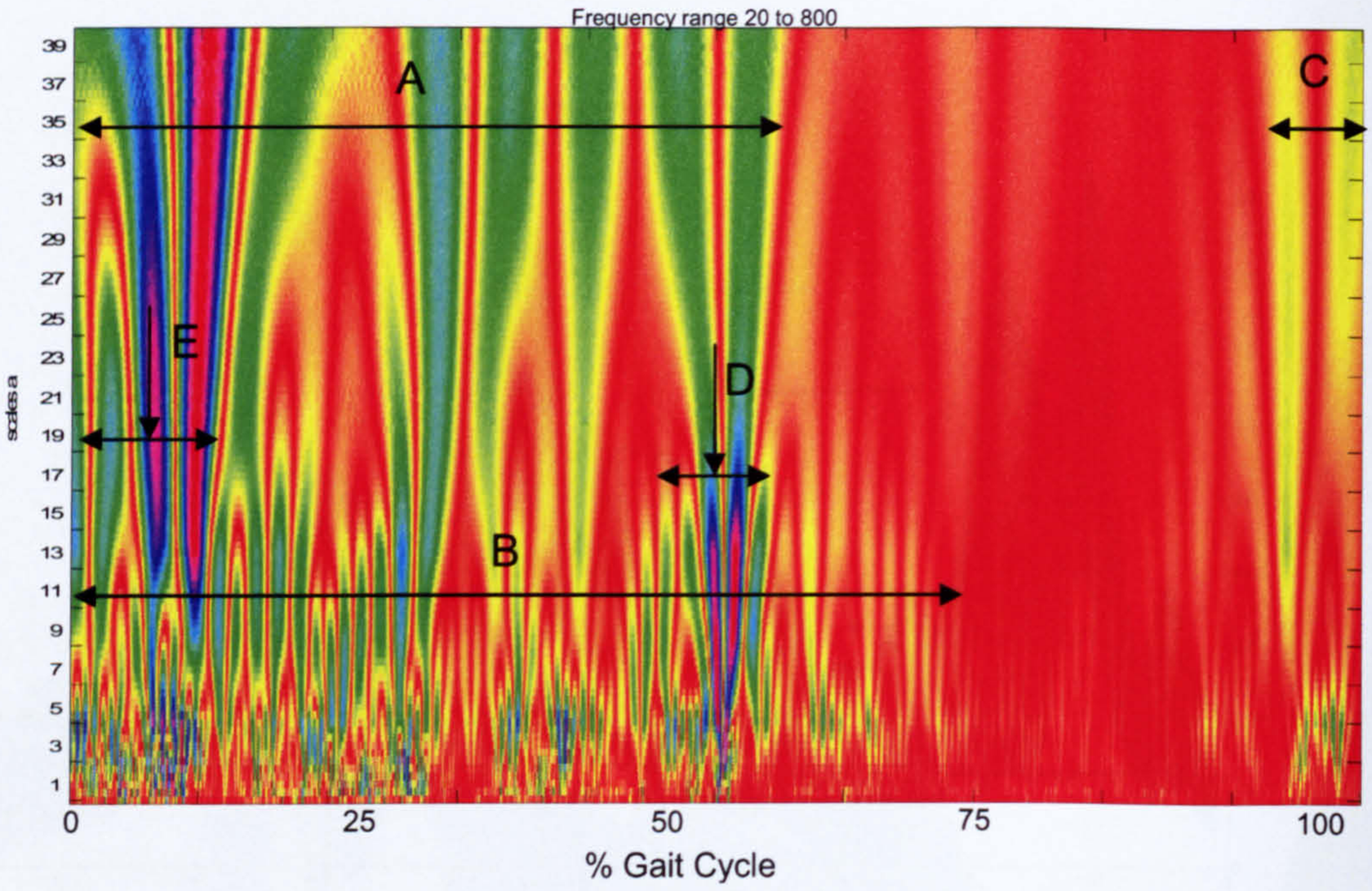

Appendix Figure 32 CVA03 time frequency representation of the tibialis anterior muscle activity. Continuous low frequency activity can be seen during swing phase, shown by A, which is commensurate with high frequency bursts. Continuous activity is visible during the swing phase, shown by B. A small cross frequency burst of activity is visible at toe off shown by C. D shows a burst related to foot strike. E shows activity related toe off and foot clearance.

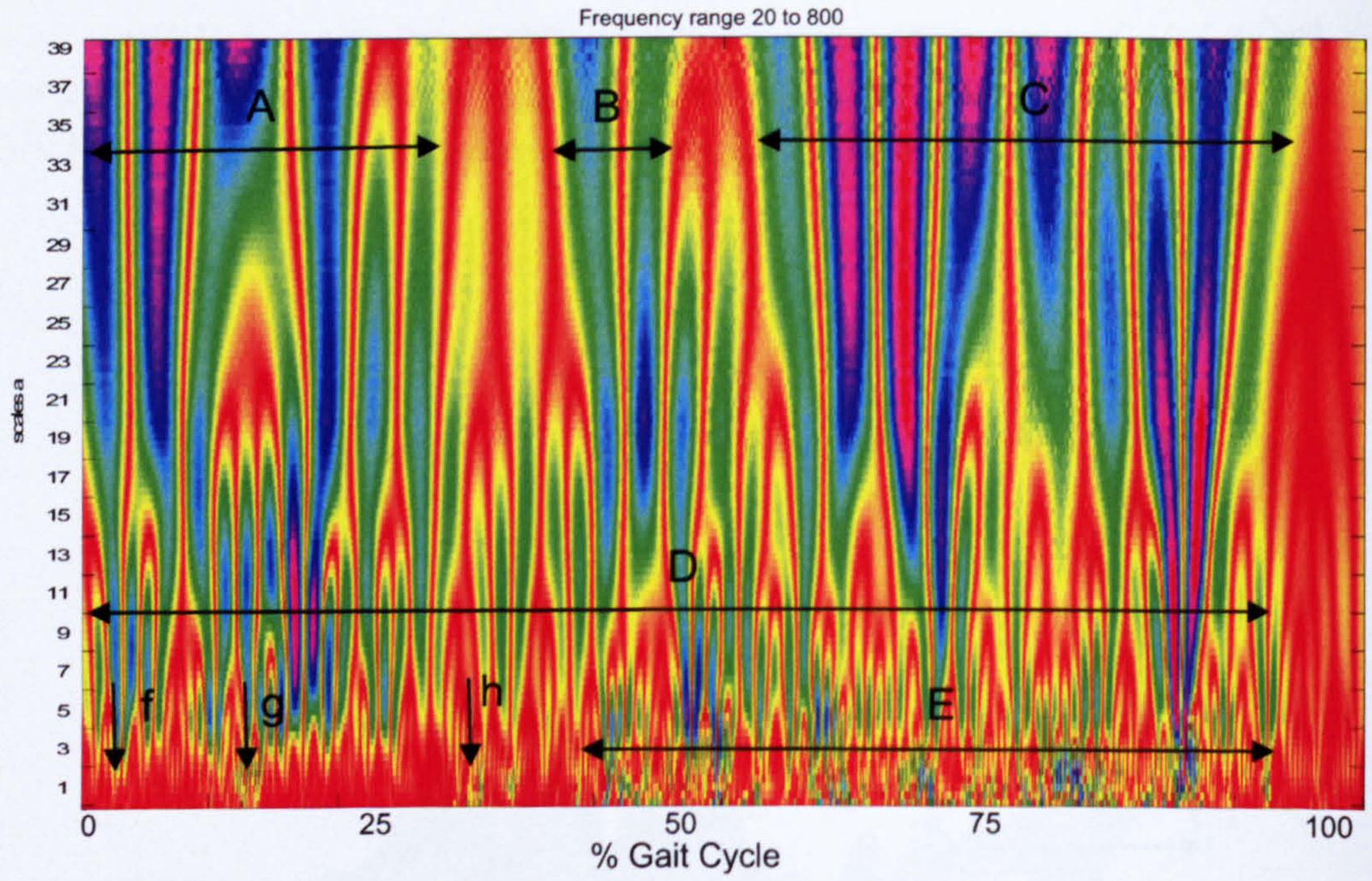

Appendix Figure 33 CVA03 time frequency representation of the gastrocnemius muscle activity. There is almost continuous activity throughout the stride shown by D, however, the highest activity occurs from late swing to terminal stance shown by E. Where the period E shows the highest frequency, A, B and C show three periods of greatest low frequency activity. Points f and g are two bursts of high frequency activity that appear in the swing phase.

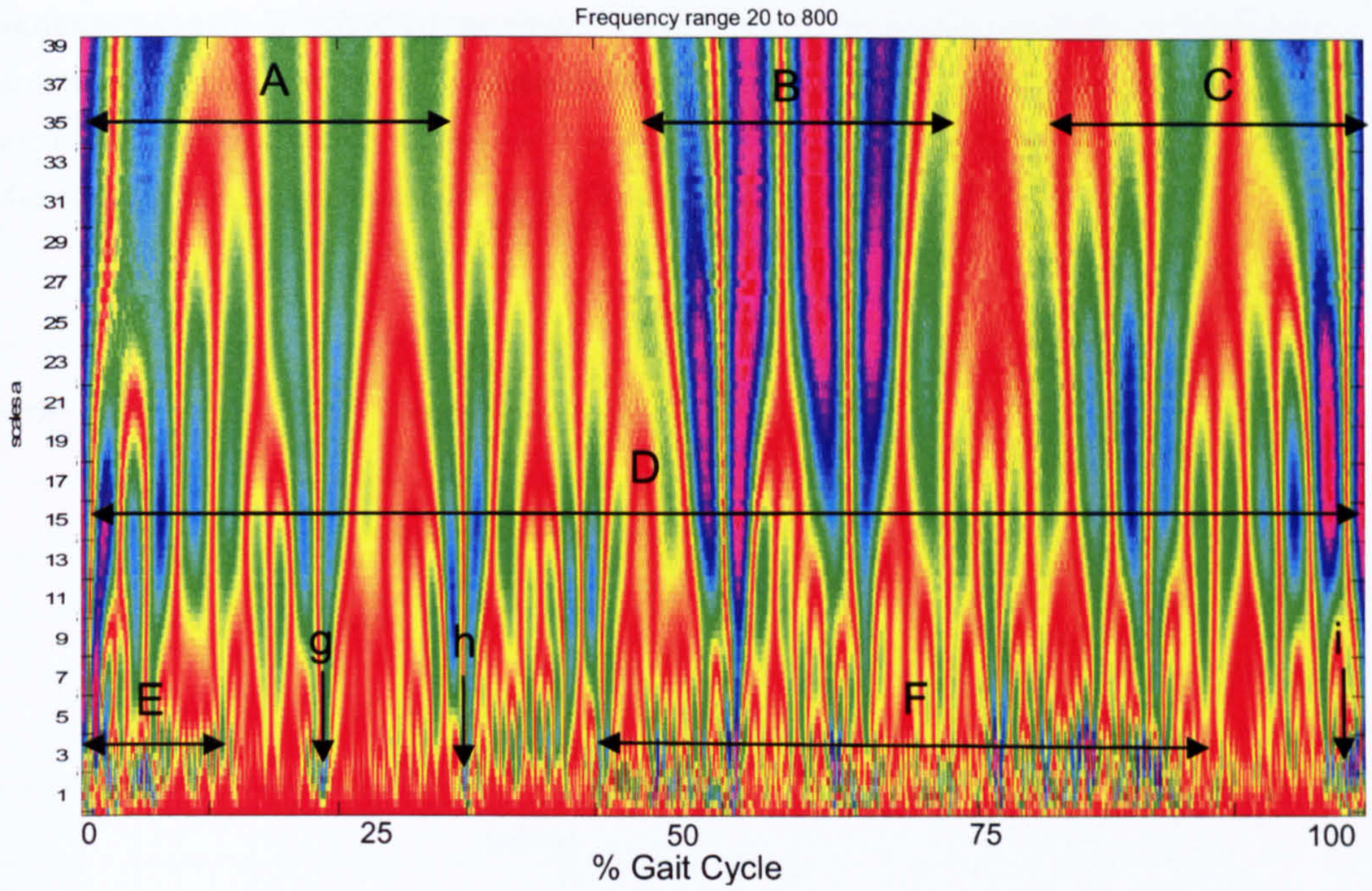

Appendix Figure 34 CVA03 time frequency activity of the soleus muscle. Similarly to the gastrocnemius muscle, the soleus shows continuous large coefficients throughout the stride Shown by period D. Again the activity in the highest scale (1 – 6) occurs between terminal swing to terminal stance and is shown in period F. Several small bursts of activity in the high frequency bins occur at toe off (period E and point i) during the swing phase (points g and h) and foot strike (period F). Three burst of lower frequency activity can be observed during periods A, B and C.

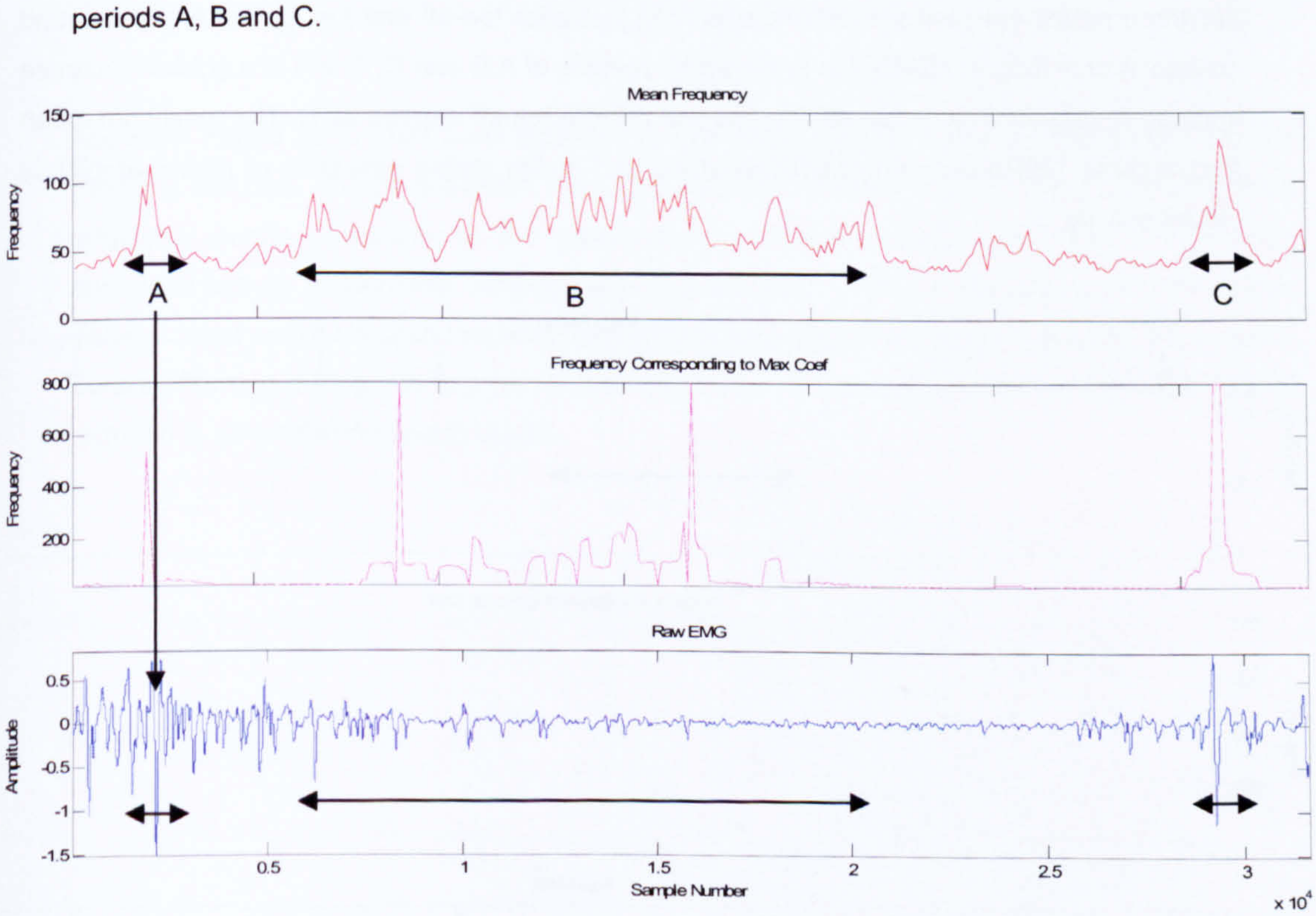

Appendix Figure 35 CVA03 instantaneous mean frequency of the tibialis anterior muscle. The mean frequency increases from toe-off in relation to increased amplitude sEMG, shown by period A. The amplitude of the mean frequency subsequently decreases only to rise again. This increase corresponds to low amplitude sEMG activity during terminal swing phase and foot-strike. This period is shown by B. There is a final increase in mean amplitude corresponding to

an increase in sEMG amplitude just prior to toe-off as shown by period C. The maximum mean frequency is approximately 125Hz occurring prior to toe-off.

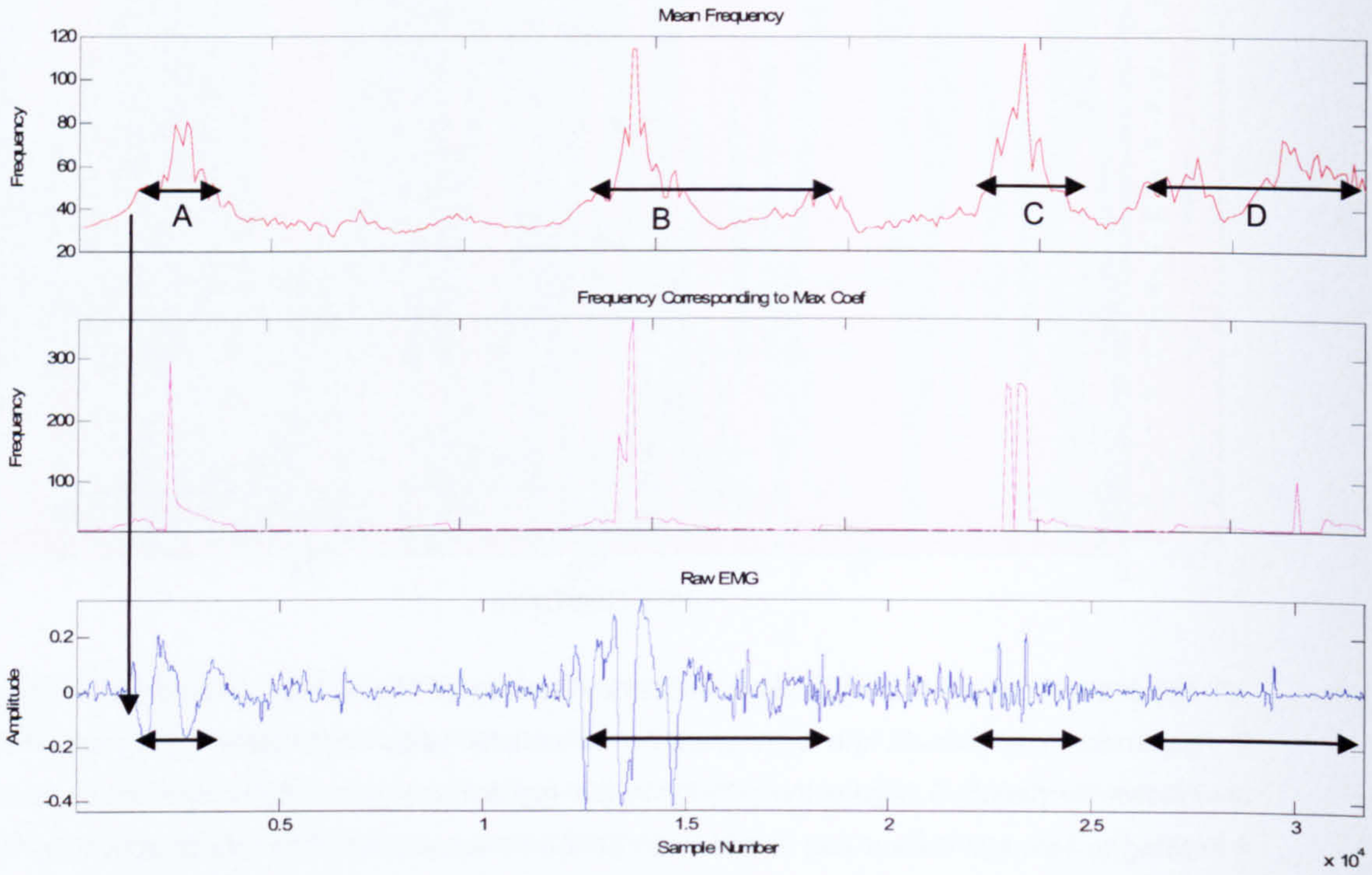

Appendix Figure 36 CVA03 instantaneous mean frequency of the gastrocnemius muscle. There are three prominent peaks of activity occurring just after toe-off and just before foot strike and cessation of activity in sEMG this is shown by periods of A,B and C. There is a gradual increase in mean frequency in terminal stance and just prior to toe-off marked as D. The maximum mean frequency is 120Hz occurring near foot-strike and at the visible cessation of higher amplitude sEMG activity.

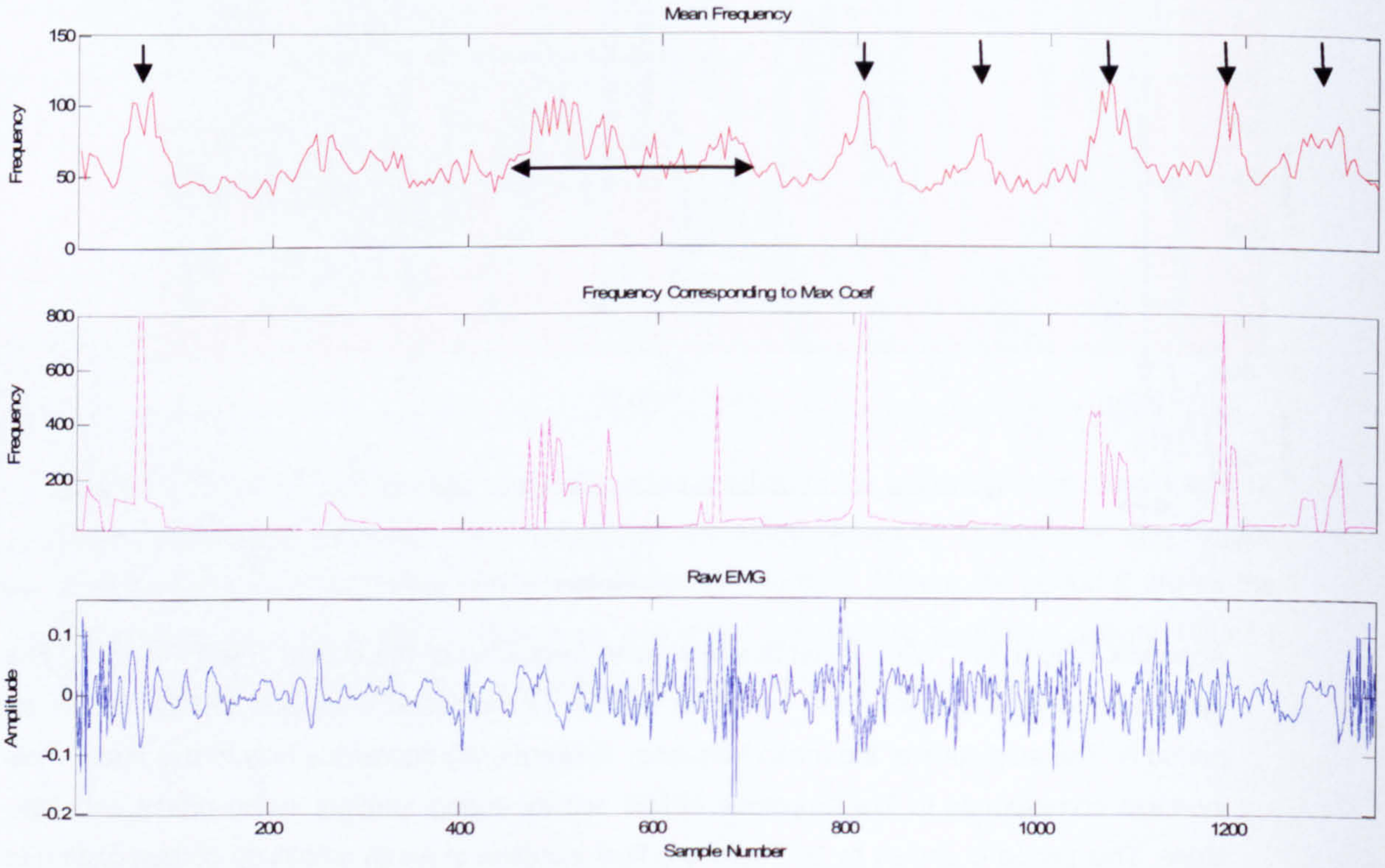

Appendix Figure 37 CVA03 instantaneous mean frequency of the soleus muscle. Activity is sustained throughout the stride, in particular activity is seen during the swing phase and increases slightly towards foot-strike. The activity has a pulsatile characteristic especially during the stance phase. The maximum mean frequency is approximately 120Hz.

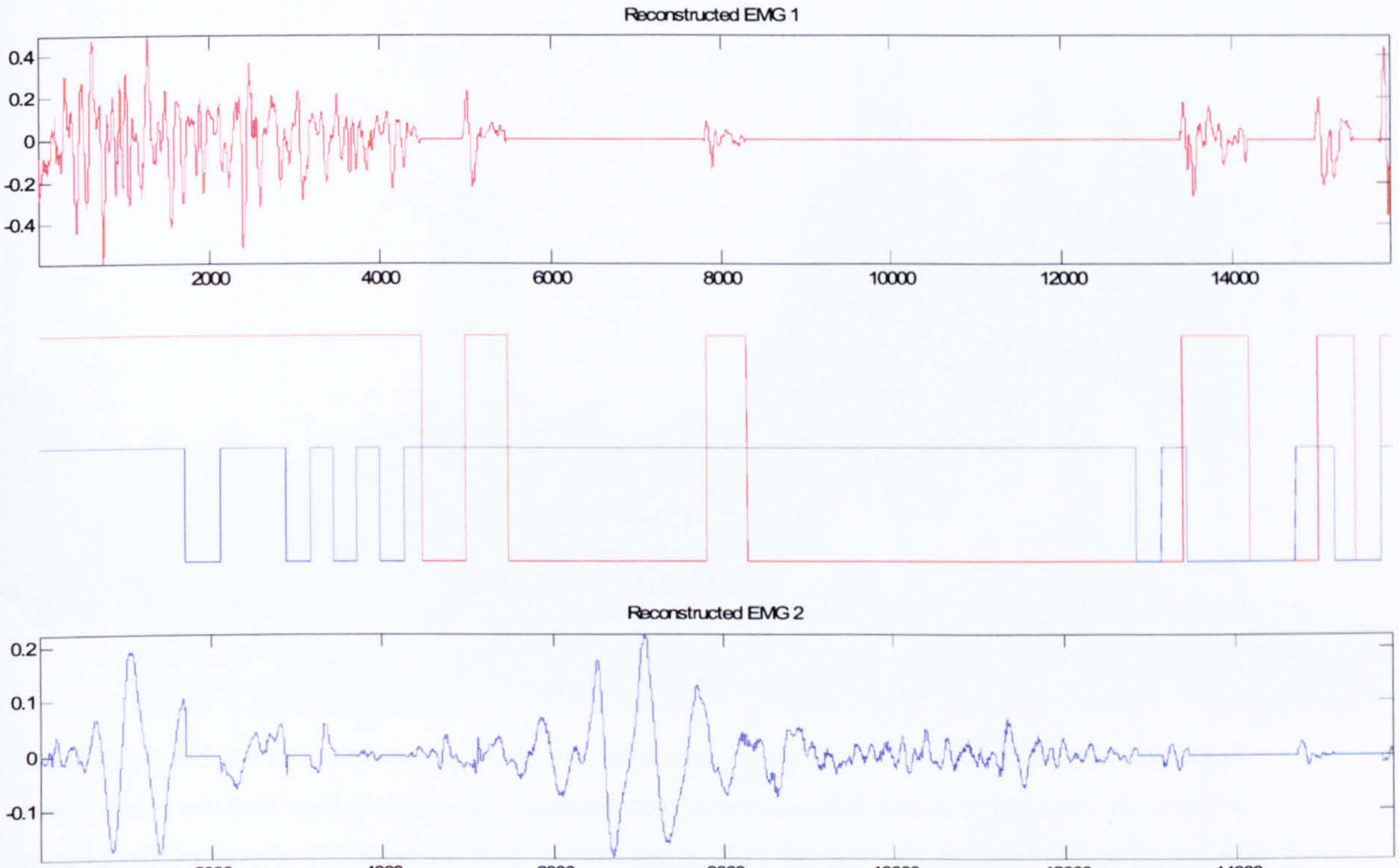

Appendix Figure 38 CVA03 burst locations of the tibialis anterior (top) and the gastrocnemius (bottom) muscles. The co-activation ratio for these two muscles is 0.31. The method identifies additional bursts of activity in the gastrocnemius muscle during swing phase. The most sustained activity is identified between approximately 30 – 70% of the gait cycle. The tibialis anterior burst activity is predominately restricted to the early swing phase with only short epoch bursts occurring during mid and terminal swing phase. The activity in terminal stance has been reduced to several short epoch bursts.

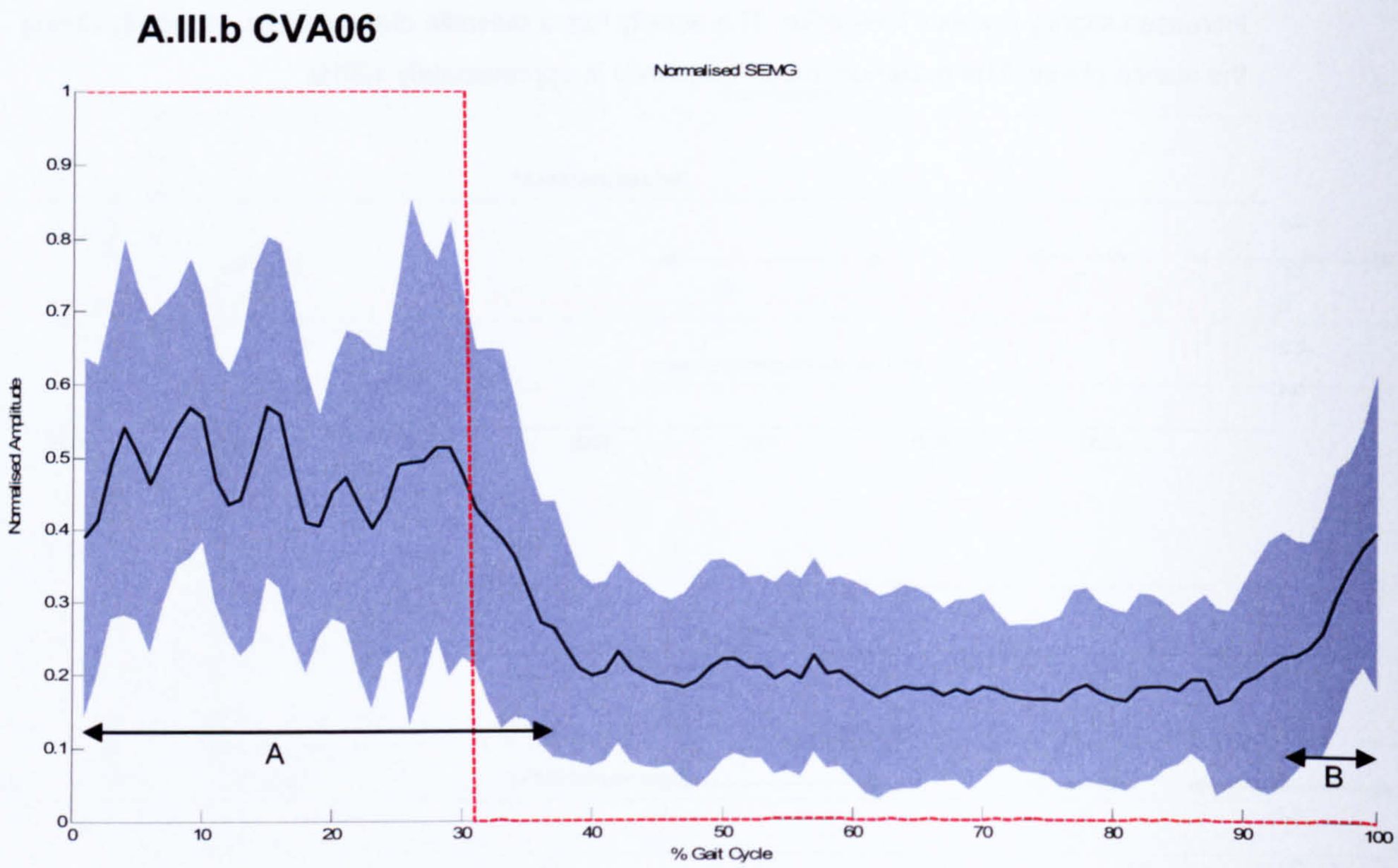

Appendix Figure 39 CVA06 mean linear envelope and standard deviation of the tibialis anterior muscle. shows activity of the tibialis anterior with standard deviation in blue and the mean linear envelope value displayed as the solid black line. Mean footswitch data is shown by the broken red line. Most activity is seen in the swing phase, shown by period A. Activity returns in the last 10% of the gait cycle shown by period B.

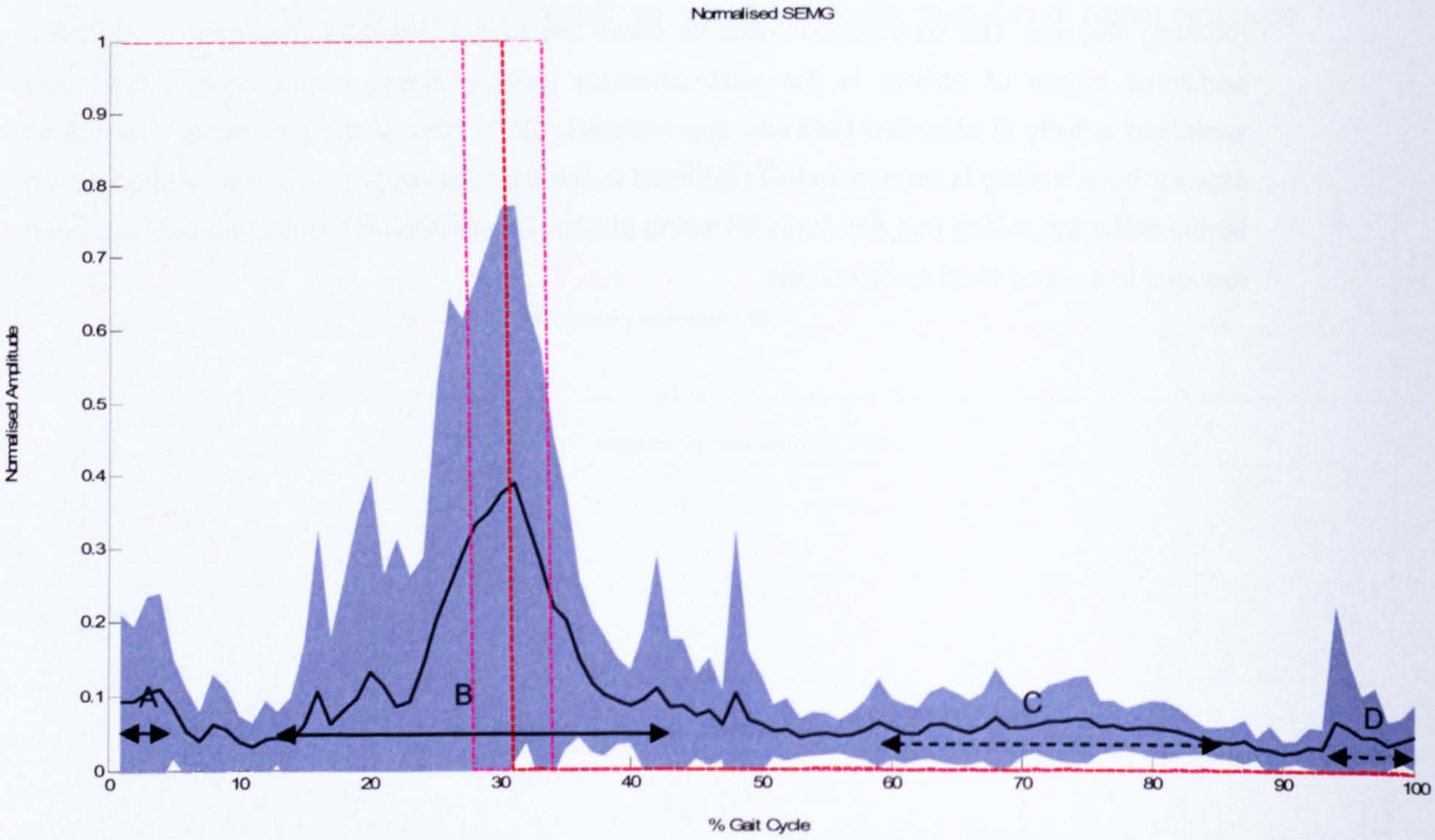

Appendix Figure 40 CVA06 linear envelope activity for the gastrocnemius muscle. There is one prominent burst around foot strike shown by period B. There are smaller, less prominent, bursts

of activity in early the early swing phase shown by period A. Period C and D, during the stance phase, also relate to small increases in amplitude.

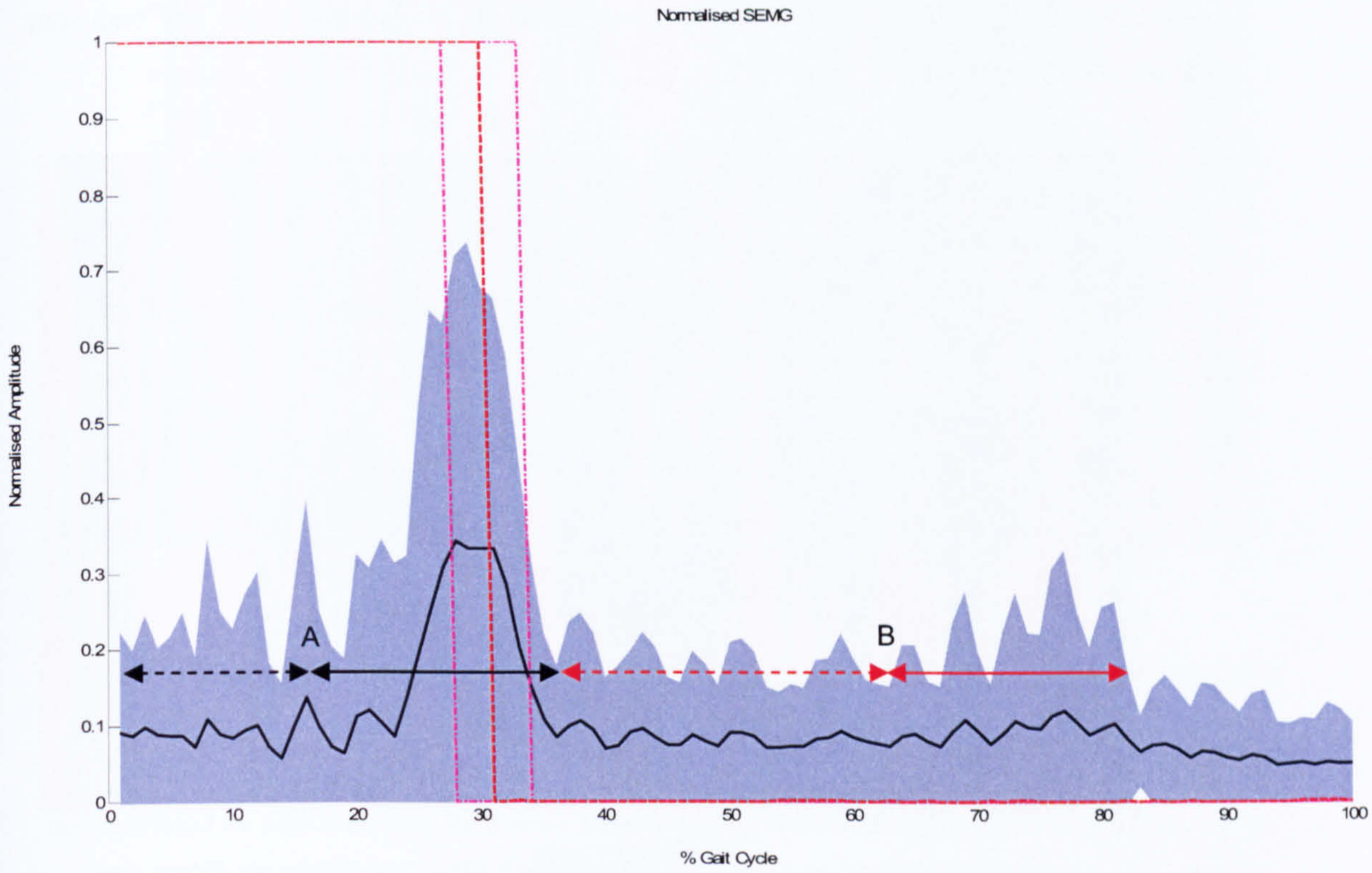

Appendix Figure 41 CVA06 linear envelope activity of the soleus muscle. A single prominent burst of activity is visible around foot strike and is shown during period A. The broken line displaying period A denotes an uncertain period of activity. Period B displays a second period of reduced amplitude activity; again the broken line displays a uncertain period of activity.

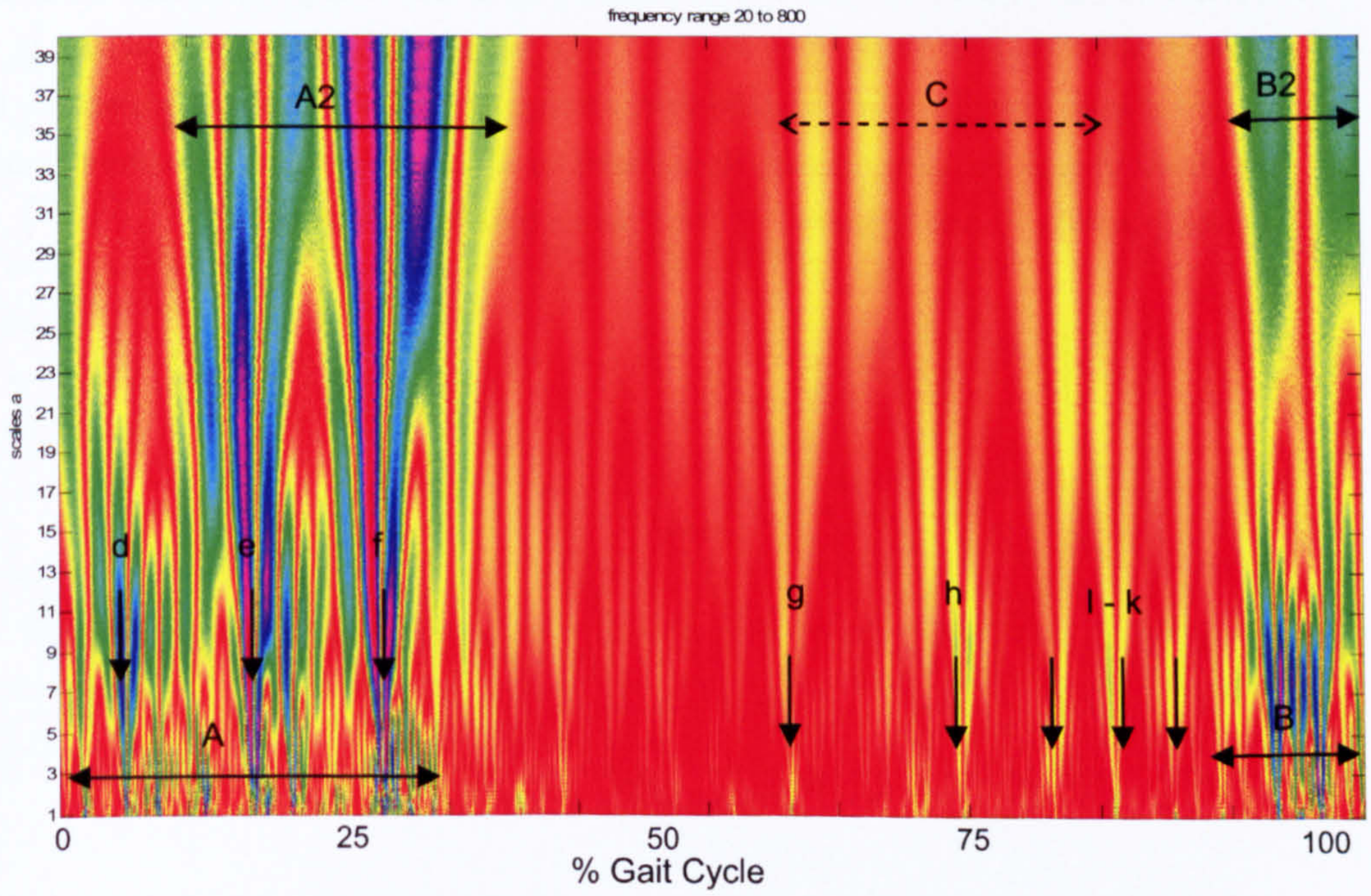

Appendix Figure 42 CVA06 Time-frequency activity of the tibialis anterior muscle. Two prominent bursts of activity can be seen in period A and period B. Within the first burst the maximum coefficients exist in the mid to low frequency bands with short epochs of high

frequency activity shown by points d, e and f. The second burst contains large coefficients mainly in the moderate high frequency bands. Low frequency burst activity can be seen related to high frequency bursts shown by periods A2 and B2. Points g – k relate to lower amplitude coefficients of burst activity and relate to lower amplitude coefficients in the low frequency bands, shown by period C

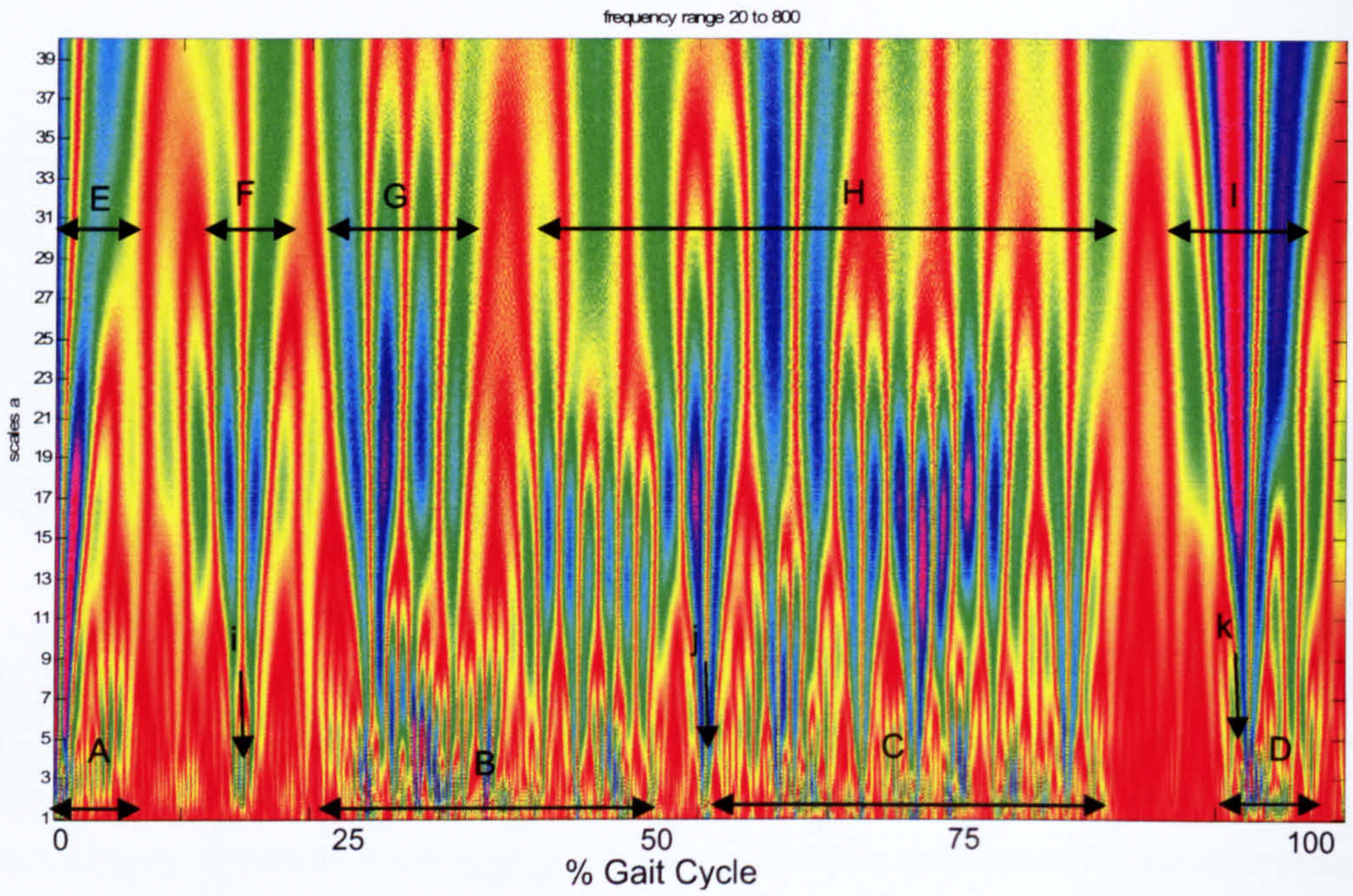

Appendix Figure 43 CVA06 Time-frequency activity in the gastrocnemius muscle. The graph reveals high frequency activity of the gastrocnemius muscle at to off. A period of high frequency activity can be seen designated by B and C. This is punctuated a large burst at point f. There is a final burst of high frequency activity with associated high amplitude coefficients at low frequencies during period D and I. This period begins with a large amplitude burst at point k. Although relatively low in amplitude there are four periods of low frequency activity E, F and H. Period I shows high coefficient amplitude low frequency activity. During early stance there is a short burst of high frequency activity designated by A. Just prior to the prominent period of high frequency activity (B and C) there is a short epoch burst shown by point j.

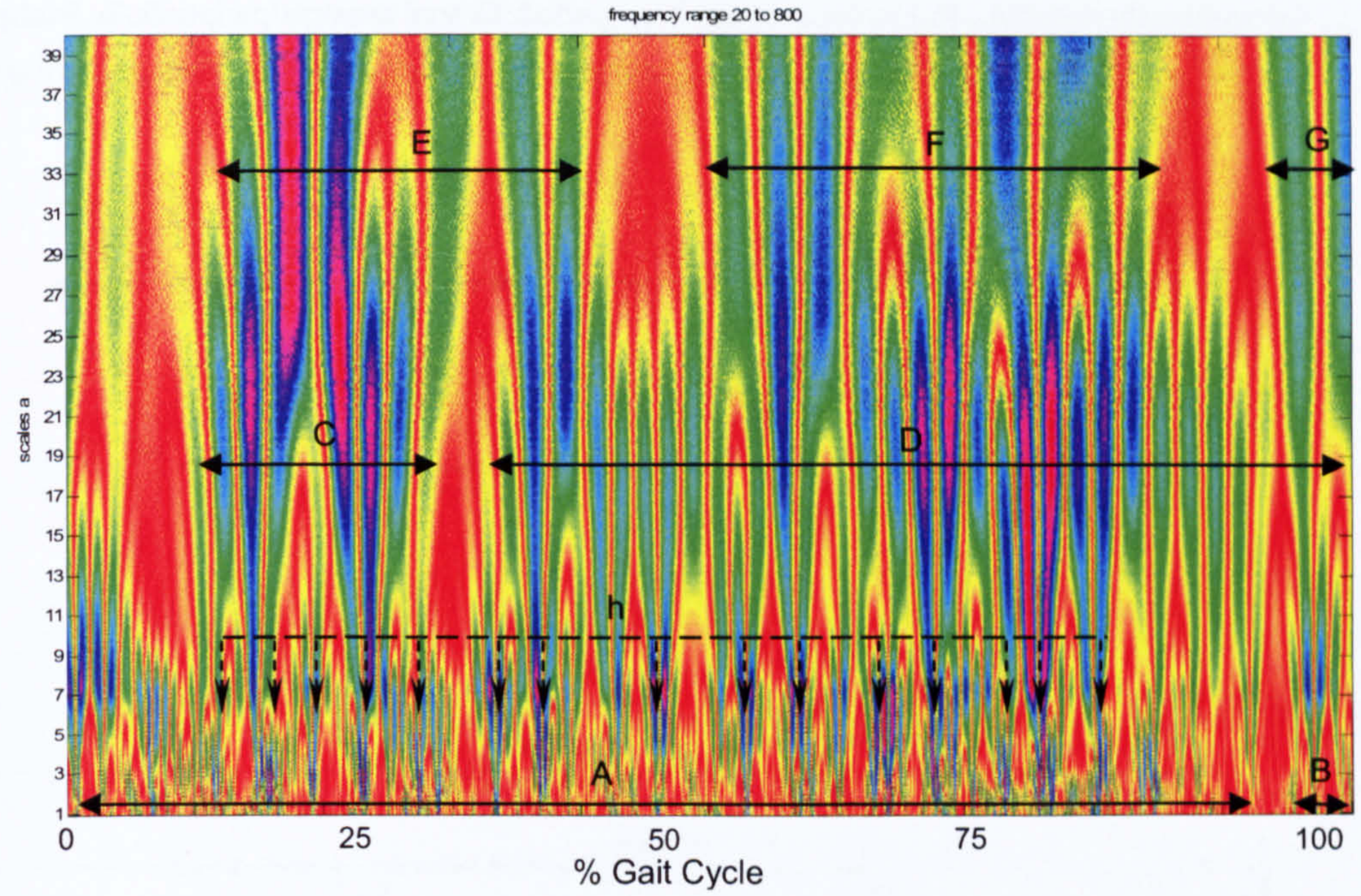

Appendix Figure 44 CVA06 time-frequency results for the soleus muscle. The graph displays the time frequency activity of the soleus muscle. There is almost continuous high frequency (scale 1-3) and moderate high (scale 5-9) frequency activity across the stride. This activity is designated by period A. High frequency activity seems to diminish after period A although some lower amplitude coefficients exist during period B. Three prominent low frequency bursts can be seen in periods E, F and G. Moderate frequency activity can be seen during periods C and D. This time frequency activity is characterised by many short epoch bursts during period A represented by the points h.

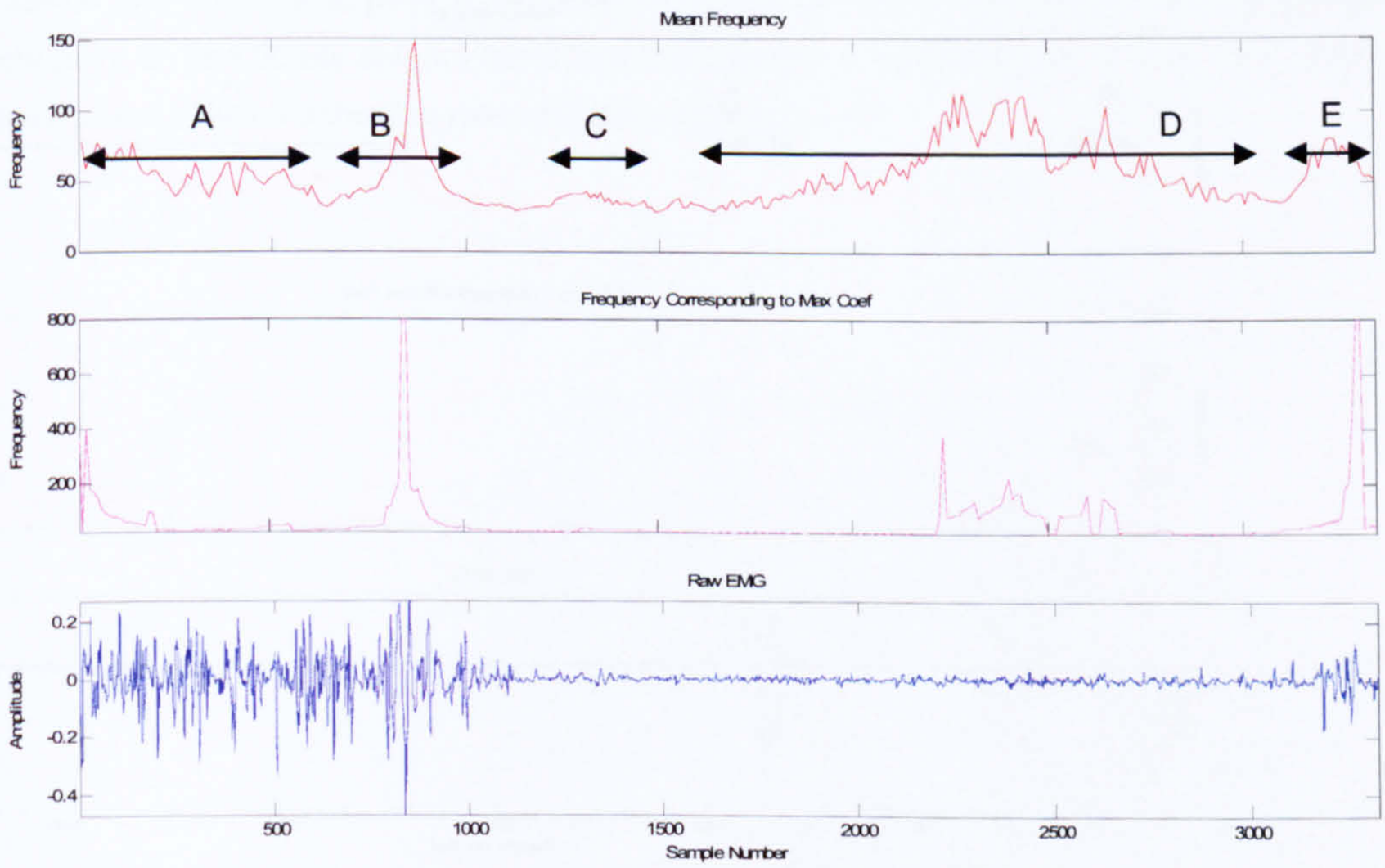

Appendix Figure 45 CVA06 mean frequency results for the tibialis anterior muscle. The graph shows instantaneous mean frequency activity across a stride for the tibialis anterior muscle. The mean frequency diminishes from toe-off denoted by period A. A peak frequency can then be seen at the termination of the first burst of sEMG activity, shown by period B. The mean

frequency then begins to increase again from period C and through period D. A final peak of activity can be seen at toe off, denoted by period E.

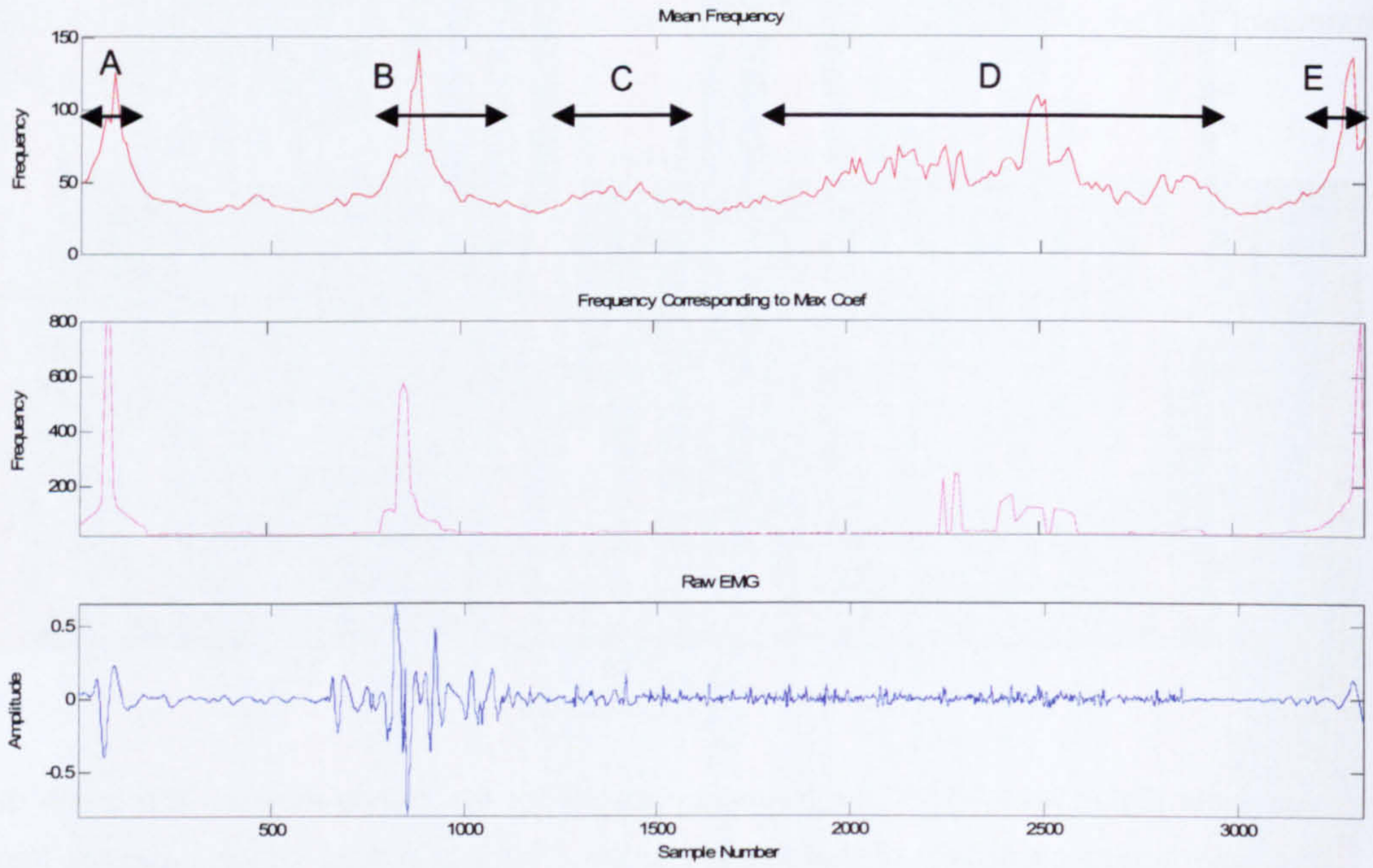

Appendix Figure 46 CVA06 mean frequency results for the gastrocnemius muscle. The graph shows instantaneous mean frequency of the gastrocnemius muscle. Mean frequency activity increases to a maximum concurrent sEMG burst activity during period A and B. Activity increases towards the end of the period of raw sEMG activity, shown by period C and D, and then again finally at toe-off, period E.

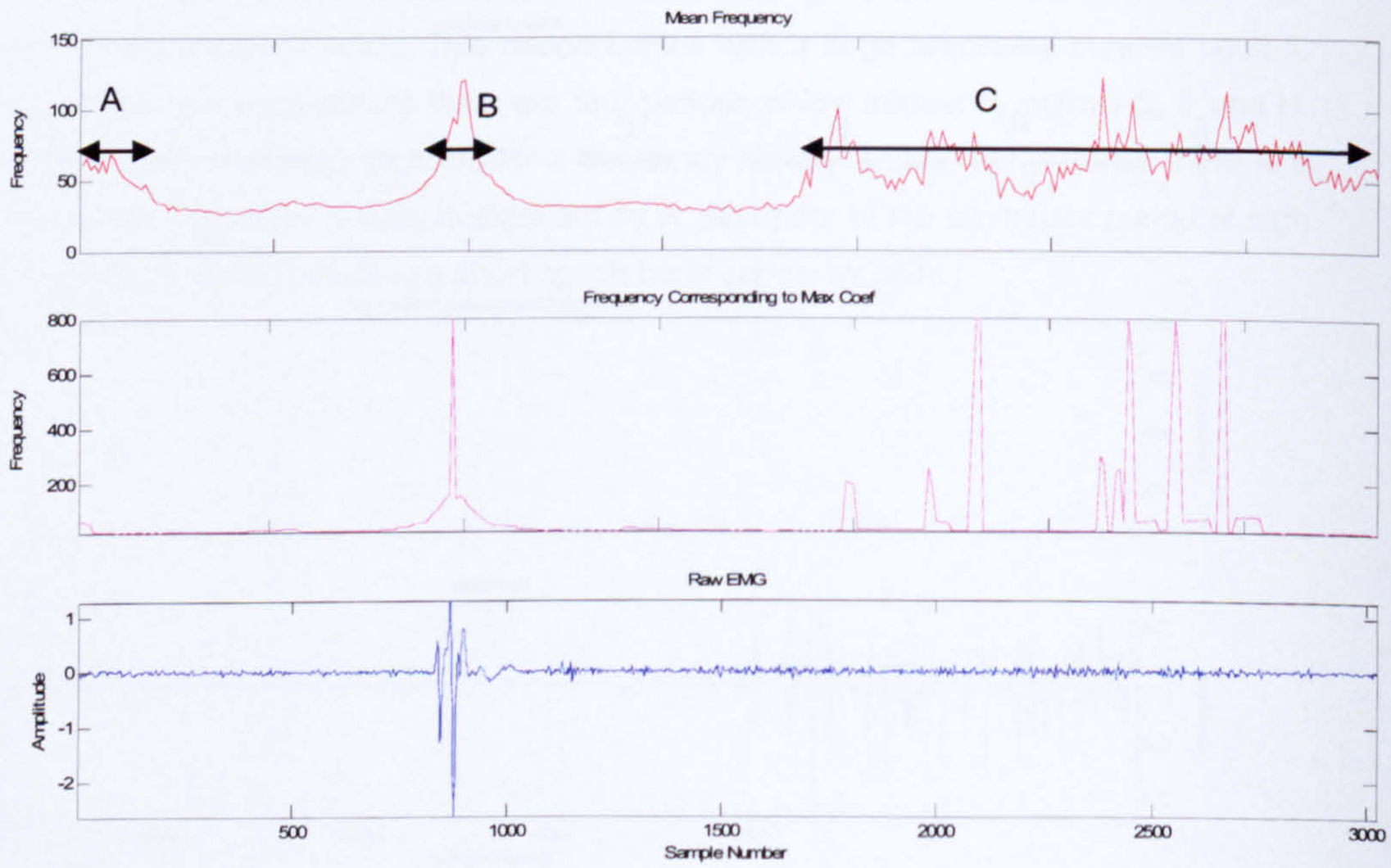

Appendix Figure 47 CVA06 mean frequency results for the soleus muscle. The graph shows the instantaneous mean frequency of the soleus muscle. The Figure shows a peak of activity during period A.. The second significant increase in mean frequency occurs at foot strike shown by

period B. Subsequently there is a sustained period of increased mean frequency to toe off this is denoted by period C. This period is characterised by a periodic increases in amplitude.

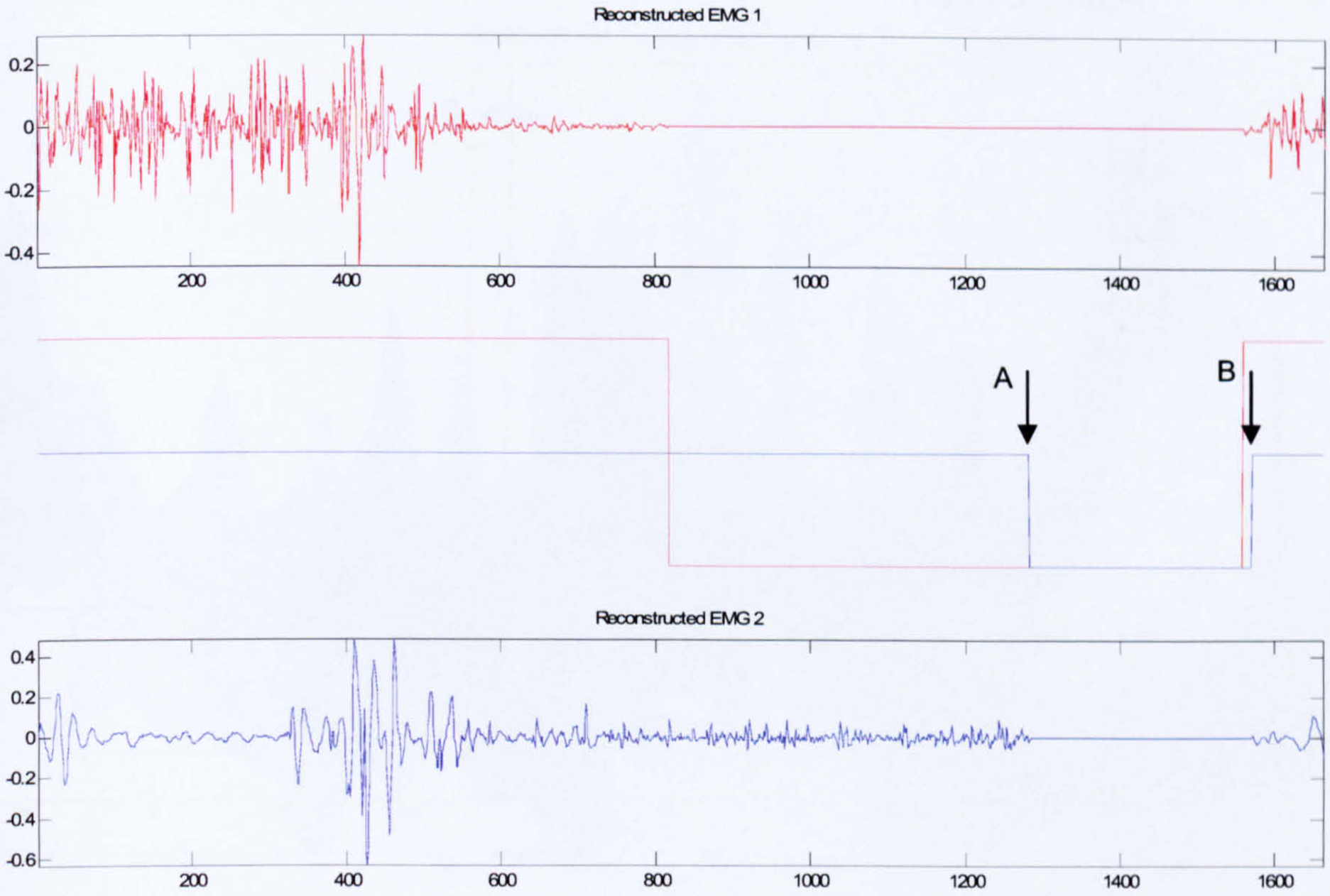

Appendix Figure 48 CVA06 Burst activity of the tibialis anterior and gastrocnemius. The graph displays the burst locations from the gastrocnemius and the tibialis anterior muscles. The Figure shows that the tibialis anterior burst locations are well defined. Burst locations of the gastrocnemius are less well defined. The gastrocnemius burst locations are calculated to begin at toe-off and continue to point A. An additional burst can be observed at the end of the gait cycle point B. The tibialis anterior burst locations identify a sustained period of activity into the stance phase. The co-activation ratio of these muscles is 0.66.

A.III.c CVA07

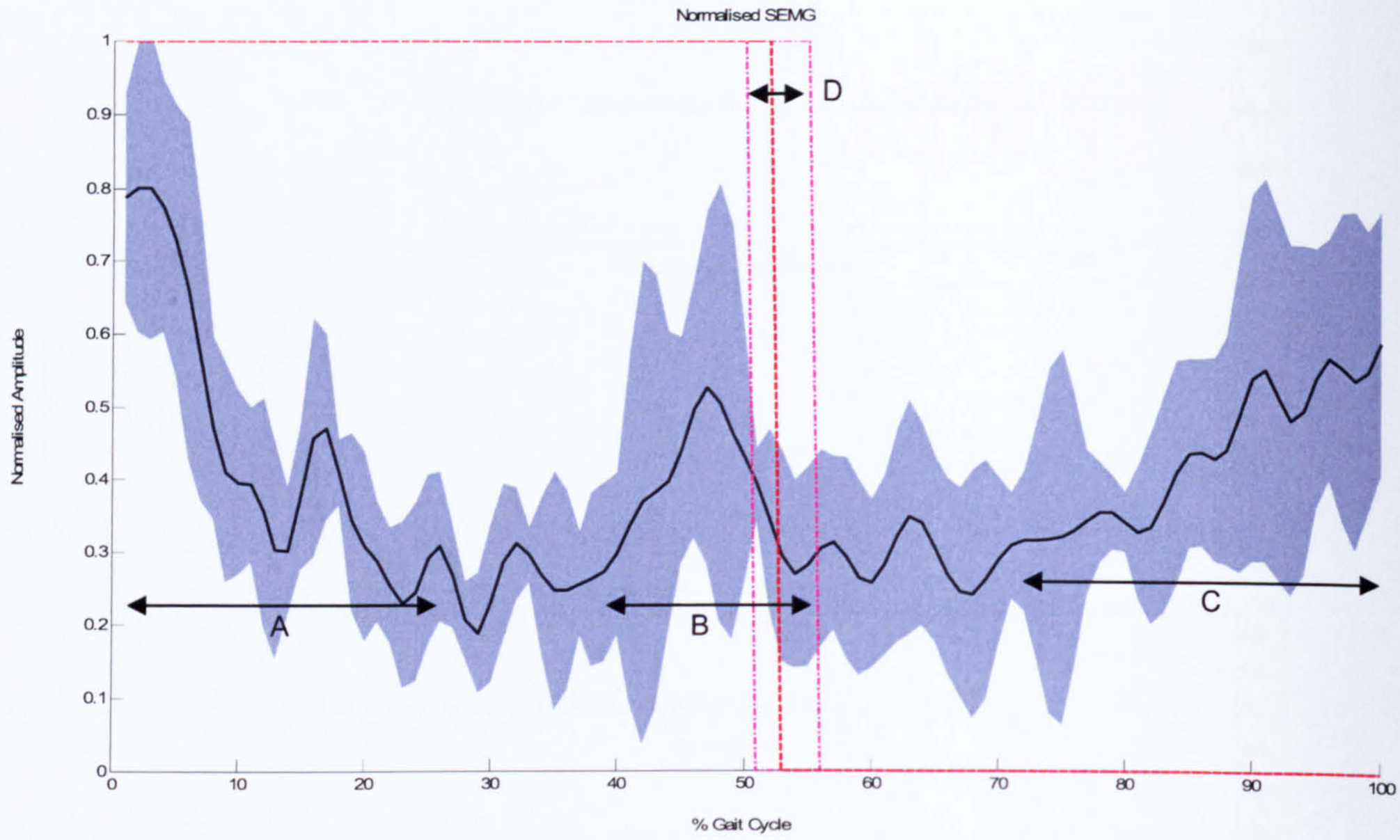

Appendix Figure 49 shows for CVA07 the mean linear envelope and standard deviation of the tibialis anterior. Two prominent bursts of activity can be seen during period A and period C. One smaller burst of activity can be observed during period B just prior to foot strike. The red broken line shows the average foot strike. The mauve broken lines show the variation in foot strike location and can be seen between period D.

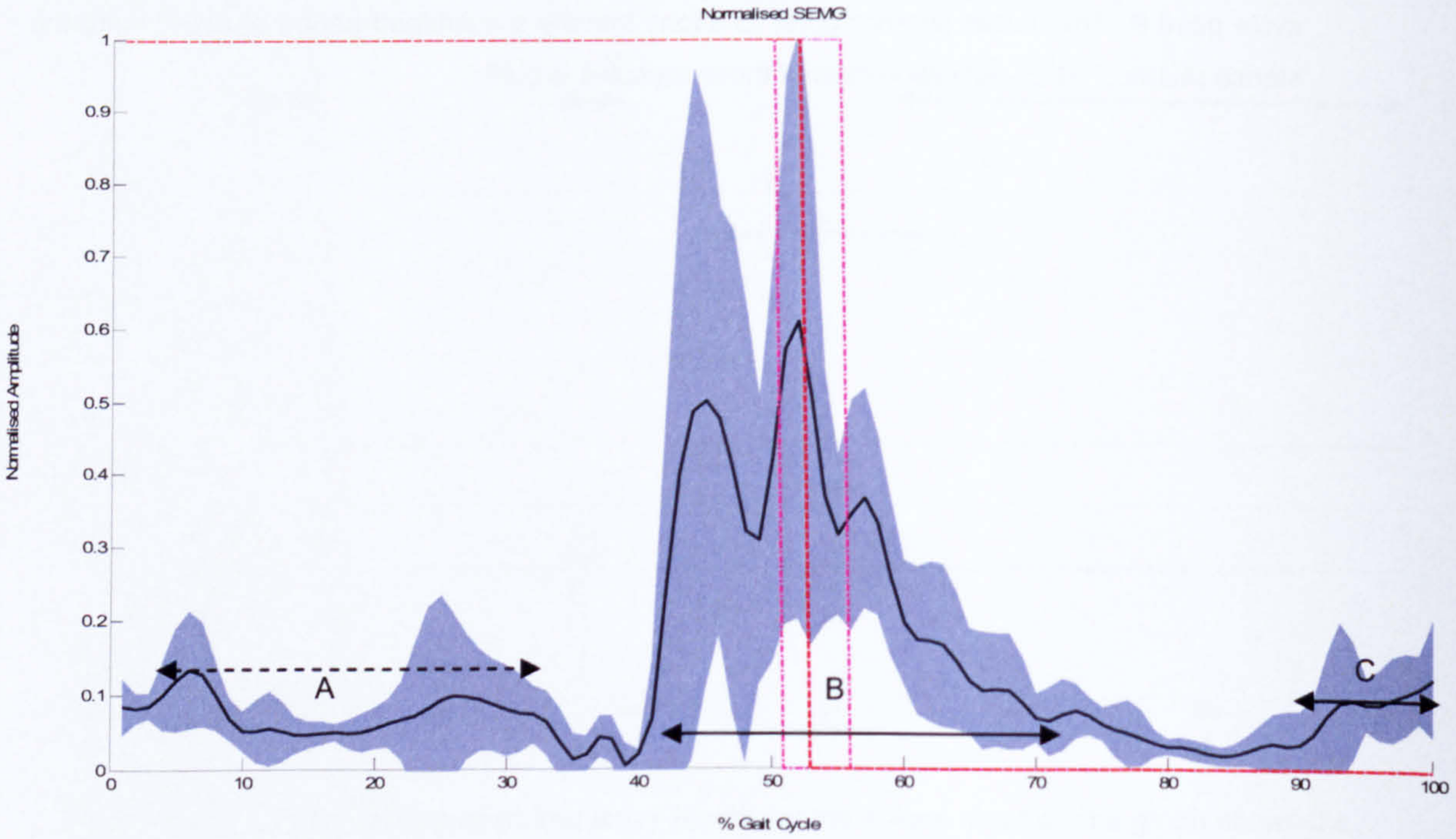

Appendix Figure 50 shows for CVA07 the mean linear envelope and standard deviation of the gastrocnemius muscle a prominent burst can be seen in period B. There is a comparatively small amplitude burst of activity during the first part of the gait cycle and denoted by period A.

There is a small increase in amplitude in the last portion of the gait cycle and shown by period C.

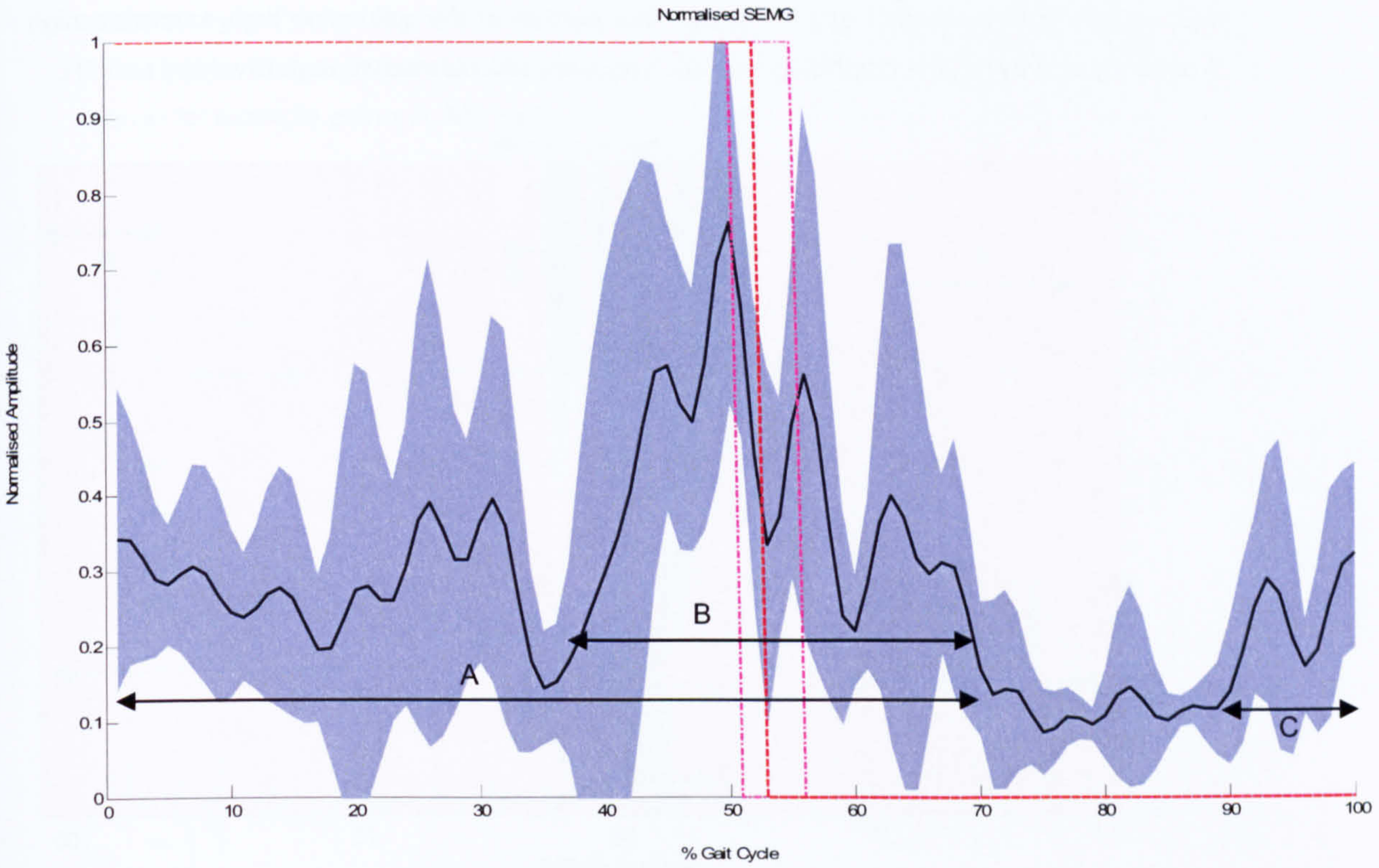

Appendix Figure 51 shows for CVA07 the mean linear envelope and standard deviation of the soleus muscle. Activity can be seen over period A. This activity is made up of two prominent bursts the second shown by period B. There is a period of relative quiescence followed a final burst of activity denoted by C.

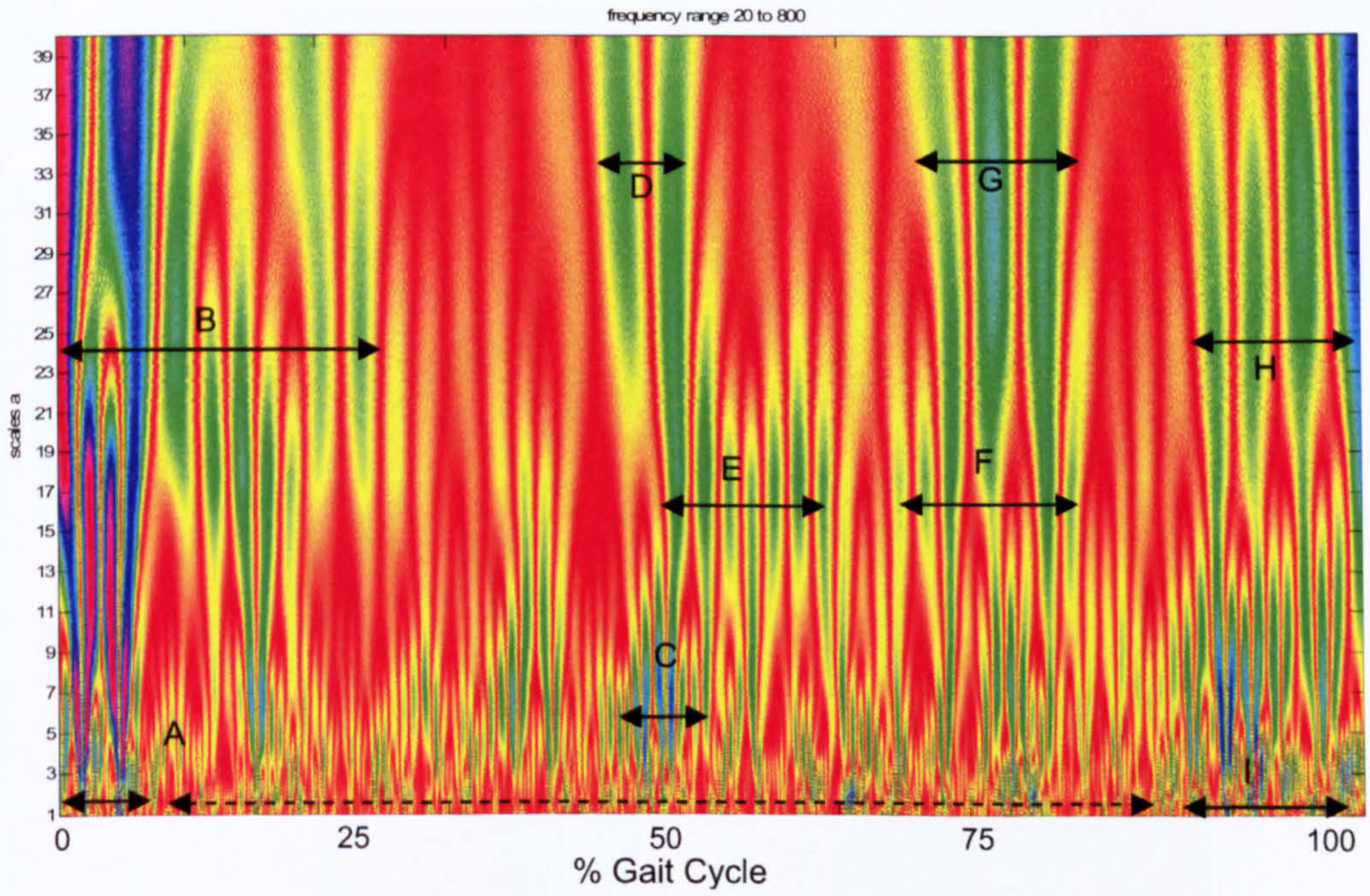

Appendix Figure 52 shows for CVA07 the time-frequency representation of tibialis anterior activity. There are two prominent bursts in the high frequency activity that form the activity in period A. The high frequency activity continues but at a lower amplitude shown by the dotted

line. Low frequency activity ranges period B and three further low frequency bursts are shown by D, G and H. There is one medium high frequency burst of activity shown by period C which coincides with period D and E. Periods E and F show moderate frequency activity coinciding respectively with periods D and G. In the final portion of the gait cycle high amplitude high frequency activity returns coinciding with low frequency activity shown respectively by I and H.

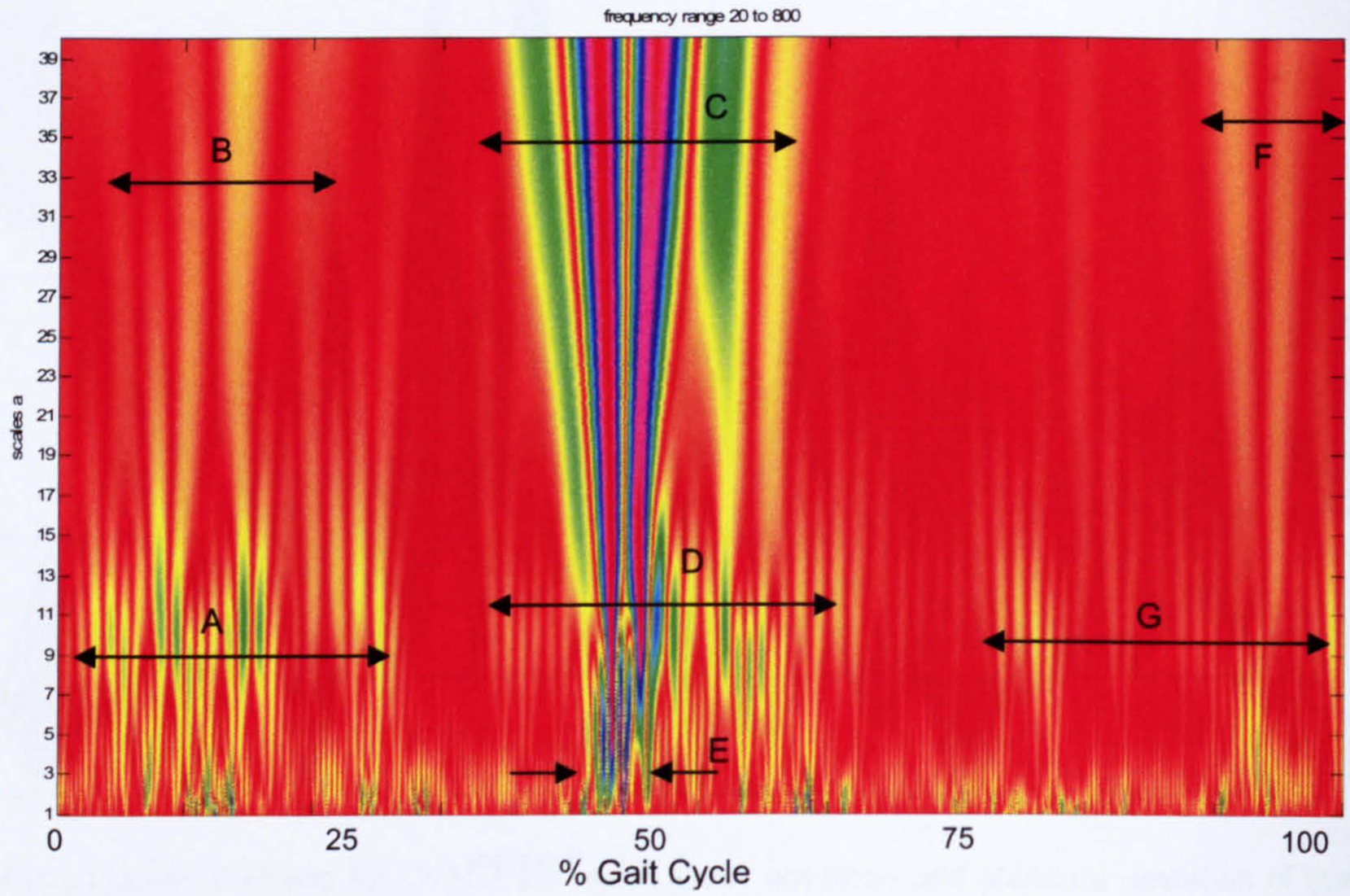

Appendix Figure 53 shows for CVA07 the time-frequency representation of the gastrocnemius muscle. Over period C there is a very prominent burst of activity. This activity extends across all the frequency bins and consists of very large coefficients in comparison to the rest of the stride. The commensurate low frequency activity extends over period C, yet in the higher frequency bands activity exists predominantly over period E. There are several smaller short epoch bursts of activity for example over period A, and G. Over period A, D and G there is an increased level of activity in the midrange frequency bins.

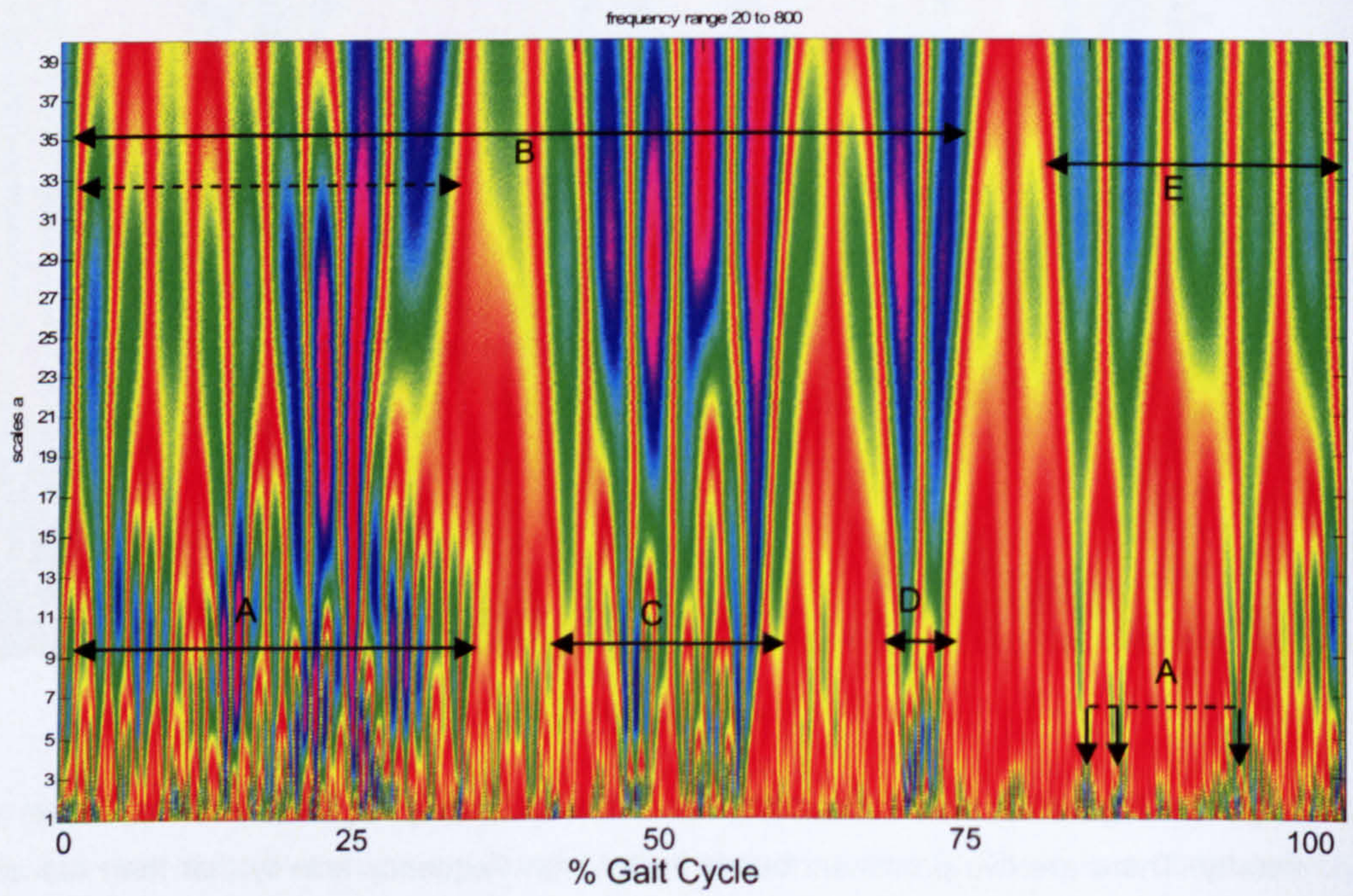

Appendix Figure 54 shows for CVA07 the time-frequency representation of the soleus muscle. There are three high frequency periods of activity shown by periods A, C and D. These relate to two low frequency periods of activity shown by B and E. period B might be split into two periods as shown by the dotted line. Between periods A and C there is lower amplitude activity present in the higher frequency bands but less prominent. Again, several short epoch bursts can be seen at for example points A. Mid range activity is clearer during the first part of the gait cycle.

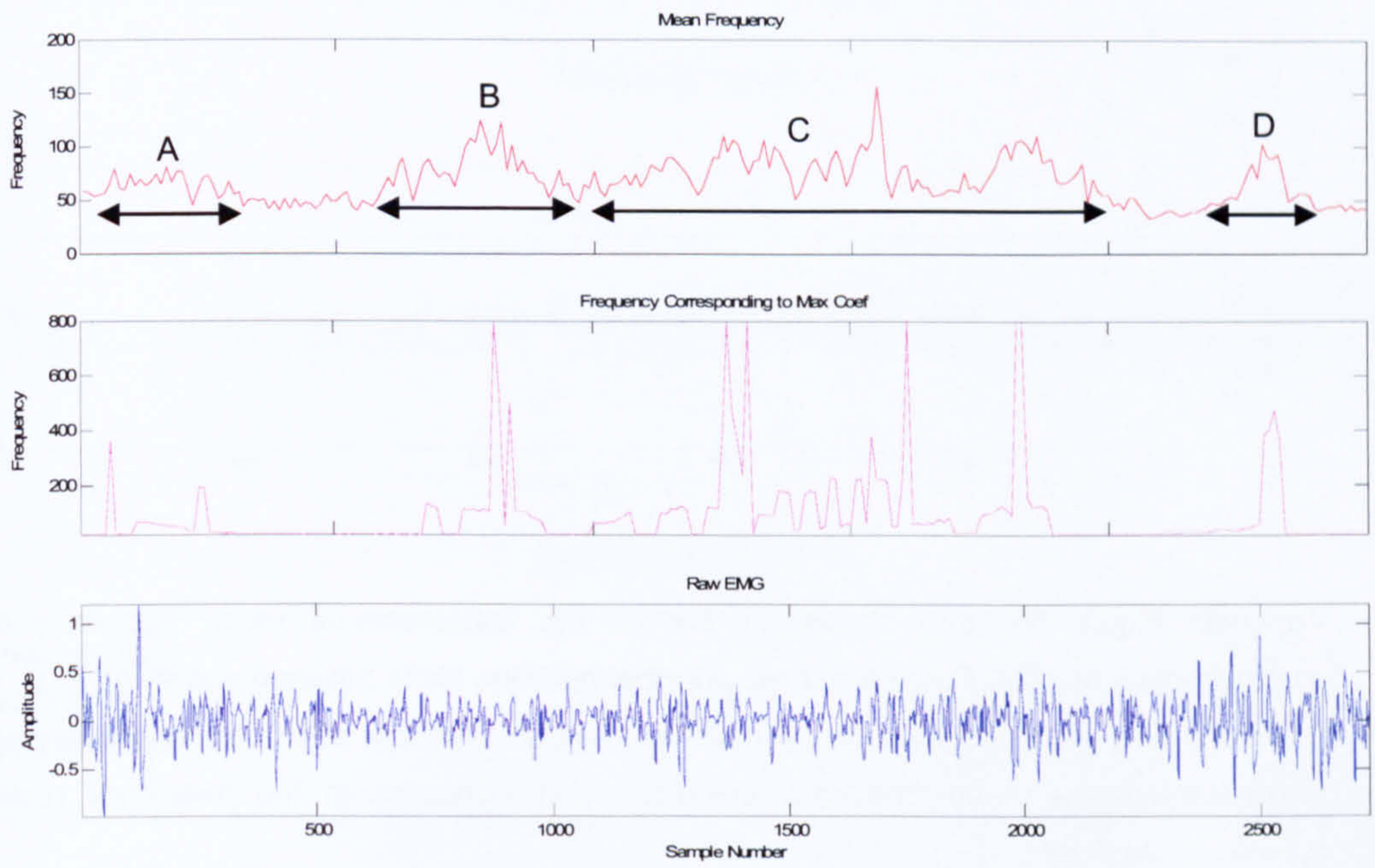

Appendix Figure 55 (top) shows for CVA07 the instantaneous mean frequency of the tibialis anterior muscle. There are three base line shifts between period A, period B and C and period D. Periods A and D are temporally related to subtle bursts of activity seen in the raw sEMG. Period A of the mean instantaneous frequency Figure displays less activity compared to the rest of the graph, equivalently there is little activity seen in the frequency related to maximum coefficient Figure (middle). The base line shifts coincide with increases in the frequency related to maximum coefficient.

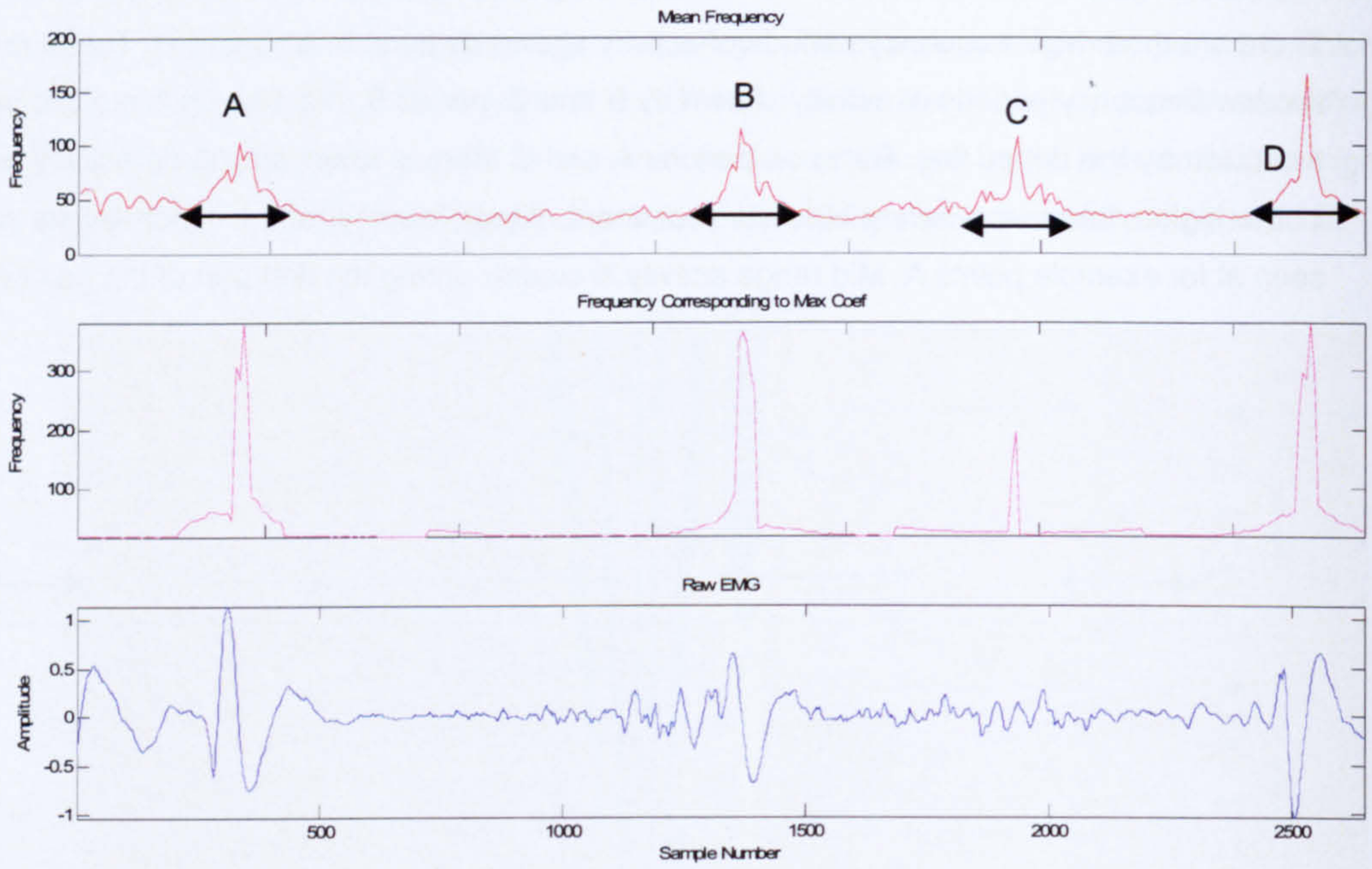

Appendix Figure 56 (top) shows for CVA07 the instantaneous mean frequency of the gastrocnemius muscle. There are three principal baseline shifts between shown by A, B, C and D. Period A, B and D coincide with prominent artefact in the raw sEMG signal. Activity seen in the instantaneous mean frequency coincides with increases in the frequency related to maximum coefficient.

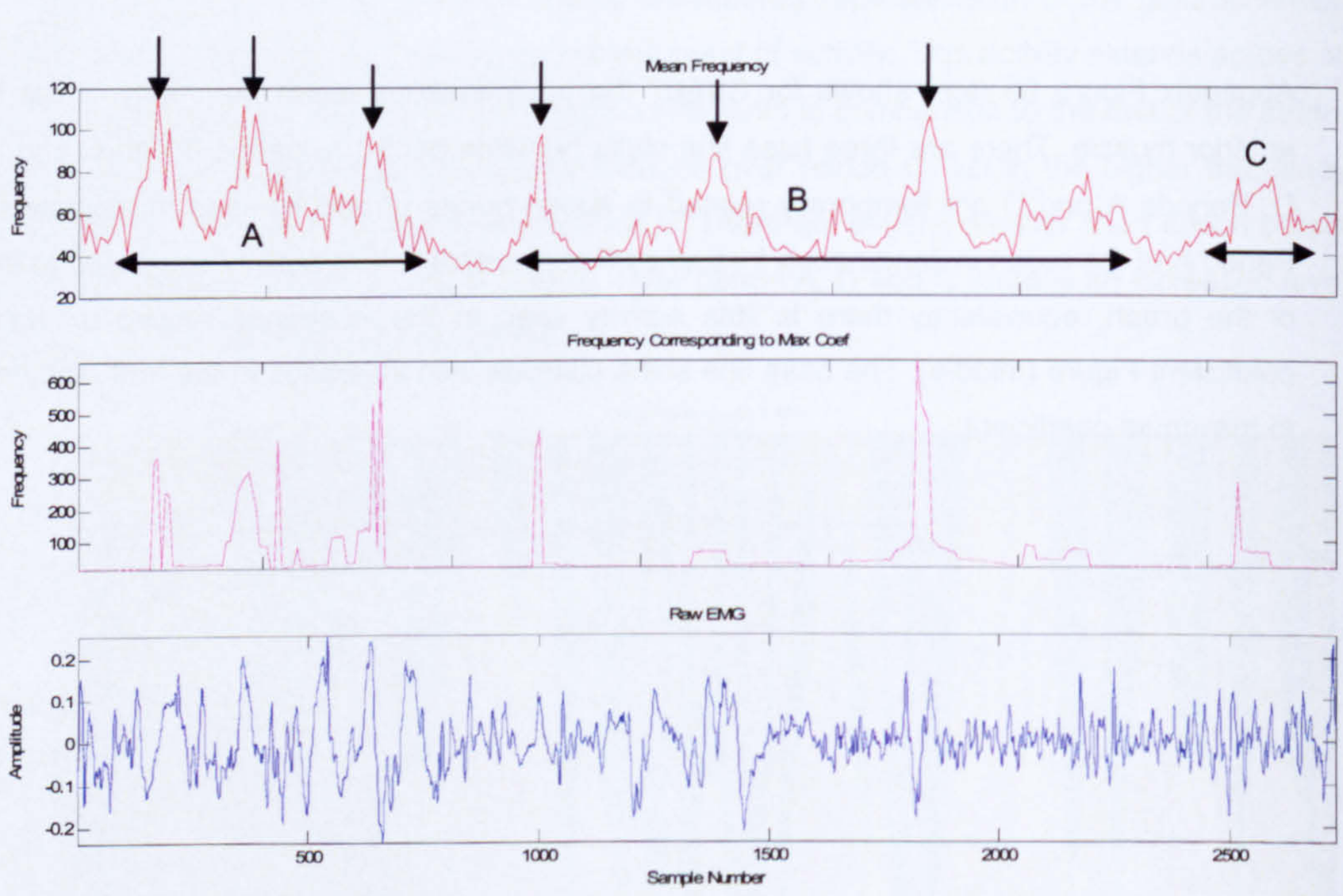

Appendix Figure 57 (top) shows for CVA07 the instantaneous mean frequency of the soleus muscle. A baseline shift can be seen over period A. Subsequently, the mean frequency signal is characterised by periodic peaks, identified by down arrows in the graph, that correspond to peaks of coefficients corresponding to max coefficients. The frequency corresponding to max coefficients (Figure 49 middle) display an increase in the baseline during the first period A. There are then periodic peaks similar to that seen in the mean frequency graph.

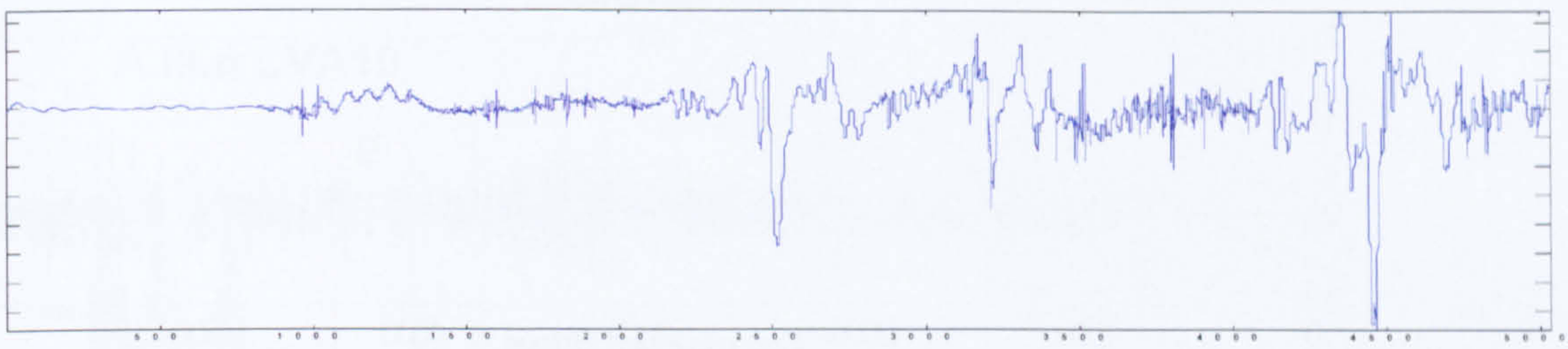

Appendix Figure 58 represent sub-band filtering for the gastrocnemius muscle for three strides from standing in which no clear activity bursts are evident. Raw sEMG is shown in Figure 50 (top). Figure 50 (middle) shows the raw signal decomposed at wavelet level 7 and Figure 50 (bottom) shows the raw signal decomposed to wavelet level 8. In Figure 50 (bottom) three periods of activity are evident in the signal decomposition at wavelet level 8. These periods are denoted on the on the figure.

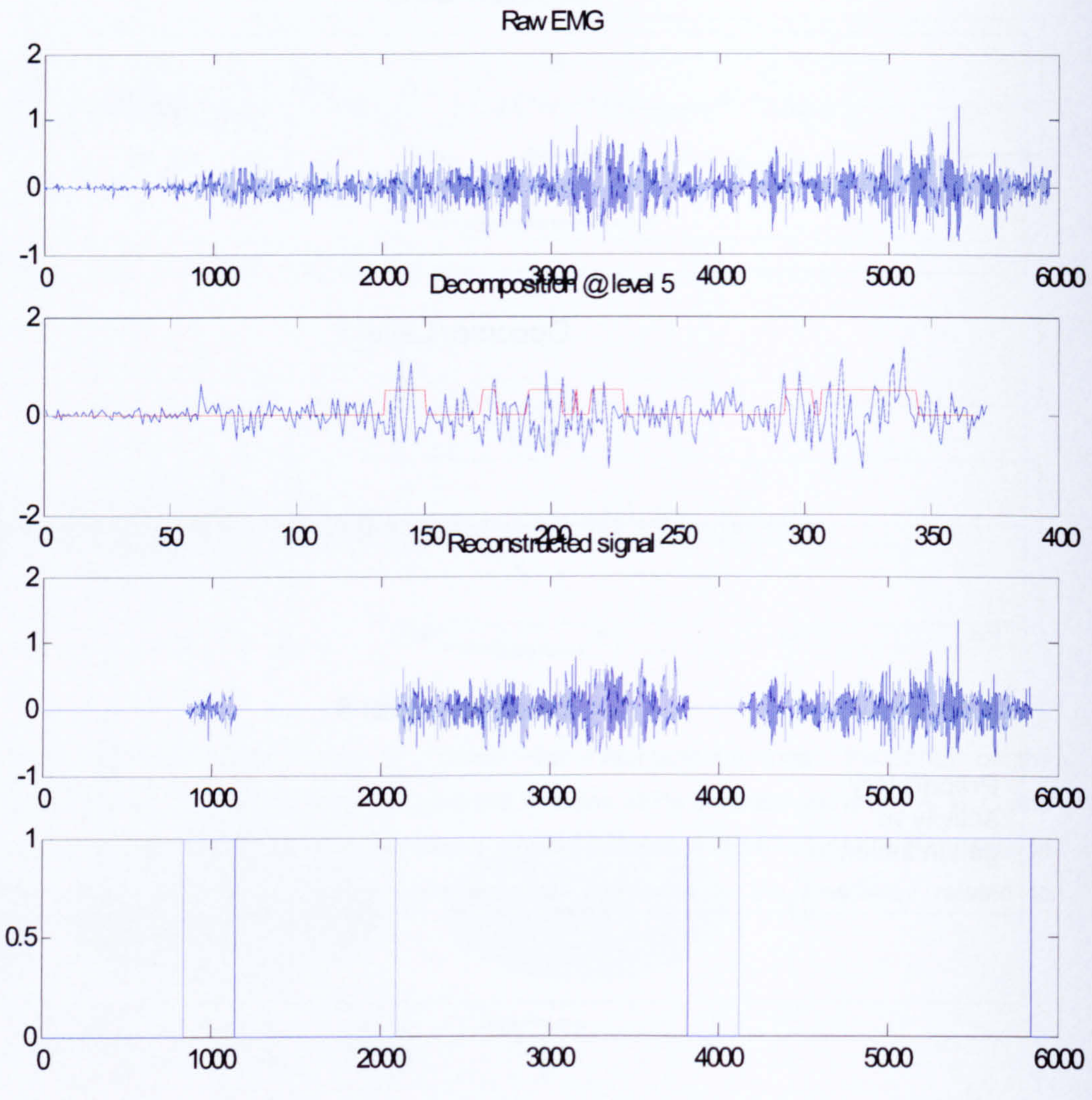

Appendix Figure 59 shows the steps of a signal decomposition for the tibialis anterior muscle for three strides from standing. The beginning of the Figure 51 (top) shows the level of background sEMG activity which indicates increased activity throughout the three strides. Figure 51 (upper middle) shows the raw signal decomposed at level 5 (scale 2^5) the red line displays areas predicted to be burst and inter-bursts periods of the sEMG signal at level 5. Figure 51 (lower middle) shows the result of the combined sub-band filtering across all scales. Figure 51 (bottom) shows the result of the sub-band filtering in terms of burst and inter-burst periods. These graphs display that burst activity can be identified from arguably continuous activity.

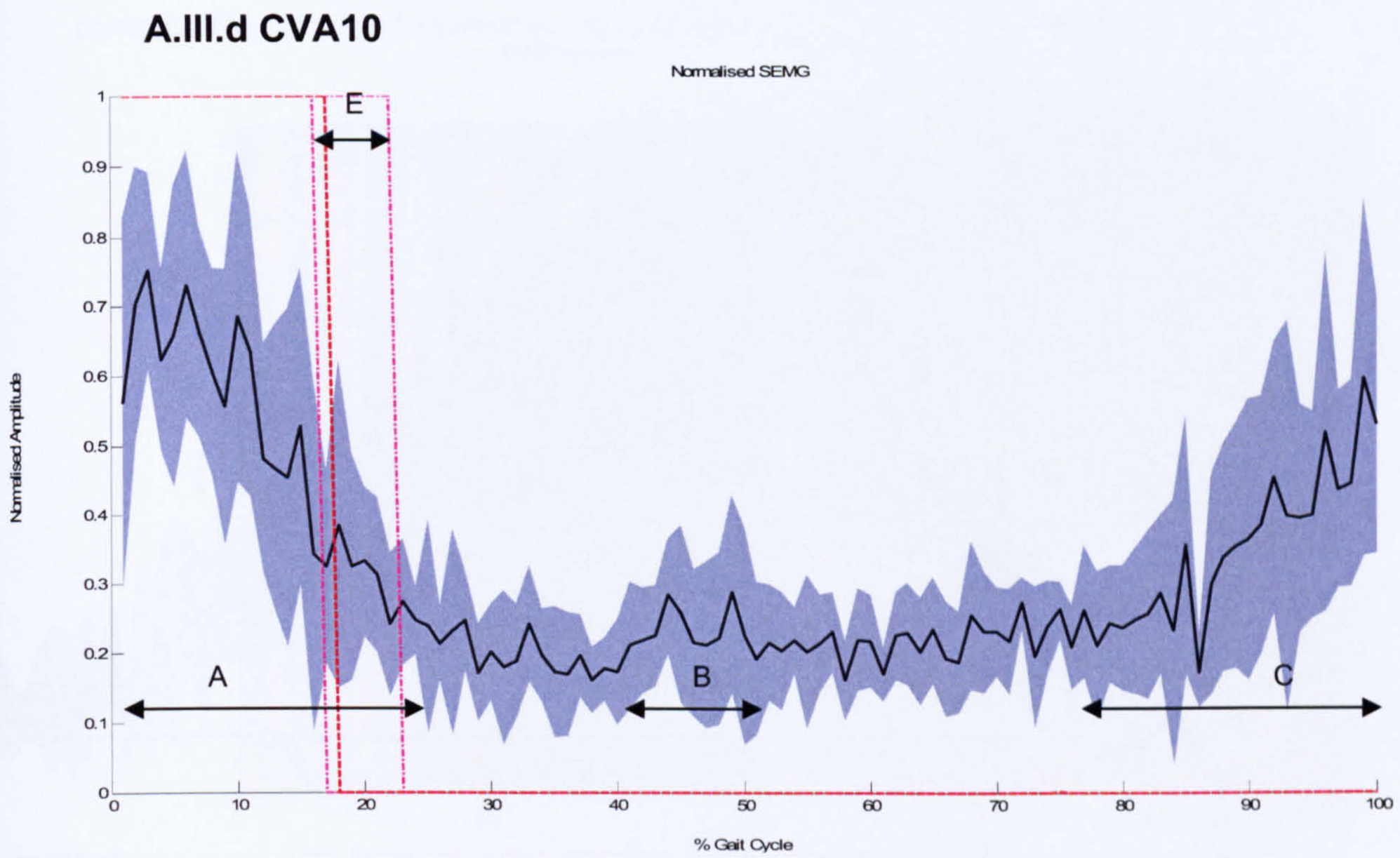

Appendix Figure 60 shows for CVA10 the mean linear envelope and standard deviation of the tibialis anterior. Minimum and maximum foot switch information are displayed by the two broken mauve lines and the mean footswitch value is given by the broken red line. The gait cycle variation can be seen between maximum and minimum foot strike locations shown by E. Tibialis activity is seen to occur between period A and in the final period of the gait cycle, period C. An additional small burst of activity is apparent during the middle part of the gait cycle shown by period B.

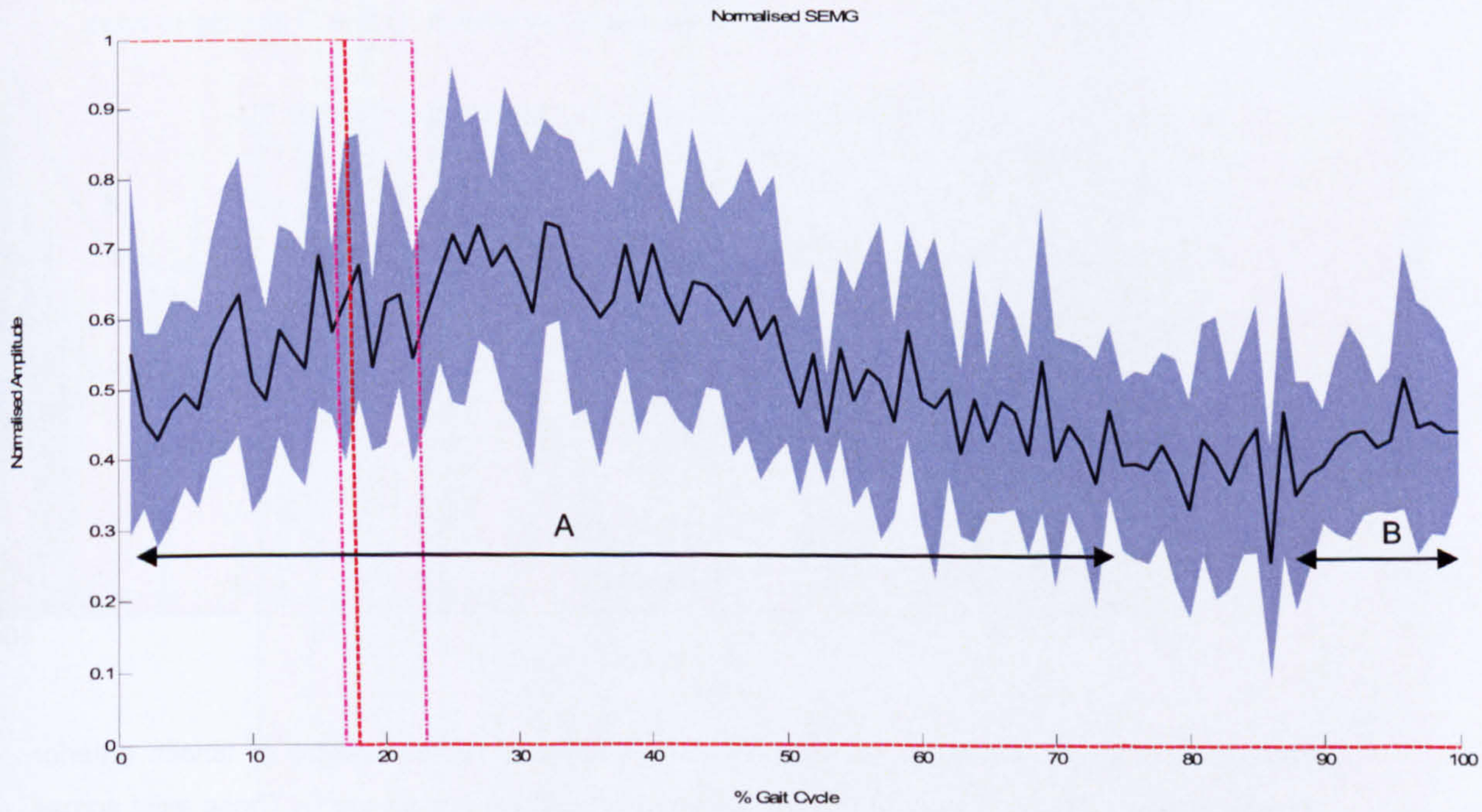

Appendix Figure 61 shows for CVA10 the mean linear envelope and standard deviation of the gastrocnemius muscle activity. Activity can be seen to be slightly more prominent between period A. There appears to be activity ramping up during the swing phase then reducing during

stance phase. There appears to be a small increase in activity during terminal stance shown by period B.

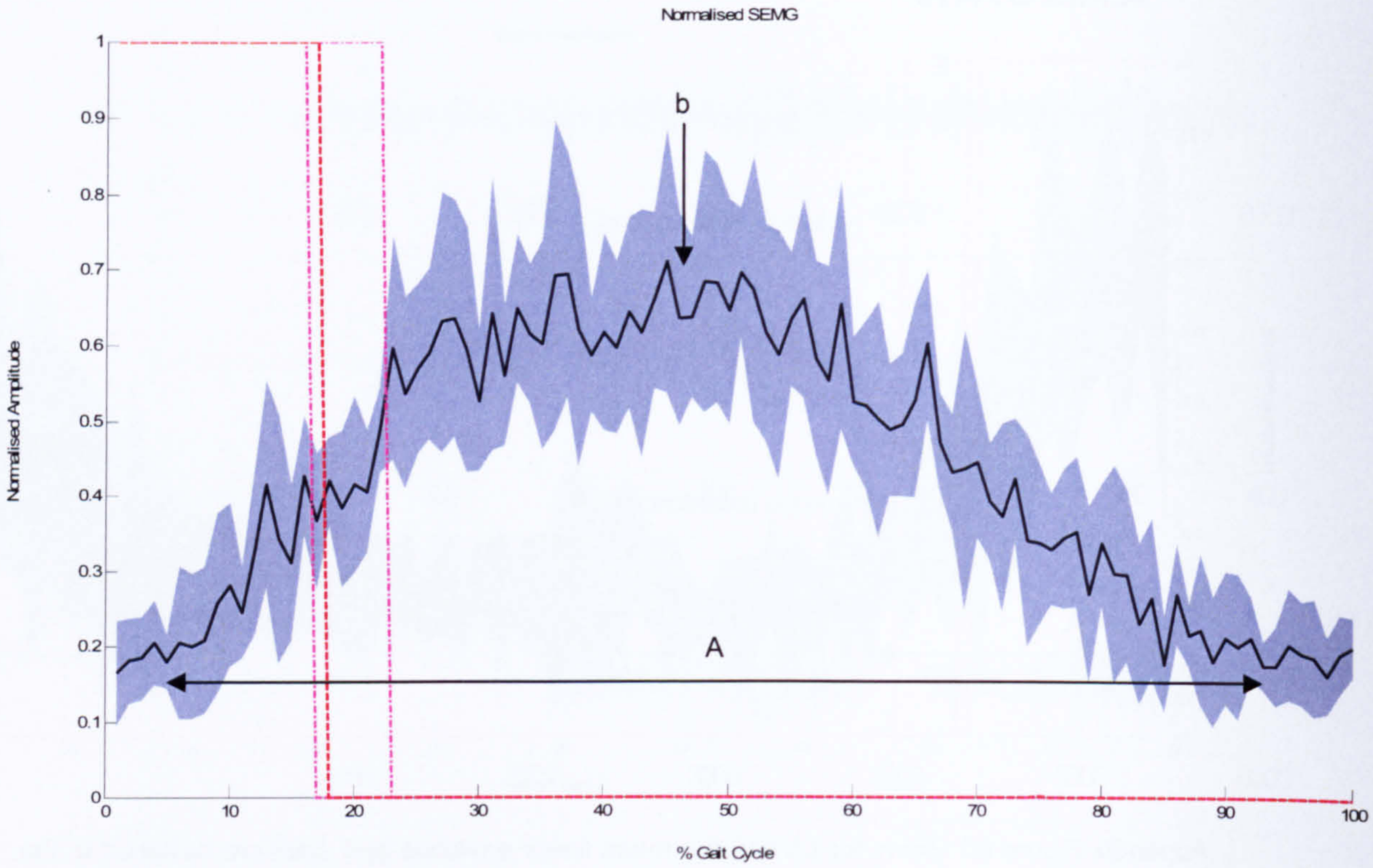

Appendix Figure 62 shows for CVA10 the mean linear envelope and standard deviation of the soleus muscle. Activity is seen to rise from toe off to peak at point b and then reduce until the following toe off. There is activity across the stride and shown by period A.

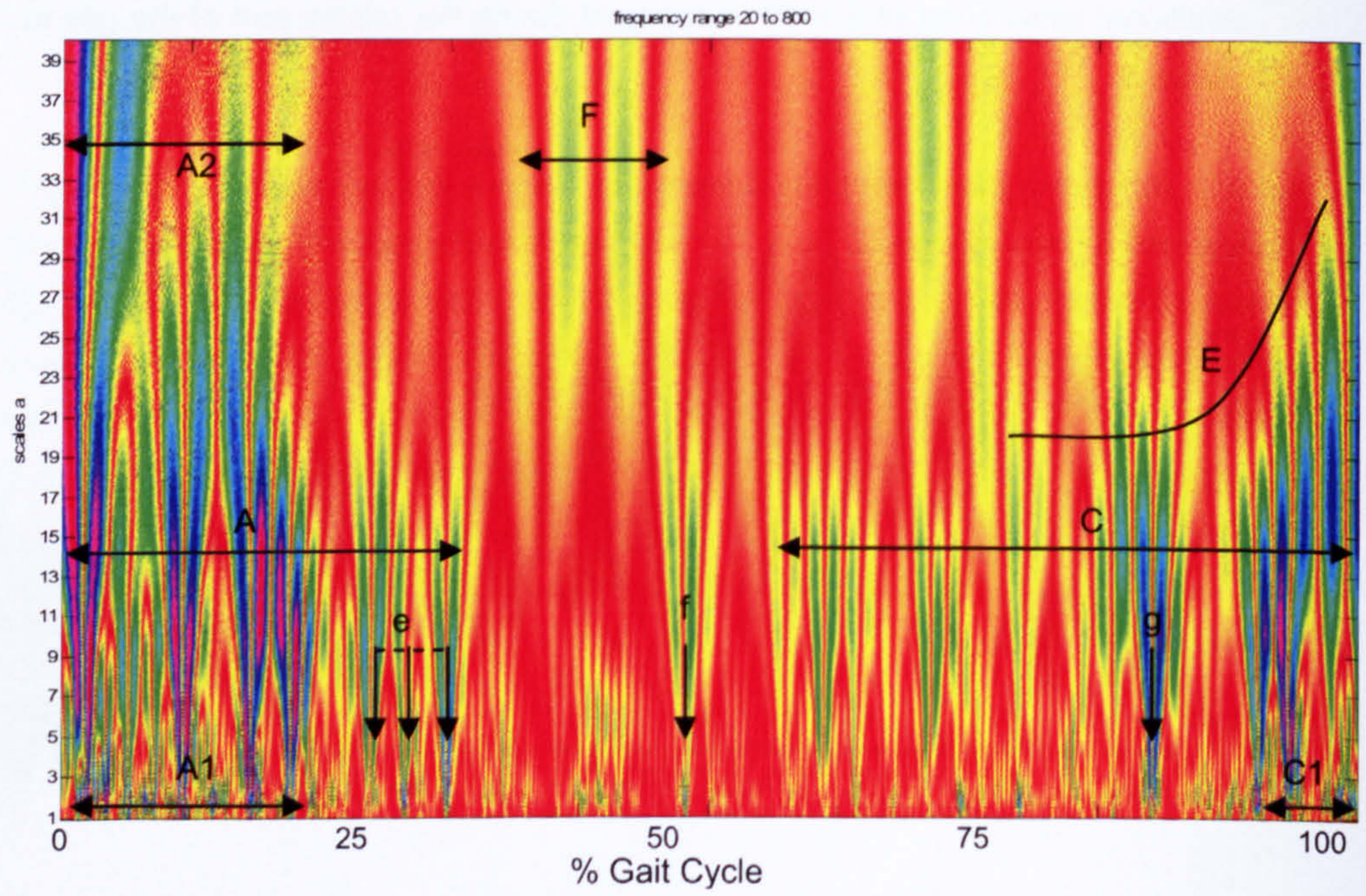

Appendix Figure 63 shows for CVA10 the time-frequency representation of tibialis anterior muscle activity. Two prominent bursts can be seen in period A and period C. These exist across the frequency bins but are maximum in the mid range. Period A1 show the extent of the high frequency activity in the first period and A2 show the lowest frequency during period of A. similarly C1 shows the highest frequency components of period C. E displays the increase in

lower frequency components towards the end of the gait cycle. Points e, f and g show small and short epoch burst of activity in the high frequency region. These small high frequency bursts correspond to mid range frequency activity and appear to characterise the pattern of activation.

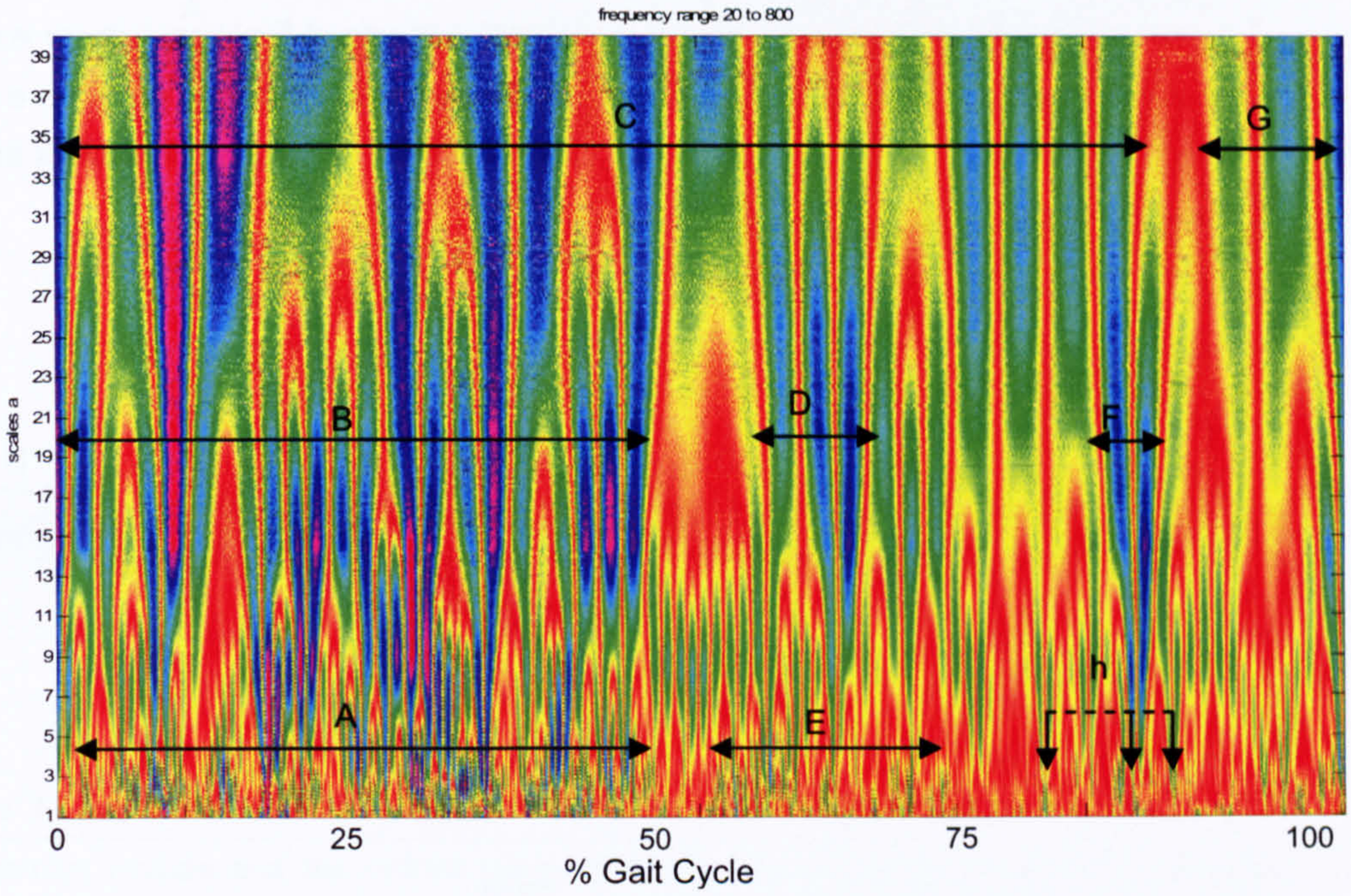

Appendix Figure 64 shows for CVA10 the time-frequency representation of the gastrocnemius muscle activity. Activity can be seen throughout the stride and across all frequency bins. Across the high frequency bins there increased amplitude coefficients over period A and to a lesser extent over period E. Between these two periods a continuous moderate high frequency period of activity exists. The intensity of the high frequency activity reduces across the rest of the gait cycle. Three bursts of mid range activity can be seen during periods B D and F with lower amplitude activity separating them. Two distinguishable periods of low frequency activity can be seen in periods C and G. Examples of short epoch bursts are represented by points h.

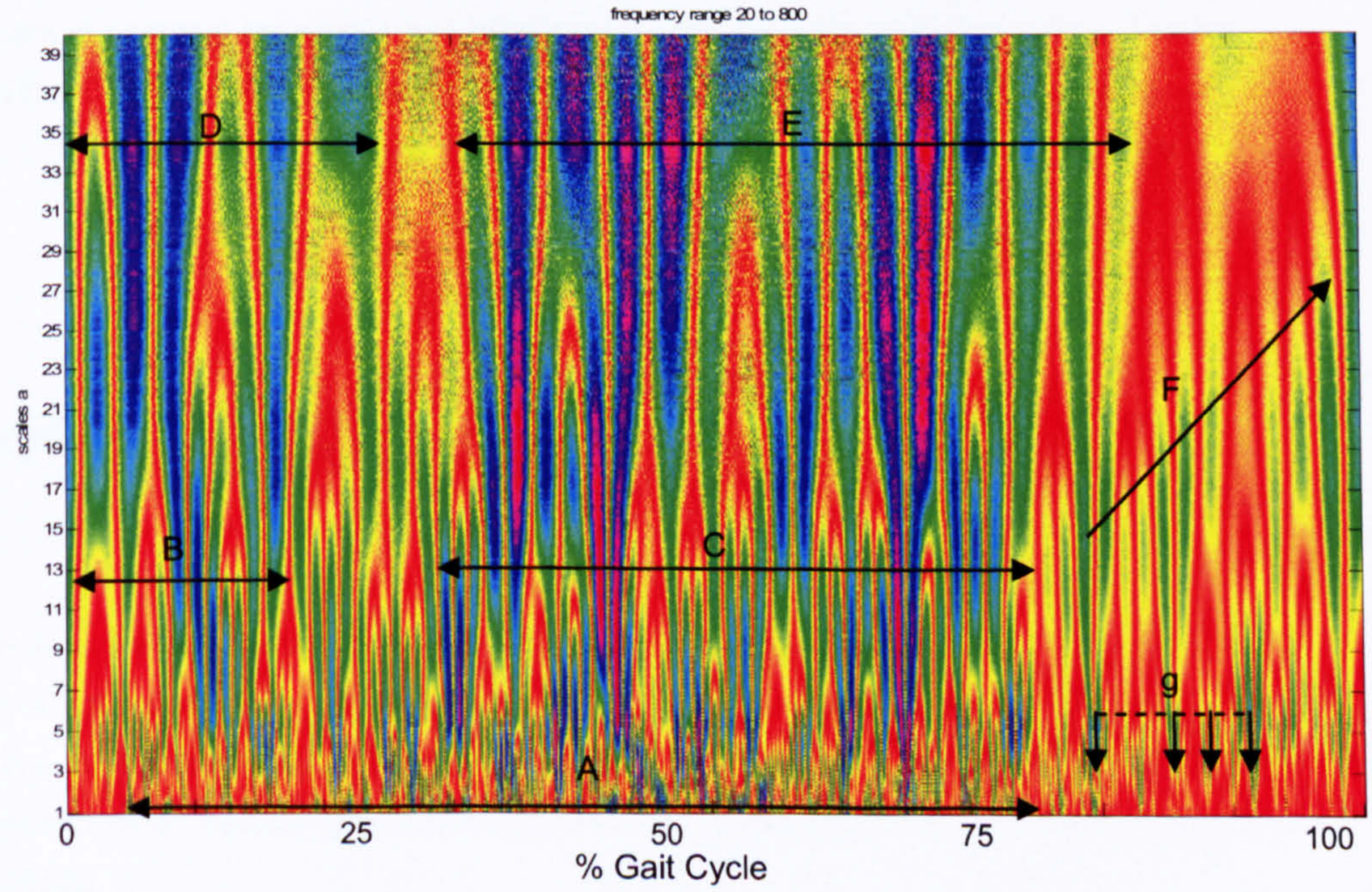

Appendix Figure 65 shows for CVA10 the time-frequency representation of the soleus muscle activity. Although there is activity across the stride, the amplitude of high to moderate high frequency increases during period B and reduces towards the end of period C. Maximum amplitude of coefficients of high frequency bins can be seen during period A. Low frequency activity exists most prominently between period D and period E although there is an argument that this constitutes one burst. Again the characteristic short epochs of activity are seen at g. At this time period F reveals an increase in lower frequency coefficient amplitudes at increasingly lower frequencies.

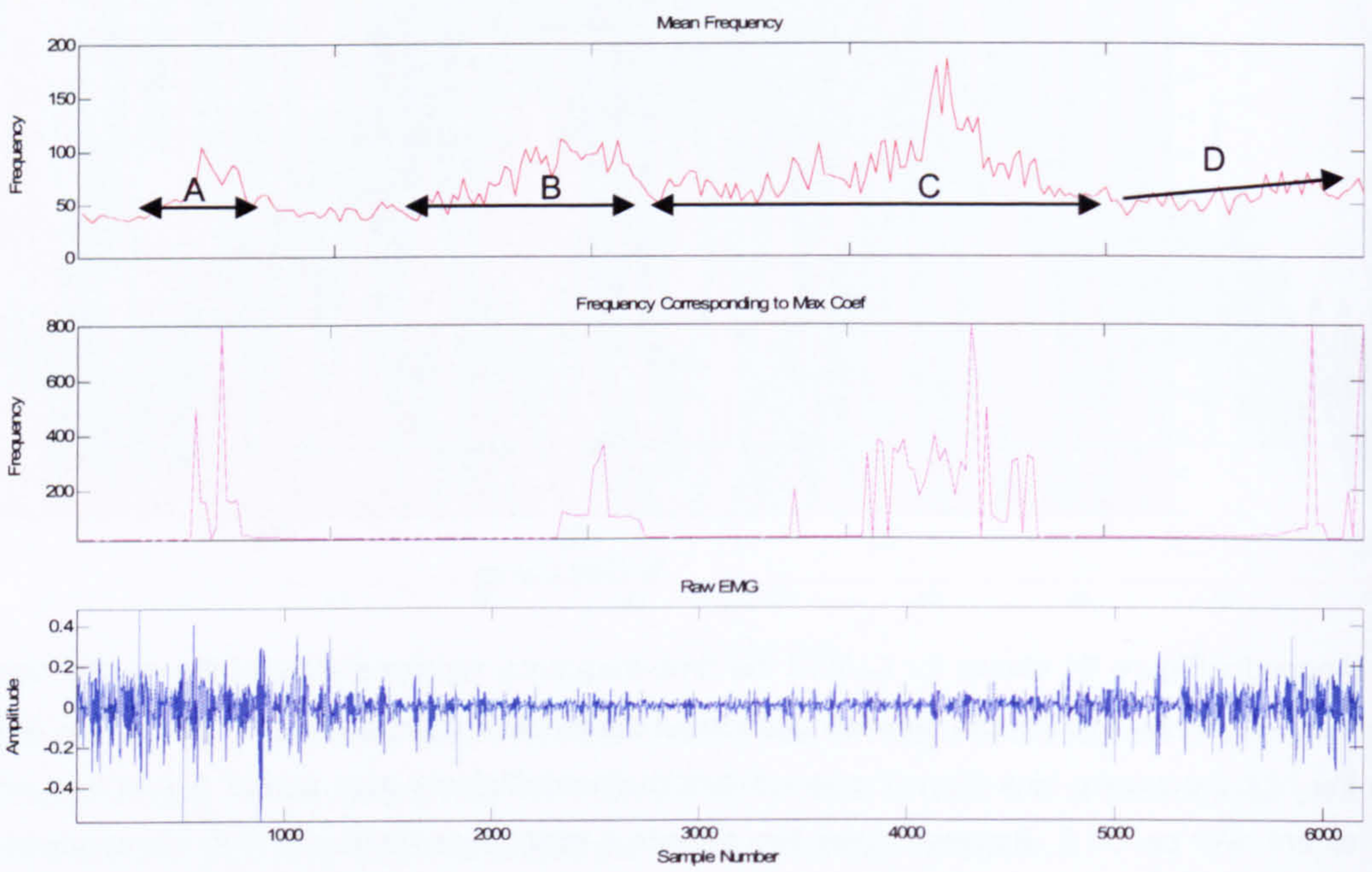

Appendix Figure 66 shows for CVA10 the instantaneous mean frequency of the tibialis anterior muscle. The baseline mean frequency increases over period A, which occurs at the time as the mid point of increased amplitude sEMG. Subsequently the instantaneous mean frequency increases over period B. This is followed by a third and prominent increase in mean frequency over period C. Both B and C relate to a relatively quiescent periods of SMEG activity. Period D shows a gradual increase during stance relating to an increase in sEMG activity

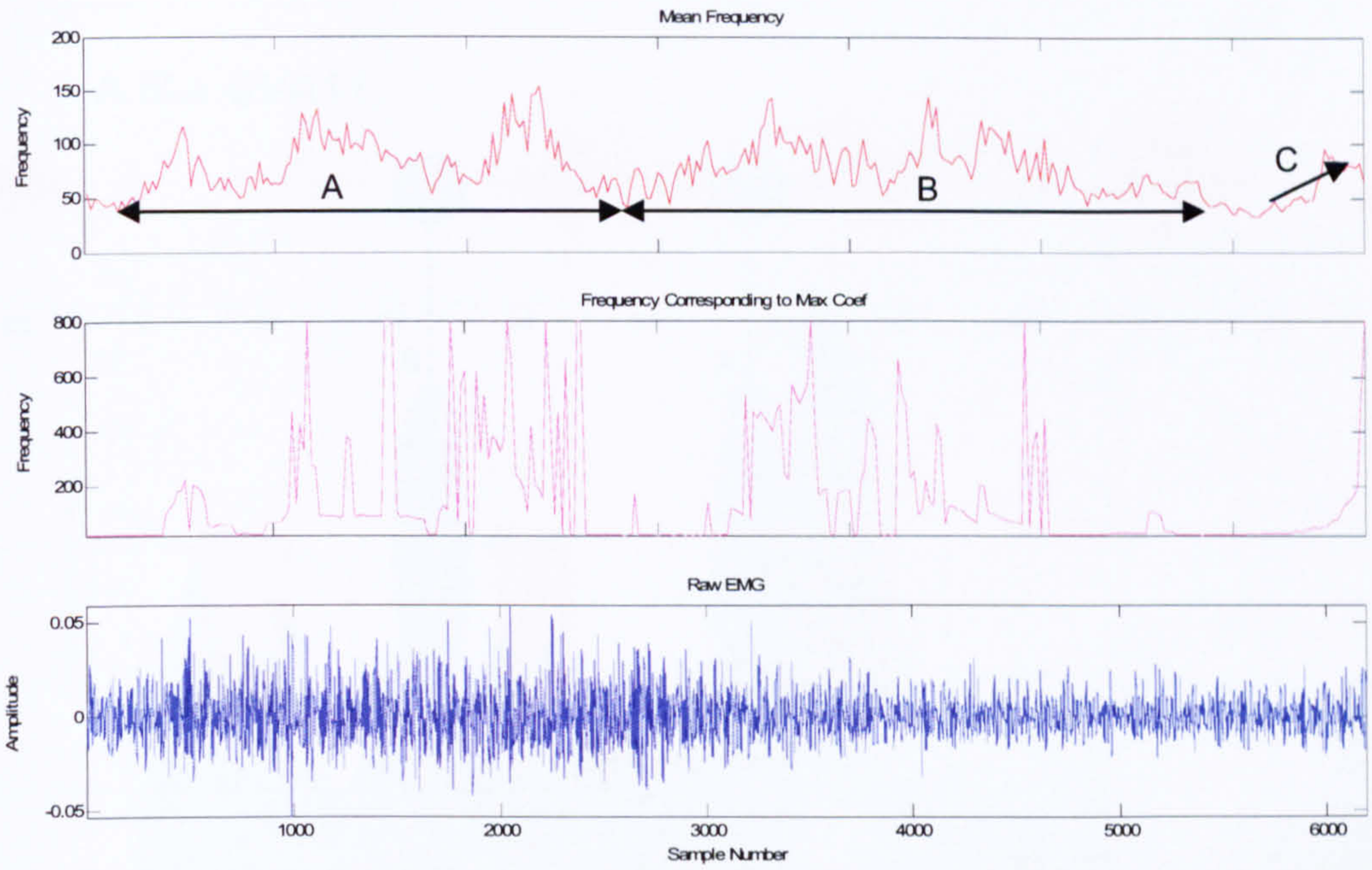

Appendix Figure 67 shows for CVA10 the instantaneous mean frequency activity of the gastrocnemius muscle and the related mean instantaneous frequency. The mean frequency increases over period A. The mean frequency increases again over period B The activity has a pulsatile characteristic increasing and decreasing over the stride. There is a gradual increase again the part of the gait cycle denoted by C. The activity extends over a large proportion of the stride.

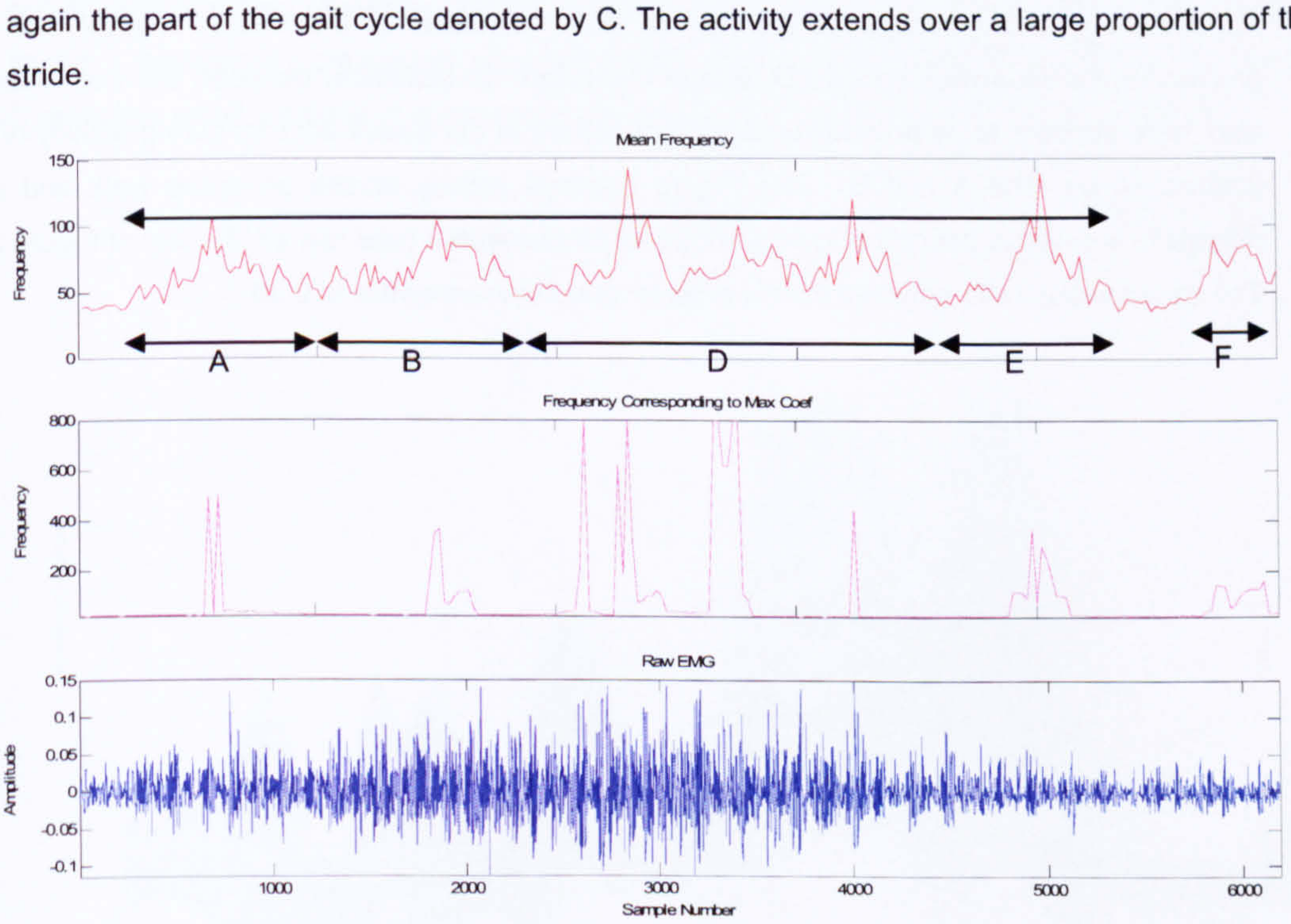

Appendix Figure 68 shows for CVA10 the instantaneous mean frequency for the soleus muscle. There is a extended period of increased mean frequency that can be subdivided into four periods A – E. This activity is consistent to increased amplitude sEMG activity. Period F shows an increase in mean frequency at the end of the stride and relates to a period of quiescence in the raw sEMG.

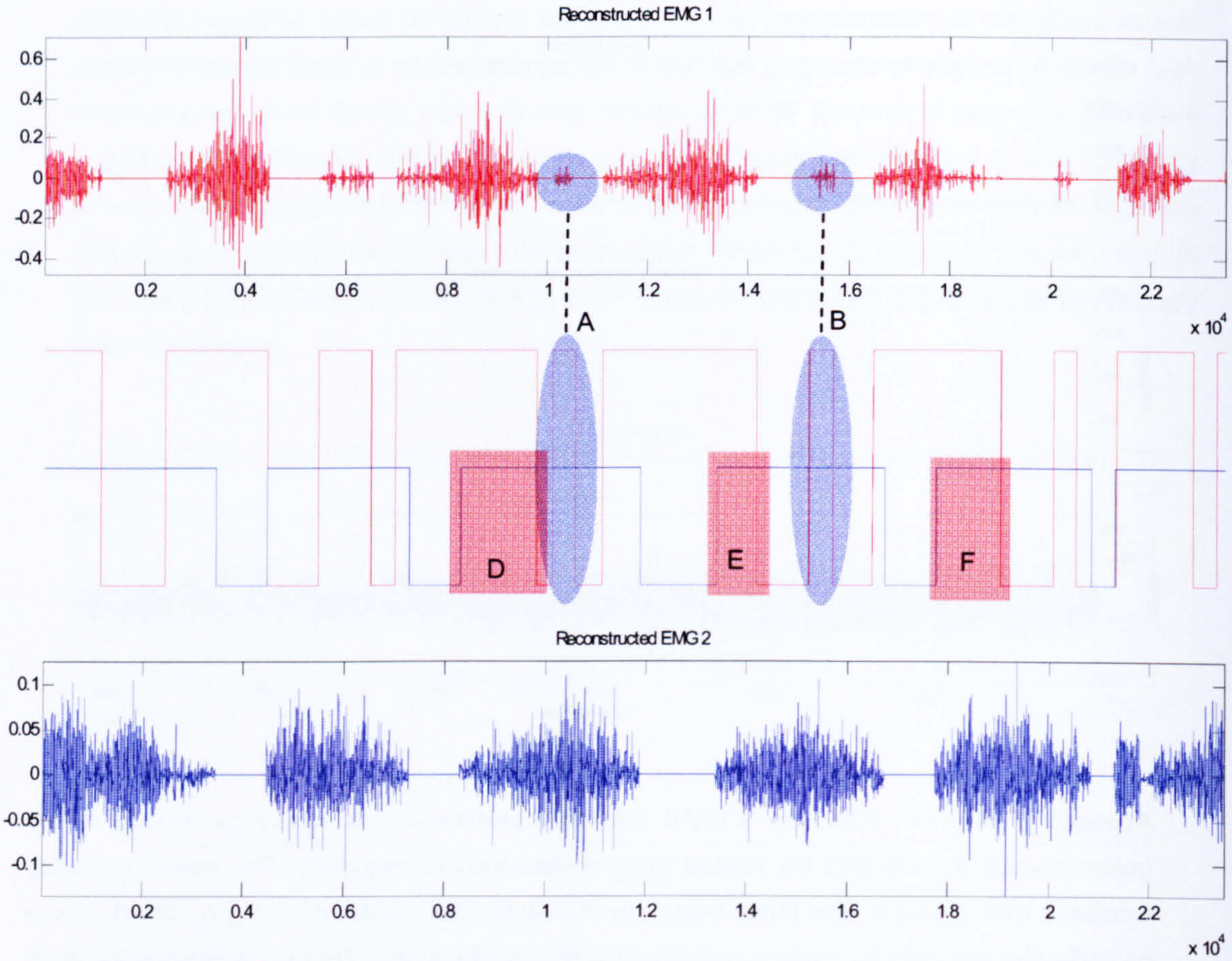

Appendix Figure 69 shows for CVA10 the burst locations of the tibialis anterior and the gastrocnemius muscles. Periods D, E and F indicate co-activation between the two muscles also there appears to be an additional burst of activity of the tibialis anterior during activity of the gastrocnemius (see A and B). This Figure displays activity across an entire walk and also reveals how artificial periods of quiescence can be generated (see raw sEMG plot of Figure 38). The co-activation ratio between tibialis anterior and Gastrocnemius is 0.38.

A.III.e CVA11

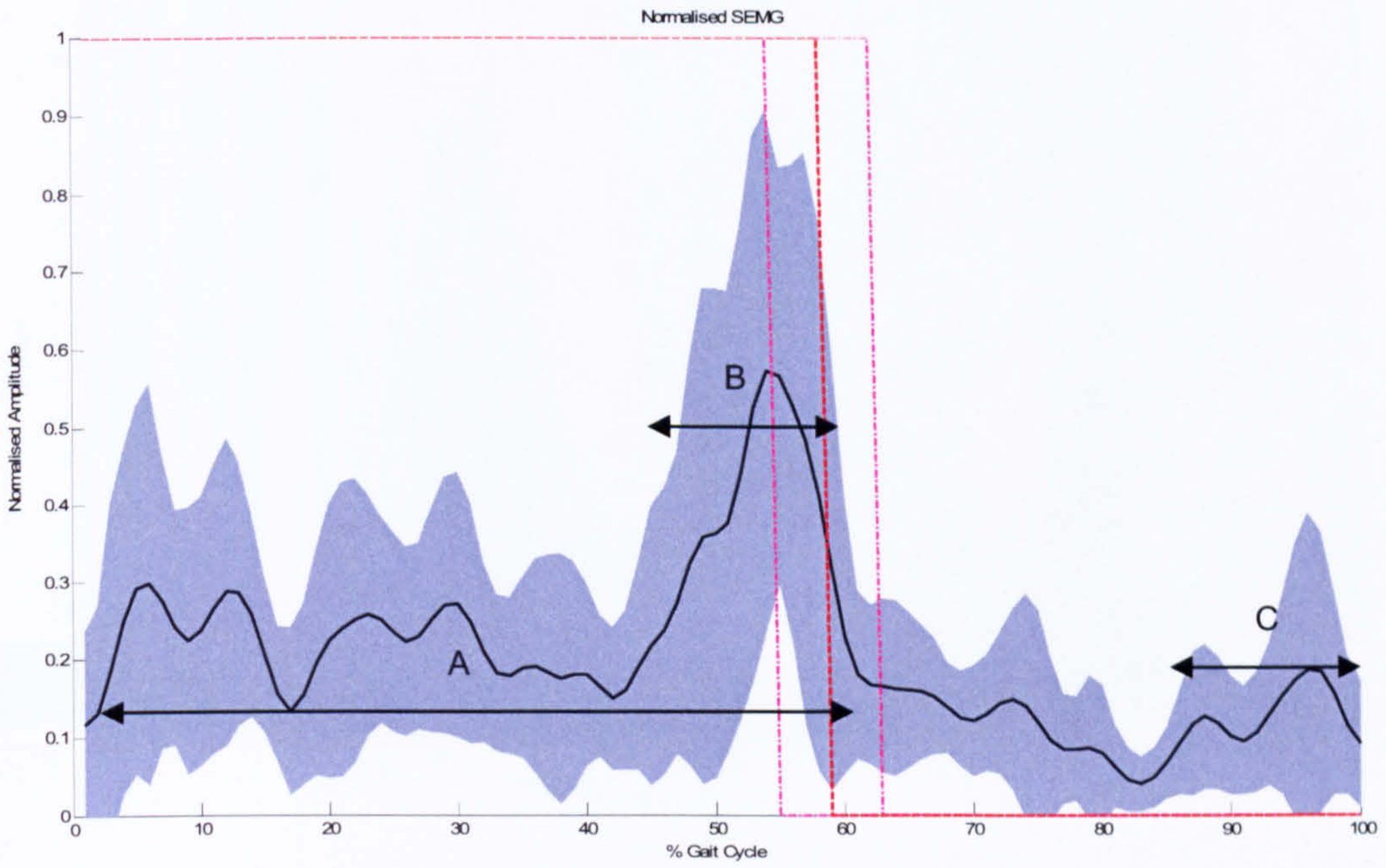

Appendix Figure 70 CVA11 linear envelope representation of the mean tibialis anterior muscle activity and standard deviation. Tibialis anterior activity can be seen during period A. Period B shows a substantial increase just prior to foot-strike after which subsequently diminishes. Period C reveals a small increase in linear envelope amplitude towards the end of the gait cycle.

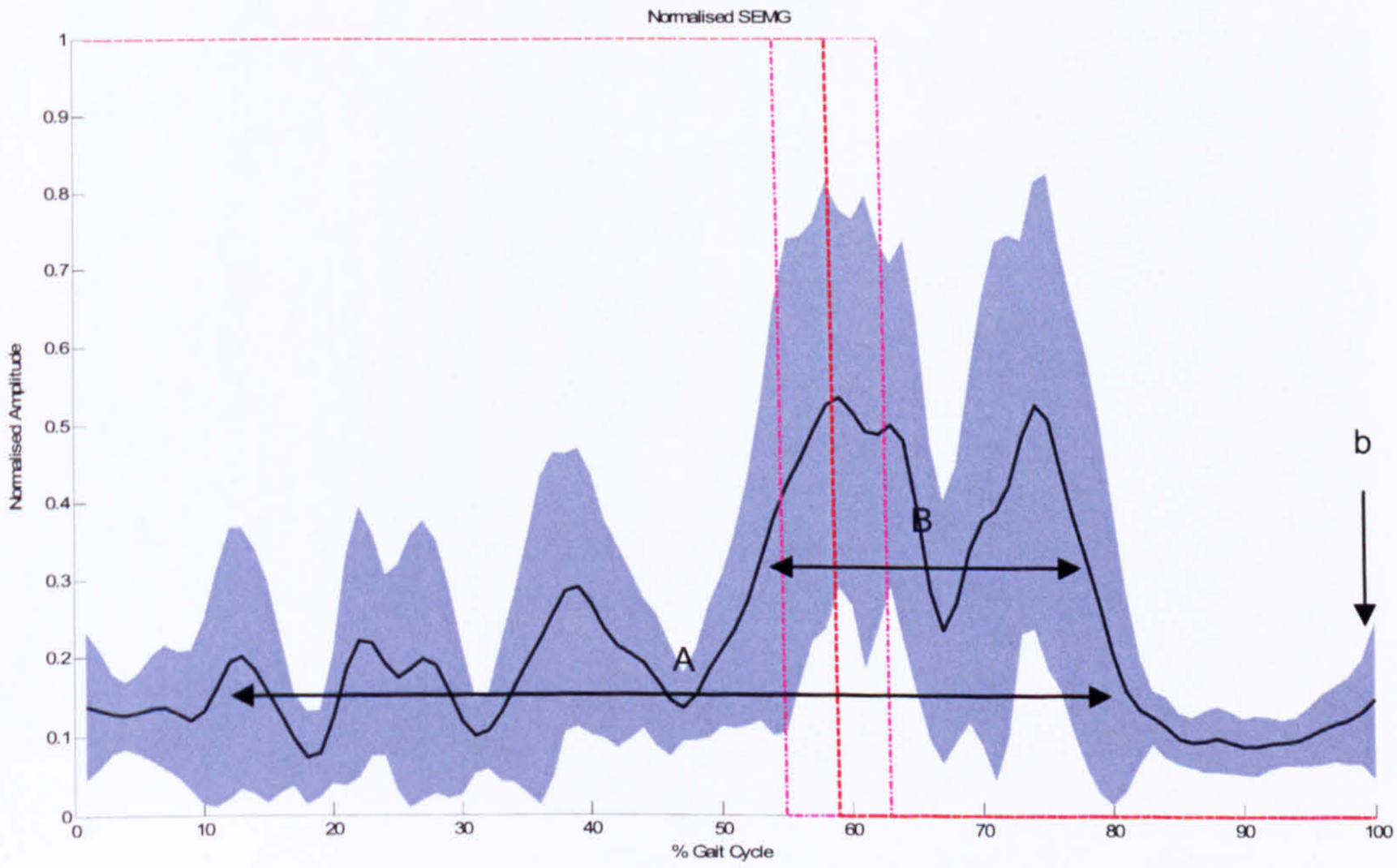

Appendix Figure 71 CVA11 activity form the gastrocnemius muscle. Periodic bursts of activity exist during period A, activity gradually increases from toe-off peaking at foot strike. Two large bursts of activity are sustained through period B where it rapidly diminishes. There is a small increase during terminal stance designated by point b.

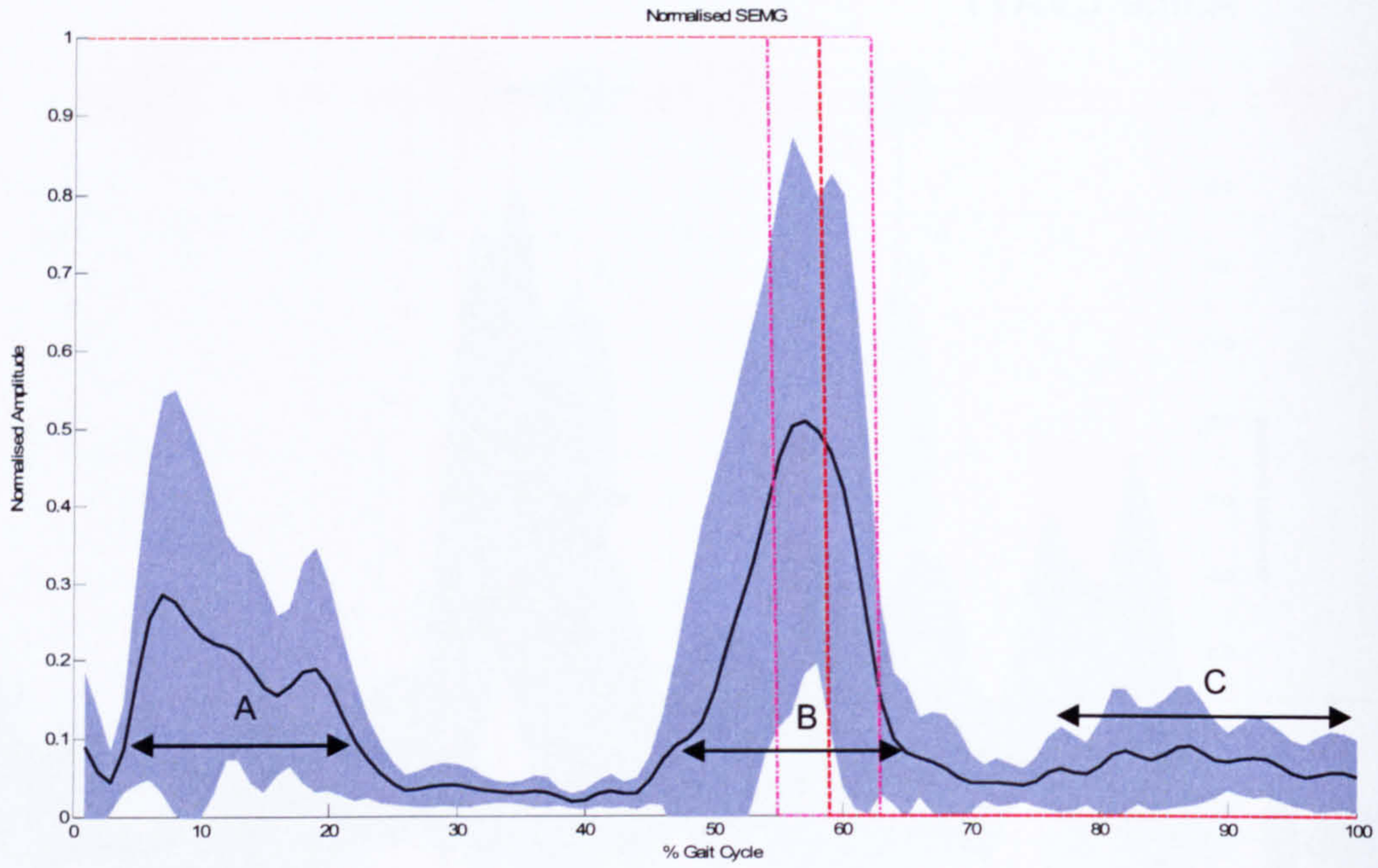

Appendix Figure 72 CVA11 linear envelope activity of the soleus and footswitch data. Activity can be seen in early swing phase were subsequently it diminishes to zero, this is denoted by period A. Activity then increases just prior to foot strike (Period B) and once more diminishes. A small level of activity can be seen in the final period of the stance phase and is shown by period C. The mean foot strike location is shown to be increased from normal.

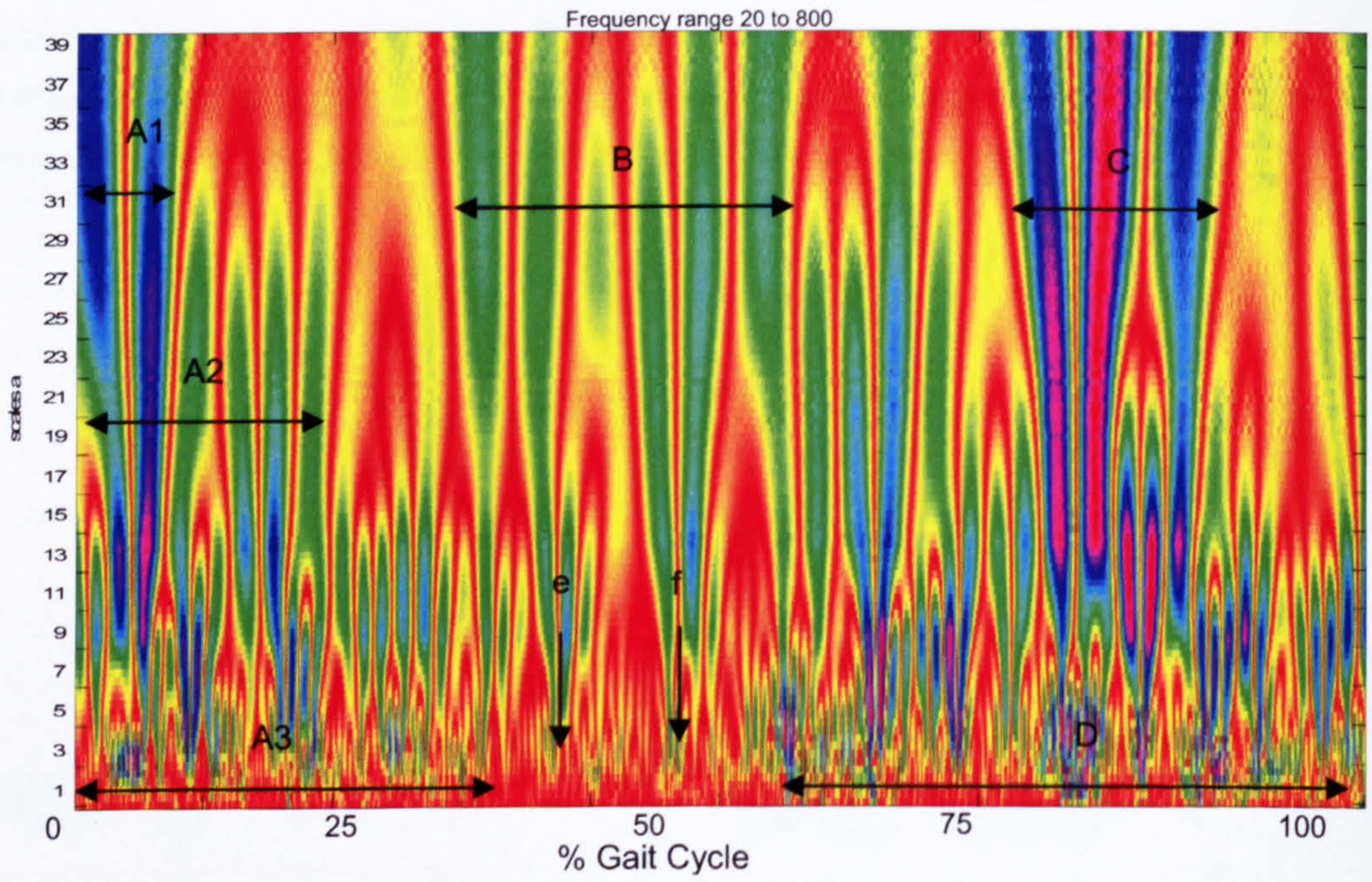

Appendix Figure 73 CVA11 time frequency activity of the tibialis anterior muscle. This reveals sporadic bursts of high frequency activity during period A3 of the gait cycle concurrent with low frequency activity, A2 and A1, this ceases being replaced by lower amplitude coefficients period B and points e and f, when the sporadic high frequency activity returns. During period D the

high and moderate frequency activity is temporally related to a high amplitude low frequency burst, C. The high frequency activity is more prominent in the stance phase (period D).

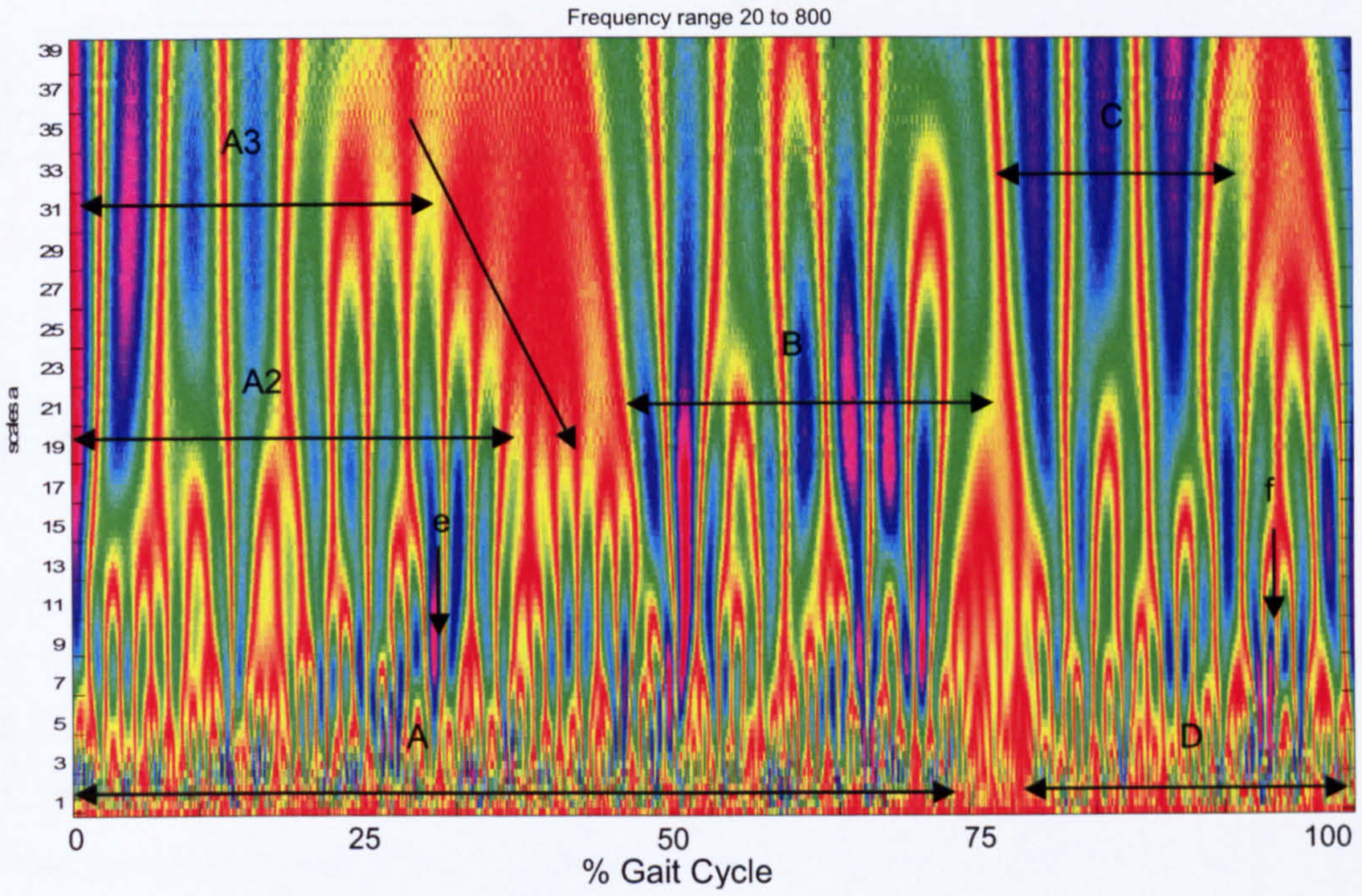

Appendix Figure 74 CVA11 time frequency activity for the gastrocnemius muscle. There is activity throughout the higher frequencies ceasing momentarily shown by periods A and D. Three bursts of low frequency activity can be seen in early swing either side of foot strike and in the stance phase, these are shown by periods A2/A3, B and C. At points e and f there are bursts of moderate to high frequency activity present which are not concurrent with a large low frequency burst.

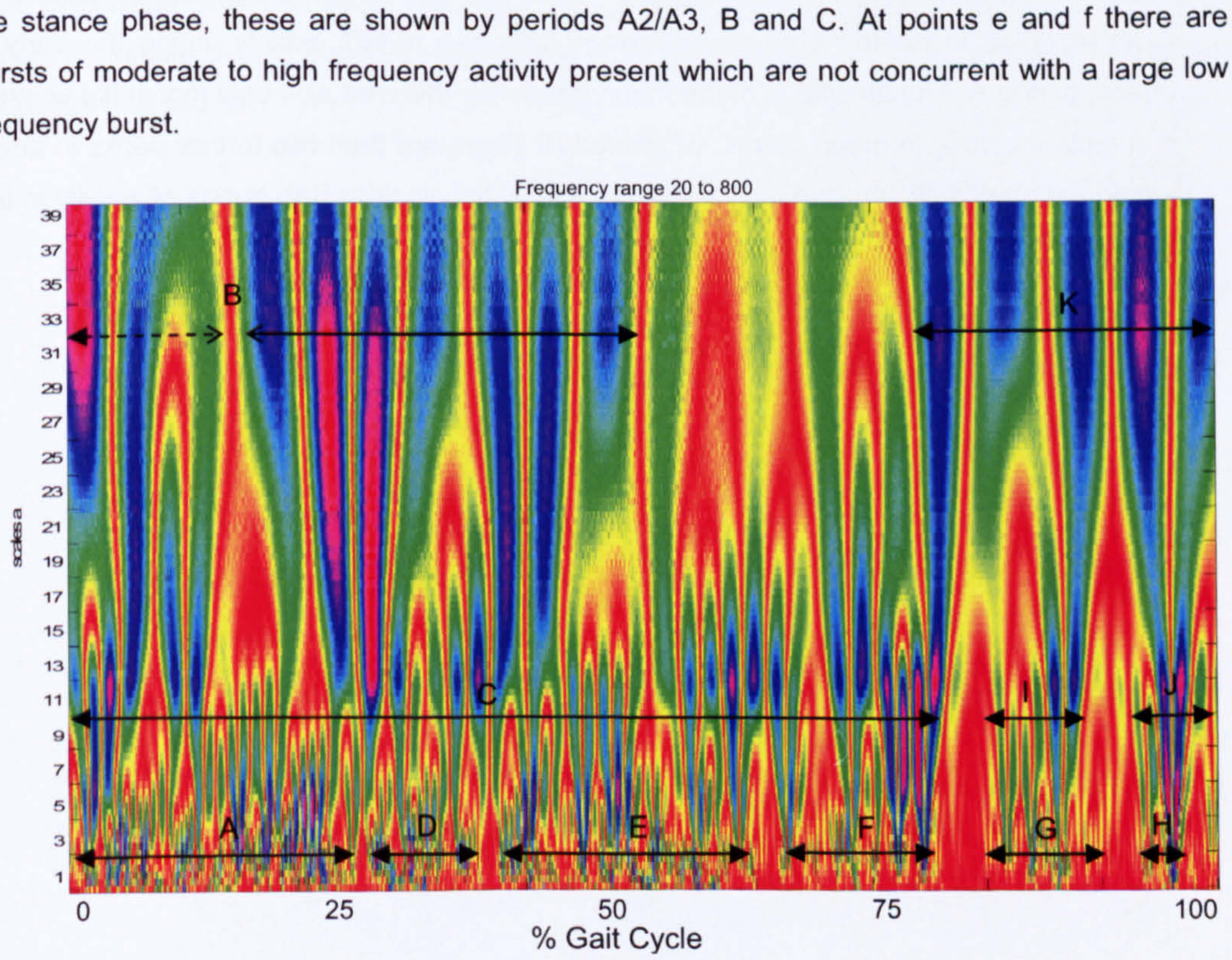

Appendix Figure 75 CVA11 time frequency activity for the soleus muscle. There is activity throughout all frequency bins and across the stride. The largest coefficients occur at the lower frequencies during period B (which might be viewed as two separate periods) and during period K (The intervening period also displays some lower level activity). Moderate to high frequency

activity may be viewed as three prominent periods of activity; C I and J. The high frequency activity is constructed of several bursts (periods A, D, E, F, G and H)

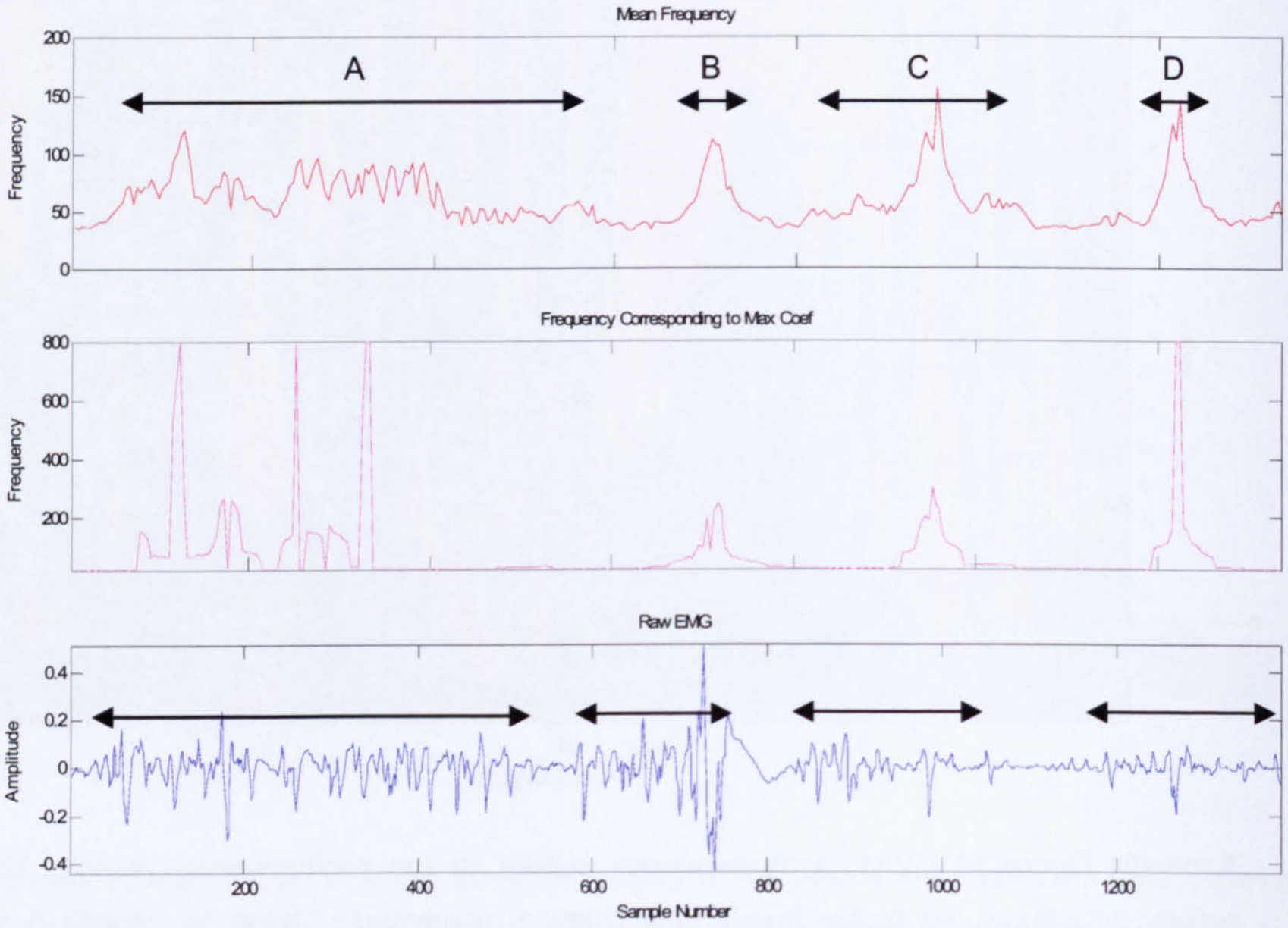

Appendix Figure 76 CVA11 instantaneous mean frequency of the tibialis anterior muscle. There is an increase in mean frequency consistent with raw sEMG activity during the early swing phase, period A. The amplitude of the mean frequency then reduces until foot strike where there is a rapid increase in mean frequency, period B. There are then two further peaks in amplitude during the stance phase, period C and D. This activity coincides with bursts of activity in the raw sEMG.

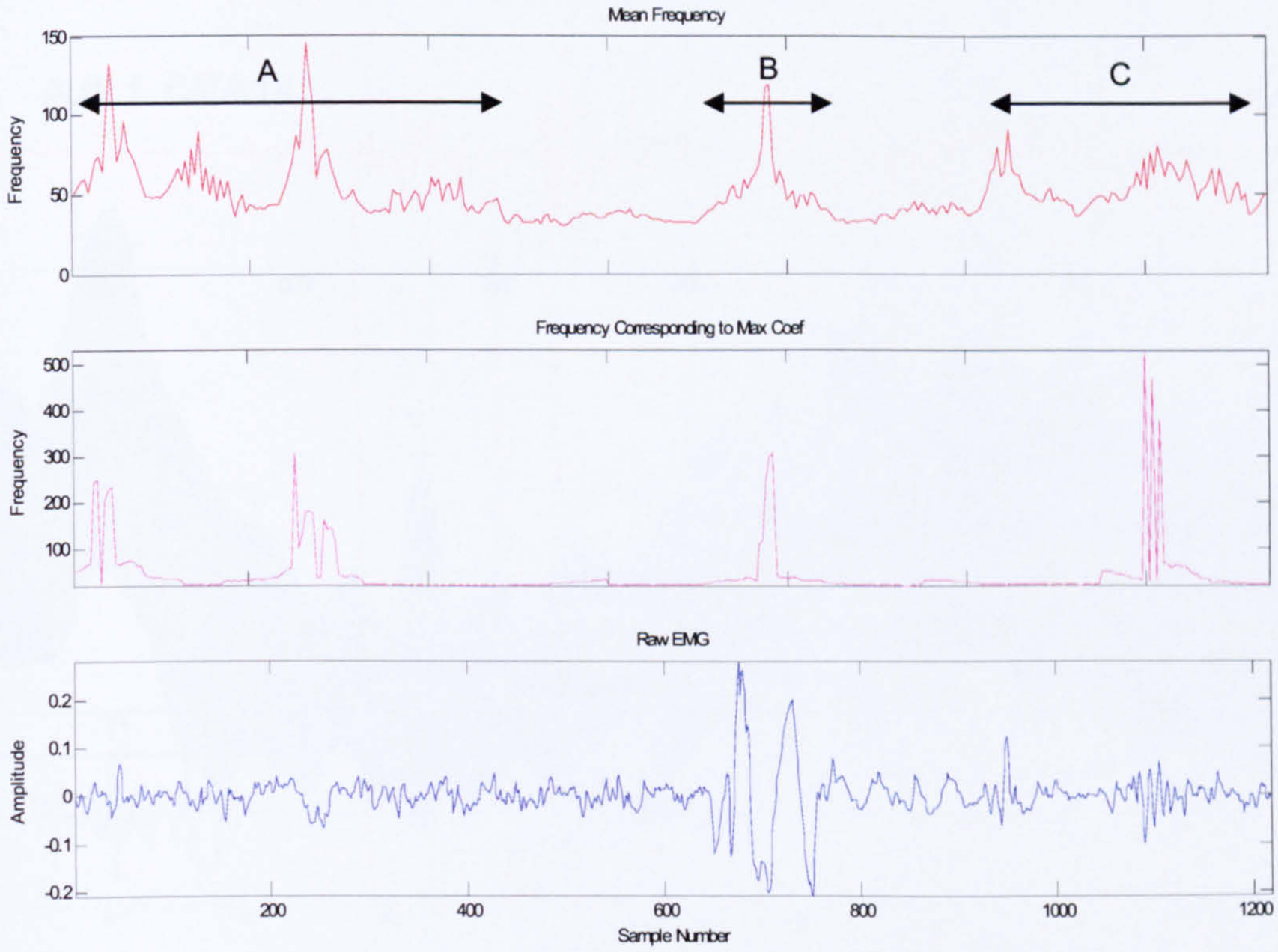

Appendix Figure 77 CVA11 instantaneous mean frequency of the gastrocnemius muscle. There is an increase in mean frequency during the swing phase denoted by period A. The amplitude then diminishes until foot strike where there is a prominent increase in amplitude shown by period B. Finally during period C there is an increase in amplitude of mean frequency that continues until toe off.

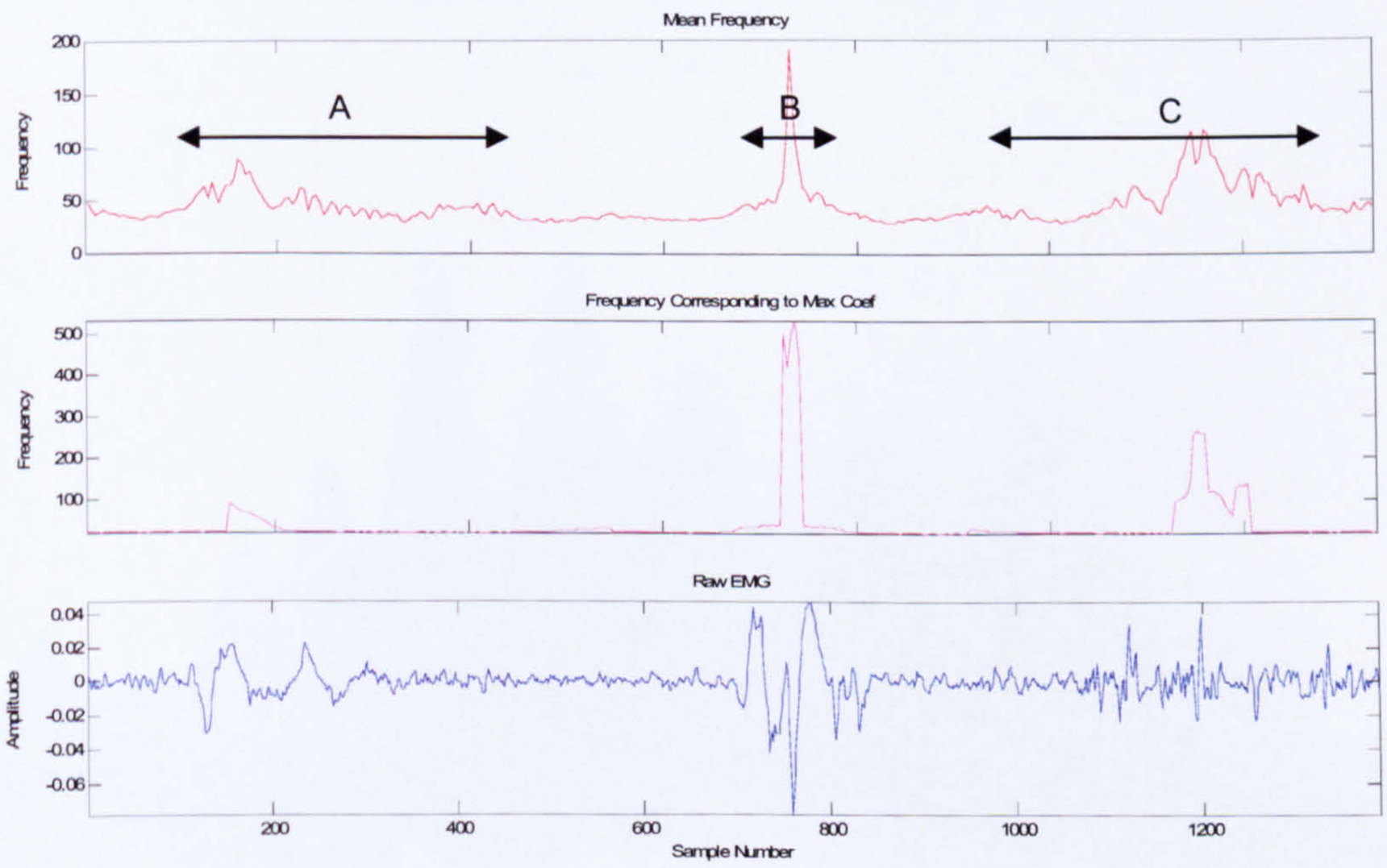

Appendix Figure 78 CVA11 instantaneous mean frequency of the soleus muscle. The signal is characterised by three peaks of mean frequency. The first occurs in early stance, period A, the second high amplitude peak occurs at foot strike, period B. Finally the third peak of activity occurs in the final 25% of the gait cycle prior to toe-off period C.

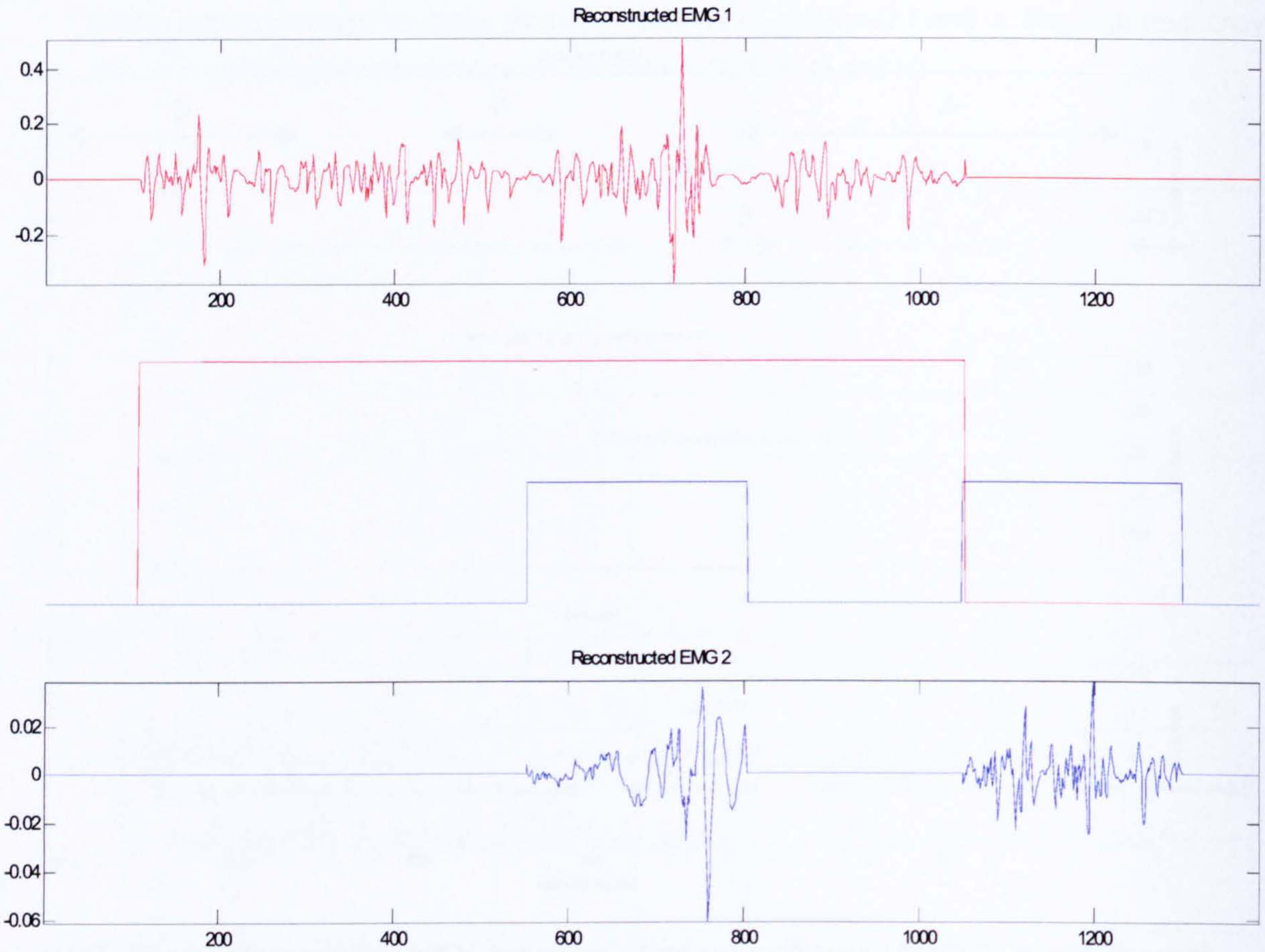

Appendix Figure 79 CVA11 burst locations of both tibialis anterior and gastrocnemius. Burst locations for the tibialis anterior are well defined. Gastrocnemius burst locations are less well defined. The burst locations of the gastrocnemius appear overlapping the tibialis anterior bursts. The co-activation ratio for these muscles is 0.21. The technique does not identify activity in the swing phase of the gait cycle visible in the raw sEMG signal.

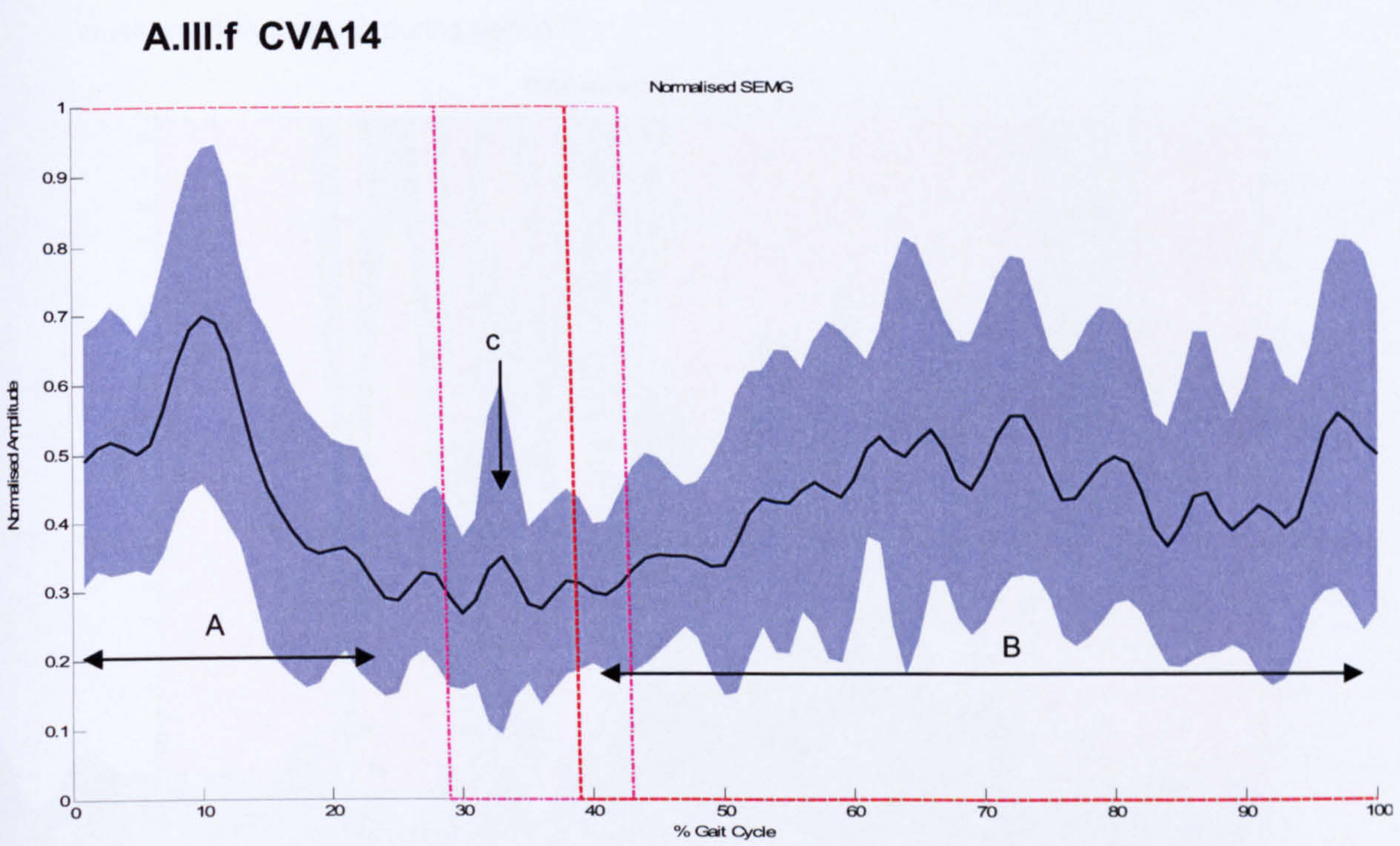

Appendix Figure 80 shows for CVA14 the linear envelope representation of the tibialis anterior muscle with mean amplitude and standard deviation. Activity can be seen during the swing phase with a prominent burst in period A and a smaller burst represented by point c. During the stance phase there is an increase in the linear envelope amplitude that is sustained until toe-off and represented by period B. The red dashed line displays the mean footswitch activity and shows the swing phase is reduced.

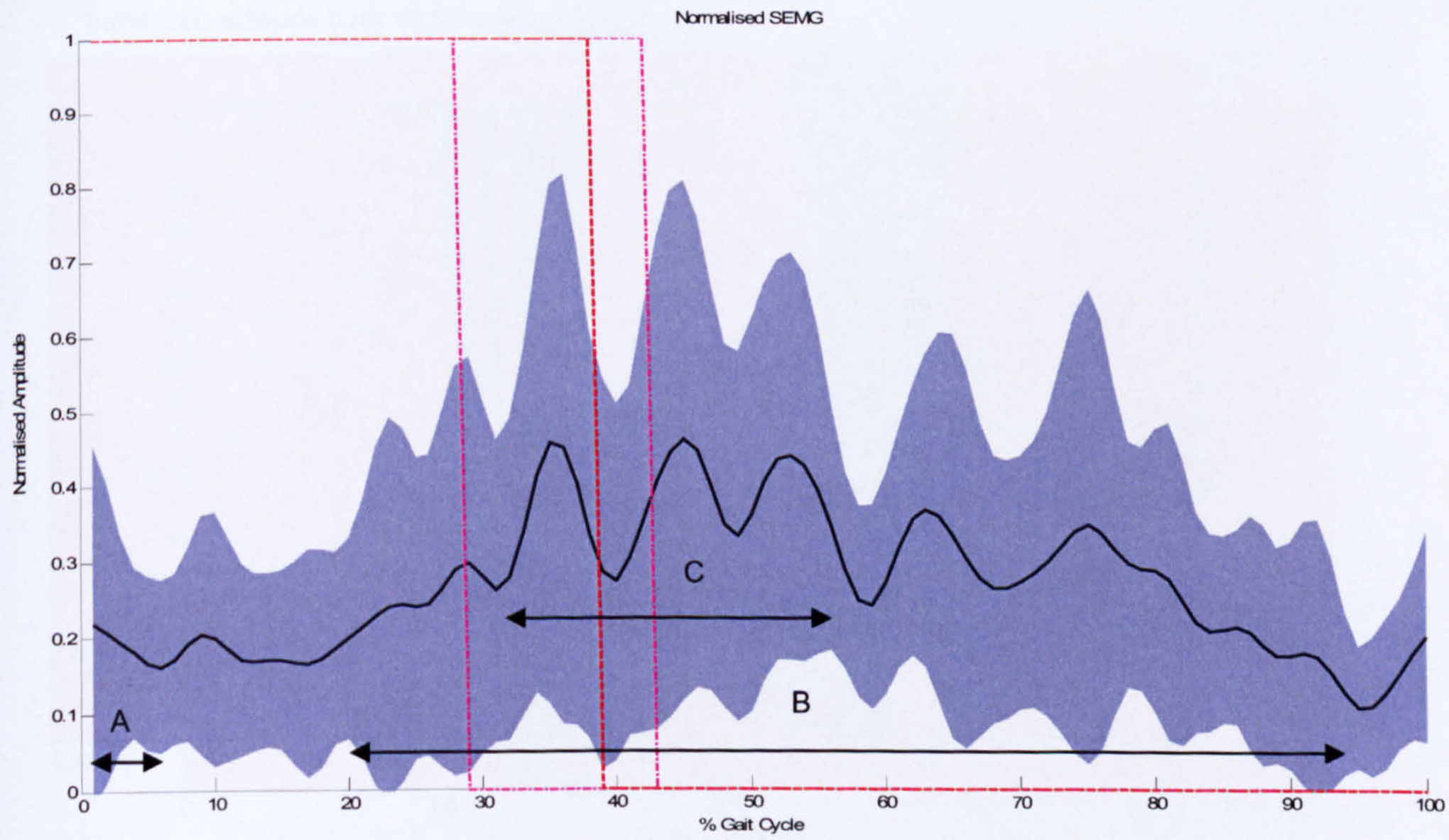

Appendix Figure 81 shows for CVA14 the mean and standard deviation of the linear envelope representation of the gastrocnemius muscle. There is a small increase just after toe off shown

by period A The activity increases from early swing and remains active until terminal stance., shown by period B The activity reaches a maximum during period C.

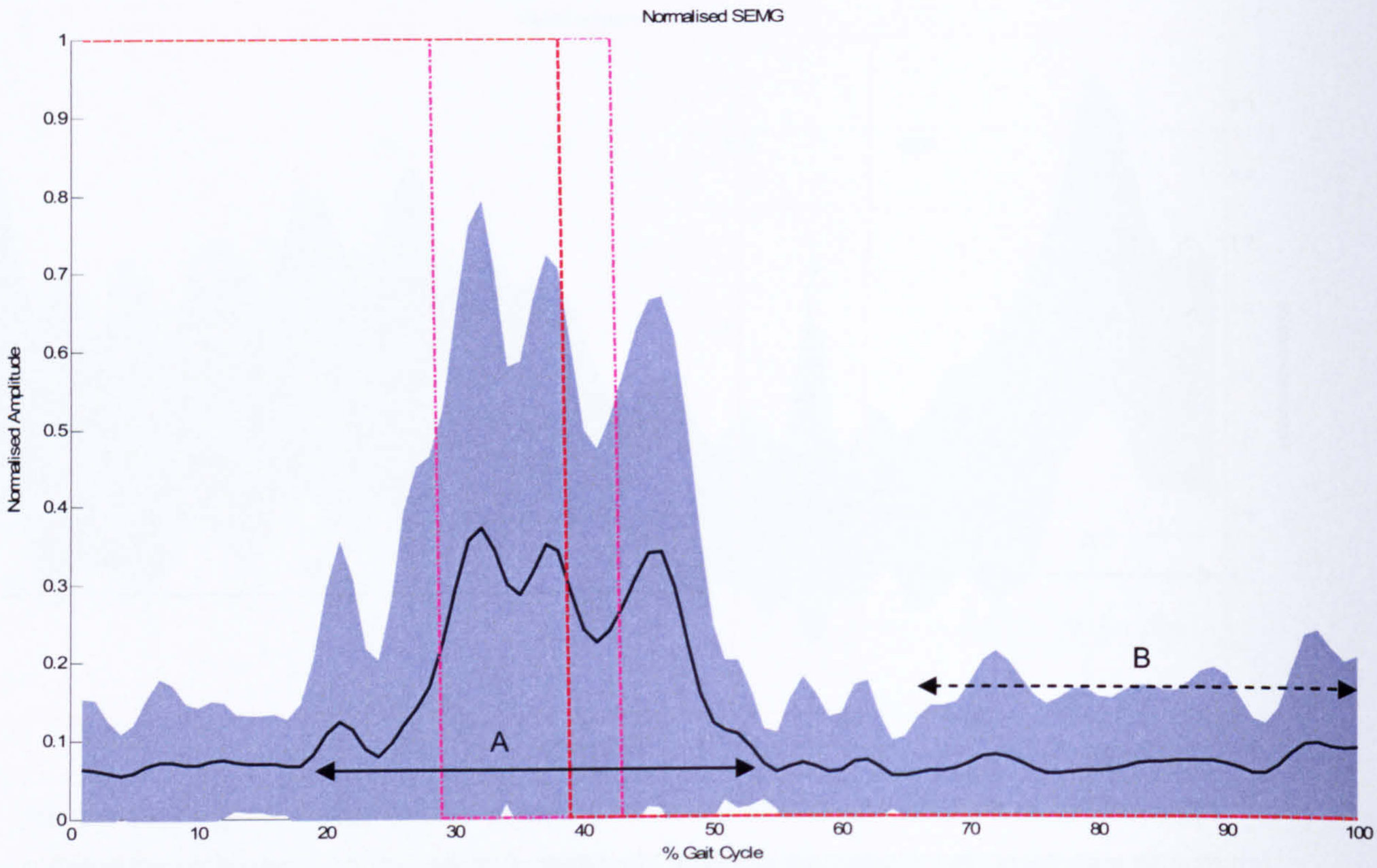

Appendix Figure 82 shows for CVA14 the mean and standard deviation of the linear envelope representation of the soleus muscle. Activity is restricted to period A and boarders the mean foot strike. There is appears to be a small level of activity during the stance phase represented by the broken line B

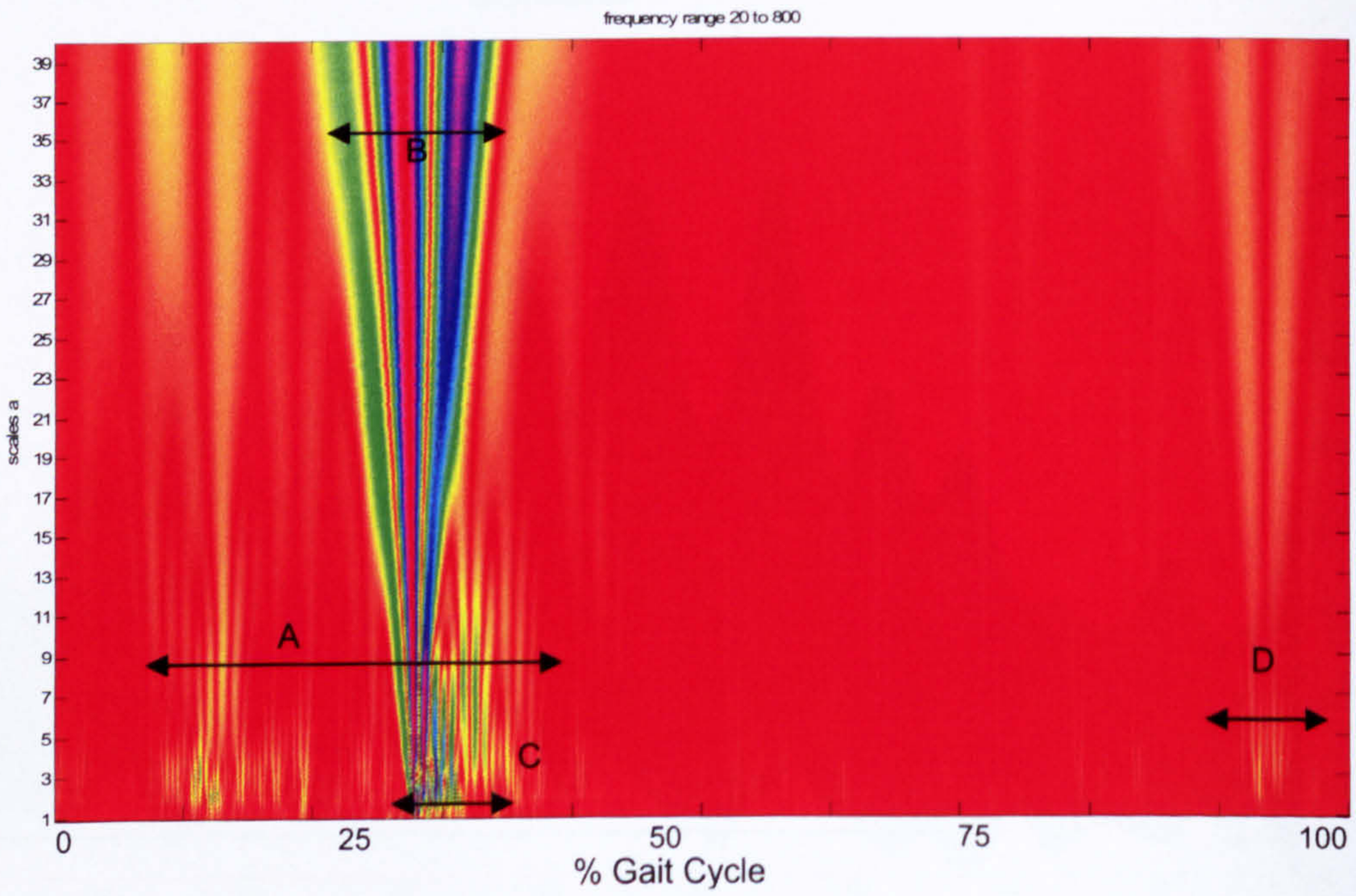

Appendix Figure 83 shows for CVA14 the time-frequency representation of the tibialis anterior muscle. A prominent burst of activity that extends across all frequency bands is present during period b and C. There is additional activity that extends over period A, the activity contains

smaller amplitude coefficients but are greatest in the higher to moderate frequency bands though do extend into the lower frequency bands. There is a final burst of activity with very small coefficient values during period D.

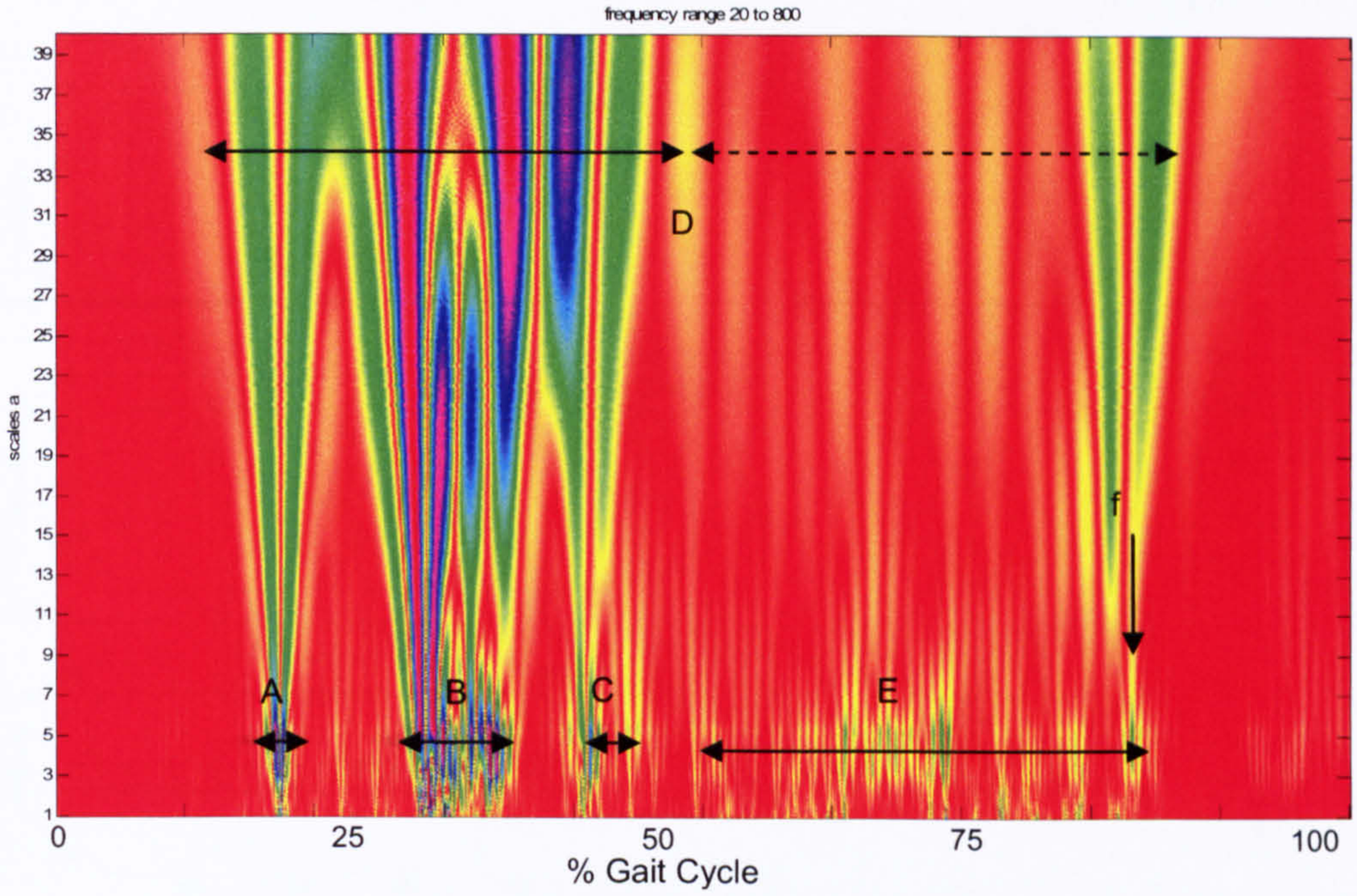

Appendix Figure 84 shows for CVA14 the time-frequency representation of the gastrocnemius muscles. Activity extends over period D, the activity is most concentrated within the solid line. There are three prominent bursts of activity represented by periods A, B and C, these extend across all frequency bands and are constructed of high amplitude coefficients. Activity then reduces in amplitude but is clearly visible in the higher frequency bands; small coefficients are visible in the lower frequency bands shown by period E. At point f there is another prominent burst that extends over all frequency bands

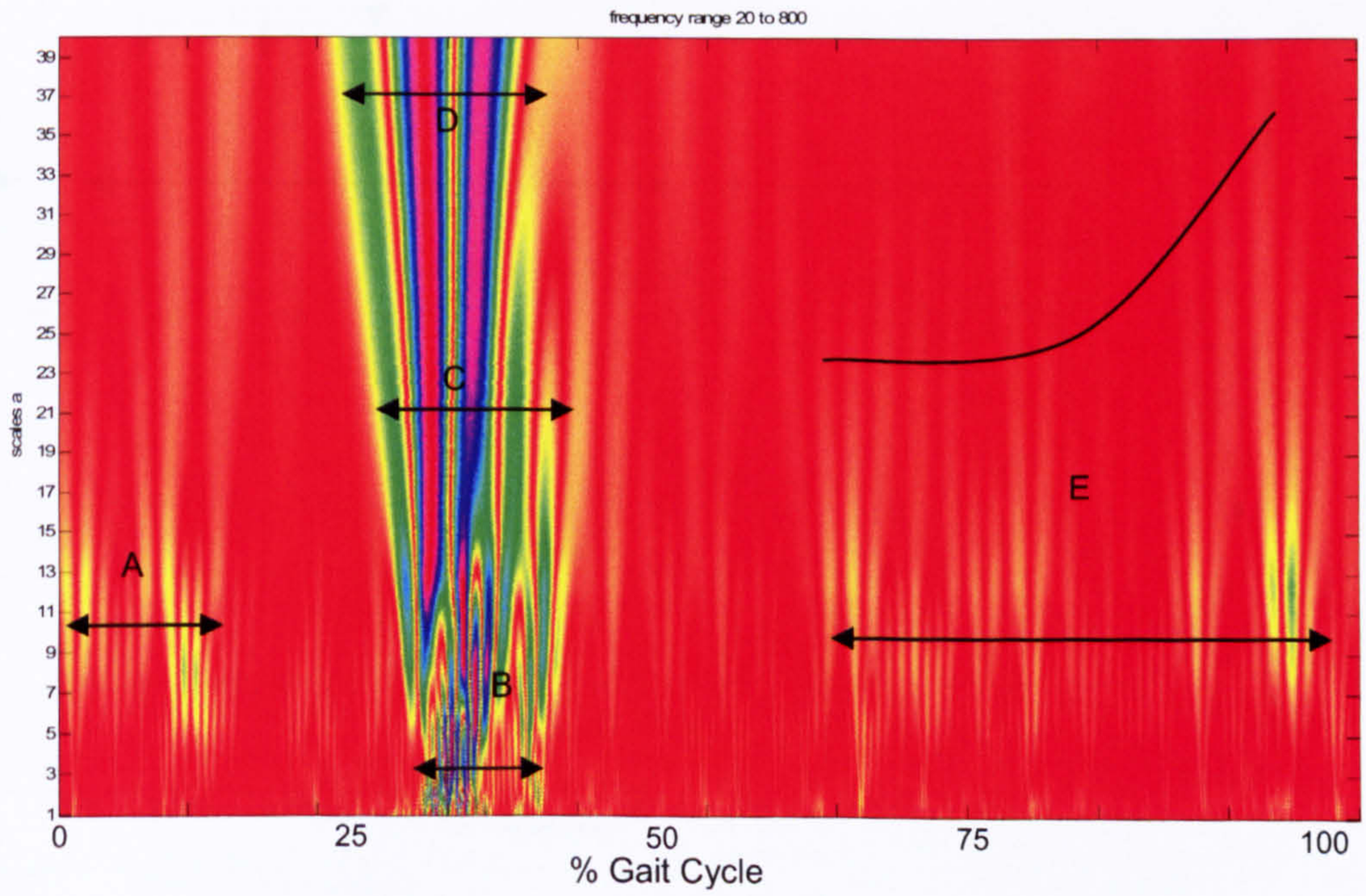

Appendix Figure 85 shows for CVA14 the time-frequency representation of the soleus muscles. There is moderate amplitude activity over period A that exists in the moderate high frequency

range. There is a prominent increase in coefficient amplitude across all frequency bands shown by periods B, C and D. Activity then reduces in amplitude. High amplitude activity is visible as short epoch bursts. Over period E there is an increase in amplitude that moves towards lower frequency bands.

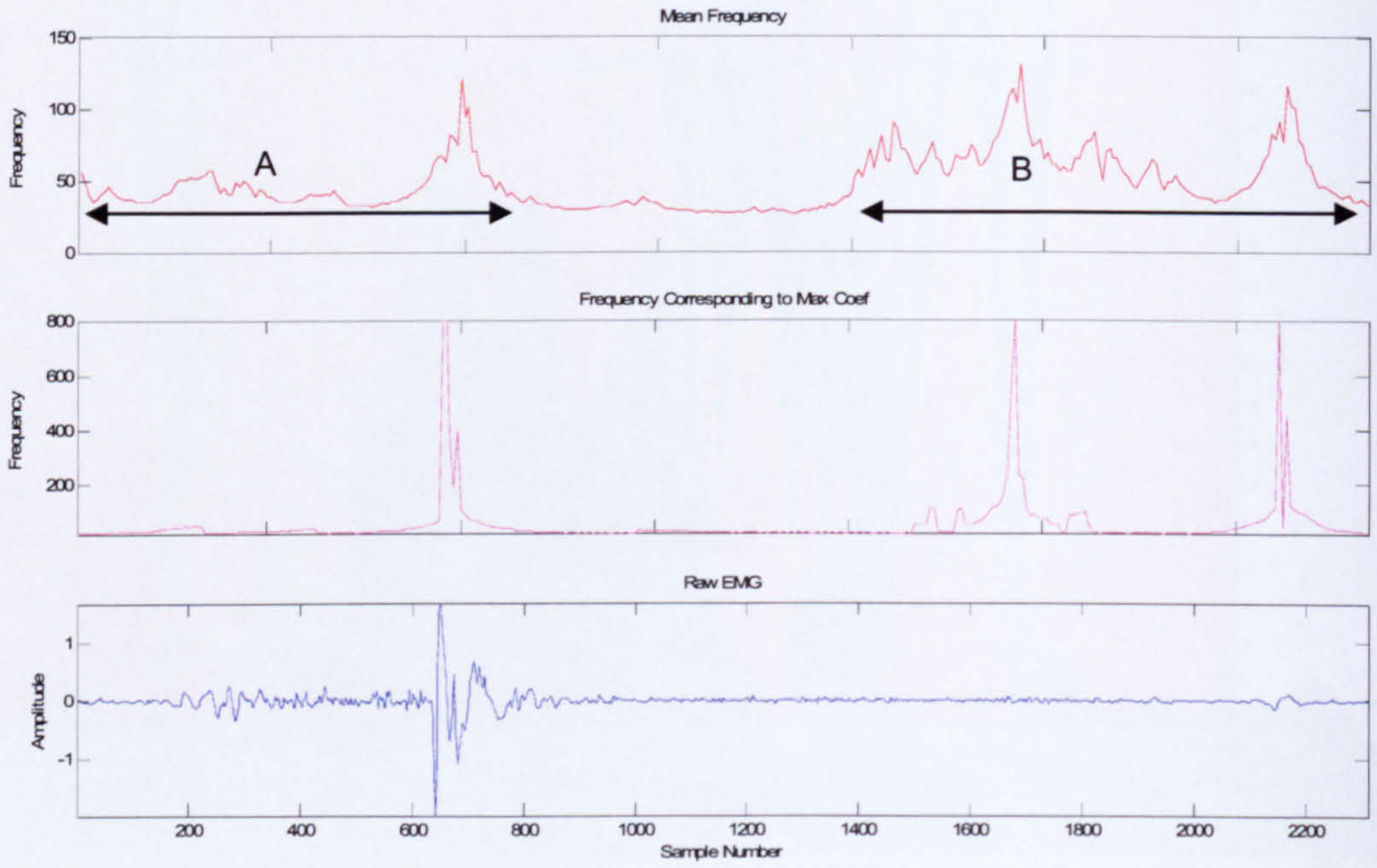

Appendix Figure 86 shows for CVA14 the instantaneous mean frequency of the tibialis anterior muscle. There are two periods of activity, the first occurs at foot strike and is denoted by period A. The second period of activity, shown by period B begins in the stance phase and exists in a period of apparent raw signal latency

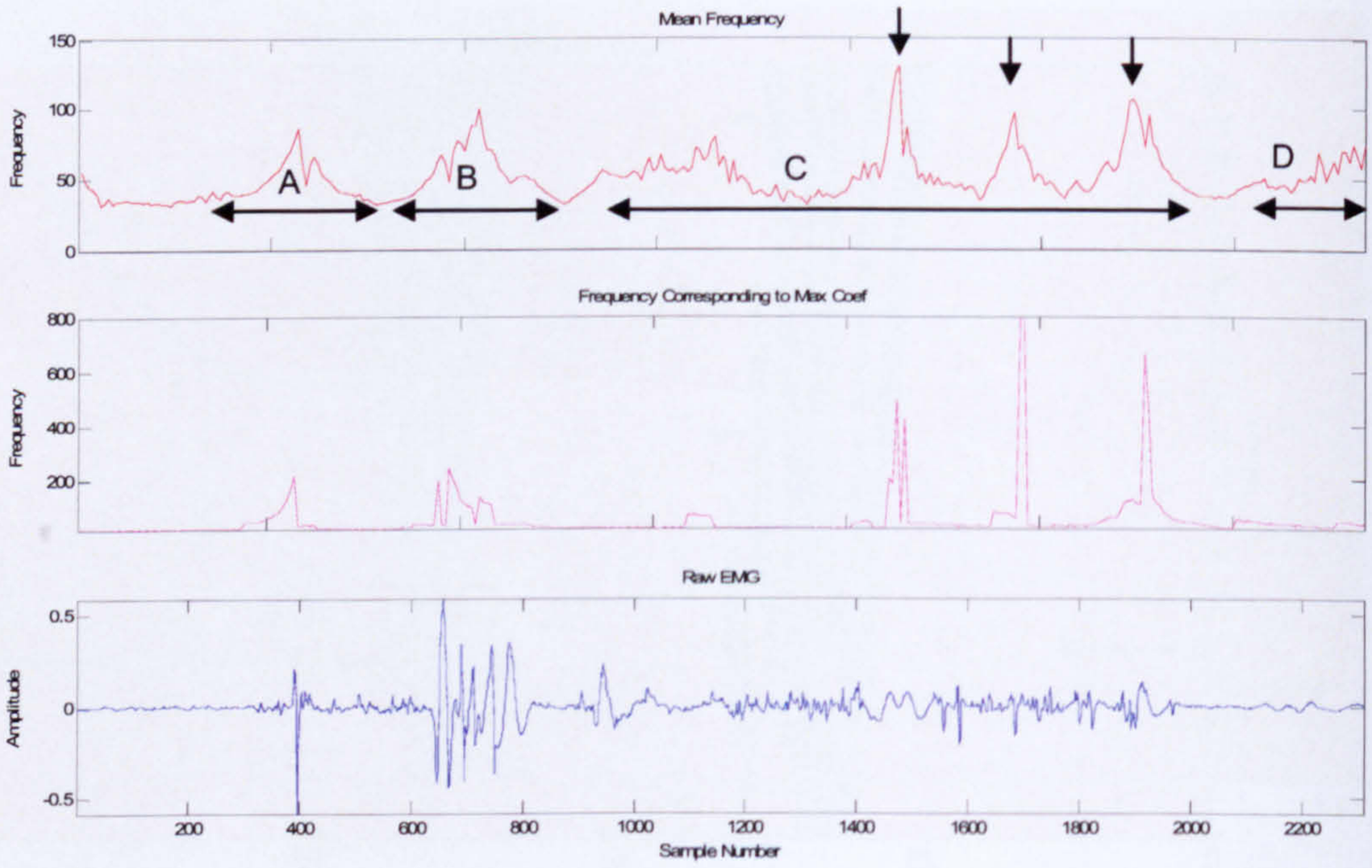

Appendix Figure 87 shows for CVA14 the instantaneous mean frequency of the gastrocnemius muscle. There are two peaks of mean frequency during the swing phase corresponding to the

initiation of sEMG activity and foot strike these are denoted by periods A and B. Post foot strike there is an increase in the level of mean frequency. This is shown by periods C and D. There are three prominent peaks of activity associated with low amplitude sEMG activity during this period shown by the down arrows.

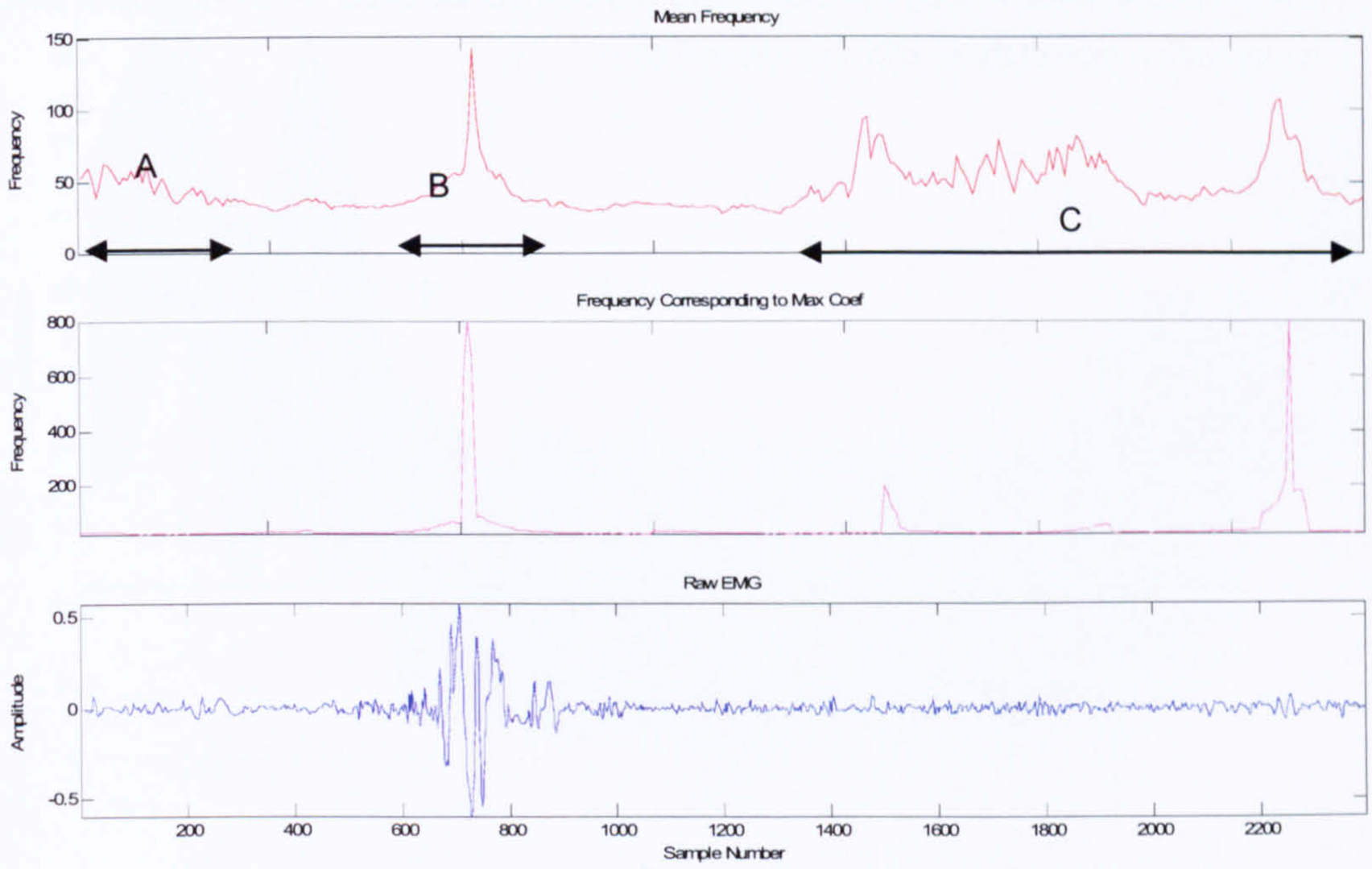

Appendix Figure 88 shows for CVA14 the instantaneous mean frequency of the soleus muscle. The mean frequency reduces from toe off shown by period A. subsequently there is a large amplitude burst that rapidly diminishes shown by period B There is a period of quiescence until the start of period C when the amplitude again increases corresponding with a small increase in sEMG amplitude this then diminishes but again almost immediately increases just prior to toe-off

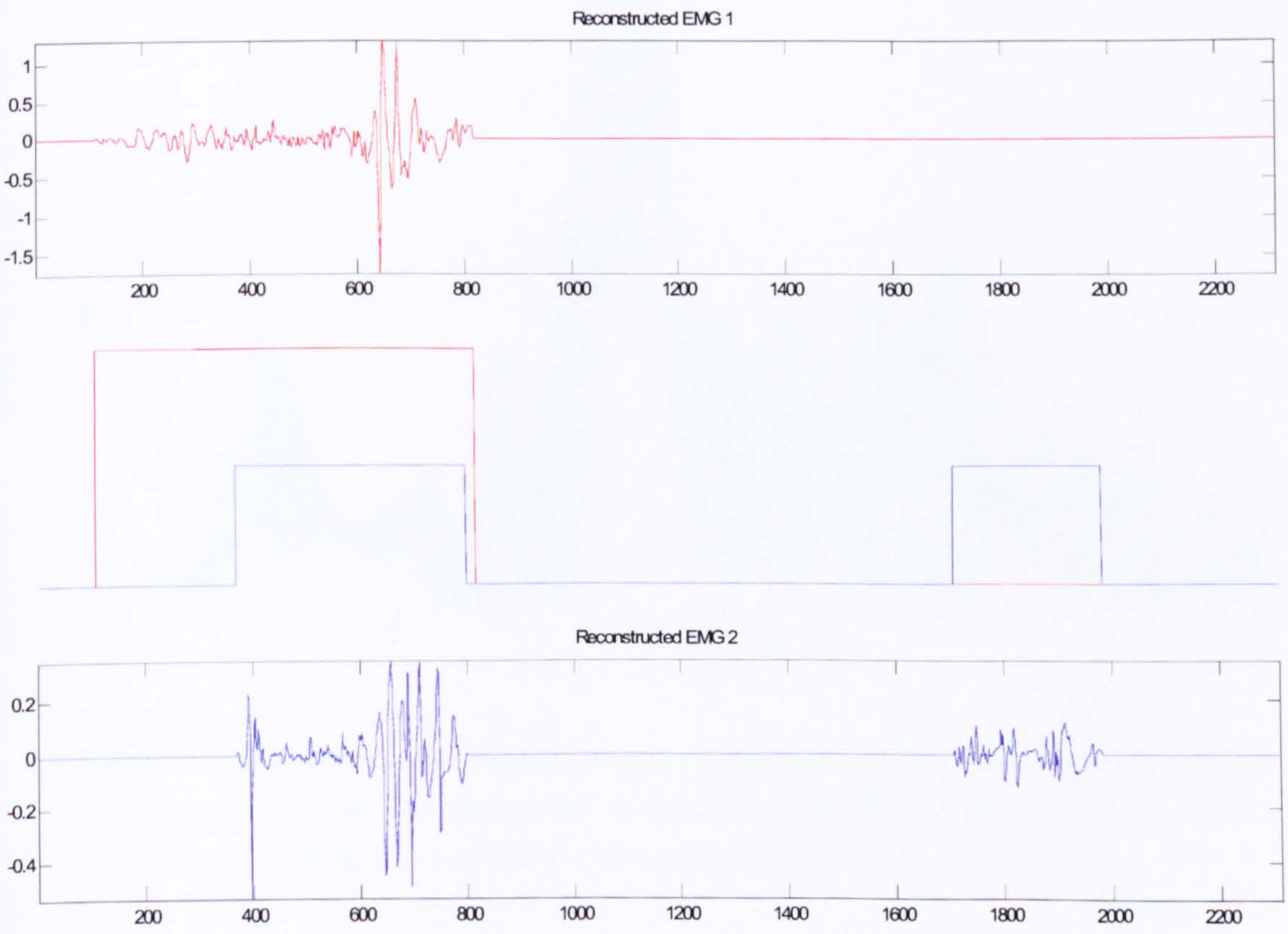

Appendix Figure 89 shows for CVA14 the burst locations calculated form sub-band filtering the tibialis anterior and gastrocnemius muscles. Tibialis anterior activity is clearly identified during the swing phase. The gastrocnemius activity is identified during early swing and foot strike; there is a second period of activity identified during mid stance. A period of activity during mid stance visible in the raw sEMG (see Figure 69) was not identified as an inter-burst period, the co-activation ratio of these two muscles is 0.43

A.III.g CVA15

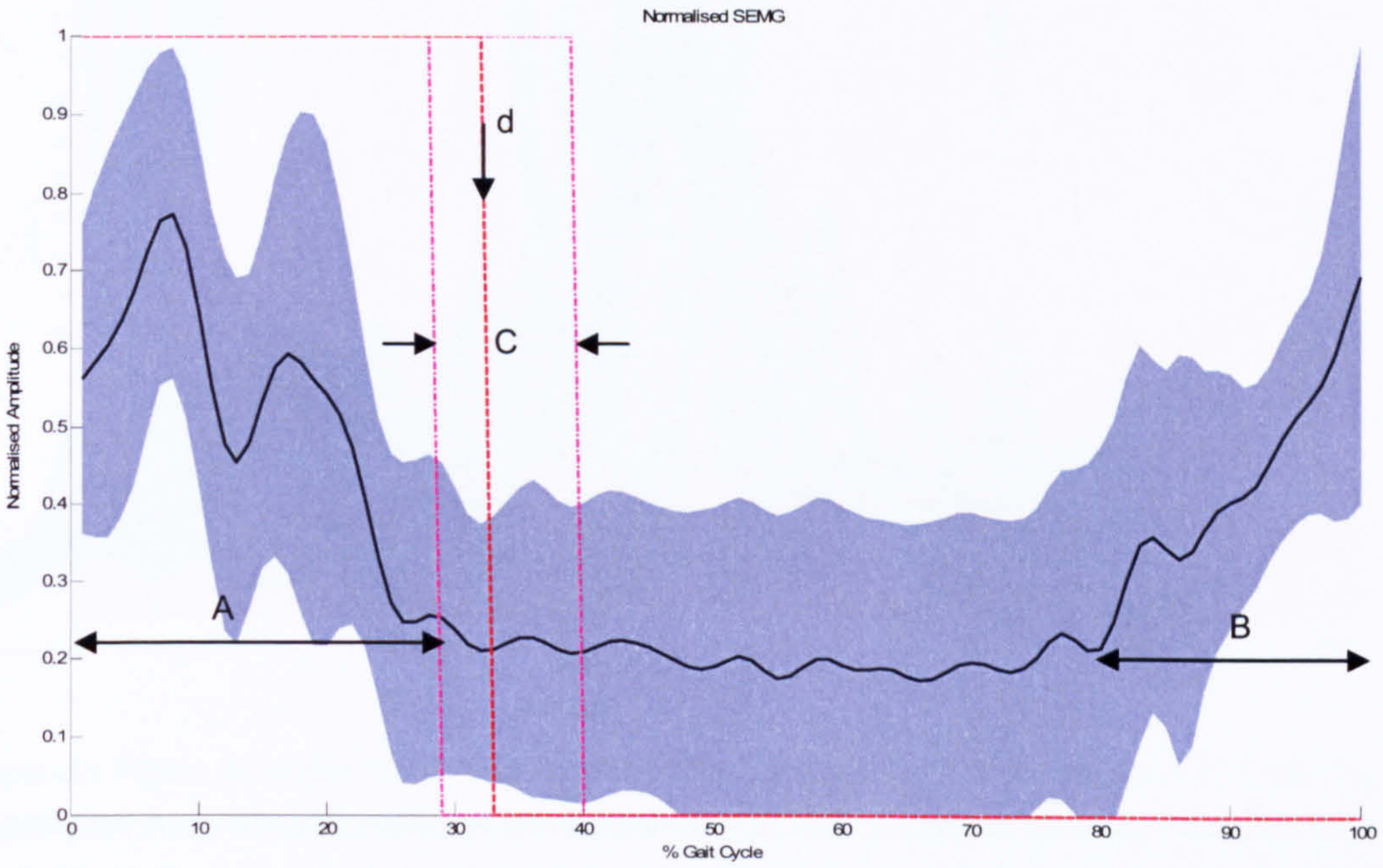

Appendix Figure 90 shows for CVA15 the mean linear envelope and standard deviation of the tibialis anterior. Two prominent peaks of activity can be seen over periods A and B. The red broken line displays the mean foot switch activity that appears at point d the variation of the location of foot strike, shown by the broken mauve line is given by period C.

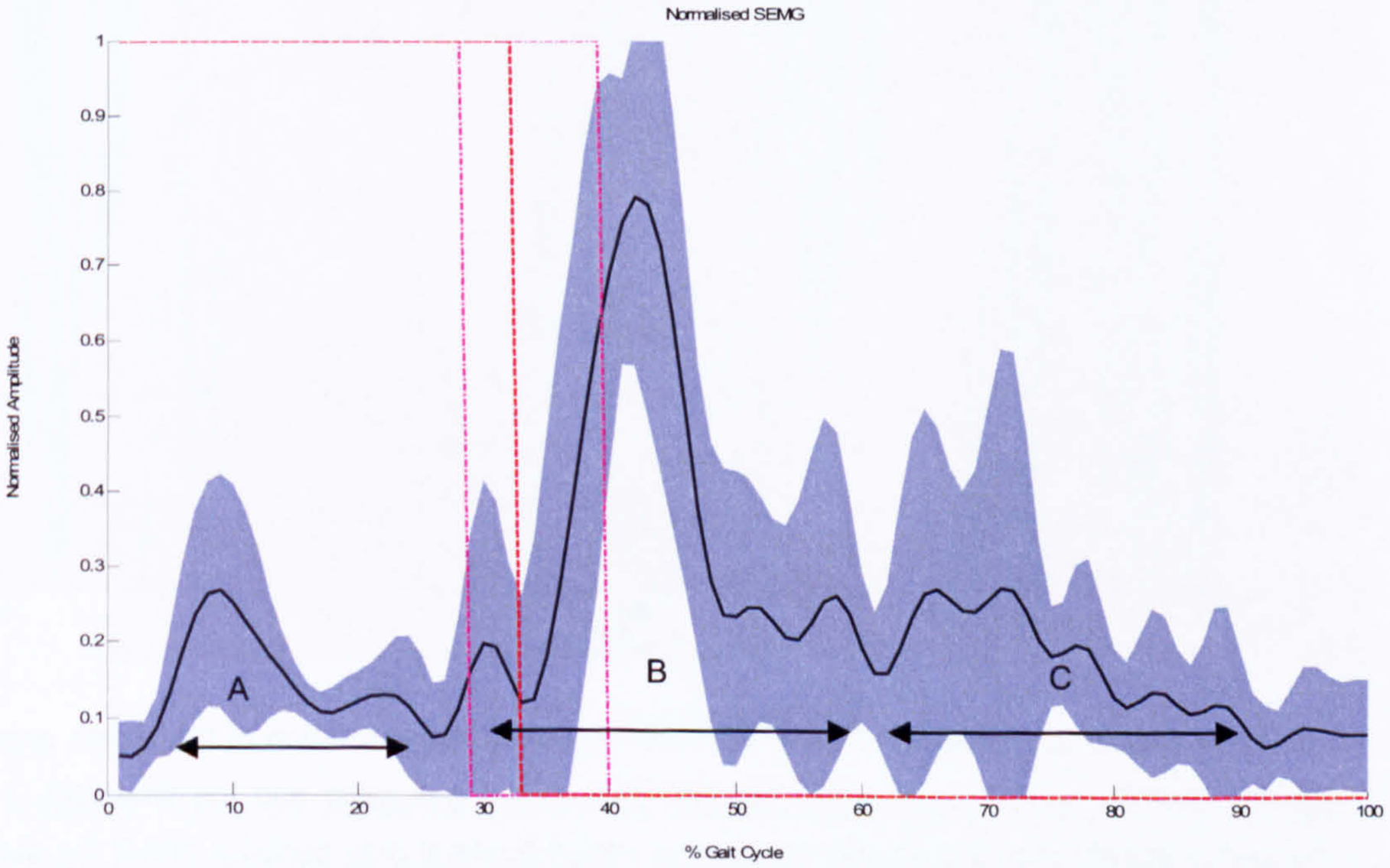

Appendix Figure 91 shows for CVA15 the mean linear envelope and standard deviation of the gastrocnemius muscle. The main period of activity can be seen between periods B and C. A smaller burst of activity can be observed during period A in early swing phase

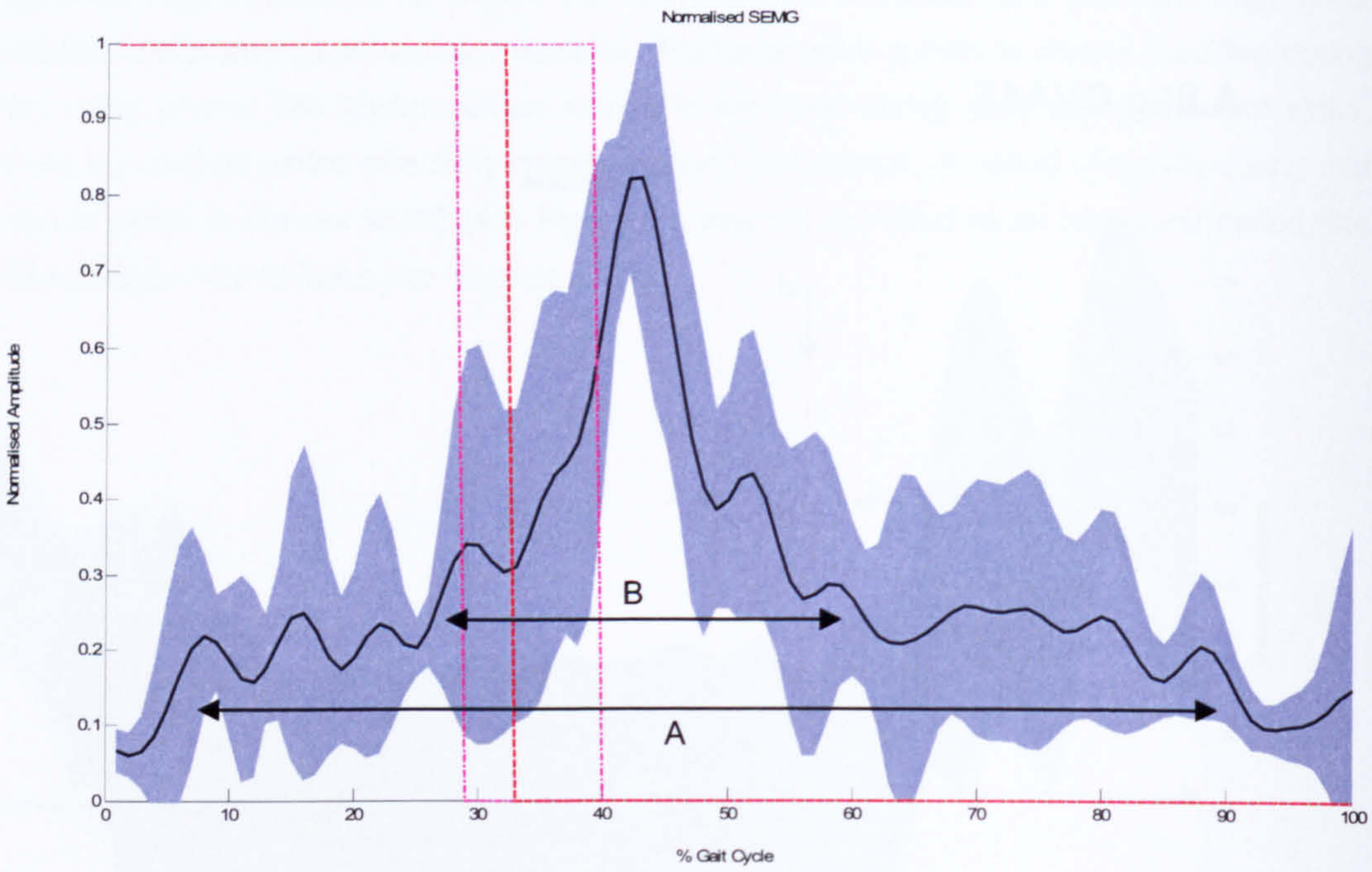

Appendix Figure 92 shows for CVA15 the mean linear envelope and standard deviation of the soleus muscle. Activity appears to be present during period A. The main peak of activity exists during period B.

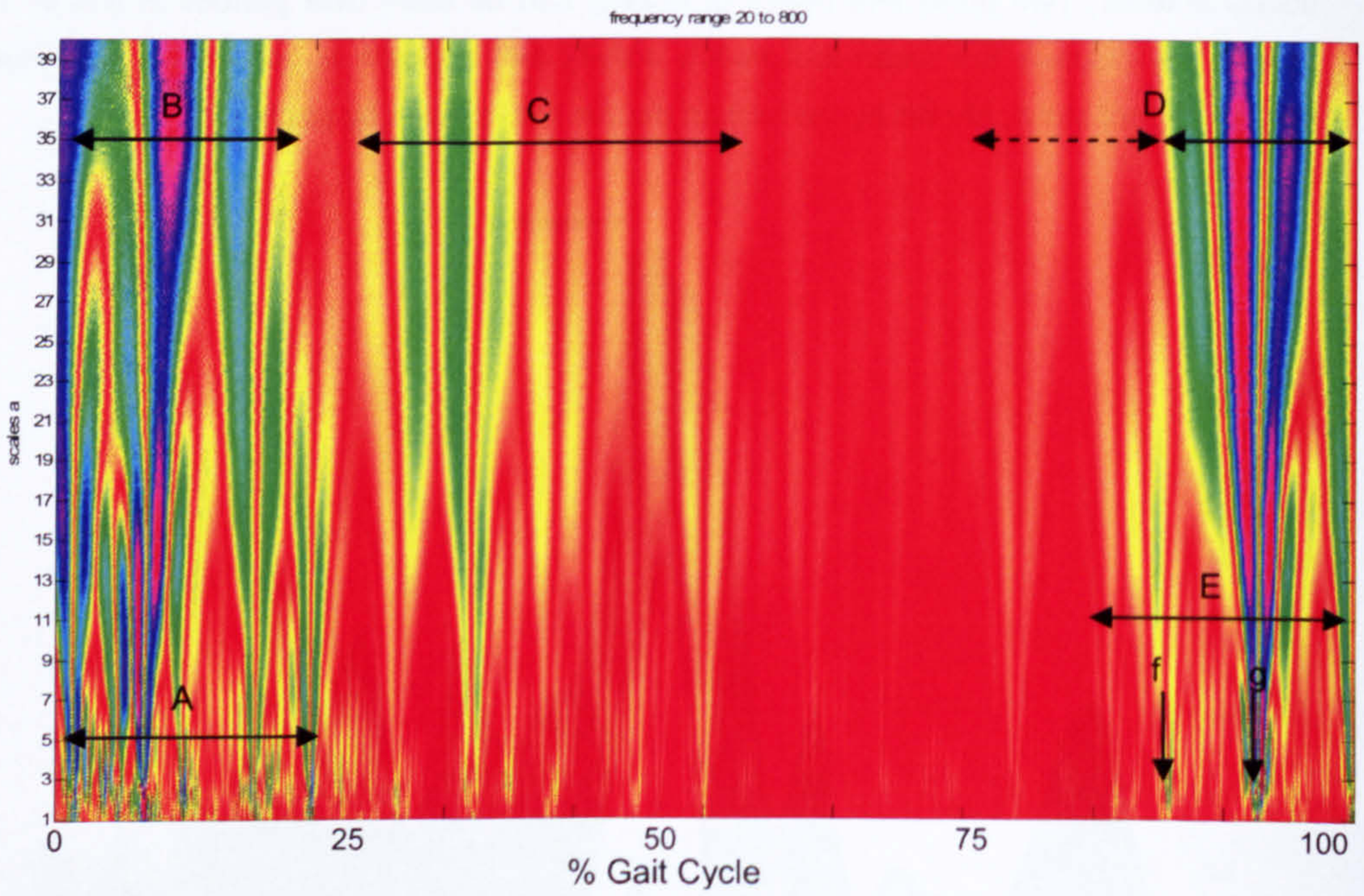

Appendix Figure 93 shows for CVA15 the time-frequency representation of the tibialis anterior muscle. Activity can be seen within the first 50% of the gait cycle and the final 20%. High frequency activity occurs predominately during period A where over period A and B the activity exists throughout all frequency bands. Short epoch bursts of activity appear over period C which appear as larger coefficients in the mid to low frequency bands. Similarly short epoch high frequency bursts produce large coefficients in the mid to low frequency bands over period E. Prominent low frequency activity can be seen over period D where the broken line reflects reduced amplitude activity.

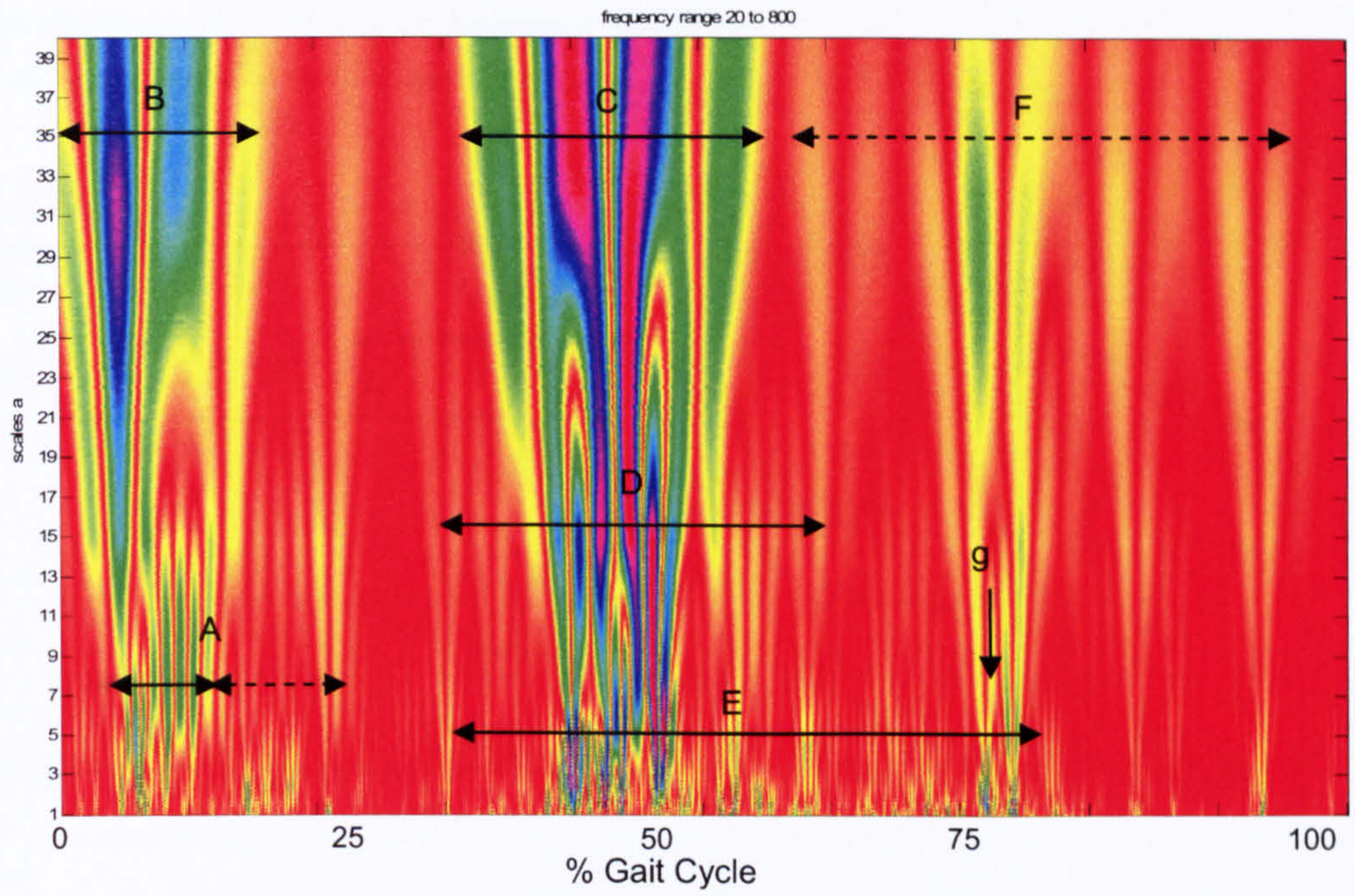

Appendix Figure 94 shows for CVA15 the time-frequency activity of the gastrocnemius muscle. Three prominent bursts of activity are visible and shown as period B, C and point g. High frequency activity can be observed over period E and during period A. However, only the former high frequency burst translate to high coefficients in the mid to low frequency bands. Several other short epoch high frequency low amplitude bursts can be observed at that produce low amplitude activity in the mid to low frequency bands

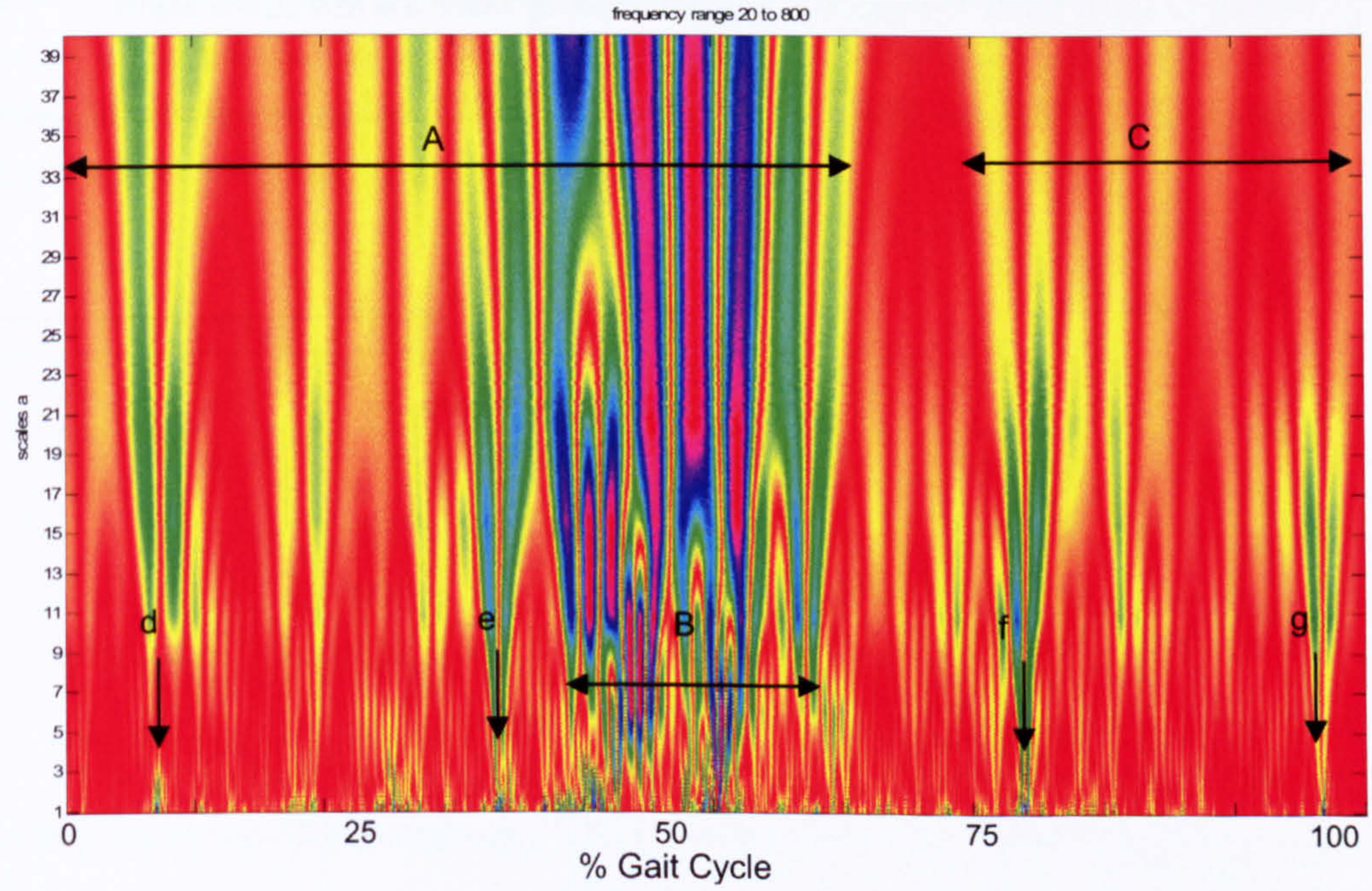

Appendix Figure 95 shows for CVA15 the time-frequency activity from the soleus muscle. Bursts of activity can be seen throughout the stride. During period B, these produce high amplitude responses across the frequency bands. Similarly, high frequency bursts at points d, e, f and g produce mid to low frequency responses. Low frequency activity exists over period A and to a lesser extent over period C.

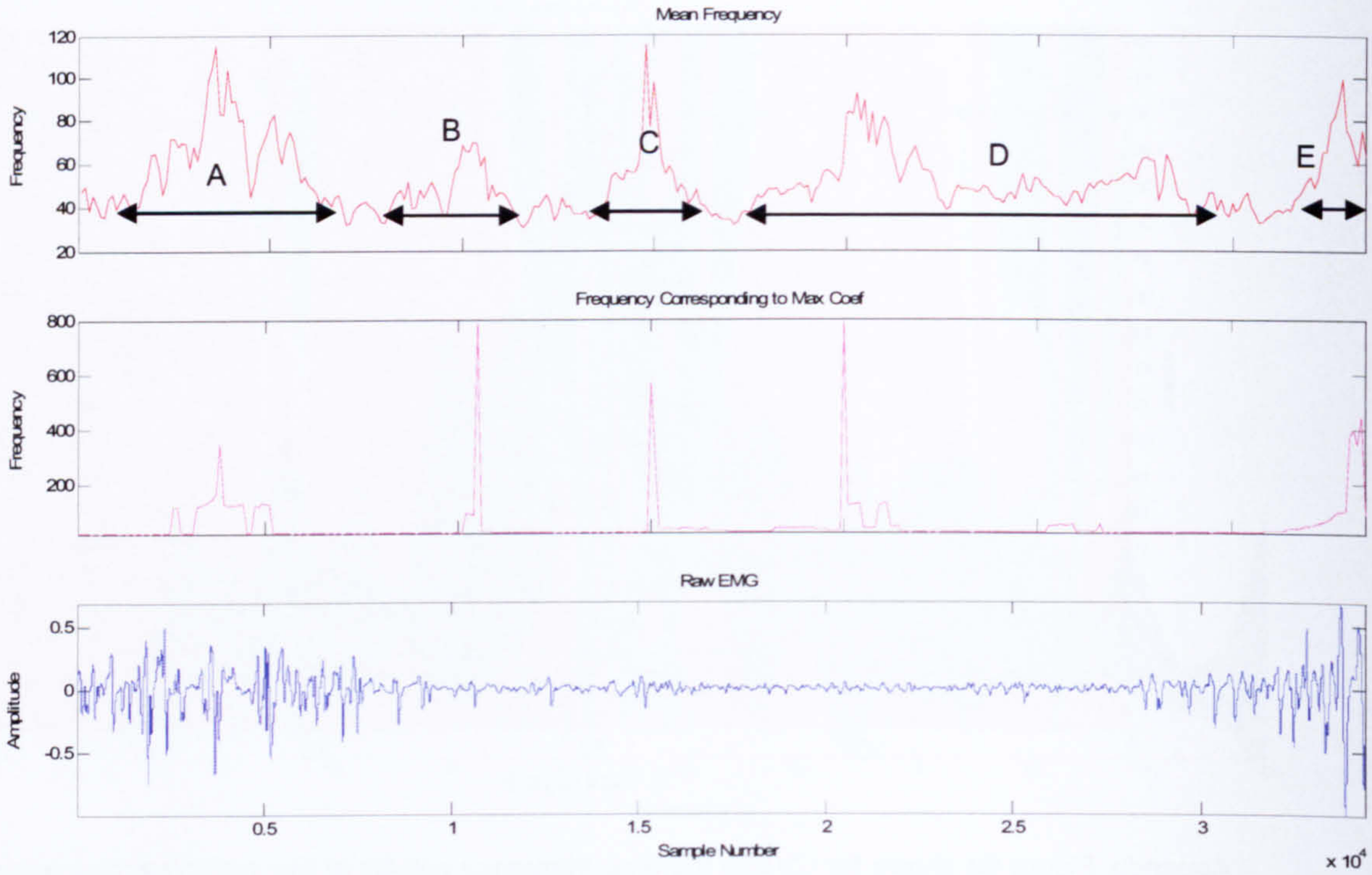

Appendix Figure 96 shows for CVA15 the instantaneous mean frequency of the tibialis anterior muscle. There is a gradual increase in mean frequency over period A and extends into the stance phase. Additional peaks of activity are seen in periods B and C. D corresponds to an extended period a activity. During terminal stance there is a final peak of mean frequency shown by period E Periods A, B and E corresponds to an increase in activity of the raw sEMG. Periods C and D relate to periods of apparent latency within the raw sEMG signal.

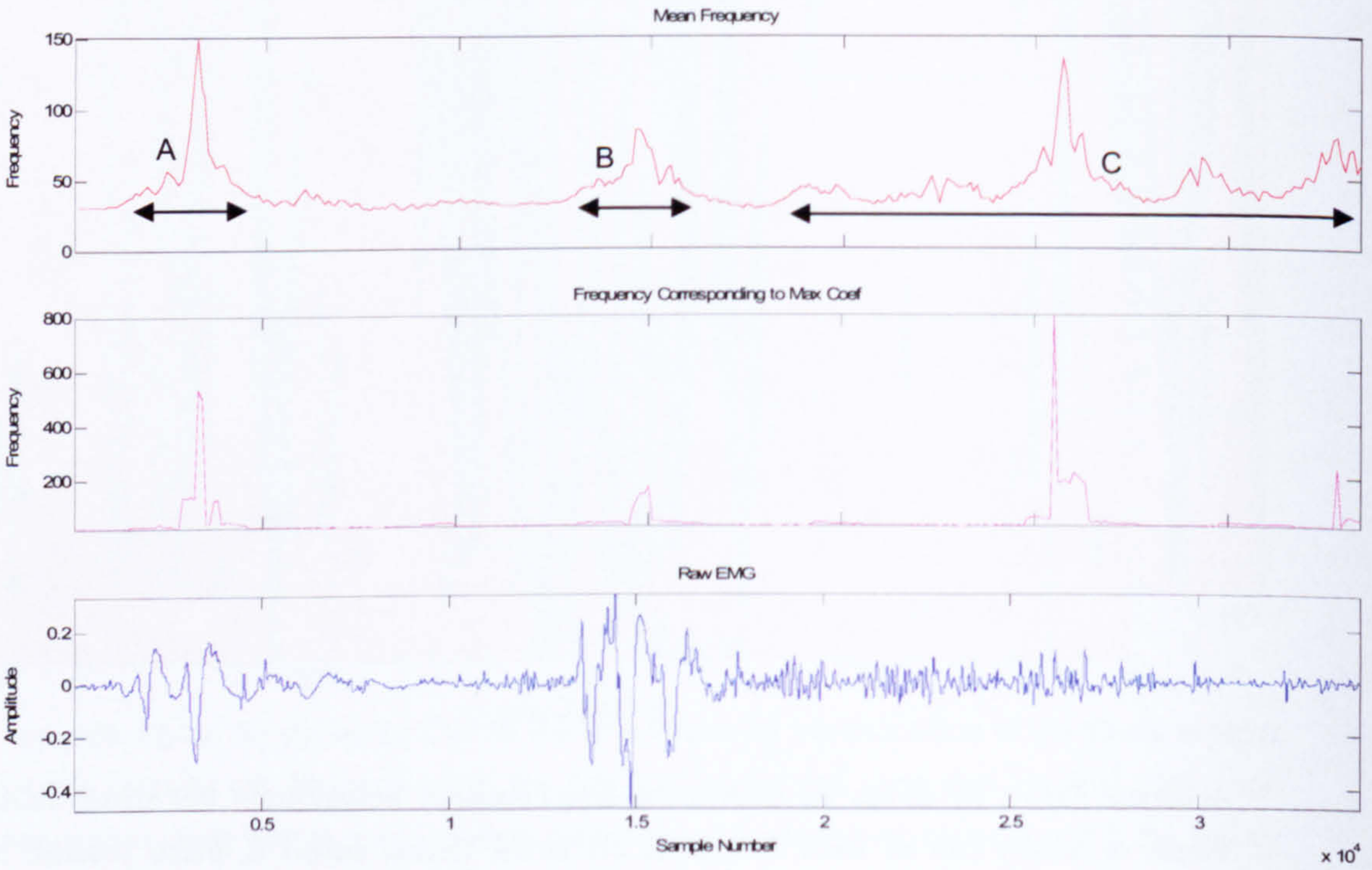

Appendix Figure 97 shows for CVA15 the instantaneous mean frequency across a stride of the gastrocnemius muscle. Three peaks of activity characterise the signal; the first occurs just after toe-off and shown by period A. The second period of increased mean frequency occurs at foot

strike shown period B. Finally the third peak of activity occurs at the end of period of the sEMG activity and extends to terminal stance; this is represented by period C.

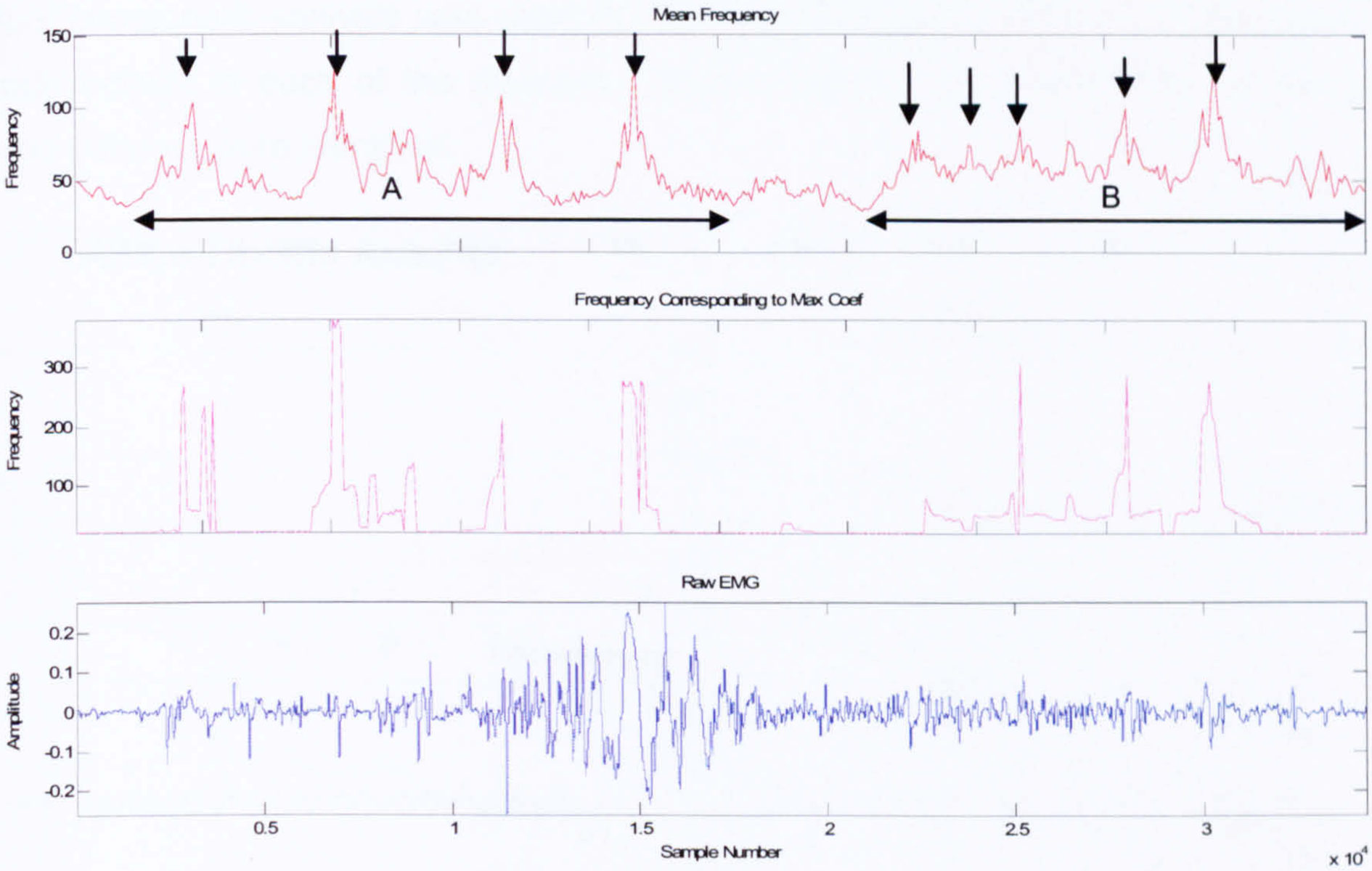

Appendix Figure 98 shows for CVA15 the instantaneous mean frequency across a stride of the soleus muscle. An increase in mean frequency can be seen subsequent to toe-off during period A. which is characterised by periodic bursts of increased amplitude. There is a final significant increase in activity over period B as the raw sEMG activity reduces. Again this is characterised by burst activity and is identified by down arrows.

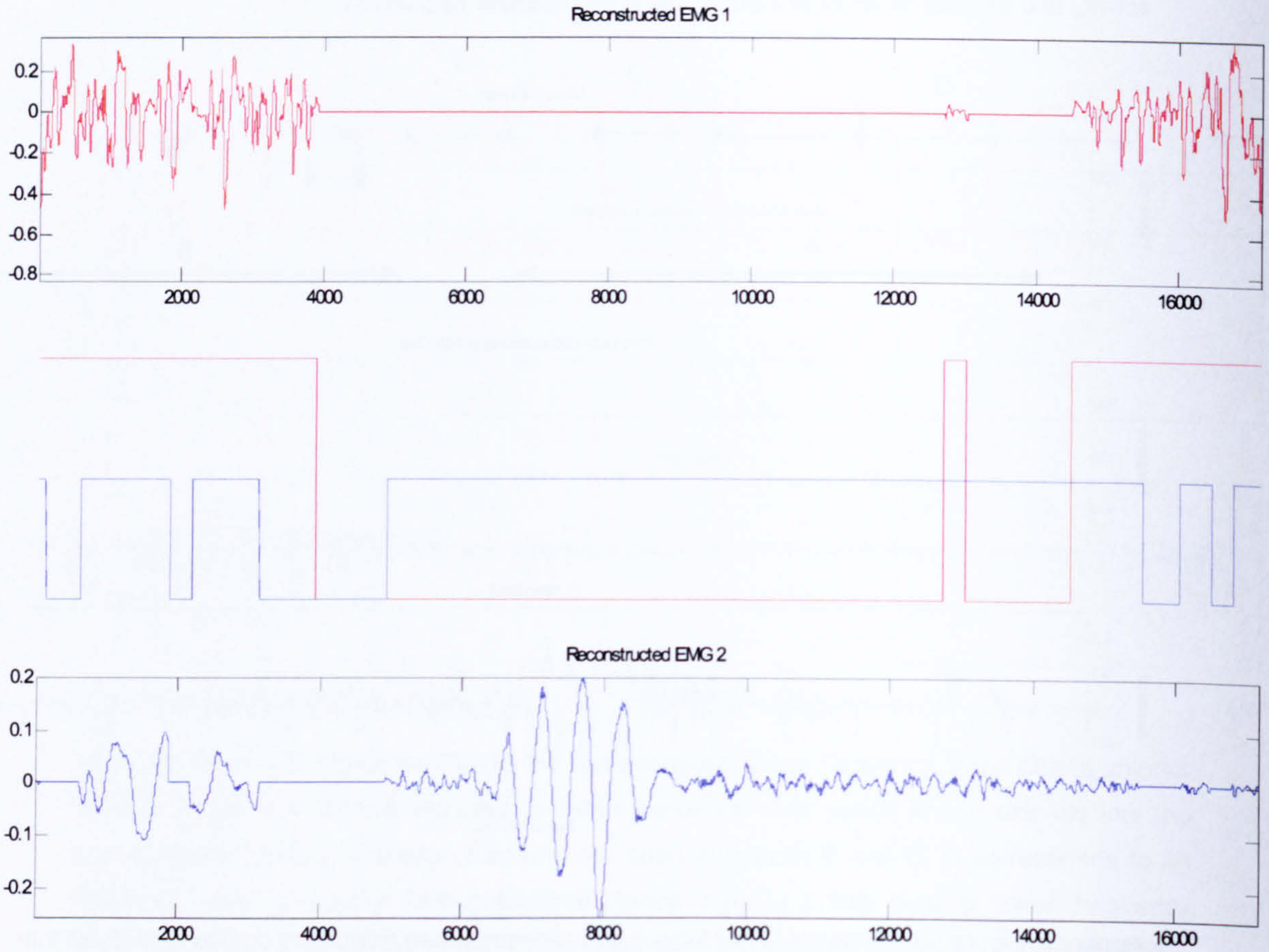

Appendix Figure 99 shows for CVA15 the burst locations for the tibialis anterior and gastrocnemius muscles. The Tibialis anterior shows good discrimination between burst and inter-burst periods. The method identifies many periods of activity over the stride. The most prominent period of activity is seen to exist between the prominent bursts of the tibialis anterior. The tibialis anterior activity is shown over the swing phase. Two additional bursts are then reported during early stance. In terminal stance several periods of activity are identified. The co-activation ratio for these two muscles is 0.27

A.IV Principal Component Analysis

Principal component analysis was used to find characteristic patterns to describe linear envelope activity in each of the muscles. Concentrating on the ankle musculature the following patterns were identified.

A.IV.a Tibialis Anterior

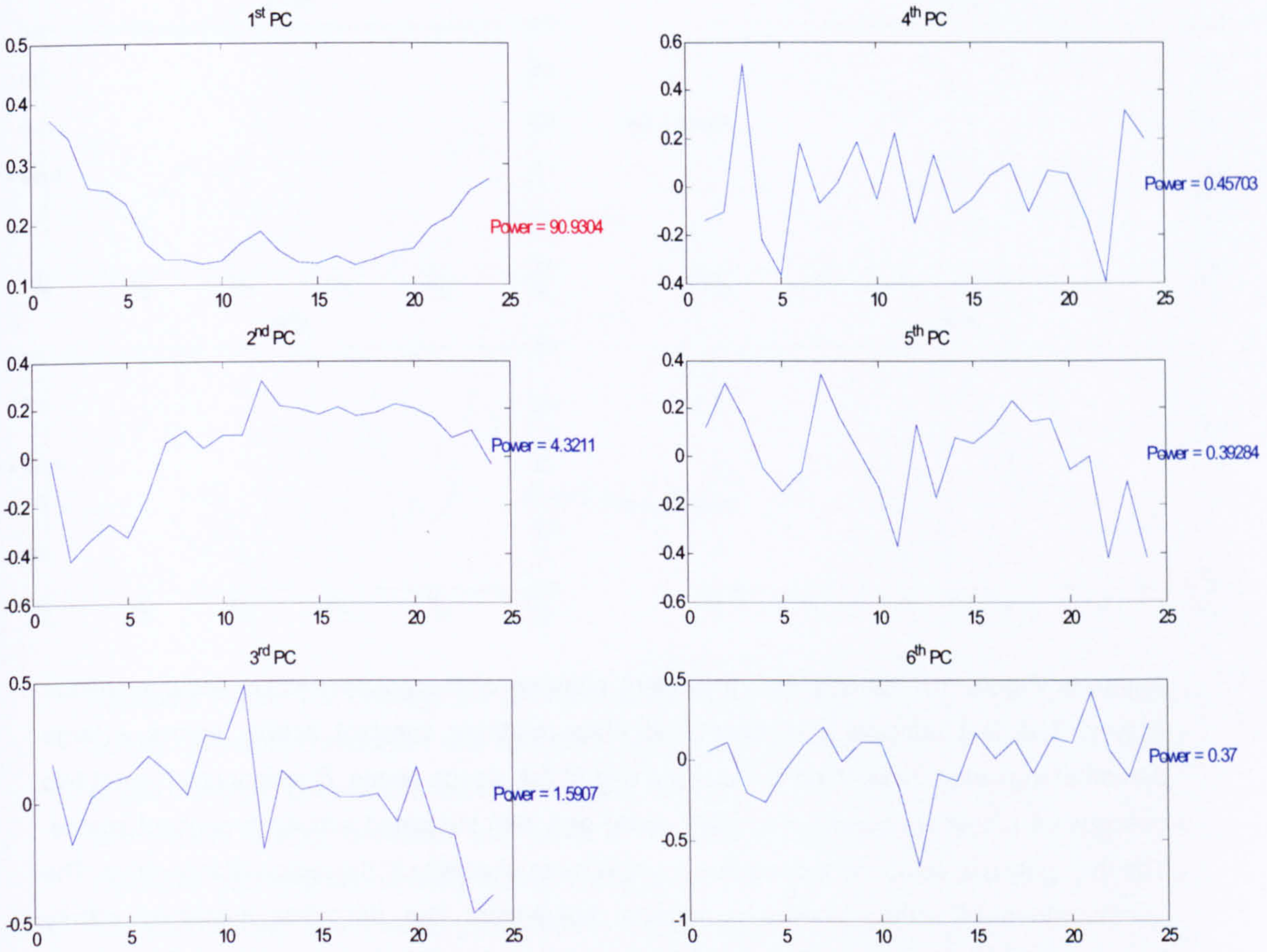

Appendix Figure 100 reveals three prominent patterns of the tibialis anterior linear envelope activity. The first principal component shows activity during early swing and during late stance and a degree of activity at foot-strike. Principal component 2 describes a pattern where the majority of the activity is in the swing phase and very little activity during late stance. The third principal component characterises activity with a prominent burst at foot strike. The final three principal components have a power less than 1 and are therefore excluded, however, they do modify the patterns already described. Principal component four contributes to more complex activity across the stride, principal component five modifies swing phase activity and principal component six modifies stance phase activity.

A.IV.b Gastrocnemius

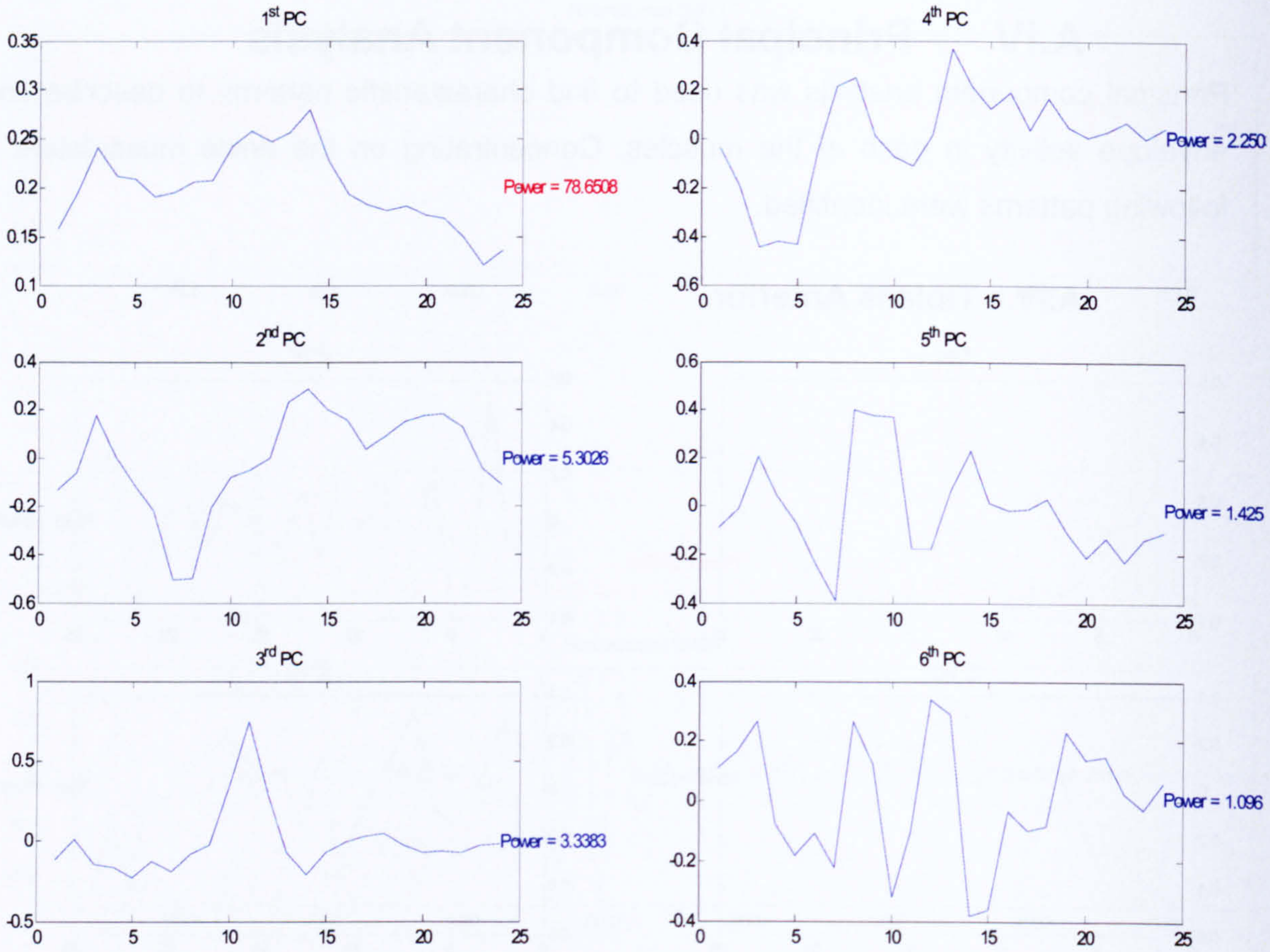

Appendix Figure 101 reveals four prominent patterns of the gastrocnemius linear envelope activity. The first principal component describes relatively constant activity across a large portion of the stride diminishing towards the end of the stance phase. Principal component two describes a prominent burst during early swing and then sustained activity throughout stance. The third principal component describes a single burst of activity in the region of foot-strike. The fourth pattern of activity shown in principal component four describes sustained activity throughout the stance phase and some activity in late swing. Principal components five and six are considered to be modifiers of the other components and predominately add additional complexity to the swing phase activity and specifically to activity at foot-strike.

A.IV.c Soleus

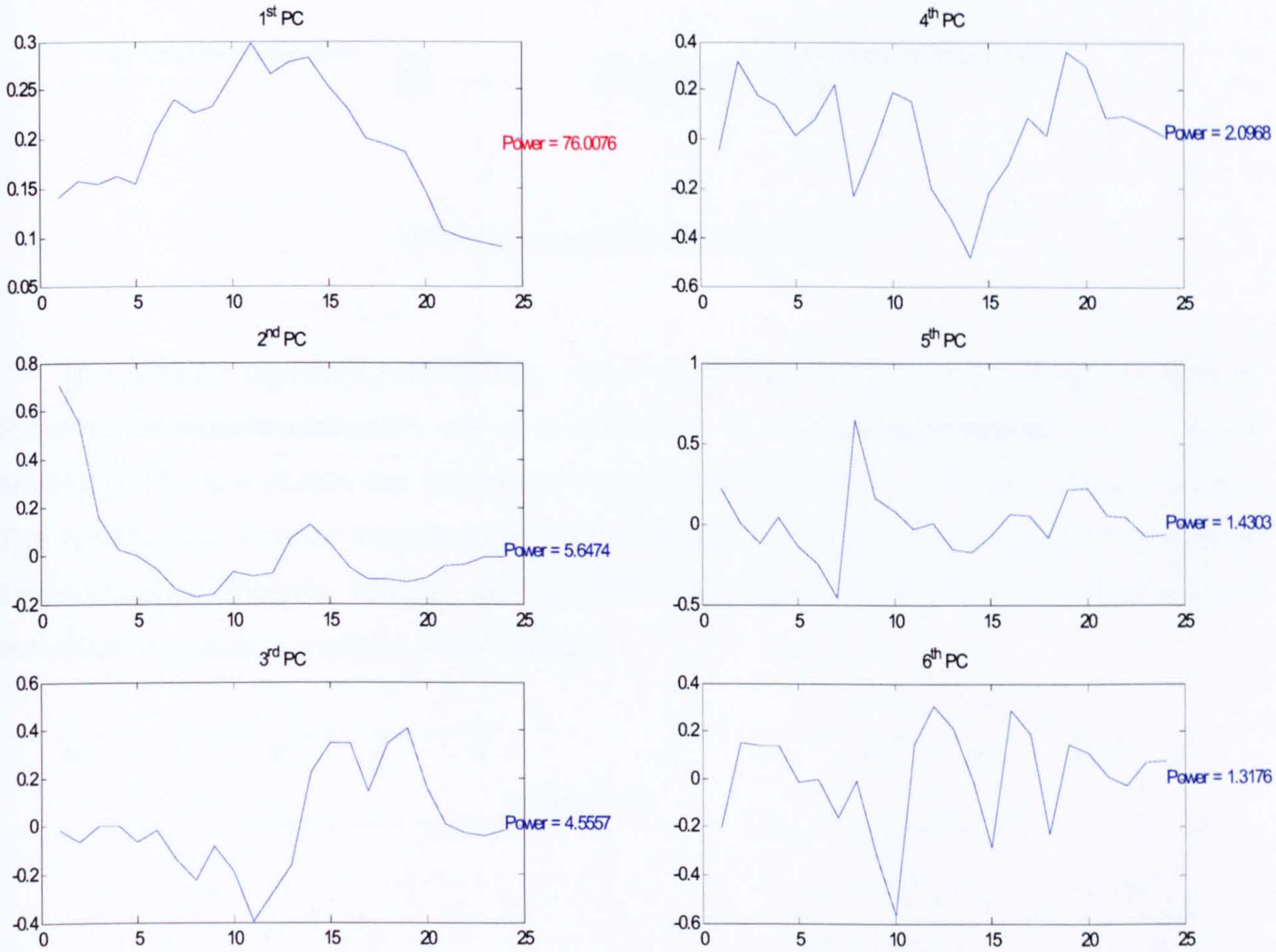

Appendix Figure 102 displays the principal components describing the soleus linear envelope activity. Principal component one describes activity during late swing phase and early stance phase. Principal component two shows bursts of activity at toe-off and in the early swing phase and activity during foot-strike and early in the stance phase. Principal component three describes activity predominately during the stance phase. Principal component four represents sustained activity in the swing phase and a second period of activity during the stance phase. Principal components five and six are again thought to be modifiers. Principal component five amplifies activity at foot-strike and the stance phase, principal component six introduces complexity to the stance phase activity.

A.IV.d Reconstruction

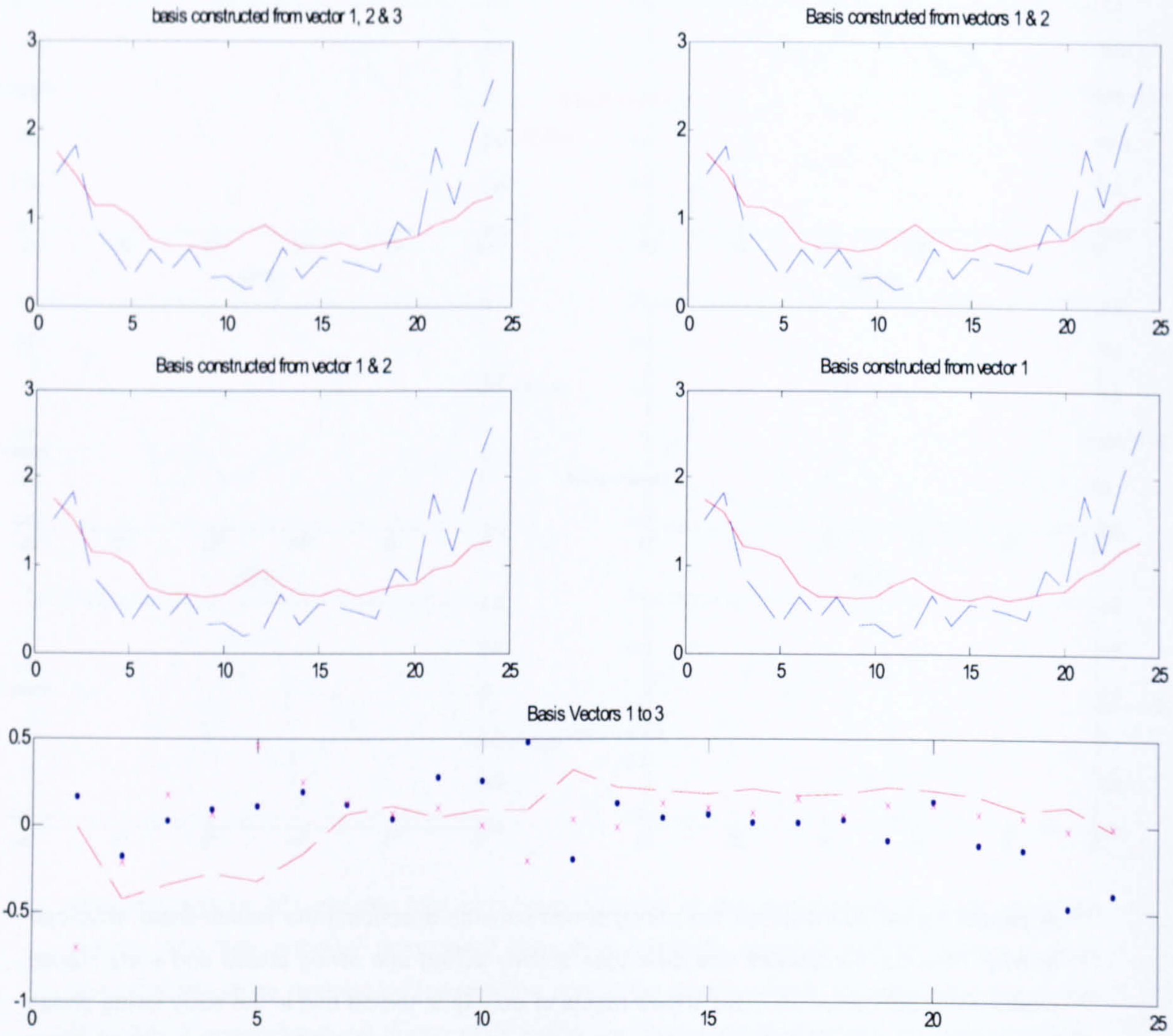

Appendix Figure 103 indicates the reconstruction of a signal not used to generate the principal components and therefore represents the ability of the principal components to capture the underlying characteristics of the linear envelope data set. The Mean square error between the two signals shown in the upper left hand Figure (red = reconstructed signal and blue = first, second and third principal components) is 21%. The bottom Figure displays the three highest power basis vectors or principal components used to reconstruct the signal.

B Appendix

Un-Impaired Subject Data

This section presents results from walking assessments from un-impaired subjects. Patterns of muscle activation within a stride are given, firstly, in the form of a linear envelope. Multiple strides are combined for each subject and for the three ankle muscles. The results from Fourier frequency analysis are then presented followed by the results of time-frequency analysis. Finally, examples for results from the sub-band filtering and co-activation calculation method are presented.

B.I Linear Envelope representation

B.I.a NOP1

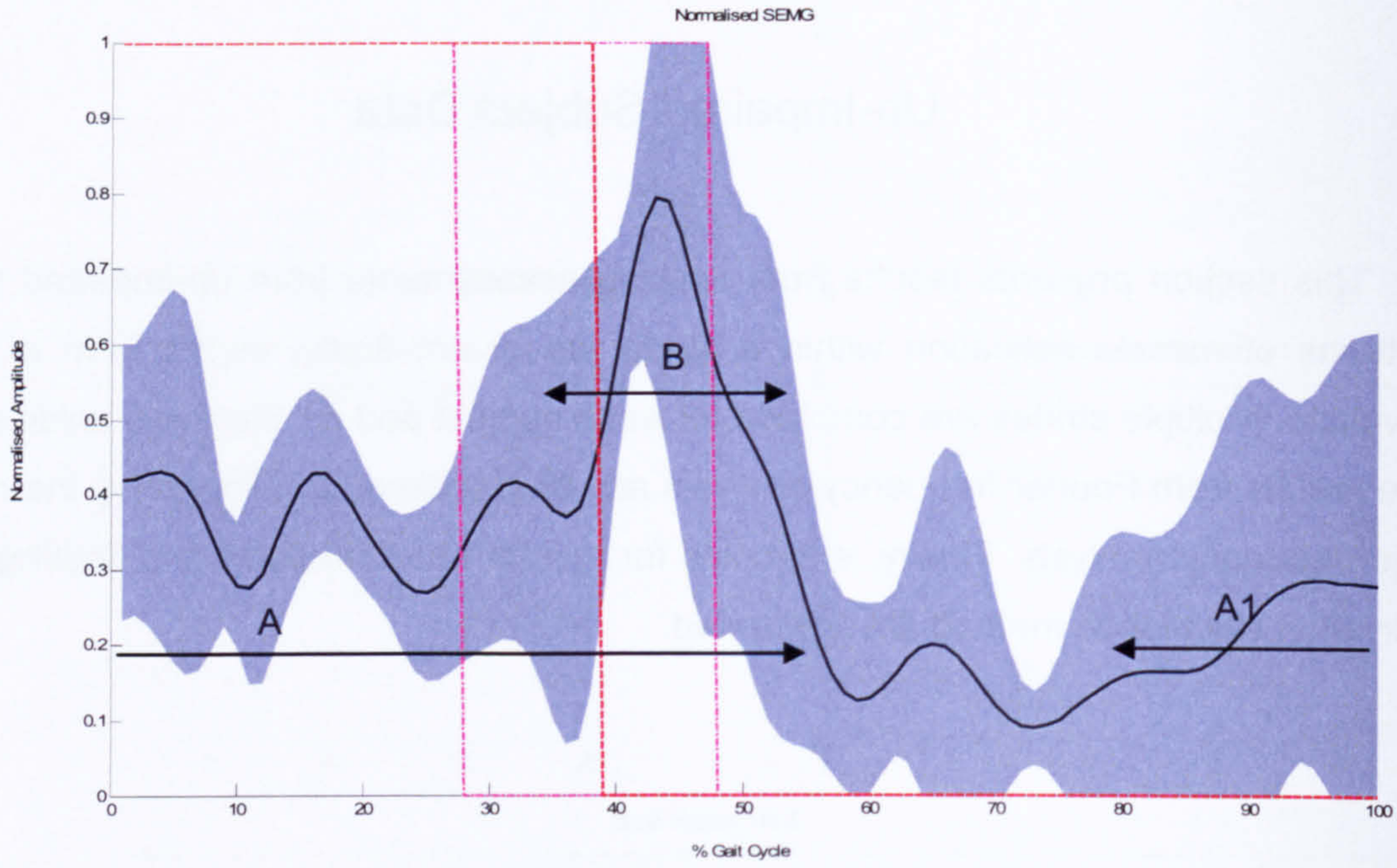

Appendix Figure 104 Normalised Linear Envelope of the Tibialis Anterior for NOP1. Activity occurs in the latter period of stance and is sustained throughout the swing phase; this is denoted by period A. There is a peak of activity after the mean location of foot-strike this occurs during the prominent burst denoted by period B.

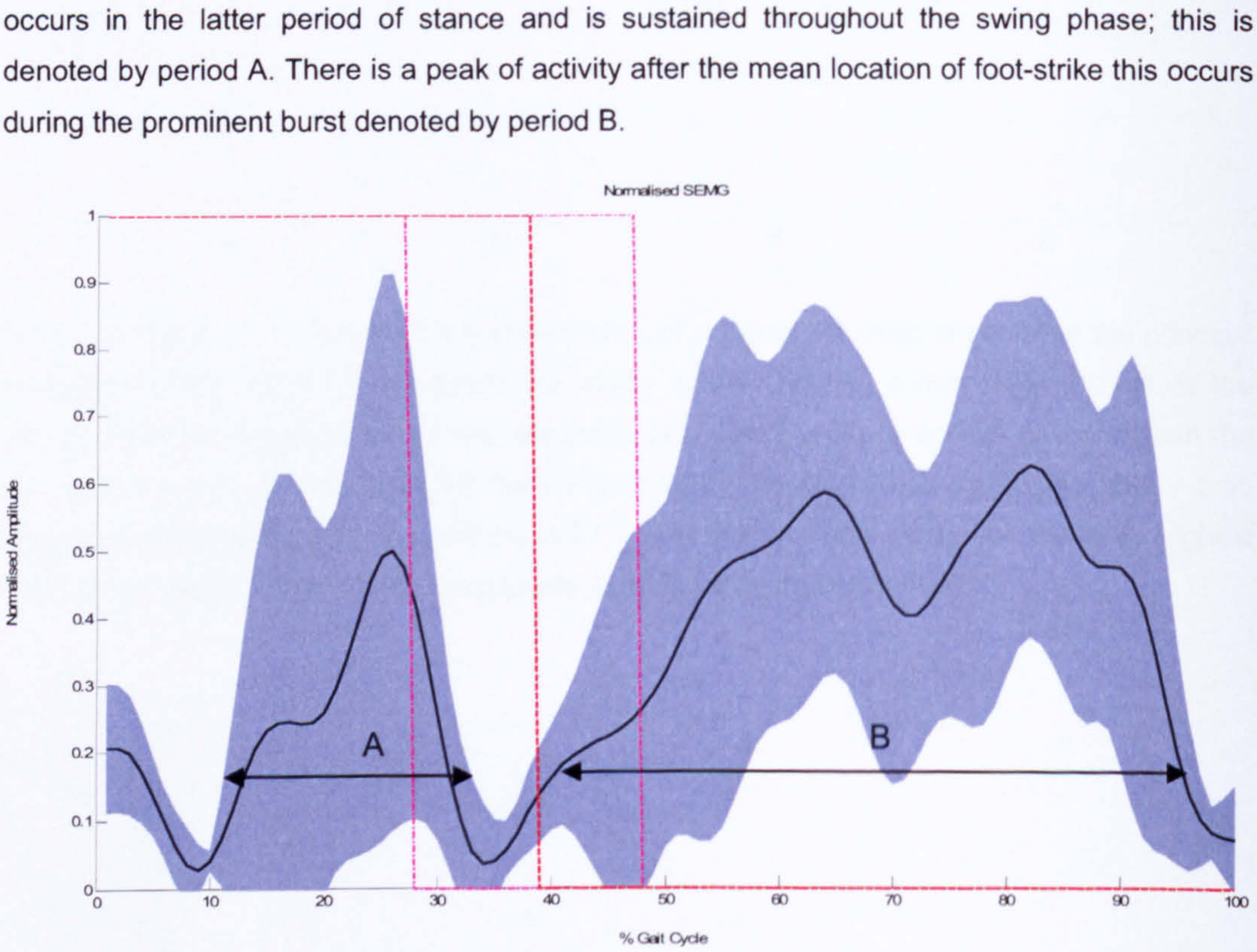

Appendix Figure 105 Normalised Linear Envelope of the Gastrocnemius for NOP1 shows normalised linear envelope and standard deviation of the gastrocnemius. There is a predominant burst of activity during the swing phase which is itself consists of a double burst of activity B. Contrary to expectation there is an additional prominent burst of activity between period A during the stance phase.

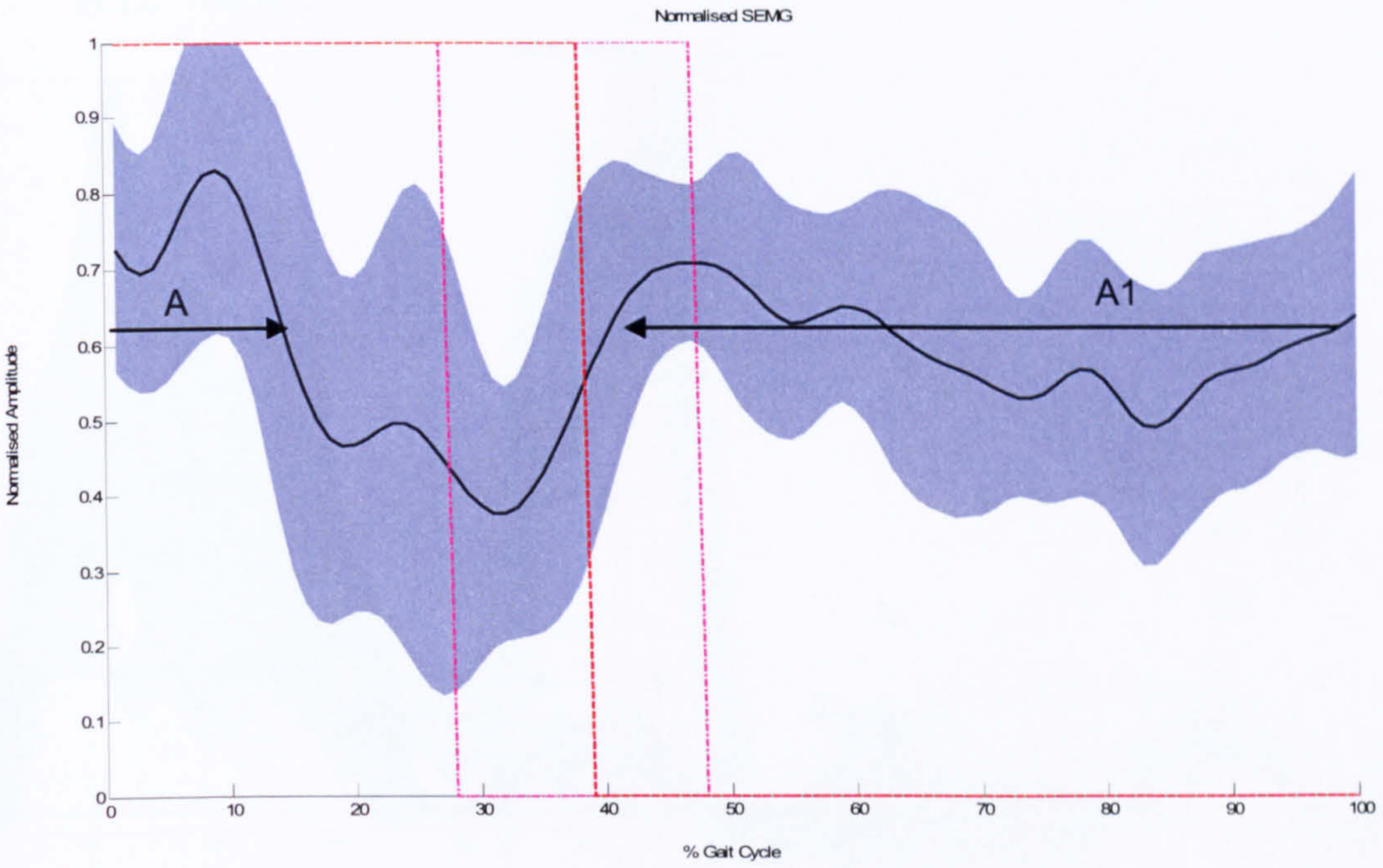

Appendix Figure 106 shows the normalised linear envelope activity of the soleus muscle for NOP1 Soleus activity can be seen throughout the stance phase and continues into the swing phase were there is an additional burst of activity. This is denoted by period period A

B.I.b NOP2

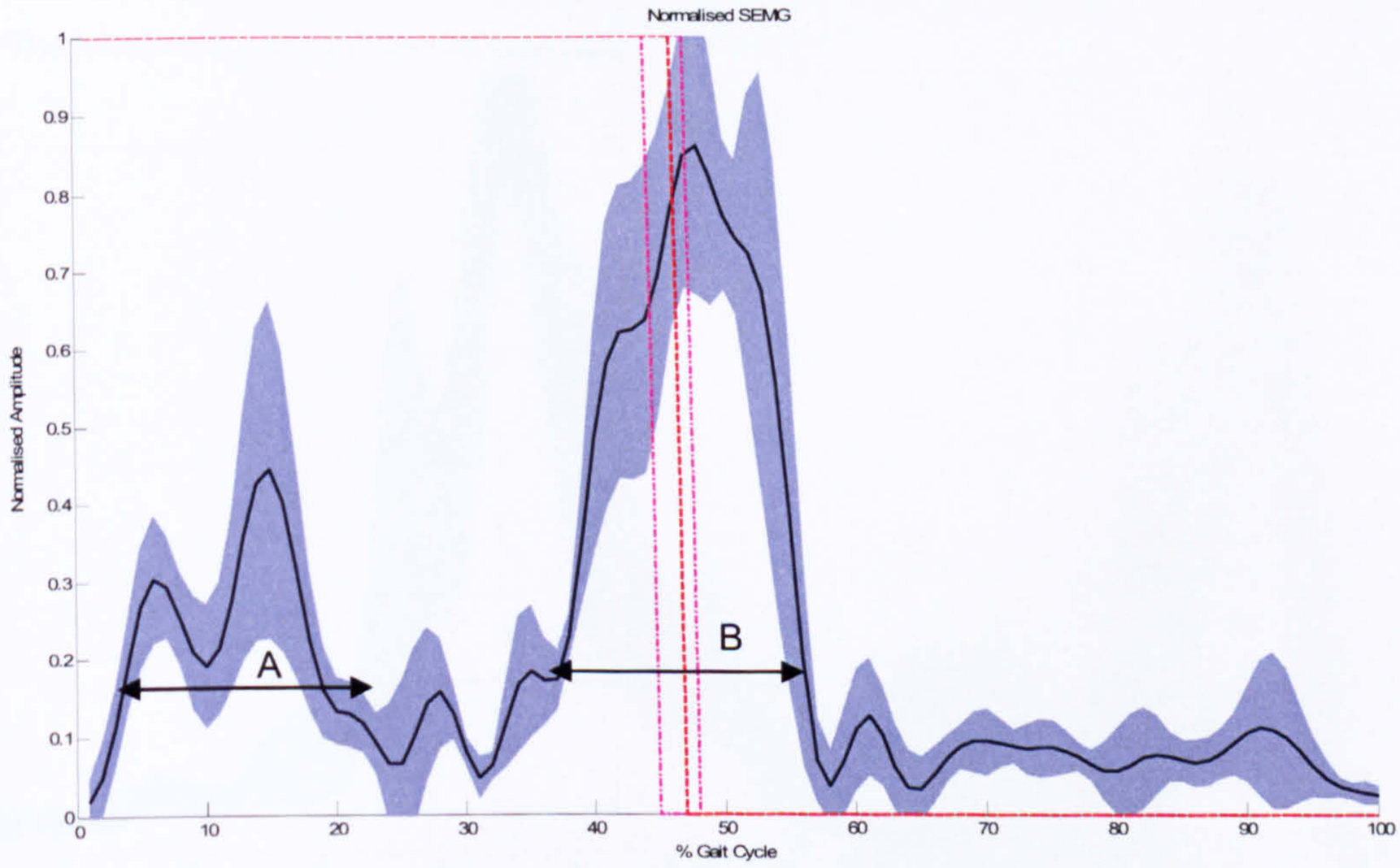

Appendix Figure 107 shows the normalised linear envelope representation of the tibialis anterior for NOP2 displays activity is isolated to the swing phase with little or no apparent increase in activity toward the end of the stance phase. The activity of the muscle appears as two prominent bursts occurring during period A and period B.

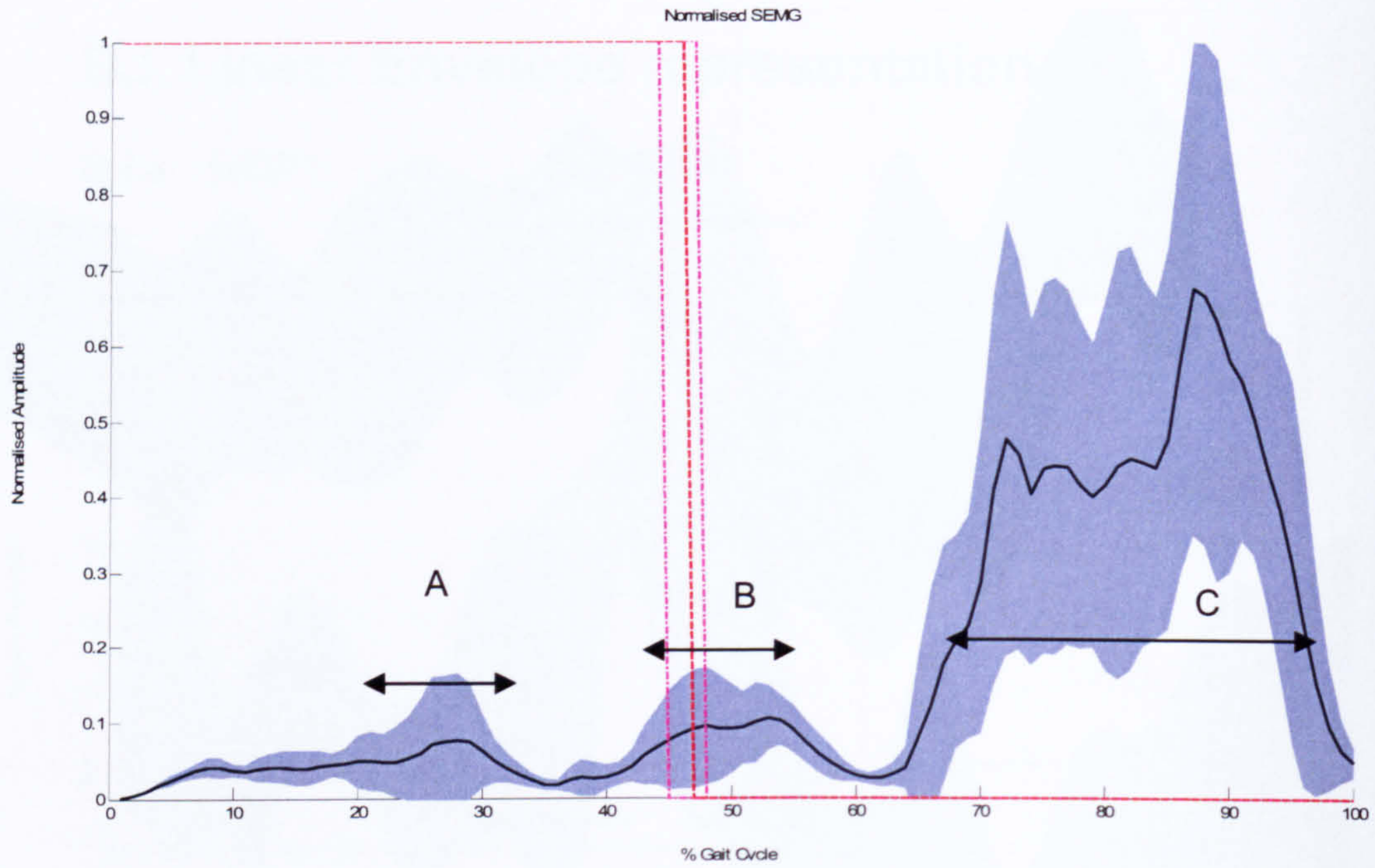

Appendix Figure 108 shows the normalised linear envelope representation of the gastrocnemius for NOP2 shows a single prominent burst of activity of the gastrocnemius in late stance shown by period C. Period B reveals a small increase in amplitude consistent the period of foot-strike. There is the suggestion of a very small amount of activity during mid swing which is not consistent across all strides represented by period A.

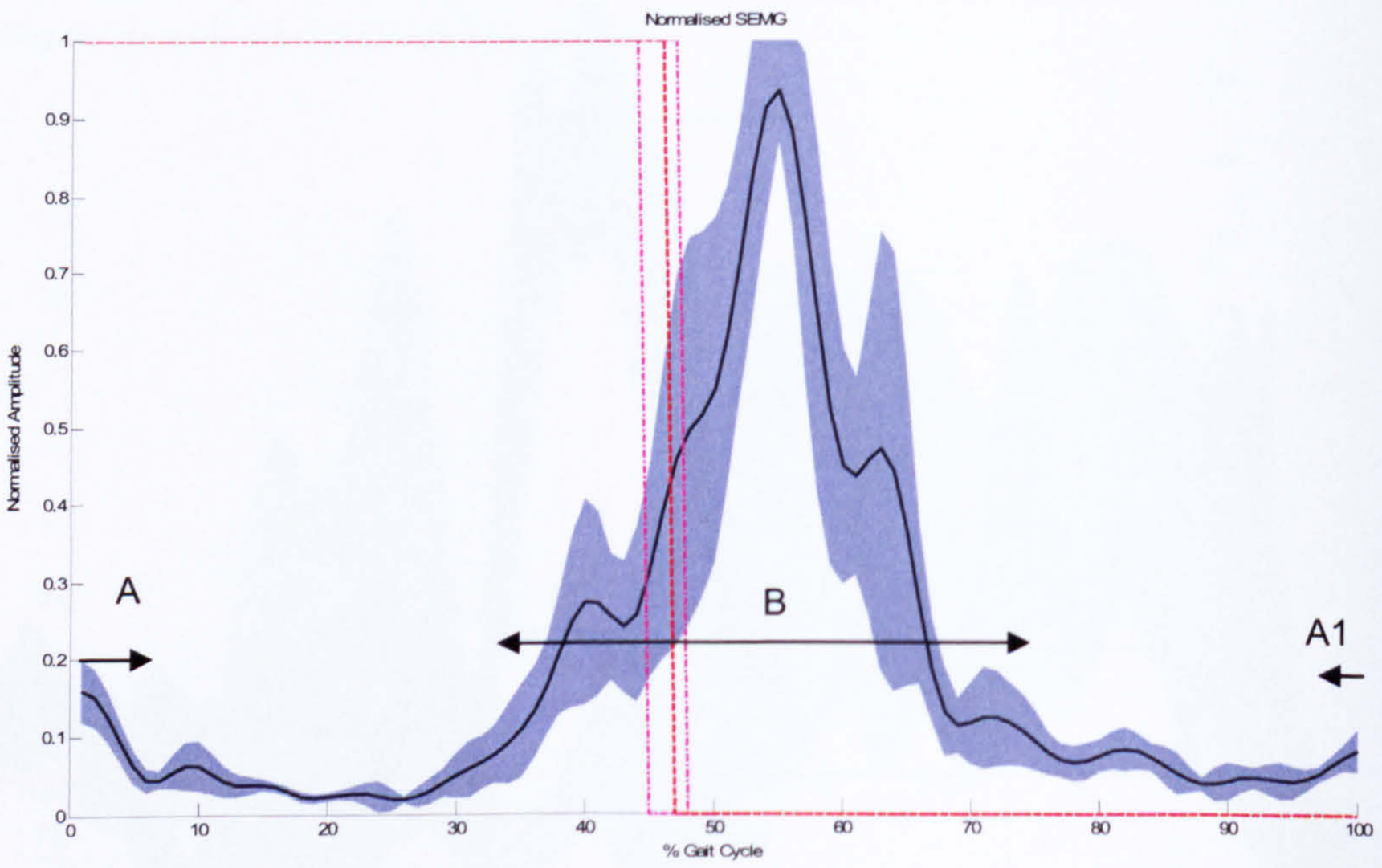

Appendix Figure 109 shows the mean linear envelope representation of the Soleus activity for NOP2. A prominent preiod of activity is shown be B that exists over the swing / stance transition. Period A shows a slight increase in activity that begins in terminal stance and early swing.

B.I.c NOP3

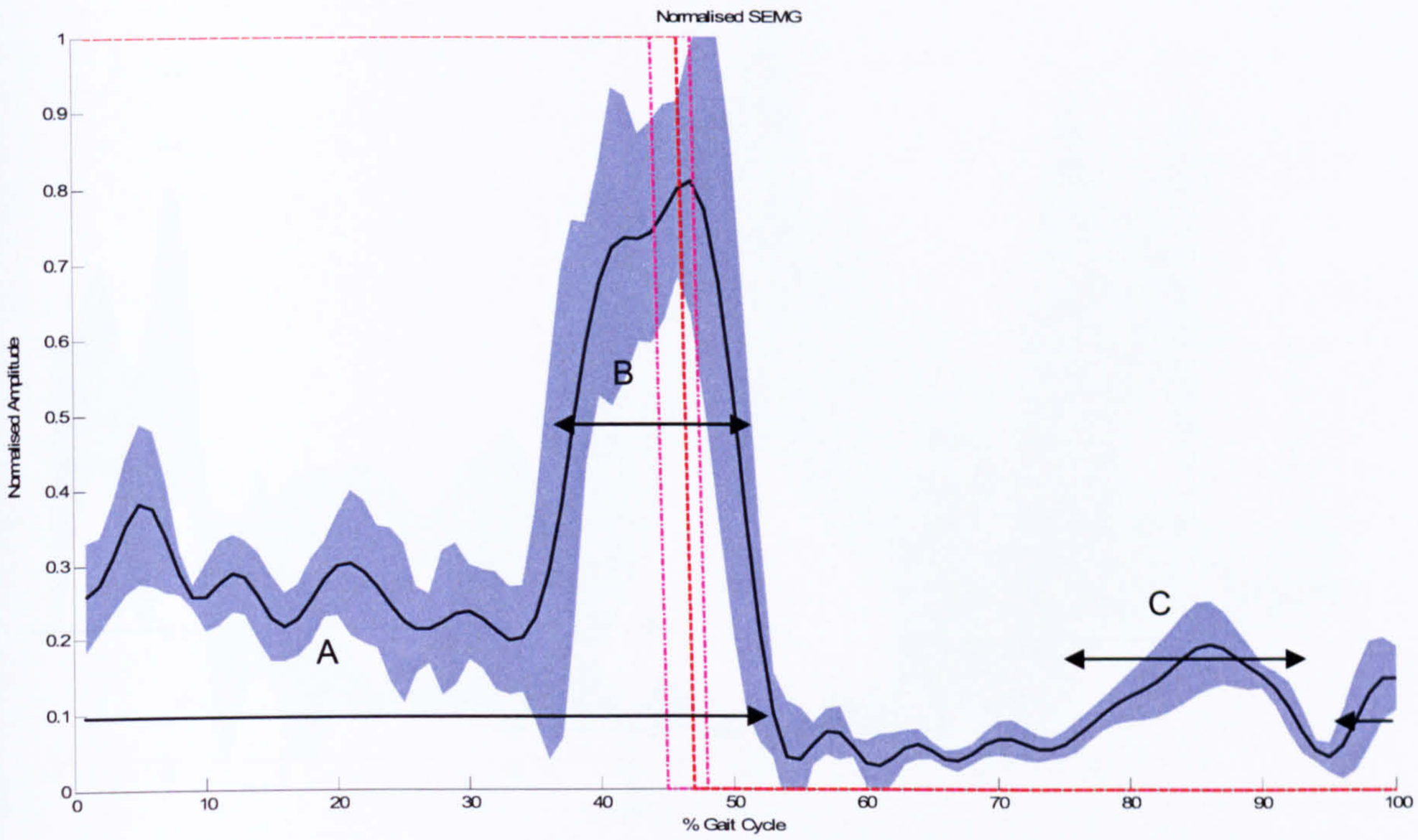

Appendix Figure 110 normalised linear envelope representation of the tibialis anterior activity for NOP3. During the swing phase activity increases from toe off to a maximum amplitude at foot strike and is shown by period A. A prominent burst of activity occurs during period B and relates to the preparation for foot-strike. There is a small degree of activity towards terminal stance as the foot is being prepared for the dorsiflexion component of early swing phase shown by period C. The initiation of period A can be seen at terminal stance.

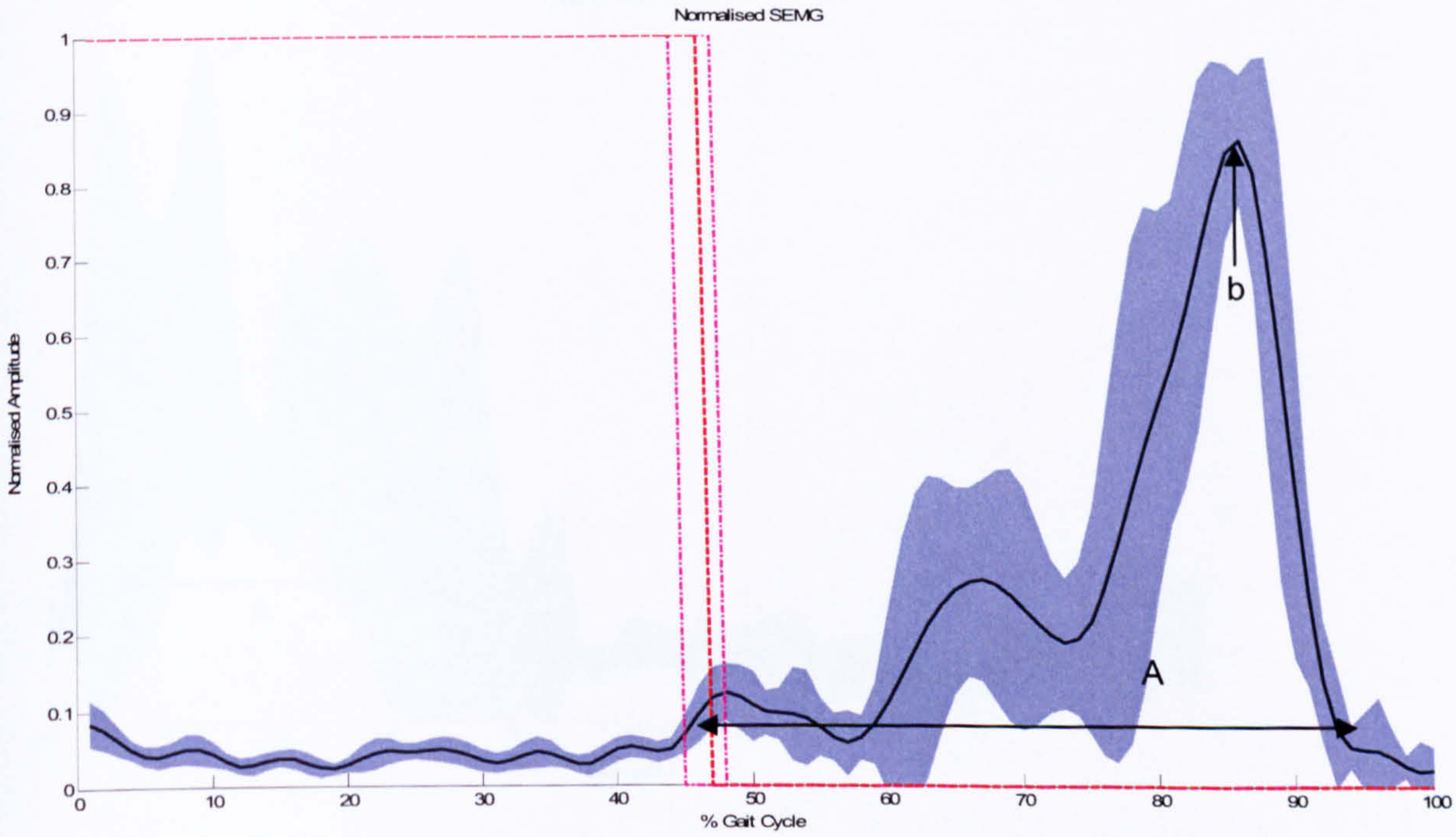

Appendix Figure 111 normalised linear envelope representation of the gastrocnemius for NOP4. Activity can be seen to start at foot strike and continue throughout period A. The activity peaks at point b where the activity then diminishes rapidly to zero just prior to toe off and during the transference of the body's weight to the contralateral leg.

B.I.d NOP4

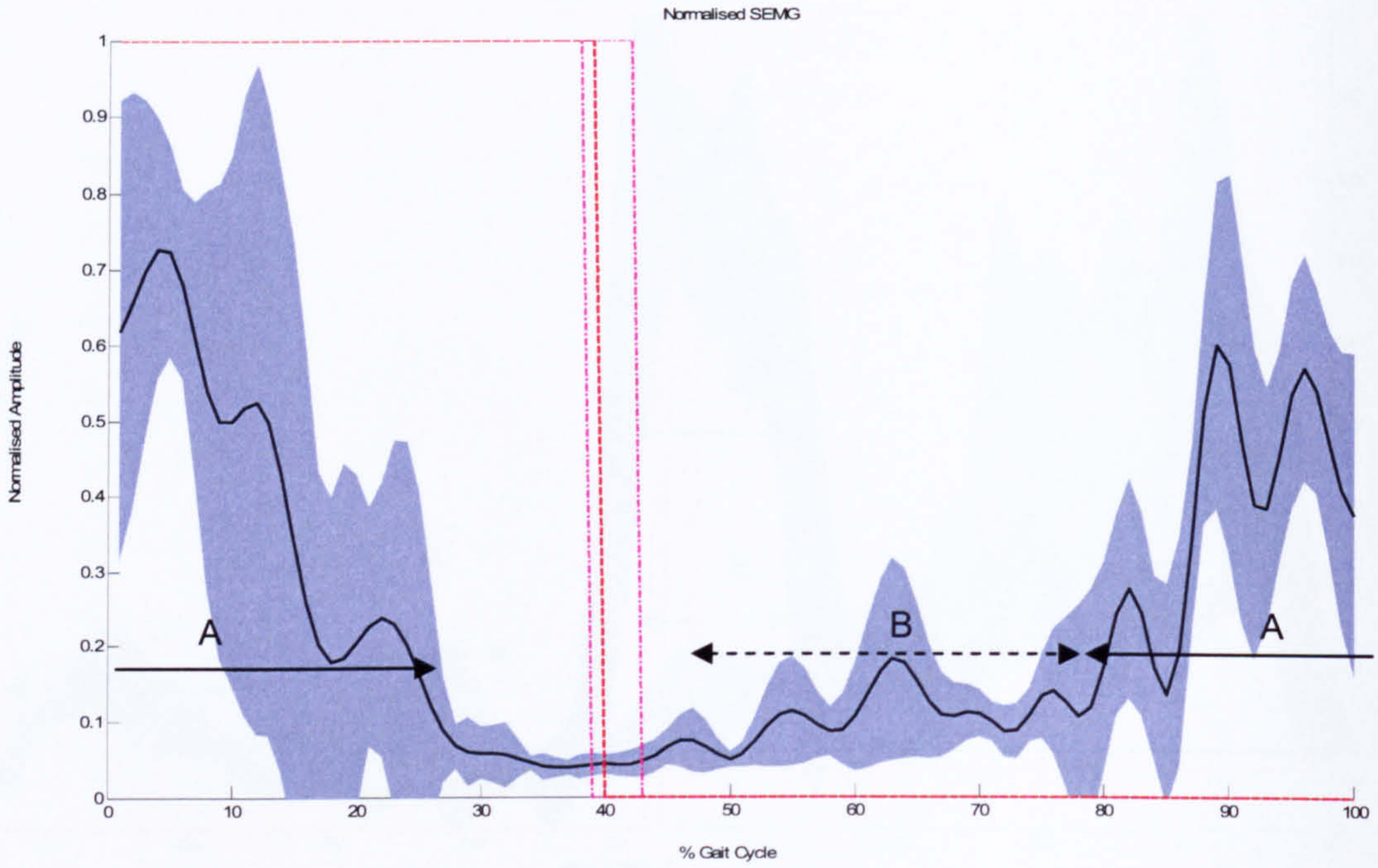

Appendix Figure 112 Linear envelope representation of Tibialis Anterior for NOP4 Activity is observed during the swing phase of gait, denoted by period A, discontinuing just prior to foot strike. Activity is not present during the early to mid stance phase then increases in terminal stance to toe off. The initial onset of this activity is shown by period B and subsequently the prominent onset of period A.

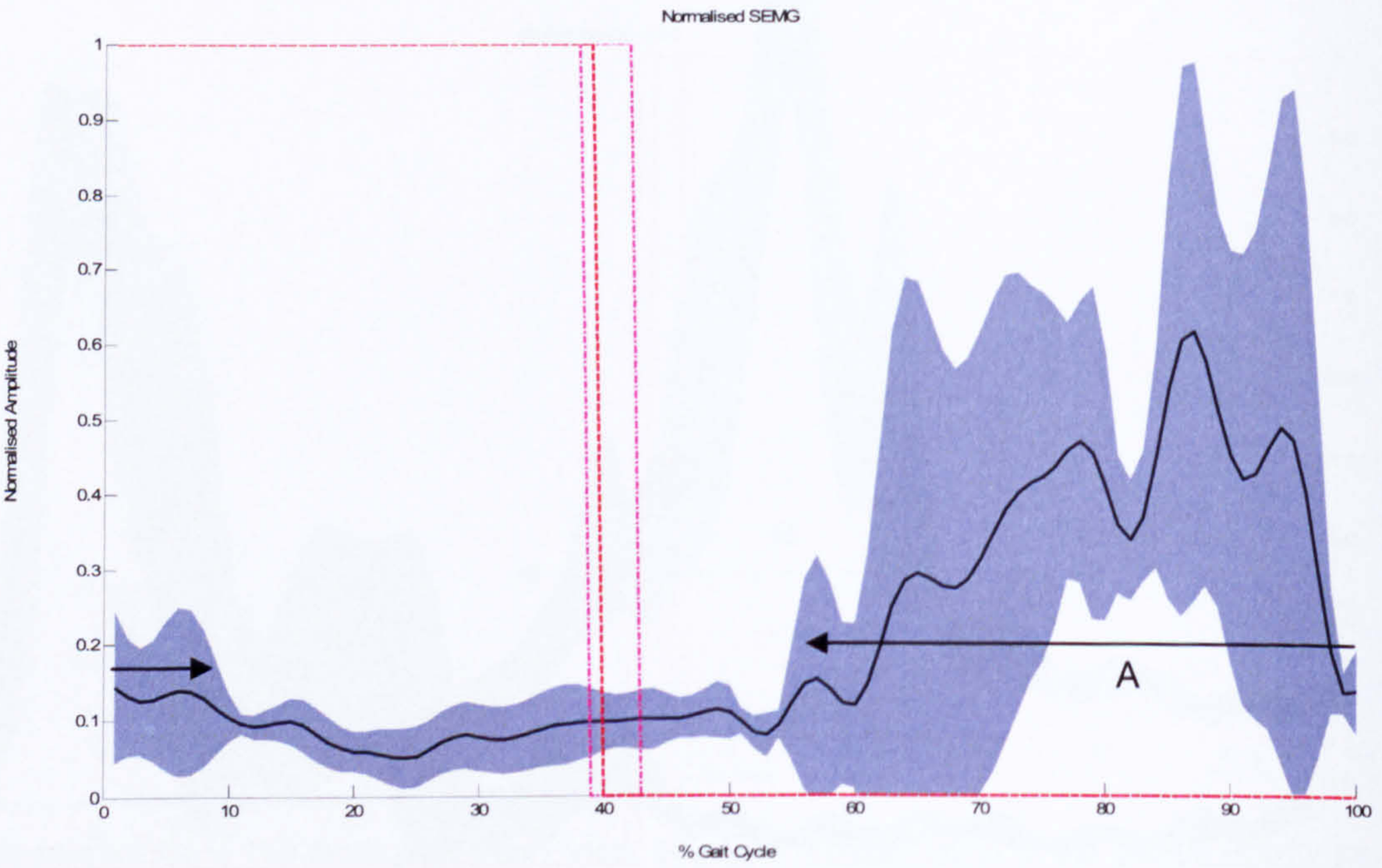

Appendix Figure 113 Linear envelope representation Gastrocnemius NOP4 shows activity for the gastrocnemius during the entire stance phase, indicated by period A that continues subtlety into the swing phase. there is little apparent activity during the remainder of the swing phase.

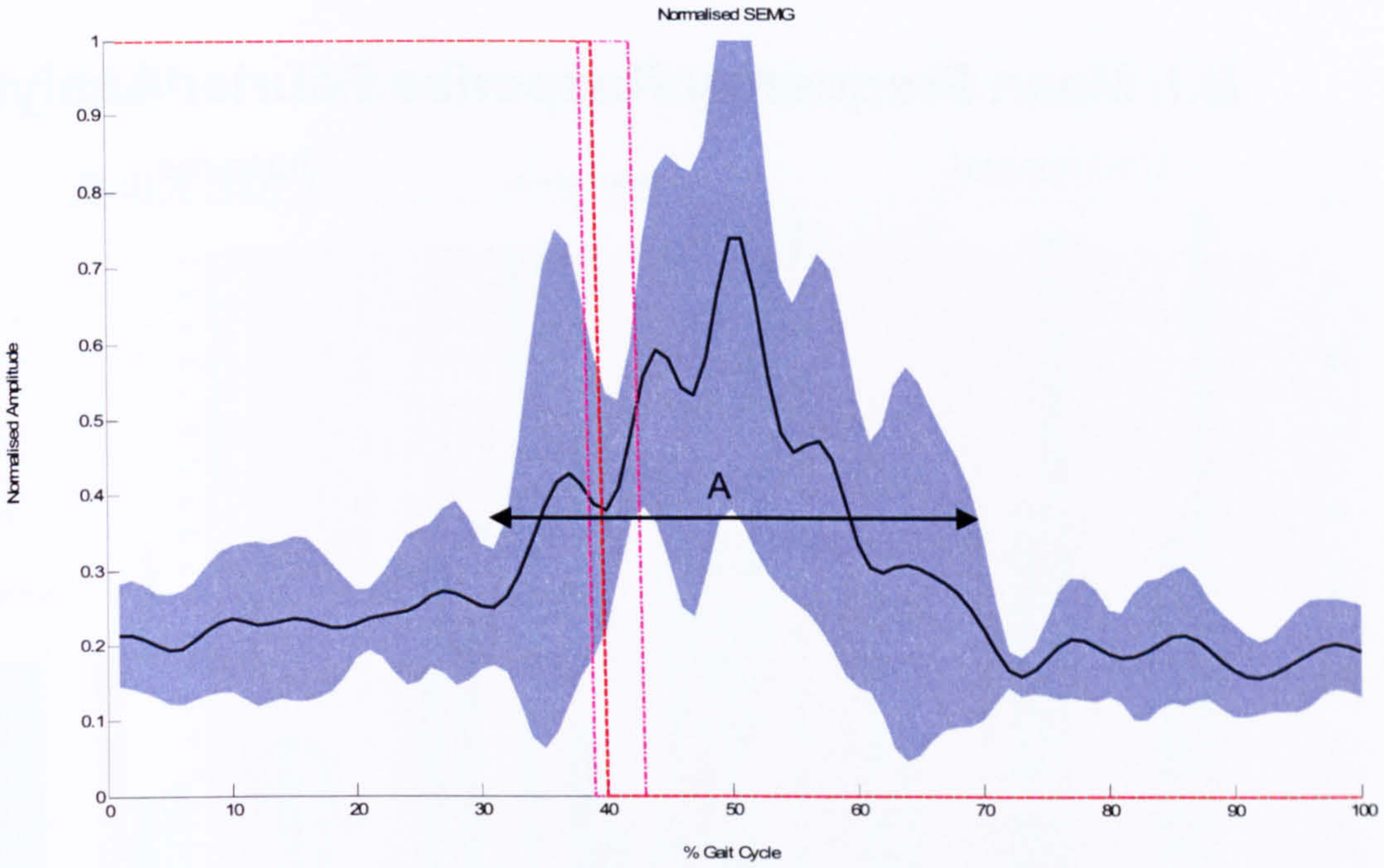

Appendix Figure 114 Linear envelope representation of the Soleus for NOP4. A small level of activity is seen in throughout the gait cycle; however, the prominent burst of activity begins just prior to foot-strike and is denoted by period A.

B.II Mean Frequency Response Fourier Analysis

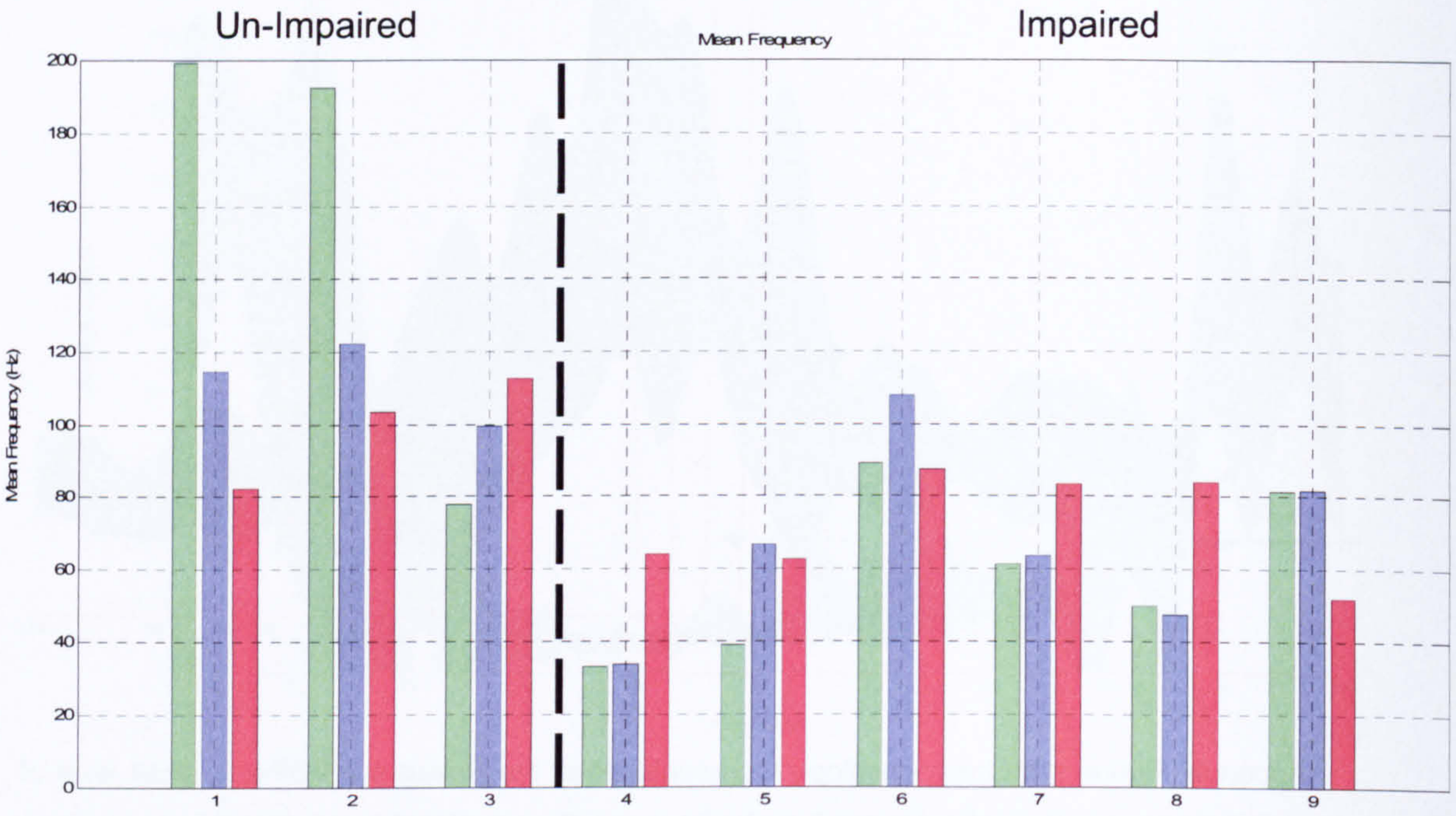

Appendix Figure 115 Mean frequency of the tibialis anterior (green), Gastrocnemius (Blue) and Soleus (Red) generated using Fourier analysis Results from Fourier frequency analysis are shown in graph 12. The graph displays results from three un-impaired subjects and six impaired subjects. Each group (1-9 x-axis) represents average SEMG frequency from three muscles and from an individual over four strides from one walk. The tibialis anterior is shown in green, the gastrocnemius is shown in blue and the soleus muscle is shown in red. The broken black line differentiates between the un-impaired subjects (left) and impaired subjects (right).

B.III Time-Frequency Analysis

B.III.a NOP1

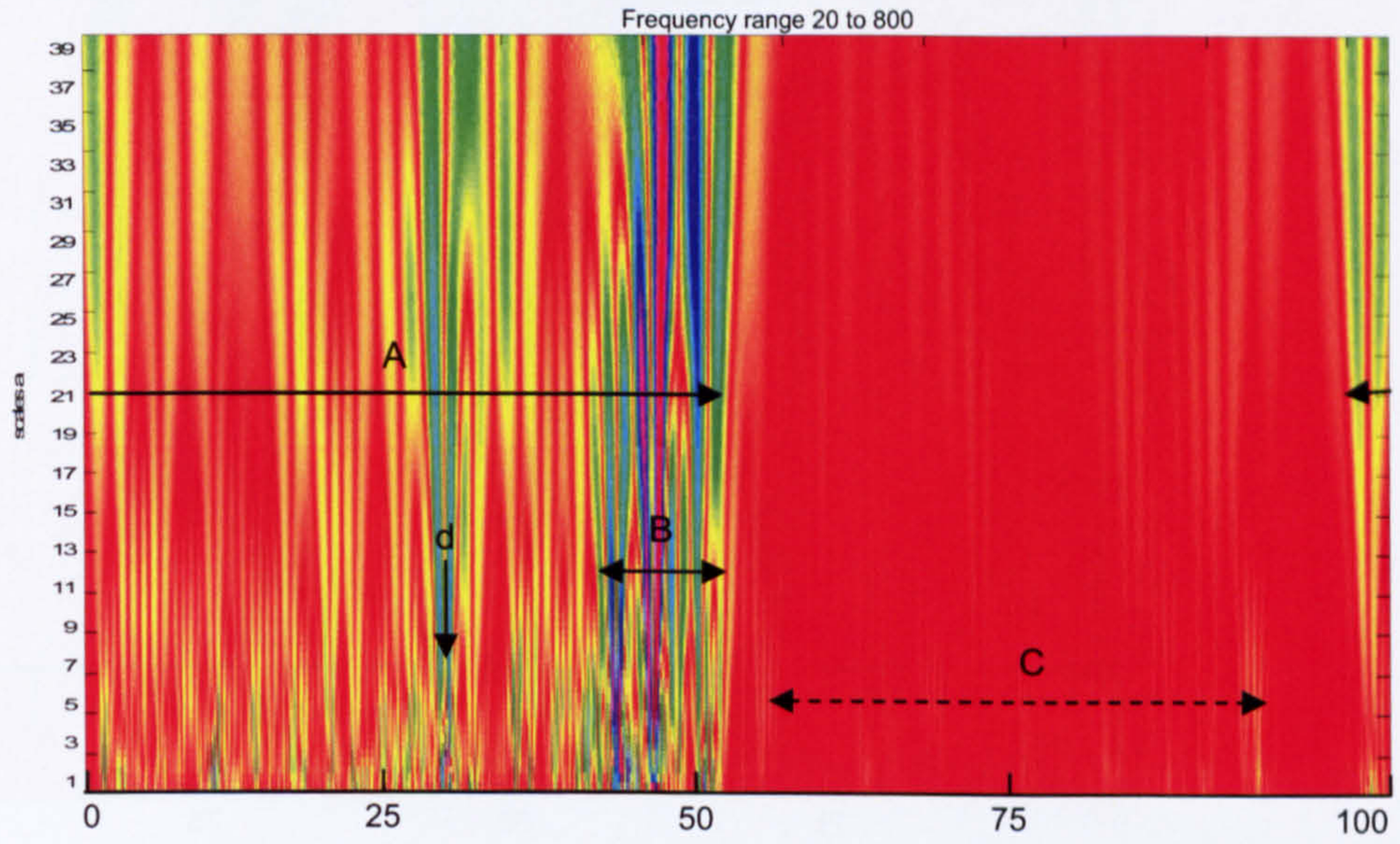

Appendix Figure 116 shows the time-frequency representation of the tibialis muscle activity for subject NOP 1. Activity can be seen over the swing phase and just prior to toe off, this is represented by period A. The highest frequencies coefficients appear at foot strike and exist originate at the high frequency scale, shown by period B. Prior to foot-strike an additional prominent burst is shown by point d. There is continuous higher frequency activity throughout swing phase. Period C shows low level activity across the frequency bands during the stance phase.

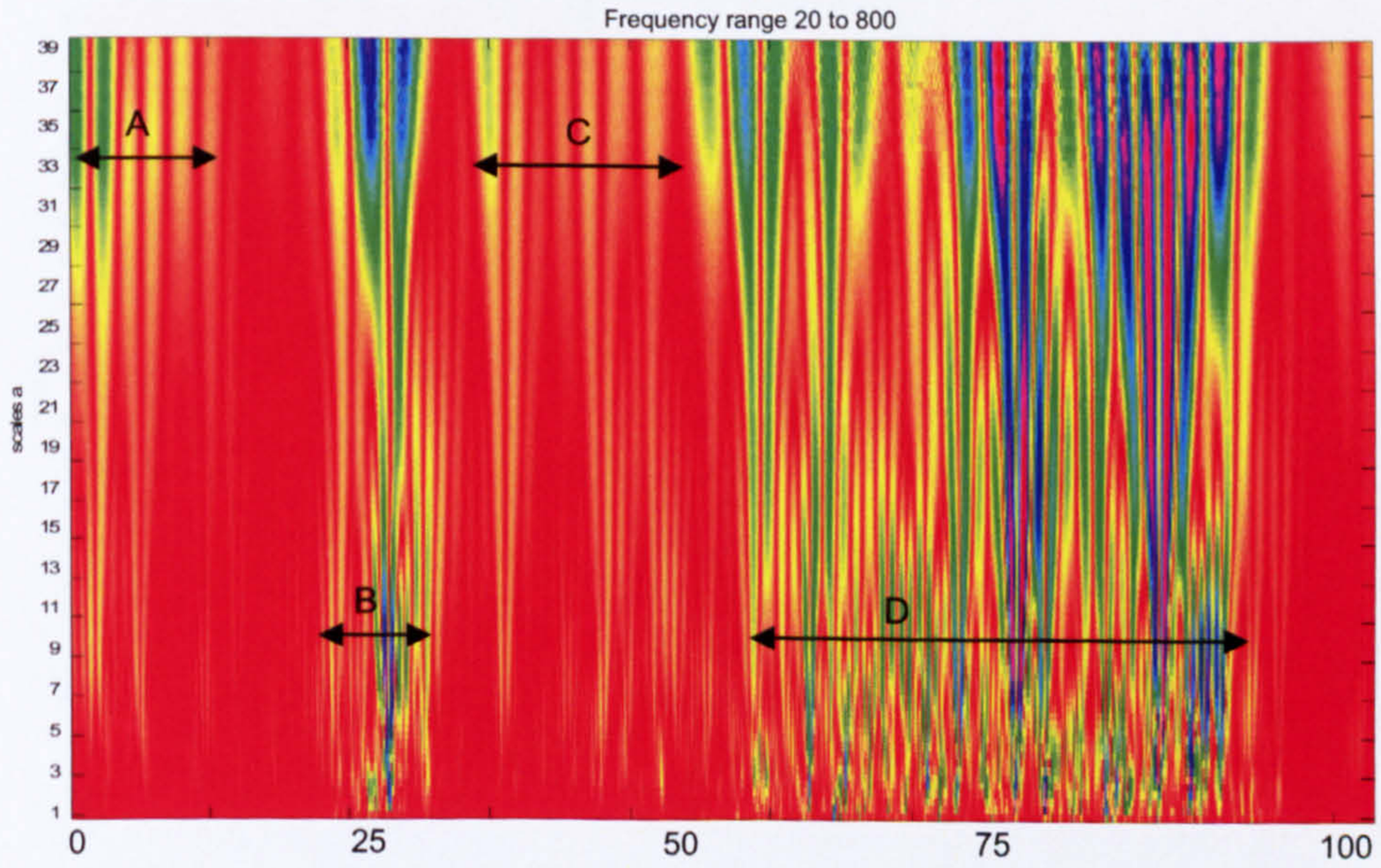

Appendix Figure 117 similarly shows the time-frequency representation of the gastrocnemius muscle activity. A prominent high frequency component can be seen during mid swing and shown by period B. During the stance phase, activity can be seen across the frequency bins peaking at mid stance and terminal stance were prominent large scale (low frequency) coefficients are visible as well as high frequency coefficients, shown by period D. There are low

amplitude coefficients present in early swing, represented by period A, and in the vicinity of foot-strike, shown by period C.

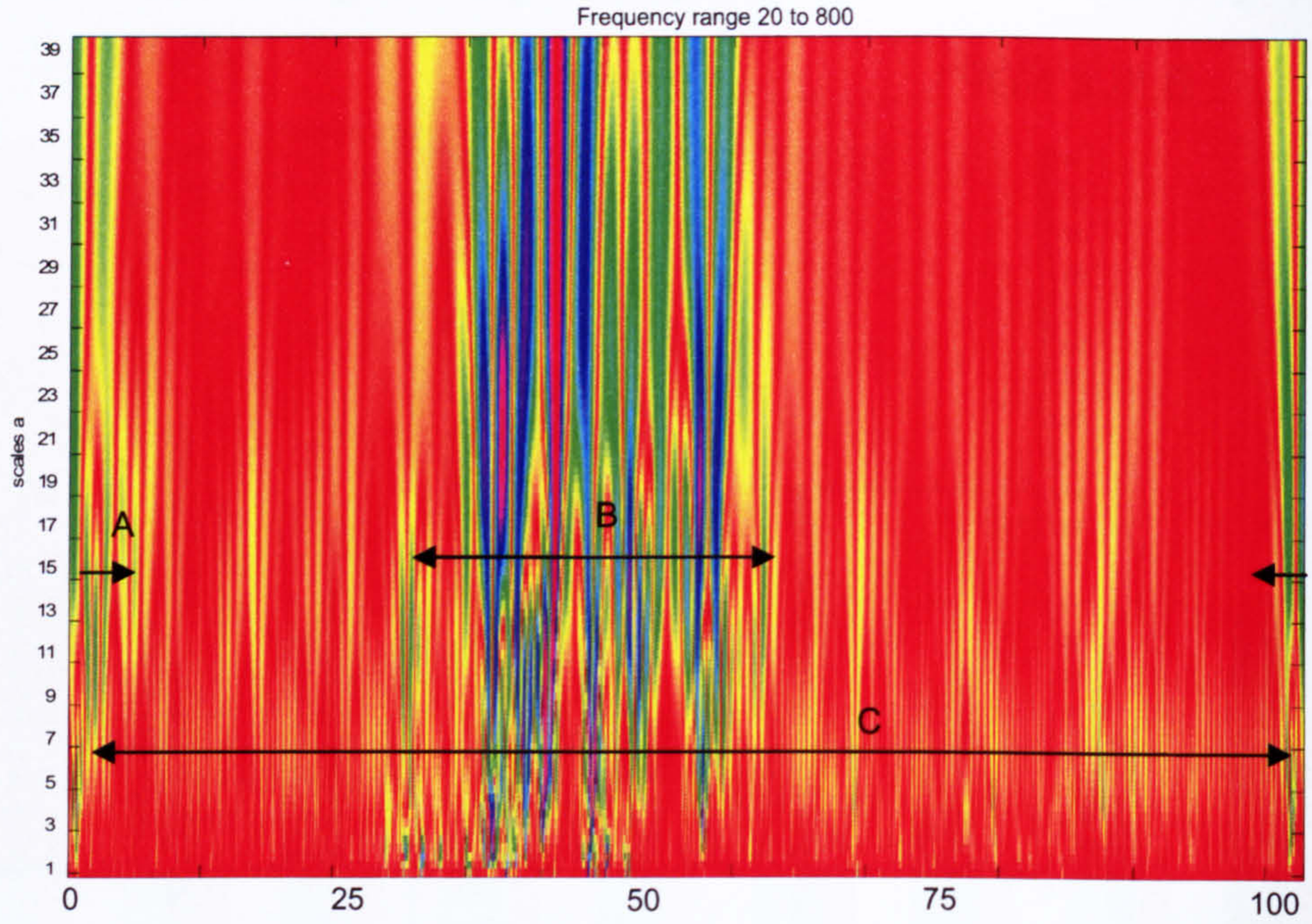

Appendix Figure 118 represents the time-frequency representation of the soleus muscle activity. The most prominent activity that spans all frequency bins occurs at approximately foot-strike spanning the swing, stance phase transition, shown by period B. There is also low amplitude activity across the entire stride, shown by period C, with two moderate amplitude bursts occurring at the beginning and end of the gait cycle, shown by period A.

B.III.b NOP2

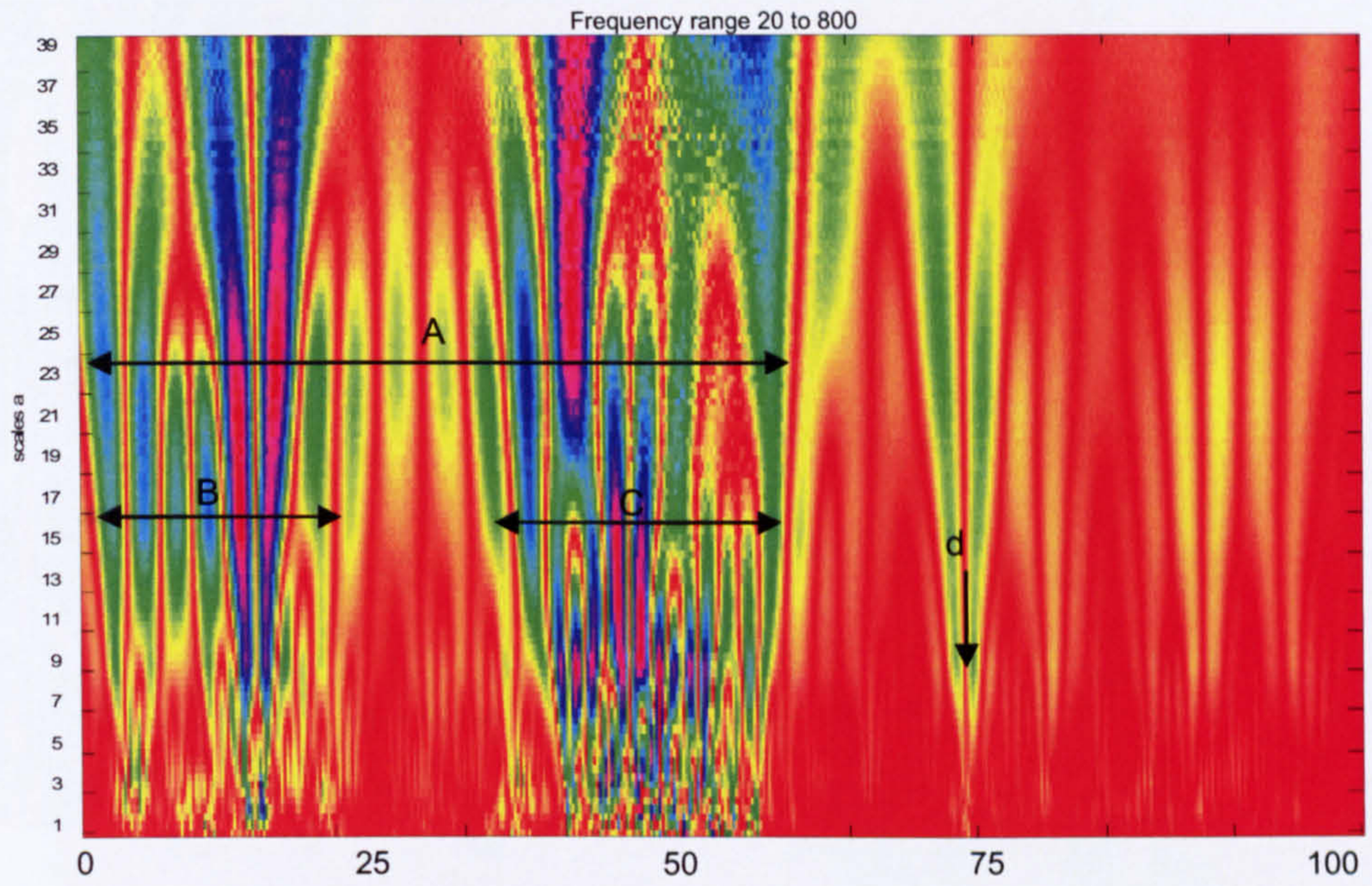

Appendix Figure 119 displays the time-frequency representation for the tibialis anterior muscle activity for subject NOP 2. Activity can be seen in the swing phase, period A, consisting of two periods of high frequency activity, periods B and C, the second of these being more prominent. The second burst contains the largest coefficients at lower scales, although continuous and large coefficient values are found at the highest frequencies unlike the first burst where continuous activity is not seen until the lower frequency bands. There is a single burst of activity represented by point d during the stance phase.

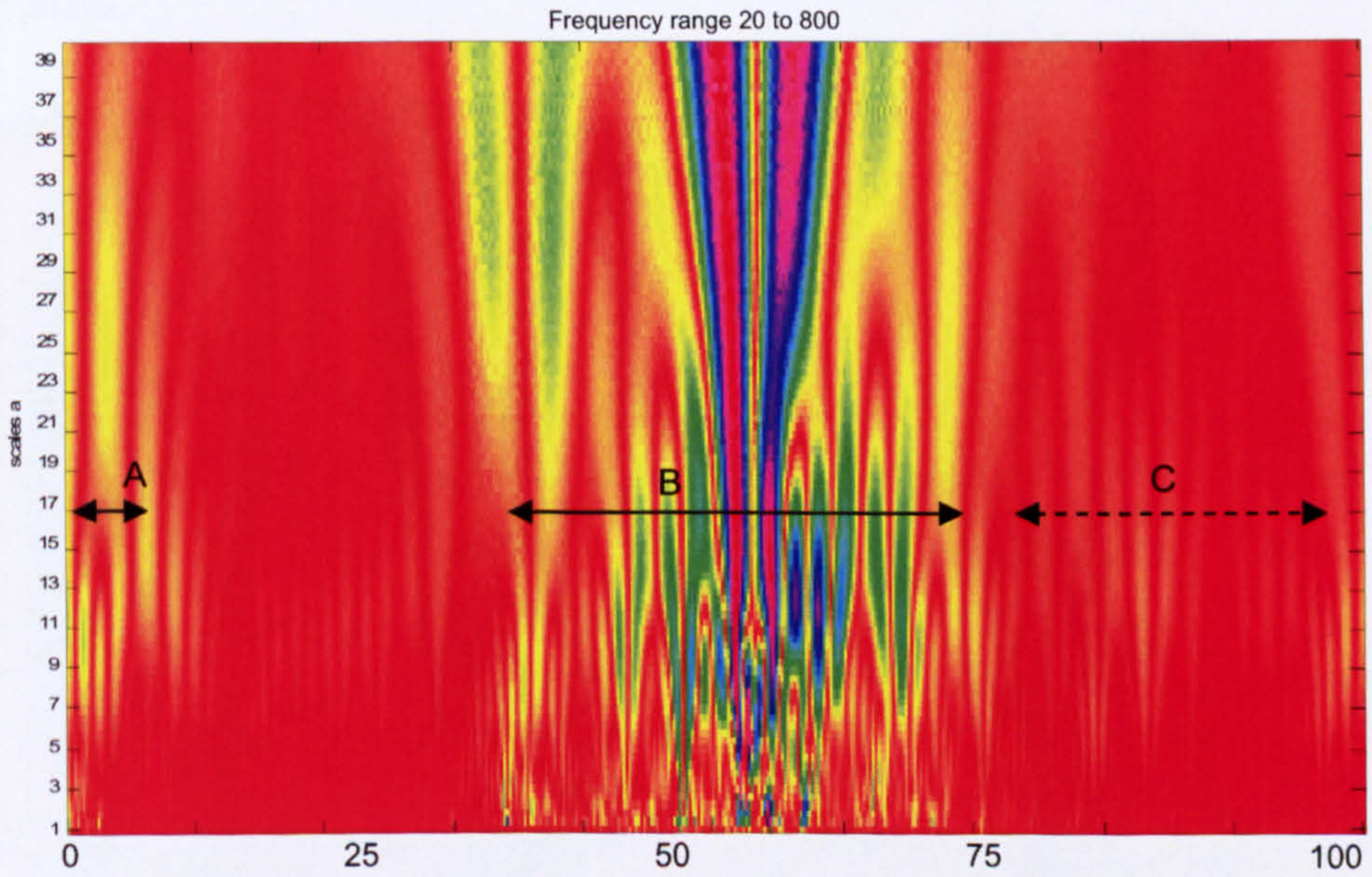

Appendix Figure 120 shows time-frequency representation for the soleus muscle activity of subject NOP2. High frequency activity is seen to increase from the swing phase peaking at approximately foot strike and then reducing during early stance, period B. The largest amplitude coefficients are seen at the lowest frequencies although continuous mid range frequency coefficients are also visible. Period A shows a small period of activity early in the stance phase.

Very low amplitude activity can be seen in the remainder of the stance phase, shown by period C.

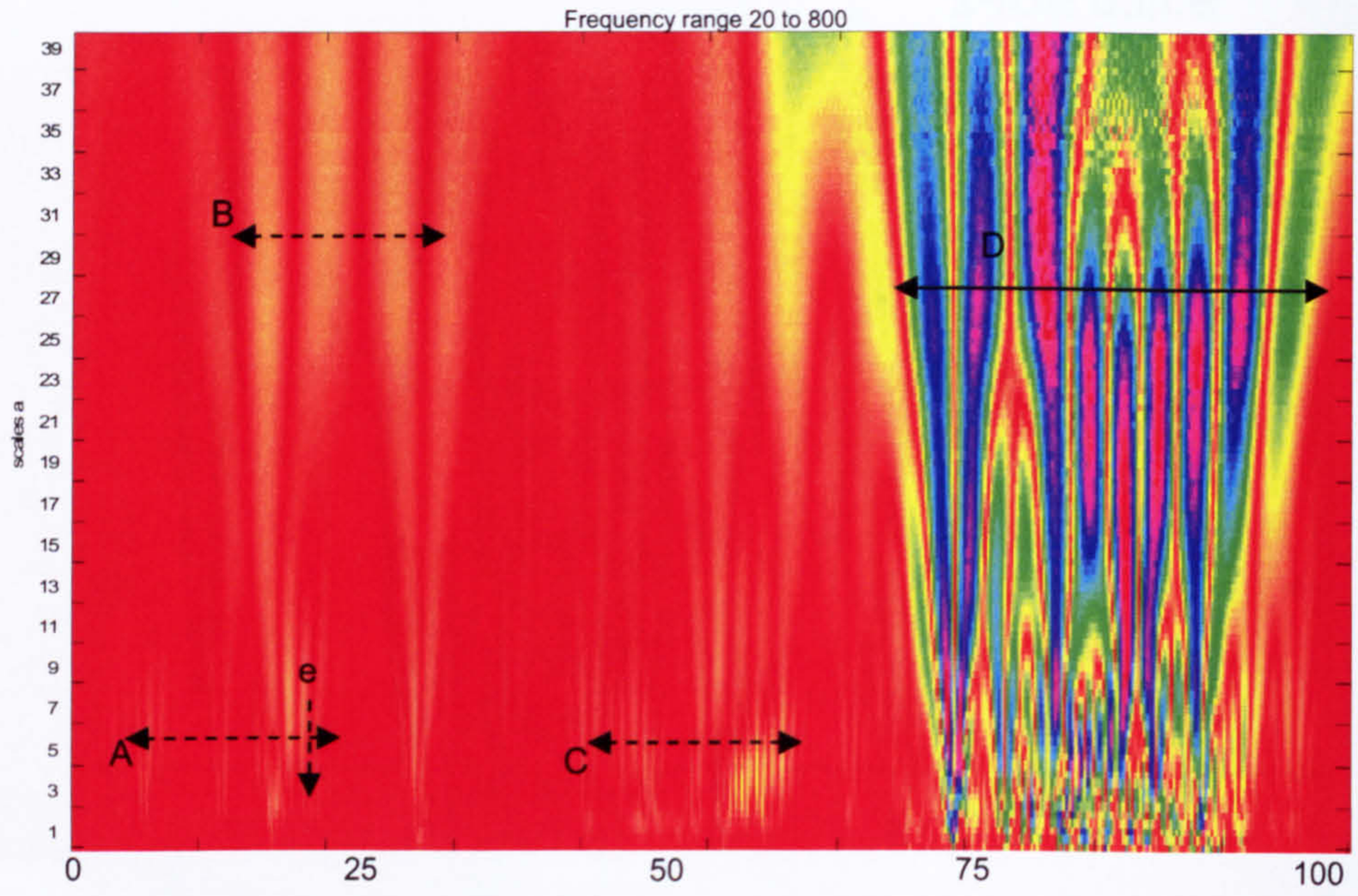

Appendix Figure 121 displays the time-frequency representation of the gastrocnemius muscle activity for NOP2. Continuous large value coefficients are visible at the lowest scale values and are present across all frequency bins, period D. The large-scale coefficients are present during early to terminal stance in the low frequency regions and contracted within the high frequency regions. Low levels of activity are also present in periods A, B and C. Periods A and C reveals high frequency activity where period B shows low frequency activity originating from point e and activity in period A.

B.III.c NOP3

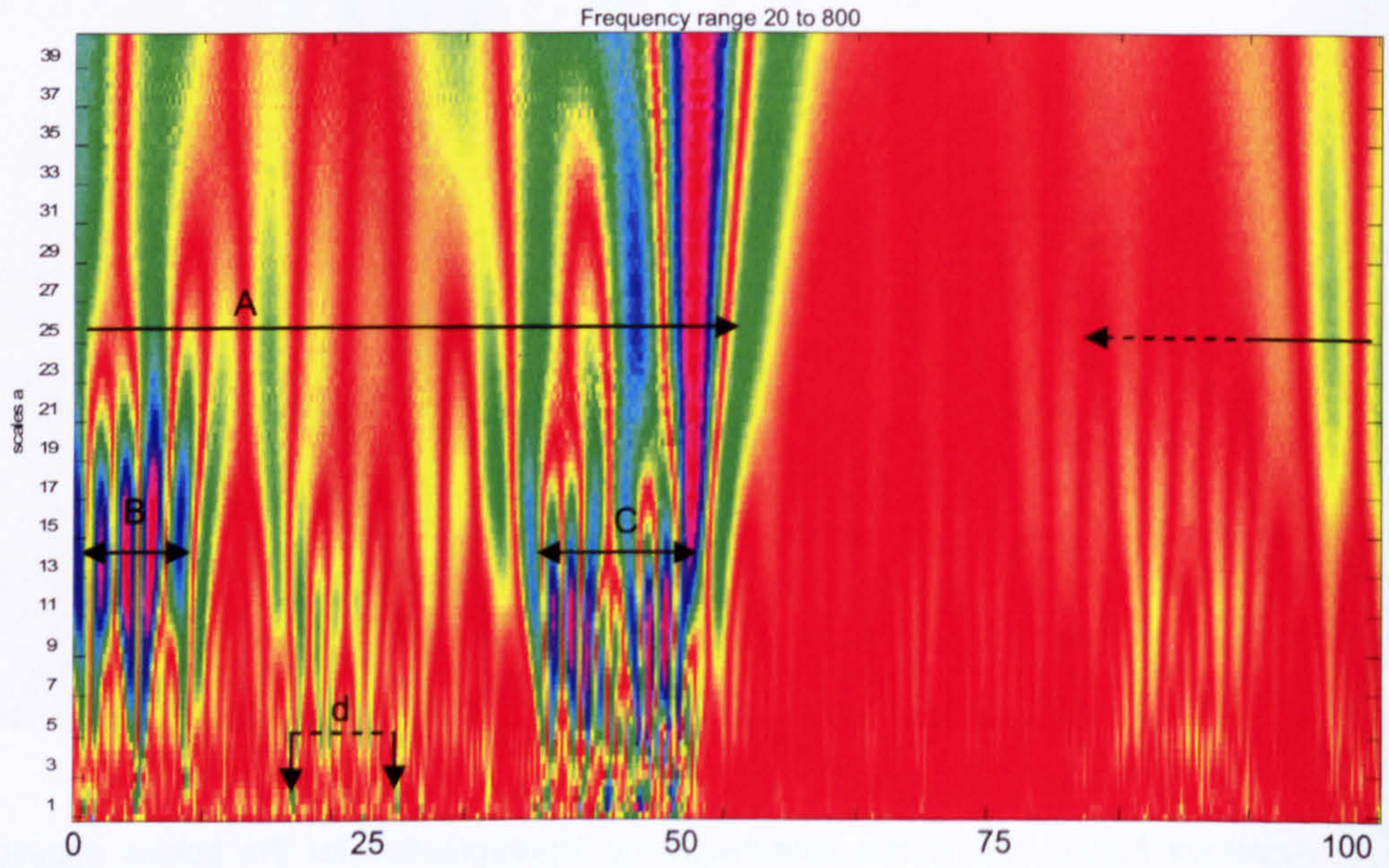

Appendix Figure 122 shows the time-frequency representation of the tibialis anterior muscle activity for NOP3. One prominent burst can be seen during period A which begins in the final period of the stance phase. This activity begins as relatively high frequency activity though low in coefficient amplitude. The activity shows large coefficients in the moderate to high frequency

bands. In the low frequency bands the activity is present over period A. The first burst of activity on the gait cycle is during period B, where again large coefficients can be seen in the moderate high frequency bands. This activity appears to extend to the high frequency bands as short epoch bursts, example points d.

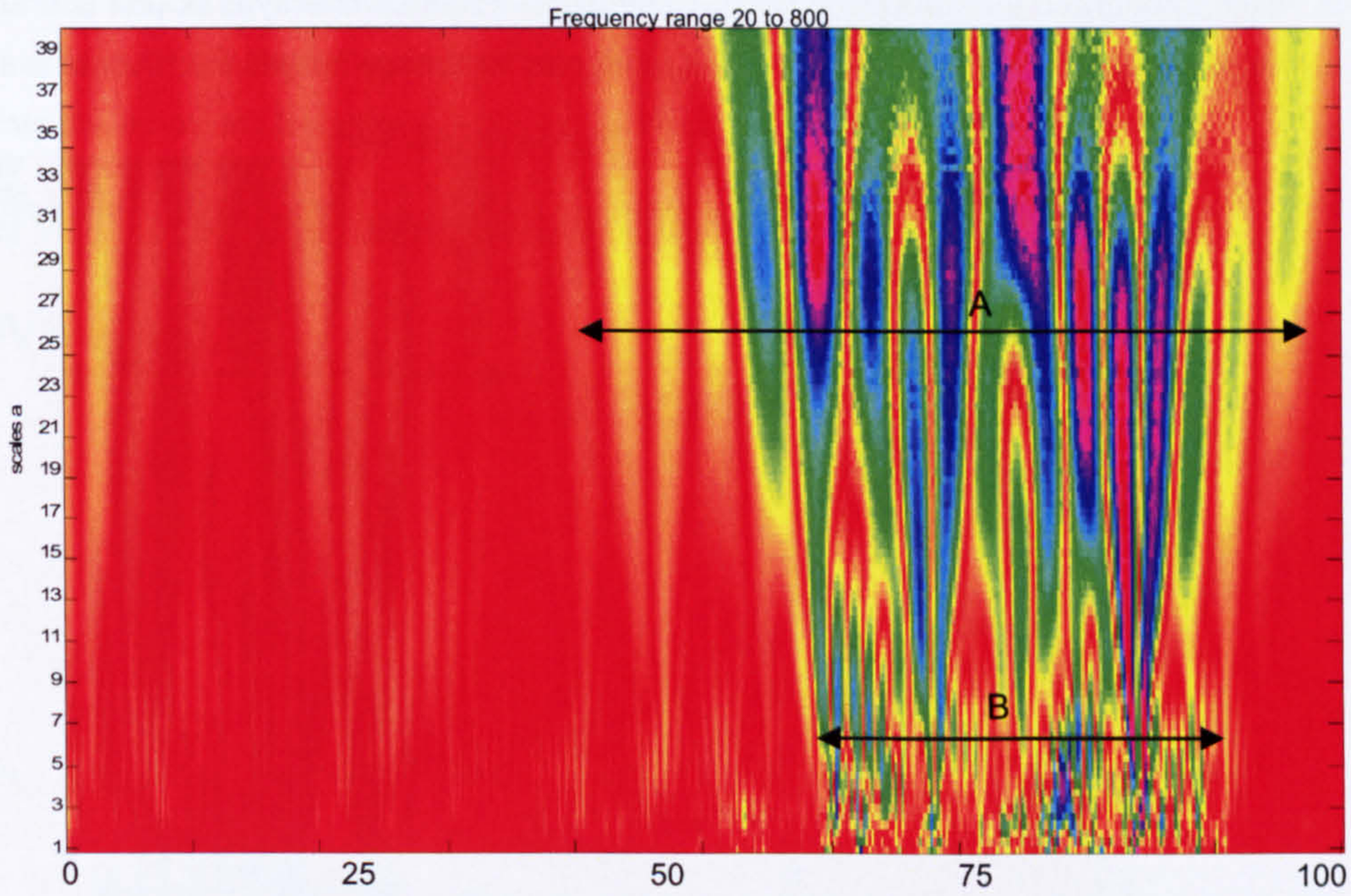

Appendix Figure 123 shows the time-frequency representation of the gastrocnemius muscle activity for NOP3. There is one prominent burst, shown by period B, with respect to the high frequency band. In the low frequency range, the activity extends and is shown by period A. High frequency activity seen in period A has the largest coefficients present as short epochs, in the low frequency bands the large coefficients are almost continuous. Low level activity can be seen in the swing phase.

B.III.d NOP4

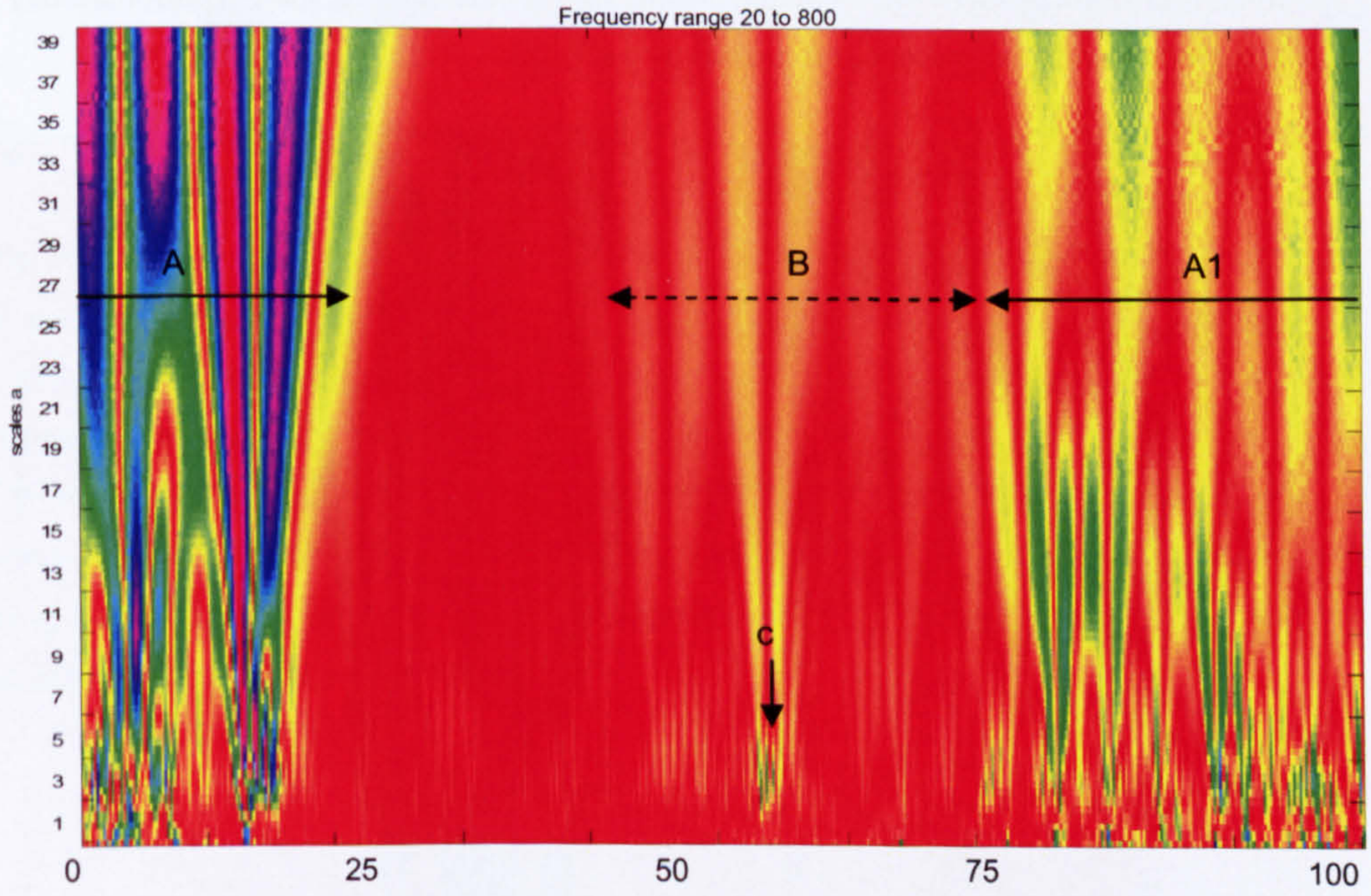

Appendix Figure 124 shows the time -frequency representation of the tibialis anterior muscle activity for NOP4. Three prominent bursts of activity can be seen. The first of which (Period A)

consists of two separate bursts when viewed with respect to the high frequency bands. In the low frequency bands large value coefficients exist over period A. A short epoch burst is seen at point c, the moderate amplitude coefficients exist throughout all frequency bands but is most prominent in the moderate high band. Over period B and A1 moderate amplitude coefficients exist throughout the frequency bands. The high frequency activity is at first sporadic becoming more continuous towards toe-off. In the moderate frequency ranges the reverse is seen.

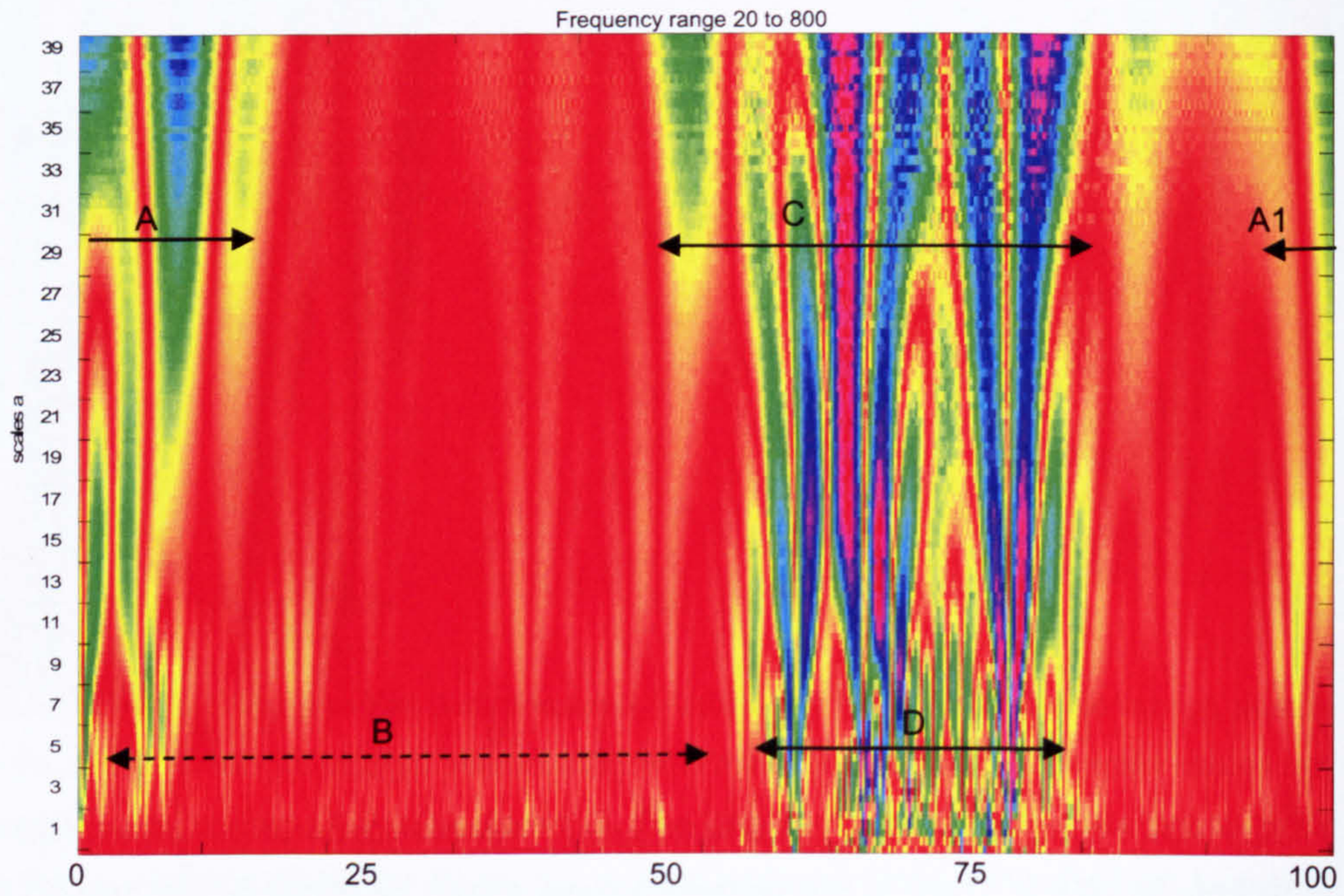

Appendix Figure 125 shows the time frequency activity of the gastrocnemius muscle for NOP4. Again three bursts can be identified, the first period A (originating for A1). There is low frequency activity extending over period C. This appears as prominent high frequency activity over period D. Over period D the activity exists throughout the all frequency ranges. At the highest frequency this burst can be seen to be constructed of an initial short epoch then sustained burst of activity. Over the swing phase low level activity, predominantly in the high frequency bands, is present and shown by period B.

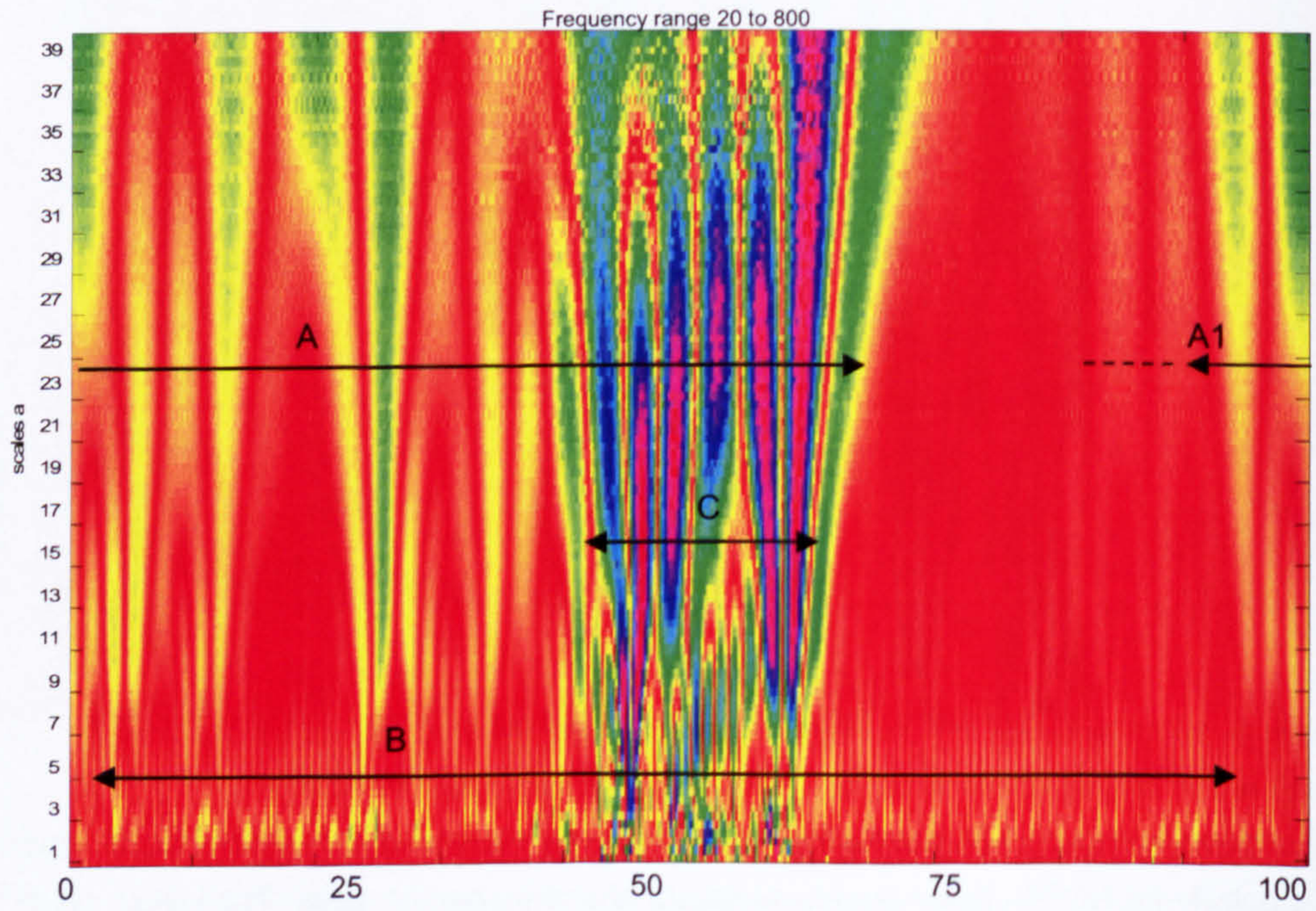

Appendix Figure 126 shows the time-frequency representation of the soleus muscle activity for subject NOP4. Low frequency activity can be seen almost thought the entire stride period B. However, in the moderate to high frequency ranges activity is restricted to a multitude of short epoch bursts over period A. Over period C there is a prominent burst of activity that exists throughout all frequency bands. With respect to the low frequency bands this activity is extended in time. There finally some low frequency activity is seen over period A1 this activity extends into the moderate frequency rages as moderate amplitude coefficients.

B.IV Sub-band filtering

B.IV.a NOP1

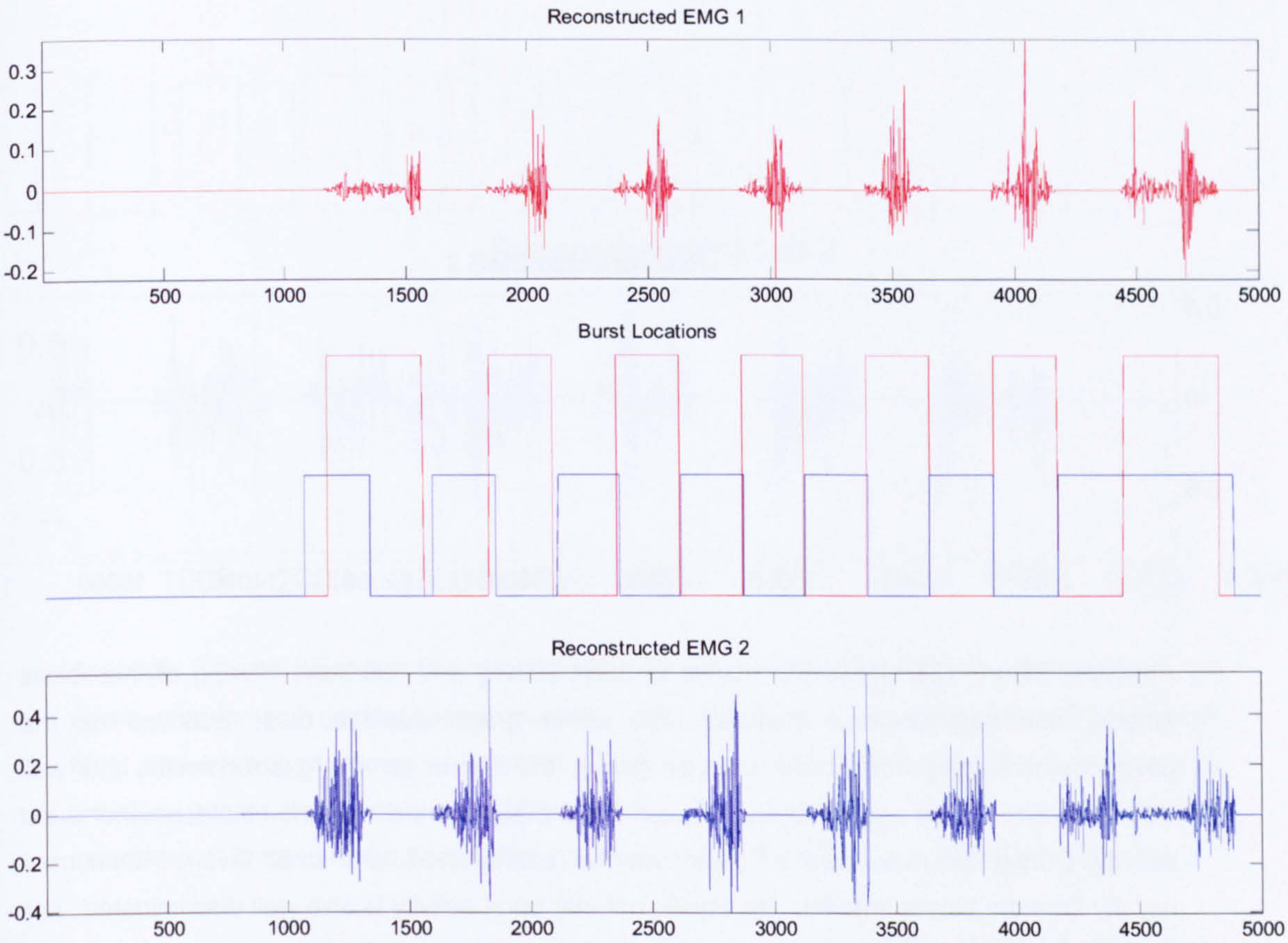

Appendix Figure 127 shows the results of burst activity and sub-band filtering of the tibialis anterior and gastrocnemius muscles. Tibialis anterior activity (Red plot) is well defined and shows burst locations between the gastrocnemius burst locations (Blue plot). The gastrocnemius burst activity displays a failure to discriminate between burst and inter-burst activity in the final two bursts. It is interesting to note that in the first and last bursts of gastrocnemius activity there is overlap between the two muscles that does not occur during the intervening bursts during the walk. The co-activation value is 0.16, this value is influenced by the false activity shown in the final stride.

B.IV.b NOP2

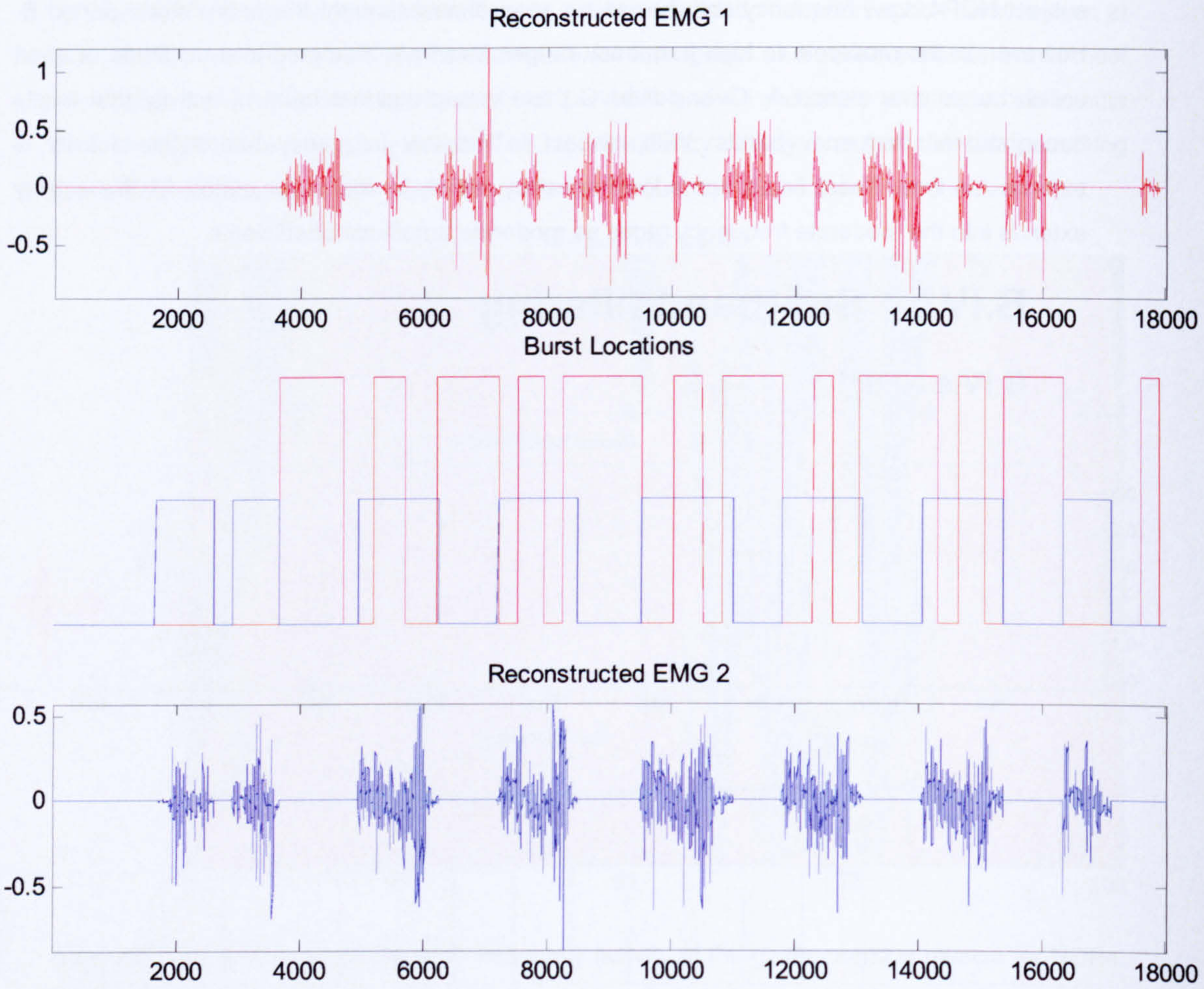

Appendix Figure 128 shows the results of burst activity and sub-band filtering of the tibialis anterior and gastrocnemius muscles. The upper graph displays burst locations for the gastrocnemius (red) and tibialis anterior (blue), the bursts for the gastrocnemius are well discriminated with an additional short epoch burst that occurs during the tibialis anterior burst activity. During the main burst of gastrocnemius activity there is a small level of concurrent activity from the tibialis anterior. The tibialis anterior burst activity is also well discriminated. The co-activation index is 0.24.

B.IV.c NOP3

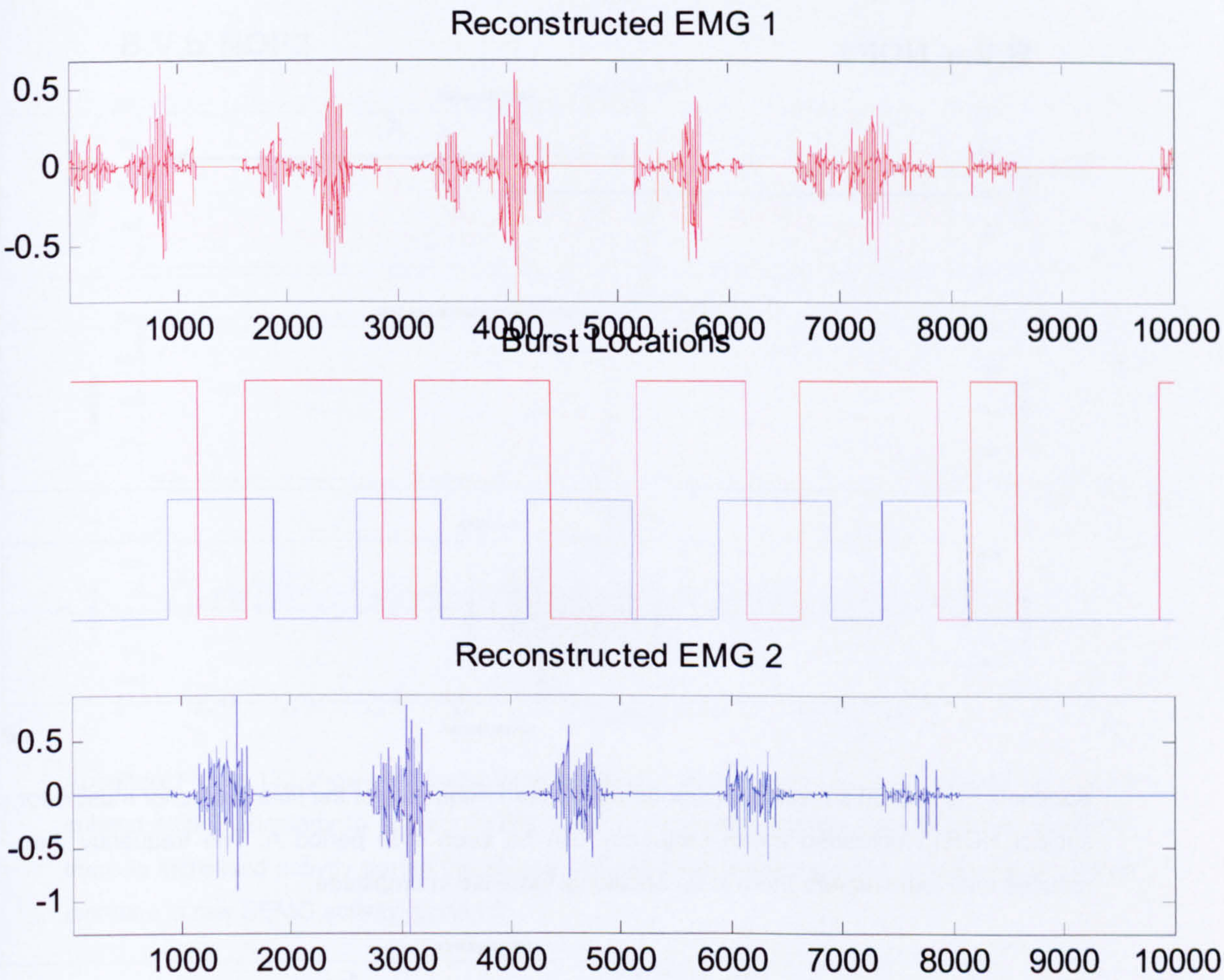

Appendix Figure 129 shows the burst locations and burst time frequency representation of the tibialis anterior and gastrocnemius muscles. Both signals show good discrimination between burst and inter-burst intervals. There is an extension of the inter-burst period of the tibialis anterior greater than would be estimated by visual inspection. There are false positive responses at the end of the tibialis anterior burst activity (red plot). (co-activation = 0.26.

B.V Mean Frequency over Stride

B.V.a NOP1

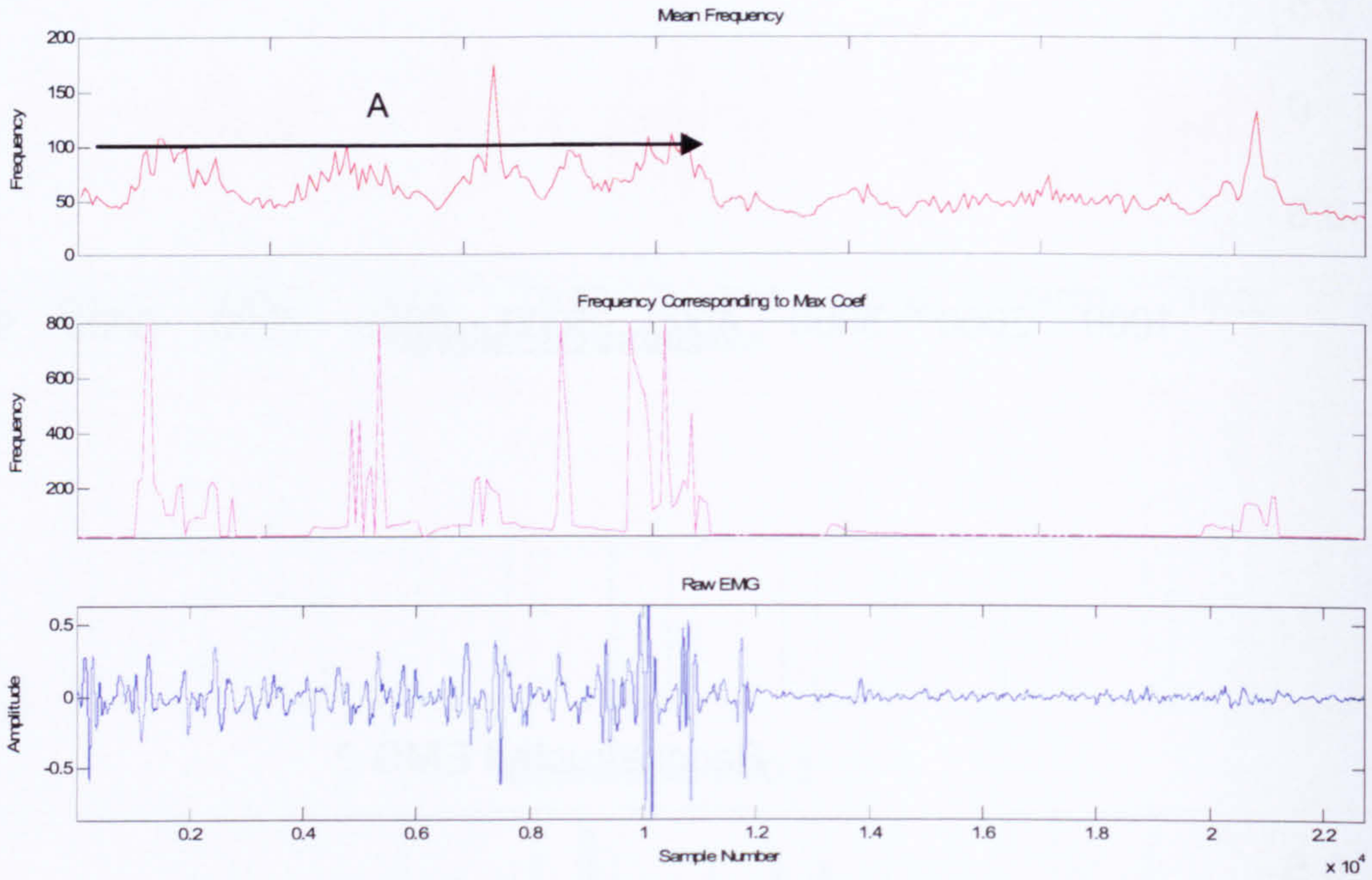

Appendix Figure 130 shows the instantaneous mean frequency of the tibialis anterior muscle for subject NOP1. Increased mean frequency can be seen over period A. The frequency then reduces until toe-of where there is an additional increase in amplitude.

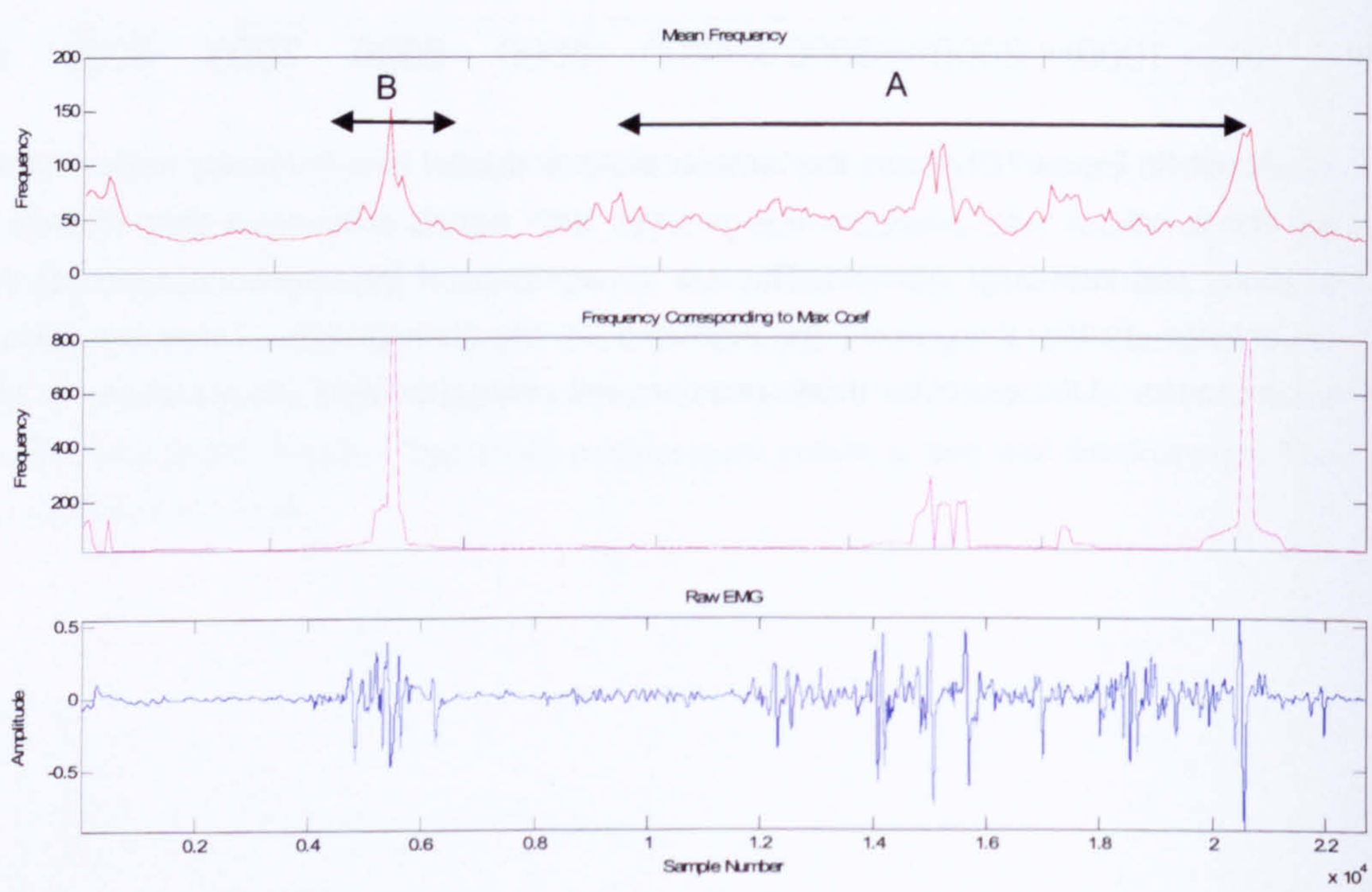

Appendix Figure 131 displays the instantaneous mean frequency of the gastrocnemius muscle for subject NOP1. The activity is characterised by an increase in activity over period A where there is a prominent increase in amplitude consistent with toe-off. There is an additional burst of activity during mid swing corresponding with SEMG activity period B.

B.V.b NOP2

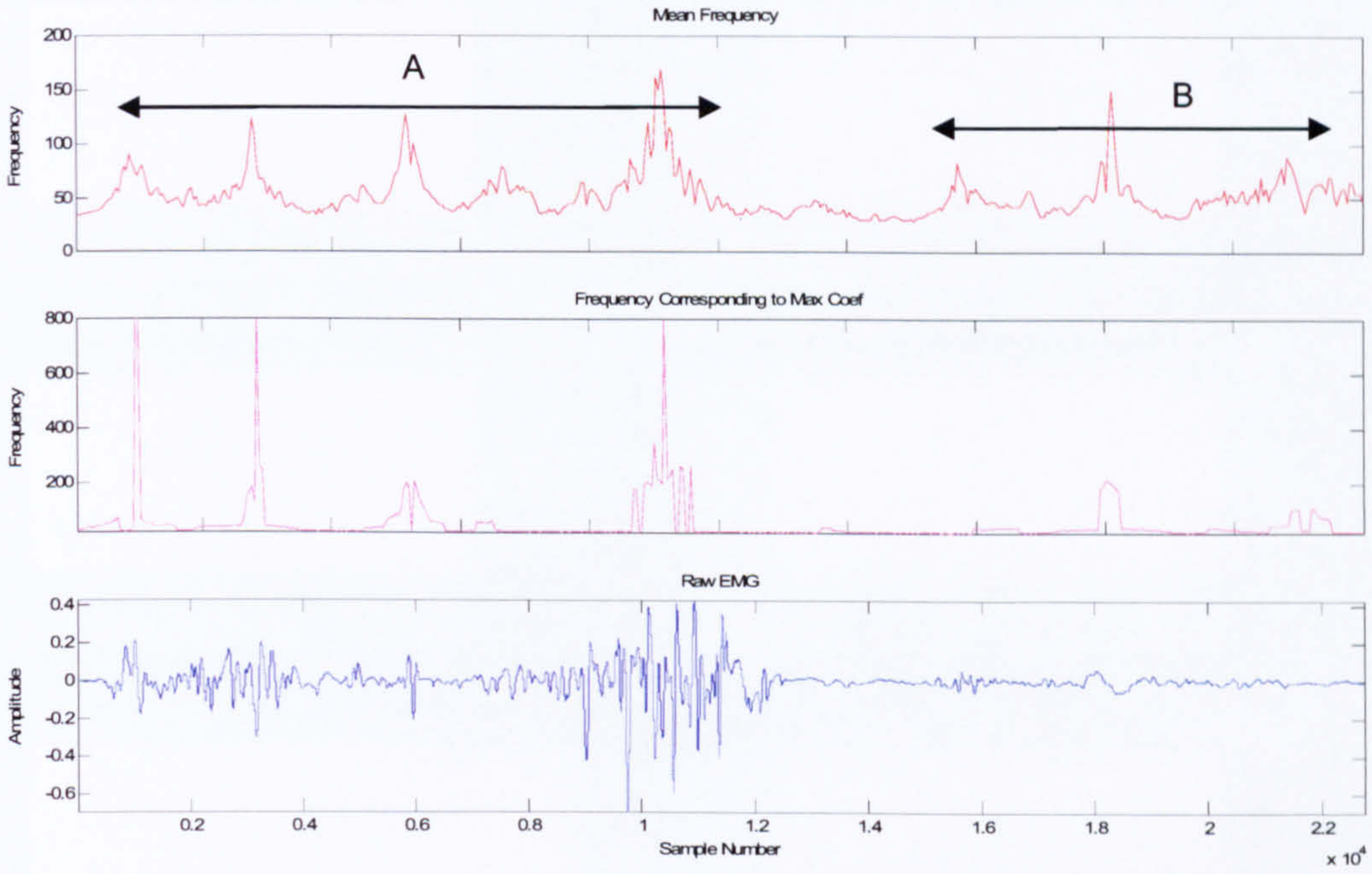

Appendix Figure 132 shows the instantaneous mean frequency of the tibialis anterior muscle for subject NOP2. Similarly to subject NOP1 there is increased activity over period A. However, there is increased activity during the stance phase which is not associated with any prominent increase in raw SEMG activity, period B.

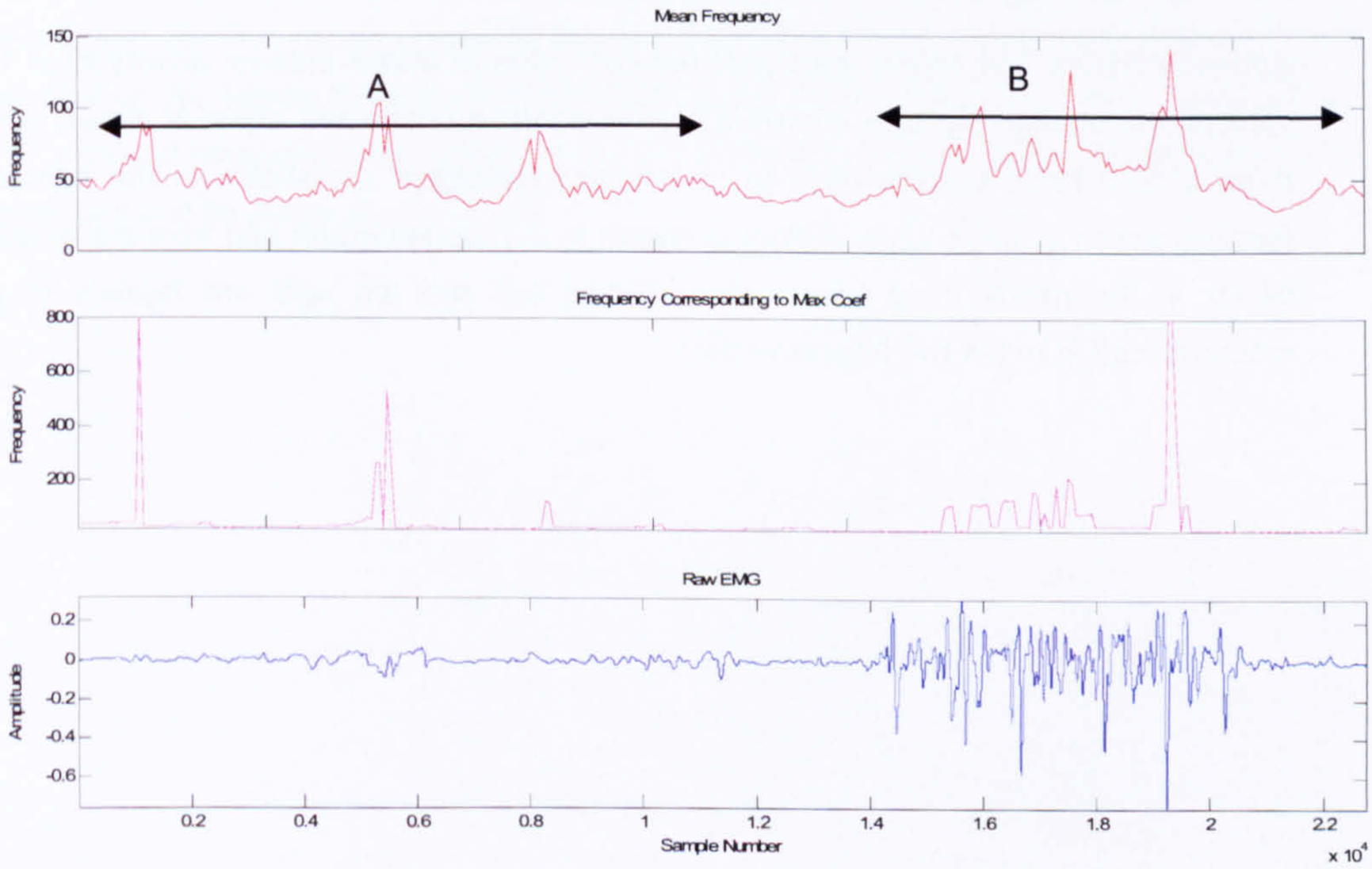

Appendix Figure 133 displays the mean instantaneous frequency for the gastrocnemius of subject NOP2. There are three prominent bursts of activity during the swing phase the first associated with toe off. The second an third appear to be associated to small perturbations in the raw SEMG, reflected by period A. over period B there is an increase in mean frequency corresponding to increase in the raw SEMG amplitude

B.VI Principal Component analysis

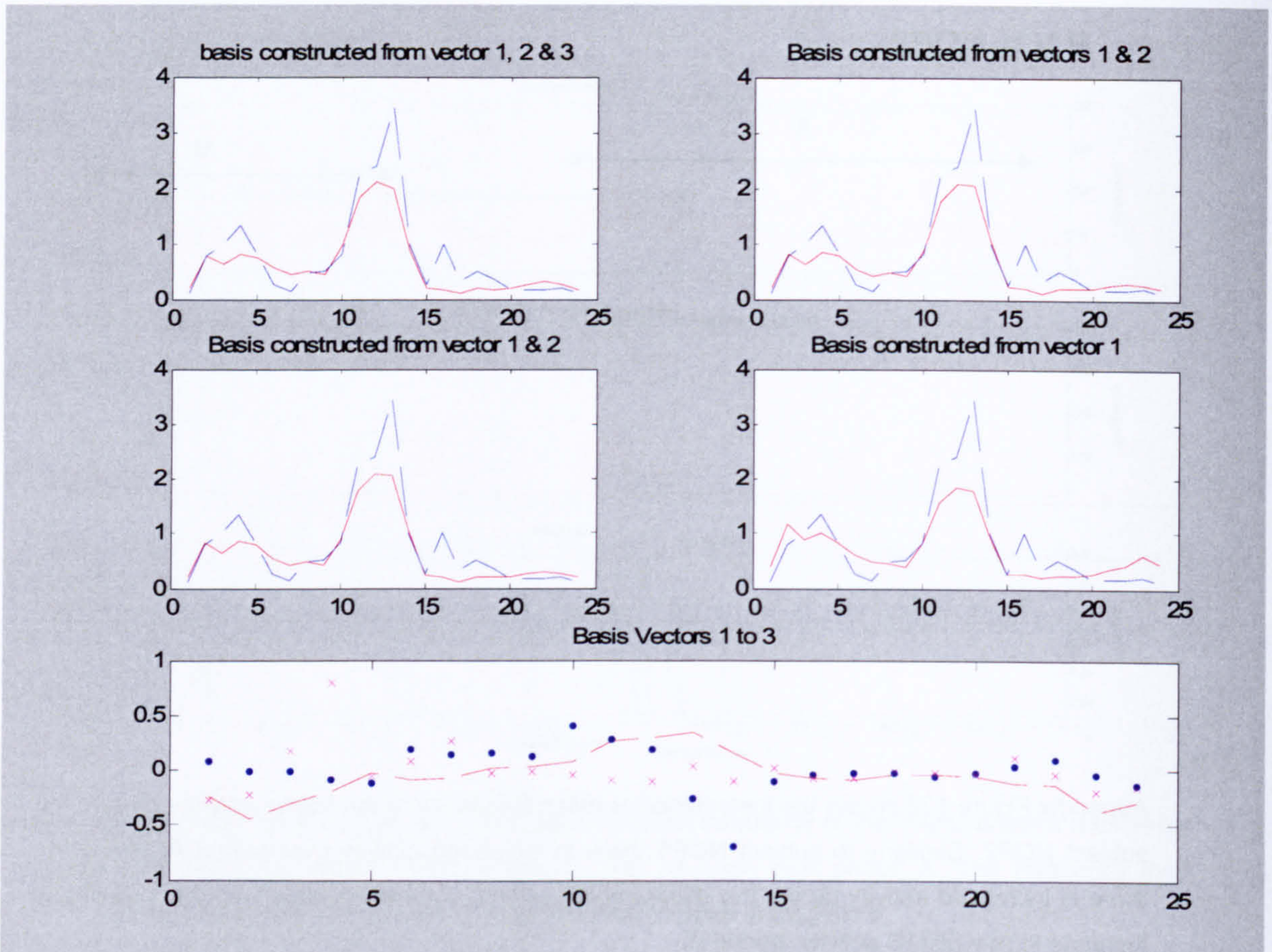

Appendix Figure 134 shows the signal reconstruction of tibialis anterior activity from 1-3 basis vectors, the original signal is shown in blue and the reconstructed signal is shown in red. The three largest basis vectors used to reconstruct the signal are shown in the bottom graph. Reconstruction from all three vectors is shown in the top left graph and from the single largest vector in the middle right hand graph. Middle left and top right are repeats of a signal reconstructed from the two largest vectors.

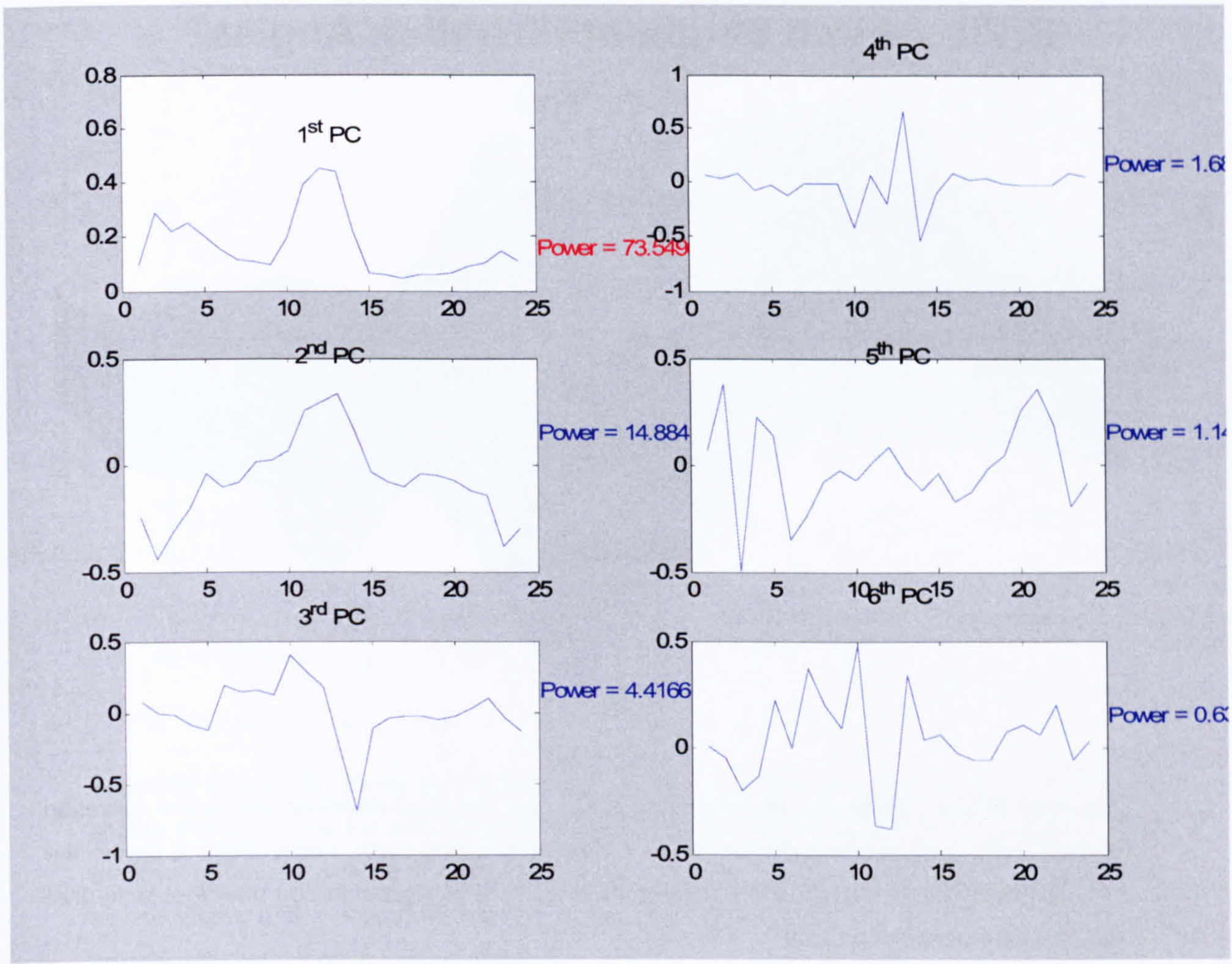

Appendix Figure 135 displays the principal components used to construct the basis vectors seen in graph 28. The values printed to the left of the graphs are the power of each principal component or the degree to which each principal component contributes to the original signal. The 1st principal component, the component that contributes most strongly, is shown in the top left hand plot and its power shown in red.

B.VII Limb Segment Elevation Angles

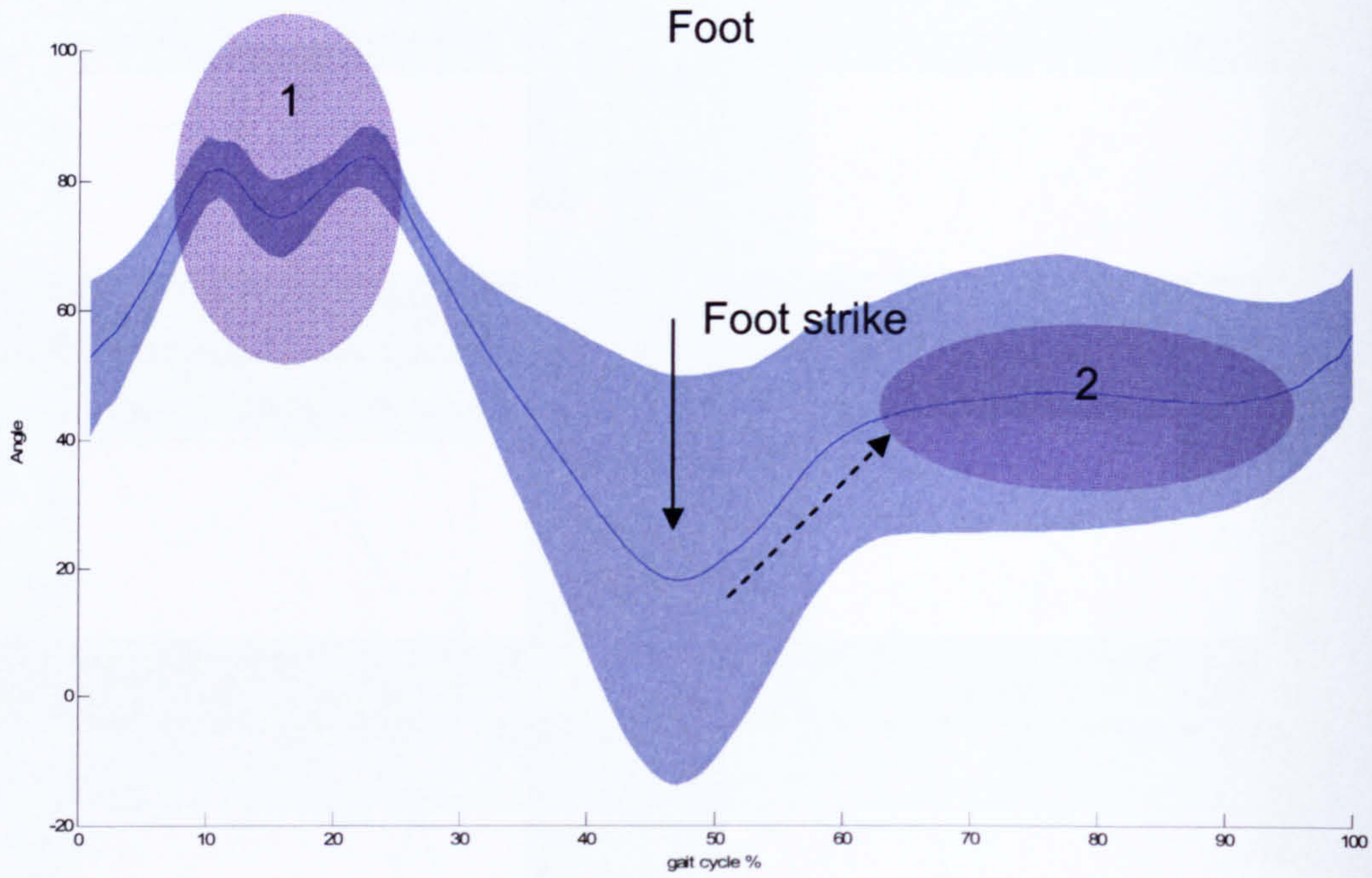

Appendix Figure 136 shows the combined mean and standard deviation of the foot elevation angles. Point 1 shows dorsiflexion for foot clearance during early swing. Point 2 shows the period of foot flat. The dashed line represents the period of plantar flexion after foot-strike that results in the period of foot flat.

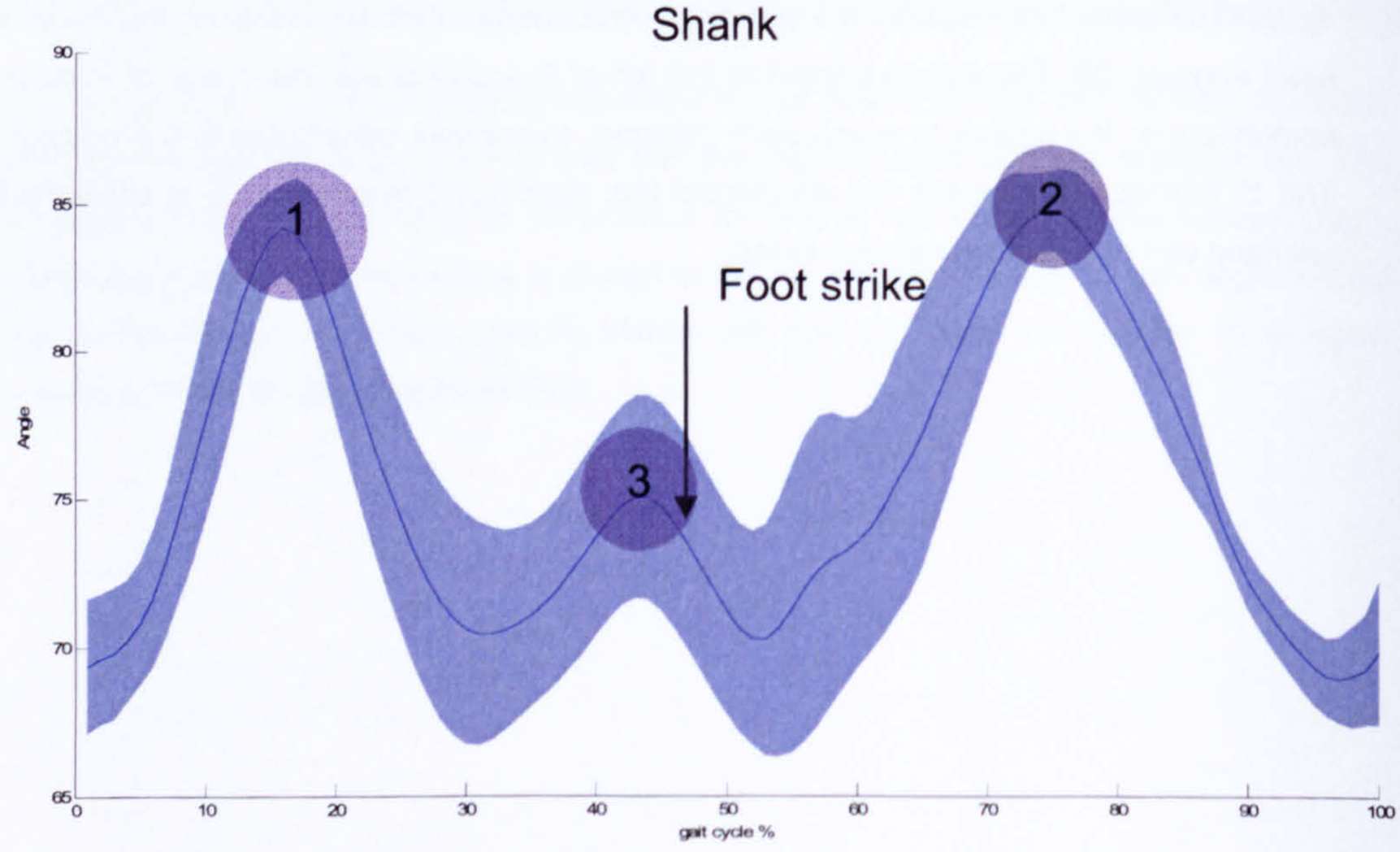

Appendix Figure 137 shows the combined mean and standard deviation of the shank elevation angles. Points 1 & 2 show the times at which the shank passes the midline of the body and are therefore mid-swing and mid-stance respectively. Point 3 shows a small level of posterior rotation of the shank about the knee just prior to foot-strike.

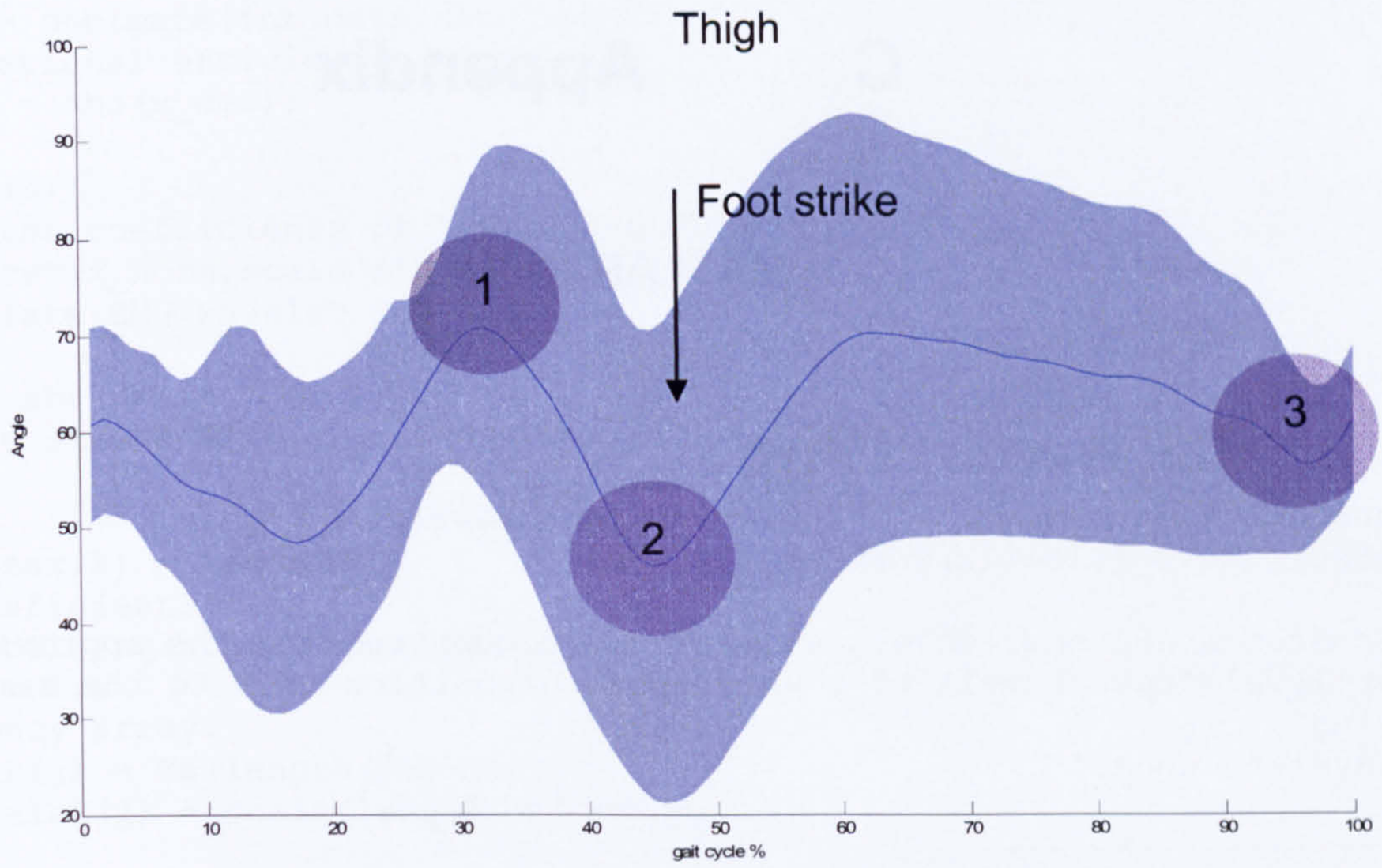

Appendix Figure 138 shows the combined mean and standard deviation of the thigh elevation angles. Point 1 shows the time at which the thigh passes the mid line of the body, point 2 shows the level of forward rotation of the thigh prior to foot strike. Point 3 shows that at the end of the stance phase and the gradual rotation of the thigh posteriorly prior to the beginning of the anterior rotation during the swing phase.

C Appendix

MATLAB CODE

C.I Wavelet Filter

```
function wrec = Wave_filter(X,wname,reconLevel)
%wrec = Wave_filter(X,wname,reconLevel)
%
%Generates a linear envelope (wrec) by reconstructing the approximation
%at level 'reconLevel' of a wavelet decomposition of X to the same level
using
%wavelet 'wname'

%--------------------
    %wname = 'dmey';
    %reconLevel = 6;
    %X = EMG_abs;
%--------------------

[C,L] = wavedec(X,reconLevel,wname);
wrec = wrcoef('a',C,L,wname,reconLevel);
%plot(wrec);
```

C.II Continuous Wavelet Transform

```
function [mfreqs, smfreqs] = cont_wave_2(data,chan,dec)

wname = 'gaus3';                                    %wavelet type
decomlevel=9;                                       %decomposition level, wavelet
level
dec_level = dec;                                    %decimation factor
scale_max = 40;                                     %maximum wavelet scale
scale_delta = 0.1;                                    %scale interval
scale_min    = 1;                                   %minimum wavelet scale level
delta_t = 0.0005;                                   %sampling frequency
scale = [scale_min:scale_delta:scale_max];          %calculate value for scale
[dr dc] = size(data);

if dc > dr
    data = data';                                   % Transpose data if required
    disp('data transposed');
else
    disp('NO TRANSPOSE');
end

if dc == 1
    x = data;                                       % Data only consists of one
muscle
elseif dc > 1
    x = data(1:length(data),chan);                  % Select muscle.
else
    error('data format error')                      % Catch all
end
```

```
clear dr dc;
x_dec = decimate(int_data,dec_level);          %decimate array for
computational efficiency. Default 1;
x_norm = abs(x_dec);                           %generate RMS EMG.

figure(3)
%plot the coefficients of the wavelet transform
CWT = cwt(x_norm,scale_min:scale_delta:scale_max,wname,'abslvl');
%calculate EMG wavelet coefficients

aCWT = abs(CWT);
[m,n] = size(aCWT);                            %calculate array sizes.
                                               % m = frequency bins
                                               % n = sample number
%[CWT_max,I] = max(aCWT);                      %Calculate the scale relating
max coeficient.
Fa = scal2frq(scale,wname,delta_t);            %Real frequency Hz.
for j = 1:m                                    %Reverse the scale and
frequency array.
    FaR(j) = Fa(length(Fa)-(j-1));
    scaleR(j) = scale(length(scale)-(j-1));
end

%-------------------------------------------------------------------------
-
% Use to look for maximum from bottom to top
%for j = 1:n
    %for i = 1:m
        %RaCWT(i,j) = aCWT(m-(i-1),j); % Reverse coeficients
    %end
%end
%[CWT_max,I] = max(RaCWT);                      %Calculate the scale
relating max coeficient.
%-------------------------------------------------------------------------
-

% calculate mean frequency
for i = 1:n                                    %Calculate mean and median
frequency.
    for j = 1:m
        coefs(j) = aCWT(j,i);
        freqs(j) = aCWT(j,i)*Fa(j); %*maxCWT;
    end
    scalefreq(i) = max(aCWT(:,i));
    mfreqs(i) = (sum(freqs)/sum(coefs));
    smfreqs(i) = (sum(freqs)/sum(coefs))*scalefreq(i);    % Scaled
frequency
    [CWT_max(i), I(i)] = max(aCWT(:,i));
end
FaMax = Fa(I);     %Convert scale related to max coef frequency.

%Plot Stuff

title(['frequency range ',num2str(floor(FaR(1))),' to
',num2str(floor(FaR(length(FaR))))]);
%set(gca,'YTickLabel',[scale_min scale_max/2 scale_max]);
%set(gca,'XTickLabel',[]); XLabel('');
xscale = [1:n]; colormap('hsv');

figure(2)
subplot(311); plot(xscale,mfreqs,'r'); ylabel('Frequency'); XLim([0 n]);
set(gca,'XTickLabel',[]);
    title('Mean Frequency');
```

```
subplot(312); plot(xscale,FaMax,'m'); ylabel('Frequency'); XLim([0
n]);set(gca,'XTickLabel',[]);
    title('Frequency Corresponding to Max Coef'); axis tight;
%subplot(312); plot(xscale,smfreqs,'m'); ylabel('weighted Frequency');
XLim([0 n]);set(gca,'XTickLabel',[]);
    %title('Weighted Frequency');
subplot(313); plot(x),'b';xlabel('Sample Number'); ylabel('Amplitude');
XLim([0 n]);
    title('Raw EMG'); axis tight;

%figure(4)
%contourf(RaCWT);
```

C.III Principal Component Analysis

```
function covarience_calcs(data,data_2,numfeatures);
[m,n] = size(data);
%numfeatures = 10;
features = get_features(data, numfeatures);

R = features * features' * (1/m);   % Calculate correlation matrix of
"features"

[V,D] = eig(R);                     % Get eigenvectors (V) of the correlation
matrix.
                                    % These act the basis vectors
                                    % V = vectors, D = values
[mV, nV] = size(V);
x = 1:mV;
weight_coefs = V' * features;   % Calculate the weighting coeficients

%-------------------------------------------------------------------
--

new_features = get_features(data_2, numfeatures);
new_data = data_2(:,1);                             % Construct new data
new_R = new_features * new_features' * (1/m);   % Create new Covarience
matrix
[new_V,new_D] = eig(new_R);                         % Calculate new
eigenvaluees and eigenvectors

weight_coefs_2 = new_V' * new_features;     % Generate new weighting
coeficients
[power fraction] = VectorPower(V,D);        % Calculate power
contribution

ev_1 = V(:,nV)* fraction(mV,nV);            % Weight each of the basis
eigenvalues
ev_2 = V(:,nV-1)* fraction(mV-1,nV-1);      %
ev_3 = V(:,nV-2)* fraction(mV-2,nV-2);      %
ev_4 = V(:,nV-3)* fraction(mV-3,nV-3);      %

basis_1 = ev_1 + ev_2 + ev_3;           % Construct Basis vector from the
three largest eigen values
basis_2 = ev_1 + ev_2;                  %
basis_3 = ev_1;                         %

recon_sig_3 = basis_3 * weight_coefs_2';    % Reconstruct signal
recon_sig_2 = basis_2 * weight_coefs_2';    %
recon_sig_1 = basis_1 * weight_coefs_2';    %

mse = meanSquareError(new_features, recon_sig_1(:,nV))
```

```
%-------------------------------------------------------------------------
--
%-------------------------------Plot Data---------------------------------
--

figure('name','Principal components')
subplot(321); plot(V(:,nV));
    title('1^s^t PC'); text(length(V(:,nV)),mean(V(:,nV)),['Power = ',
num2str(power(mV,nV))],'color','r');
subplot(322); plot(V(:,nV-4));
    title('4^t^h PC'); text(length(V(:,nV-4)),mean(V(:,nV-4)),['Power = ',
num2str(power(mV-4,nV-4))],'color','b');
subplot(323); plot(V(:,nV-1));
    title('2^n^d PC'); text(length(V(:,nV-1)),mean(V(:,nV-1)),['Power = ',
num2str(power(mV-1,nV-1))],'color','b');
subplot(324); plot(V(:,nV-5));
    title('5^t^h PC'); text(length(V(:,nV-5)),mean(V(:,nV-5)),['Power = ',
num2str(power(mV-5,nV-5))],'color','b');
subplot(325); plot(V(:,nV-2));
    title('3^r^d PC'); text(length(V(:,nV-2)),mean(V(:,nV-2)),['Power = ',
num2str(power(mV-2,nV-2))],'color','b');
subplot(326); plot(V(:,nV-6));
    title('6^t^h PC'); text(length(V(:,nV-6)),mean(V(:,nV-6)),['Power = ',
num2str(power(mV-6,nV-6))],'color','b');

figure('name','Reconstruction')
subplot(321); plot( x ,recon_sig_1(:,nV),'r-', x ,new_features,'b--');
    xlabel(''); title('basis constructed from vector 1, 2 & 3');

subplot(322); plot( x ,recon_sig_2(:,nV),'r-', x ,new_features,'b--');
    xlabel(''); title('Basis constructed from vectors 1 & 2');

subplot(323); plot( x ,recon_sig_2(:,nV),'r-', x ,new_features,'b--');
    xlabel(''); title('Basis constructed from vector 1 & 2');

subplot(324); plot( x ,recon_sig_3(:,nV),'r-', x ,new_features,'b--');
    xlabel(''); title('Basis constructed from vector 1');

subplot(313); plot( x ,V(:,nV-1),'r--', x ,V(:,nV-2),'b.', x ,V(:,nV-
3),'mx');
    title('Basis Vectors 1 to 3');
```

C.IV Sub-Band Filtering

```
function [ba_norm, burstlocation, Xrec] = de_burst_5(X,win,win2)
clc
wname = 'dmey';                     % Define mother wavelet
N = 8;                              % Decomp scale
window = win;  %31                  % Burst detection window
window2 = win2; %21
halfwindow = (window/2)-0.5;        % Defines number of values from window
centre to end
halfwindow2 = (window2/2)-0.5;  % Defines number of values from window
centre to end
X = X - mean(X);
disp('creating coeficients')
[Ca Cd]   = dwt( X ,wname,'mode','per');
[Ca2 Cd2] = dwt(Ca ,wname,'mode','per');
[Ca3 Cd3] = dwt(Ca2,wname,'mode','per');
[Ca4 Cd4] = dwt(Ca3,wname,'mode','per');
[Ca5 Cd5] = dwt(Ca4,wname,'mode','per');
[Ca6 Cd6] = dwt(Ca5,wname,'mode','per');
[Ca7 Cd7] = dwt(Ca6,wname,'mode','per');
[Ca8 Cd8] = dwt(Ca7,wname,'mode','per');
```

```
d8 = Cd; d7 = Cd2; d6 = Cd3; d5 = Cd4; d4 = Cd5; d3 = Cd6; d2 = Cd7; d1 =
Cd8;

%-------------------------------------------------------------------------
--
%---------------------------- First threshold ----------------------------
--
%------------------------------------ d5 -----------------------------------
--
disp('Thresh 1 - d5')
std_d5 = std(abs(d5));
max_d5 = max(d5);                          % Get value of max coeficients
mean_d5 = mean(abs(d5));
thresh_d5 = std_d5/4;                        % Set threshold to 1/3 max
coeficient level
d5_burst_activity = 0;
for i = 1:length(d5) - halfwindow2
    if i < window2
        if std(d5(i : i + halfwindow2)) < thresh_d5
            d5_burst_activity(i) = 0;    % inter - burst zone
        else
            d5_burst_activity(i) = 1;    % burst zone
        end
    else
        val = std(d5(i - halfwindow2 : i + halfwindow2));
        if val < thresh_d5
            d5_burst_activity(i) = 0;    %inter-burst zone
        else
            d5_burst_activity(i) = 1;    %burst zone
        end
    end
end
clear max_d5 thresh_d5 val i                    %tidy up
%-------------------------------------------------------------------------
--
%---------------------- Calculate the inter-burst power Pa ---------------
--
%-------------------- Pa = 1/N(inter-burst) sigma (coef j)^2 ------------
--
%------------------------------------ d5 -----------------------------------
--
burst_index = find(d5_burst_activity == 0);
for i = 1:length(burst_index)
    coefd5(i) = d5(burst_index(i)).^2;
end
coefd5intburst = sum(coefd5)/length(burst_index);
clear burst_index coefd5
%-------------------------------------------------------------------------
--
%---------------------- Calculate the burst power Ps ---------------------
--
%-----------------Ps = 1/N(Burst) sigma (coef j)^2 - Pa(j) ------------
--
%------------------------------------ d5 -----------------------------------
--
burst_index = find(d5_burst_activity == 1);
%get the indexes of burst periods
for i = 1:length(burst_index)
    coefd5(i) = d5(burst_index(i)).^2;
%square the coeficents
end
coefd5burst = (sum(coefd5) - coefd5intburst)/length(burst_index);
%sum of the squared coefs / number of coefs
```

```
clear burst_index coefd5
%tidy up
%-------------------------------------------------------------------
--
%----------------- Second threshold using power calculations -----------
--
%---------------------------------- d5 ------------------------------
--
for i = 1:length(d5) - halfwindow
    if i < window
        if d5(i : i + halfwindow).^2 < coefd5burst
            d5_burst_activity2th(i) = 0;                    % Inter -
burst zone
        else
            d5_burst_activity2th(i) = 1;                    % Burst zone
    end
elseif i + halfwindow >length(d5)
    j =  (i + (halfwindow))-length(d5);
    val = d5(i - (halfwindow) : i + ((halfwindow) - j)).^2;
    if val < coefd5burst
        d5_burst_activity2th(i) = 0;
    else
        d5_burst_activity2th(i) = 1;
    end
else
    val = d5(i - halfwindow : i + halfwindow).^2;
    if val < coefd5burst
        d5_burst_activity2th(i) = 0;
    else
        d5_burst_activity2th(i) = 1;
    end
end
clear val i j
clear coefd5burst coefd5intburst burst_index
%-------------------------------End for d5-------------------------------
--
%-------------------------------------------------------------------
--

d6_burst_activity = round(interpft(d5_burst_activity,length(d6)));
%-------------------------------------------------------------------
--
%---------------------- Calculate the inter-burst power Pa -------------
--
%-------------------- Pa = 1/N(inter-burst) sigma (coef j)^2 ------------
--
%---------------------------------- d6 ------------------------------
--
burst_index = find(d6_burst_activity == 0);
for i = 1:length(burst_index)
    coefd6(i) = d6(burst_index(i)).^2;
end
coefd6intburst = sum(coefd6)/length(burst_index);
clear burst_index coefd6
%-------------------------------------------------------------------
--
%---------------------- Calculate the burst power Ps -------------------
--
%------------------Ps = 1/N(Burst) sigma (coef j)^2 - Pa(j) -------------
--
%---------------------------------- d6 ------------------------------
--
```

```
burst_index = find(d6_burst_activity == 1);
%get the indexes of burst periods
for i = 1:length(burst_index)
    coefd6(i) = d6(burst_index(i)).^2;
%square the coeficents
end
coefd6burst = (sum(coefd6) - coefd6intburst)/length(burst_index);
%sum of the squared coefs / number of coefs
clear burst_index coefd6
%tidy up
%-------------------------------------------------------------
--
%----------------- Second threshold using power calculations -----------
--
%---------------------------------- d6 ---------------------------------
--
disp('Thresh 2 - d6')
for i = 1:length(d6)
    if i < halfwindow*2 + 1
        if mean(d6(i : i + (halfwindow*2)).^2) < coefd6burst
            d6_burst_activity2th(i) = 0;                    % Inter -
burst zone
        else
            d6_burst_activity2th(i) = 1;                    % Burst zone
        end
    elseif i + halfwindow*2 >length(d6)
        j =  (i + (halfwindow*2))-length(d6);
        val = mean(d6(i - (halfwindow*2) : i + ((halfwindow*2) - j)).^2);
        if val < coefd6burst
            d6_burst_activity2th(i) = 0;
        else
            d6_burst_activity2th(i) = 1;
        end
    else
        val = mean(d6(i - (halfwindow*2) : i + (halfwindow*2)).^2);
        if val < coefd6burst
            d6_burst_activity2th(i) = 0;
        else
            d6_burst_activity2th(i) = 1;
        end
    end
end
clear val i j
clear coefd6burst coefd6intburst burst_index
%-------------------------------End for d6---------------------------
--
%-------------------------------------------------------------
--

d7_burst_activity = round(interpft(d6_burst_activity,length(d7)));
%-------------------------------------------------------------
--
%---------------------- Calculate the inter-burst power Pa -------------
--
%-------------------- Pa = 1/N(inter-burst) sigma (coef j)^2 ------------
--
%---------------------------------- d7 ---------------------------------
--
burst_index = find(d7_burst_activity == 0);
for i = 1:length(burst_index)
    coefd7(i) = d7(burst_index(i)).^2;
end
coefd7intburst = sum(coefd7)/length(burst_index);
clear burst_index coefd7
```

```
%-------------------------------------------------------------------
--
%--------------------- Calculate the burst power Ps ----------------
--
%-----------------Ps = 1/N(Burst) sigma (coef j)^2 - Pa(j) ----------
--
%---------------------------------- d7 -------------------------------
--
burst_index = find(d7_burst_activity == 1);
%get the indexes of burst periods
for i = 1:length(burst_index)
    coefd7(i) = d7(burst_index(i)).^2;
%square the coeficents
end
coefd7burst = (sum(coefd7) - coefd7intburst)/length(burst_index);
%sum of the squared coefs / number of coefs
clear burst_index coefd7
%tidy up
%-------------------------------------------------------------------
--
%----------------- Second threshold using power calculations -----------
--
%---------------------------------- d7 -------------------------------
--
disp('Thresh 2 - d7')
for i = 1:length(d7)
    if i < halfwindow*4 + 1
        if mean(d7(i : i + (halfwindow*4)).^2) < coefd7burst
            d7_burst_activity2th(i) = 0;                    % Inter -
burst zone
        else
            d7_burst_activity2th(i) = 1;                    % Burst zone
        end
    elseif i + halfwindow*4 >length(d7)
        j =  (i + (halfwindow*4))-length(d7);
        val = mean(d7(i - (halfwindow*4) : i + ((halfwindow*4) - j)).^2);
        if val < coefd7burst
            d7_burst_activity2th(i) = 0;
        else
            d7_burst_activity2th(i) = 1;
        end
    else
        val = mean(d7(i - (halfwindow*4) : i + (halfwindow*4)).^2);
        if val < coefd7burst
            d7_burst_activity2th(i) = 0;
        else
            d7_burst_activity2th(i) = 1;
        end
    end
end
clear val i j
clear coefd7burst coefd7intburst burst_index
%-------------------------------End for d7-------------------------------
--
%-------------------------------------------------------------------
--

d8_burst_activity = round(interpft(d7_burst_activity,length(d8)));
%-------------------------------------------------------------------
--
%---------------------- Calculate the inter-burst power Pa ------------
--
%-------------------- Pa = 1/N(inter-burst) sigma (coef j)^2 ------------
--
```

```
%------------------------------------ d8 ------------------------------------
--
burst_index = find(d8_burst_activity == 0);
for i = 1:length(burst_index)
    coefd8(i) = d8(burst_index(i)).^2;
end
coefd8intburst = sum(coefd8)/length(burst_index);
clear burst_index coefd8
%----------------------------------------------------------------------------
--
%--------------------- Calculate the burst power Ps ---------------------
--
%-----------------Ps = 1/N(Burst) sigma (coef j)^2 - Pa(j) ------------
--
%------------------------------------ d8 ------------------------------------
--
burst_index = find(d8_burst_activity == 1);
%get the indexes of burst periods
for i = 1:length(burst_index)
    coefd8(i) = d8(burst_index(i)).^2;
%square the coeficents
end
coefd8burst = (sum(coefd8) - coefd8intburst)/length(burst_index);
%sum of the squared coefs / number of coefs
clear burst_index coefd8
%tidy up
%----------------------------------------------------------------------------
--
%----------------- Second threshold using power calculations -----------
--
%------------------------------------ d8 ------------------------------------
--
disp('Thresh 2 - d8')
for i = 1:length(d8)
    if i < halfwindow*8 + 1
        if mean(d8(i : i + (halfwindow*8)).^2) < coefd8burst
            d8_burst_activity2th(i) = 0;                    % Inter -
burst zone
        else
            d8_burst_activity2th(i) = 1;                    % Burst zone
        end
    elseif i + halfwindow*8 >length(d8)
        j =  (i + (halfwindow*8))-length(d8);
        val = mean(d8(i - (halfwindow*8) : i + ((halfwindow*8) - j)).^2);
        if val < coefd8burst
            d8_burst_activity2th(i) = 0;
        else
            d8_burst_activity2th(i) = 1;
        end
    else
        val = mean(d8(i - (halfwindow*8) : i + (halfwindow*8)).^2);
        if val < coefd8burst
            d8_burst_activity2th(i) = 0;
        else
            d8_burst_activity2th(i) = 1;
        end
    end
end
clear val i j
clear coefd8burst coefd8intburst burst_index
%-----------------------------End for d8-------------------------------
--
%----------------------------------------------------------------------------
--
```

```
%--------------------------- Get Burst locations ----------------------
--
disp('Calculating Burst locations')
ba8 = round(interpft(d8_burst_activity2th,length(d5)));
ba7 = round(interpft(d7_burst_activity2th,length(d5)));
ba6 = round(interpft(d6_burst_activity2th,length(d5)));
ba5 = round(interpft(d5_burst_activity2th,length(d5)));
ba = ba5 + ba6 + ba7 + ba8;
ba_norm = ba;

for i = 1 : length(ba_norm)
    if ba_norm(i)<1
        ba_norm(i) = 0;
    else
        ba_norm(i) = 1;
    end
end

%ba_norm = d5_burst_activity2th;

clear i ba8 ba7 ba6 ba5
%----------------------------------------------------------------------
--

%----------------------------------------------------------------------
--
%--------------------------- Filter lower subbands ----------------------
--
%----------------------------------------------------------------------
--
disp('Filter lower subbands')
ba_norm = round(interpft(ba_norm,length(d4)));
d4_burst_activity  = ba_norm;
%----------------------------------------------------------------------
--
%---------------------- Calculate the inter-burst power Pa ------------
--
%-------------------- Pa = 1/N(inter-burst) sigma (coef j)^2 ------------
--
%---------------------------------- d4 ----------------------------------
--
disp('d4')
burst_index = find(d4_burst_activity == 0);
for i = 1:length(burst_index)
    coefd4(i) = d4(burst_index(i)).^2;
end
coefd4intburst = sum(coefd4)/length(burst_index);
clear burst_index coefd4
%----------------------------------------------------------------------
--
%---------------------- Calculate the burst power Ps --------------------
--
%------------------Ps = 1/N(Burst) sigma (coef j)^2 - Pa(j) -------------
--
%---------------------------------- d4 ----------------------------------
--
burst_index = find(d4_burst_activity == 1);
%get the indexes of burst periods
for i = 1:length(burst_index)
    coefd4(i) = d4(burst_index(i)).^2;
%square the coeficents
end
```

```
coefd4burst = (sum(coefd4) - coefd4intburst)/length(burst_index);
%sum of the squared coefs / number of coefs
clear burst_index coefd4
%tidy up
%------------------------ De-noise burst ------------------------------
--
%------------------------------ d4 ------------------------------------
--
burst_index = find(d4_burst_activity == 1);          % Get the indexes of
burst periods
for i = 1:length(burst_index)
    if d4(burst_index(i)) < coefd4intburst
        d4(burst_index(i)) = 0;                      % Set to zero if
noise
    elseif abs(d4(burst_index(i))) > 2*coefd4burst
        d4(burst_index(i)) = 0;
    else
        'not noise';
    end
end
%---------------------------- End d4 ------------------------------------
--
%------------------------------------------------------------------------
--
ba_norm = round(interpft(ba_norm,length(d3)));
d3_burst_activity  = ba_norm;
%------------------------------------------------------------------------
--
%---------------------- Calculate the inter-burst power Pa -------------
--
%-------------------- Pa = 1/N(inter-burst) sigma (coef j)^2 -----------
--
%------------------------------------ d3 ------------------------------
--
disp('d3')
burst_index = find(d3_burst_activity == 0);
for i = 1:length(burst_index)
    coefd3(i) = d3(burst_index(i)).^2;
end
coefd3intburst = sum(coefd3)/length(burst_index);
clear burst_index coefd3
%------------------------------------------------------------------------
--
%---------------------- Calculate the burst power Ps --------------------
--
%-----------------Ps = 1/N(Burst) sigma (coef j)^2 - Pa(j) -------------
--
%------------------------------------ d3 ------------------------------
--
burst_index = find(d3_burst_activity == 1);
%get the indexes of burst periods
for i = 1:length(burst_index)
    coefd3(i) = d3(burst_index(i)).^2;
%square the coeficents
end
coefd3burst = (sum(coefd3) - coefd3intburst)/length(burst_index);
%sum of the squared coefs / number of coefs
clear burst_index coefd3
%tidy up
%------------------------ De-noise burst ------------------------------
--
%------------------------------ d3 ------------------------------------
--
```

```
burst_index = find(d3_burst_activity == 1);          % Get the indexes of
burst periods
for i = 1:length(burst_index)
    if abs(d3(burst_index(i))) < coefd3intburst
        d3(burst_index(i)) = 0;                      % Set to zero if
noise
    elseif abs(d3(burst_index(i))) > 2*coefd3burst
        d3(burst_index(i)) = 0;
    else
        'not noise';
    end
end
%------------------------ End d3 ------------------------------------
--
%--------------------------------------------------------------------
--
ba_norm = round(interpft(ba_norm,length(d2)));
d2_burst_activity  = ba_norm;
%--------------------------------------------------------------------
--
%---------------------- Calculate the inter-burst power Pa ----------
--
%-------------------- Pa = 1/N(inter-burst) sigma (coef j)^2 ----------
--
%---------------------------------- d2 ----------------------------
--
disp('d2')
burst_index = find(d2_burst_activity == 0);
for i = 1:length(burst_index)
    coefd2(i) = d2(burst_index(i)).^2;
end
coefd2intburst = sum(coefd2)/length(burst_index);
clear burst_index coefd2
%--------------------------------------------------------------------
--
%--------------------- Calculate the burst power Ps -----------------
--
%------------------Ps = 1/N(Burst) sigma (coef j)^2 - Pa(j) ----------
--
%---------------------------------- d2 ----------------------------
--
burst_index = find(d2_burst_activity == 1);
%get the indexes of burst periods
for i = 1:length(burst_index)
    coefd2(i) = d2(burst_index(i)).^2;
%square the coeficents
end
coefd2burst = (sum(coefd2) - coefd2intburst)/length(burst_index);
%sum of the squared coefs / number of coefs
clear burst_index coefd2
%tidy up
%------------------------ De-noise burst ----------------------------
--
%---------------------------------- d2 ----------------------------
--
burst_index = find(d2_burst_activity == 1);          % Get the indexes of
burst periods
for i = 1:length(burst_index)
    if abs(d2(burst_index(i))) < coefd2intburst
        d2(burst_index(i)) = 0;                      % Set to zero if
noise
    elseif abs(d2(burst_index(i))) >2*coefd2burst
        d2(burst_index(i)) = 0;
    else
```

```
        'not noise';
    end
end
%------------------------ End d2 ------------------------------------
--

ba_norm = round(interpft(ba_norm,length(d1)));
d1_burst_activity  = ba_norm;
%--------------------------------------------------------------------
--
%---------------------- Calculate the inter-burst power Pa ----------
--
%-------------------- Pa = 1/N(inter-burst) sigma (coef j)^2 ----------
--
%---------------------------------- d1 ------------------------------
--
disp('d1')
burst_index = find(d1_burst_activity == 0);
for i = 1:length(burst_index)
    coefd1(i) = d1(burst_index(i)).^2;
end
coefd1intburst = sum(coefd1)/length(burst_index);
clear burst_index coefd1
%--------------------------------------------------------------------
--
%--------------------- Calculate the burst power Ps -----------------
--
%-----------------Ps = 1/N(Burst) sigma (coef j)^2 - Pa(j) ----------
--
%---------------------------------- d1 ------------------------------
--
burst_index = find(d1_burst_activity == 1);
%get the indexes of burst periods
for i = 1:length(burst_index)
    coefd1(i) = d1(burst_index(i)).^2;
%square the coeficents
end
coefd1burst = (sum(coefd1) - coefd1intburst)/length(burst_index);
%sum of the squared coefs / number of coefs
clear burst_index coefd1
%tidy up
%------------------------ De-noise burst ----------------------------
--
%---------------------------------- d1 ------------------------------
--
burst_index = find(d1_burst_activity == 1);          % Get the indexes of
burst periods
for i = 1:length(burst_index)
    if abs(d1(burst_index(i))) < coefd1intburst
        d1(burst_index(i)) = 0;                      % Set to zero if
noise
    elseif abs(d1(burst_index(i))) >2*coefd1burst
        d1(burst_index(i)) = 0;
    else
        'not noise';
    end
end
%------------------------ End d1 ------------------------------------
--
disp('Reconstructing signal')
C = [Ca8; d1; d2; d3; d4; d5; d6; d7; d8];
%disp('C')
L = [length(Ca8); length(d1); length(d2); length(d3); length(d4);
length(d5); length(d6); length(d7); length(d8); length(X)];
```

```
%disp('L')
Xrec = waverec(C,L,wname);
%disp('Xrec')

ba_norm = round(interpft(ba_norm,length(Xrec)));
%ba_norm = round(interpft(d5_burst_activity2th,length(Xrec)));
burst_index = find(ba_norm == 0);
for i = 1:length(burst_index)
    Xrec(burst_index(i)) = 0;                                    %square
the coeficents
end

ba_norm = round(interpft(ba_norm,length(Xrec)));
%-------------------------------------------------------------------
--
%-------------------------------------------------------------------
--
disp('Generating normalised burst locations')
burstlocation = [];                                  % create zero length
array
i = 1;
while i < length(ba_norm)
    if ba_norm(i) == 0
        i = i + 1;
        %disp(i);
    else
        burstlocation(length(burstlocation)+1) = i;
        inburst = 1;
        %disp('inburst')
        while inburst == 1 % && i+1 <= length(d6_burst_activity)
            if i+1 >= length(ba_norm)
                burstlocation(length(burstlocation)+1) = i;
                i = i + 1;
                %disp('Break')
                break
            elseif ba_norm(i+1) == 1
                i = i + 1;
                inburst = 1;
                %disp('inburst')
            else
                burstlocation(length(burstlocation)+1) = i;
                i = i + 1;
                inburst = 0;
                %disp('inter burst')
            end
        end
    end
end
disp('End')
function EMG_normal = EMG_Norm_Amp(EMG_abs)
%Generates normalised EMG in amplitude
%EMG_Norm_Amp(EMG_abs), EMG_abs array representing RMS EMG

[m,n] = size(EMG_abs);              % Get size of the EMG signal array.
Length (samples and number of channels
                                    % m = number of samples
                                    % n = channel number

for i = 1:n
    max_amp(i) = max(EMG_abs(:,i));      % Find max valu from each channel
end

max_amp = max(max_amp(:));      % Make max amplitude value of maximum from
all channels
```

```
for i = 1:n
    for j = 1:m
    EMG_normal(j,i) = EMG_abs(j,i)/max_amp; % Make each sample a
porportion of max value
    end
end
```

C.V Time Normalisation

```
function Time_Norm_EMG = EMG_Norm_Time(EMG_norm, Num_points)
% Normalise EMG signal in time. n = the re-sample factor
% This must be called after calling EMG_Norm_Amp()

if Num_points < 1
    error('Number of interpolation points must be greater than zero')
else
    disp(['   Number of points = ' num2str(Num_points)])
end

m=0; n=0; %reset m and n (don't know if strictly nec.)

[m,n] = size(EMG_norm);      % Get size of the EMG signal array. Length
(samples and number of channels
                             % m = number of samples
                             % n = channel number

if n > m
    EMG_norm = EMG_norm';    %Transpose the array if wrong orientation.
    [m,n] =size(EMG_norm);
    disp('      Array transposed')
else
    disp('      no transpose')
end

if n >= 2    %check the number of channels if more than one iterate
through channels
    for i = 1:n
        Time_Norm_EMG(:,i) = interpft(EMG_norm(:,i), Num_points); % re-
samples EMG_norm to produce n equally spaced points (100 in this case)
    end
    disp(['      ' num2str(i) ' channels']);
elseif n == 0
    error('Input array must be non zero');
else
    Time_Norm_EMG = interpft(EMG_norm, Num_points);
    disp('      Single channel');
end
plot(Time_Norm_EMG);
title('normalised SEMG'); xlabel('Time'); ylabel('Amplitude');
end
```

C.VI Surface EMG Processing MATLAB

```
function EMG_LE = GetEMG(data, Num_points,DeBurst)
% Converts data to correct channels and linear envelope representation
% GetEMG(data), data 2d matrix of raw EMG cols = chan

[m,n] = size(data);
%-----------------depending on the format the EMG was saved format
channels---------------------------
if n == 9
    EMG = [data(:,5) data(:,4) data(:,3) data(:,2) data(:,8) data(:,7)];
%first should be 5, select relavent channels
```

```
elseif n == 11
    EMG = [data(:,7) data(:,6) data(:,5) data(:,4) data(:,10) data(:,9)];
%first should be 7, select relevant channels
else
    EMG = data;
end
m=0; n=0; %reset m and n (don't know if strictly nec.)
[m,n] = size(EMG);              % Get size of the EMG signal array. Length
(samples and number of channels
                                % m = number of samples
                                % n = channel number
for i = 1:n                     % Check to see if any array is zero
    Z_array(m,1) = 0;           % Create zero array
    if EMG(:,i)== Z_array       % Compare each channel
        EMG(:,i) = 0.1;         % If array zero then make not zero
    end
end
if m > 10000                    % For efficiency if array greater than 10000
samples
    for i = 1:n                 % Decimate the array
       EMG_dec(:,i) = decimate(EMG(:,i),20);    % Decimate the array by
factor 20
       EMG_abs(:,i) = abs(EMG_dec(:,i));        % Get RMS value for the
EMG
   end
else
    for i = 1:n
        EMG_abs(:,i) = abs(EMG(:,i));       % Create RMS anyway
    end
end
m=0; n=0; %reset m and n (don't know if strictly nec.)
[m,n] = size(EMG_abs);          % Get size of the EMG_norm signal array.
Length (samples and number of channels
                                % m = number of samples
                                % n = channel number
b = ones(1,50)/50;              % Coefficients for 50 point moving average
filter denominator
a = 1;                          % Numerator
for i = 1:n
    %EMG_LE(:,i) = filter(b,a,EMG_norm(:,i));        % Application of 50
point moving average filter
    %EMG_abs = EMG_filter(EMG_abs, 1, Hd);
    if DeBurst == 1
        [EMG_abs(:,i),C] = DeBurst(EMG_abs(:,i),6,'dmey',0.0005,0.2);
    else
        'no DeBurst';
    end
    EMG_abs(:,i) = Wave_filter(EMG_abs(:,i),'dmey',6);
end
EMG_abs = NormaliseLE(EMG_abs);                     % Get amplitude
normalised EMG
EMG_LE = EMG_Norm_Time(EMG_abs, Num_points);        % Re-samples the LE
to produce n points describing the LE
```

C.VII Plotting Linear Envelopes (Ensemble Average)

```
function ThesisPlotLE_STNDDEV(data,average,footswitch)

%invert footswitch
%for i = 1:length(footswitch)
%    if footswitch(i) < 0.5
```

```
%         footswitch(i) =1;
%     else
%         footswitch(i) = 0;
%     end
%end
[row col] = size(data);
if row ~= 100
    data = interpft(data,100);
else
x = 1:100;
% Calculate the standard deviation of the data
stddev = std(data');
stddev = stddev';
stndplus = average + stddev;
stndminus = average - stddev;
figure(1)
hold on
pixls = [x' stndplus; x(end:-1:1)' stndminus(end:-1:1)];
h = fill(pixls(:,1),pixls(:,2),[ 0.561 0.655 0.796 ]);
set(h, 'EdgeColor', [ 0.561 0.655 0.796 ]);
%plot(x,abs(data),'-b','LineWidth',0.5);
ylim([0 1]);
plot(x,abs(average),'-k','LineWidth',1.5);
plot(x,footswitch(:,1),'-.m',x,footswitch(:,2),'-.m',x,footswitch(:,3),'-
-r','LineWidth',2);
title('Normalised SEMG'); xlabel('% Gait Cycle'); ylabel(' Normalised
Amplitude');
%legend('SEMG LE','Average LE','Gait Phase',1);
hold off
```

D Appendix

LabVIEW Code

D.I Video Module

NEW_GAIT_FP_3.vi Front panel

Block Diagram

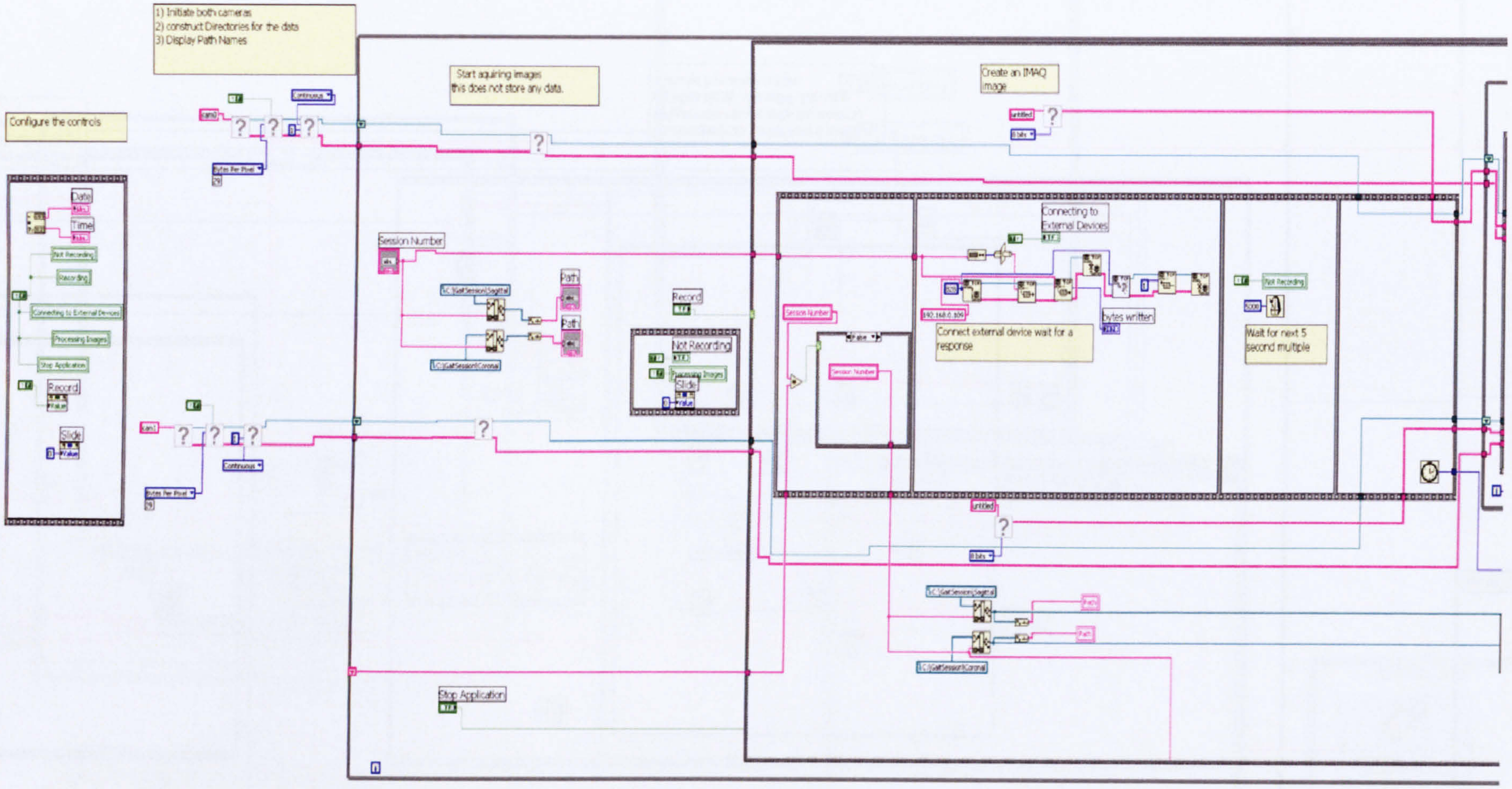
1) Initiate both cameras
2) construct Directories for the data
3) Display Path Names
Configure the controls
Start aquiring images
this does not store any data.
Create an IMAQ image
Session Number
Record
Not Recording
Processing Images
Slide
Connecting to External Devices
Connect external device wait for a response
bytes written
Wait for next 5 second multiple
Stop Application

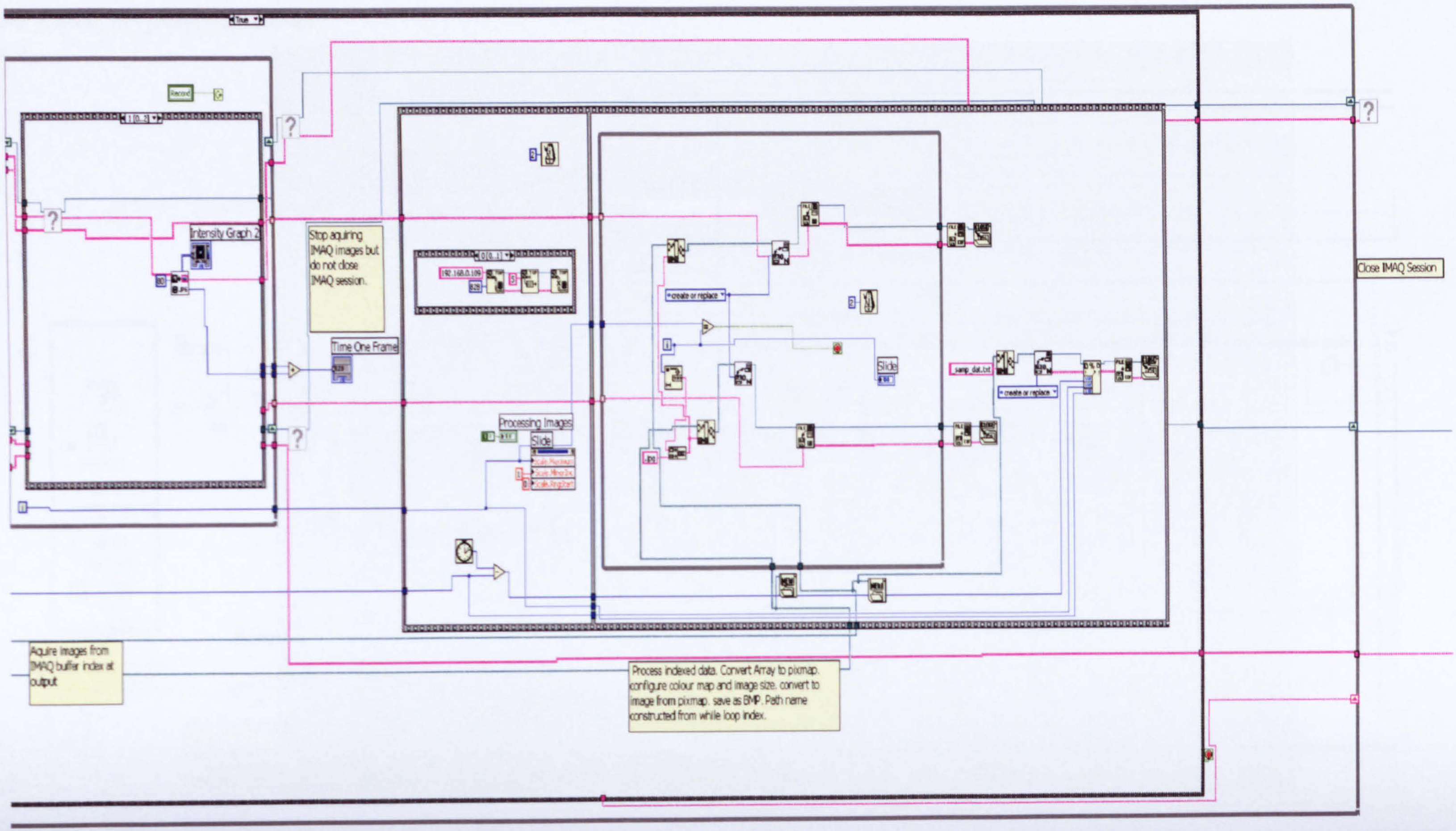
True
Record
Intensity Graph 2
Stop aquiring IMAQ images but do not close IMAQ session.
Time One Frame
Processing Images
Slide
create or replace
Close IMAQ Session
Aquire images from IMAQ buffer index at output
Process indexed data. Convert Array to pixmap. configure colour map and image size. convert to image from pixmap. save as BMP. Path name constructed from while loop index.

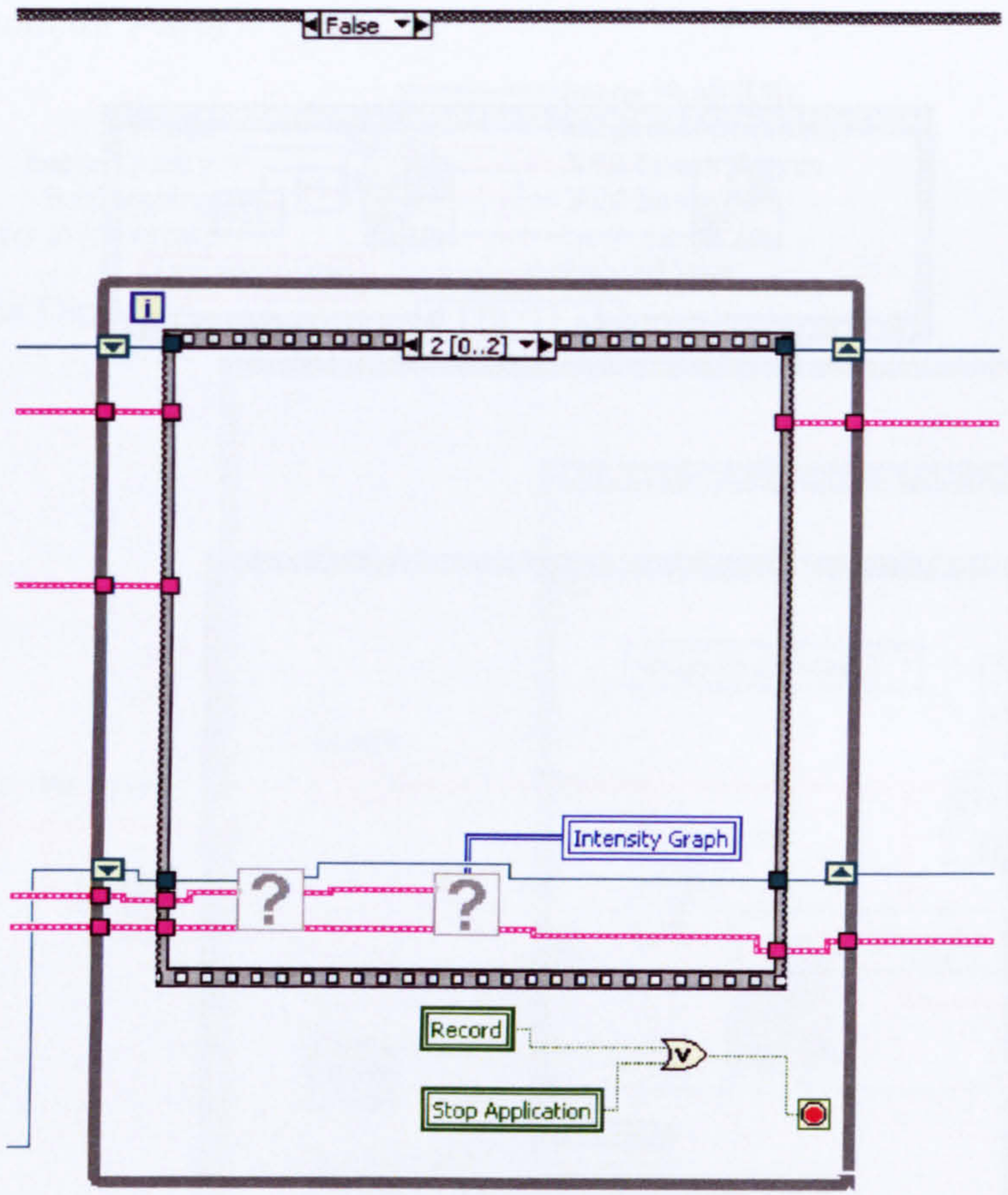

Get an image from IMAQ buffer and convert to 8 bit bitmap. Display on intensity graph

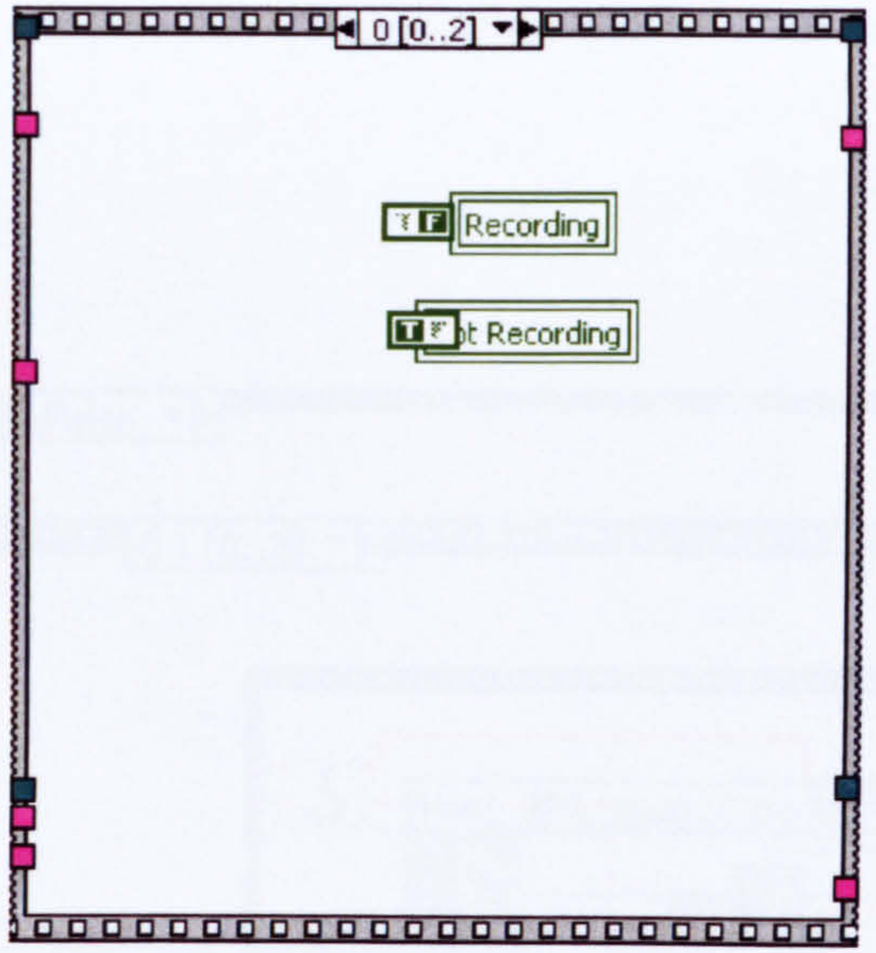

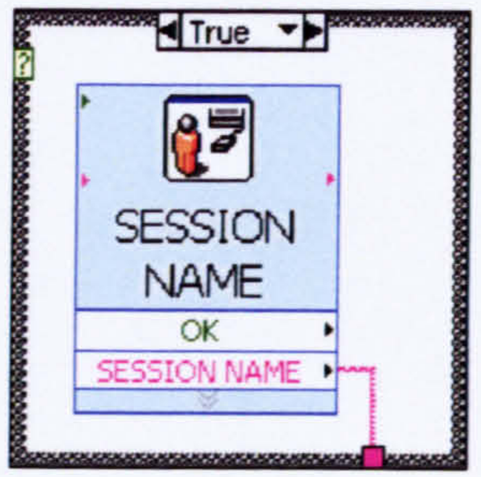

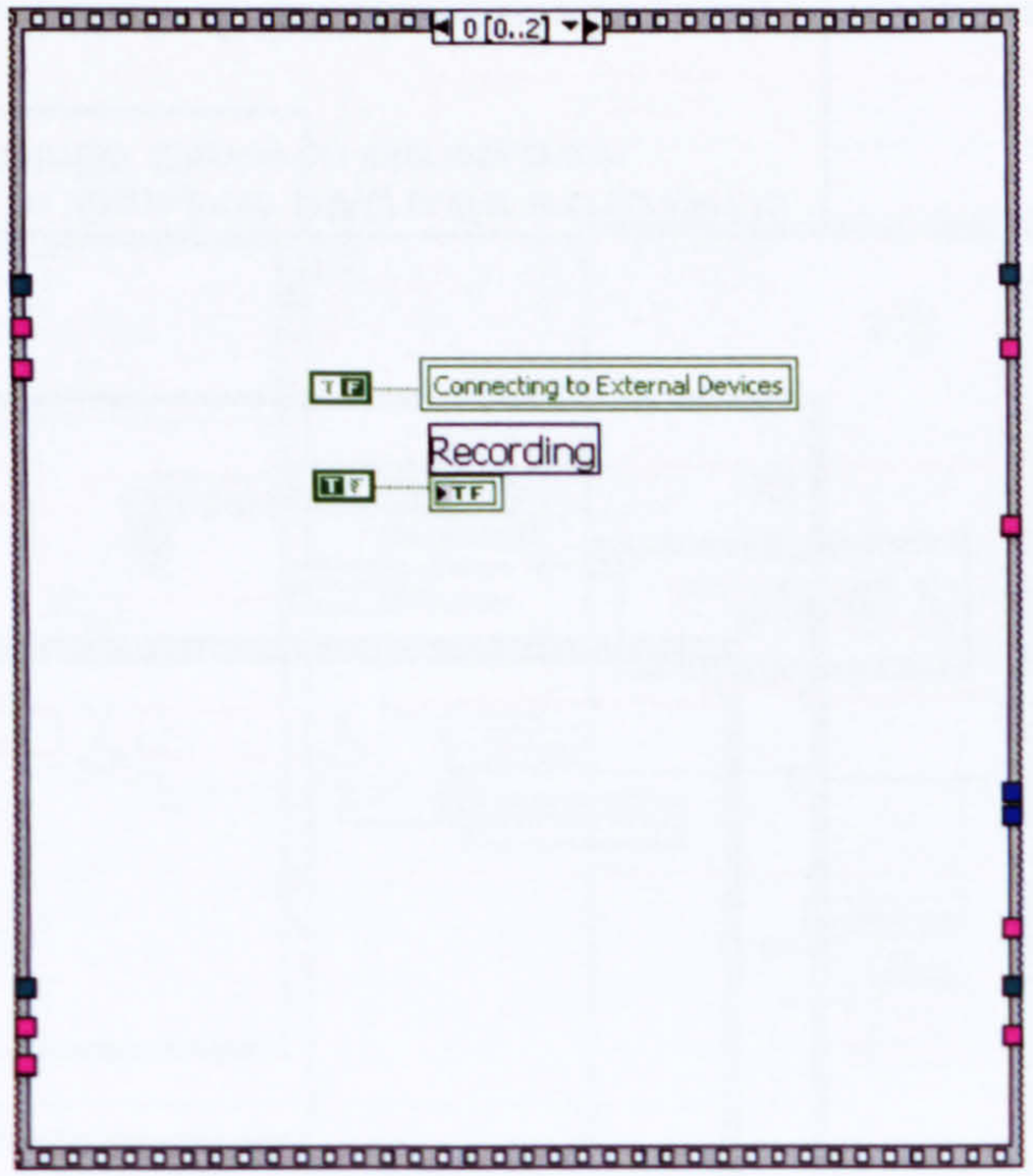
0 [0..2]
Connecting to External Devices
Recording

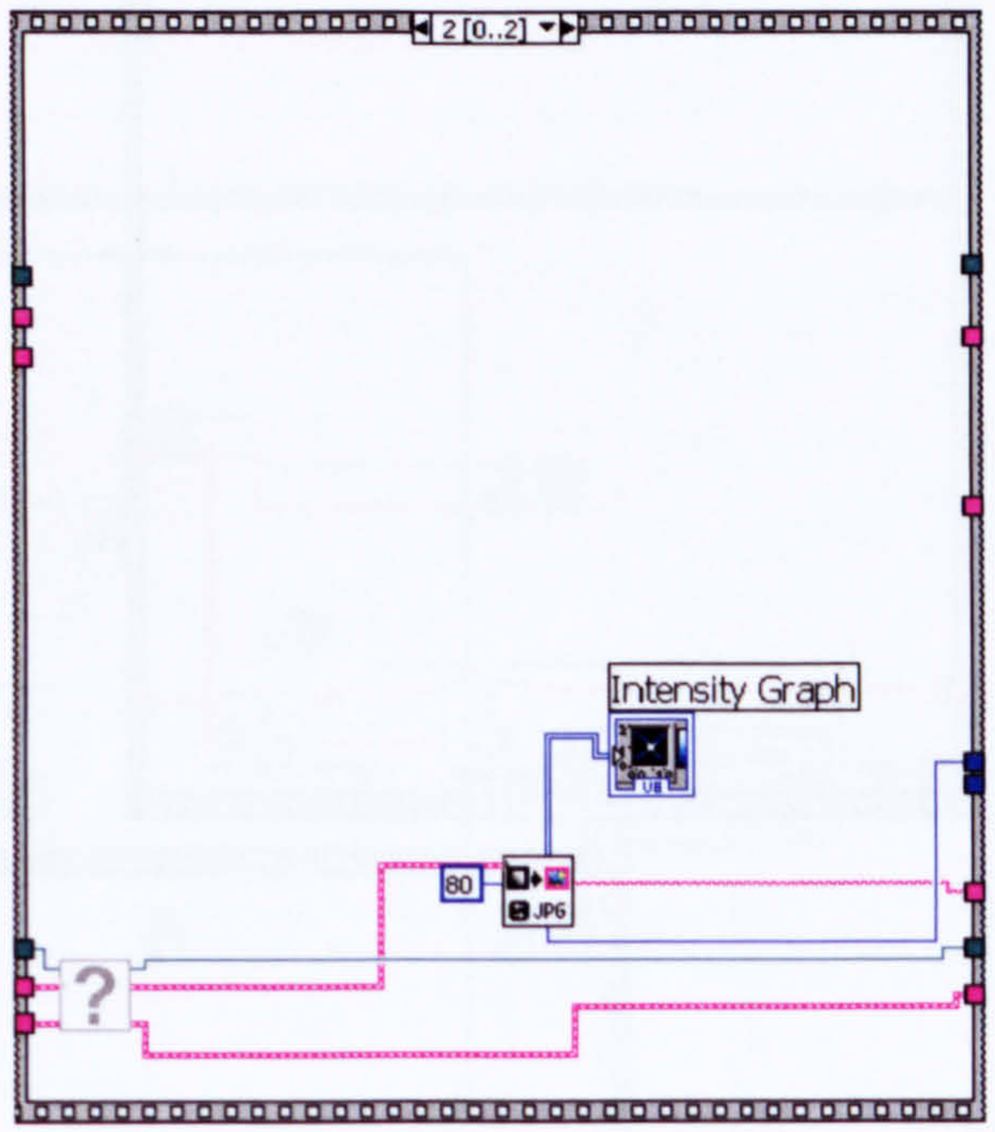
2 [0..2]
Intensity Graph
80
JPG
?

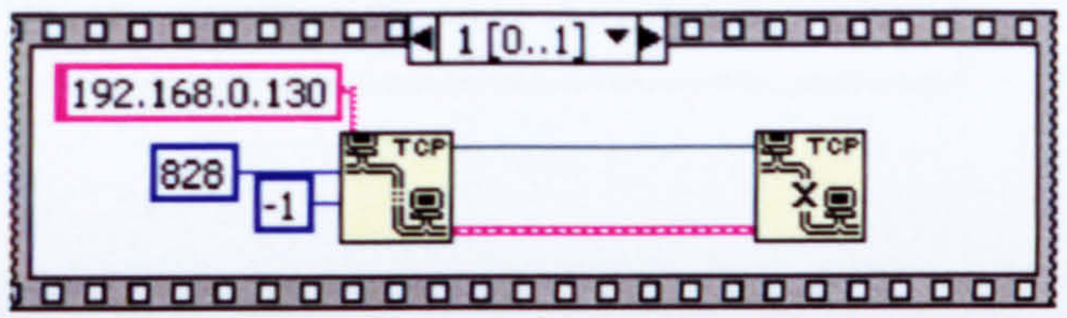
1 [0..1]
192.168.0.130
828
-1
TCP
TCP

Connector Pane

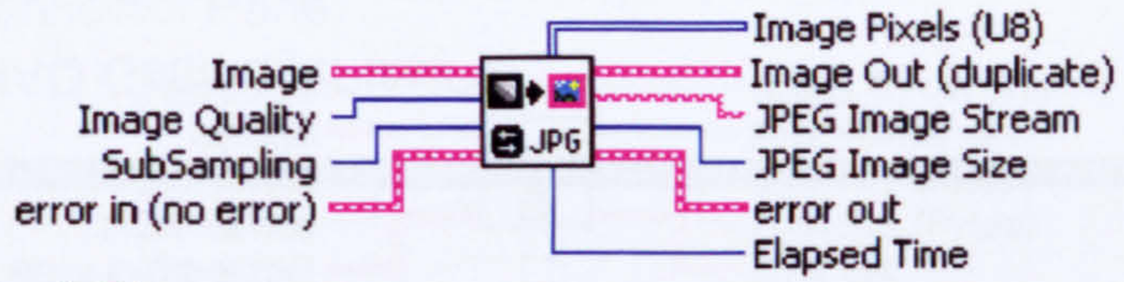

Block Diagram

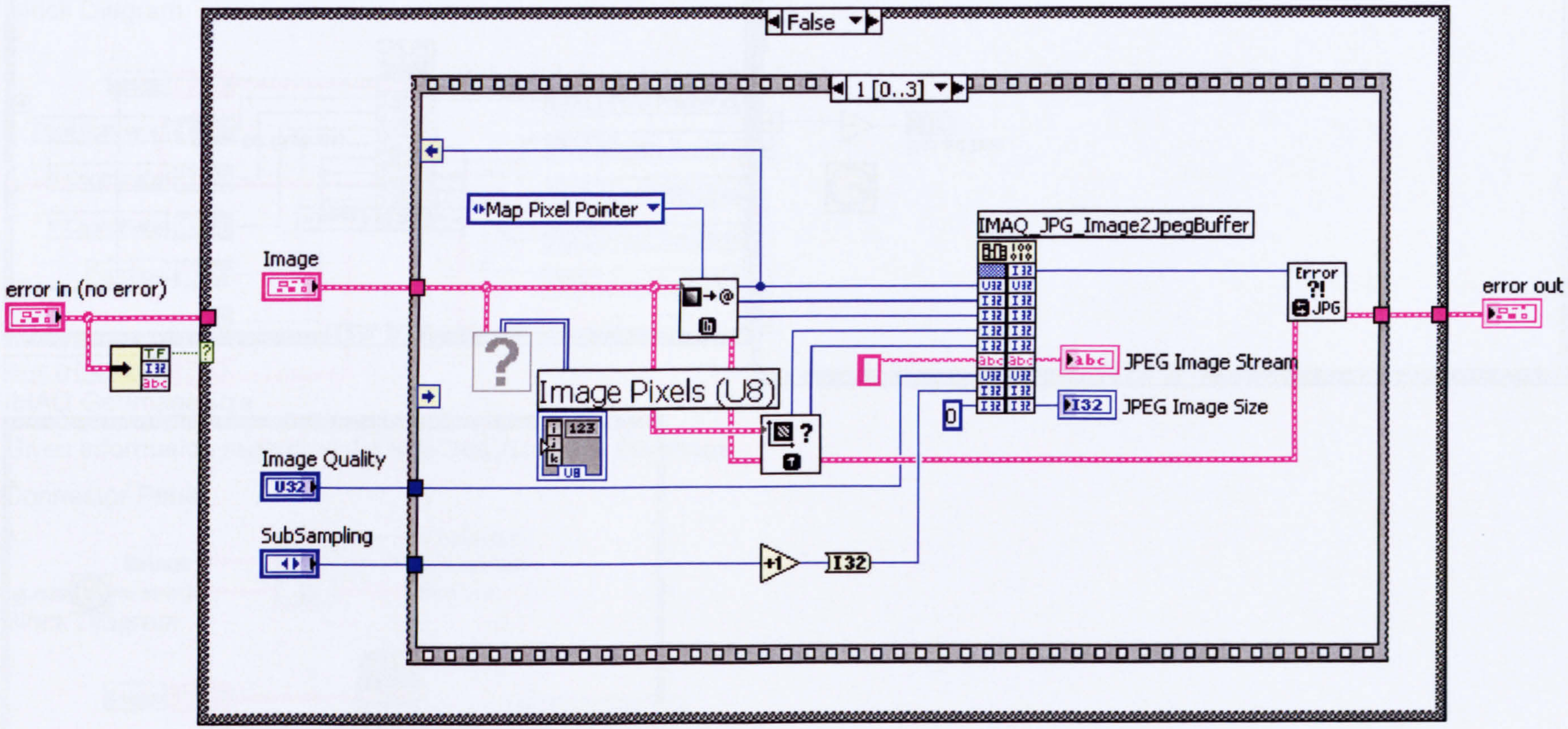

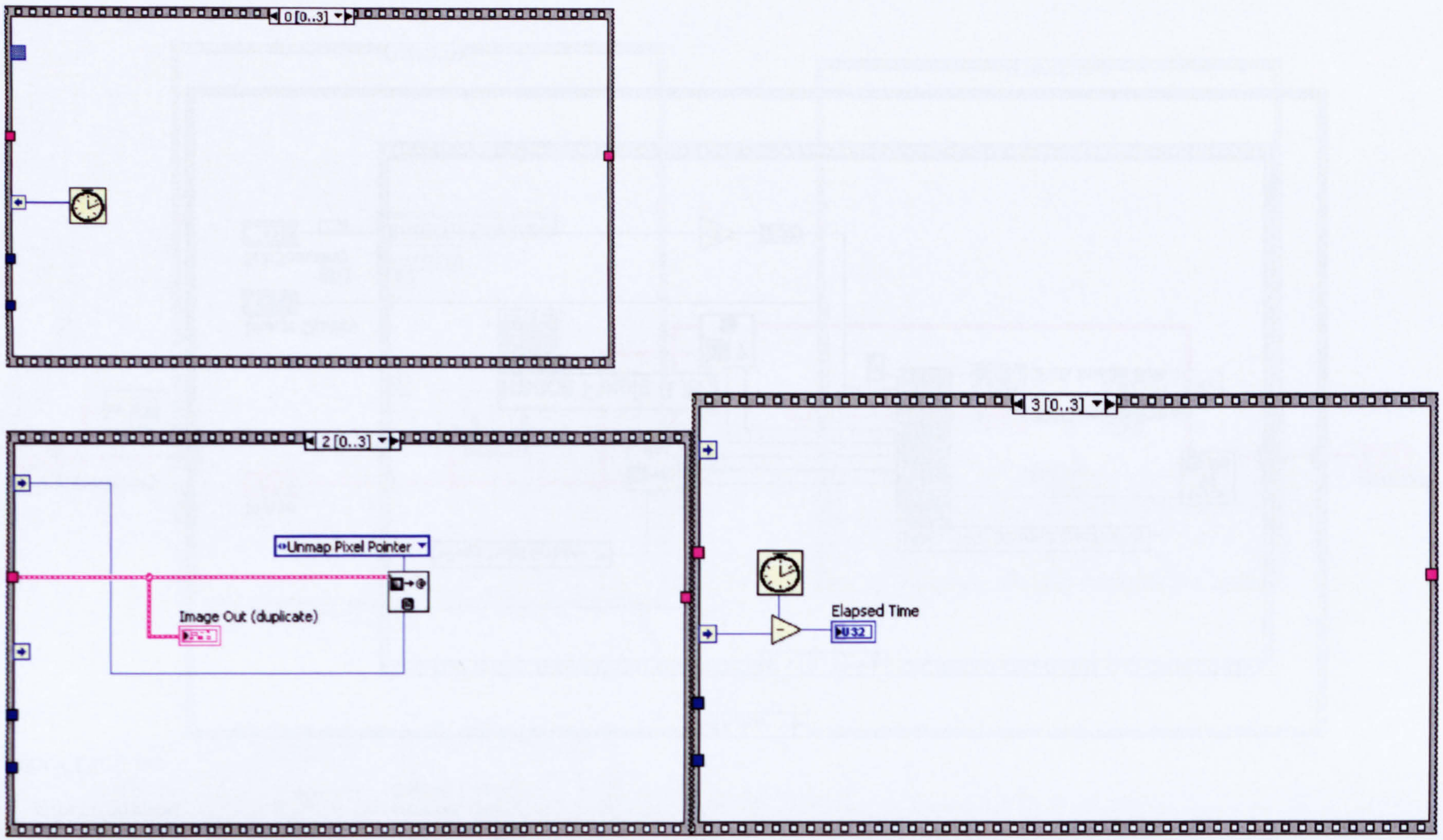

IMAQ GetImagePixelPtr

Obtains a pointer on the pixels of an image.

Connector Pane

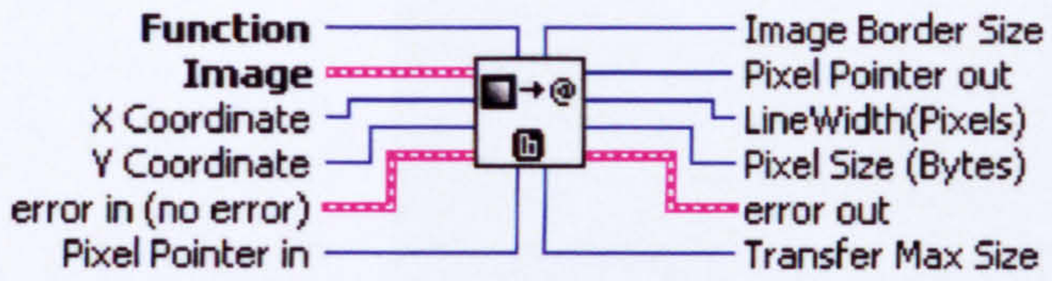

Block Diagram

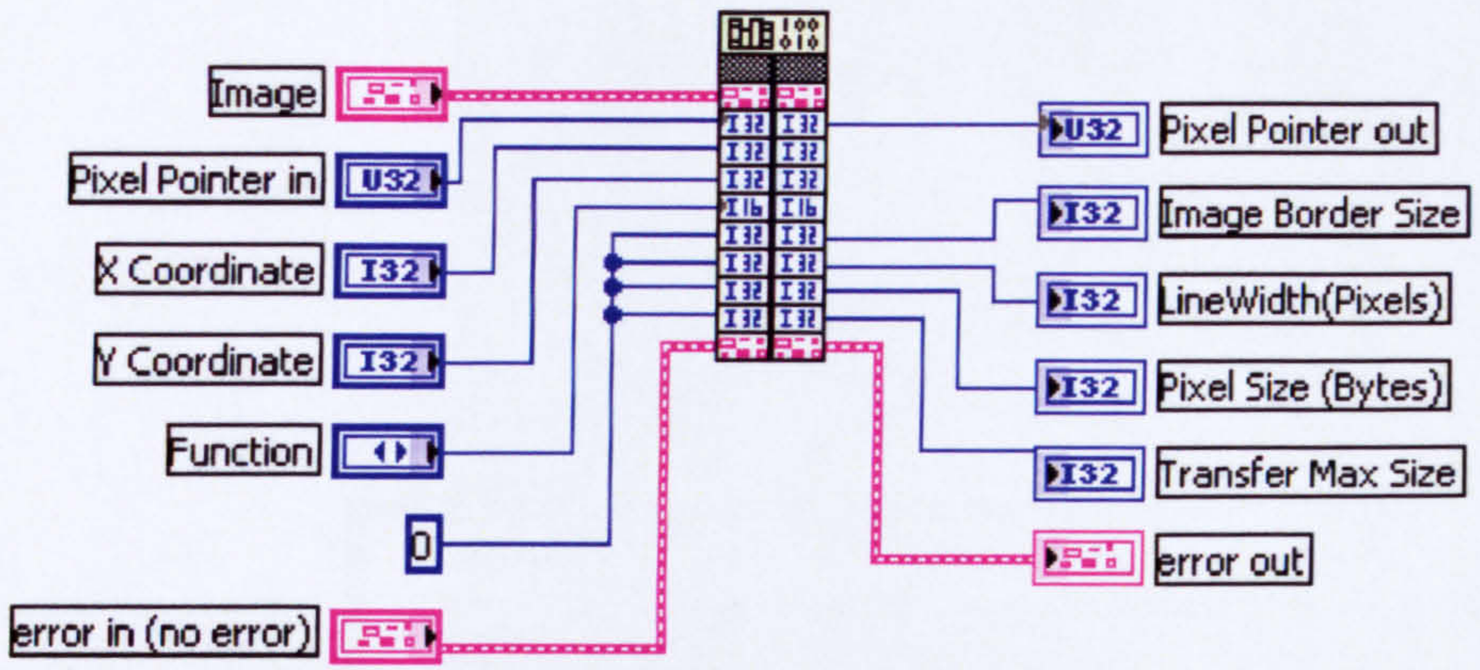

IMAQ GetImageSize

Gives information regarding the size (resolution) of the image.

Connector Pane

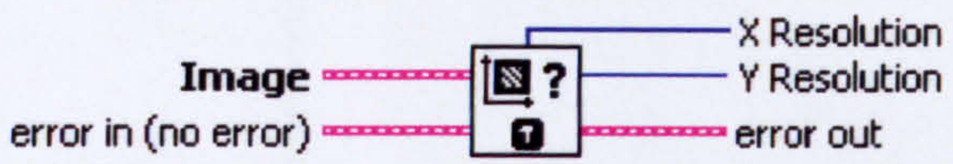

Block Diagram

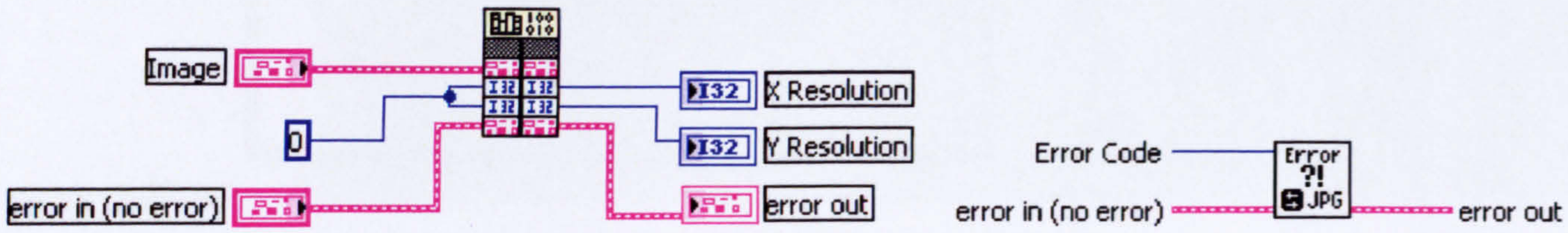

Block Diagram

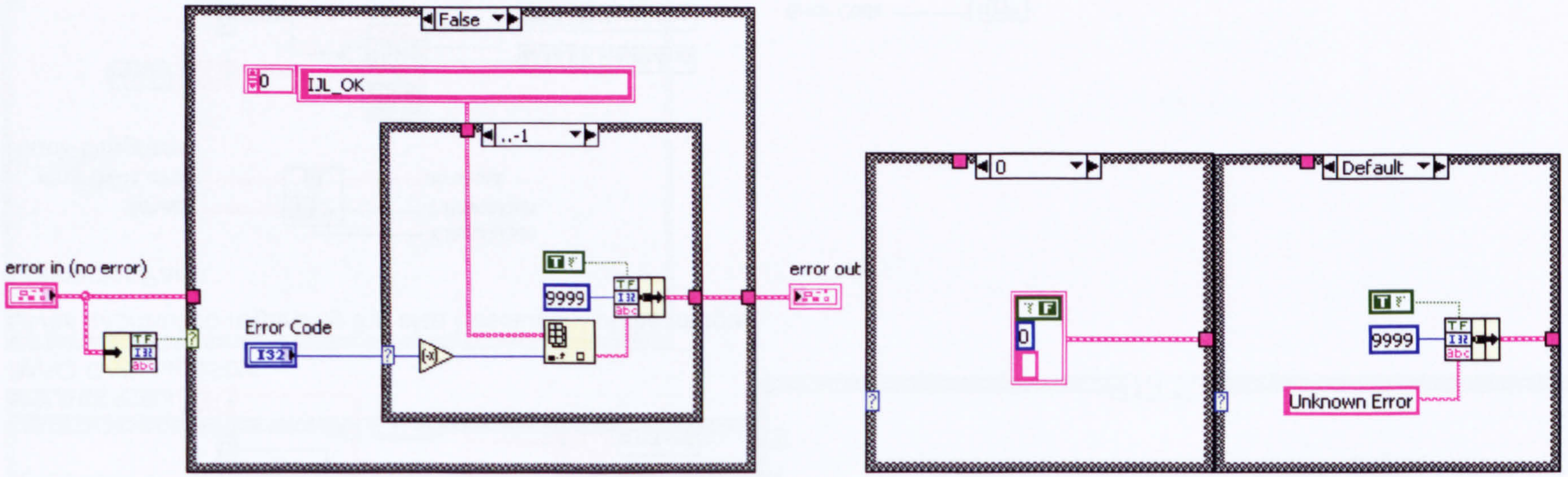

D.II Motion Analysis Module

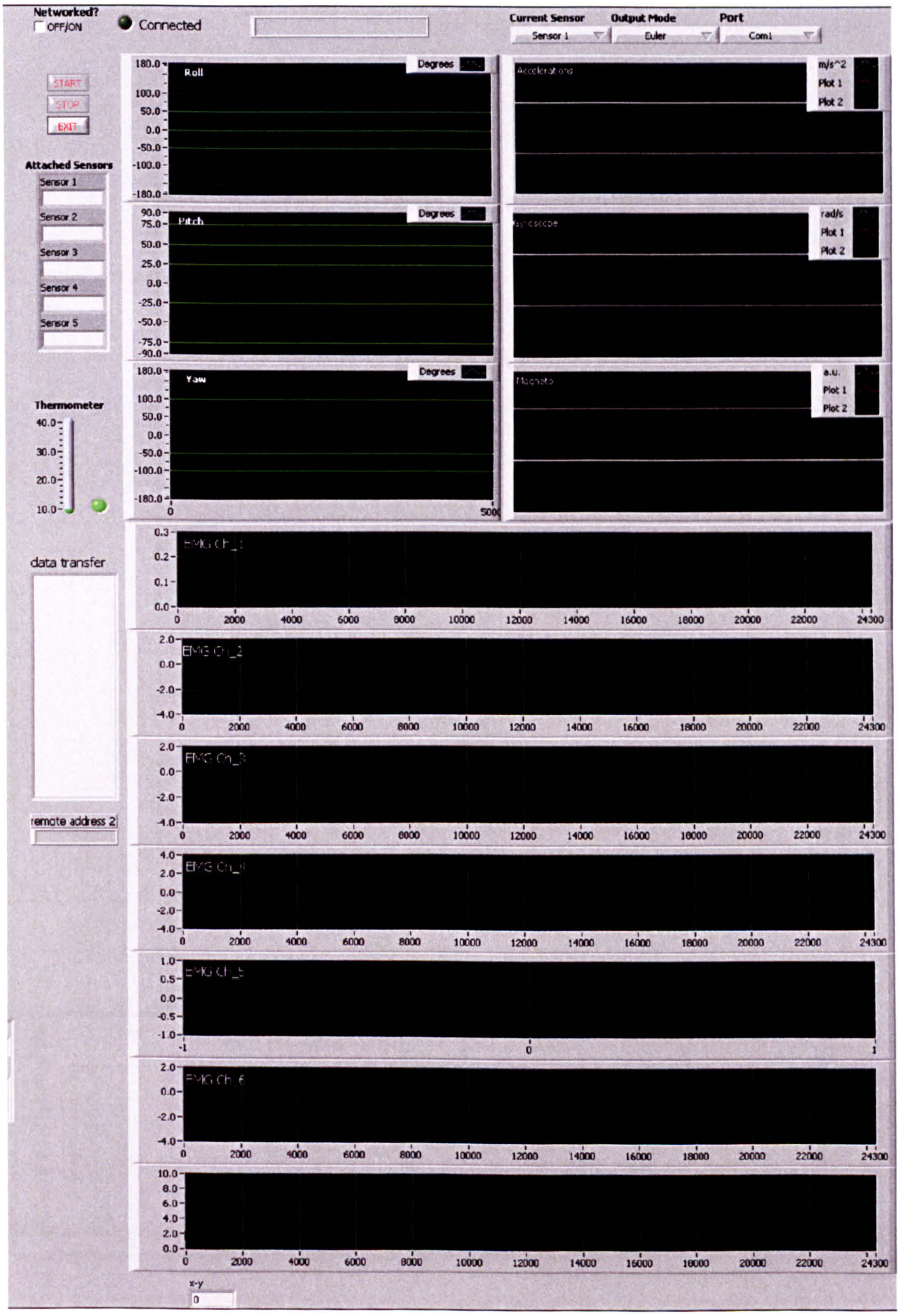

Block Diagram

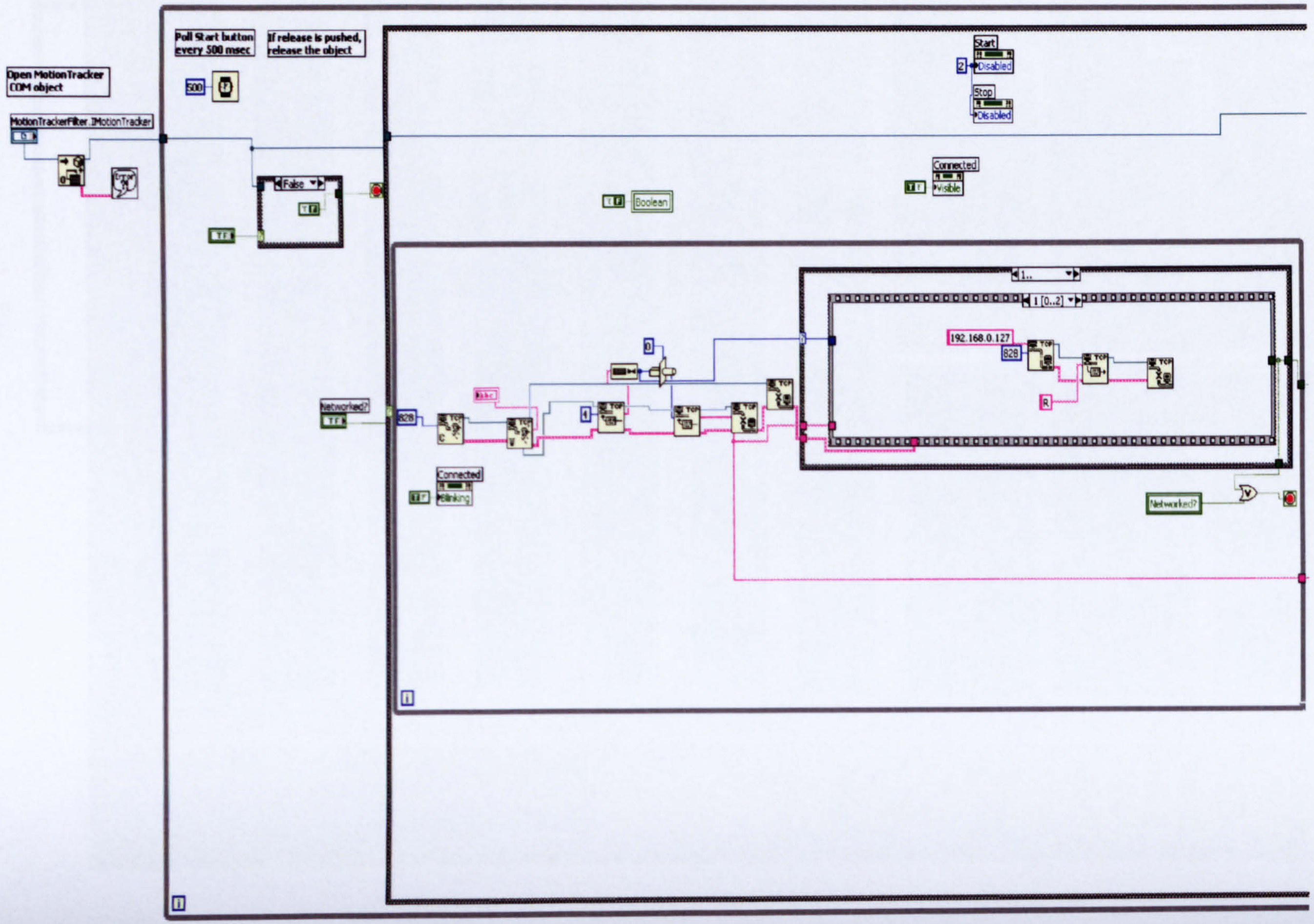

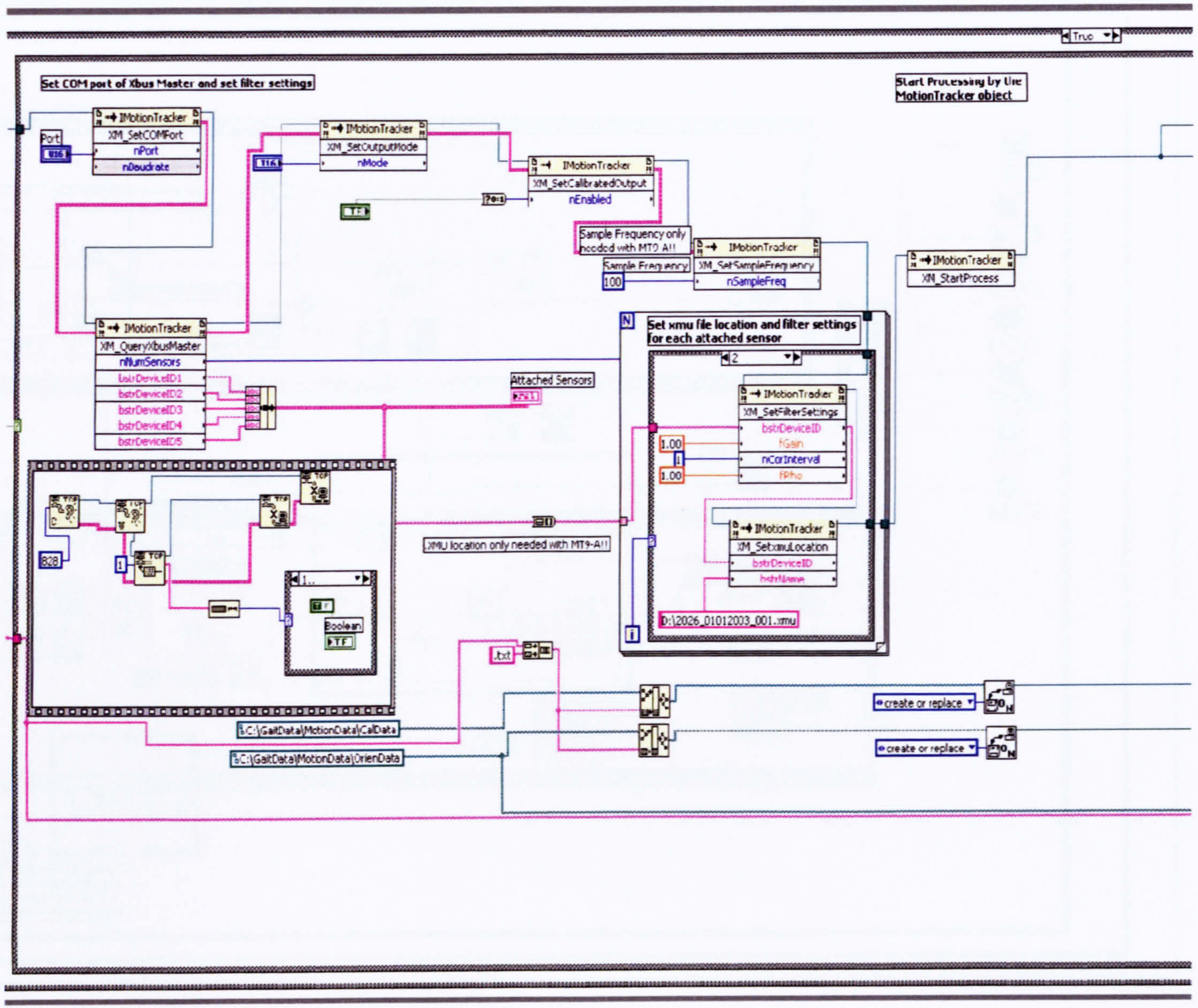
True
Set COM port of Xbus Master and set filter settings
Start Processing by the MotionTracker object
IMotionTracker
XM_SetCOMPort
nPort
nBaudrate
Port
XM_SetOutputMode
nMode
XM_SetCalibratedOutput
nEnabled
Sample Frequency only needed with MT9-A!!
Sample Frequency
100
XM_SetSampleFrequency
nSampleFreq
XM_StartProcess
XM_QueryXbusMaster
nNumSensors
bstrDeviceID1
bstrDeviceID2
bstrDeviceID3
bstrDeviceID4
bstrDeviceID5
Attached Sensors
Set xmu file location and filter settings for each attached sensor
XM_SetFilterSettings
bstrDeviceID
fGain
nCorInterval
fPho
XM_SetXmuLocation
bstrFileName
D:\2026_01012003_001.xmu
XMU location only needed with MT9-A!!
828
Boolean
.txt
C:\GaitData\MotionData\CalData
C:\GaitData\MotionData\OrienData
create or replace
create or replace

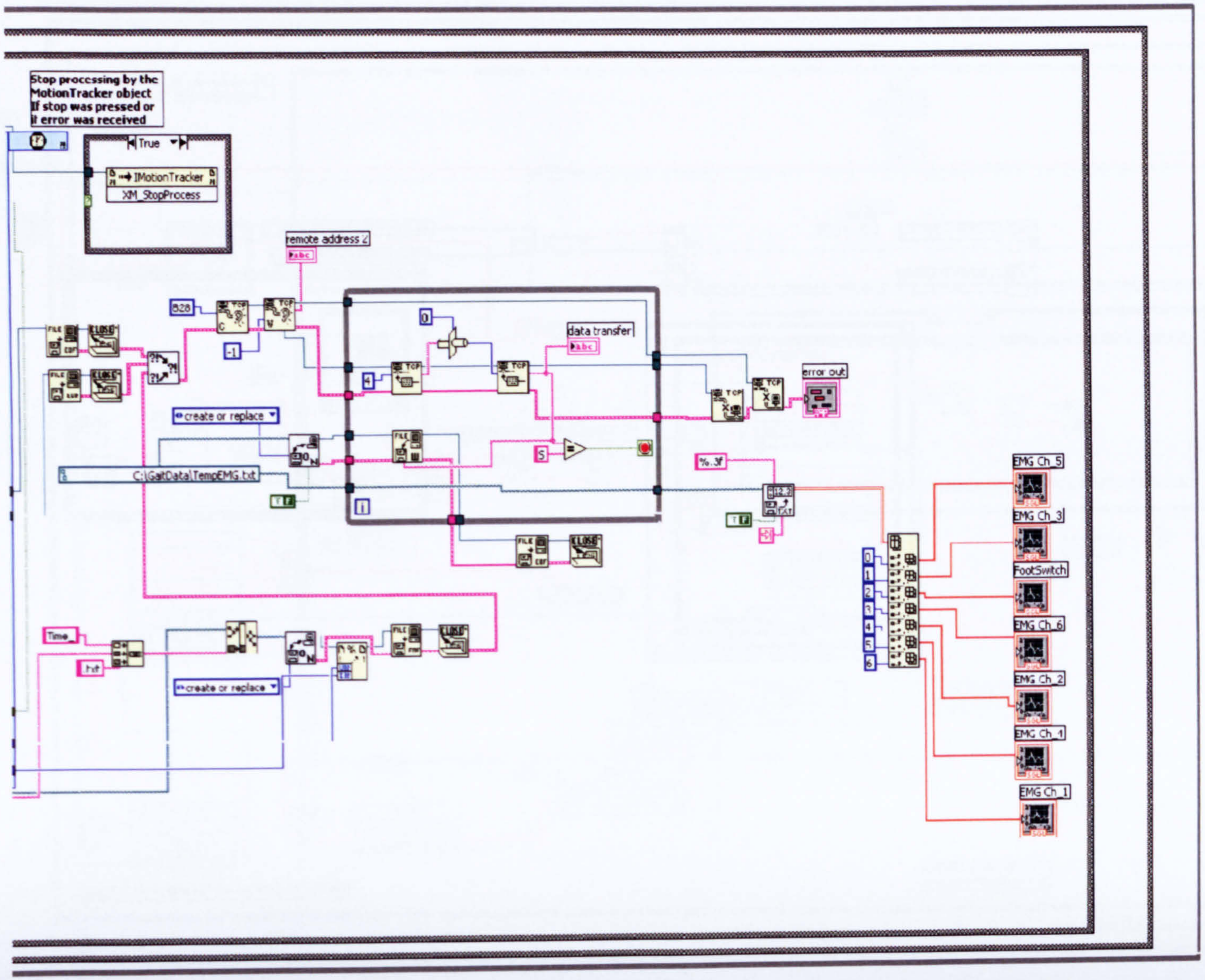
Stop processing by the MotionTracker object If stop was pressed or if error was received
True
IMotionTracker
XM_StopProcess
remote address
828
-1
data transfer
error out
create or replace
C:\GaitData\TempEMG.txt
%.3f
Time_
.txt
create or replace
EMG Ch_5
EMG Ch_3
FootSwitch
EMG Ch_6
EMG Ch_2
EMG Ch_1
EMG Ch_1

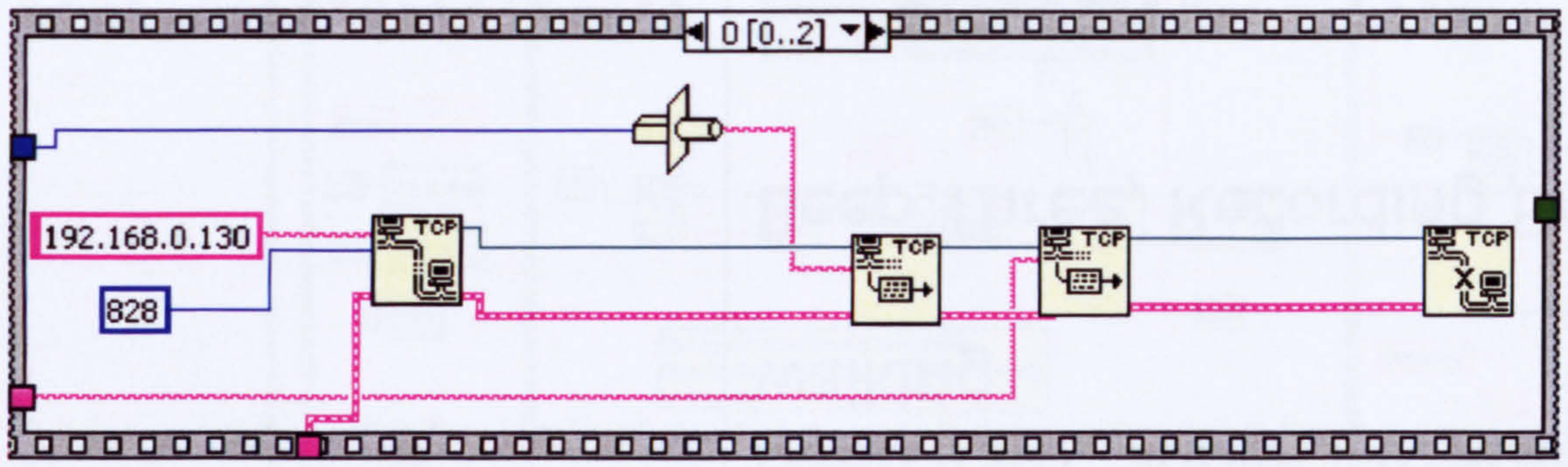
0 [0..2]
192.168.0.130
828
TCP
TCP
TCP
TCP

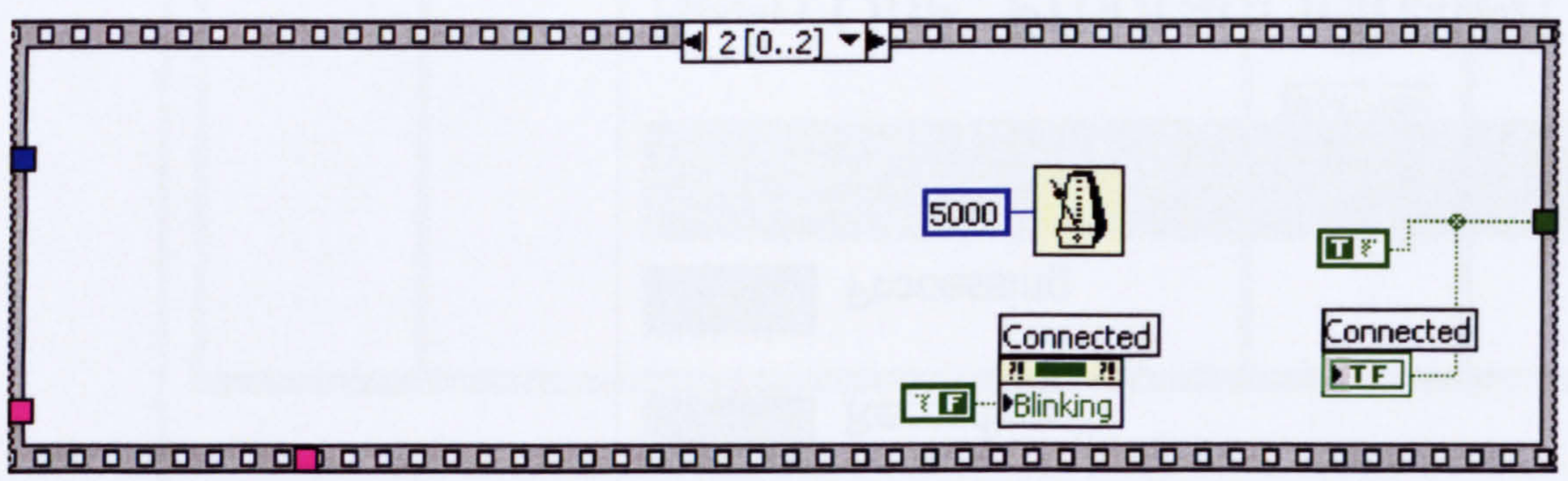
2 [0..2]
5000
Connected
Blinking
Connected
TF

D.III Surface EMG Module

PDA_EMG_V4.vi Front Panel

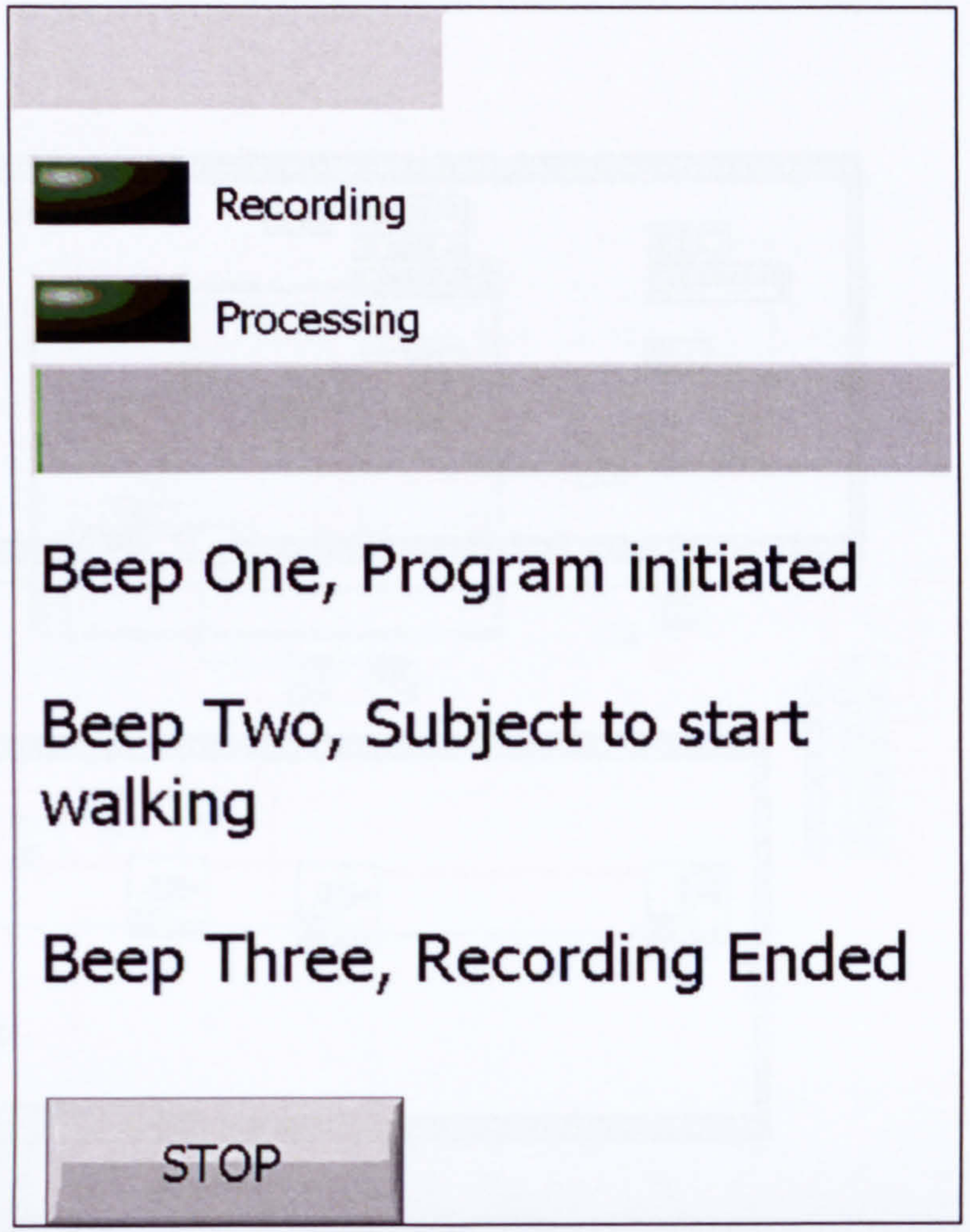

Block Diagram

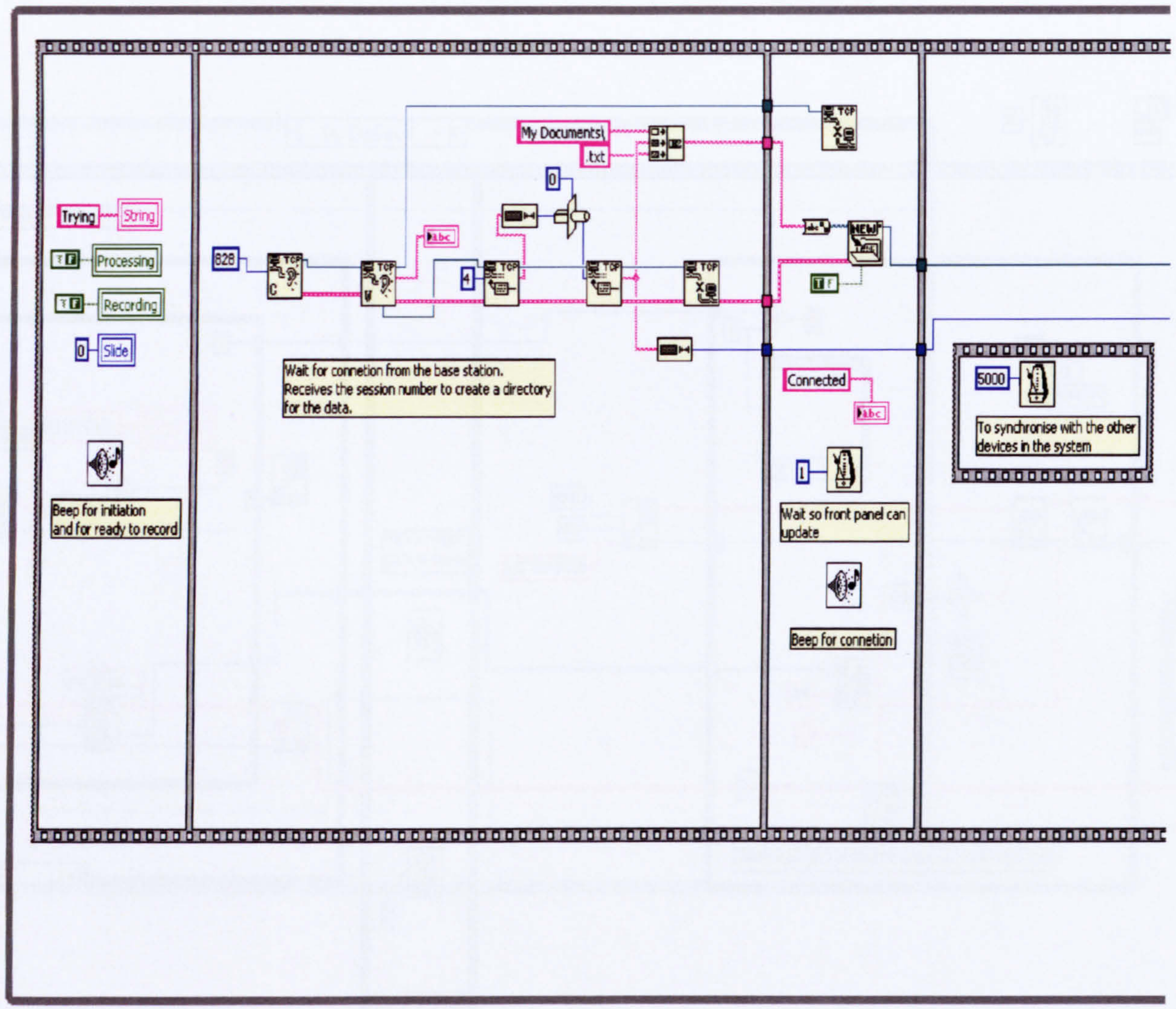
Trying
String
Processing
Recording
Slide
Beep for initiation and for ready to record
My Documents\
.txt
0
828
4
Wait for connetion from the base station. Receives the session number to create a directory for the data.
Connected
1
Wait so front panel can update
Beep for connetion
5000
To synchronise with the other devices in the system

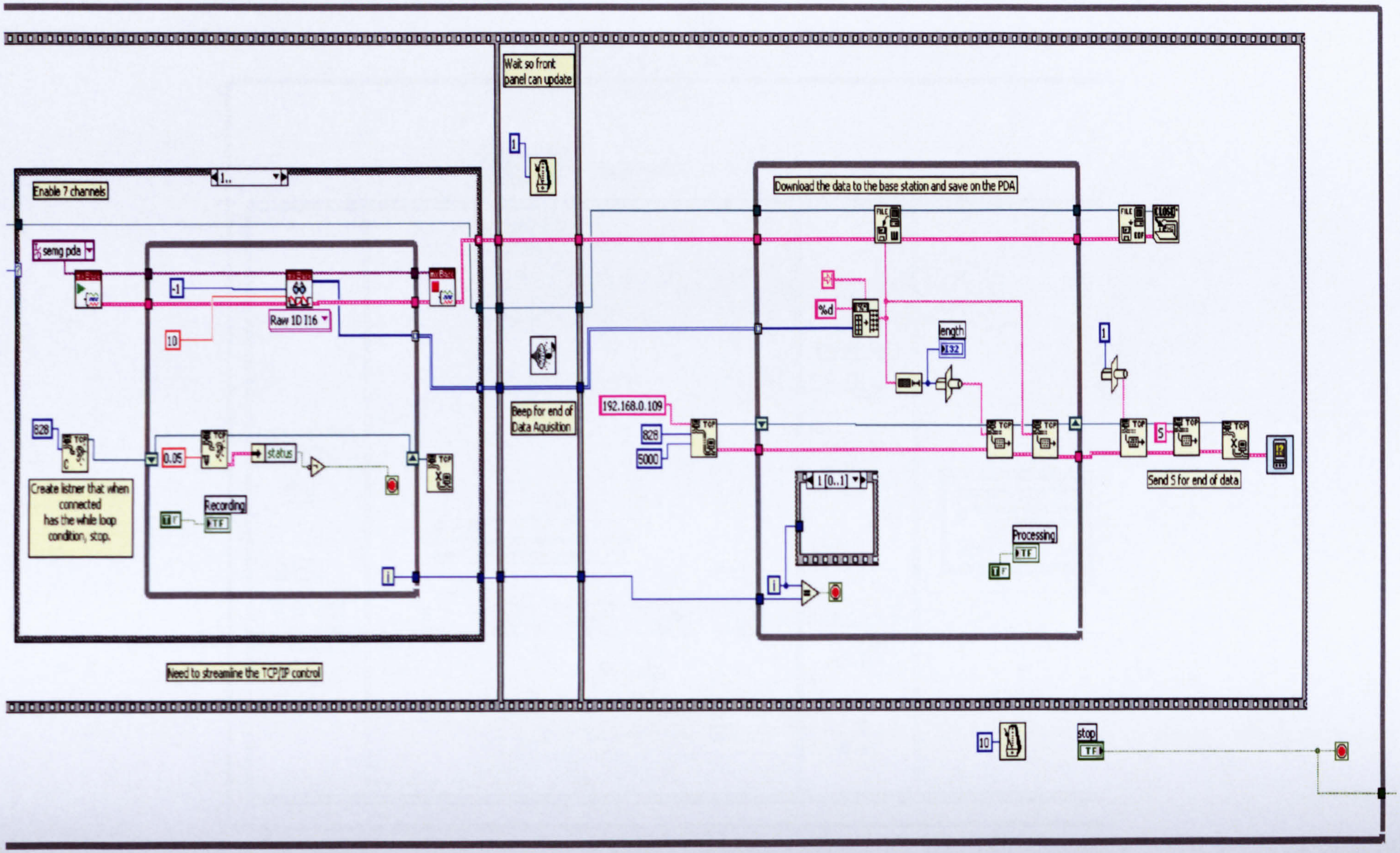
Wait so front panel can update
Enable 7 channels
semg pda
Raw 1D I16
Create listner that when connected has the while loop condition, stop.
Recording
status
Beep for end of Data Aquisition
Download the data to the base station and save on the PDA
192.168.0.109
828
5000
length
Send 5 for end of data
Processing
stop
Need to streamline the TCP/IP control

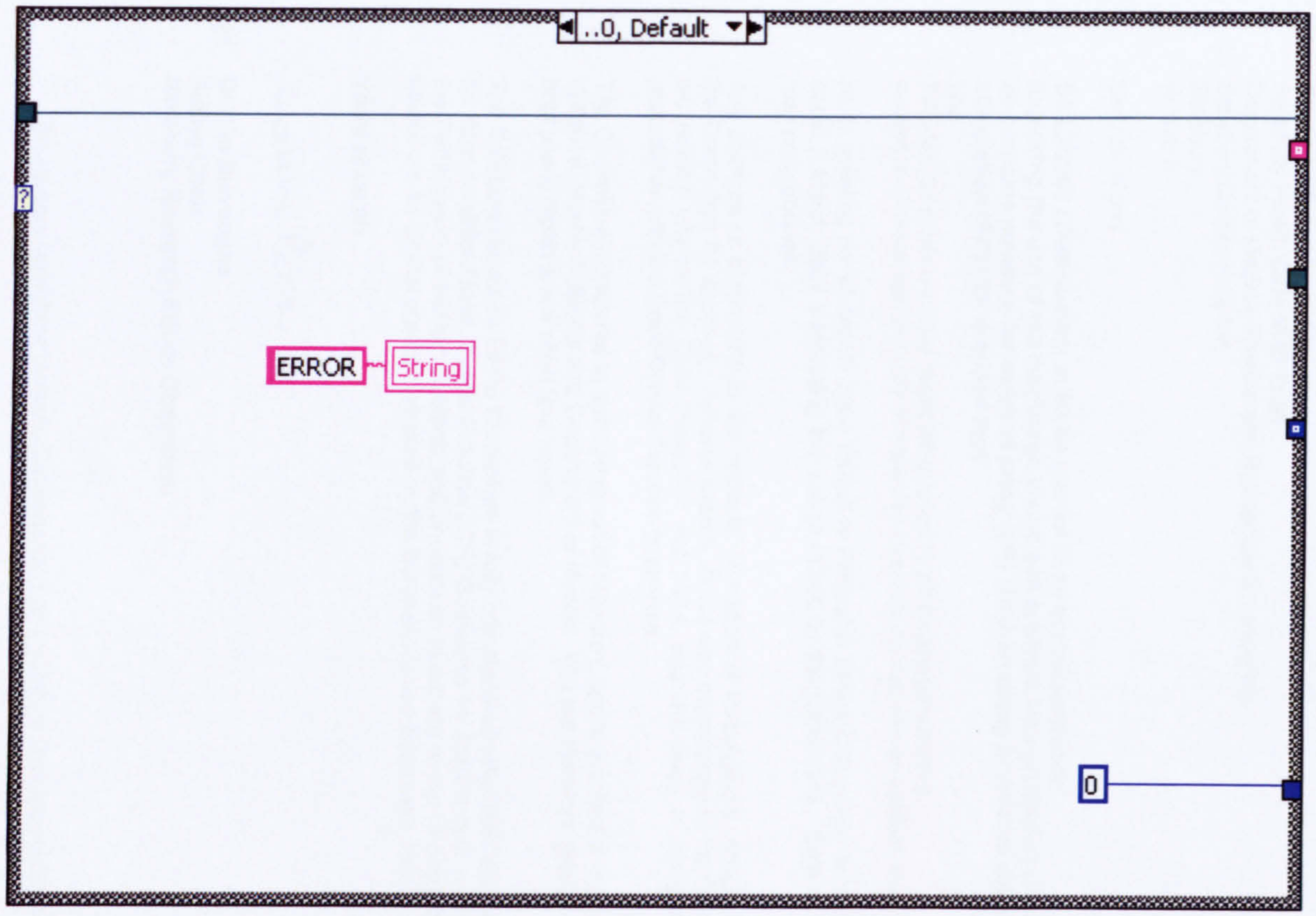
..0, Default
ERROR
String
0

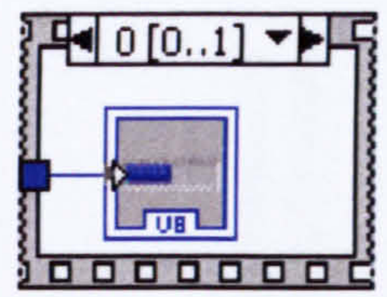
0 [0..1]
VB

E Appendix

Ethics

E.I Ethics Committee Favourable Opinion

Salisbury Research Ethics Committee (REC)
Kennet and North Wiltshire Primary Care Trust
Southgate House
Pans Lane
Devizes
Wiltshire
SN10 5EQ

Direct Line: 01380 733767
Fax: 01380 733779

SB/kp/SA 52/2003 and 53/2003

6 April 2004

Dr Duncan Wood
Principal Clinical Engineer
Salisbury Health Care NHS Trust
Department of Medical Physics and Biomedical Engineering
Salisbury District Hospital
Salisbury
Wiltshire

Dear Dr Wood

SA 52/2003 **(This number must be quoted in all correspondence)**
Exploring the use of the Edinburgh visual gait analysis interval testing (GAIT) scale as an outcome measure for cerebral palsy (CP) children using functional electrical stimulation (FES) for dropped foot
and
SA 53/2003 **(This number must be quoted in all correspondence)**
Analysis of electrical activity in muscles to characterise abnormalities during walking

At its meeting on 31 March 2004 Salisbury Research Ethics Committee received your letter dated 9 March 2004 addressing the issues raised by the Committee. Both of these studies may now proceed.

Any changes or extensions to the protocol, or additional investigators, should be notified to the Committee for approval. Adverse events should also be reported to the Committee. May we remind you of the Data Protection Act 1984, and the need to conduct the trial in accordance with the Good Clinical Practice guidelines.

The Committee is required to audit progress of research, and to produce a yearly report to the Wiltshire Health Authority and Department of Health. You are therefore required to provide a brief yearly report and a short final report.

The Salisbury Research Ethics Committee is fully compliant with the International Conference on Harmonisation/Good Clinical Practice (ICH) Guidelines for the Conduct of Trials Involving the Participation of Human Subjects and undertakes to adhere to the relevant clauses of the guidelines for clinical practice adopted by the European Union in January 1997.

Yours sincerely

Kirsten Peck

pp **Dr Sue Burroughs**
Acting Chair
Salisbury Research Ethics Committee

E.II Assessment Flow Diagram

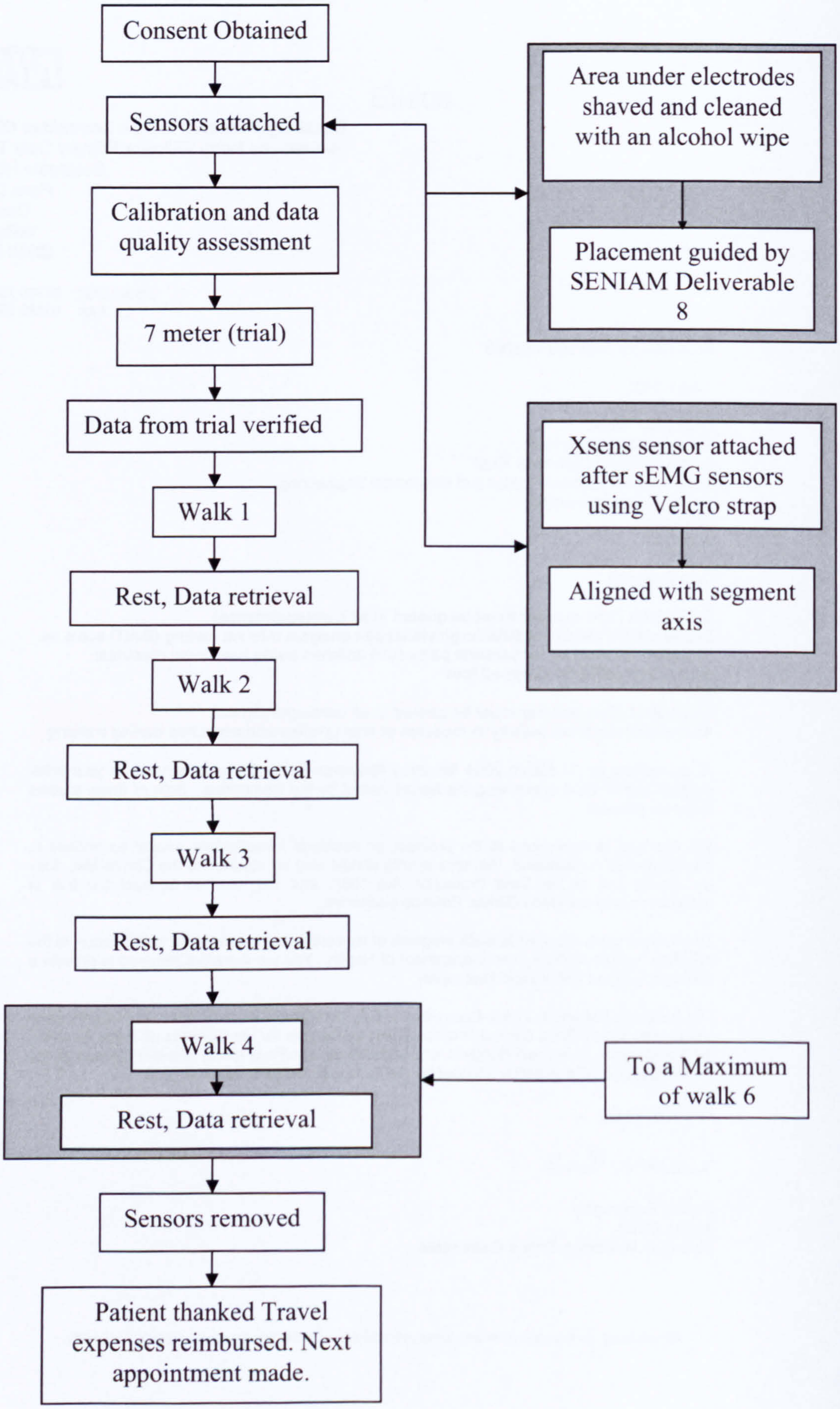

F Appendix

Observational Gait analysis Scale

F.I Rivermead Visual Gait Assessment Form

Rivermead Visual Gait Assessment Form

Patient or Video ID: Date

Scoring 0 = normal **Deviations** 1 = mild, 2 = moderate, 3 = severe

For trunk deviations 0 = midline

Upper Limb Position				**0**	**1**	**2**	**3**	
1 Shoulder Depressed/Retracted/Elevated				☐	☐	☐	☐	
2 Elbow flexed ≤ 45° (=0) 45° to 90° (=1) >90° (=2)				☐	☐	☐	☐	
Stance Phase								
3. Trunk Flexed / Extended								
Inclined:	**3** ☐	**2** ☐	**1** ☐	**0** ☐	**1** ☐	**2** ☐	**3** ☐	
	Backward ←					→ *Forward*		
4. Trunk Side Flexed								
Direction:	**3** ☐	**2** ☐	**1** ☐	**0** ☐	**1** ☐	**2** ☐	**3** ☐	
	Left ←					→ *Right*		
5. Trunk & Pelvis: lateral displacement								
Amount:	**3** ☐	**2** ☐	**1** ☐	**0** ☐	**1** ☐	**2** ☐	**3** ☐	
	Excessive ←					→ *Reduced*		
6. Contralateral drop pelvis				**0** ☐	**1** ☐	**2** ☐	**3** ☐	
7. Hip **extension** decreased				☐	☐	☐	☐	
With backward rotation				☐	☐	☐	☐	
Knee **flexion** excessive:								
9a. *at initial contact*				☐	☐	☐	☐	
10a. *through Range*				☐	☐	☐	☐	
OR								
Knee **extension** excessive:								
9b. *at initial contact*				☐	☐	☐	☐	
10b. *through range*				☐	☐	☐	☐	
11a. Ankle in excess **plantar** flexion				☐	☐	☐	☐	

Stance Phase Continued ...

	0	1	2	3
11b. Ankle excess dorsi flexion	☐	☐	☐	☐
12. Inversion excessive	☐	☐	☐	☐
13. Planter flexion decreased at toe off	☐	☐	☐	☐

Swing Phase

For trunk deviations 0 = midline

14. Trunk flexed		3 ☐	2 ☐	1 ☐	0 ☐	1 ☐	2 ☐	3 ☐
	Direction	*Backward* ←					→	*Forward*
15. Trunk side flexed		3 ☐	2 ☐	1 ☐	0 ☐	1 ☐	2 ☐	3 ☐
	Direction	*Left*		←			→	*Right*

	0	1	2	3
16. Hike pelvis (elevation)	☐	☐	☐	☐
17. Backward rotation pelvis	☐	☐	☐	☐
18. Decreased **hip** flexion	☐	☐	☐	☐
19. Decreased **knee** flexion	☐	☐	☐	☐
20. Ankle in excess **plantar** flexion	☐	☐	☐	☐
21. Ankle inverts excessively	☐	☐	☐	☐

Reference Limb: _____

Walking Aid:

F.II Los Amigos Gait Analysis Form

GAIT ANALYSIS: FULL BODY

RANCHO LOS AMIGOS MEDICAL CENTER
PHYSICAL THERAPY DEPARTMENT

Reference Limb:
L [X] R [ ]

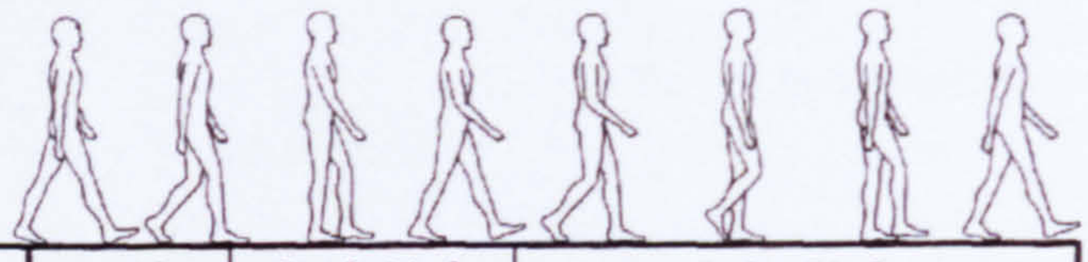

Major Deviation
Minor Deviation

		Weight Accept		Single Limb Support		Swing Limb Advancement			
		IC	LR	MSt	TSt	PSw	ISw	MSw	TSw
Trunk	Lean: B/F								
	Lateral Lean: R/L								
	Rotates: B/F								
Pelvis	Hikes								
	Tilt: P/A								
	Lacks Forward Rotation								
	Lacks Backward Rotation								
	Excess Forward Rotation								
	Excess Backward Rotation								
	Ipsilateral Drop								
	Contralateral Drop								
Hip	Flexion: Limited								
	Excess							✓	
	Inadequate Extension								
	Past Retract								✓
	Rotation: IR/ER								
	Ad/Abduction: Ad/Ab								
Knee	Flexion: Limited		✓						
	Excess								
	Inadequate Extension								✓
	Wobbles								
	Hyperextends								
	Extension Thrust								
	Varus/Valgus: Vr/Vl								
	Excess Contralateral Flex								
Ankle	Forefoot Contact	✓							
	Foot-Flat Contact								
	Foot Slap								
	Excess Plantar Flexion		✓				✓	✓	✓
	Excess Dorsiflexion								
	Inversion/Eversion: Iv/Ev								
	Heel Off								
	No Heel Off								
	Drag								
	Contralateral Vaulting								
Toes	Up								
	Inadequate Extension								
	Clawed								

MAJOR PROBLEMS:

Weight Acceptance

forefoot contact
limited knee flexion

Single Limb Support

Swing Limb Advancement

inadequate knee extension
excess plantar flexion

Excessive UE Weight Bearing [ ]

Name

(L) tibia & fibula fx

Diagnosis

G Appendix

Sensor Placement

MUSCLE

Name	Gastrocnemius
Subdivision	Medialis

MUSCLE ANATOMY

Origin	Proximal and posterior part of medial condyle and adjacent part of the femur, capsule of the knee joint.
Insertion	Middle part of posterior surface of calcaneus.
Function	Flexion of the ankle joint and assist in flexion of the knee joint.

Electrode location on the muscle

RECOMMENDED SENSOR PLACEMENT PROCEDURE

Starting posture	Lying on the belly with the face down, the knee extended and the foot projecting over the end of the table.
Electrode size	Maximum size in the direction of the muscle fibres: 10 mm.
Inter electrode distance	20 mm.
Electrode placement	
- location	Electrodes need to be placed on the most prominent bulge of the muscle.
- orientation	In the direction of the leg (see picture).
- fixation on the skin	(Double sided) tape / rings or elastic band.
- reference electrode	On / around the ankle or the proc. spin of C7.
Clinical test	Plantar flexion of the foot with emphasis on pulling the heel upward more than pushing the forefoot downward. For maximum pressure in this position it is necessary to apply pressure against the forefoot as well as against the calcaneus.
Remarks	The SENIAM guidelines include a separate sensor placement procedure for the lateral gastrocnemius.

MUSCLE

Name	Tibialis anterior
Subdivision	

MUSCLE ANATOMY

Origin	Lateral condyle and proximal 1/2 of lateral surface of tibia, interosseus membrane, deep fascia and lateral intermuscular septum.
Insertion	Medial and plantar surface of medial cuneiform bone, base of first metatarsal bone.
Function	Dorsiflexion of the ankle joint and assistance in inversion of the foot.

Electrode location on the muscle

RECOMMENDED SENSOR PLACEMENT PROCEDURE

Starting posture	Supine or sitting.
Electrode size	Maximum size in the direction of muscle fibres: 10 mm.
Inter electrode distance	20 mm.
Electrode placement	
- location	The electrodes need to be placed at 1/3 on the line between the tip of the fibula and the tip of the medial malleolus.
- orientation	In the direction of the line between the tip of the fibula and the tip of the medial malleolus.
- fixation on the skin	(Double sided) tape / rings or elastic band.
- reference electrode	On / around the ankle or the proc. spin. of C7.
Clinical test	Support the leg just above the ankle joint with the ankle joint in dorsiflexion and the foot in inversion without extension of the great toe. Apply pressure against the medial side, dorsal surface of the foot in the direction of plantar flexion of the ankle joint and eversion of the foot.

MUSCLE

Name	Quadriceps femoris
Subdivision	Rectus femoris

MUSCLE ANATOMY

Origin	Straight head from anterior inferior iliac spine. Reflected head from groove above rim of acetabulum.
Insertion	Proximal border of the patella and through patellar ligament.
Function	Extension of the knee joint and flexion of the hip joint.

Electrode location on the muscle

RECOMMENDED SENSOR PLACEMENT PROCEDURE

Starting posture	Sitting on a table with the knees in slight flexion and the upper body slightly bend backward.
Electrode size	Maximum size in the direction of the muscle fibres: 10 mm.
Inter electrode distance	20 mm.
Electrode placement	
- location	The electrodes need to be placed at 50% on the line from the anterior spina iliaca superior to the superior part of the patella
- orientation	In the direction of the line from the anterior spina iliaca superior to the superior part of the patella.
- fixation on the skin	(Double sided) tape / rings or elastic band.
- reference electrode	On / around the ankle or the proc. spin. of C7.
Clinical test	Extend the knee without rotating the thigh while applying pressure against the leg above the ankle in the direction of flexion.
Remarks	The SENIAM guidelines include also a separate sensor placement procedure for the vastus medialis and the vastus lateralis muscle.

MUSCLE

Name	Soleus
Subdivision	

MUSCLE ANATOMY

Origin	Posterior surfaces of the head of the fibula and proximal 1/3 of its body, soleal line and middle 1/3 of medial border of tibia and tendinous arch between tibia and fibula.
Insertion	With tendon of gastrocnemius into posterior surface of calcaneus.
Function	Plantar flexion of the ankle joint.

Electrode location on the muscle

RECOMMENDED SENSOR PLACEMENT PROCEDURE

Starting posture	Sitting with the knee approximately 90 degrees flexed and the heel / foot of the investigated leg on the floor.
Electrode size	Maximum size in the direction of muscle fibres: 10 mm.
Inter electrode distance	20 mm
Electrode placement	
- location	The electrodes need to be placed at 2/3 of the line between the medial condylis of the femur to the medial malleolus.
- orientation	In the direction of the line between the medial condylis to the medial malleolus.
- fixation on the skin	(Double sides) tape / rings or elastic band.
- reference electrode	On / around the ankle or the proc. spin. of C7.
Clinical test	Put a hand on the knee and keep / push the knee downward while asking the subject / patient to lift the heel from the floor.

MUSCLE

Name	Biceps femoris
Subdivisions	Long head and short head

MUSCLE ANATOMY

Origin	Long head: distal part of sacrotuberous ligament and posterior part of tuberosity Short head: lateral lip of linea aspera, proximal 2/3 of supracondylar line and lateral intermuscular septum.
Insertion	Lateral side of head of fibula, lateral condyle of tibia, deep fascial on lateral side of leg.
Function	Flexion and lateral rotation of the knee joint. The long head also extends and assists in lateral rotation of the hip joint.

Electrode location on the muscle

RECOMMENDED SENSOR PLACEMENT PROCEDURE

Starting posture	Lying on the belly with the face down with the thigh down on the table and the knees flexed (to less than 90 degrees) with the thigh in slight lateral rotation and the leg in slight lateral rotation with respect to the thigh.
Electrode size	Maximum size in the direction of the muscle fibres: 10 mm.
Inter electrode distance	20 mm.
Electrode placement	
- location	The electrodes need to be placed at 50% on the line between the ischial tuberosity and the lateral epicondyle of the tibia.
- orientation	In the direction of the line between the ischial tuberosity and the lateral epicondyle of the tibia.
- fixation on the skin	(Double sided) tape / rings or elastic band.
- reference electrode	On / around the ankle or the proc. spin. of C7.
Clinical test	Press against the leg proximal to the ankle in the direction of knee extension.

MUSCLE

Name	Quadriceps femoris
Subdivision	Vastus lateralis

MUSCLE ANATOMY

Origin	Proximal parts of intertrochanteric line, anterior and inferior borders of greater trochanter, lateral lip of gluteal tuberosity, proximal half of lateral lip of linea aspera, and lateral intermuscular septum.
Insertion	Proximal border of the patella and through patellar ligament.
Function	Extension of the knee joint.

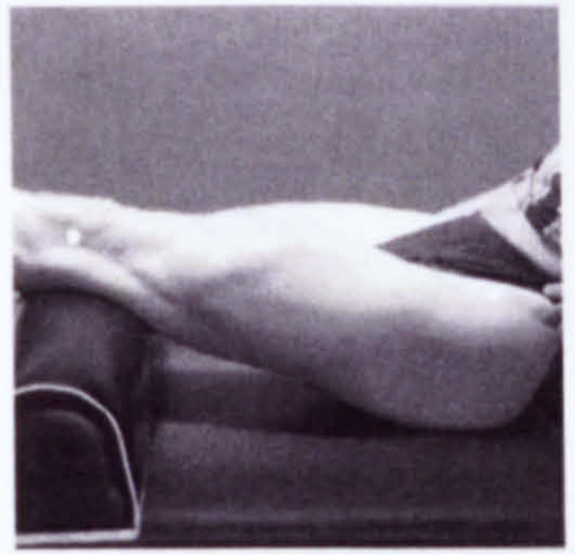

Electrode location on the muscle

RECOMMENDED SENSOR PLACEMENT PROCEDURE

Starting posture	Sitting on a table with the knees in slight flexion and the upper body slightly bend backward.
Electrode size	Maximum size in the direction of the muscle fibres. 10 mm.
Inter electrode distance	20 mm.
Electrode placement	
- location	Electrodes need to be placed at 2/3 on the line from the anterior spina iliaca superior to the lateral side of the patella.
- orientation	In the direction of the muscle fibres
- fixation on the skin	(Double sided) tape / rings or elastic band.
- reference electrode	On / around the ankle or the proc. spin. of C7.
Clinical test	Extend the knee without rotating the thigh while applying pressure against the leg above the ankle in the direction of flexion.
Remarks	The SENIAM guidelines include also a separate sensor placement procedure for the vastus medialis and the rectus femoris muscle.